

**Finite Element Analysis Model for Determination of In-situ and Mining  
Induced Stresses as a Function of Two Different Mining Methods Used at  
Diavik Diamond Mine**

by

Mohammadali Sepehri

A thesis submitted in partial fulfillment of the requirements for the degree of

Doctor of Philosophy

in

Mining Engineering

Department of Civil and Environmental Engineering  
University of Alberta

## ABSTRACT

One of the essential components of the underground excavation design process, which directly influences the performance and stability of underground constructions, is knowledge of the in-situ and mining-induced stress. Knowing the magnitudes and directions of these stresses can help determine suitable shapes and orientations for tunnels (drifts) and stopes. In addition, knowing the stress regime in the rock mass can be used to predict the type of rock failure that may occur in the future and identify potential rockbursting zones. The problem statement for this geomechanical research thesis is: *“The determination of in-situ and mining-induced stress regimes as a function of two different underground mining methods used at Diavik Diamond Mine”*

In this research, the main objective is to develop an engineering methodology to estimate the in-situ and mining-induced stress regimes in the host rock and orebody using the finite element analysis method. A case study of Diavik Diamond Mine is used to illustrate the estimation procedure and to implement the proposed methodology.

In order to reach the objectives of this research, a full realistic three dimensional finite element model of the case study mine was developed. This finite element analysis model was used to determine the in-situ and mining-induced stress regimes at the case study mine. Some laboratory tests have been conducted on Kimberlite samples to calibrate the material strength properties (such as elastic

and strength parameters). Finally, the results from the developed finite element model are validated by comparing them to actual field data and site observations.

The main contributions of this study include developing and implementing an engineering methodology for estimating in-situ and mining-induced stresses, providing a better understanding of the stress distribution regime in a mine and investigating the role of mining methods on mining-induced stress fields. The outcomes of this research will enhance the body of knowledge regarding the effect of stress ratio (the ratio between horizontal to vertical stress) and stress heterogeneity regimes on the stability of underground excavations and possible zones of failure.

## **PREFACE**

This thesis is an original work by Mohammadali Sepehri. No part of this thesis has been previously published. This study was supported by the Natural Sciences and Engineering Research Council of Canada (NSERC) under Collaborative Research and Development (CRD) Grant [Number RES0017513]. This collaborative research was led by Professor Derek Apel at University of Alberta with guidance from the industrial collaborator represented by Mr. Jan Romanowski, the superintendent of mine technical services at Diavik Diamond Underground Mine.

## DEDICATION

This thesis is dedicated to:

*My Lovely Parents Sara and Daryoush*

*My Lovely Wife Azadeh*

*My Sister Setareh and Brother-in-law Ali*

*And to Azadeh's Parents Fereshteh and Mahmood*

## ACKNOWLEDGMENTS

I would like to thank my supervisor Dr. Derek Apel for his continued encouragements and guidance during this research. Without his leadership, support, time and energy he committed to helping me, I would not be able to accomplish this research.

I would like to thank my late co-supervisor Dr. Jozef Szymanski for his kindness and valuable suggestions.

I would like to express my gratitude and appreciation to the thesis examining committee members: Dr. Vivek Bindiganavile, Dr. Greg Galecki, Dr. Yashar Pourrahimian and Dr. Wei Liu for their precious time and constructive criticisms and comments. They brought out the best in me.

I would like to thank Dr. Rick Chalaturnyk for providing the access to coring equipment.

I would like to thank one of my best friends and research colleague Paul Leveille. His help during the rock mechanics laboratory tests is acknowledged.

This study was supported by the Natural Sciences and Engineering Research Council of Canada (NSERC) under Collaborative Research and Development (CRD) Grant [Number RES0017513]. The supports from NSERC, Diavik Diamond Mine and Rio Tinto are acknowledged.

Mr. Jan Romanowski, the superintendent of mine technical services at Diavik Diamond underground mine is specially acknowledged for his support and technical inputs throughout this research.

I would like to thank Mr. Cristian Gherghel, the superintendent of mine technical services at Diavik Diamond underground mine for supporting the original idea for this research.

I would like to thank Dr. Amir Karami, the senior underground geotechnical engineer at Diavik Diamond Mine for his assistance with data gathering and his

valuable technical inputs. Also the support provided by Mr. Robbie McGregor and Mr. Roger Young the underground mine geologists, Mr. Aaron Elderkin the drill and blast engineer and Ms. Olga Druecker the geotechnical engineer at Diavik diamond mine is acknowledged.

Mr. Greg Miller and Mr. Camron West, the Structural Engineering Technologists, are acknowledged for their professional support during rock mechanics laboratory tests.

This research has been enabled by the use of computing resources provided by WestGrid and Compute/Calcul Canada. I would like to thank Dr. Masao Fujinaga, and Dr. Doug Phillips, the WestGrid's support team members, for their outstanding work helping me to use the supercomputers during this research.

I would like to thank Dr. Doug Booth and Dr. Samer Adeeb for answering my questions regarding to three-dimensional modeling and Abaqus respectively.

I am most thankful to my parents, Sara and Daryoush, for their lifetime unconditional love, support and encouragements. I would like to thank my sister, Setareh, for her moral and emotional support during this course of study.

Finally, I owe my love and gratitude to my lovely wife, Azadeh, who believed in me and stood by my side to pursuing my dreams. I thank her for the patience and continuous encouragements and inspirations during this research.

Mohammadali Sepehri, September 2016

# Table of Contents

|  |           |
|--|-----------|
| ABSTRACT.....  | ii        |
| PREFACE.....   | iv        |
| DEDICATION.....  | v         |
| ACKNOWLEDGMENTS.....   | vi        |
| LIST OF TABLES.....  | xiv       |
| LIST OF FIGURES.....   | xv        |
| LIST OF ABBREVIATIONS.....   | xxiv      |
| LIST OF SYMBOLS.....   | xxvi      |
| <b>CHAPTER 1: INTRODUCTION.....</b>  | <b>1</b>  |
| 1.1 General Background and Statement of the Problem.....                       | 2         |
| 1.2 Objectives of the Study.....   | 4         |
| 1.3 Research Methodology.....  | 5         |
| 1.4 Organization of Thesis.....  | 7         |
| <b>CHAPTER 2: LITERATURE REVIEW.....</b>                                       | <b>10</b> |
| 2.1 Conventional methods of stress analysis around underground structures..... | 12        |
| 2.1.1 In-situ stress.....  | 12        |
| 2.1.1.1 Vertical stress.....   | 12        |
| 2.1.1.2 Horizontal stress.....   | 13        |
| 2.1.1.3 Direction of the in-situ stress.....                                   | 16        |
| 2.1.1.4 World stress map.....  | 18        |
| 2.1.2 Analytical methods of induced stress estimation.....                     | 18        |
| 2.1.2.1 Circular excavation shape.....   | 18        |
| 2.1.3 Zone of influence of a tunnel.....                                       | 20        |
| 2.1.4 Standard Stress Measurement Techniques.....                              | 21        |
| 2.1.4.1 Flatjack measurement technique.....                                    | 21        |

|   |           |
|---|-----------|
| 2.1.4.2 Hydraulic fracturing technique.....   | 22        |
| 2.1.4.3 Overcoring techniques (USBM and CSIRO).....                                       | 24        |
| 2.2 Underground stability analysis methods.....   | 26        |
| 2.2.1 Analytical methods of excavation design.....  | 26        |
| 2.2.1.1 Beam theory.....  | 26        |
| 2.2.1.2 Voussoir arch theory.....   | 27        |
| 2.2.1.3 Hoek-Brown failure criterion.....   | 30        |
| 2.2.1.4 Mohr-Coulomb failure criterion.....   | 32        |
| 2.2.1.5 Relationship between the Mohr-Coulomb and the Hoek-Brown criteria.....            | 34        |
| 2.2.2 Empirical methods of open stope stability analysis.....                             | 34        |
| 2.2.2.1 Rock mass classification design schemes.....                                      | 34        |
| 2.2.2.2 Rock mass rating (also known as geomechanics classification).....                 | 35        |
| 2.2.2.3 Rock tunneling quality index system and the modified tunneling quality index..... | 35        |
| 2.2.2.4 Geological strength index.....  | 38        |
| 2.2.2.5 Mathews stability graph.....  | 39        |
| 2.2.3 Observational method.....   | 43        |
| 2.3 Numerical modeling in rock mechanics.....   | 45        |
| 2.3.1 Introduction.....   | 45        |
| 2.3.2 Finite element method.....  | 47        |
| 2.4 A review of current state-of-the-art rock mechanics modeling approaches.....          | 53        |
| <b>CHAPTER 3: FINITE ELEMENT ANALYSIS MODEL FOR THE</b>                                   |           |
| <b>DETERMINATION OF IN-SITU AND MINING-INDUCED STRESS – A CASE</b>                        |           |
| <b>STUDY OF DIAVIK DIAMOND MINE.....</b>  | <b>55</b> |
| 3.1 Introduction.....   | 56        |
| 3.2 A case study: Diavik Diamond Mine.....  | 56        |
| 3.2.1 Sublevel open stoping and blasthole stoping.....                                    | 58        |
| 3.2.2 Sublevel longhole retreat mining method.....  | 59        |



|  |            |
|--|------------|
| 4.4.1.1. <i>Potential rockbursting in Zone 1</i> .....   | 115        |
| 4.4.1.2. <i>Potential rockbursting in Zone 2</i> .....   | 118        |
| 4.4.1.3. <i>Potential rockbursting in Zone 3</i> .....   | 120        |
| 4.4.2 Potential rockbursting in the Kimberlite pipes .....   | 123        |
| 4.4.2.1. <i>Potential rockbursting in the A154 North Kimberlite pipe</i> .....   | 124        |
| 4.4.2.2. <i>Potential rockbursting in the A154 South Kimberlite pipe</i> .....   | 126        |
| 4.4.3 Rockburst potentials in the sill pillar .....  | 127        |
| 4.5 Summary and conclusion .....   | 130        |
| <b>CHAPTER 5: PREDICTION OF MINING-INDUCED SURFACE SUBSIDENCE<br/>AND GROUND MOVEMENTS AT DIAVIK DIAMOND MINE USING A FULL<br/>3D ELASTOPLASTIC FINITE ELEMENT MODEL .....</b> | <b>131</b> |
| 5.1 Introduction .....   | 132        |
| 5.2 Diavik Diamond Mine .....  | 133        |
| 5.2.1 Mining Method .....  | 133        |
| 5.3 Methodology .....  | 135        |
| 5.3.1 Model geometry .....   | 135        |
| 5.3.2 Finite element mesh .....  | 137        |
| 5.3.3 Constitutive model and material properties .....   | 140        |
| 5.3.4 Simulation steps .....   | 141        |
| 5.3.5 In-situ stresses (simulating the initial stress state) .....   | 143        |
| 5.4 Calibration of the finite element model .....  | 145        |
| 5.5 Results and discussion .....   | 148        |
| 5.5.2 Verification of the results .....  | 151        |
| 5.6 Conclusion .....   | 155        |
| <b>CHAPTER 6: STOPE STABILITY ASSESSMENT, YIELDING AND<br/>RELAXATION ZONES, AND SENSITIVITY ANALYSIS USING THE FINITE<br/>ELEMENT MODEL .....</b>                             | <b>157</b> |
| 6.1 Introduction .....   | 158        |

|   |            |
|---|------------|
| 6.1.1 Case study: Diavik Diamond Mine.....  | 159        |
| 6.1.2 Problem definition and objectives.....  | 159        |
| 6.2 Overview of the stability graph method.....                                       | 160        |
| 6.3 Stability assessment using the stability graph method.....                        | 161        |
| 6.3.1 Stress factor ( <i>A</i> ).....   | 162        |
| 6.3.2 Joint orientation factor ( <i>B</i> ).....                                      | 163        |
| 6.3.3 Gravity adjustment factor ( <i>C</i> ).....                                     | 164        |
| 6.4 Results of the assessment using the stability graph .....                         | 164        |
| 6.4.1 Results for the first section (0 to 30 m of the stope length) .....             | 164        |
| 6.4.2 Stability assessment for the second section (30 to 114 m of the stope length).. | 165        |
| 6.5 Overview of the numerical approach: finite element method.....                    | 167        |
| 6.5.1 Numerical model.....  | 167        |
| 6.5.2 Input data assumptions and defining elements .....                              | 169        |
| 6.5.3 Simulation steps.....   | 170        |
| 6.6 Results of the stability assessments using the numerical model.....               | 170        |
| 6.6.1 Yielding zones .....  | 171        |
| 6.6.2 Relaxation zones .....  | 171        |
| 6.7 Sensitivity analysis.....   | 173        |
| 6.7.1 Yielding zone.....  | 173        |
| 6.7.2 Relaxation zones .....  | 174        |
| 6.8 Discussion and conclusions .....  | 175        |
| <b>CHAPTER 7: VERIFICATION, VALIDATION AND DISCUSSION OF THE RESULTS .....</b>        | <b>176</b> |
| 7.1 Introduction.....   | 177        |
| 7.2 Verification .....  | 178        |
| 7.2.1 Pre-mining state of stress .....  | 178        |
| 7.3 Discussion and validation of the finite element model results.....                | 180        |

|   |            |
|---|------------|
| 7.3.1 Surface subsidence at the N9280 bench: discussion and validation of the results .....       | 181        |
| 7.3.2 S9125 South wall movements and failure: Bottom of the pit .....                             | 186        |
| 7.3.3 Fall of ground at the N9225-118 drift.....  | 191        |
| 7.3.4 Rockburst failure incident at the S9050-940 drift and finite element model prediction ..... | 192        |
| 7.4 Summary and conclusion .....  | 193        |
| <b>CHAPTER 8: SUMMARY, CONCLUSIONS AND RECOMMENDATIONS.....</b>                                   | <b>194</b> |
| 8.1 Summary of the research .....   | 195        |
| 8.2 Research conclusions .....  | 199        |
| 8.3 Significance and contributions of the research .....  | 201        |
| 8.4 Recommendations for future work .....   | 203        |
| <b>BIBLIOGRAPHY .....</b>   | <b>204</b> |
| <b>Appendix A: Rock Mechanics Laboratory Tests Results.....</b>                                   | <b>215</b> |
| <b>Appendix B: WORLD STRESS MAP .....</b>   | <b>255</b> |
| <b>Appendix C: The Support Chart Based on the Tunnelling Quality Index Q.....</b>                 | <b>257</b> |
| <b>Appendix D: ABAQUS CODE – SIMULATION STEPS .....</b>   | <b>258</b> |

## LIST OF TABLES

|  |     |
|--|-----|
| Table 2.1 Popular rock mass classification systems for underground design .....  | 36  |
| Table 2.2 Guidelines for excavations and support in rock tunnels (after Bieniawski, 1989)<br>.....                       | 37  |
| Table 3.1 Kimberlite sample rock types .....   | 60  |
| Table 3.2 Uniaxial compressive strength test results .....   | 65  |
| Table 3.3 Brazilian test results.....  | 70  |
| Table 3.4 Results of the triaxial test on the PKX Kimberlite rock type.....  | 74  |
| Table 3.5 Triaxial compressive test results on intact core specimens.....  | 79  |
| Table 3.6 Estimated rock mass properties for each Kimberlite rock type .....   | 87  |
| Table 3.7 Material properties defined in the FE model .....  | 87  |
| Table 3.8 Mesh scenarios used to perform a mesh convergence study .....  | 90  |
| Table 3.9 CPU time for the first iteration* .....  | 92  |
| Table 3.10 Cost and Time of Calculations.....  | 103 |
| Table 4.1 Rockburst hazard rating system proposed by Miao et al. (2016).....   | 109 |
| Table 4.2 Rockburst tendency prediction using the rock brittleness coefficient .....                                     | 110 |
| Table 4.3 Rockburst tendency prediction using the tangential stress criterion (Wang and<br>Park, 2001).....              | 111 |
| Table 4.4 Estimation of the critical strain energy for granite.....  | 114 |
| Table 4.5 Depth of each monitoring point in Zone 1 .....   | 116 |
| Table 4.6 Depth of each monitoring point in Zone 2.....  | 118 |
| Table 4.7 Average critical energy values for both Kimberlite pipes (from Leveille, 2015;<br>Leveille et al., 2016) ..... | 123 |
| Table 4.8 Average UCS values estimated from laboratory tests on Kimberlite samples                                       | 123 |
| Table 5.1 Mesh Scenarios used to perform a Mesh Convergence Study (MCS).....   | 138 |
| Table 5.2 CPU Time for the First Iteration* .....  | 139 |
| Table 5.3 Material properties .....  | 141 |
| Table 5.4 Comparison between finite element model results and the measured data.....                                     | 155 |
| Table 6.1 Value of the modified tunneling quality index .....  | 161 |
| Table 6.2 Proposed stope dimensions.....   | 162 |
| Table 6.3 Calculated shape factor.....   | 162 |
| Table 6.4 Joint orientation factor .....   | 164 |
| Table 6.5 Gravity adjustment factor .....  | 164 |

|   |     |
|---|-----|
| Table 6.6 Stability parameters for section 1 (0 to 30 m).....                                       | 164 |
| Table 6.7 Stability parameters for section 2 (30 to 114 m).....                                     | 166 |
| Table 6.8 Material properties.....  | 169 |
| Table 7.1 Compression of the analytical and finite element model solutions.....                     | 179 |
| Table 7.2 Comparison between the measured data and the finite element model's<br>calculations ..... | 186 |
| Table D-1 The Value of ESR proposed by Barton et al., (1974).....                                   | 257 |

## LIST OF FIGURES

|   |    |
|---|----|
| Figure 2.1 Variation with depth of measured values of in-situ vertical stress (after Hoek<br>and Brown, 1980) .....   | 13 |
| Figure 2.2 Variation with depth of ratio of horizontal to vertical stresses (after Hoek and<br>Brown, 1980) .....   | 14 |
| Figure 2.3 Ratio of the average horizontal to vertical stress based on Sheory (1994) and<br>Hoek and Brown (1980).....  | 15 |
| Figure 2.4 State of the principal stresses near an open fracture (after Hudson et al., 2003)<br>.....   | 16 |
| Figure 2.5 State of in-situ stress around different types of faults .....   | 17 |
| Figure 2.6 Breakouts around a horizontal wellbore in different in-situ stress regimes<br>(after Wikel, 2011).....   | 17 |
| Figure 2.7 Problem geometry for estimating the stress and displacement around a circular<br>excavation in a biaxial stress field (after Brady and Brown, 2004)..... | 19 |
| Figure 2.8 Stress distribution around a circular excavation in a hydrostatic stress field<br>(after Brady and Brown, 2004).....                                     | 20 |
| Figure 2.9 Flatjack test setup .....  | 22 |
| Figure 2.10 Hydraulic fracturing test (after Thompson et al., 2004).....  | 23 |
| Figure 2.11 USBM borehole deformation gauge.....  | 24 |
| Figure 2.12 Simple beam theory diagram.....   | 27 |
| Figure 2.13 Free body diagrams of the Voussoir beam (mid-span of the left side of the<br>beam is shown) (after Diederichs and Kaiser, 1999).....                    | 28 |
| Figure 2.14 The complete procedure for the determination of deflection and stability of a<br>Voussoir beam (after Diederichs and Kaiser, 1999).....                 | 31 |

|  |    |
|--|----|
| Figure 2.15 Estimation of the generalized Hoek-Brown parameters for an undisturbed rock mass (from Hoek et al., 1995).....   | 33 |
| Figure 2.16 Mohr-Coulomb failure envelope .....  | 33 |
| Figure 2.17 Mathews stability graph design factors: (a) stress factor ( $A$ ), (b) joint orientation adjustment factor ( $b$ ), (c) gravity adjustment factor for gravity fall and slabbing failure mode, and (d) gravity factor for sliding failure mode (after Potvin, 1988) ..... | 41 |
| Figure 2.18 The modified stability graph (after Stewart and Forsyth, 1995) .....   | 42 |
| Figure 2.19 Choice of continuum or discontinuum methods (after Bobet et al., 2009)....   | 46 |
| Figure 2.20 Discretization of the domain using finite elements and forming a mesh.....   | 48 |
| Figure 2.21 A linear triangular element .....  | 48 |
| Figure 2.22 Pascal triangle for 2D cases (after Liu et al., 2003).....   | 52 |
| Figure 2.23 Pascal pyramid for 3D cases (after Liu et al., 2003) .....   | 52 |
| Figure 2.24 Flowchart of a rock mechanics modeling and rock engineering design approach (after Feng and Hudson, 2011).....   | 53 |
| Figure 3.1 Aerial image of Diavik Diamond Mine (courtesy of Diavik Diamond Mine)   | 57 |
| Figure 3.2 Location of three Kimberlite pipes .....  | 57 |
| Figure 3.3 An illustration of the SLR mining method (after Diavik Dialogue, 2011).....   | 59 |
| Figure 3.4 Test specimen preparation workflow .....  | 61 |
| Figure 3.5 Example results from a UCS test (Sample ID: PK-UCS3).....   | 64 |
| Figure 3.6 Example of mode of failure from a UCS test (Sample ID: PK-UCS3) .....   | 64 |
| Figure 3.7 Uniaxial compressive test results - Note: SD stands for standard deviation ...  | 66 |
| Figure 3.8 Young's modulus estimations from UCS test - Note: SD stands for Standard Deviation.....   | 66 |
| Figure 3.9 Poisson's ratio estimations from UCS test - Note: SD stands for Standard Deviation.....   | 67 |
| Figure 3.10 Apparatus used for the Brazilian test.....   | 68 |
| Figure 3.11 Example results of a Brazilian test, its mode of failure and corresponding calculations (Sample ID: MRK - T5).....   | 69 |
| Figure 3.12 Error bars for Tensile strength test results - Note: SD stands for Standard Deviation.....   | 69 |
| Figure 3.13 Hoek-Franklin triaxial cell and its cutaway view .....   | 71 |
| Figure 3.14 Triaxial test settings using the Hoek-Franklin cell .....  | 72 |
| Figure 3.15 Triaxial stress state for each PKX Kimberlite specimen .....   | 76 |

|   |     |
|---|-----|
| Figure 3.16 Failure mode of each PKX Kimberlite core specimen (obtained from triaxial testing regime) .....   | 77  |
| Figure 3.17 The linear relationship between the major and minor principal stresses for PKX Kimberlite .....   | 78  |
| Figure 3.18 Mohr-Coulomb failure envelope for intact PKX Kimberlite.....  | 78  |
| Figure 3.19 Summary of the FE analysis methodology.....   | 80  |
| Figure 3.20 Full 3D model of the mine constructed in Abaqus .....   | 81  |
| Figure 3.21 Full 3D models of the underground structures constructed in Abaqus: two Kimberlite pipes, two mining methods (BHS and SLR), sill pillar, crown pillar, haulage drifts and ramps ..... | 82  |
| Figure 3.22 Full 3D models of the A154 North pipe, sill pillar, crown pillar, CRF cap and BHS stopes.....   | 84  |
| Figure 3.23 Full 3D model of the A154 North pipe with SLR stopes .....  | 85  |
| Figure 3.24 Methodology for estimating the rock mass strength of Kimberlite.....  | 88  |
| Figure 3.25 FE mesh .....   | 89  |
| Figure 3.26 Mesh convergence study on maximum displacement .....  | 90  |
| Figure 3.27 MCS on vertical stress at a monitoring node.....  | 91  |
| Figure 3.28 MCS: active yield flag at the monitoring node.....  | 92  |
| Figure 3.29 Initial state of stress as simulated in step 1 (geostatic step).....  | 94  |
| Figure 3.30 Contact between granite and the A154 North Kimberlite Pipe at mine level N9275.....   | 95  |
| Figure 3.31 Mining Block A sequence and simulation steps * .....  | 98  |
| Figure 3.32 Mining Block B sequence and simulation steps* .....   | 99  |
| Figure 3.33 Sequence of mining and simulation steps for mine level S9100 of the A154 South pipe* (using SLR).....   | 100 |
| Figure 3.34 Sequence of mining and simulation steps for mine level S9075 of the A154 South pipe (using SLR).....  | 101 |
| Figure 3.35 Sequence of mining and simulation steps for mine level S9050 of the A154 South pipe (using SLR).....  | 102 |
| Figure 4.1 Schematic representation of rockburst potentials (after Castro et al., 2012) .   | 107 |
| Figure 4.2 Typical UCS hysteresis looping test curve (after Kwasniewski et al., 1994)   | 108 |
| Figure 4.3 Proposed methodology for rockburst prediction .....  | 113 |
| Figure 4.4 Identified zones of rockburst potentials in the granite-Kimberlite contact at the A154 South pipe .....  | 115 |

|   |     |
|---|-----|
| Figure 4.5 Rockburst potential Zone 1 and monitored points.....   | 115 |
| Figure 4.6 Energy storage density at the monitoring points in Zone 1 throughout the simulation.....                                 | 116 |
| Figure 4.7 Burst potential index at the monitoring points at Zone 1 throughout the simulation steps.....                            | 117 |
| Figure 4.8 Rockburst tendency evaluation based on the tangential stress criterion.....  | 117 |
| Figure 4.9 Rockburst potential Zone 2 and monitored points.....   | 118 |
| Figure 4.10 Energy storage rate at the monitoring points in Zone 2 throughout the simulation.....                                   | 119 |
| Figure 4.11 Burst potential index at the monitoring points in Zone 1 throughout the simulation.....                                 | 119 |
| Figure 4.12 Rockburst tendency evaluation based on the tangential stress criterion at the A154 South-granite contact in Zone 2..... | 120 |
| Figure 4.13 Rockburst potential in Zone 3 and monitored points.....   | 121 |
| Figure 4.14 Energy storage rate at the monitoring points in Zone 3 throughout the simulation steps.....                             | 121 |
| Figure 4.15 Burst potential index (BPI) in the monitoring point at zone 3.....  | 122 |
| Figure 4.16 Rockburst tendency evaluation based on the tangential stress criterion at the A154 South-granite contact in Zone 3..... | 122 |
| Figure 4.17 Estimation of the burst potential index and energy storage density in the A154 North Kimberlite pipe.....               | 124 |
| Figure 4.18 Maximum tangential stress distribution and estimated rockburst tendency for the A154 North Kimberlite pipe.....         | 125 |
| Figure 4.19 Estimation of the burst potential index and energy storage density at the A154 South Kimberlite pipe.....               | 126 |
| Figure 4.20 Maximum tangential stress distribution and estimated rockburst tendency for the A154 South Kimberlite pipe.....         | 127 |
| Figure 4.21 Estimation of the burst potential index and energy storage density in the sill pillar.....                              | 128 |
| Figure 4.22 Variation of the energy storage rate along the circumferential path.....  | 128 |
| Figure 4.23 Variation of the burst potential index along the circumferential path.....  | 129 |
| Figure 4.24 Maximum tangential stress distribution and estimated rockburst tendency in the sill pillar.....                         | 129 |
| Figure 5.1 Blasthole Stopping Method (After Diavik Diamond Mine fact book 2012) ...   | 134 |

|   |     |
|---|-----|
| Figure 5.2 Full 3D model of the mine in Abaqus .....  | 135 |
| Figure 5.3 3D geometry of the A154N Kimberlite pipe created in abaqus .....   | 136 |
| Figure 5.4 The A154 North Kimberlite surface crown pillar at mine elevation N9225 m to N9290 m .....  | 136 |
| Figure 5.5 3D geometries of blasthole stopes created in Abaqus .....  | 137 |
| Figure 6 Mesh Convergence Study on Maximum Displacement .....   | 138 |
| Figure 5.7 MCS on Vertical Stress at a monitoring node at the back of N9175 Undercut drift.....   | 139 |
| Figure 5.8 The Mohr-Coulomb Failure Criterion .....   | 140 |
| Figure 5.9 Estimation of the Mohr-Coulomb parameters (Hoek et al. 1995) for Kimberlite using RocLab software .....  | 142 |
| Figure 5.10 Mining sequence and simulation steps .....  | 143 |
| Figure 5.11 Initial State of Stress- Simulated in Step one (Geostatic Step) .....   | 144 |
| Figure 5.12 Ground movement extensometer data measured at N9175- S118's undercut .....  | 145 |
| Figure 5.13 Movements of the calibration point on the back of the N9175-118 drift ....  | 146 |
| Figure 5.14 Ground movement extensometer data measured at the N9175- S148 undercut .....  | 147 |
| Figure 5.15 Movements of the calibration point on the back of the N9175-118 drift ....  | 148 |
| Figure 5.16 Displacement on the pit surface predicted by the finite element model.....  | 149 |
| Figure 5.17 Predicted surface subsidence along the monitoring nodes path in different simulation steps.....   | 150 |
| Figure 5.18 Curve fitting of the numerical predictions.....   | 150 |
| Figure 5.19 Cross section of BHS mining and induced movements. Mining Block A is located at the A154 North pipe between mine levels N9175 and N9275 ..... | 151 |
| Figure 5.20 Location of the monitoring prisms on the bench used for finite element model verification.....  | 152 |
| Figure 5.21 Comparison of the magnitude of displacement for Monitoring Zone 1 .....   | 153 |
| Figure 5.22 Comparison of the magnitude of displacement for Monitoring Zone 2 .....   | 153 |
| Figure 5.23 Comparison of the magnitude of displacement of the 280-10 prism.....  | 154 |
| Figure 5.24 Comparison of the magnitude of displacement of the 280-12 prism.....  | 154 |
| Figure 6.1 Rock stress factor for different values of $\sigma_c/\sigma_v$ (after Mathews et al., 1981)  | 163 |
| Figure 6.2 The dominant structure sets.....   | 163 |

|  |     |
|--|-----|
| Figure 6.3 Stability assessment using Mathews stability graph for section 1 using GDA software.....  | 165 |
| Figure 6.4 Stability assessment using Mathews stability graph for section 2 using GDA software.....  | 166 |
| Figure 6.5 Full 3D model of the mine in Abaqus (left) and aerial view of the mine.....   | 168 |
| Figure 6.6 Simplified model of the A154 North Kimberlite pipe and Mining Block A.  | 168 |
| Figure 6.7 Targeted stope P1-185 is located between mine levels N9225 and N9250...   | 169 |
| Figure 6.8 Mining sequence and simulation steps .....  | 170 |
| Figure 6.9 Yielding zones around each stope block .....  | 171 |
| Figure 6.10 Relaxation zones around each stope block .....   | 172 |
| Figure 6.11 Development of the relaxed zone after the excavation of Stope Block 3....  | 172 |
| Figure 6.12 The extent of the yielding zones around Block 1 with different $k$ values ...  | 173 |
| Figure 6.13 Average relaxation depth for different stress regimes .....  | 174 |
| Figure 6.14 Average relaxation depth for different stress regimes .....  | 174 |
| Figure 7.1 Method of specifying the in-situ state of stress relative to a set of global references axes (after Brady and Brown, 2004)..... | 178 |
| Figure 7.2 Compression of the analytical and finite element model solutions .....  | 180 |
| Figure 7.3 Surface subsidence displacements calculated by the finite element model for the N9280 bench .....                               | 181 |
| Figure 7.4 Mining-induced surface subsidence growth throughout the finite element model simulation.....                                    | 182 |
| Figure 7.5 Curve fitting of the finite element model results for N9280's mining-induced surface subsidence .....                           | 182 |
| Figure 7.6 Comparison of monitored displacements at Monitoring Zone 1 versus the finite element model's calculated values .....            | 184 |
| Figure 7.7 Comparison of monitored displacements at Monitoring Zone 2 versus the finite element model's calculated values.....             | 184 |
| Figure 7.8 Comparison of monitored displacements of the 280-10 prism and the finite element model's calculated values.....                 | 185 |
| Figure 7.9 Comparison of monitored displacements of the 280-12 prism and the finite element model's calculated values.....                 | 185 |
| Figure 7.10 Surface settlements predicted by the finite element model for the S9125 South and North wall failure.....                      | 187 |

|   |     |
|---|-----|
| Figure 7.11 The extent of the mining-induced surface subsidence predicted by the finite element model.....  | 188 |
| Figure 7.12 Crack meters installed in the S9125-920 drift by the mine (courtesy of Diavik Diamond Mine).....  | 189 |
| Figure 7.13 Measured displacements along the horizontal and vertical crack meters (CM 6 and CM5, respectively).....                                     | 190 |
| Figure 7.14 The S9125 South wall failure (from the S9125 prisms data; photo courtesy of Diavik Diamond Mine).....                                       | 190 |
| Figure 7.15 fall of ground at the N9225-118 drift and the finite element model predictions for this drift (photo courtesy of Diavik Diamond Mine) ..... | 191 |
| Figure 7.16 Ground failure at S9050 SLR (A154 South) and the finite element model predictions (photo courtesy of Diavik Diamond Mine).....              | 192 |
| Figure 8.1 Visual summary of the research methodology .....   | 196 |
| Figure A-1 Sample No. PK - UCS 1 .....  | 216 |
| Figure A-2 Sample No. PK - UCS 2.....   | 216 |
| Figure A-3 Sample No. PK - UCS 3.....   | 217 |
| Figure A-4 Sample No. PKX-UCS 1 .....   | 217 |
| Figure A-5 Sample No. PKX-UCS 2.....  | 218 |
| Figure A-6 Sample No. PKX-UCS3.....   | 218 |
| Figure A-7 Sample No. MK-UCS1 .....   | 219 |
| Figure A-8 Sample No. MK-UCS2 .....   | 219 |
| Figure A-9 Sample No. MK-UCS3 .....   | 220 |
| Figure A-10 Sample No. MRK-UCS1 .....   | 220 |
| Figure A-11 Sample No. MRK-UCS2.....  | 221 |
| Figure A- 12 Sample No. MRK-UCS3.....   | 221 |
| Figure A-13 Sample No. MRK-UCS4.....  | 222 |
| Figure A-14 Sample No. MRK-UCS5.....  | 222 |
| Figure A-15 Sample No. MRK-UCS6.....  | 223 |
| Figure A-16 Sample No. BMVK-UCS1 .....  | 223 |
| Figure A-17 Sample No. BMVK-UCS2.....   | 224 |
| Figure A-18 Sample No. BMVK-UCS3 .....  | 224 |
| Figure A-19 Uniaxial Compressive Strength Tests Results - Failure Modes for PK, PKX and MK Rock Types .....   | 225 |

|  |     |
|--|-----|
| Figure A-20 Uniaxial Compressive Strength Tests Results - Failure Modes for BMVK and MRK Rock Types .....      | 226 |
| Figure A-21 Brazilian Test - Sample No. MRK - T1 .....   | 227 |
| Figure A-22 Brazilian Test - Sample No. MRK – T2.....  | 227 |
| Figure A-23Brazilian Test - Sample No. MRK - T3 .....  | 228 |
| Figure A-24 Brazilian Test - Sample No. MRK - T4 .....   | 228 |
| Figure A-25 Brazilian Test - Sample No. MRK - T5 .....   | 229 |
| Figure A-26 Brazilian Test - Sample No. MRK - T6 .....   | 229 |
| Figure A-27 Brazilian Test - Sample No. MK – T1 .....  | 230 |
| Figure A-28 Brazilian Test - Sample No. MK – T2 .....  | 230 |
| Figure A-29 Brazilian Test - Sample No. MK – T3 .....  | 231 |
| Figure A-30 Brazilian Test - Sample No. MK – T4 .....  | 231 |
| Figure A-31 Brazilian Test - Sample No. MK – T5 .....  | 232 |
| Figure A-32 Brazilian Test - Sample No. MK – T6 .....  | 232 |
| Figure A-33Brazilian Test - Sample No. BMVK – T1.....  | 233 |
| Figure A-34 Brazilian Test - Sample No. BMVK – T2.....   | 233 |
| Figure A-35 Brazilian Test - Sample No. BMVK – T3.....   | 234 |
| Figure A-36 Brazilian Test - Sample No. BMVK – T4.....   | 234 |
| Figure A-37 Brazilian Test - Sample No. BMVK – T5.....   | 235 |
| Figure A-38 Brazilian Test - Sample No. BMVK – T6.....   | 235 |
| Figure A-39 Brazilian Test - Sample No. BMVK – T7.....   | 236 |
| Figure A-40 Brazilian Test - Sample No. PKX – T4.....  | 236 |
| Figure A-41 Brazilian Test - Sample No. PKX – T5.....  | 237 |
| Figure A-42 Brazilian Test - Sample No. PKX – T6.....  | 237 |
| Figure A-43 Brazilian Test - Sample No. PKX – T7.....  | 238 |
| Figure A.44 Axial Stress vs Piston Displacement for Each Specimen – Rock Type PK239                            |     |
| Figure A.45 Axial Stress vs. Confinement Pressure for Each Specimen - Rock Type: PK .....                      | 240 |
| Figure A.46 The linear relationship between the major and minor principal stresses for PK Kimberlite .....     | 241 |
| Figure A.47 Mohr-Coulomb failure envelope for intact PK Kimberlite (based on the Average Acceptable data)..... | 241 |
| Figure A.48 Failure Mode of Each Core Specimen - PK Kimberlite - Triaxial Test .....                           | 242 |

|   |     |
|---|-----|
| Figure A.49 Axial Stress vs Piston Displacement for Each Sample – Rock Type BMVK<br>.....   | 243 |
| Figure A.50 Axial Stress vs. Confinement Pressure for Each Specimen - Rock Type:<br>BMVK .....  | 244 |
| Figure A.51 The linear relationship between the major and minor principal stresses for<br>BMVK Kimberlite .....   | 245 |
| Figure A.52 Mohr-Coulomb failure envelope for intact BMVK Kimberlite (based on the<br>Average Acceptable data) .....                                      | 245 |
| Figure A.53 Failure Mode of Each Core Specimen - BMVK Kimberlite - Triaxial Test<br>.....   | 246 |
| Figure A.54 Axial Stress vs Piston Displacement for Each Sample – Rock Type MRK   | 247 |
| Figure A.55 .....   | 248 |
| Figure a.56 The linear relationship between the major and minor principal stresses for<br>MRK Kimberlite .....  | 249 |
| Figure A.57 Mohr-Coulomb failure envelope for intact MRK Kimberlite (based on the<br>Average Acceptable data) .....                                       | 249 |
| Figure A.58 Failure Mode of Each Core Specimen - MRK Kimberlite - Triaxial Test   | 250 |
| Figure A.59 Axial Stress vs Piston Displacement for Each Sample – Rock Type MK  | 251 |
| Figure A.60 Axial Stress vs. Confinement Pressure for Each Specimen - Rock Type: MK<br>.....  | 252 |
| Figure A.61 The linear relationship between the major and minor principal stresses for<br>MRK Kimberlite .....  | 253 |
| Figure A.62 Mohr-Coulomb failure envelope for intact MRK Kimberlite (based on the<br>Average Acceptable data) .....                                       | 253 |
| Figure A.63 Failure Mode of Each Core Specimen - MRK Kimberlite - Triaxial Test   | 254 |
| Figure B-1 North America Stress Map (Heidbach et al. 2008).....   | 255 |
| Figure B-2 World Stress Map (Heidbach et al. 2008) .....  | 256 |
| Figure D-1 Estimation of Support parameters based on tunnelling quality index Q (After<br>Grimstad and Barton 1993, From Palmstrom and Broch, 2006) ..... | 257 |

## **LIST OF ABBREVIATIONS**

|       |  |
|-------|--|
| 2D    | Two-Dimensional  |
| 3D    | Three-Dimensional  |
| ARD   | Average Relaxation Depth                                   |
| ASTM  | American Society for Testing and Materials                 |
| BEM   | Boundary Element Method                                    |
| BHS   | Blasthole Stopping   |
| BMVK  | Black Macrocrystic Volcaniclastic Kimberlite               |
| BPI   | Burst Potential Index                                      |
| CPU   | Central Processing Unit                                    |
| CRF   | Cemented Rockfill  |
| CSIRO | Council of Scientific and Industrial Research Organization |
| DEM   | Discrete Element Method                                    |
| DFN   | Discrete Fracture Network                                  |
| ESR   | Energy Storage Rate  |
| FDM   | Finite Difference Method                                   |
| FE    | Finite Element   |
| FEM   | Finite Element Method                                      |
| GSI   | Geological Strength Index                                  |
| HR    | Hydraulic Radius   |
| HTPF  | Hydraulic Testing of Pre-existing Fractures                |
| ISRM  | International Society for Rock Mechanics                   |
| MCS   | Mesh Convergence Study                                     |

|      |  |
|------|--|
| MK   | Magnetic Lapilli Rich Macrocrystic Volcaniclastic Kimberlite |
| MRK  | Mud-Rich Volcaniclastic Kimberlite                           |
| NATM | New Austrian Tunneling Method                                |
| PK   | Pyroclastic Kimberlite                                       |
| PKX  | Olive & Macrocrystic-rich Pyroclastic Kimberlite             |
| RAM  | Random Access Memory   |
| RMR  | Rock Mass Rating   |
| RQD  | Rock Quality Designation                                     |
| SED  | Strain Energy Density  |
| SLR  | Sublevel Longhole Retreat                                    |
| SRF  | Stress Reduction Factor                                      |
| UCS  | Uniaxial Compressive Strength                                |
| URF  | Uncemented Rockfill  |
| USBM | United States Bureau of Mines                                |
| V&V  | Verification and Validation                                  |
| WSM  | World Stress Map   |

## LIST OF SYMBOLS

|                 |  |
|-----------------|--|
| $A$             | Stress factor  |
| $a$             | Hoek-Brown criterion constant for rock mass  |
| $\alpha$        | Dip angle from the horizontal  |
| $B$             | Joint orientation factor   |
| [B]             | Strain-displacement matrix   |
| $C$             | Gravity adjustment factor  |
| [C]             | Constitutive matrix  |
| $c$             | Cohesion (cohesive strength)   |
| $D$             | Original un-deformed Diameter of specimen  |
| $D_e$           | Equivalent dimension parameter   |
| $\Delta D$      | Change in the measured diameter  |
| $\Delta L$      | Change in measured axial gauge length  |
| $\delta_{\max}$ | Maximum vertical deflection at the centre of the roof  |
| $E$             | Young's modulus  |
| $E_h$           | Average deformation modulus of the upper part of the earth's crust measured in horizontal direction. |
| $E_t$           | Tangent Young's modulus  |
| $E_{av}$        | Average Young's modulus  |
| $E_s$           | Secant Young's modulus   |
| $e_c$           | Critical energy  |
| $\varepsilon$   | Strain   |
| $\varepsilon_a$ | Axial strain   |

|              |   |
|--------------|---|
| $\epsilon_l$ | Lateral strain  |
| $F$          | Ratio of elastic energy to dissipated energy  |
| $G$          | Modulus of rigidity   |
| $\gamma$     | Unit weight of the rock   |
| $\gamma_e$   | effective unit weight of the rock   |
| $J_n$        | Joint set number  |
| $J_r$        | Joint roughness number  |
| $J_a$        | Joint alteration number   |
| $J_w$        | Joint water reduction factor  |
| [K]          | Stiffness matrix  |
| $k$          | Ratio of the average horizontal stress to vertical stress                             |
| $L$          | Original un-deformed axial gauge length   |
| $m_i$        | Hoek-Brown criterion material constant  |
| $m_b$        | Reduced value of the Hoek-Brown criterion material constant material constant $m_i$ . |
| $N'$         | Modified stability number   |
| NT           | Average thickness of the compressive arch   |
| [O]          | Operation matrix  |
| $\nu$        | Poisson's ratio of the rock   |
| $P$          | Uniformly applied support pressure (in Voussoir arch theory)                          |
| $\phi$       | Angle of friction   |
| $\phi_{sp}$  | Elastic energy stored in the rock   |
| $\phi_{st}$  | Dissipated energy in creation of the plastic deformation                              |
| $Q$          | Rock tunneling quality index  |

|                         |  |
|-------------------------|--|
| $Q'$                    | Modified rock tunneling quality index            |
| S                       | Stope surface shape factor                       |
| s                       | Hoek-Brown criterion constant for rock mass      |
| SD                      | Standard Deviation                               |
| $\sigma_1$              | Major principal stress                           |
| $\sigma_2$              | Intermediate principal stress                    |
| $\sigma_3$              | Minimum principal stress                         |
| $\sigma'_1$             | Major principal stress                           |
| $\sigma'_3$             | Minimum principal stress                         |
| $\sigma'_{3\max}$       | The upper limit of confining stress              |
| $\sigma_c$              | Uniaxial compressive strength                    |
| $\sigma_{ci}$           | Uniaxial compressive strength of the intact rock |
| $\sigma'_{cm}$          | Global rock mass strength                        |
| $\sigma_h$              | In-situ horizontal stress                        |
| $\sigma_{h\max}$        | Maximum in-situ horizontal stress                |
| $\sigma_{h\min}$        | Minimum in-situ horizontal stress                |
| $\sigma_{\max}$         | Maximum normal stress at the abutments           |
| $\sigma_n$              | Normal stress                                    |
| $\sigma_{rr}$           | Mining-induced radial stress.                    |
| $\sigma_{r\theta}$      | Mining-induced shear stress.                     |
| $\sigma_t$              | Tensile strength of the specimen                 |
| $\sigma_{\theta\theta}$ | Mining-induced tangential stress.                |
| $\sigma_v$              | In-situ vertical stress                          |
| t                       | Thickness of the roof layer                      |

|            |  |
|------------|--|
| $T$        | Normal thickness of the single layer   |
| $T_s$      | Tangential stress criterion            |
| $\Theta$   | Dip of the stopes face                 |
| $\tau_p$   | Peak-shear strength                    |
| $U_r$      | Mining-induced radial displacement     |
| $U_\theta$ | Mining-induced tangential displacement |
| $u$        | Complete element displacement          |
| $u_i$      | Degree of freedom in x direction       |
| $u_e$      | Vector of the nodal displacement       |
| $v_i$      | Degree of freedom in y direction       |
| $z$        | Depth below the surface                |
| $Z$        | Moment arm                             |
| $Z_0$      | Initial moment arm                     |

# CHAPTER 1: INTRODUCTION

*This chapter provides an overview of the research. It discusses the general background of the study; the statement of the problem; the objectives of the study, and the proposed methodology. At the end, the organization of the thesis is outlined.*

## 1.1 General Background and Statement of the Problem

Canada is the third-largest diamond-producing country in the world based on value. According to Natural Resources Canada, the value of diamonds produced in Canada in 2013 was \$1.9 billion. Many of the developed Canadian diamond mines approached depths where they had to switch from surface mining to a more challenging underground mining environment. Because of the geological environment of underground diamond mines, most operators have chosen sublevel open stoping and sublevel longhole retreat as their primary underground mining methods.

Sublevel open stoping is the most common underground mining method in Canada. According to Potvin et al. (2001), the popularity of this method is due to its ability to achieve high production levels by employing large-sized excavations and using mechanized equipment. As the size of the stopes increases, more production can be achieved; on the other hand, with bigger stopes, the stability of the open stopes will reach its critical point.

The assessment of the stability of these open stopes is a critical task for geotechnical and mining engineers. In the sublevel longhole retreat method, the mined-out area will be not backfilled; therefore, in this method the stability of the host rock and orebody is of great concern. The performance and stability of underground excavations are directly influenced by the rock mass stress regime around the underground constructions.

There are two kinds of rock stresses: in-situ stress and mining-induced stress. The loading system for underground excavation is formed by in-situ stresses, which are initial stresses prior to excavation (also called pre-mining stresses). Due to mining activity, there is a disruption in the stress field around the underground excavations. This disruption is caused by a new set of stresses which is called mining-induced stresses. Depending on the magnitude of the in-situ stresses, mining method, shape and size of the underground openings, the magnitude and directions of the induced stresses are different (Brady et al., 2004).

Knowing the magnitudes and directions of these stresses can help determine suitable shapes and orientations of underground constructions and assess their stability. In addition, knowing the stress regime in the rock mass can help predict the type of failure which may occur in the future and identify potential rockbursting zones.

Four types of stress measurement techniques have been suggested by the International Society for Rock Mechanics (ISRM), and they have been documented by several researchers such as Kim et al. (1987), Hudson et al. (2003), Sjoberg et al. (2003), Haimson et al. (2003), Christiansson et al. (2003), and Brady and Brown (2004). These methods will be reviewed in chapter 2 of this thesis. These standard techniques are usually difficult and costly to use. Most of these techniques measure stress at a point in a rock mass, and this has been proven to produce a large scatter. In addition, there are some analytical methods of induced stress calculations such as Kirsch Equations (Kirsch, 1898) and Bray's equations (Bray, 1977). Most of these analytical methods assume simple two-dimensional (2D) excavation geometries, and the main assumption is that the materials are homogeneous with elastic behavior. However, in reality the excavation geometries are more complicated and the rock mass is heterogeneous with elastoplastic behavior.

In summary, the problem statement for this geomechanical research thesis is: "The determination of in-situ and mining-induced stress regimes as a function of two different underground mining methods used at Diavik Diamond Mine". The research question that drives this dissertation thesis is:

*"Is it possible to develop, implement and verify an integrated engineering methodology to estimate the in-situ and mining-induced stresses as the function of mining methods and simulate the complete stress-strain path throughout entire mine domain and during mine life, using the finite element method, and use this methodology as a reliable predictive design tool?"*

## 1.2 Objectives of the Study

In this research, the main objective is to develop, implement and verify an integrated engineering methodology to estimate the in-situ and mining-induced stress regimes in the host rock and orebody using a finite element (FE) analysis model. The goal is to seek a detailed understanding of stress (in-situ and mine-induced) distribution regimes in a mine as a function of mining methods. A case study of the Diavik Diamond Mine is used to illustrate the estimation procedure and to implement the proposed methodology.

In summary, the main objectives of this thesis are to develop, implement and verify an integrated engineering methodology which focuses on:

- Determination of in-situ and mining-induced stress regimes in the host rock and orebody.
- Analysis of the influence of the stress heterogeneity regime on: (i) the stability of open stopes; and (ii) the propagation and extension of the yielding and relaxation zones around the underground excavations.
- Estimation of mining-induced energy and development of an integration approach to combine FE analysis modeling and conventional criteria to predict and identify zones of potential rockbursting in the mine.
- Prediction of the mining-induced surface subsidence and ground movements caused by different underground mining methods (i.e. in this case, BHS and SLR mining methods).
- Verify and validate the developed numerical model using measured field data and observations.

Finally, the resultant methodology, developed in this research, can be used to assess the stability of surface crown pillars and sill pillars with respect to the mine stress distribution regime (both in-situ and mining-induced stresses). Recovery of

the surface crown pillars and sill pillars is the common problem between underground mines.

### **1.3 Research Methodology**

To reach the objectives of this research dissertation, a full realistic three dimensional (3D) elastoplastic finite element model of a case study mine has been developed. This FE analysis model was used to determine the in-situ and mining-induced stress regime at the case study mine.

Abaqus (Dassault Systèmes) software was used to develop the full 3D FE model of the mine. Abaqus is a powerful general-purpose FE simulation program which can solve a wide range of linear and nonlinear problems including geomechanical problems. Moreover, it has a high graphic resolution which increases its ability as a visualization tool.

RocLab Software (Rocscience Inc.) was used for initial estimations of rock mass strength parameters based on the latest version of generalized Hoek-Brown failure criterion. The constitutive rock model supported by Abaqus is the Mohr-Coulomb criterion. RocLab provides a simple and intuitive implementation of the Hoek-Brown failure criterion, allowing users to easily obtain reliable estimates of Mohr-Coulomb rock mass properties. However, to calibrate the rock mass properties, some Kimberlite samples were collected from the mine site and shipped to the University of Alberta for required rock mechanics tests.

To estimate the strength properties of Kimberlite, three main laboratory tests were performed: (i) uniaxial compressive strength (UCS) test; (ii) indirect tensile strength test (also called Brazilian test); and (iii) triaxial compressive test. The results from these tests were used to calibrate and estimate the rock mass properties to be used as the input parameters in the FE model.

In addition, to validate the results of the FE model, some ground movement monitoring instruments were installed at the desired locations. The input stresses were adjusted to give a best fit to field stress change data.

To achieve the objectives of this research, the following research tasks have been completed:

- **Literature review:** An extensive review of all relevant pre-existing conventional methods of assessing in-situ and mining-induced stresses along with all relevant up-to-date underground excavation design methods have been reviewed during this task. In addition, numerical methods in rock mechanics and current state-of-the-art rock mechanics modeling have been reviewed.
- **Initial site investigations to collect required input data:** This research task involved gathering data required to create a realistic 3D geometry of the mine, gathering data regarding rock mass classifications (RMR, Q, GSI), initial estimation of the rock mass strength parameters using Hoek-Brown criterion and RocLab software, collecting data regarding the in-situ state of stresses to develop initial assumptions and identifying any significant geological features (i.e. faults) relevant to the problem.
- **Laboratory testing:** This task consisted of three parts:
  - 1) Preparing the test specimens from bulk samples gathered during the previous step.
  - 2) Estimating the strength properties of Kimberlite thorough three main rock mechanics laboratory tests: (i) UCS test; (ii) indirect tensile strength (also called Brazilian test) test; and (iii) triaxial test.
  - 3) Obtaining modeling input parameters for rock mass behavior from the laboratory tests. The results were used to calibrate the initial input values of the FE model.
- **Develop a Finite Element Analysis Model:** Based on the data collected in step 2, a full realistic 3D FE model using Abaqus was

developed. The model captures the true geometry of the problem (including two pits, two Kimberlite pipes, drifts, stopes, etc.).

- ***Defining the Simulation Steps:*** The sequence of mining (excavation and backfilling) was defined according to real-life operations and the mine production plan. Detailed analyses were conducted mainly focusing on (i) the assessment of the stress distribution regime (both in-situ and mining-induced) and its impact on the stability of the open stopes; (ii) estimation of the mining-induced energy and prediction of potential rockbursting zones; and (iii) prediction of possible mining-induced surface subsidence.
- ***Conducting a sensitivity analysis:*** This research task proposed new scenarios such as new in-situ stress regimes to study the impact of the horizontal to vertical stress ratio on the propagation and extension of the yielding and relaxation zones around the underground excavations.
- ***Verification, Calibration and Validation of the FE model:*** Based on the laboratory tests, actual ground movement data and visual observations, the FE model was calibrated and the results were validated.

#### 1.4 Organization of Thesis

**Chapter 1** of this thesis provides an overview of the research. It discusses the general background of the study, the problem statement, the objectives of the study and the proposed methodology.

**Chapter 2** provides the literature review based on the objectives of this research study. The major focuses are on: (i) conventional methods of stress analysis around underground openings; (ii) underground stability analysis methods and rock mass failure criteria; (iii) application of numerical methods in rock mechanics and rock engineering; (iv) the theory behind the FE analysis method; and (v) current state-of-the-art rock mechanics modeling.

**Chapter 3** presents a case study of Diavik Diamond Mine, which was used to implement the research methodology. A full 3D FE model of the mine was constructed step by step. Some rock mechanics laboratory tests were performed on Kimberlite samples from Diavik Mine to measure the intact properties of Kimberlite. The results of these laboratory tests were used to estimate the rock mass properties and calibrate the modeling input parameters of the FE analysis. This chapter presents a methodology to obtain the modeling input parameters for rock masses from laboratory tests on intact rock samples.

**Chapter 4** presents an evaluation of mining-induced energy and rockburst prediction using the developed FE analysis model. Rockburst is an instantaneous and violent failure of rock which occurs when a volume of rock is strained beyond its elastic limit. It poses a serious threat to the safety of underground personnel. In this chapter, a review of current state-of-the-art methods for rockburst prediction is presented. Then, a methodology is proposed to evaluate the extent and magnitude of mining-induced strain energy and its accumulation in rock masses to predict the rockburst potentials in an underground mine.

**Chapter 5** presents a prediction of mining-induced surface subsidence and ground movements at Diavik Mine using a full 3D elastoplastic FE model. Prediction of the surface subsidence profile and its magnitude is a critical task for rock mechanics engineers, and it is crucial in the planning of underground mining operations. In this chapter, the forecast capacity of the developed numerical model for the prediction of mining-induced surface subsidence and ground movements in a real case study is presented. The developed FE model was used to predict surface-induced ground movements due to underground blasthole stoping activities. The developed model was calibrated using two extensometers installed on the back of two secondary undercut drifts in one of the Kimberlite pipes. Finally, the results of the calibrated model were verified using pit surface prism monitoring system data. The comparison between the predicted results of the FE model and monitoring data showed the predictive capacity of the numerical model as a valuable tool in stability and design analysis of underground mines.

**Chapter 6** focuses on stope stability assessment and the effect of horizontal to vertical stress ratio on the yielding and relaxation zones around underground open stopes. Prediction of the stability of the open stopes can be one of the most challenging tasks for underground mine engineers. For decades, the Mathews stability graph method has been used as the first step of open stope design around the world. However, there are some shortcomings with this method. In this study, both empirical and numerical methods were used to assess the stability of an open stope located at Diavik Mine. Finally, a sensitivity analysis was performed to investigate the impact of the stress ratio on the extent of the yielding and relaxation zones around underground openings.

**Chapter 7** presents the verification of the developed FE model code through a process referred to as numerical algorithm verification. In addition, the results of the FE model were validated by comparing the FE model results to actual field data and site observations. The main objective is to find the answers to the following two questions: (i) Did I build the model right? (Verification process) and (ii) Did I build the right model? (Validation process).

**Chapter 8** provides the thesis summary and research conclusions. The significance and contributions of this research are discussed. In addition, it contains recommendations for future work in determining in-situ and mining-induced stresses in an underground mine.

## CHAPTER 2: LITERATURE REVIEW

*Throughout this chapter, based on the objectives of this research study, the literature review is provided, focusing on the following three major topics:*

- 1) Conventional methods of stress analysis around underground openings*
- 2) Underground stability analysis methods and rock mass failure criteria*
- 3) Numerical modeling in rock mechanics*

# **PART ONE:**

## **CONVENTIONAL METHODS OF STRESS ANALYSIS AROUND UNDERGROUND OPENINGS**

*This section reviews the following topics related to in-situ and mining-induced stresses:*

- *Conventional methods of determining in-situ and mining-induced stresses around underground structures*
- *Factors influencing the direction of in-situ stresses*
- *Zones of influence of tunnels*
- *Stress paths around underground openings*
- *Standard methods of stress determination*

## 2.1 Conventional methods of stress analysis around underground structures

One of the essential components of the underground excavation design process, which directly influences the performance and stability of underground openings, is knowledge of in-situ and mining-induced stresses. Knowing the magnitudes and directions of these stresses can help determine a suitable shape, orientation and mining sequence for underground openings (such as tunnels, drifts, stopes, etc.). In addition, knowing the stress regime in the rock mass can help predict the type of rock failure that may occur in the future and identify potential rockburst zones.

This section provides an overview of the conventional methods for determining the magnitude and direction of in-situ and mining-induced stresses. It outlines the application and importance of in-situ and mining-induced stresses for the prediction of the failure mode and stress path around underground openings. Finally an overview of the standard methods for stress measurement in the field is provided.

### 2.1.1 In-situ stress

In-situ stress components (vertical and horizontal) can be estimated using elasticity theory. Here the assumption is that the shear stress components are zero; therefore, the vertical and horizontal stresses are the principal stresses ( $\sigma_1, \sigma_2, \sigma_3$ ).

#### 2.1.1.1 Vertical stress

The results of the state of vertical in-situ stress in different mining, petroleum and civil engineering sites around the world were first reported by Hoek and Brown (1980) and are presented in figure 2.1. This figure has been updated by other researchers (Aydan and Kawamoto, 1997; Aydan, 2014). The average trend line of this figure (and on the updated figures) can be expressed using equation (2.1):

$$\sigma_v = 0.027.z \quad (2.1)$$

where  $z$  is the depth (m) below the surface.

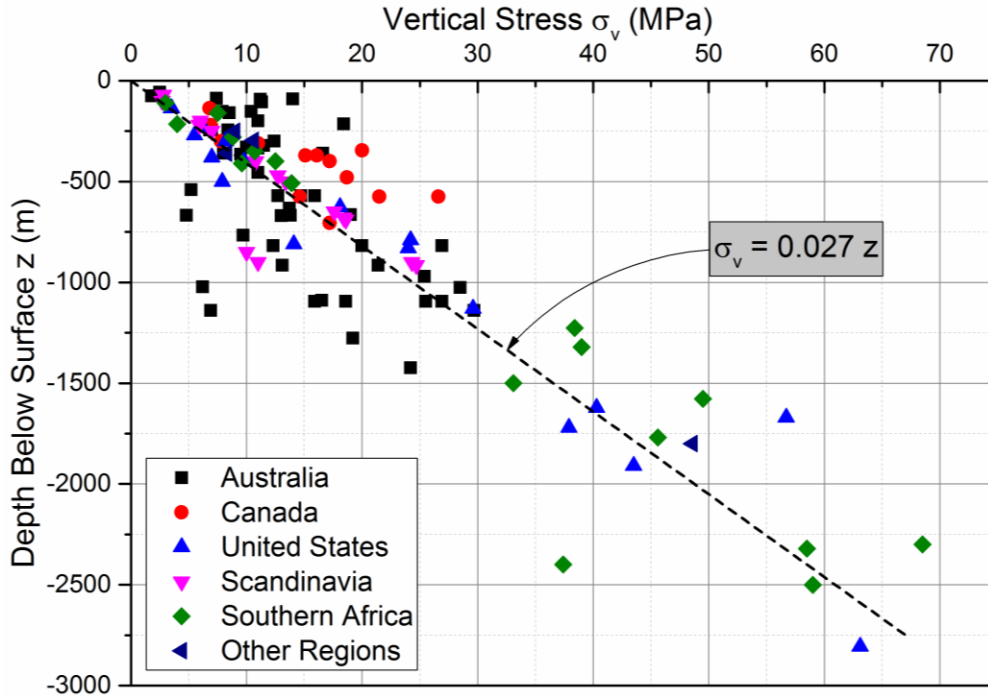


**Figure 2.1** Variation with depth of measured values of in-situ vertical stress (after Hoek and Brown, 1980)

Since the average unit weight for most rocks can be reasonably assumed to be  $0.027 \text{ MN/m}^3$ , the vertical component of in-situ stress ( $\sigma_v$ ) can be estimated based on the unit weight of the overburden rock using equation (2.2):

$$\sigma_v = \gamma \cdot z \quad (2.2)$$

where  $\gamma$  is the unit weight of the rock ( $\frac{\text{MN}}{\text{m}^3}$ ) and  $z$  is the depth (m).

### 2.1.1.2 Horizontal stress

The general equation which can be used to estimate horizontal stress ( $\sigma_h$ ) is as follows:

$$\sigma_h = k \sigma_v \quad (2.3)$$

where  $k$  is defined as the ratio of the average horizontal stress to vertical stress.

For perfect elastic and isotropic rocks,  $k$  can be assumed to be independent of the depth and can be calculated from the following equation proposed by Terzaghi et al. (1952):

$$k = \frac{\nu}{1-\nu} \quad (2.4)$$

where  $\nu$  is the Poisson's ratio of the rock.

A collection of measurements of in-situ stresses from the fields of mining, drilling and civil engineering has been presented by Hoek and Brown (1980) as shown in figure 2.2.

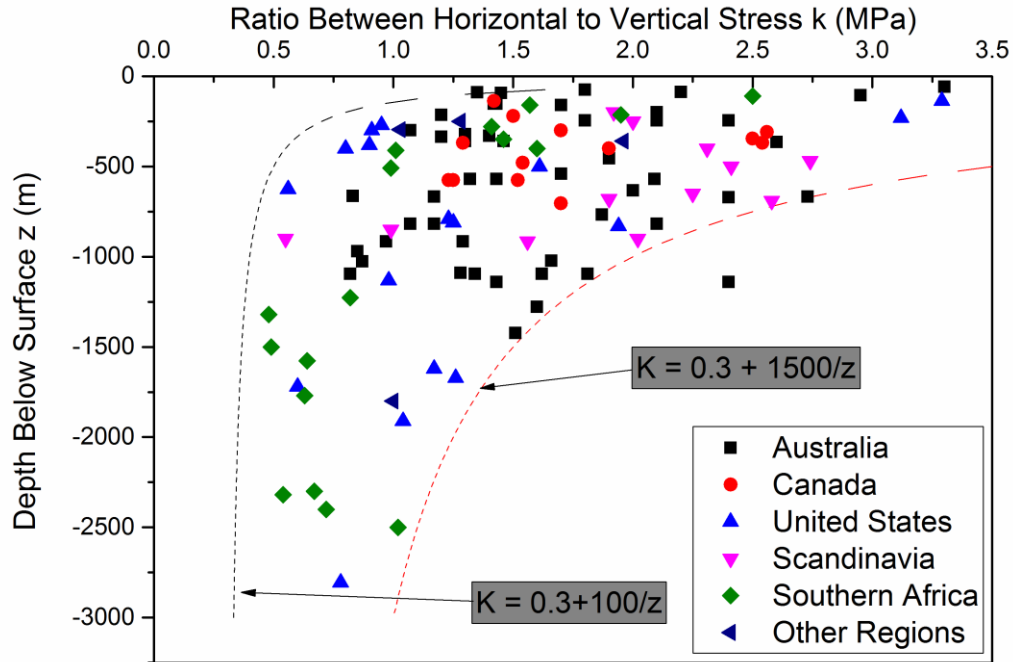


**Figure 2.2** Variation with depth of ratio of horizontal to vertical stresses (after Hoek and Brown, 1980)

Based on this collection, it is possible to estimate the possible range for  $k$  as follows:

$$0.3 + \frac{100}{z} < k < 0.5 + \frac{1500}{z} \quad (2.5)$$

In addition, Sheorey (1994) introduced an approach for estimating  $k$  as follows:

$$k = 0.25 + 7 E_h \left( 0.001 + \frac{1}{z} \right) \quad (2.6)$$

where  $z$  is the depth (m) below surface and  $E_h$  is the average deformation modulus (GPa) of the upper part of the earth's crust measured in the horizontal direction. A plot of equation (2.5) is shown in figure 2.3 and is compared with the proposed ranges by Hoek and Brown (1980).

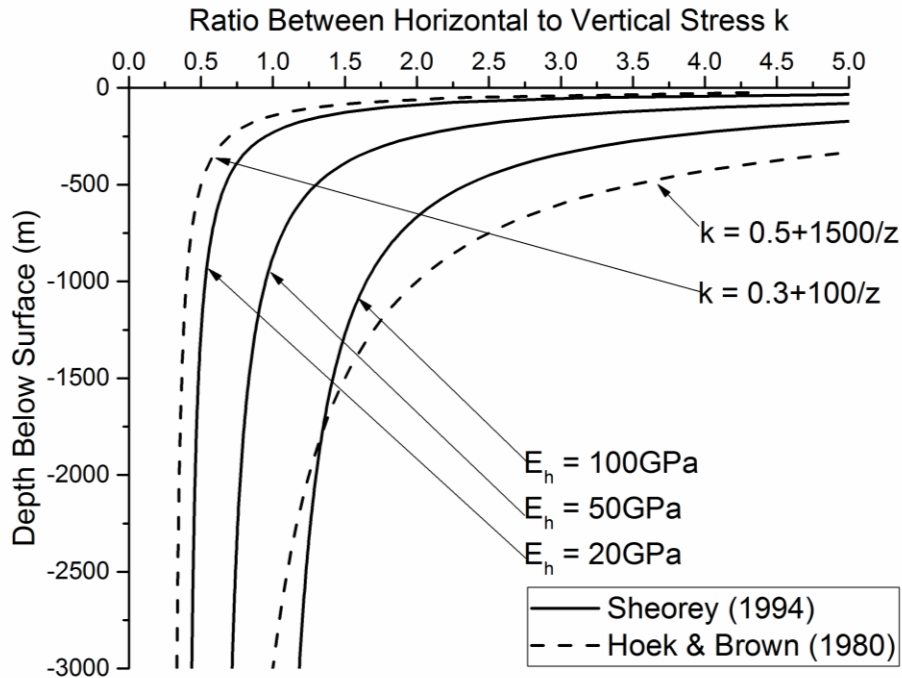


**Figure 2.3** Ratio of the average horizontal to vertical stress based on Sheorey (1994) and Hoek and Brown (1980)

It should be noted that at geological feature sites (such as faults, fractures, erosions, etc.) the value of  $k$  could be greater than 1. In such cases, the vertical component of the stress will no longer be the major principal stress; therefore, simply estimating the  $k$  value using the above theories, in some cases, can be very misleading and result in serious and catastrophic underground design errors.

Some examples of geological features which can create zones of high horizontal stress are given by Hudson and Harrison (1997) as outlined below:

- Tectonics (i.e. reverse faults)
- Fractures
- Anisotropy (i.e. transverse isotropic, orthotropic)
- Erosion

These are beyond the scope of this research and will not be discussed. However, in the following section, important geotechnical features affecting the magnitude and direction of in-situ stress are briefly discussed.

### 2.1.1.3 Direction of the in-situ stress

The general assumption is that the direction of principal in-situ stresses are vertical and horizontal. However, this assumption is valid as long as there are no geological (and geotechnical) features. Martin et al. (1993) reported that in the existence of geological structures, even for a homogeneous rock, the direction and the magnitude of the in-situ stress could be highly variable.

At the site of geotechnical features, the directions of the principal stresses can be inferred. Figure 2.4 shows that in the case of open fractures in the rock mass, the direction of the principal stresses from state A, which is the general assumption, will rotate to states B and C. From figure 2.4, it can be seen that the magnitude of the principal stresses also change in that the horizontal stresses become the major principal stresses.

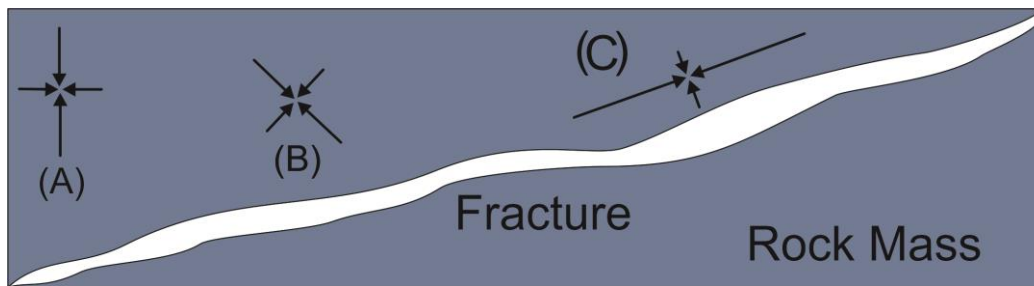


**Figure 2.4** State of the principal stresses near an open fracture (after Hudson et al., 2003)

In the case of normal faults, figure 2.5a, the vertical stress ( $\sigma_v$ ) and the maximum and minimum horizontal stresses ( $\sigma_H$  and  $\sigma_h$ , respectively) are normal to the trace of fault (Goodman, 1989). In this case, vertical stress is the major principal stress ( $\sigma_v > \sigma_H > \sigma_h$ ). Reverse faults, figure 2.5b, occur due to the high magnitude of horizontal stresses. In this case, vertical stress is the minimum principal stress ( $\sigma_H > \sigma_h > \sigma_v$ ) (Singh, 2006). In the case of strike-slip faults, figure 2.5c, the vertical stress is the intermediate stress state, the maximum horizontal stress is the major principal stress and the minimum horizontal stress is the minimum principal stress ( $\sigma_H > \sigma_v > \sigma_h$ ) (Taherynia et al., 2016).

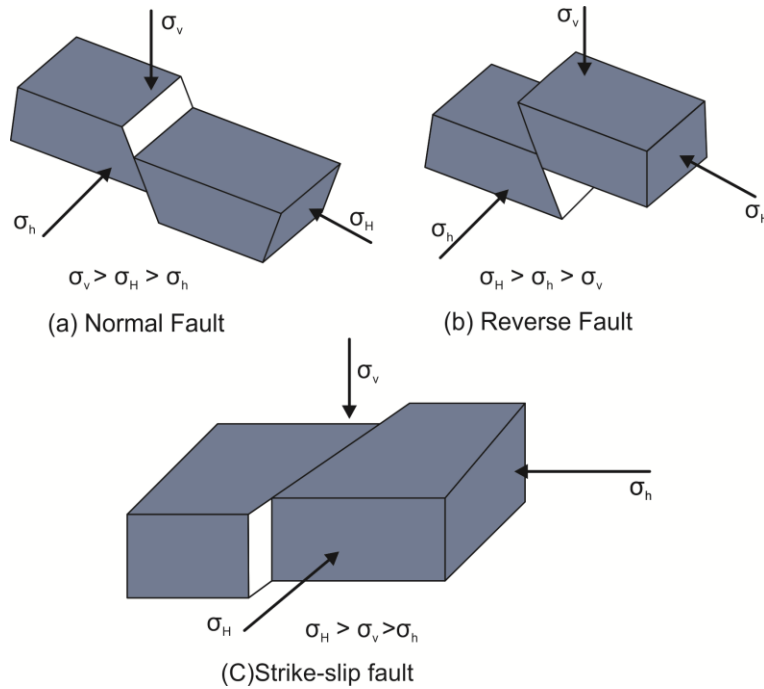


**Figure 2.5** State of in-situ stress around different types of faults

It is possible to determine in-situ stress directions, particularly determine the direction of the major principal stress, from the occurrence of rock breakage on borehole walls (and wellbores). This phenomenon is called breakouts (figure 2.6) and occurs when the rock fails to hold the compressive stress concentrations around the borehole.

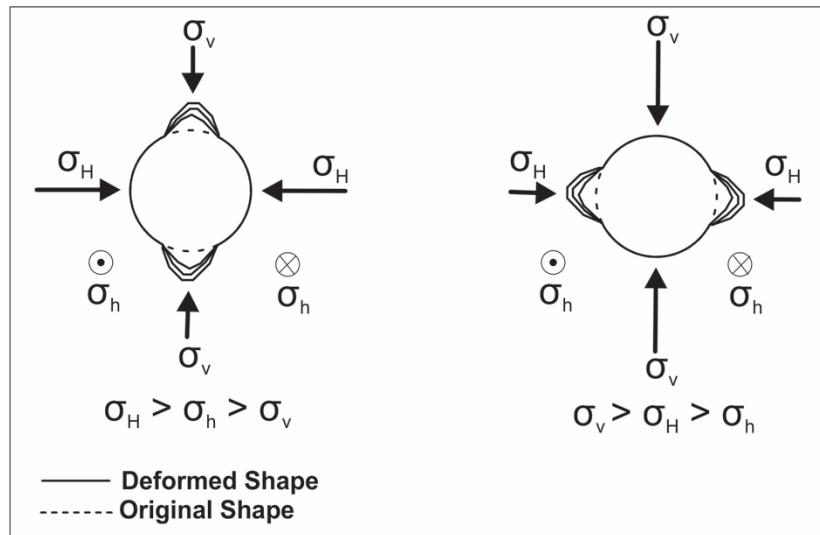


**Figure 2.6** Breakouts around a horizontal wellbore in different in-situ stress regimes (after Wikel, 2011)

### 2.1.1.4 World stress map

The world stress map (WSM) is a global database of the tectonic stress of the earth's crust from a wide range of stress indicators in civil, petroleum and mining engineering (Heidbach et al., 2008). It shows the orientation of the horizontal stresses and the stress regimes superimposed on a topographical map of different regions of the earth. It has a wide range of application in rock engineering and rock mechanics, particularly in geo-modeling. However, data in this map are limited to international engineering sites with a substantial amount of in-situ stress measurements. This map is available in Appendix B.

### 2.1.2 Analytical methods of induced stress estimation

When an excavation operation is occurring in rock, a new set of stresses called induced stresses will be created. In this case, there is a disruption in the stress field around the underground opening. Depending on the shape and size of the opening, the magnitude, direction and the zone of influence of this disruption is different.

The use of Kirsch equations is the most popular analytical method of estimating mining-induced stresses around a circular-shaped opening. The following review has been provided from Brady and Brown (2004).

#### 2.1.2.1 Circular excavation shape

The closed-form solution for estimating the stress and displacement around a circular opening (figure 2.7) is universally known as the Kirsch equations. It was first given by Kirsch (1898) as follows:

Assuming the in-situ vertical stress is  $P$  and the horizontal stress is  $kP$ ,

$$\sigma_{rr} = \frac{P}{2} \left[ (1+k) \left( 1 - \frac{a^2}{r^2} \right) - (1-k) \left( 1 - 4 \frac{a^2}{r^2} + \frac{3a^4}{r^4} \right) \cos 2\theta \right] \quad (2.7)$$

$$\sigma_{\theta\theta} = \frac{P}{2} \left[ (1+k) \left( 1 + \frac{a^2}{r^2} \right) + (1-k) \left( 1 + \frac{3a^4}{r^4} \right) \cos 2\theta \right] \quad (2.8)$$

$$\sigma_{r\theta} = \frac{P}{2} \left[ (1-k) \left( 1 + \frac{2a^2}{r^2} - \frac{3a^4}{r^4} \right) \sin 2\theta \right] \quad (2.9)$$

$$U_r = -\frac{Pa^2}{4Gr} \left[ (1+k) - (1-k) \left\{ 4(1-\nu) - \frac{a^2}{r^2} \right\} \cos 2\theta \right] \quad (2.10)$$

$$U_{\theta} = -\frac{Pa^2}{4Gr} \left[ (1-k) \left\{ 2(1-2\nu) + \frac{a^2}{r^2} \right\} \sin 2\theta \right] \quad (2.11)$$

where  $a$  is radius of the tunnel,  $r$  is the distance at which stress and displacement are being estimated,  $\nu$  is Poisson's ratio,  $G$  is the modulus of rigidity,  $U_r$  and  $U_{\theta}$  are mining-induced displacements and  $\sigma_{rr}$ ,  $\sigma_{\theta\theta}$ ,  $\sigma_{r\theta}$  are radial, tangential and shear stresses, respectively.

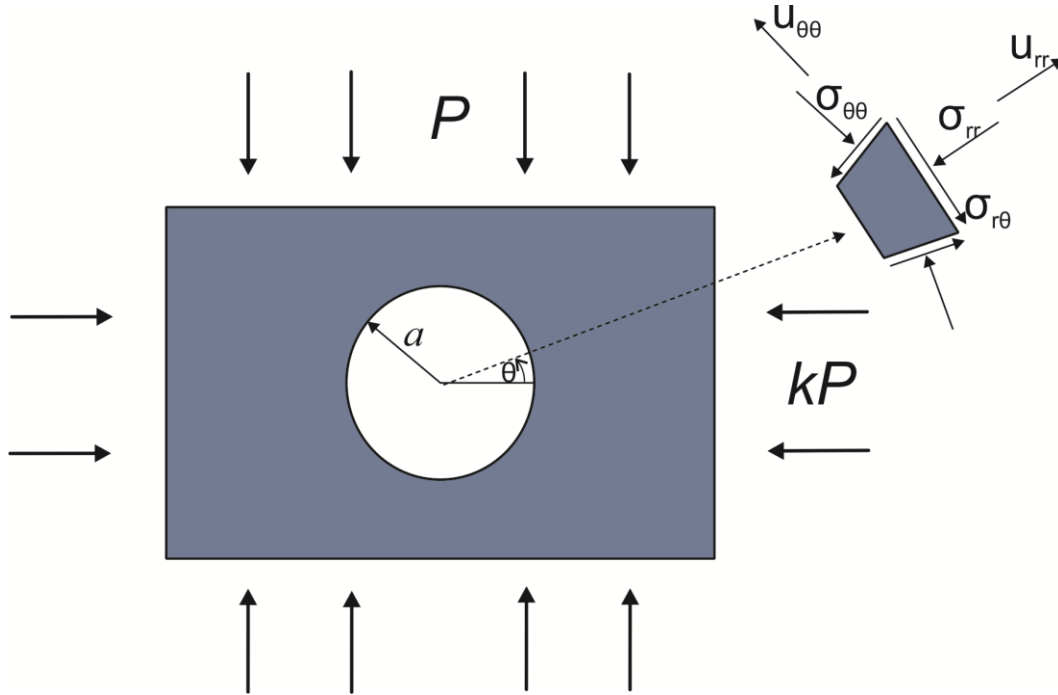


**Figure 2.7** Problem geometry for estimating the stress and displacement around a circular excavation in a biaxial stress field (after Brady and Brown, 2004)

The state of stresses on the boundary of the tunnel ( $r = a$ ) can be calculated as follows:

$$\sigma_{r\theta} = 0 \quad (2.12)$$

$$\sigma_{\theta\theta} = P[(1+k) + 2(1-k)\cos 2\theta] \quad (2.13)$$

$$\sigma_{rr} = 0 \quad (2.14)$$

In addition, from equation 2.13, it can be inferred for the hydrostatic stress field ( $k = 1$ ) that the magnitude of the stress at the boundary of the excavation is independent of angle  $\theta$  and it is always equal to  $\sigma_{\theta\theta} = 2P$ .

### 2.1.3 Zone of influence of a tunnel

One of the main design issues in underground mining activities is evaluating the interaction between underground structures. It is important to estimate the zone of influence of excavations to determine a safe distance between underground openings. For instance, in a hydrostatic stress field ( $k = 1$ ), the stress distribution around a circular excavation can be calculated from Kirsch equations as follows:

$$\sigma_{rr} = P \left( 1 - \frac{a^2}{r^2} \right) \quad (2.15)$$

$$\sigma_{\theta\theta} = P \left( 1 + \frac{a^2}{r^2} \right) \quad (2.16)$$

Stress distribution around a circular excavation is illustrated in figure 2.8 using equations (2.15) and (2.16). As seen from this figure, from  $r = 6a$ , the state of stress is not significantly changed from the virgin stress field (Brady and Brown, 2004). In other words, the limit of the zone of influence of a circular tunnel in a hydrostatic stress field with a radius of  $a$  is equal to  $6a$ .

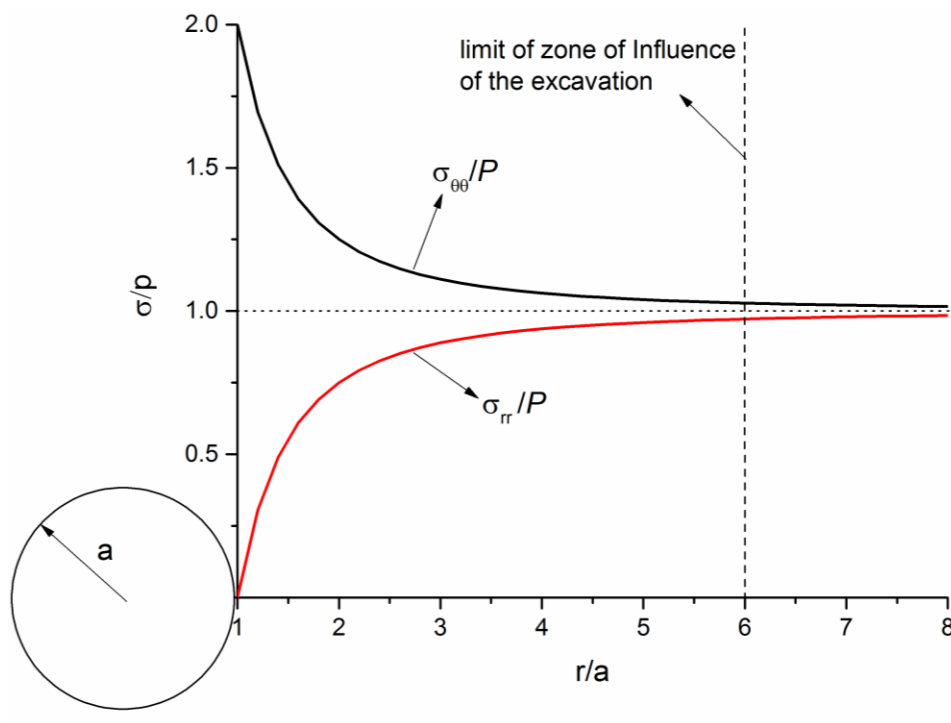


**Figure 2.8** Stress distribution around a circular excavation in a hydrostatic stress field (after Brady and Brown, 2004)

In conclusion, it has been shown that the zone of influence of an opening is related to both in-situ stresses and excavation shape.

#### **2.1.4 Standard Stress Measurement Techniques**

Four methods have been suggested by the ISRM (prepared by Christiansson and Hudson, 2003; Hudson et al., 2003; Haimson and Cornet, 2003; Sjöberg et al., 2003) for rock stress measurement as follows:

- The flatjack technique
- The hydraulic fracturing technique
- The USBM-type drillhole deformation gauge
- The CSIRO-type cell with 9 or 12 strain gauges

A more comprehensive discussion about these methods is beyond the scope of this research thesis; however, in the following sections a brief review of each one is presented.

##### ***2.1.4.1 Flatjack measurement technique***

In this method normal stress can be measured. To calculate the shear components, the normal stress in different directions must be measured. Therefore, to determine the stress tensor, six measurements in six different directions are required. According to Singh et al. (2006), the major assumptions in this method are that: (i) the rock is perfect elastic; and (ii) the in-situ stress directions are vertical and horizontal. A brief procedure of this method is provided by Goodman (1989) as described below.

In this method, normal in-situ stresses can be measured by unloading and reloading the rock through cutting a slot. The normal stress can be calculated from the pressure required to null the displacement as a result of cutting. For instance, if we assume the initial distance between the pins is  $d_0$ , after cutting the slot, the distance will begin to decrease (figure 2.9). After cutting the slot, the Flatjack is inserted into the slot and pressured is applied until the distance of the pins returns to the initial value  $d_0$ . The pressure at this point, called cancellation pressure of

the jack, can be used as an approximate estimation for the average normal stress to the jack. The complete procedure can be found in ASTM D4729-08.

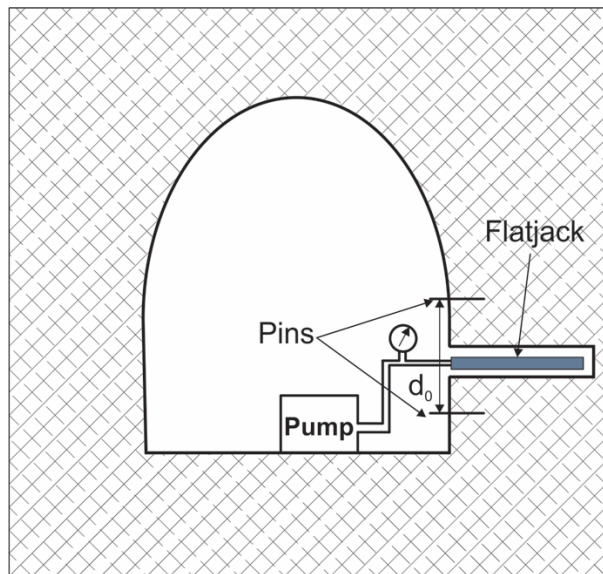


**Figure 2.9** Flatjack test setup

The shortcomings of this method are: (i) the stress tensor at the excavation wall is being measured, which is under the influence of the mining-induced stresses and cannot represent the in-situ stress state. In fact, it is likely to represent the mining-induced stress (Hudson and Harrison, 1997); (ii) to access to the exposed rock surface an underground excavation is needed; and (iii) the assumption that the behavior of the rock is perfectly elastic.

#### **2.1.4.2 Hydraulic fracturing technique**

The complete name of this method is hydraulic testing of pre-existing fractures (HTPF). Using the HTPF method, all six components of the stress can be evaluated (Hudson et al., 2003). A brief description of this method is provided herein.

First, using two inflatable rubber packers, a section of a borehole is sealed. Then, this sealed section is pressurized using a hydraulic fluid, which is usually water, until a fracture occurs. Finally, there are two pressures which are used to evaluate the magnitude of the principal stresses: the breakdown pressure which is the

pressure required to open the fracture and the shut-in pressure which is the pressure at which the fracture closes.

The two main advantages of this method are: (i) this method is most suitable for situations where there are no underground access to the rock surface (i.e. shafts, tunnels) and for depths more than 50 m; and (ii) the elastic properties of the rock are not required.

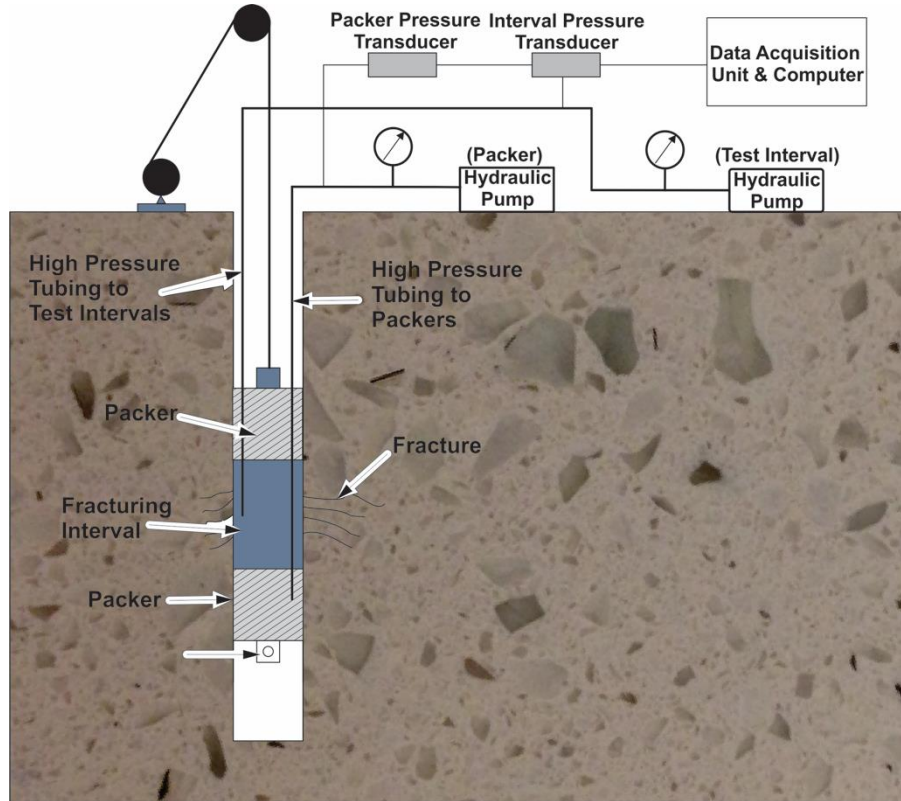


**Figure 2.10** Hydraulic fracturing test (after Thompson et al., 2004)

The main disadvantages of this method are: (i) this method assumes that the principal stresses are parallel and perpendicular to the borehole axis; (ii) it was assumed that the vertical stresses can be evaluated from the weight of the overburden rock (Hudson, 1997); and (iii) this method is most effective in elastic, homogenous, isotropic, brittle and non-porous materials (Kim et al., 1987). On the other hand, Thompson et al. (2004) reported that this method is not effective in crystalline rock under high horizontal stress conditions.

### 2.1.4.3 Overcoring techniques (USBM and CSIRO)

Overcoring techniques can be classified into two methods: (i) the United States Bureau of Mines (USBM) borehole deformation gauge method (figure 2.11a); and (ii) the Council of Scientific and Industrial Research Organization (CSIRO) triaxial strain cell method (figure 2.11b). The basic principle of these methods is to estimate the stress state from strain measurements in boreholes. To do this, the elastic properties of the rock are required. The assumptions for these methods are that the rock is perfect elastic, continuum, homogeneous and isotropic.

The procedure of this method is given by Hudson et al. (2003), which can be summarized in four steps: (i) a borehole is drilled at the location of the measurement (e.g. in the CSIRO overcoring technique, the diameter of the borehole is 86 mm); (ii) a pilot hole which has a smaller diameter (e.g. in the CSIRO overcoring technique, 38mm) is drilled. Then, the measurement cell (strain cell) is installed in it; (iii) The strain cell is overcored. Consequently, the stress acting on the rock will be relieved, and the strain can be measured; and (iv) the recovered core, containing the strain cell, is used to measure the elastic properties of the rock, which is required for calculation. Unlike the flatjack and hydraulic fracturing methods, in this method the elastic properties of the rock are required. With the combination of these elastic properties of the rock and the measurements of the drillhole deformation during overcoring, it is possible to calculate the principal stress components. The complete procedures of overcoring techniques can be found in Hudson et al. (1997), Sjöberg et al. (2003) and ASTM D4623-08.



(a) USBM Gauge



(b) CSIRO Strain Gauge

**Figure 2.11** USBM borehole deformation gauge

# **PART TWO:**

## **UNDERGROUND STABILITY**

### **ANALYSIS METHODS**

*This section reviews state-of-the-art underground stability analysis methods. There are four main approaches for underground excavation design:*

- *Analytical methods*
- *Empirical methods*
- *Observational methods*
- *Numerical methods*

*This section reviews the first three methods. Numerical methods are covered in part three of this chapter.*

## 2.2 Underground stability analysis methods

There are four main approaches for underground excavation design: (i) analytical methods; (ii) empirical methods; (iii) observational methods; and (iv) numerical methods. The following sections provide a brief review of the first three methods. Numerical methods are covered in part three of this chapter.

### 2.2.1 Analytical methods of excavation design

The most popular analytical methods of excavation design are:

- Kirsch equations
- Beam theory
- Voussoir arch theory
- Hoek-Brown failure criterion
- Mohr-Coulomb failure criterion

Kirsch equations were discussed in part one of this chapter.

#### 2.2.1.1 Beam theory

One way to estimate the safe span length of an underground opening in a laminated rock mass is using the simple beam theory (figure 2.12). The basic assumption here is that the laminated roof structure will remain in a completely continuous and elastic state after excavation. In this case, the maximum value of vertical deflection and the maximum normal stress for a single opening is given by Obert and Duvall (1967) as follows:

$$\sigma_{\max} = \frac{\gamma S^2}{2t} \quad (2.17)$$

$$\delta_{\max} = \frac{\gamma S^4}{32Et^2} \quad (2.18)$$

where  $\sigma_{\max}$  is the maximum normal stress at the abutments (MPa) (compression at the bottom of the beam and tension on the top of the beam),  $\delta_{\max}$  is the maximum vertical deflection at the center of the roof (m),  $E$  is the Young's modulus of the

rock (MPa),  $\gamma$  is the specific weight ( $\text{MN}/\text{m}^3$ ),  $S$  is the horizontal span (m) and  $t$  is the thickness of the roof layer (m).

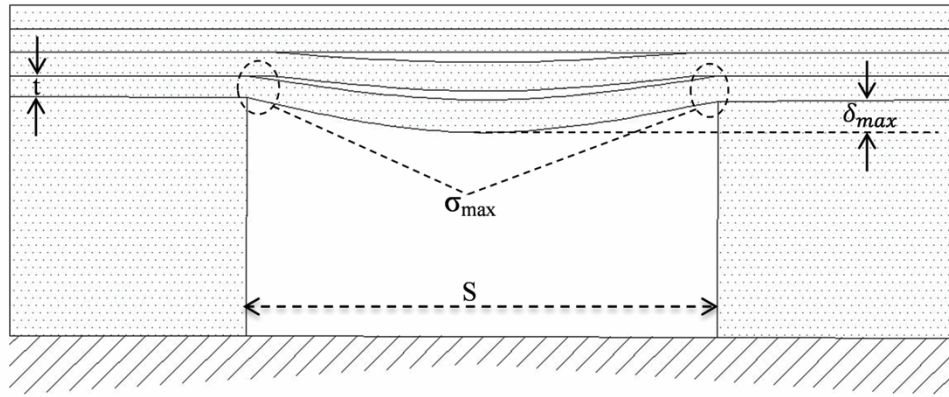


**Figure 2.12** Simple beam theory diagram

In some cases, the immediate roof (back) consists of two or more layers, where the thick roof layer is overlain by the thinner layers. Therefore, an additional load is applied on the lowest layer. To take into account this additional load, an adjusted weight density ( $\gamma_a$ ) has been proposed by Obert and Duvall (1967):

$$\gamma_a = \frac{E_1 t_1^2 (\gamma_1 t_1 + \gamma_2 t_2 + \dots + \gamma_n t_n)}{E_1 t_1^3 + E_2 t_2^3 + \dots + E_n t_n^3} \quad (2.19)$$

where  $E_1, E_2, \dots, E_n$  are the elastic Young's moduli,  $t_1, t_2, \dots, t_n$  are the thicknesses of the layers and  $\gamma_1, \gamma_2, \dots, \gamma_n$  are the unit weights.

### 2.2.1.2 Voussoir arch theory

In practice, it is rare that a laminated roof structure will remain in a completely continuous and elastic state after excavation. The presence of cross joints makes it difficult to assume that the rock will remain continuous after excavation. Moreover, these cross-cut joints decrease the sustainability of the rock's tensile stress significantly. Therefore, the simple beam theory cannot answer questions regarding the stability of underground openings.

Evan (1941) proposed a design procedure for roof beams that are jointed or cracked inasmuch that it is impossible to consider them as simple beams. The method was then modified by Beer and Meek (1982). A simplified version of the

Beer and Meek method (1982) was proposed by Brady and Brown (1993). More detailed analyses were performed by Sofianos (1996) and Diederichs and Kaiser (1999). These researchers identified some limitations and errors with the previous method proposed by Brady and Brown (1993). Consequently, they proposed alternative procedures to predict the roof stability using the Voussoir beam theory. Here the procedure proposed by Diederichs and Kaiser (1999) is presented.

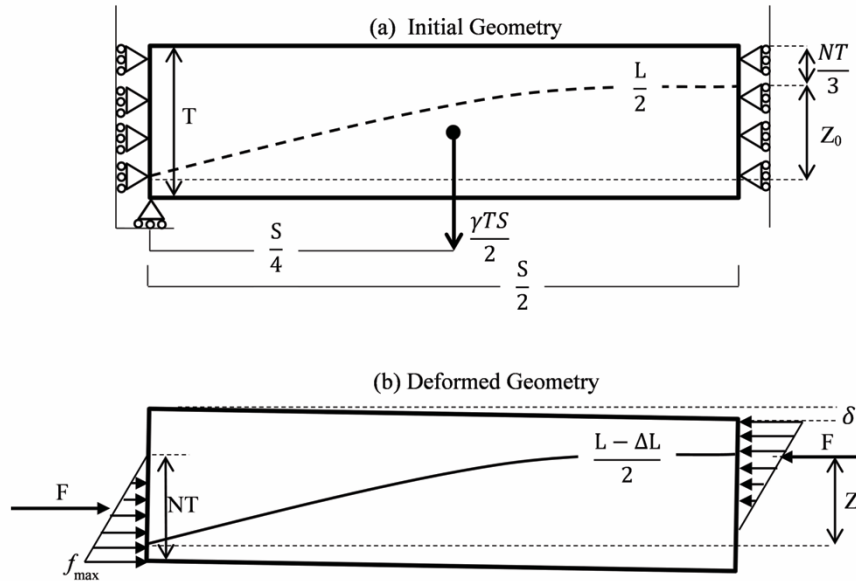


**Figure 2.13** Free body diagrams of the Voussoir beam (mid-span of the left side of the beam is shown) (after Diederichs and Kaiser, 1999)

The left side of the symmetric Voussoir beam model is shown in figure 2.13. The basic assumption of the Voussoir beam theory is that a compression arch structure develops within the beam, rising from the abutments to a high point at the mid-span, as can be seen from figure 2.13. Moreover, it is assumed that this arch will carry all the loads and will transmit them to the abutments. Four modes of failure are assumed to be: i) crushing at the mid-span or the abutments; ii) buckling (snap-through) failure; iii) sliding between the block at the abutments; and iv) diagonal fracturing. The complete procedure for determining deflection and stability of a Voussoir beam has been proposed by Diederichs and Kaiser (1999) (figure 2.14).

As shown in figure 2.14, the input data needed to perform the analysis are: the horizontal span ( $S$ ); the normal thickness of the single layer ( $T$ ); the Young's modulus of the rock ( $E$ ); the specific weight ( $\gamma$ ); the dip (angle from the horizontal) of the lamination plan ( $\alpha$ ); the unconfined compressive strength (UCS) of the rock ( $\sigma_c$ ); the friction angle ( $\phi$ ); and the uniformly applied support pressure ( $p$ ), if applicable.

Referencing figure 2.14, first, it is essential to estimate an effective specific weight ( $\gamma_e$ ) (steps 1 and 2 in the chart). Then, the loop starts: the average thickness of the compressive arch ( $NT$ ) is initially unknown.  $N$  varies between 0.01 and 1. To start the loop, the initial value of  $N$  is assumed to be 0.01. The initial moment arm ( $Z_\theta$  in figure 2.13a) prior to deflection is unknown and can be calculated in step 3. In step 4, the length of the reaction arch ( $L$ ) is calculated. The initial value for the elastic shortening of the arc ( $\Delta L$ ) is assumed to be zero (begin the secondary loop). The purpose of step 5 is to check the sign of the term under the square root ( $Z_{chk}$ ) in the formula presented in step 6. If  $Z_{chk} < 0$ , it means that the critical beam deflection has been exceeded. In this case, snap-through failure would occur for the specified value of  $NT$ . Consequently, the loop should be started again (the current value of  $N$  should be aborted, and the next value of  $N$  should be taken). If there are no values of  $N$  between 0.01 and 1, for which a stable solution can be obtained, the ultimate collapse of the beam is assumed to occur. In other words, stability is impossible because there is no arch thickness ( $NT$ ) which yields an equilibrium solution. If the  $Z_{chk} > 0$ , then the new reaction moment arm  $Z$  can be calculated in step 6. The maximum stress acting in the beam ( $f_m$ ) and the average stress along the reaction line ( $f_{av}$ ) can be estimated through steps 7 and 8, respectively. The initial value for  $\Delta L$  will be saved as  $\Delta L_{prev}$  in step 9. The new value of  $\Delta L$  can be calculated in step 10. Then these two values, the  $\Delta L_{prev}$  and the new value of  $\Delta L$ , will be compared; if there is no difference and  $N \geq 1$ , then the loop will be ended.

Finally, design parameters such as the buckling limit (which is a percentage of values of  $N$  within the range of 0 to 1 for which a solution cannot be obtained), factor of safety with respect to crushing at abutments and at the mid-span

(*F.S.Crush*), factor of safety with respect to vertical sliding for the unsupported beam under self-weight along joints at the abutments (*F.S.slide*) and the mid-span deflection can be estimated through steps 11 to 14, respectively. Diederichs and Kaiser (1999) showed that ultimate failure happens at a buckling limit of 100%, corresponding to a displacement equivalent to approximately 0.25 T.

### **2.2.1.3 Hoek-Brown failure criterion**

Hoek and Brown (1980a, 1980b) proposed an empirical failure criterion for rock. This criterion was developed based on the results of a paper presented by Hoek (1968) on brittle failure of rock as well as a paper presented by Brown (1970) on model studies of jointed rock mass behavior. According to Hoek et al. (2007), the original proposed Hoek-Brown equation had been used as early as 1936 to describe the failure of concrete. The significant contribution of this criterion was to link this equation to geological observations by means of available rock mass classification charts.

Furthermore, Hoek (1994) and Hoek et al. (1995) introduced the generalized Hoek-Brown criterion. This research recognized that the rock mass rating (RMR) system proposed by Bieniawski was no longer adequate as a means to relate the criterion to geological observations in the field for poor-quality rock masses. Consequently, to overcome the limitation of the RMR, the geological strength index (GSI) was introduced by Hoek (1994) and Hoek et al. (1995).

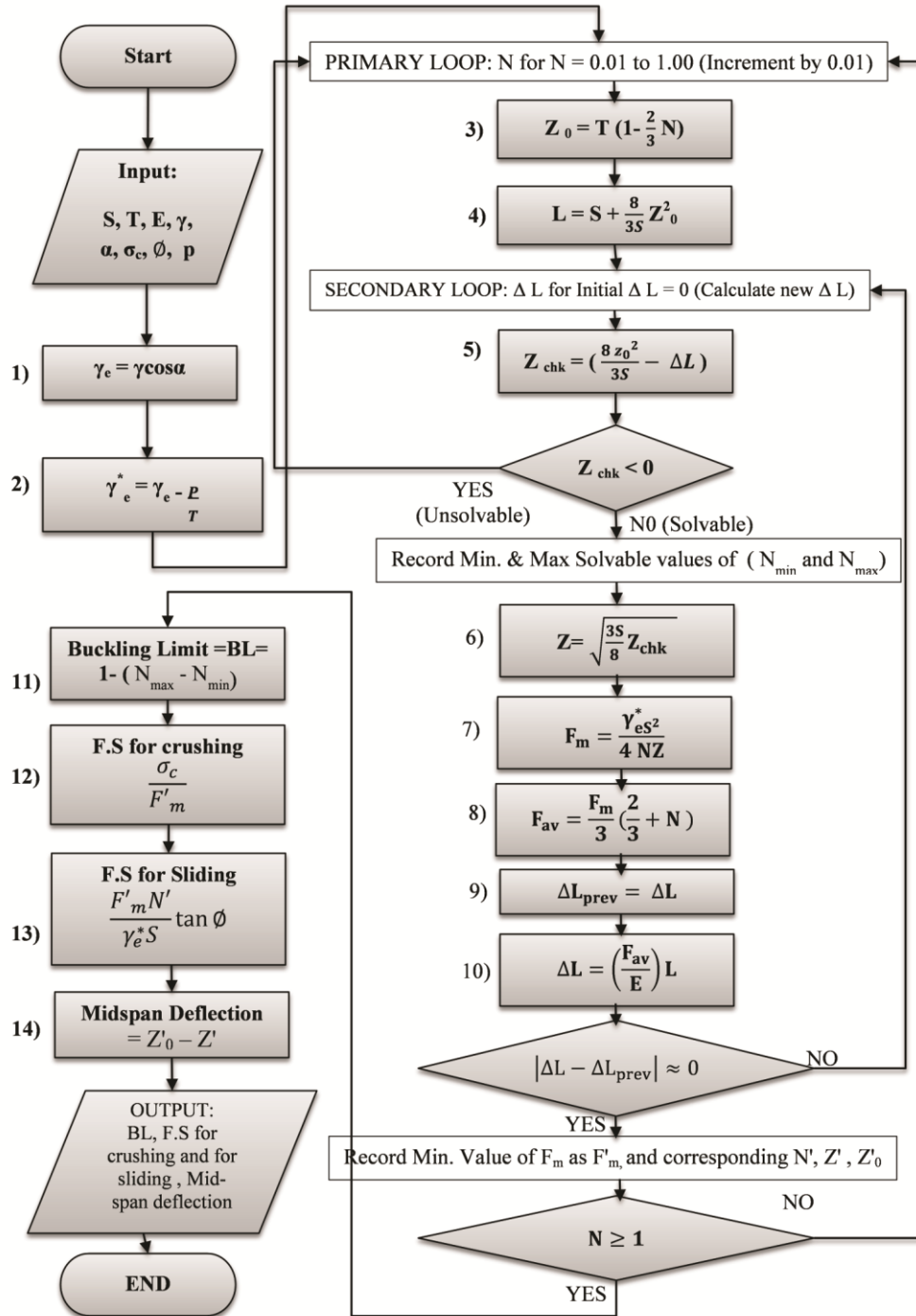


**Figure 2.14** The complete procedure for the determination of deflection and stability of a Voussoir beam (after Diederichs and Kaiser, 1999)

Finally, a new generalized Hoek-Brown criterion was introduced by Hoek et al. (2002) as follows:

$$\sigma'_1 = \sigma'_3 + \sigma_{ci} \left( m_b \frac{\sigma'_3}{\sigma_{ci}} + s \right)^a \quad (2.20)$$

where  $\sigma'_1$  and  $\sigma'_3$  are the major and minor effective principal stresses at failure, respectively,  $\sigma_{ci}$  is the UCS of the intact rock and  $m_b$  is a reduced value of the material constant  $m_i$  and can be estimated as follows:

$$m_b = m_i \exp\left(\frac{GSI-100}{28-14D}\right) \quad (2.21)$$

$s$  and  $a$  are constants:

$$s = \exp\left(\frac{GSI-100}{9-3D}\right) \quad (2.22)$$

$$a = \frac{1}{2} + \frac{1}{6} \left( e^{\frac{-GSI}{15}} - e^{\frac{-20}{3}} \right) \quad (2.23)$$

$D$  is the disturbance factor which depends on the stress relaxation and blast damage. It varies from 0 to 1. For undisturbed rock masses the value of  $D$  is 0 and for very disturbed rock masses the value of  $D$  is 1. (A guideline for the selection of the  $D$  factor has been provided by Hoek et al. (2002)). A practical and useful table has been provided by Hoek et al. (1995) to estimate the Hoek-Brown parameters ( $s$ ,  $a$ ,  $\frac{m_b}{m_i}$  GSI) and elastic properties of rock (deformation modulus,  $E$ , and Poisson's ratio,  $\nu$ ) based on rock mass structure and discontinuity surface conditions (figure 2.15).

#### **2.2.1.4 Mohr-Coulomb failure criterion**

The Mohr-Coulomb failure criterion is the combination of the Coulomb failure criterion presented by Coulomb (1773) and Mohr (1900). The basic assumption in this model is that shear failure depends on the normal stress. The Mohr's circles can be plotted for states of principal stresses (minimum and maximum). The Mohr-Coulomb failure criterion is the best straight (linear) envelope that touches the Mohr's circles (figure 2.16). The equation of this linear envelope can be written as:

$$\tau_p = C + \sigma_n \tan\phi \tag{2.24}$$

where  $\sigma_1$  and  $\sigma_3$ , shown in figure 2.16, are the maximum and minimum principal stresses, respectively,  $\tau_p$  is the peak shear stress or shear strength,  $\sigma_n$  is the normal stress,  $c$  is the cohesion of the rock materials and  $\phi$  is the angle of friction.

| GENERALISED HOEK-BROWN CRITERION   |   | STRUCTURE  | SURFACE CONDITION                            | VERY GOOD<br>Very rough, unweathered surfaces | GOOD<br>Rough, slightly weathered, iron stained surfaces | FAIR<br>Smooth, moderately weathered or altered surfaces | POOR<br>Slackensided, highly weathered surfaces with compact coatings or fillings containing angular rock fragments | VERY POOR<br>Slackensided, highly weathered surfaces with soft clay coatings or fillings |
|--|---|--|--|---|--|--|---|--|
| $\sigma_1' = \sigma_3' + \sigma_c \left( m_b \frac{\sigma_3'}{\sigma_c} + s \right)^a$ <p><math>\sigma_1'</math> = major principal effective stress at failure<br/> <math>\sigma_3'</math> = minor principal effective stress at failure<br/> <math>\sigma_c</math> = uniaxial compressive strength of intact pieces of rock<br/> <math>m_b</math>, <math>s</math> and <math>a</math> are constants which depend on the composition, structure and surface conditions of the rock mass</p> |   |  |  |   |  |  |   |  |
|   | BLOCKY - very well interlocked undisturbed rock mass consisting of cubical blocks formed by three orthogonal discontinuity sets     | $m_b/m_i$<br>$s$<br>$a$<br>$E_m$<br>$v$<br>$GSI$ | 0.60<br>0.190<br>0.5<br>75,000<br>0.2<br>85  | 0.40<br>0.062<br>0.5<br>40,000<br>0.2<br>75   | 0.26<br>0.015<br>0.5<br>20,000<br>0.25<br>62             | 0.16<br>0.003<br>0.5<br>9,000<br>0.25<br>48              | 0.08<br>0.0004<br>0.5<br>3,000<br>0.25<br>34  |  |
|    | VERY BLOCKY - interlocked, partially disturbed rock mass with multifaceted angular blocks formed by four or more discontinuity sets | $m_b/m_i$<br>$s$<br>$a$<br>$E_m$<br>$v$<br>$GSI$ | 0.40<br>0.062<br>0.5<br>40,000<br>0.2<br>75  | 0.29<br>0.021<br>0.5<br>24,000<br>0.25<br>65  | 0.16<br>0.003<br>0.5<br>9,000<br>0.25<br>48              | 0.11<br>0.001<br>0.5<br>5,000<br>0.25<br>38              | 0.07<br>0<br>0.53<br>2,500<br>0.3<br>25   |  |
|   | BLOCKY/SEAMY - folded and faulted with many intersecting discontinuities forming angular blocks                                     | $m_b/m_i$<br>$s$<br>$a$<br>$E_m$<br>$v$<br>$GSI$ | 0.24<br>0.012<br>0.5<br>18,000<br>0.25<br>60 | 0.17<br>0.004<br>0.5<br>10,000<br>0.25<br>50  | 0.12<br>0.001<br>0.5<br>6,000<br>0.25<br>40              | 0.08<br>0<br>0.5<br>3,000<br>0.3<br>30                   | 0.06<br>0<br>0.55<br>2,000<br>0.3<br>20   |  |
|   | CRUSHED - poorly interlocked, heavily broken rock mass with a mixture of angular and rounded blocks                                 | $m_b/m_i$<br>$s$<br>$a$<br>$E_m$<br>$v$<br>$GSI$ | 0.17<br>0.004<br>0.5<br>10,000<br>0.25<br>50 | 0.12<br>0.001<br>0.5<br>6,000<br>0.25<br>40   | 0.08<br>0<br>0.5<br>3,000<br>0.3<br>30                   | 0.06<br>0<br>0.55<br>2,000<br>0.3<br>20                  | 0.04<br>0<br>0.60<br>1,000<br>0.3<br>10   |  |

Figure 2.15 Estimation of the generalized Hoek-Brown parameters for an undisturbed rock mass (from Hoek et al., 1995)

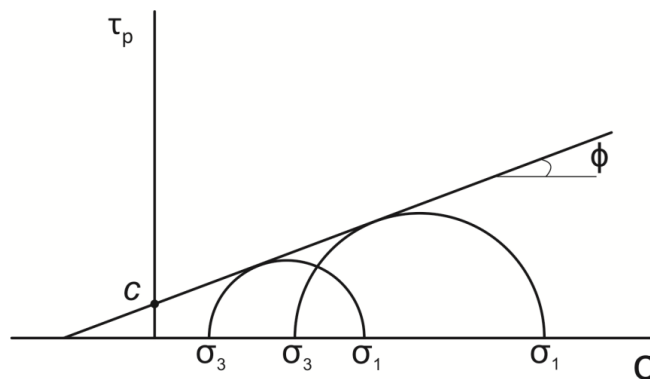


Figure 2.16 Mohr-Coulomb failure envelope

### 2.2.1.5 Relationship between the Mohr-Coulomb and the Hoek-Brown criteria

Since most geotechnical software packages and Abaqus use the Mohr-Coulomb failure criterion, there is a need to convert the Hoek-Brown parameters to the Mohr-Coulomb parameters. For this purpose, Hoek et al. (2002) presented the relationships between the Mohr-Coulomb and the Hoek-Brown criteria. Moreover, software called RocLab (Rocscience Inc.) was developed using the abovementioned research, includes all the proposed conversion equations and can be used to assess the Mohr-Coulomb failure criterion parameters. The proposed equations by Hoek et al. (2002) are as follows:

$$\phi = \sin^{-1} \left[ \frac{6am_b(S+m_b\sigma'_{3n})^{a-1}}{2(1+a)(2+a)+6am_b(S+m_b\sigma'_{3n})^{a-1}} \right] \quad (2.25)$$

$$C = \frac{\sigma_{ci}[(1+2a)s+(1-a)m_b\sigma'_{3n}](S+m_b\sigma'_{3n})^{a-1}}{(1+a)(2+a)\sqrt{1+(6am_b(S+m_b\sigma'_{3n})^{a-1})/((1+a)(2+a))}} \quad (2.26)$$

$$\text{where } \sigma'_{3n} = \frac{\sigma'_{3max}}{\sigma_{ci}}$$

An extensive discussion has been presented by Hoek et al. (2002) on the determination of  $\sigma'_{3max}$  for two different specific applications: tunnels and slopes.

## 2.2.2 Empirical methods of open slope stability analysis

Many empirical methods in rock mechanics are based on the past experiences and case histories related to the specific problem. The most popular empirical method of open slope design is proposed by Mathews et al. (1981). Initially, this method was developed based on only 26 case histories. Potvin et al. (1988) modified the initial model and increased the case histories to 176. The most updated stability graph, which is based on 400 case histories, was presented by Mawdesley et al. (2001). The main input data for most of the empirical open slope design methods (such as Mathews stability graph), is the rock mass classification design schemes.

### 2.2.2.1 Rock mass classification design schemes

Rock mass classification schemes can be used to characterize the rock mass quality according to the parameters influencing stability and the support

requirements in underground openings. The chronological development of popular rock mass classification schemes is shown in table 2.1. A discussion about all of these schemes is beyond the scope of this research. In the subsequent sections, only the RMR system and the tunnelling quality index (Q and Q') will be discussed.

### ***2.2.2.2 Rock mass rating (also known as geomechanics classification)***

One of the geomechanical rock mass classification systems widely used in mining is the RMR system developed by Bienawski (1973). It was modified by Bienawski over the years based on new case histories. The most updated version of the RMR system is presented by Bienawski (1989).

The RMR system is based on six input parameters: 1) the UCS of rock materials; 2) rock quality designation (RQD); 3) spacing of discontinuities; 4) condition of discontinuities; 5) groundwater conditions; and 6) orientation of discontinuities. Bienawski (1989) provided guidelines for the selection of rock reinforcement for tunnels based on the value of RMR. These guidelines are presented in table 2.2.

### ***2.2.2.3 Rock tunneling quality index system and the modified tunneling quality index***

The rock tunneling quality index (also known as the Q system) was proposed by Barton et al. (1974). The updated version of this system (Grimstad and Barton, 1993; Grimstad et al., 2002) is based on a large number of case histories of underground excavations in Norway, Switzerland and India.

The Q system is defined as:

$$Q = \frac{RQD}{J_n} \times \frac{J_r}{J_a} \times \frac{J_w}{SRF} \quad (2.27)$$

where RQD is the rock quality designation (defined in table 2.1),  $J_n$  is the joint set number,  $J_r$  is the joint roughness number,  $J_a$  is the joint alteration number,  $J_w$  is the joint water reduction factor and  $SRF$  is the stress reduction factor.

**Table 2.1** Popular rock mass classification systems for underground design

| <b>Classification System</b>                 | <b>Developer</b>     | <b>Application and description</b>   |
|--|----------------------|--|
| <b>Terzaghi's rock mass classification</b>   | Terzaghi, 1946       | Design of tunnel support based on the descriptive rock mass classification (i.e. intact rock, stratified rock, moderately jointed rock, blocky / seamy rock, crushed rock, squeezing rock and swelling rock)   |
| <b>Lauffer classification</b>                | Lauffer, 1958        | Introduced the concept of stand-up time into the design of tunnel support. This concept is important because as the span increases, the time to install support decreases.   |
| <b>Rock quality designation (RQD) index</b>  | Deer et al., 1967    | Estimation of rock mass quality from core logs, one of the key input data required to assess RMR, Q and Q'. RQD is define as percentages of intact core pieces longer than 10 cm in the total length of a core sample.   |
| <b>Rock structure rating (RSR)</b>           | Wichham et al., 1972 | Design of the support, based on the concept of rating the important parameters: parameter A (geology), Parameter B (geometry) and Parameter C (groundwater and joint conditions). Consequently, $RSR = A+B+C$ . Wichham et al. (1972) developed a design chart which the support parameters (such as shotcrete thickness, rockbolt spacing, steel rib spacing) can be estimated based on the RSR number. |
| <b>Rock mass rating (RMR) system</b>         | Bieniawski, 1973     | Design of underground structures (details in section 2.2.1.1)  |
| <b>Rock tunnelling quality index (Q, Q')</b> | Barton et al., 1974  | Design of support for underground structures, one of the key input data necessary to assess open stope stability using Mathews stability graph (details in section 2.2.1.2)  |
| <b>Geological strength index (GSI)</b>       | Hoek, 1994           | A key parameter to assess the Hoek-Brown failure criterion parameters. The lowest value of GSI is 10 for very poor rock masses and the maximum value of GSI is 100 for intact rock.  |

**Table 2.2** Guidelines for excavations and support in rock tunnels (after Bieniawski, 1989)

| Rock mass class           | RMR    | Excavation  | Rockbolts (20mm diameter, fully grouted)   | Support shotcrete                                     | Steel sets  |
|---------------------------|--------|---|--|---|---|
| <b>I – Very good rock</b> | 81-100 | Full face, 3 m advance  | <i>Generally no support required except for occasional spot bolting</i>                    |   |   |
| <b>II-Good rock</b>       | 61-80  | Full face 1.0-1.5 m advance. Complete support 20 m from face  | Locally bolts in crown 3 m king, spaced 2.5 m with occasional wire mesh                    | 50 mm in crown where required                         | None  |
| <b>III- Fair rock</b>     | 41-60  | Top heading and bench, 1.5-3 m advance in top heading. Commence support after blast. Complete support 10 m from face                          | Systematic bolts 4 m long, spaced 1.5-2 m in crown and walls with wire mesh in crown       | 50- 100 mm in crown and 30 mm in slides               | None  |
| <b>IV- Poor rock</b>      | 21-40  | Top heading and bench 1.0- 1.5 m advance in top heading. Install support concurrently with excavation 10m from face                           | Systematic bolts 4-5 m long, spaced 1-1.5m in crown and walls with wire mesh               | 100-150 mm in crown and 100 mm in sides               | Light to medium ribs spaced 1.5 m where required  |
| <b>V – Very poor rock</b> | ≤ 20   | Multiple drifts. 0.5-1.5 m advance in top heading. Install support concurrently with excavation. Shotcrete as soon as possible after blasting | Systematic bolts 5-6 m long, spaced 1-1.5 m in crown and walls with wire mesh. Bolt invert | 150-200 mm in crown, 150 mm in sides and 50mm on face | Medium to heavy ribs spaced 0.75 m with steel lagging and fore-poling if required. Close invert |

The above six parameters can be estimated from surface mapping and core logging by means of a design chart developed by Barton et al. (1974).

The mostly used Q system application is the estimation of the support parameters. For this purpose Barton et al. (1974) introduced a parameter called equivalent dimension ( $D_e$ ) which is defined as:

$$D_e = \frac{\text{Excavation Span or Height (m)}}{ESR} \quad (2.28)$$

where  $ESR$  is the excavation support ratio, which is some sort of safety factor related to the purpose of the excavation. Barton et al. (1974) provided suggested values for  $ESR$ , which is presented in Appendix C.

The modified tunnelling quality index (Q') system is exactly the same as the Q system, except the stress reduction factor ( $SRF$ ) is set to 1 (Potvin, 1988). Moreover, the Q' system is designed for dry rock mass conditions. Consequently, the joint water reduction factor is assumed to be 1. The Q' system is one of the key important parameters for the Mathews stability graph.

$$Q' = \frac{RQD}{J_n} \times \frac{J_r}{J_a} \quad (2.29)$$

#### 2.2.2.4 Geological strength index

The geological strength index (GSI) is a key parameter to assess the Hoek-Brown failure criterion parameters. It was first introduced by Hoek (1994) as a characterization system based on geological observations of rock mass structures and discontinuity surface conditions. The relationship between Bieniawski's 1976 and 1989 RMR of given by equations (2.30) and (2.31) as follows:

$$GSI = RMR_{76}, \text{ for } RMR_{76} > 18 \quad (2.30)$$

$$GSI = RMR_{89} - 5 \text{ for } RMR_{89} > 23 \quad (2.31)$$

The lowest value of GSI is 10 for very poor rock masses and the maximum value of GSI is 100 for intact rock. Most updated version of the GSI index chart is presented by Hoek. et al. (2013).

### 2.2.2.5 Mathews stability graph

The stability graph method for open stope design was initially introduced by Mathews et al. (1981), almost three decades ago. The method was modified and calibrated by Potvin (1988) and Nickeson (1992). The Mathews stability graph was updated (figure 2.18) by Stewart and Forsyth (1995) and by Hadjigeorgiou et al. (1995). Today, the extended version of the method, given by Trueman et al. (2000) and Mawdesley et al. (2001), is based on more than 400 case histories collected from underground hard rock mines.

This method has been used widely as the first step in the open stope design procedure. However, reviews by several researchers such as Hutchinson and Diederichs (1996), Suorineni et al. (2001), Suorineni (2010), and Mitri et al. (2011) showed that there are still many shortcomings with the Mathews stability graph. There is a need for factors that account for stope stand-up time, geological features (i.e. faults) and blast damage. Also, in this graph, there is no procedure for determining the stability of stope surfaces that are made of backfill.

The design procedure using the stability graph is based on the calculation of two factors: the modified stability number ( $N$ ) and the shape factor ( $S$ , also called the hydraulic radius,  $HR$ ).

The modified stability number ( $N'$ ), which represents the ability of the rock to stand up without support under a given stress condition, is defined by Potvin (1988) as follows:

$$N' = Q' \times A \times B \times C \quad (2.32)$$

where  $Q'$  is the modified tunneling quality index introduced by Barton et al. (1974),  $A$  is the stress factor,  $B$  is the joint orientation adjustment factor and  $C$  is the gravity adjustment factor. The design chart for evaluating each factor is shown in figure 2.17.

Factor  $A$  (figure 2.17a), the stress factor, accounts for the effect of the induced stresses around the stope surfaces. To estimate  $A$ , two input data are required: the UCS ( $\sigma_c$ ) and the vertically induced compressive stress at the centre-line of the

stope surface ( $\sigma_v$ ). Based on the ratio  $\sigma_c / \sigma_v$  and using figure 2.17a,  $A$  can be estimated. This factor varies between 0.1 for high compressive stress and 1 for relaxed conditions.

Factor  $B$  (figure 2.17b) accounts for the influence of the joint orientation on the stope stability. It can be defined as a measure of the relative difference in dip between the stope surface and the critical joint set affecting wall stability.

Factor  $C$ , the gravity adjustment factor, depends on the mode of failure. Three general modes of failure are assumed: gravity fall, slabbing (figure 2.17c) and sliding (figure 2.17d). The gravity adjustment factor for wedge falls and slabbing can also be estimated using equation (2.33) below:

$$C = 8 - 6\cos\theta \quad (2.33)$$

where  $\theta$  is the dip of the stope's face.

The hydraulic radius ( $HR$ ), or the stope surface shape factor ( $S$ ), accounts for the influence of the shape and size of a stope surface. It can be calculated as follows:

$$S = \frac{\text{Area of the given stope surface}}{\text{perimeter of the stope surface}} \quad (2.34)$$

The modified stability number ( $N'$ ) and the shape factor ( $S$ ) must be calculated for each stope surface. Consequently, using figure 2.18, the stability of each stope surface (hanging wall, footwall, back and vertical walls) should be assessed independently. Stewart and Forysth (1995) proposed four stability zones (figure 2.18) and three transition zones (gray shaded area) for the Mathew's stability graph: (i) potentially stable, (ii) transition zone between potentially stable and potentially unstable, (iii) potentially unstable, (iv) transition zone between potentially unstable and potentially major failure, (v) potentially major failure, (vi) transition zone between potentially major failure and potentially caving, and (vii) potential caving.

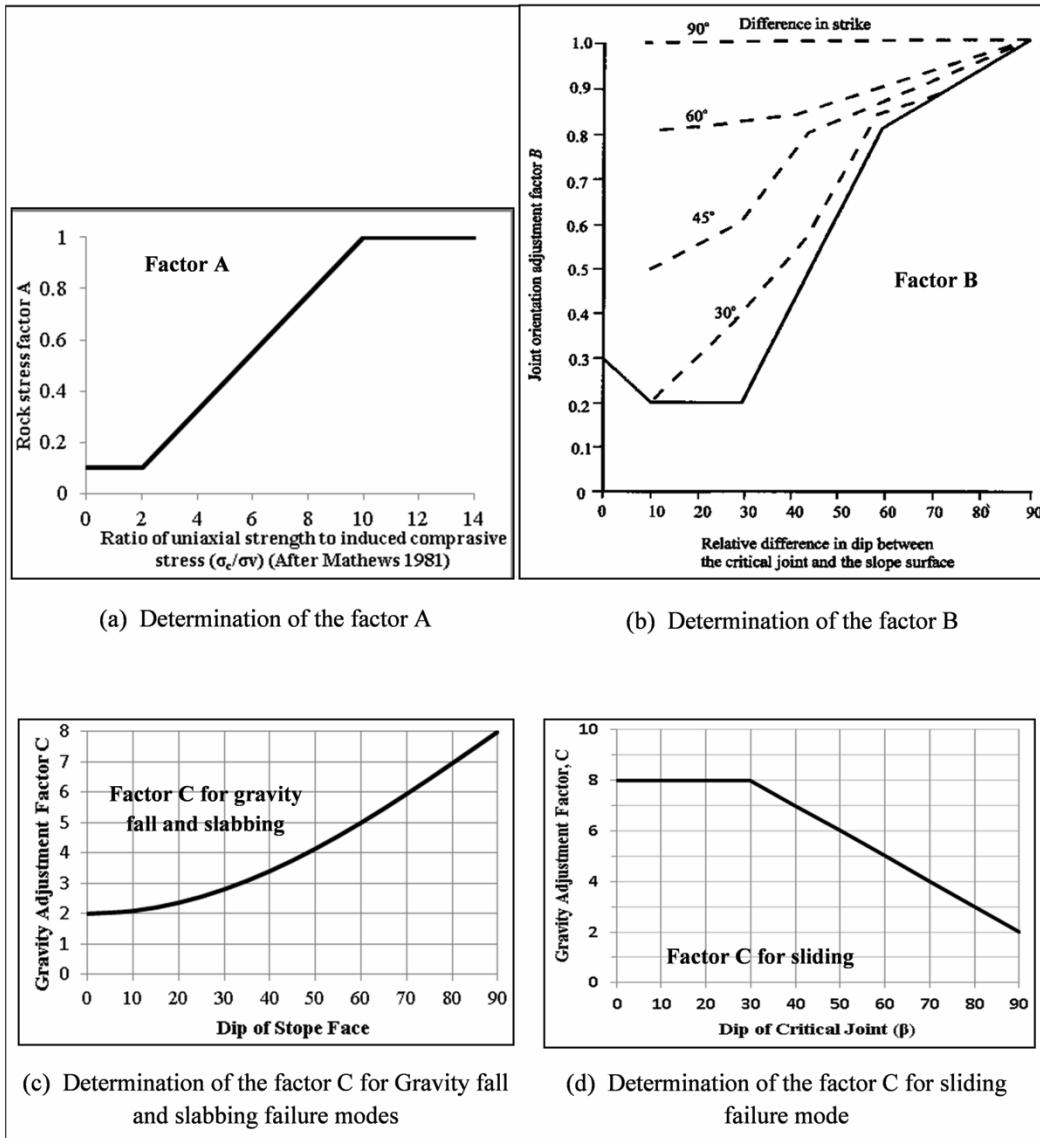


**Figure 2.17** Mathews stability graph design factors: (a) stress factor (*A*), (b) joint orientation adjustment factor (*B*), (c) gravity adjustment factor for gravity fall and slabbing failure mode, and (d) gravity factor for sliding failure mode (after Potvin, 1988)

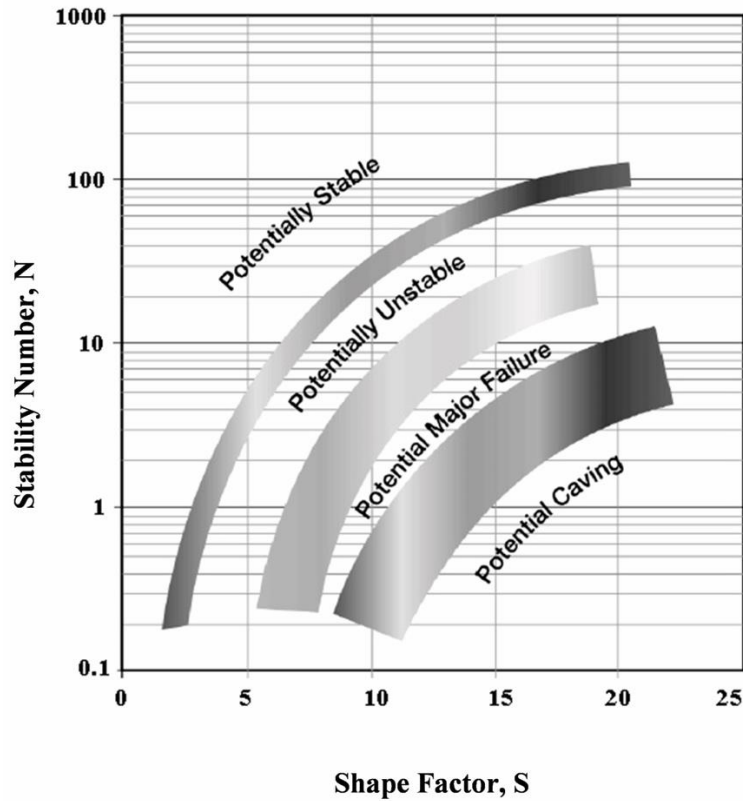


**Figure 2.18** The modified stability graph (after Stewart and Forsyth, 1995)

Reviews by several researchers (Hutchinson and Diederichs, 1996; Suorineni et al., 2001; Suorineni, 2010; Mitri et al., 2011) show that there are still many shortcomings with this method, such as: (i) the stability graph method does not account for the relaxation zones around the stopes; (ii) the stand-up time is not considered in this method; (iii) effects of geological features such as faults and shear zones are neglected; (iv) blasting effects are ignored; (v) it is difficult (and sometimes impossible) to use for complex stope geometry; (vi) this method cannot be used to evaluate the stability of the high walls made of backfill. Therefore, in the sublevel mining method which is performed in a primary/secondary manner, the interaction between the backfilled primaries and the ore body cannot be assessed by using this method; and (vii) this method cannot be used for the last stage of mining to assess the stability of the sill pillars and surface crown pillars.

### 2.2.3 Observational method

The observational method is the only way to assess the performance of the underground excavations and to verify the design predictions using the other three methods. The first practical use of this method was shown by Terzaghi and Peck (1948). Later the method was formalized by Peck in 1969.

The observational method is based on the monitoring and observation of the excavation and rock mass performance during construction and modifying the design and support parameters as the project proceeds. Observations can be made either visually or by means of instruments. One of the well-known examples of this method is the New Austrian Tunneling Method (NATM).

NATM was developed by Rabcewicz (1964) and Pacher (1975). Basically, this method provides a procedure to assess the excavation design parameters and to estimate the required support parameters based on observation of the excavation performance. Based on these observations, the design parameters are continuously adjusted to the encountered conditions. However, there are some shortcomings with NATM and because of that this method is not widely accepted in rock mechanics design. Whitney et al. (1983) provided a good discussion regarding the strengths and weaknesses of NATM.

Observational methods are the best way to calibrate a numerical model and to confirm and verify the predictions made using numerical methods. Brady and Brown (2004) provided a comprehensive review of the techniques of rock mass performance monitoring. Discussion about these methods is beyond the scope of this research proposal. Finally, a good critical review of this method is given by Spross (2014).

# **PART THREE**

## **NUMERICAL MODELING IN ROCK MECHANICS**

*This section reviews the application of numerical methods in rock mechanics and rock engineering. The focus is on the theory behind the finite element analysis method. The current state-of-the-art in rock mechanics modeling is reviewed.*

## 2.3 Numerical modeling in rock mechanics

### 2.3.1 Introduction

In the past three decades, numerical methods have become popular due to rapid advancements in computer technology. The suitability of these methods for analysis and design of very complex geotechnical problems is another reason why they are popular. Many conventional methods in rock mechanics are applicable to situations similar to the ones for which they were developed. However, there are many problems for which no past experience is available (Pande and Beer, 1990). In such cases, numerical methods are the best option to solve the design problems. Moreover, numerical methods should be used as a complementary method along with analytical and empirical methods.

According to Jing and Hudson (2002), numerical methods in rock mechanics can be classified into continuum, discontinuum and hybrid methods as described below:

Continuum methods are:

- The finite element method (FEM)
- The finite difference method (FDM)
- The boundary element method (BEM)

Discontinuum methods are:

- Discrete (or Distinct) elements method (DEM)
- Discrete fracture network (DFN)

Hybrid methods are:

- Hybrid FEM/BEM
- Hybrid DEM/BEM
- Hybrid FEM/DEM

The choice of continuum or discontinuum methods depends on the problem scale and the fracture system geometry. For example, in figure 2.19a the displacement field is continuous and the medium has no discontinuities; thus, continuum numerical methods would be appropriate. Discontinuum methods are suitable for moderately fractured rock masses where large-scale displacements of individual blocks are possible (Jing, 2003). For example, in figure 2.19b the displacement is determined by a slip along the discontinuities and rotation of the blocks; in this case, discontinuum methods would be appropriate.

There is no absolute guide on which method is better than another and when one or another should be used. However, the disadvantages of each type can be avoided by using hybrid methods. In figure 2.19c the displacement field would be continuous inside each area; however, it may be discontinuous across the areas, so in this case, hybrid methods would be a good choice (Bobet et al., 2009).

FEM is a well-recognized numerical method which can be used for rock mechanics and geomechanical design problems. It has the ability to deal with material heterogeneity, anisotropy, non-linearity, complex boundary conditions, in-situ stresses and gravity (Jing and Hudson, 2002). For these reasons, in this research, FEM will be used as the main numerical method to perform the numerical analysis.

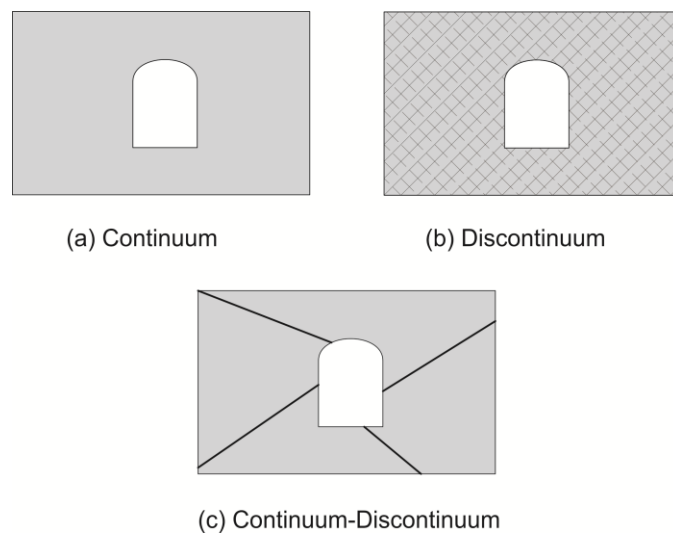


**Figure 2.19** Choice of continuum or discontinuum methods (after Bobet et al., 2009)

### 2.3.2 Finite element method

FEM is a well-recognized numerical method which can be used for rock mechanics and rock engineering problems. It has the ability to deal with material heterogeneity, anisotropy, non-linearity, complex boundary conditions, in-situ stresses and gravity (Jing et al., 2002).

FEM is the numerical solution of the mathematically weak form of a problem in engineering, which mainly consists of six steps as described briefly below (Singiresu, 2004):

- **Step 1: Discretization of the domain**

The domain will be divided into small (finite) elements. Elements are connected at points called *nodes*. The particular arrangement of elements is called a mesh (figure 2.20).

- **Step 2: Selection of a proper shape function**

The unknown variable is interpolated with certain shape functions that are localized to those finite elements.

- **Step 3: Calculating the element stiffness matrices (or, in general, element characteristic matrices)**

Element stiffness matrices will be assembled in the next step to give the global stiffness matrix or the stiffness matrix of the structure.

- **Step 4: The assemblage of elements (global stiffness matrix)**

The assemblage of element stiffness matrices is called the stiffness matrix of a structure. With this, the overall equilibrium equations will be obtained. The stiffness matrix of a structure against a particular degree of freedom is the value and direction of the set of forces needed to produce a unit displacement or rotation in that particular degree of freedom.

- **Step 5: Find the displacement for each node**

- **Step 6: Calculation of element stresses and strains (if desired)**

Steps 5 and 6 will be discussed later through an example.

FEM provides an approximate solution. The solution can be improved by using more elements to represent the structure (Cook et al., 2001).

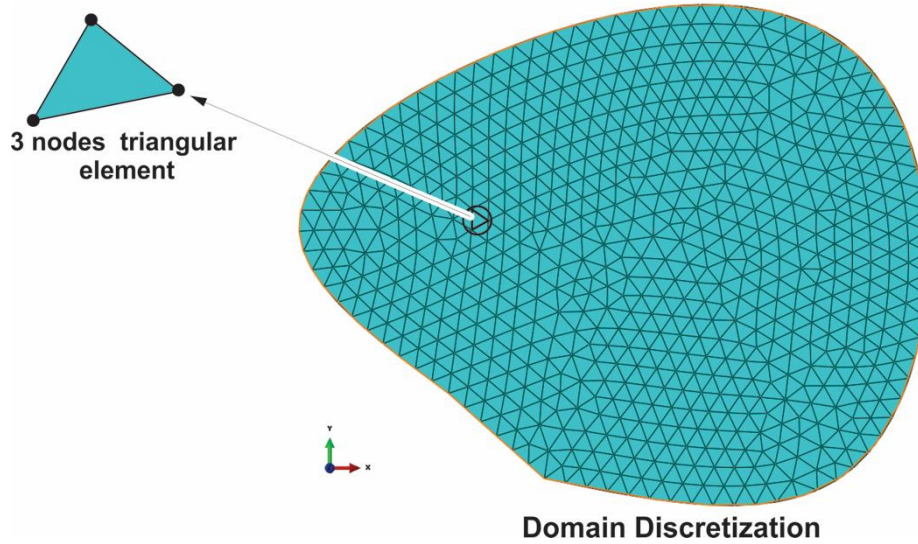


**Figure 2.20** Discretization of the domain using finite elements and forming a mesh

To illustrate the abovementioned steps, an example is given below.

Assuming a 2D problem, the domain is discrete with a number of triangular elements (step 1), as shown in figure 2.20. A linear triangular element is shown in figure 2.21.

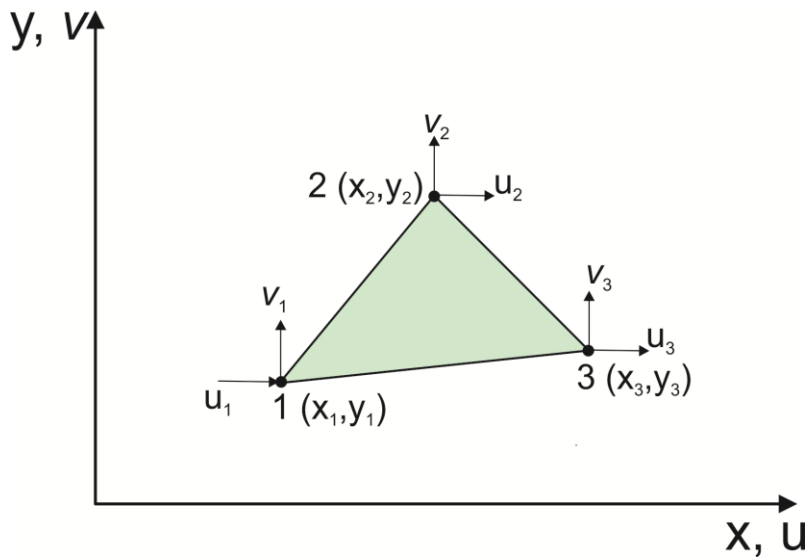


**Figure 2.21** A linear triangular element

The process to find the interpolation functions (shape functions, step 2) is explained as follows (Adeeb, 2010):

To calculate the shape functions, generally there are two methods: the intuitive method and rigorous structured method. Both are the same, but the rigorous structured method is most suitable for higher order elements. For this example, the latter method is only discussed.

According to the number of degree of freedom (for example, for the linear triangular element shown in figure 2.21, we have  $u_1, u_2, u_3$  and  $v_1, v_2, v_3$ ), the interpolation functions based on the Pascal triangle (figures 2.22 and 2.23) are chosen as below:

$$u(x,y) = a_1 + a_2x + a_3y \quad (2.35)$$

$$v(x,y) = b_1 + b_2x + b_3y \quad (2.36)$$

$$\begin{Bmatrix} u \\ v \end{Bmatrix} = \begin{pmatrix} 1 & 0 & x & 0 & y & 0 \\ 0 & 1 & 0 & x & 0 & y \end{pmatrix} \begin{Bmatrix} a_1 \\ b_1 \\ a_2 \\ b_2 \\ a_3 \\ b_3 \end{Bmatrix} \quad (2.37)$$

$$u = Xa \quad (2.38)$$

$$\begin{Bmatrix} u_1 \\ v_1 \\ u_2 \\ v_2 \\ u_3 \\ v_3 \end{Bmatrix} = \begin{pmatrix} 1 & 0 & x_1 & 0 & y_1 & 0 \\ 0 & 1 & 0 & x_1 & 0 & y_1 \\ 1 & 0 & x_2 & 0 & y_2 & 0 \\ 0 & 1 & 0 & x_2 & 0 & y_2 \\ 1 & 0 & x_3 & 0 & y_3 & 0 \\ 0 & 1 & 0 & x_3 & 0 & y_3 \end{pmatrix} \begin{Bmatrix} a_1 \\ b_1 \\ a_2 \\ b_2 \\ a_3 \\ b_3 \end{Bmatrix} \quad (2.39)$$

$$u_e = Aa, u_e \text{ is a vector of the nodal displacements.} \quad (2.40)$$

$$a = A^{-1}u_e \quad (2.41)$$

$$u = Xa = X A^{-1} u_e \quad (2.42)$$

Therefore, the shape function  $N_i$  is equal to:

$$N = X A^{-1} \quad (2.43)$$

$$N = \begin{bmatrix} N_1 & 0 & N_2 & 0 & N_3 & 0 \\ 0 & N_1 & 0 & N_2 & 0 & N_3 \end{bmatrix}$$

After calculating the shape functions, now the stiffness matrix of the element should be calculated (step 3). The elemental stiffness matrices will be assembled to give the global stiffness matrix. The global stiffness matrix is used to determine the global force and displacement. To calculate the element stiffness matrix, the following steps should be taken:

As shown in equation (2.42), the complete element displacement ( $u$ ) is:

$$u = N \cdot u_e$$

Therefore, the stiffness matrix of the previous example is:

$$K = \int B^T \cdot C \cdot B \cdot dv = t \int B^T \cdot C \cdot B \cdot dA = t \int_{-1}^1 \int_{-1}^1 B^T \cdot C \cdot B \cdot dydx \quad (2.44)$$

where the constitutive matrix  $[C]$  contains elastic constants. The dimension of the  $[C]$  matrix depends on the strain components. For example in 2D problems, strain has three components ( $\epsilon_{xx}, \epsilon_{yy}, \gamma_{xy}$ ) so the dimension of  $[C]$  is  $3 \times 3$ . For 3D problems, the strain components are 6 so the dimension of  $[C]$  is  $6 \times 6$ .

For plane stress:

$$c = \frac{E}{1-\nu^2} \begin{bmatrix} 1 & \nu & 0 \\ \nu & 1 & 0 \\ 0 & 0 & \frac{1-\nu}{2} \end{bmatrix} \quad (2.45)$$

And for plane strain:

$$c = \frac{E}{(1+\nu)(1-2\nu)} \begin{bmatrix} 1-\nu & \nu & 0 \\ \nu & 1-\nu & 0 \\ 0 & 0 & \frac{1-2\nu}{2} \end{bmatrix} \quad (2.46)$$

The matrix  $[B]$  is called the strain-displacement matrix. It is defined as:

$$[B] = [O] \cdot [N] \quad (2.47)$$

The  $[O]$  matrix is the operation matrix. For this example, it can be defined as:

$$[O] = \begin{bmatrix} \frac{\partial}{\partial x} & 0 \\ 0 & \frac{\partial}{\partial y} \\ \frac{\partial}{\partial y} & \frac{\partial}{\partial x} \end{bmatrix} \quad (2.48)$$

$$\text{and therefore } B = \begin{bmatrix} \frac{\partial N_1}{\partial x} & 0 & \frac{\partial N_2}{\partial x} & 0 & \frac{\partial N_3}{\partial x} & 0 \\ 0 & \frac{\partial N_1}{\partial y} & 0 & \frac{\partial N_2}{\partial y} & 0 & \frac{\partial N_3}{\partial y} \\ \frac{\partial N_1}{\partial y} & \frac{\partial N_1}{\partial x} & \frac{\partial N_2}{\partial y} & \frac{\partial N_2}{\partial x} & \frac{\partial N_3}{\partial y} & \frac{\partial N_3}{\partial x} \end{bmatrix} \quad (2.49)$$

Now we can calculate the stiffness matrix of this element:

$$K = \int B^T \cdot C \cdot B \cdot dv = t \int B^T \cdot C \cdot B \cdot dA = t \int_{-1}^1 \int_{-1}^1 B^T \cdot C \cdot B \, dy \, dx$$

where  $t$  is the thickness of the element.

After calculating the element stiffness matrices, it is easy to form the assembly of the element stiffness of matrices (step 4). In this case, the global equilibrium equations are:

$$K \cdot U = F \quad (2.50)$$

where  $K$  is the global stiffness matrix,  $U$  is the vector of global displacements and  $F$  is the global vector of loads.

From equation (2.50), displacements for each node can be calculated as follows (step 5):

$$U = K^{-1} \cdot F \quad (2.51)$$

Finally, from the displacements, the strains and stress for elements can be calculated (step 6).

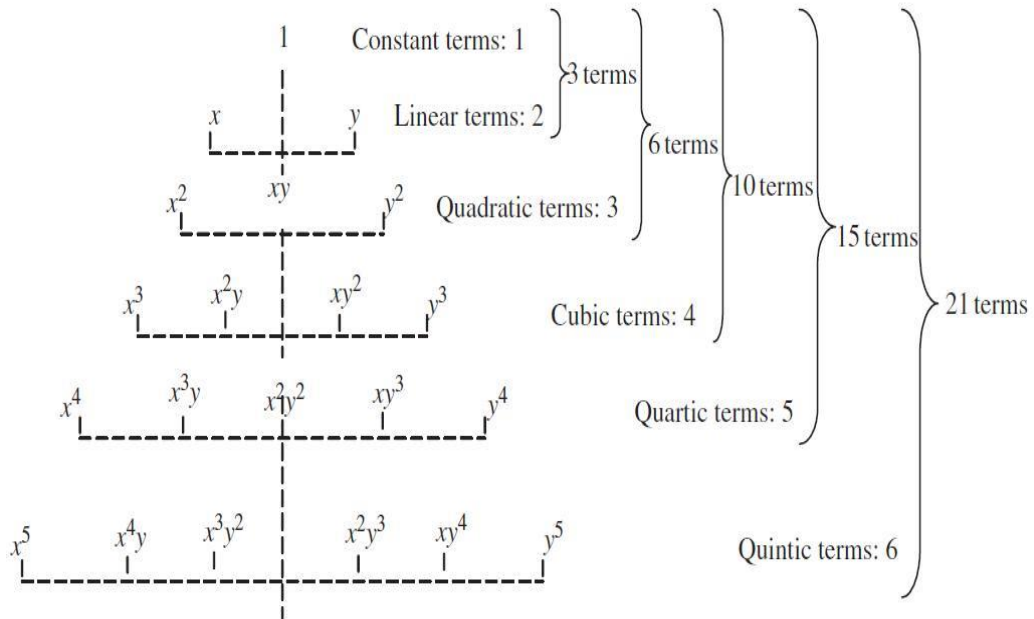


Figure 2.22 Pascal triangle for 2D cases (after Liu et al., 2003)

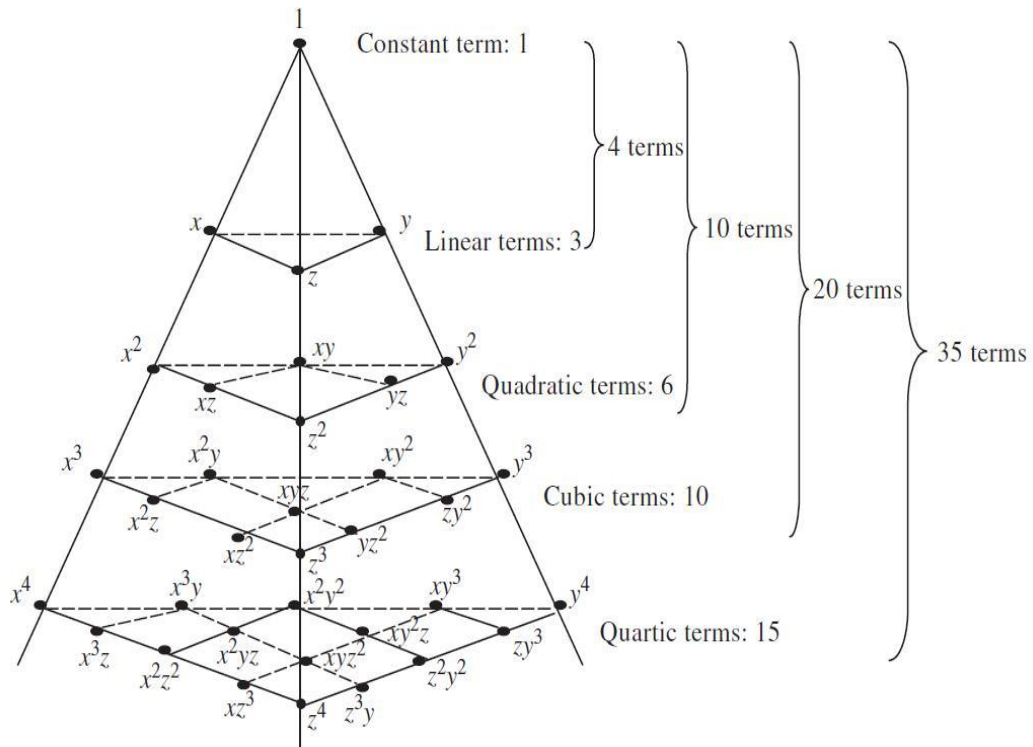
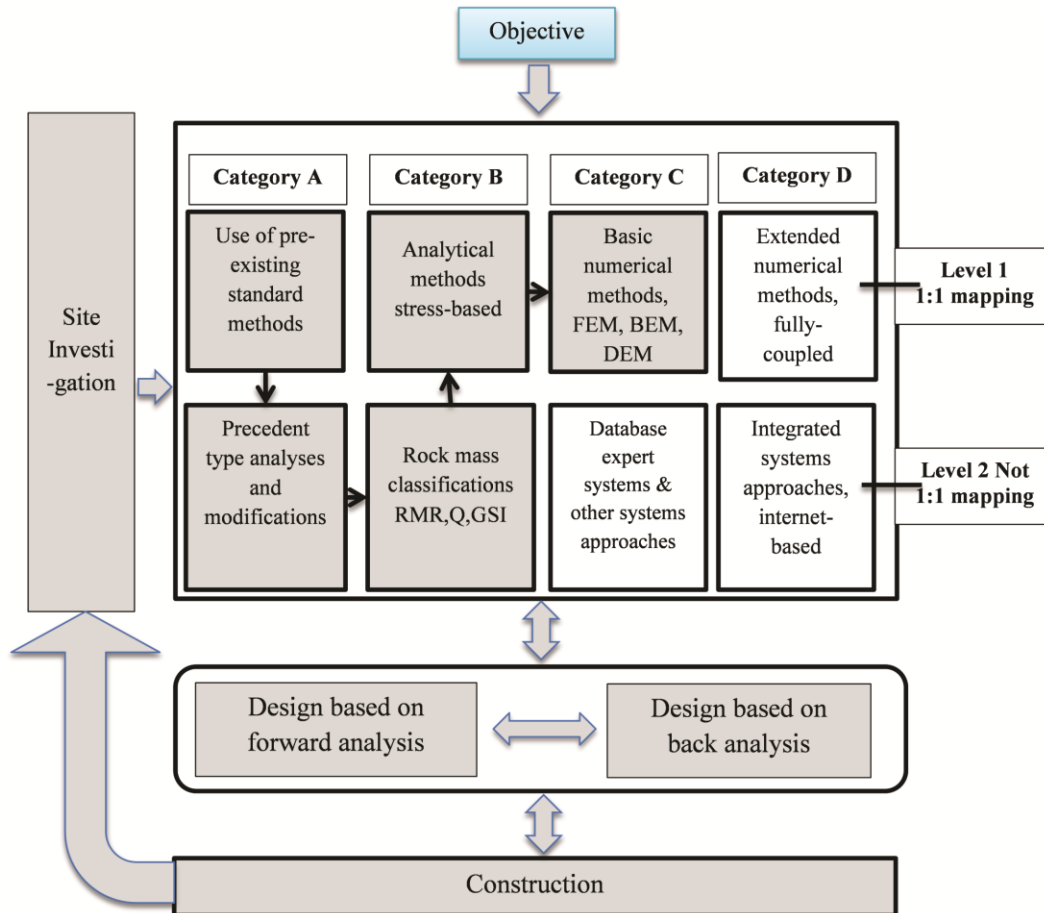


Figure 2.23 Pascal pyramid for 3D cases (after Liu et al., 2003)

## 2.4 A review of current state-of-the-art rock mechanics modeling approaches

There are several rock mechanics modeling approaches which are presented in the form of flowcharts by various researchers like Hoek and Brown (1982b), Pahl and Beitz (1984), Bieniawski (1989, 1993), Hudson (1993), Li (1998), Goricki (2003), Brady and Brown (2004), Hudson and Feng (2004, 2007, 2010) and most recently Feng and Hudson (2011).



**Figure 2.24** Flowchart of a rock mechanics modeling and rock engineering design approach (after Feng and Hudson, 2011)

In figure 2.24, the eight basic methods of modeling are classified under four categories (A to D). These categories have four levels of complexities. From left to the right, the complexity of the problems increases from simple to complicated. The framework consists of the project objectives, site investigation, design and construction. The first three categories are widely used in rock mechanics design.

The fourth category is still under development and much work needs to be done in this area. As seen in this figure, all of these categories are shown in two levels: (i) level 1, 1:1 mapping refers to those methods of modeling which try to represent the geometry and rock features on a 1:1 basis (i.e. creating a full 3D view of an underground mine with all stopes and drifts according to the reality and including major geotechnical features in the model); and (ii) level 2, not 1:1 mapping is where the modeling methods are not designed to include the geometry and mechanisms directly (i.e. rock mass classifications methods).

*This research dissertation aims to develop an integrated methodology which utilizes a combination of all the methods (the shaded boxes in figure 2.24), as needed, incorporating the advantages of the many methods available.* This methodology is discussed in Chapter 1.

# **CHAPTER 3: FINITE ELEMENT ANALYSIS MODEL FOR THE DETERMINATION OF IN-SITU AND MINING-INDUCED STRESS – A CASE STUDY OF DIAVIK DIAMOND MINE**

*In this chapter, a case study of Diavik Diamond Mine is used to implement the research methodology. A full three-dimensional finite element model of the mine is constructed step by step. Rock mechanics laboratory tests are performed on Kimberlite samples from Diavik Mine to measure the intact properties of Kimberlite. The results of these laboratory tests are used to estimate the rock mass properties and calibrate the modelling input parameters of the finite element analysis.*

## ***Appendices:***

- (i) Appendix A: Rock Mechanics Laboratory Test Results***
- (ii) Appendix D: Abaqus Code – Defining Simulation Steps***

### **3.1 Introduction**

In this chapter, a case study of Diavik Diamond Mine is used to implement the proposed research methodology. A full realistic three-dimensional (3D) elastoplastic finite element model of the mine was developed. This finite element (FE) analysis model was used to determine the in-situ and mining-induced stress regime at the mine as a function of two underground mining methods: (i) blasthole stoping (BHS); and (ii) sublevel longhole retreat (SLR). Laboratory tests were conducted on Kimberlite samples from Diavik Mine. The results of these laboratory tests were used to estimate the rock mass properties and calibrate the modeling input parameters used for the FE analysis.

The goal is to seek a detailed understanding of stress (in-situ and mining-induced) distribution regimes in the mine as a function of mining methods. The results of the developed FE model will be presented in chapters 4, 5 and 6 for predictions of possible rockbursts, mining-induced surface subsidence, and relaxation and yielding zones in the mine. Finally, the developed model will be verified and validated in chapter 7 of this thesis.

### **3.2 A case study: Diavik Diamond Mine**

Diavik Diamond Mine is located on a 20-km<sup>2</sup> island in Lac de Gras, approximately 300 km northeast of Yellowknife, Northwest Territories. Diavik reserves are contained in four diamond-bearing Kimberlite pipes named A154 North, A154 South, A418 and A21. The host rock is granite. All four pipes were located under the waters of Lac de Gras. To enable open pit mining, first the water was removed, and dikes were constructed to drain the water and prepare the surface for open pit mining. In 2002, the first dike around the A154 North and A154 South pipes was completed. Consequently, open pit mining operations started in 2003. In 2007, construction of the second dike around the A418 pipe was completed. In 2010, open pit mining of the two A154 pipes was completed and development of the underground mine commenced. The planned underground

mining methods for the A154 North, A154 South and A418 Kimberlite pipes were SLR and BHS. SLR is being used in the A154 South and A418 pipes. Figure 3.1 shows the open pits at Diavik Mine. Figure 3.2 illustrates the locations of three Kimberlite pipes: A154North, A154 South and A418.



**Figure 3.1** Aerial image of Diavik Diamond Mine (courtesy of Diavik Diamond Mine)

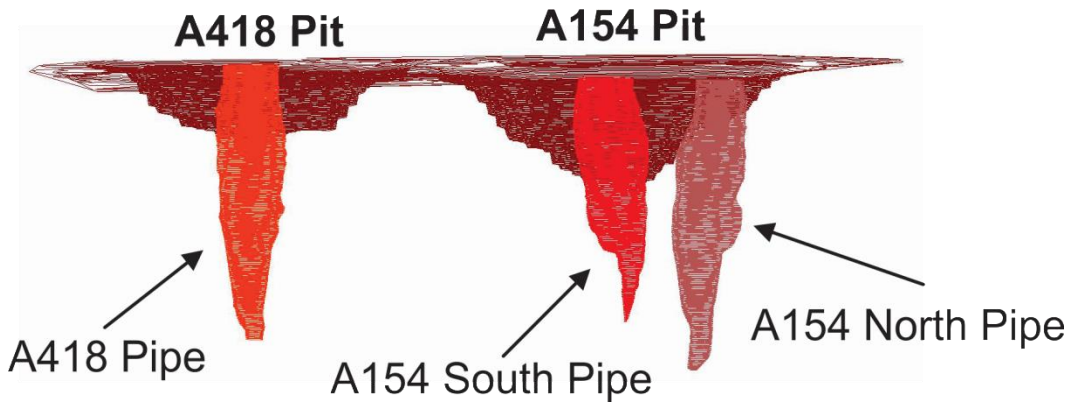


**Figure 3.2** Location of three Kimberlite pipes

### **3.2.1 Sublevel open stoping and blasthole stoping**

Sublevel open stoping is one of the most popular underground mining methods in Canada. Based on the drilling patterns and blasting direction, sublevel mining methods can be classified into three categories: (i) BHS; (ii) vertical crater retreat (VCR); and (iii) longhole stoping.

The BHS mining method is being used in the A154 North pipe at Diavik Mine. The planned BHS include primary and secondary stopes. The preliminary design calls for all of the stopes to have 7.5 m widths, strike lengths of about 100 m and heights of approximately 30 m sill to sill. Cemented rockfill (CRF) is being used to backfill the excavated stopes.

BHS generally involves two sublevels and a certain amount of preparation of the stope before actual production can proceed. One sublevel is used for drilling (overcut) and another sublevel is used for production (undercut). According to Hustrulid (2001), the BHS method is the best option when the ore body has the following characteristics:

- the dip of ore body is steep (which is the case in most Canadian underground diamond mines)
- the ore and host rock are competent (in diamond mines the host rock is often granite)
- the ore boundaries are regular
- strong hanging wall and foot wall present

Production in BHS is performed in a primary/secondary manner. First, the primary stopes are excavated. After the primary stopes are completely excavated and backfilled, excavation of the secondary stopes are initiated. After completing the mining of one level, the operation moves to the next mining level. The dimensions of the stopes are usually large in the vertical direction. Therefore, the assessment of the stability of these stopes is a critical task for geomechanical mine designers.

A horizontal section of ore, known as a sill pillar, is often left between two mining levels to support the mine working areas above the producing stopes. When sill pillars are close to the surface, they are called surface crown pillars. Recovery of surface crown and sill pillars is another challenge for mine designers.

### 3.2.2 Sublevel longhole retreat mining method

The SLR mining method is being used in the A154 South pipe. In this method, the mining levels consist of production drifts (5 m wide by 5 m high), the slot drift (same size and profile as the production drifts) and SLR stope blocks. The production drifts are developed from the main level access drift, parallel to each other. The slot drift is developed parallel to the far orebody contact and approximately parallel to the longer axis of the orebody and perpendicular to the production drifts (figure 3.3b). The SLR blocks are excavated by a series of up-hole stopes (drilled, blasted and hauled out from the production drifts on a retreat manner) starting from the far Kimberlite contact as shown in figure 3.3a. After the opening of a slot drift, stope drilling and blasting can start. Unlike the BHS method, in the SLR method, the mined-out area will not be backfilled; therefore, the stability of both the host rock and orebody is of great concern.

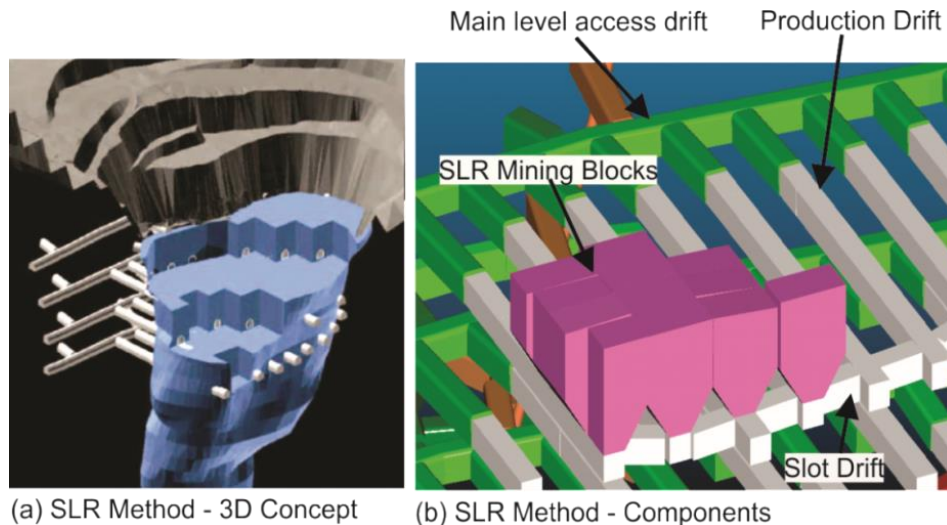


**Figure 3.3** An illustration of the SLR mining method (after Diavik Dialogue, 2011)

### 3.3 Rock mechanics laboratory tests on Kimberlite

To estimate the strength properties of Kimberlite, three main laboratory tests were performed: (i) the UCS test; (ii) indirect tensile strength test (also called Brazilian test); and (iii) triaxial compressive test. The results from these tests were used to calibrate and estimate the rock mass properties to be used as the input parameters in the FE model.

Five types of Kimberlite bulk samples were collected from the A154 South and A154 North pipes. The name of these rock types, geological descriptions and location of each rock type are presented in table 3.1.

**Table 3.1** Kimberlite sample rock types

| Rock Type | Geological Descriptions                                      | Kimberlite Pipe |
|-----------|--|-----------------|
| PK        | Pyroclastic Kimberlite                                       | A154 South      |
| PKX       | Olive & macrocrystic-rich pyroclastic Kimberlite             | A154 South      |
| MK        | Magnetic lapilli rich macrocrystic volcanoclastic Kimberlite | A154 North      |
| MRK       | Mud-rich volcanoclastic Kimberlite                           | A154 North      |
| BMVK      | Black macrocrystic volcanoclastic Kimberlite                 | A154 North      |

All of the samples were shipped to the rock mechanics laboratory at the University of Alberta. ASTM D4543-08 was followed to prepare the cylindrical core specimens, and the preparation procedure is summarized in figure 3.4. Due to the size and irregular shape of the bulk samples, the only feasible coring size was 38.1 mm (1.5 inches). However, some 63.5 mm (2.5 inches) diameter cores were also provided by the mine. As illustrated in figure 3.4, prepared cores were inspected at least two times during the preparation procedure to ensure that the ASTM requirements were met. Examples of the ASTM requirements include: (i) the specimen length-to-diameter ratio must be between 2:1 and 2.5:1 (for UCS and triaxial tests); (ii) the specimen thickness-to-diameter ratio must be between 0.2 to 0.75 (for the Brazilian test); and (iii) the shape conformance should be verified, and the end surfaces must be flat and parallel.

Due to the poor quality of some bulk samples, some cores eroded during the coring and cutting process. Therefore, the procedure had to start from beginning until the required number of cores had been met.

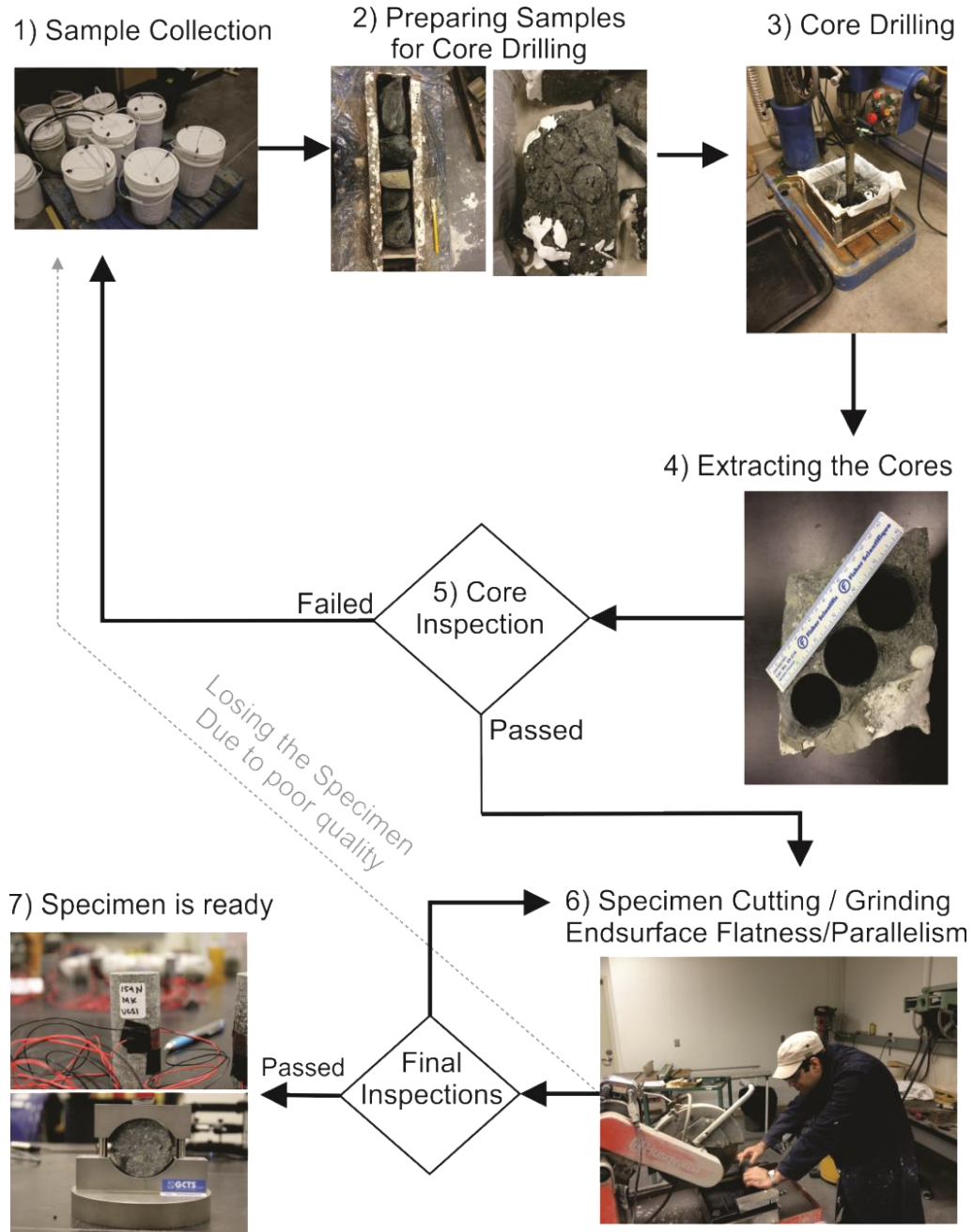


**Figure 3.4** Test specimen preparation workflow

### 3.3.1 Uniaxial compressive strength test

The UCS test is one of the most popular rock mechanics tests on rock. It is used to determine important rock strength and deformability properties such as: (i) compressive strength ( $\sigma_c$ ); (ii) Young's modulus ( $E$ ); and (iii) Poisson's ratio ( $\nu$ ).

To conduct the test, ASTM D7012-13 was followed to prepare the cylindrical specimens (specific dimensions of the core samples that meet this standard requirement have been outlined in section 3.3). Diameters of the samples were 38.1mm (1.5 inches). There were also some cores with 63.5mm (2.5 inches) provided by the mine. The required specimen length to diameter ratio is between 2.0:1 and 2.5:1 by the ASTM standards. All the core specimens are cut to the length that meets this standard requirement. A summary of the UCS test procedure is as follows:

- (i) The specimen is placed in the 1,000-ton servo-hydraulic controlled INSTRON loading frame.
- (ii) The axial load is increased continuously. The load must be applied in a stress rate (ASTM suggests between 0.5 and 1.0 MPa/s) or strain rate that produces failure of the test specimen between 2 and 15 minutes. To meet this requirement, the rate of 1.57 KN/s was defined.
- (iii) The axial and lateral deformations are recorded as a function of load until peak load and failure are obtained. For bigger samples (i.e. 63.5 mm diameter cores), a compressometer with linear variable differential transfers (LVDT) was used. For smaller samples (i.e. 38.1 mm diameter cores), strain gauges were used to read the lateral and axial deformations on the specimens.
- (iv) The maximum load sustained by the specimen was recorded ( $P$ ). The UCS ( $\sigma_c$ ) of the test specimen was calculated using as follows:

$$\sigma_c = \frac{P}{A} \quad (3.1)$$

where  $P$  is the failure load and  $A$  is the cross-sectional area of the specimen.

- (v) The axial strains ( $\epsilon_a$ ) are calculated as follows:

$$\epsilon_a = \frac{\Delta L}{L} \quad (3.2)$$

where  $\Delta L$  is the change in measured axial gauge length and  $L$  is the original undeformed axial gauge length.

- (vi) The lateral strains ( $\epsilon_l$ ) are calculated as follows:

$$\epsilon_l = \frac{\Delta D}{D} \quad (3.3)$$

where  $\Delta D$  is the change in measured diameter and  $D$  is the original undeformed diameter.

Based on the information presented above, stress-strain curves are plotted in the axial and lateral directions (figure 3.5). Using the above data, the value of  $E$  can be calculated using one of the following methods suggested by Brady and Brown (2004):

- Tangent Young's modulus ( $E_t$ ), which is the slope of the axial stress–axial strain curve at 50% of the peak strength.
- Average Young's modulus ( $E_{av}$ ) which is the average slope of the more-or-less straight line portion of the stress-strain curve.
- Secant Young's modulus ( $E_s$ ) which is the slope of a straight line joining zero to a point on the curve at some fixed percentage of the maximum strength.

The value of  $\nu$  is calculated using the following equation:

$$\nu = - \frac{\text{Slope of axial curve}}{\text{Slope of lateral curve}} = - \frac{E}{\text{Slope of lateral curve}} \quad (3.4)$$

A sample stress-strain curve and calculations of  $E$  and  $\nu$  are presented in figure 3.5. Figure 3.6 shows a mode of failure in one of the Kimberlite samples.

All five Kimberlite rock types were tested. In total, 18 UCS tests were conducted. The results are presented in table 3.2. Detailed results for each sample are presented in Appendix A.

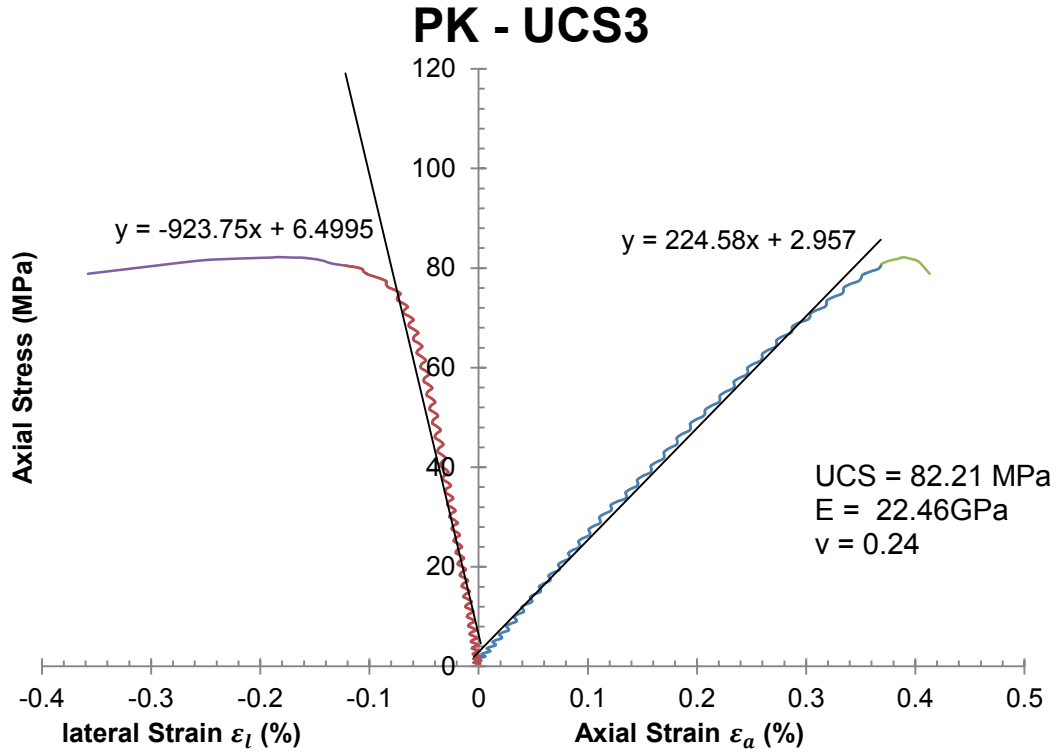


Figure 3.5 Example results from a UCS test (Sample ID: PK-UCS3)

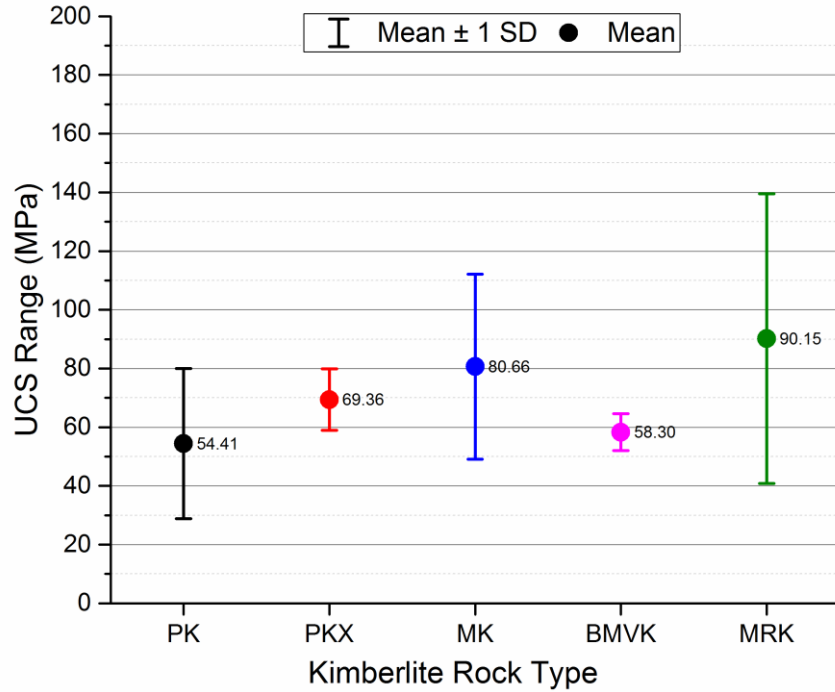


Figure 3.6 Example of mode of failure from a UCS test (Sample ID: PK-UCS3)

**Table 3.2** Uniaxial compressive strength test results

| Kimberlite Pipe | Rock Type      | Core ID      | Length (mm) | Diameter (mm)        | UCS (MPa)            | E (GPa)             | $\nu$              |      |
|-----------------|----------------|--------------|-------------|----------------------|----------------------|---------------------|--------------------|------|
| A154 South      | PK             | PK-UCS 1     | 129.06      | 63.3                 | 49.08                | 15.4                | 0.18               |      |
|                 |                | PK-UCS 2     | 128.59      | 63.38                | 31.94                | 20.66               | 0.23               |      |
|                 |                | PK-UCS 3     | 117.69      | 63.36                | 82.21                | 22.46               | 0.24               |      |
|                 | <b>Average</b> |              |             |                      | <b>54.41 ± 25.56</b> | <b>19.51 ± 3.67</b> | <b>0.22 ± 0.03</b> |      |
|                 | PKX            | PKX - UCS 1  | 132.52      | 63.37                | 74.84                | 19.1                | 0.23               |      |
|                 |                | PKX - UCS 2  | 131.01      | 63.29                | 75.96                | 18.25               | 0.27               |      |
|                 |                | PKX - UCS 3  | 127.71      | 63.42                | 57.29                | 16.06               | 0.25               |      |
|                 | <b>Average</b> |              |             |                      | <b>69.36 ± 10.47</b> | <b>17.8 ± 1.57</b>  | <b>0.25 ± 0.02</b> |      |
|                 | A154 North     | MK           | MK - UCS 1  | 88.12                | 37.78                | 112.57              | 29.72              | 0.27 |
|                 |                |              | MK - UCS 2  | 88.18                | 37.85                | 79.88               | 19.65              | 0.2  |
| MK - UCS 3      |                |              | 88.98       | 37.94                | 49.52                | 18.23               | 0.24               |      |
| <b>Average</b>  |                |              |             |                      | <b>80.66 ± 31.53</b> | <b>22.53 ± 6.25</b> | <b>0.24 ± 0.04</b> |      |
| BMVK            |                | BMVK - UCS 1 | 88.02       | 38.07                | 65.07                | 16.93               | 0.21               |      |
|                 |                | BMVK - UCS 2 | 87.77       | 38.02                | 52.72                | 17.41               | 0.25               |      |
|                 |                | BMVK - UCS 3 | 87.74       | 38                   | 57.12                | 14.41               | 0.18               |      |
| <b>Average</b>  |                |              |             |                      | <b>58.3 ± 6.25</b>   | <b>16.25 ± 1.61</b> | <b>0.21 ± 0.04</b> |      |
| MRK             |                | MRK - UCS 1  | 83.78       | 38.02                | 142.48               | 33.44               | 0.22               |      |
|                 |                | MRK - UCS 2  | 72.99       | 37.95                | 124.85               | 28.77               | 0.25               |      |
|                 |                | MRK - UCS 3  | 84.9        | 38.08                | 136.62               | 34.58               | 0.27               |      |
|                 |                | MRK - UCS 4  | 131.27      | 62.87                | 52.49                | 8.76                | 0.2                |      |
|                 |                | MRK - UCS 5  | 139.55      | 62.98                | 48.01                | 9.85                | 0.21               |      |
|                 | MRK - UCS 6    | 133.75       | 62.11       | 36.42                | 4.78                 | 0.16                |                    |      |
| <b>Average</b>  |                |              |             | <b>90.15 ± 49.36</b> | <b>20.03 ± 13.65</b> | <b>0.22 ± 0.04</b>  |                    |      |

The error bars shown in figure 3.7 provide estimations of the standard deviations of the UCS test results for each rock type. As it can be seen from this figure, there is a significant uncertainty in the results of two rock types: MK and MRK. This could be due to high variability of the Kimberlite, errors during rock sampling and preparations. The main reason for the variation in the results for MRK rock type is the inclusion of the mud in this Kimberlite rock type (MRK stands for Mud-rich volcanoclastic Kimberlite). The error can be decreased by increasing the number of samples.



**Figure 3.7** Uniaxial compressive test results - Note: SD stands for standard deviation

The error bars shown in figures 3.8 and 3.9 provide estimations of the standard deviations of the estimated Young's modulus and Poisson's ratio respectively.

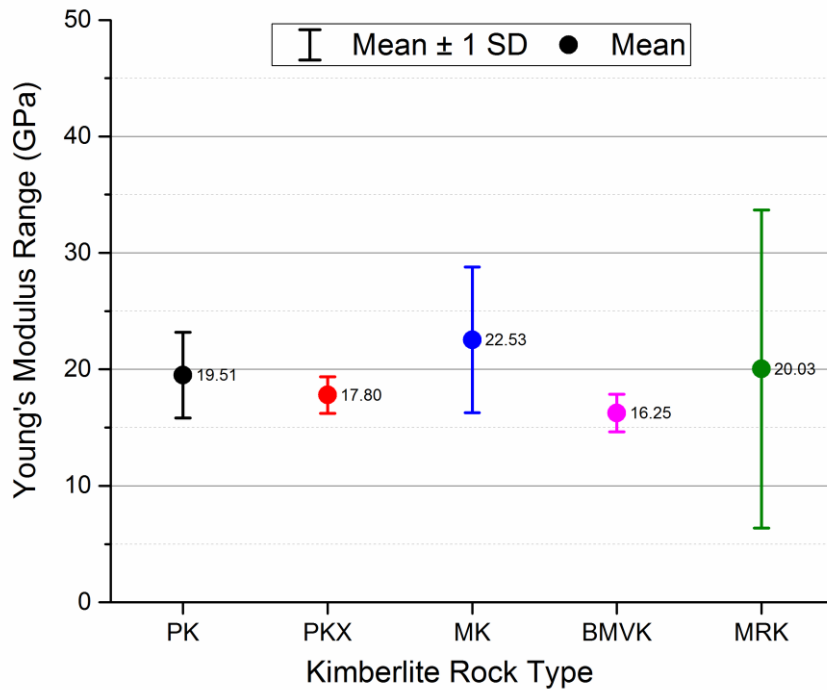


**Figure 3.8** Young's modulus estimations from UCS test - Note: SD stands for Standard Deviation

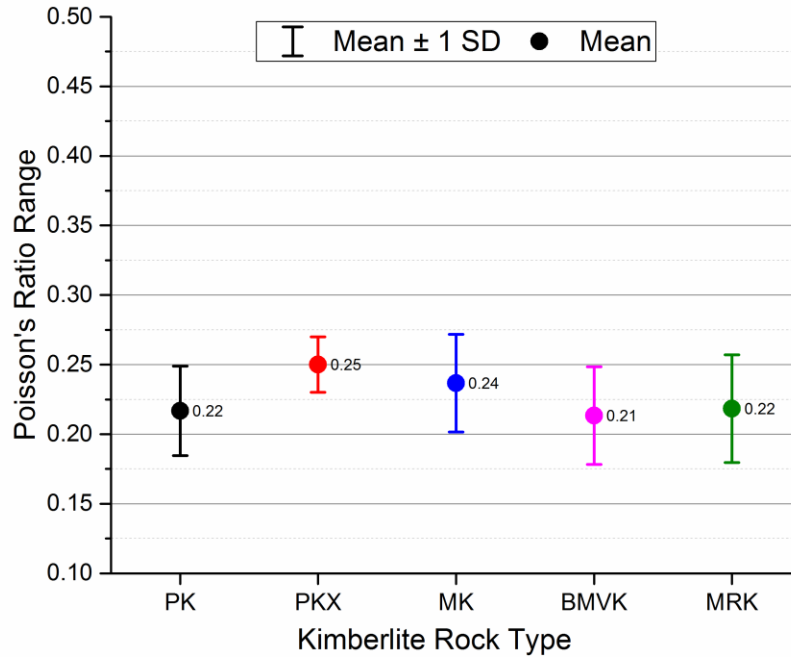


**Figure 3.9** Poisson's ratio estimations from UCS test - Note: SD stands for Standard Deviation

### 3.3.2 Brazilian test

The Brazilian test is an inexpensive and simpler method to measure the tensile strength of rock samples. The direct tensile test is expensive and often difficult to set up. However, the Brazilian test offers an acceptable alternative to the direct uniaxial tensile test (ASTM D3967-08; ISRM 1978). The purpose of this test is to indirectly measure the uniaxial tensile strength of rock specimens. Moreover, this test is more representative of the field condition, because the tensile strength of the rock specimen is obtained with the presence of compressive stresses.

The ASTM D3967-08 standard test method was followed to conduct this test. The procedure to conduct the Brazilian test can be summarized as follows:

- (i) Circular disk test specimens with a thickness-to-diameter ratio between 0.2 and 0.75 are prepared.
- (ii) The apparatus to hold and position the specimen under the loading frame is shown in figure 3.10. There are two steel loading jaws designed to contact the disc-shaped rock specimen at diametrically-

opposed surfaces. The upper jaw contains a spherical seating shaped by a 25 mm diameter half ball bearing.

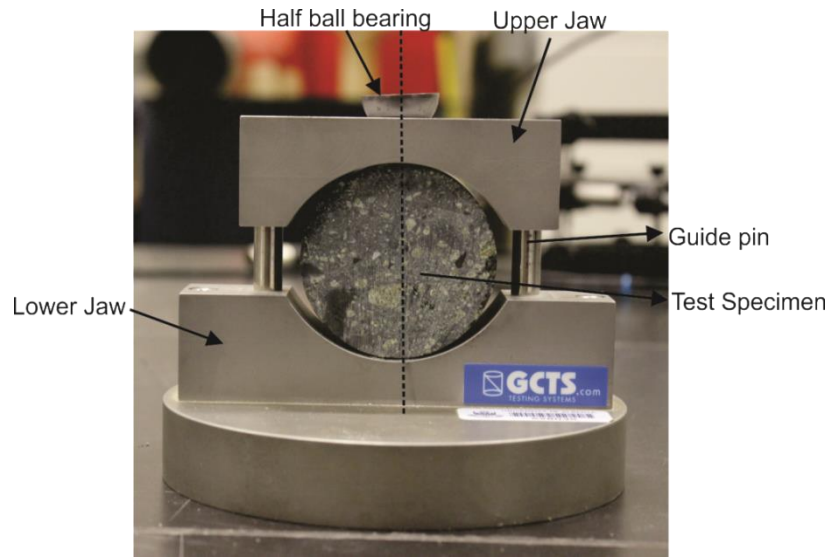


**Figure 3.10** Apparatus used for the Brazilian test

- (iii) The apparatus, with the specimen inside, is placed under the Digital Tritest 50 loading frame. The maximum capacity of this loading frame is 50 kN. The axial load is increased continuously at a constant rate of loading such that failure would occur between 1 and 10 minutes of loading (as per the ASTM requirement).
- (iv) The load at failure ( $P$ ) is recorded. The tensile strength of the specimen can be calculated using the following equation:

$$\sigma_t = \frac{2P}{\pi t D} \quad (3.5)$$

where  $\sigma_t$  is tensile strength (MPa),  $P$  is the load at failure (N),  $t$  is the thickness of the specimen (mm) and  $D$  is the diameter of the specimen (mm).

Sample test results and their respective calculations are shown in figure 3.11. In total, 29 Brazilian tests were conducted during this research. The results are presented in table 3.3. Detailed results and the mode of failure for each sample

can be found in Appendix A. The error bars for tensile strength tests on each rock types are presented in figure 3.12.

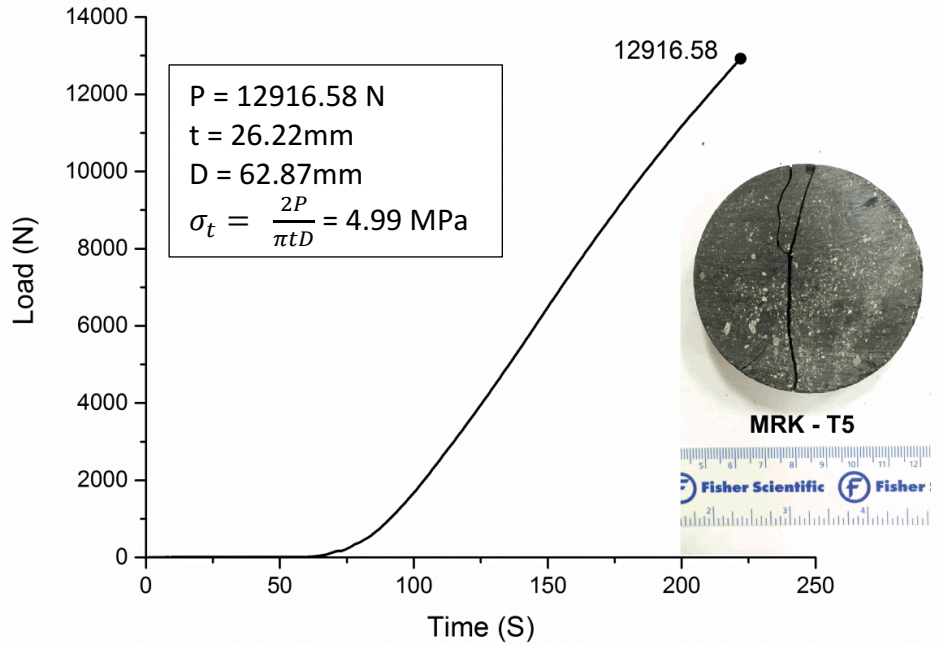


Figure 3.11 Example results of a Brazilian test, its mode of failure and corresponding calculations (Sample ID: MRK - T5)

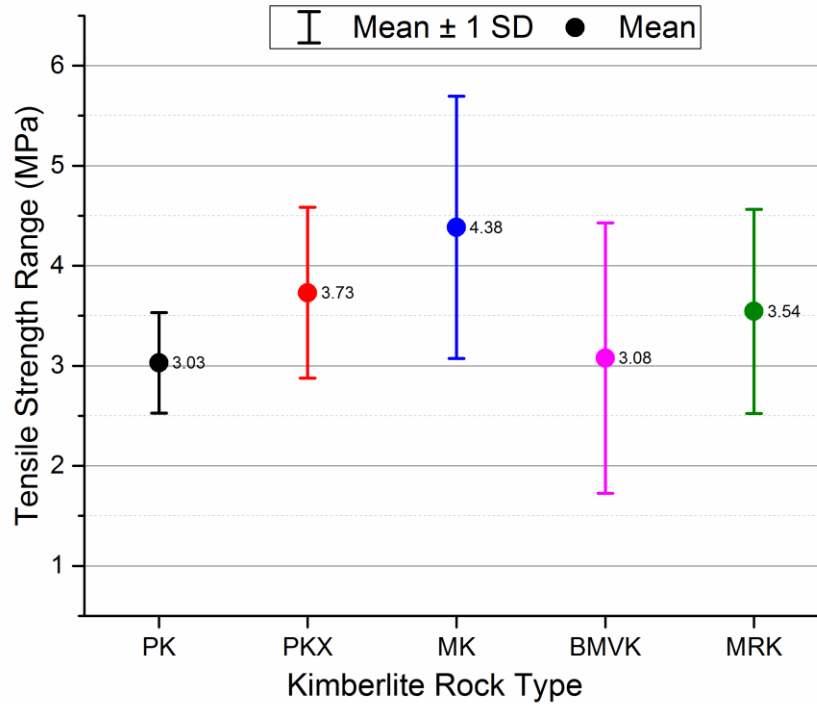


Figure 3.12 Error bars for Tensile strength test results - Note: SD stands for Standard Deviation

Table 3.3 Brazilian test results

| Kimberlite Pipe | Rock Type      | Core ID   | Thickness (mm) | Diameter (mm) | Failure Load P (N) | $\sigma_t$ (MPa)   |                    |
|-----------------|----------------|-----------|----------------|---------------|--------------------|--------------------|--------------------|
| A154 South      | PK             | PK - T1   | 38.05          | 63.28         | 10000.00           | 2.65               |                    |
|                 |                | PK - T2   | 38.07          | 63.3          | 10738.00           | 2.84               |                    |
|                 |                | PK - T3   | 37.92          | 63.32         | 13586.00           | 3.60               |                    |
|                 | <b>Average</b> |           |                |               |                    | <b>11441.33</b>    | <b>3.03 ± 0.5</b>  |
|                 | PKX            | PKX - T1  | 38.54          | 63.32         | 15318.00           | 4.00               |                    |
|                 |                | PKX - T2  | 38.44          | 63.27         | 12499.00           | 3.27               |                    |
|                 |                | PKX - T3  | 38.77          | 63.34         | 13675.00           | 3.55               |                    |
|                 |                | PKX - T4  | 21.73          | 37.99         | 3055.01            | 2.36               |                    |
|                 |                | PKX - T5  | 22.16          | 38.01         | 5350.10            | 4.05               |                    |
|                 |                | PKX - T6  | 22.5           | 38.01         | 4986.29            | 3.71               |                    |
|                 |                | PKX - T7  | 22.26          | 37.9          | 6843.31            | 5.17               |                    |
|                 | <b>Average</b> |           |                |               |                    | <b>8818.10</b>     | <b>3.73 ± 0.85</b> |
|                 | A154 North     | MK        | MK - T1        | 20.65         | 38.07              | 5747.40            | 4.66               |
|                 |                |           | MK - T2        | 20.47         | 37.83              | 6823.22            | 5.61               |
| MK - T3         |                |           | 20.41          | 37.79         | 4816.66            | 3.98               |                    |
| MK - T4         |                |           | 20.79          | 37.89         | 2528.86            | 2.04               |                    |
| MK - T5         |                |           | 20.42          | 37.88         | 6736.18            | 5.55               |                    |
| MK - T6         |                |           | 20.59          | 37.96         | 5470.63            | 4.46               |                    |
| <b>Average</b>  |                |           |                |               | <b>5353.83</b>     | <b>4.38 ± 1.31</b> |                    |
| BMVK            |                | BMVK - T1 | 22.57          | 38.11         | 7372.30            | 5.46               |                    |
|                 |                | BMVK - T2 | 23.24          | 38.11         | 5095.66            | 3.66               |                    |
|                 |                | BMVK - T3 | 23.65          | 38.13         | 4948.34            | 3.50               |                    |
|                 |                | BMVK - T4 | 22.71          | 38.11         | 3414.96            | 2.51               |                    |
|                 |                | BMVK - T5 | 22.74          | 38.07         | 4256.42            | 3.13               |                    |
|                 |                | BMVK - T6 | 23.53          | 38.09         | 1745.42            | 1.24               |                    |
|                 |                | BMVK - T7 | 21.26          | 38.15         | 2595.82            | 2.04               |                    |
| <b>Average</b>  |                |           |                |               | <b>4204.13</b>     | <b>3.08 ± 1.35</b> |                    |
| MRK             |                | MRK - T1  | 18.64          | 37.51         | 4254.19            | 3.88               |                    |
|                 |                | MRK - T2  | 18.24          | 37.51         | 3216.31            | 2.99               |                    |
|                 |                | MRK - T3  | 19.79          | 37.56         | 3089.09            | 2.65               |                    |
|                 |                | MRK - T4  | 26.31          | 62.85         | 6278.62            | 2.42               |                    |
|                 |                | MRK - T5  | 26.22          | 62.87         | 12916.58           | 4.99               |                    |
|                 |                | MRK - T6  | 26.72          | 62.87         | 11425.61           | 4.33               |                    |
| <b>Average</b>  |                |           |                |               | <b>6863.40</b>     | <b>3.54 ± 1.02</b> |                    |

### 3.3.3 Triaxial compressive test

Since the only acceptable failure criterion for rock in Abaqus is the Mohr-Coulomb failure criterion, it is necessary to determine the cohesive strengths ( $c$ ) and angle of frictions ( $\phi$ ) for each Kimberlite rock type. Therefore, the triaxial compression test is conducted on cylindrical specimens prepared in the same manner explained for the UCS test. Diameter of the core samples was 38.1mm (1.5 inches). In additions, 6 more core specimens with diameter of 63.5 (2.5 inches) were provided.

The general procedure for the triaxial compressive test is to place the cylindrical rock specimen in a chamber in which the specimen is subjected to constant lateral fluid pressure and the required axial load. However, it should be considered that the rock specimen is subjected to a homogenous state of stress in which the minor ( $\sigma_3$ ) and intermediate ( $\sigma_2$ ) principal stresses are equal ( $\sigma_1 > \sigma_2 = \sigma_3$ ).

In order to perform the test, the specimens are placed inside the triaxial cell designed by Hoek-Franklin (1968) which is illustrated in figure 3.13.

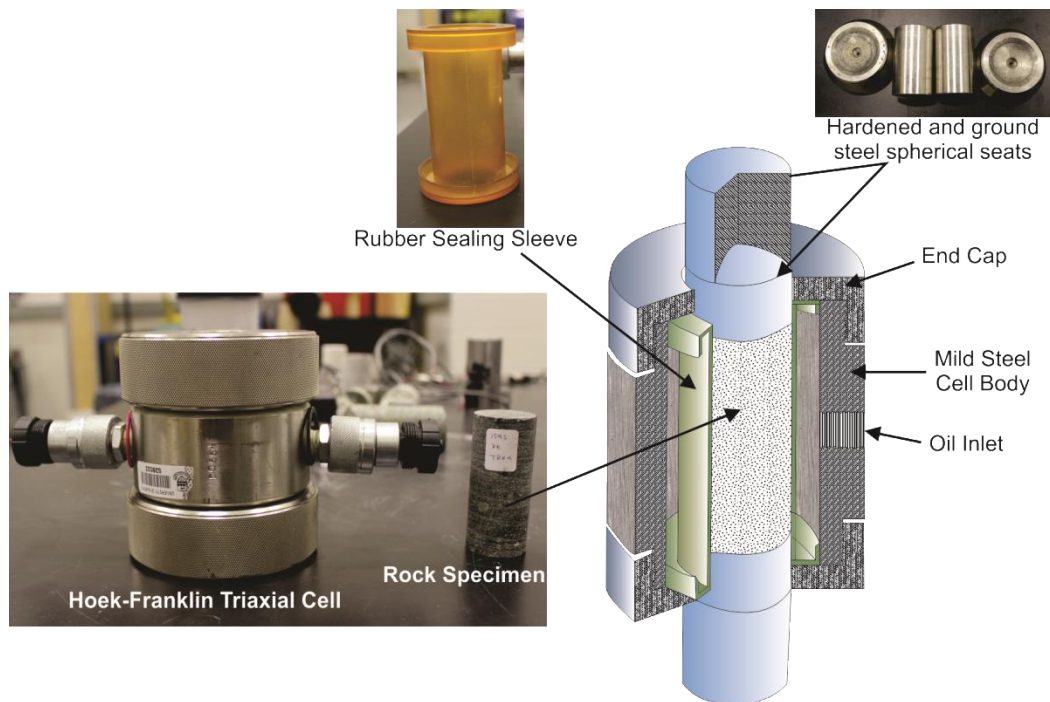
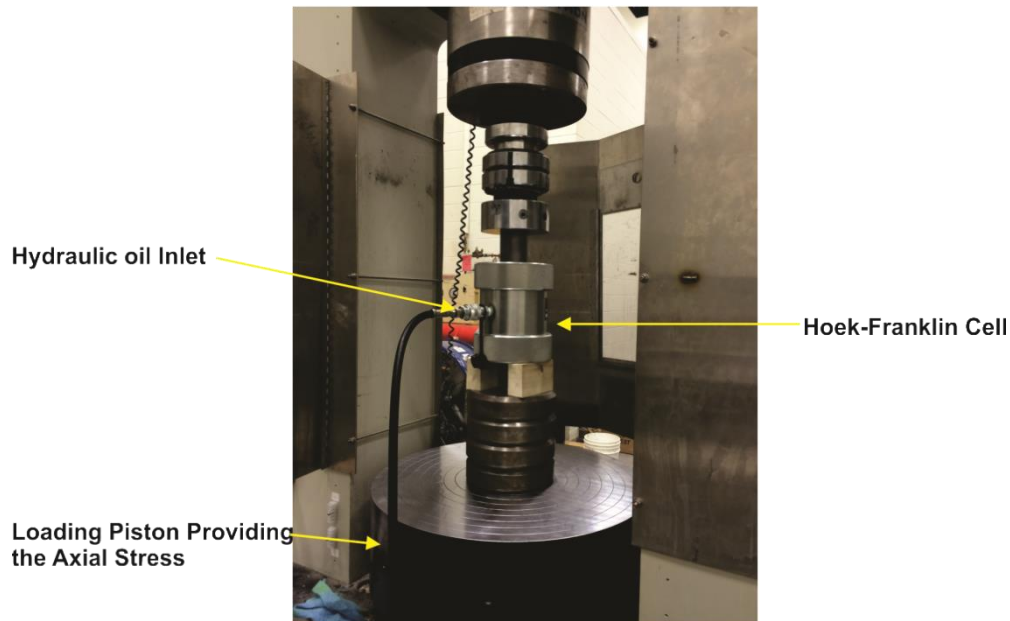
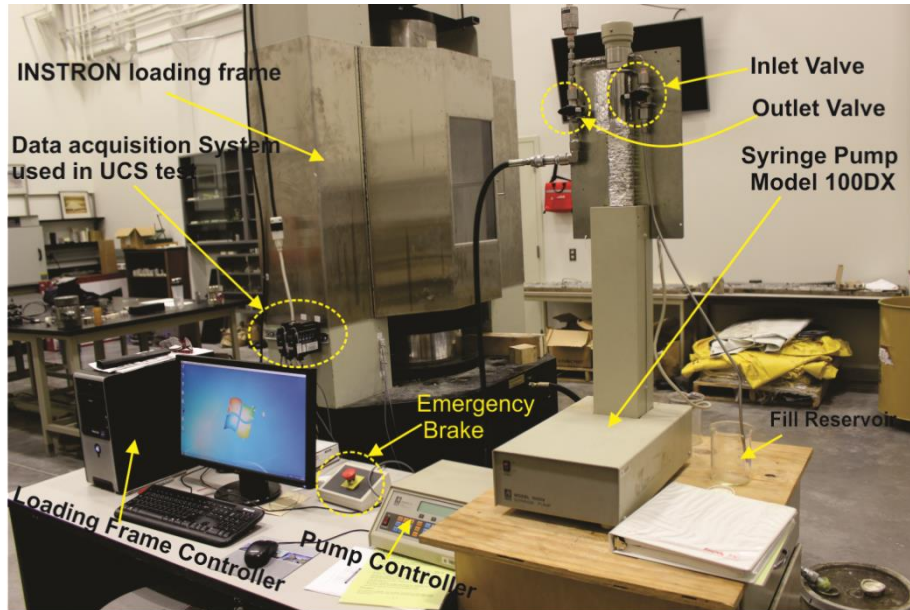


**Figure 3.13** Hoek-Franklin triaxial cell and its cutaway view

To provide the confining pressure, a syringe hydraulic pump (Model 100DX) is used. This pump has sufficient capacity to maintain the desired confining pressure within  $\pm 0.5\%$  accuracy (ASTM requirement is  $\pm 1\%$  maximum). The axial load is provided using the same INSTRON loading frame used for the UCS test. The triaxial test setup is shown in figure 3.14.



### Triaxial Test Using the Hoek -Franklin Cell

**Figure 3.14** Triaxial test settings using the Hoek-Franklin cell

A summary of the test procedure is as follows:

- (i) The test specimens are prepared according to ASTM D4543-08 as explained in section 3.3 (figure 3.4). The specimen length-to-diameter ratio is kept between 2:1 and 2.5:1
- (ii) The Hoek-Franklin cell is assembled. The cell is filled with oil by a hand pump or hydraulic pump for the first time. The main advantage of the Hoek-Franklin cell is that it does not require drainage between the tests. Therefore, a large number of tests can be conducted very fast, unless the specimen is severely deformed.
- (iii) The axial and confining pressure must be raised uniformly at the same rate to the specified confining pressure within 5 minutes.
- (iv) Once the predetermined confining pressure is reached, the test begins. The axial load will be applied in the same manner as the UCS test. Meanwhile, the confining pressure must be maintained. The syringe pump had a superb capability to maintain the pressure within an acceptable accuracy.
- (v) Finally, the maximum load sustained by the specimen is recorded. Using the cross-sectional area of the specimen, the maximum compressive strength, under the triaxial conditions, can be calculated.

All five rock types have been tested. However, because of the large variability within the Kimberlite samples, a small number of samples and associated failure modes were discarded. Detailed results of the triaxial tests are presented in Appendix A.

To illustrate the procedure used to measure  $c$  and  $\phi$  of each rock type, calculations for the PKX Kimberlite rock type is used as an example for the remainder of this section.

Six cylindrical specimens from the PKX rock bulk samples were prepared for the triaxial test. To achieve the triaxial stress state, two confining pressures, 16 MPa and 25 MPa, were used. Figure 3.15 illustrates the triaxial stress state each specimen was tested under. Table 3.4 summarizes the results of the triaxial test on the PKX rock. As presented previously in table 3.2, the UCS of this rock (compressive strength under zero confinement pressure  $\sigma_2 = \sigma_3 = 0$ ) is 69.36 MPa. The failure mode for each core specimen is shown in figure 3.16.

**Table 3.4** Results of the triaxial test on the PKX Kimberlite rock type

| Core ID | Diameter (mm) | Length (mm) | Confinement Pressure $\sigma_3$ (MPa) | Stress at Failure $\sigma_1$ (MPa) | Average Stress (MPa) |
|---------|---------------|-------------|---------------------------------------|------------------------------------|----------------------|
| TRX1    | 38.05         | 88.26       | 16                                    | 151.6                              |                      |
| TRX2    | 38.06         | 84.30       | 16                                    | 124.1                              | 142.23               |
| TRX3    | 38.14         | 90.02       | 16                                    | 151.0                              |                      |
| TRX4    | 38.18         | 89.72       | 25                                    | 182.0                              |                      |
| TRX5    | 38.14         | 89.67       | 25                                    | 216.9                              | 189.2                |
| TRX6    | 37.94         | 87.94       | 25                                    | 168.7                              |                      |

Based on the data presented in table 3.4, the best linear fit of the relationship between the major and minor principal stresses,  $\sigma_1$  and  $\sigma_3$ , is governed by equation (3.6).

$$\sigma_1 = 4.77\sigma_3 + 68.47 \quad (3.6)$$

The procedure proposed by Hoek and Brady (1997), Hoek et al. (2002) and Brady and Brown (2004) was followed to estimate the Mohr-Coulomb failure parameters. As discussed in chapter 2, the Mohr-Coulomb failure criterion defines the rock mass strength in terms of cohesive strength  $c$  and the angle of friction  $\phi$ . The shear strength of the rock ( $\tau$ ) for a given normal stress ( $\sigma_n$ ) can be defined by equation (3.7).

$$\tau = c + \sigma_n \tan \phi \quad (3.7)$$

However, the Mohr-Coulomb criterion can be defined in terms of the major and minor principal stresses ( $\sigma_1$  and  $\sigma_3$ , respectively) using equation (3.8) (Hoek et al., 2002).

$$\sigma_1 = \frac{1+\sin\phi}{1-\sin\phi} \sigma_3 + \frac{2c \cos\phi}{1-\sin\phi} \quad (3.8)$$

Comparing equations (3.6) and (3.8),  $\phi$  and  $c$  can be calculated as follows:

$$\frac{1+\sin\phi}{1-\sin\phi} = 4.77 \quad \text{Therefore: } \phi = 40.8^\circ$$

$$\frac{2c \cos\phi}{1-\sin\phi} = 68.47 \quad \text{Therefore: } c = 15.7 \text{ MPa}$$

Consequently, the Mohr-Coulomb failure criterion in terms of shear strength of rock ( $\tau$ ) for PKX rock is as follows:

$$\tau = 15.7 + \sigma_n \tan 40.8 \quad (3.9)$$

The Mohr-Coulomb failure criterion for PKX rock is illustrated in terms of principal stresses and shear stresses in figures 3.17 and 3.18, respectively.

Finally, one of the important uses of the triaxial test is to calculate the intact material constant ( $m_i$ ) of the Hoek-Brown failure criterion for Kimberlite. The Hoek-Brown criterion for intact rock specimens can be simplified as follows:

$$\sigma'_1 = \sigma'_3 + \sigma_{ci} \left( m_i \frac{\sigma'_3}{\sigma_{ci}} + 1 \right)^{0.5} \quad (3.10)$$

where  $\sigma'_1$  and  $\sigma'_3$  are the major and minor effective principal stresses at failure and  $\sigma_{ci}$  is the UCS of the intact rock.

Detailed results of the triaxial tests on the other Kimberlite samples are presented in Appendix A. Table 3.5 presents the triaxial test results for all Kimberlite rock types and the calculated values for  $c$ ,  $\phi$  and  $m_i$  for each rock type. These data will be used in section 3.4.2 to calibrate the rock mass strength to serve as input data for the FE model.

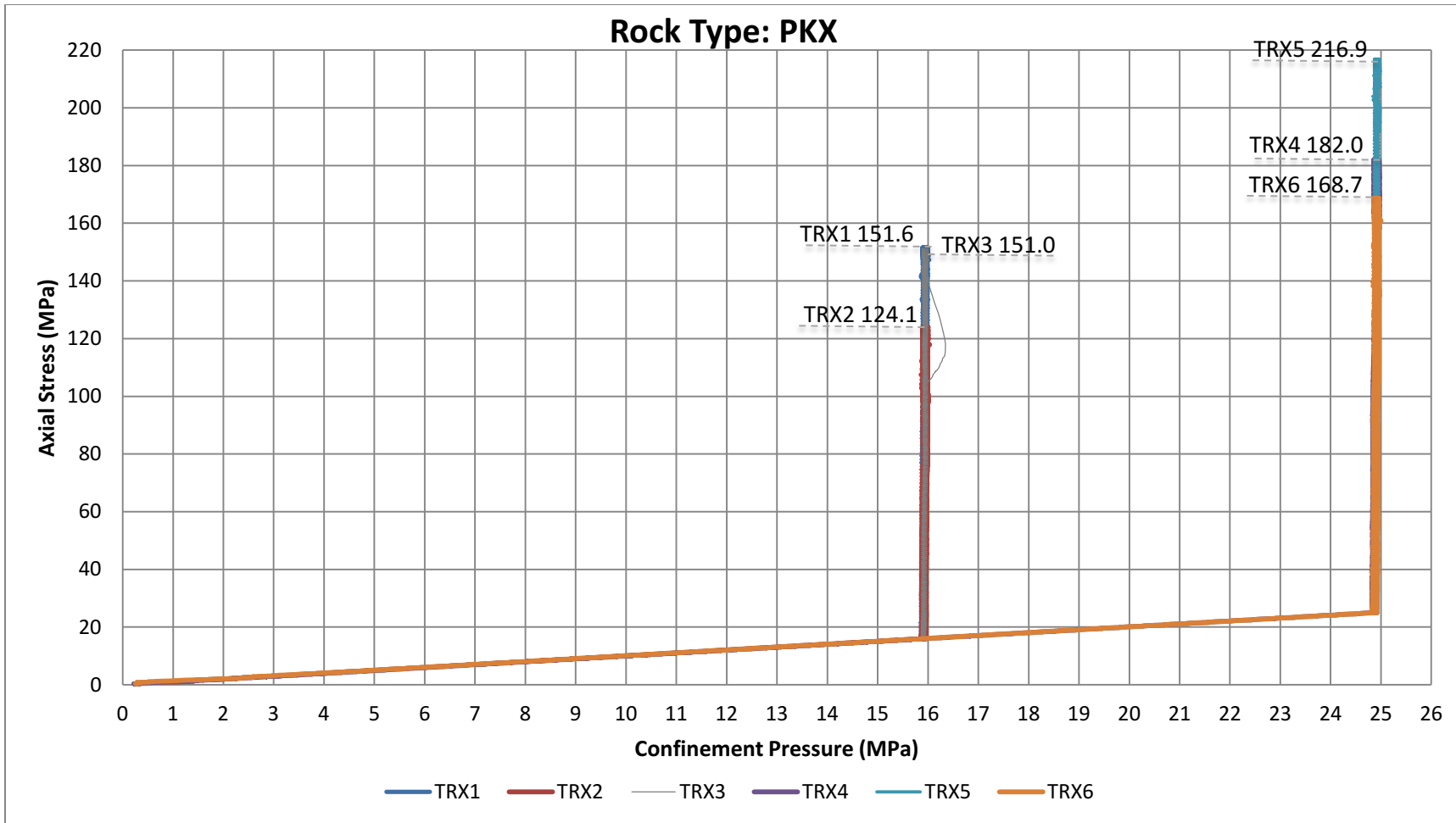
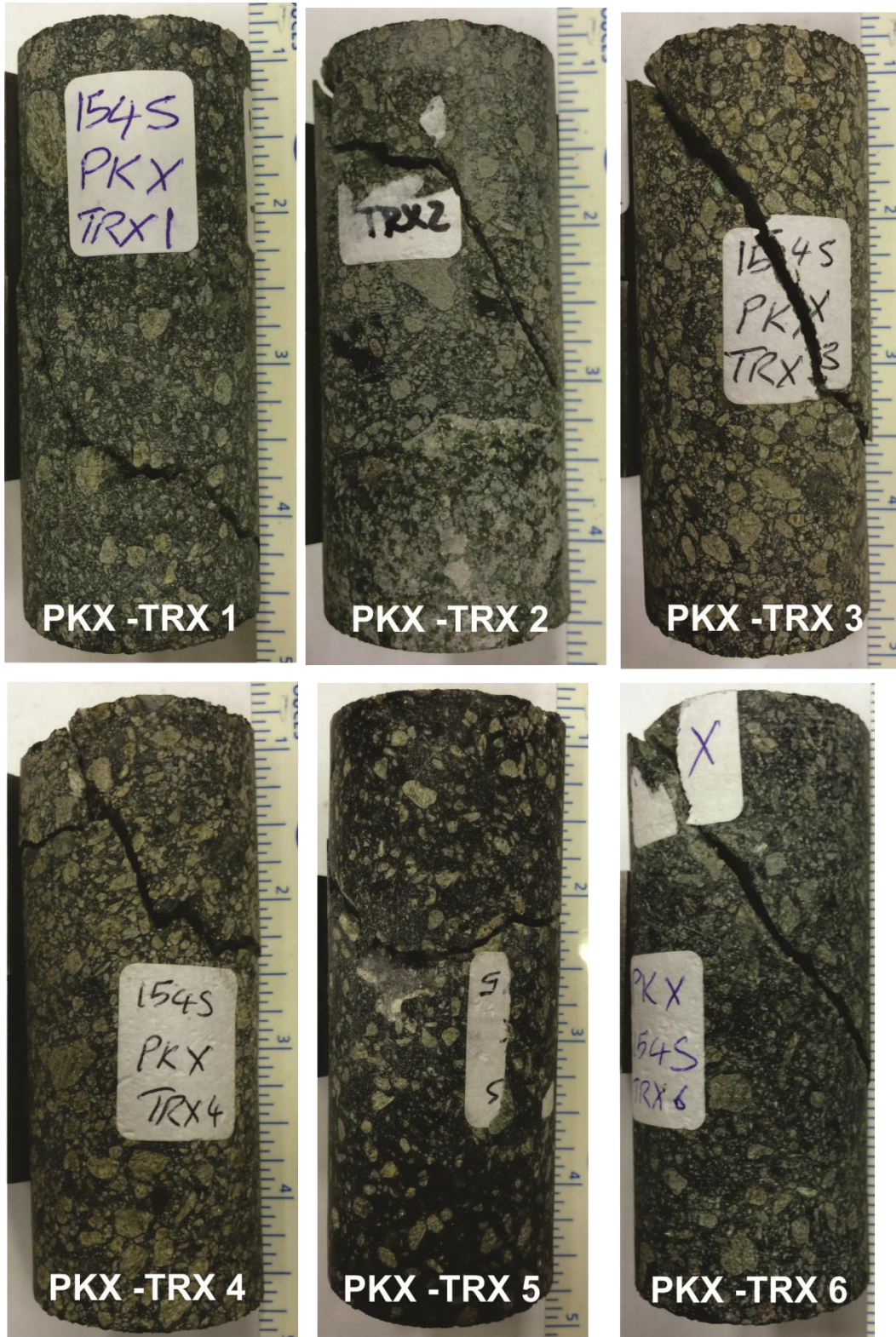
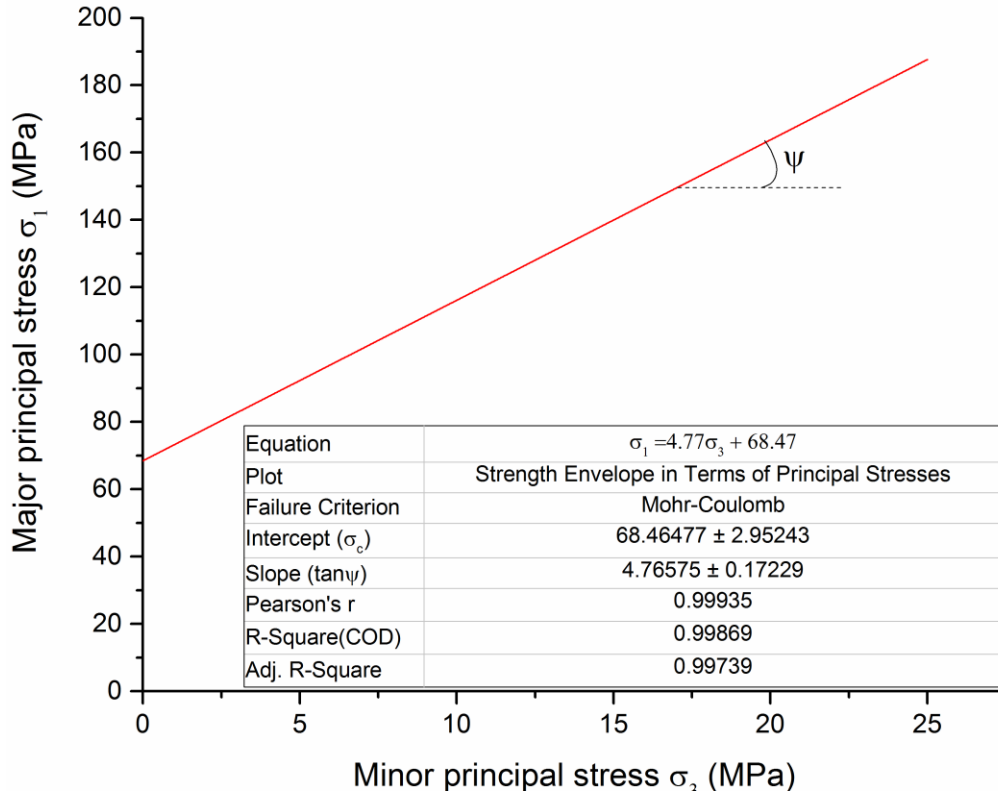


Figure 3.15 Triaxial stress state for each PKX Kimberlite specimen



**Figure 3.16** Failure mode of each PKX Kimberlite core specimen (obtained from triaxial testing regime)



**Figure 3.17** The linear relationship between the major and minor principal stresses for PKX Kimberlite

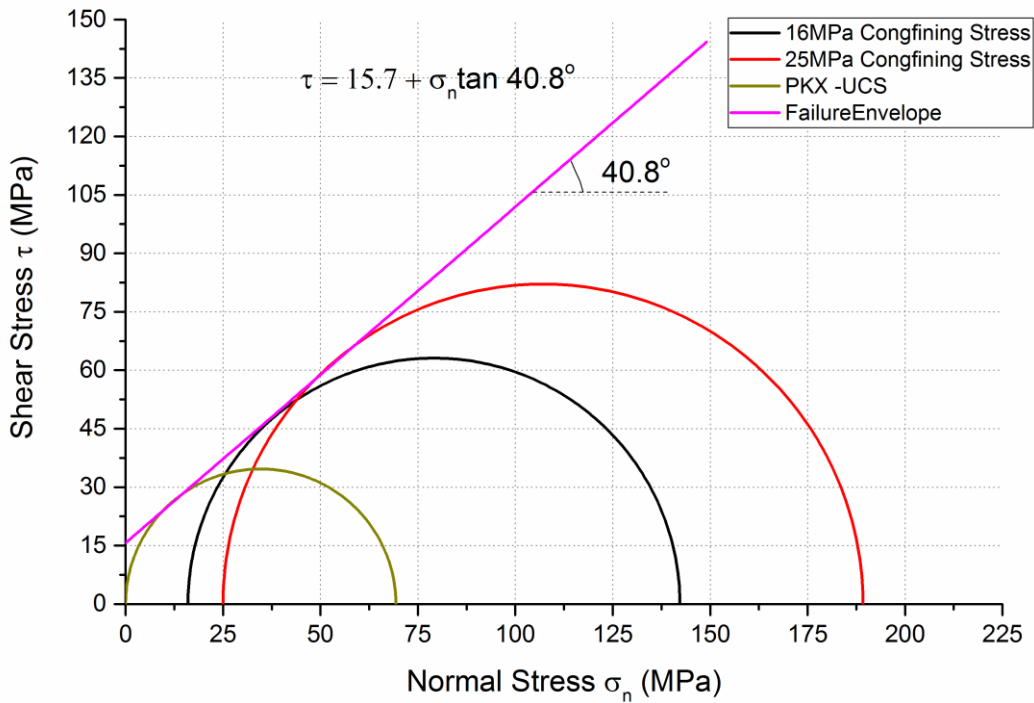


**Figure 3.18** Mohr-Coulomb failure envelope for intact PKX Kimberlite

**Table 3.5** Triaxial compressive test results on intact core specimens

| Kimberlite Pipe | Rock Type | Core ID | Diameter (mm) | Length (mm) | Confinement Pressure $\sigma'_3$ (MPa) | Stress at Failure $\sigma'_1$ (MPa) | Average Stress (MPa) | c (MPa) | $\phi^\circ$ | $m_i$ |
|-----------------|-----------|---------|---------------|-------------|--|-------------------------------------|----------------------|---------|--------------|-------|
| A154 South      | PKX       | TRX1    | 38.05         | 88.26       | 16                                     | 151.6                               | 142.2                | 15.7    | 40.8         | 12.8  |
|                 |           | TRX2    | 38.06         | 84.3        | 16                                     | 124.1                               |                      |         |              |       |
|                 |           | TRX3    | 38.14         | 90.02       | 16                                     | 151.0                               |                      |         |              |       |
|                 |           | TRX4    | 38.18         | 89.72       | 25                                     | 182.0                               | 189.2                |         |              |       |
|                 |           | TRX5    | 38.14         | 89.67       | 25                                     | 216.9                               |                      |         |              |       |
|                 |           | TRX6    | 37.94         | 87.94       | 25                                     | 168.7                               |                      |         |              |       |
|                 | PK        | TRX1    | 37.66         | 86.29       | 4                                      | 95.8                                | 95.8                 | 14.04   | 36.2         | 7.2   |
|                 |           | TRX4    | 37.8          | 87.83       | 8                                      | 99.0                                | 99.0                 |         |              |       |
|                 |           | TRX3    | 37.73         | 77.85       | 16                                     | 130.2                               | 119.9                |         |              |       |
|                 |           | TRX2    | 37.75         | 87.52       | 16                                     | 109.6                               |                      |         |              |       |
|                 |           | TRX5    | 38.08         | 88.43       | 25                                     | 161.1                               |                      |         |              |       |
|                 |           | TRX6    | 38.13         | 88.68       | 25                                     | 140.3                               | 150.7                |         |              |       |
| A154 North      | BMVK      | TRX1    | 38.1          | 87.12       | 16                                     | 99.7                                | 117.7                | 12.57   | 44.1         | 13.2  |
|                 |           | TRX2    | 38.11         | 88.96       | 16                                     | 95.3                                |                      |         |              |       |
|                 |           | TRX3    | 38.12         | 80.24       | 16                                     | 158.1                               |                      |         |              |       |
|                 |           | TRX4    | 38.16         | 85.62       | 25                                     | 198.3                               | 198.3                |         |              |       |
|                 | MRK       | TRX1    | 62.72         | 153.57      | 16                                     | 120.0                               | 107.7                | 11.75   | 35.8         | 9.5   |
|                 |           | TRX3    | 62.74         | 151.81      | 16                                     | 95.5                                |                      |         |              |       |
|                 |           | TRX6    | 62.84         | 135.1       | 25                                     | 140.8                               |                      |         |              |       |
|                 | MK        | TRX2    | 37.91         | 87.68       | 16                                     | 136.7                               | 136.7                | 22.85   | 30.9         | 5.1   |
|                 |           | TRX4    | 38.05         | 87.92       | 25                                     | 154.9                               | 154.6                |         |              |       |
|                 |           | TRX5    | 37.92         | 74.55       | 25                                     | 149.2                               |                      |         |              |       |
| TRX6            |           | 38.08   | 88.52         | 25          | 159.6                                  |                                     |                      |         |              |       |

### 3.4 Finite Element Model Implementation

A full 3D elastoplastic FE analysis model of the mine was constructed using Abaqus. Figure 3.19 illustrates the methodology used to construct a valid and reliable numerical model. Some of the highlights of this methodology are: (i) constructing the geometries at the full, realistic 3D scale; (ii) use of the rock mechanics laboratory test results to derive the rock mass properties for Kimberlite pipes; (iii) defining the sequence of mining (extraction/backfilling) according to reality and the mine production plan; and (iv) defining several monitoring points in the model to verify the results of the FE analysis. This is done by using real field data from the ground movement monitoring instruments installed at the same monitoring locations. This process will be described in Chapter 7 of this thesis.

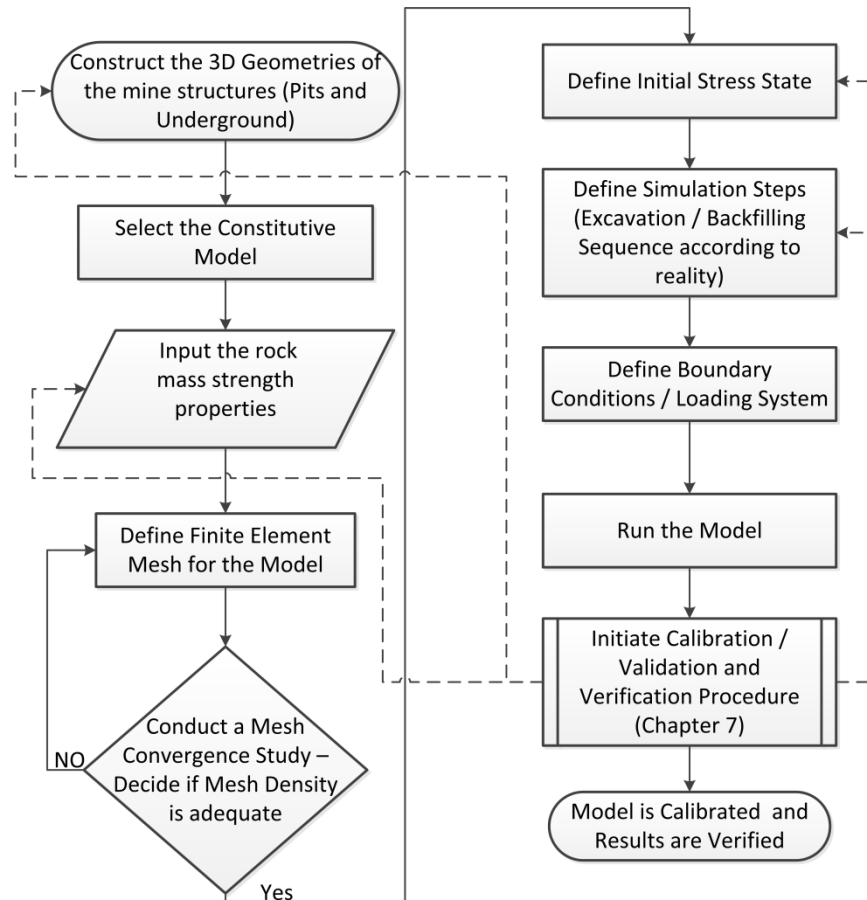


**Figure 3.19** Summary of the FE analysis methodology

### 3.4.1 Geometries

The first step in building a reliable 3D FE analysis model is to construct good representative 3D geometries of the problem. The magnitude and orientation of the mining-induced stresses directly depend on their shape, size, proximity of excavations and their 3D spatial locations (Wiles, 2006).

Despite the focus of this research on the A154 Pit, the A418 pit is also included in the model to capture the possible impacts of its geometry on the mining-induced stress field. The dimensions of the analysis domain are 2.2 km by 2.2 km and the maximum depth of the model is 800 m. The domain dimensions are sufficient to eliminate the influence of the boundaries on the model. On the vertical boundary of the model, horizontal restraints (in both the X and Y directions) are applied. Encastre boundary conditions are applied at the bottom of the model (Encastre means completely fixed in all directions). Figures 3.20 and 3.21 illustrate the 3D geometries constructed in Abaqus.

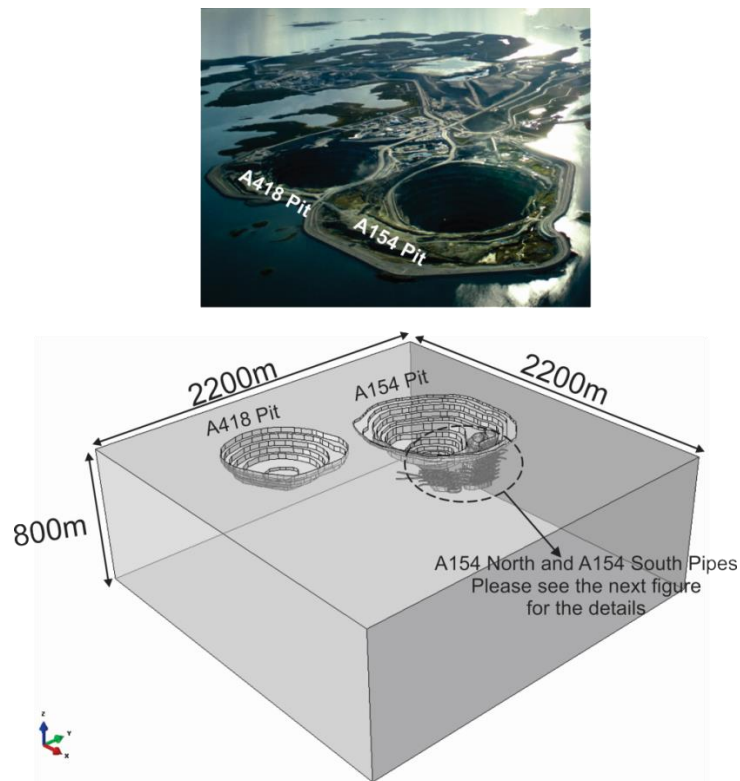


**Figure 3.20** Full 3D model of the mine constructed in Abaqus

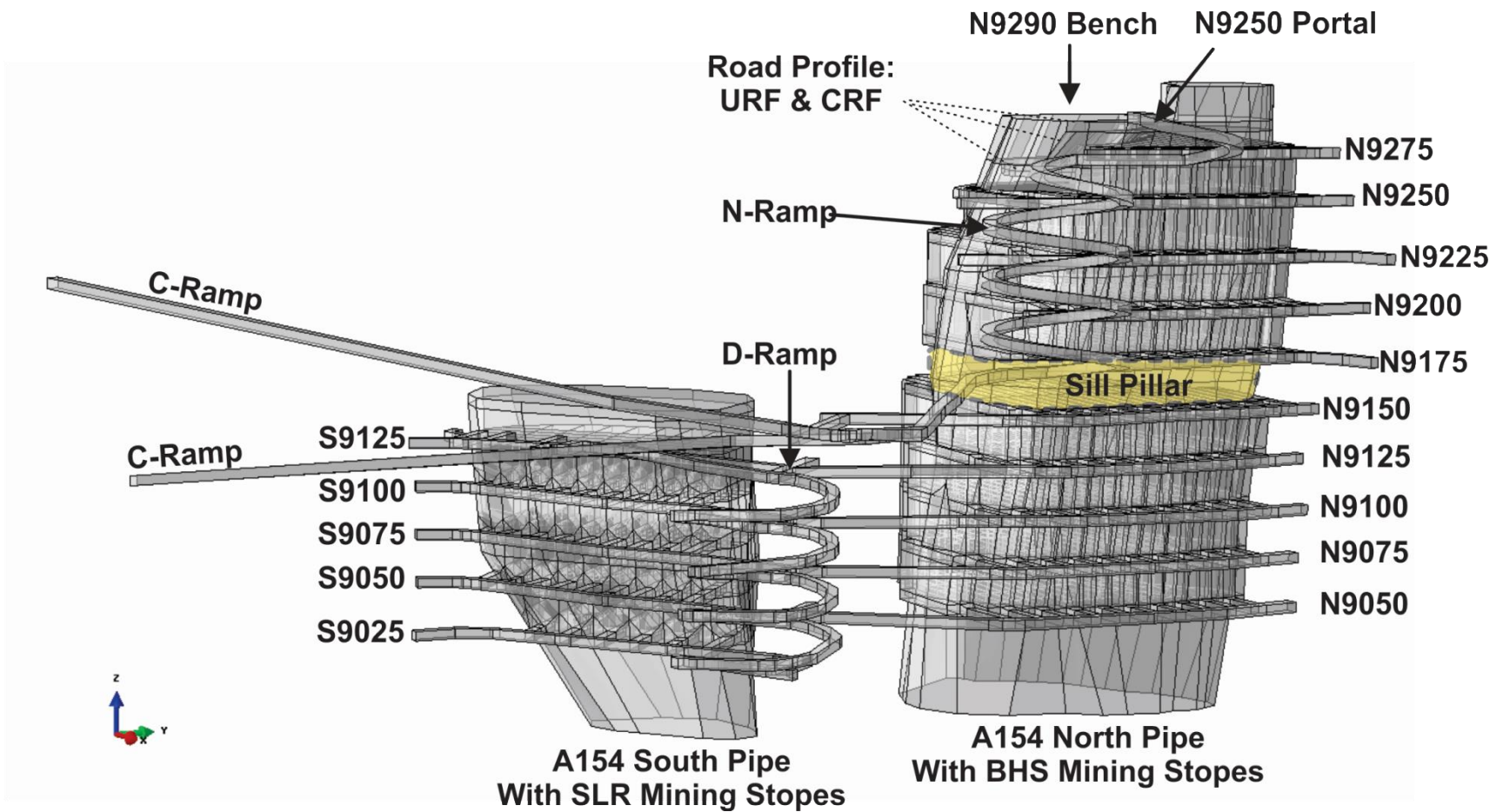


**Figure 3.21** Full 3D models of the underground structures constructed in Abaqus: two Kimberlite pipes, two mining methods (BHS and SLR), sill pillar, crown pillar, haulage drifts and ramps

Two Kimberlite pipes, A154 North and A154 South, are included in the model. The mining methods used for these two Kimberlite pipes are completely different: A154 North uses BHS and A154 South uses SLR.

#### ***3.4.1.1 A154 North Kimberlite pipe: full 3D model***

There are two BHS mining blocks (zones) at the A154 North pipe: (i) Mining Block A located between mine levels N9175 and N9275; and (ii) Mining Block B located between mine levels N9050 and N9150. A horizontal section of ore, known as sill pillar was left between two mining blocks (mining levels N9150 and N9175) to support the mine working area above the producing stopes. The surface crown pillar is located between mine levels N9275 and N9290. There is also a CRF cap to provide better support for the surface crown pillar. To build a sufficient road profile and to fill the gap between the CRF cap and N9290 bench surface, uncemented rockfill (URF) was used. The 3D geometry of these CRF and URF caps are also constructed and included in the model.

In BHS, mining is done in a primary/secondary manner. Consequently, the geometry of each primary/secondary stope was constructed separately. Finally, all the BHS stope geometries were merged together with the geometry of the A154 North pipe. Each stope has a width of 7.5 m and height of approximately 30 m. The stope is divided into three excavation blocks. The strike length of each block is less than 50 m. After mining each block, the empty excavated space will be backfilled immediately. The excavation of the next block will be initiated after the appropriate curing time of the backfilled stope has elapsed.

Figure 3.22 illustrates the details and dimensions of all the constructed 3D geometries of the A154 North pipe. Some simplifications had been made in building these 3D geometries; however, the coordinates, dimensions and strike length of the constructed features were kept in accordance with the reality.

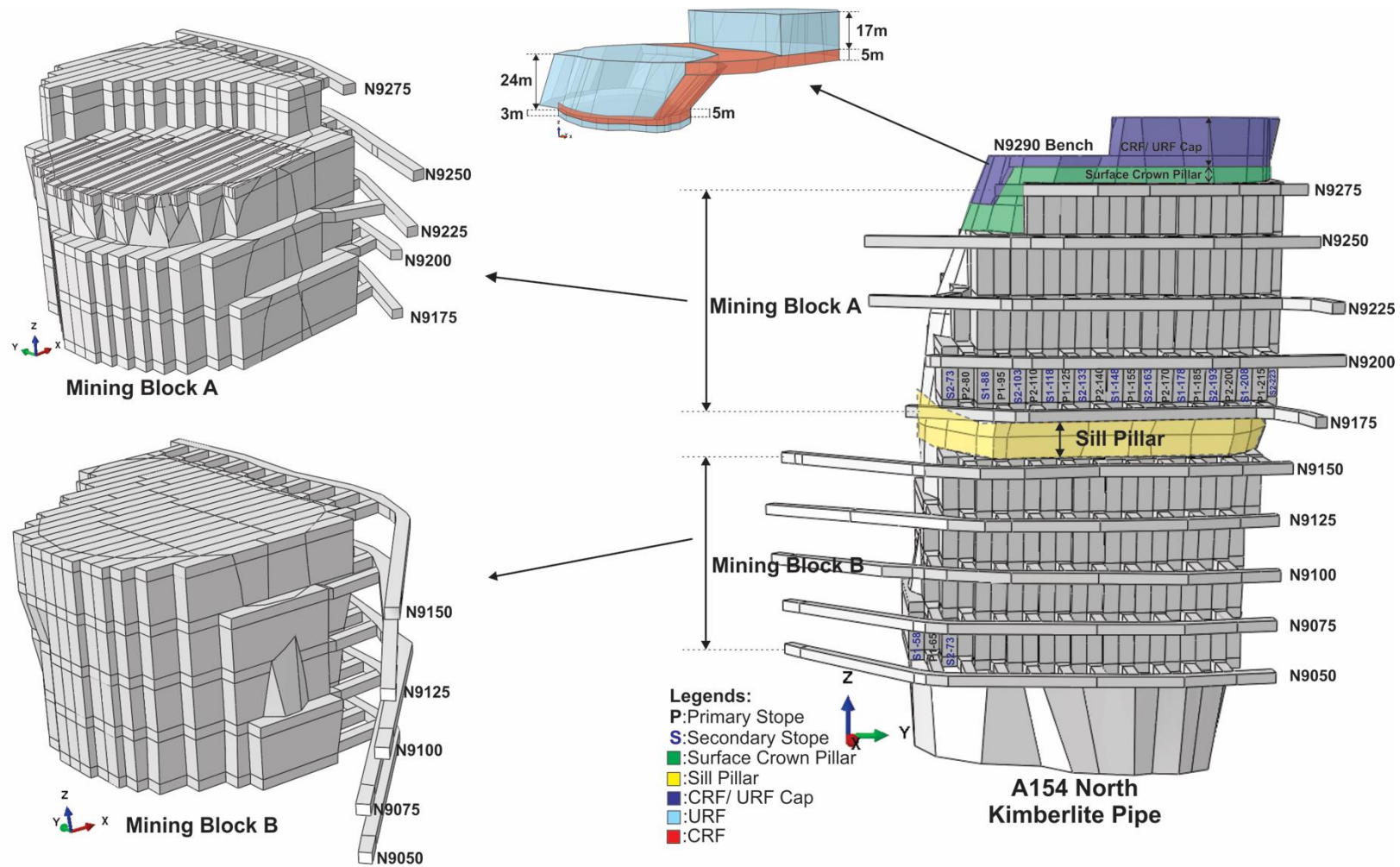


Figure 3.22 Full 3D models of the A154 North pipe, sill pillar, crown pillar, CRF cap and BHS stopes

### 3.4.1.2 A154 South Kimberlite pipe: full 3D model

The SLR method is used in the A154 South pipe. This pipe is located at the bottom of the pit. The pit bottom is located at mine level S9125, approximately 260 m below the surface. The geometry of all SLR stopes located between mining levels S9025 and S9125 are constructed and merged with the geometry of the A154 South pipe (figure 3.23). The width of each SLR block is 15 m with a height of 20 m. The production and slot drifts are 5 m wide and 5 m high. Some simplifications in the shape of the SLR stopes have been made. For instance, five to ten blasting rings in the SLR stopes were merged together to form one SLR stope.

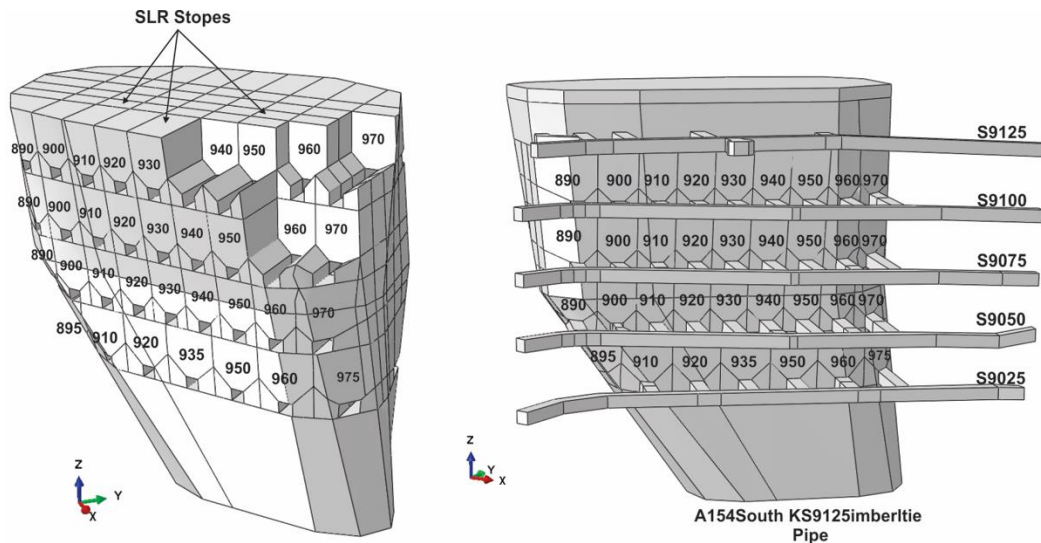


Figure 3.23 Full 3D model of the A154 North pipe with SLR stopes

### 3.4.2 Constitutive model and material properties

The behavior of the rock was assumed to be governed by an elastoplastic constitutive relation based on the elasticity theory and the Mohr-Coulomb plasticity criterion. As presented in section 3.3, the intact rock strength parameters, such as UCS, elastic Young's modulus  $E$ ,  $\nu$ , tensile strength ( $\sigma_t$ ), Cohesive strength  $c$ , angle of friction  $\phi$  and the Hoek-Brown failure criterion intact material constant ( $m_i$ ), are measured through a series of rock mechanics tests (UCS, Brazilian and triaxial tests). However, it is necessary to relate the

intact properties of the rock, measured in the laboratory, to geological observations in the field and subsequently estimate the rock mass strength properties. To do this, the generalized Hoek-Brown failure criterion, Bieniawski's rock mass rating (RMR) and the geological strength index (GSI) were used to estimate the rock mass properties (all three are reviewed extensively in chapter 2). The methodology used to estimate the rock mass properties is illustrated in figure 3.24. Herein, an example of the calculations for PKX rock are used to demonstrate the methodology.

After estimating the intact strength properties of the rock, it is essential to calculate the Hoek-Brown material constants ( $m_b$ ,  $s$  and  $a$ ). The intact material constant ( $m_i$ ) value for PKX rock is 12.76. According to the geotechnical reports available from the mine, the average  $RMR_{89}$  value for the A154 South pipe is estimated to be 55. Consequently, the average GSI value will be 50 for this pipe. The disturbance factor ( $D$ ) is estimated to be 0. (As explained in chapter 2,  $D$  is the disturbance factor depending on the blast damage and stress relaxation). Using equations (2.21), (2.22) and (2.23) presented in chapter 2, the  $m_b$  (reduced value of the material constant  $m_i$ ),  $s$  and  $a$  can be calculated as follows:

$$m_b = m_i e^{\left(\frac{GSI-100}{28-14D}\right)} = 12.76 e^{\frac{50-100}{28}} = 2.14$$

$$s = \exp\left(\frac{GSI - 100}{9 - 3D}\right) = \exp\left(\frac{50 - 100}{9}\right) = 0.0039$$

$$a = \frac{1}{2} + \frac{1}{6} \left( e^{\frac{-GSI}{15}} - e^{\frac{-20}{3}} \right) = \frac{1}{2} + \frac{1}{6} \left( e^{\frac{-50}{15}} - e^{\frac{-20}{3}} \right) = 0.51$$

The constitutive model used in Abaqus is Mohr-Coulomb criterion. Therefore, it is necessary to calculate the equivalent cohesion ( $c'$ ) and angle of friction ( $\phi'$ ) for each rock mass. As discussed in chapter 2, this can be done by using equations (2.25) and (2.26) proposed by Hoek, Carranza-Torres and Corkum (2002) as follows:

$$\phi' = \sin^{-1} \left[ \frac{6am_b(S+m_b\sigma'_{3n})^{a-1}}{2(1+a)(2+a)+6am_b(S+m_b\sigma'_{3n})^{a-1}} \right] = 29.59^\circ$$

$$c' = \frac{\sigma_{ci}[(1+2a)s+(1-a)m_b\sigma'_{3n}](S+m_b\sigma'_{3n})^{a-1}}{(1+a)(2+a)\sqrt{1+(6am_b(S+m_b\sigma'_{3n})^{a-1})/((1+a)(2+a))}} = 4.7 \text{ MPa}$$

Based on the calculated  $c'$  and  $\phi'$ , the global rock mass ( $\sigma'_{cm}$ ) can be calculated using equation (3.11):

$$\sigma'_{cm} = \frac{2c' \cos \phi'}{1 - \sin \phi'} = 13.58 \text{ MPa} \quad (3.11)$$

The above procedure was followed for all Kimberlite rock types, and the results are presented in table 3.6.

**Table 3.6** Estimated rock mass properties for each Kimberlite rock type

| Kimberlite Pipe | Rock Type      | GSI       | Rock Mass Properties |            |             |
|-----------------|----------------|-----------|----------------------|------------|-------------|
|                 |                |           | $\sigma_{cm}$ (MPa)  | $c'$ (MPa) | $\phi'$     |
| A154 South      | PK             | 50        | 8.15                 | 3.59       | 23.18       |
|                 | PKX            | 50        | 13.58                | 4.7        | 29.59       |
|                 | <b>Average</b> | <b>50</b> | <b>10.87</b>         | <b>4.2</b> | <b>26.4</b> |
| A154 North      | MK             | 60        | 13.50                | 4.55       | 26.11       |
|                 | MRK            | 60        | 9.73                 | 4.29       | 26.65       |
|                 | BMVK           | 60        | 14.4                 | 5.19       | 31.35       |
|                 | <b>Average</b> | <b>60</b> | <b>12.55</b>         | <b>4.7</b> | <b>28.1</b> |

Table 3.7 presents the material properties defined in the FE model. The Granite, CRF and URF properties have been selected from the literature as presented in the footnotes.

**Table 3.7** Material properties defined in the FE model

| Materials             | $\gamma$<br>(MN/m <sup>3</sup> ) | E (GPa) | $\nu$ | $c$<br>(MPa) | $\phi^o$ | $\sigma_c$<br>(MPa) | $\sigma_t$<br>(MPa) |
|-----------------------|----------------------------------|---------|-------|--------------|----------|---------------------|---------------------|
| Granite <sup>1</sup>  | 0.026                            | 24      | 0.3   | 9.3          | 45       | 130                 | 0                   |
| A154 North Kimberlite | 0.024                            | 19.6    | 0.22  | 4.7          | 28.1     | 79                  | 3.7                 |
| A154 South Kimberlite | 0.024                            | 18.7    | 0.24  | 4.2          | 26.4     | 66                  | 3.4                 |
| CRF <sup>2</sup>      | 0.022                            | 2       | 0.3   | 1.3          | 35       | 1.5                 | 0                   |
| URF <sup>1</sup>      | 0.026                            | 2       | 0.3   | NA           | NA       | NA                  | NA                  |

<sup>1</sup> From (Diavik technical reports, 2011; Yip and Thomson, 2015)

<sup>2</sup> From (Hassani and Archibald, 1998; Zhang and Mitri, 2008)

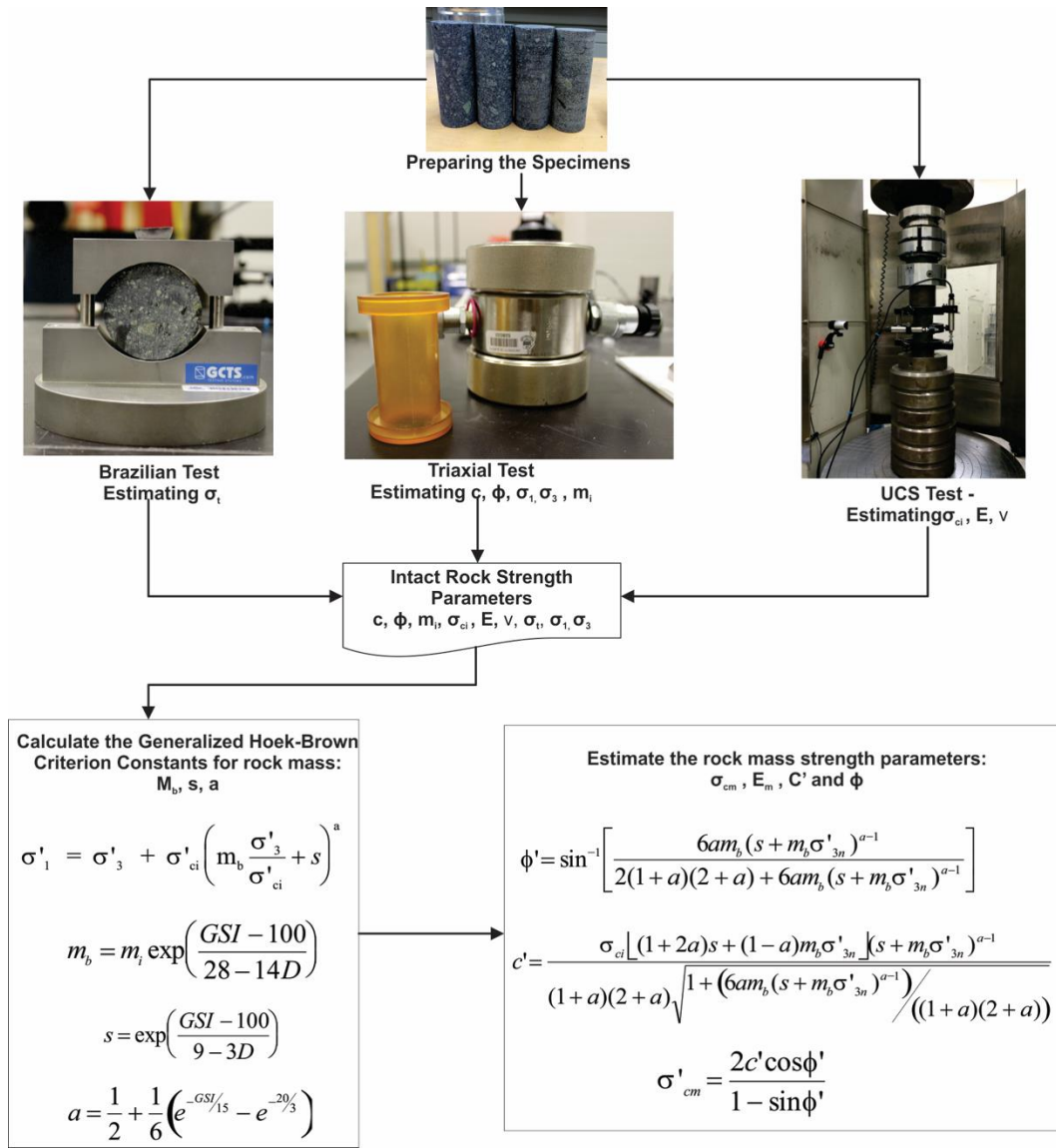


**Figure 3.24** Methodology for estimating the rock mass strength of Kimberlite

### 3.4.3 Finite element mesh and mesh convergence study

Ten-node quadratic tetrahedron element (C3D10) was used to discretize the analysis domain. The element has four corner nodes and six side nodes. Figure 3.25 illustrates the FE mesh of the model.

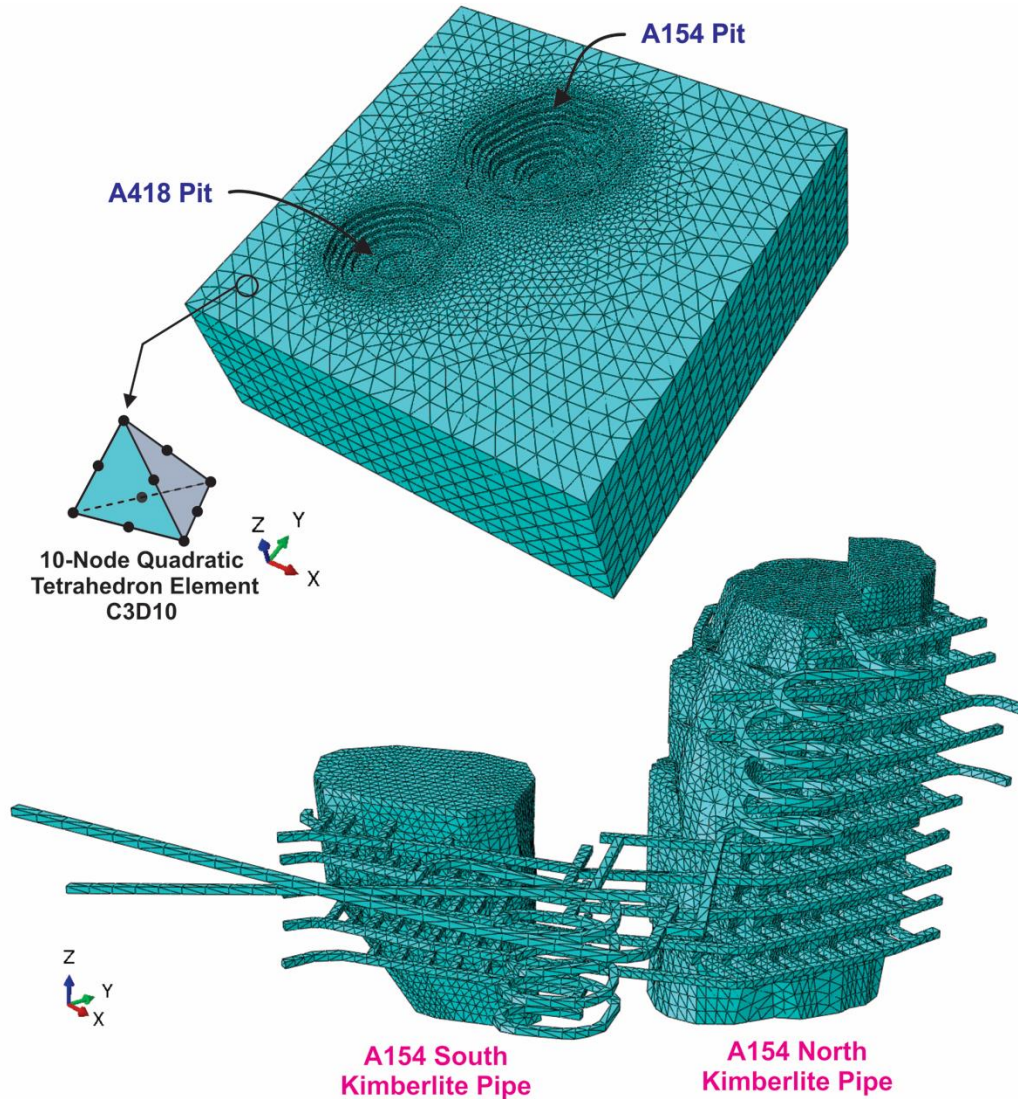


Figure 3.25 FE mesh

A mesh convergence study (MCS) was performed to ensure that a sufficient refined mesh had been used. Generally, as the density of the mesh increases, the accuracy of the results improves as well. On the other hand, as the mesh is refined, the computer resources and calculation time required to run the simulation model increase significantly. The main objective of the MCS is to

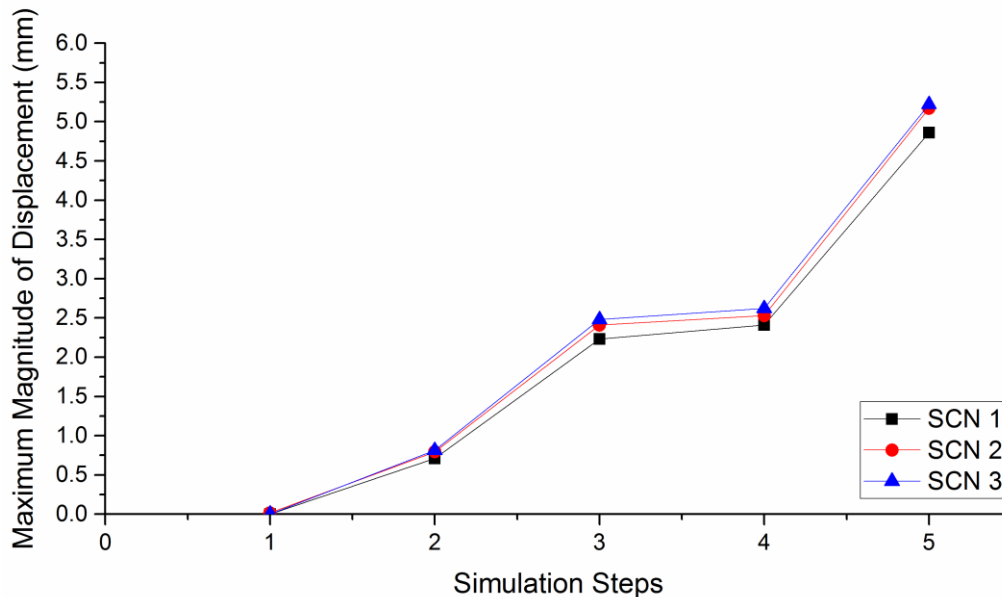
reach to an optimum meshing scenario when further mesh refinements produce a negligible change in the results.

Initially, as presented in table 3.8, three meshing scenarios (SCN) are defined. The density of the mesh increases from SCN 1 to SCN 3. In all three scenarios, mesh density varies throughout the analysis domain: a fine mesh is used around the underground drifts and stopes, while a coarse mesh is used elsewhere.

**Table 3.8** Mesh scenarios used to perform a mesh convergence study

| Scenario | Total Number of Elements | Total Number of Nodes | Number of Variables (Degree of Freedom) |
|----------|--------------------------|-----------------------|---|
| SCN 1    | 360,861                  | 492,868               | 1,478,058                               |
| SCN 2    | 817,651                  | 1,106,309             | 3,318,927                               |
| SCN 3    | 1,504,880                | 2,020,275             | 6,060,825                               |

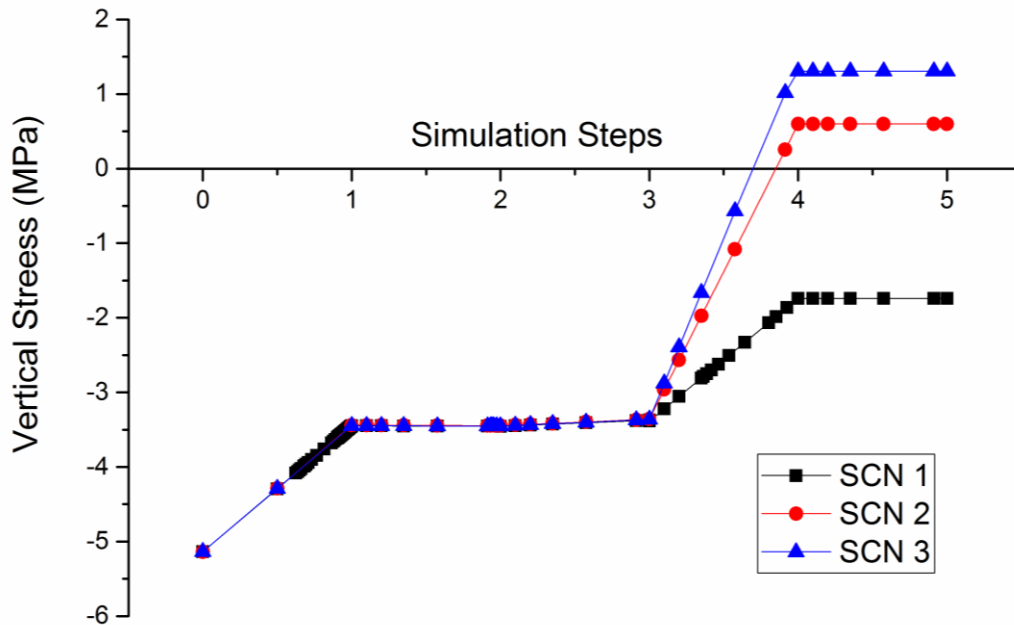
All three scenarios have been tested for the first five simulation steps out of an actual 123 simulation steps. The goal was to find the best acceptable arrangement between the accuracy of the results and the cost of finite element simulation. Here cost refers to calculation time and required computer resources.



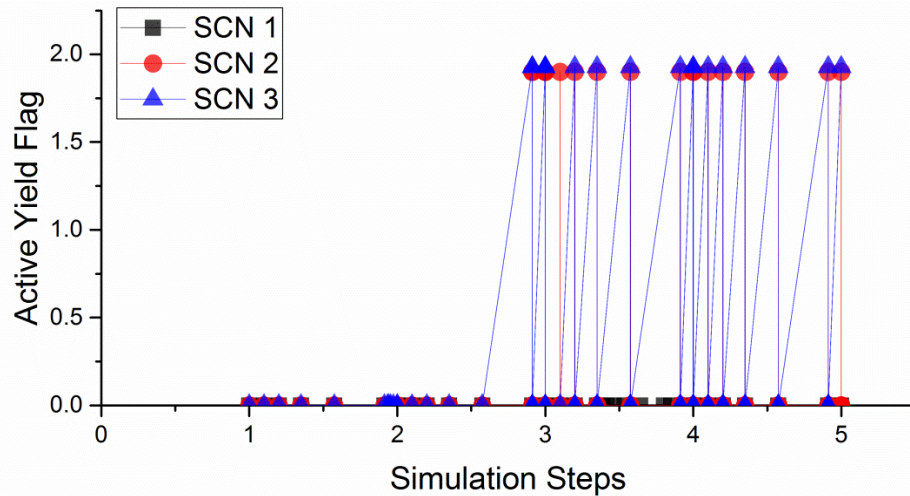
**Figure 3.26** Mesh convergence study on maximum displacement

Figure 3.26 shows the maximum magnitude of displacement generated in the first five simulation steps of the FE model under different SCNs. As can be seen, SCN2 and SCN3's graph results almost overlap each other, while SCN 1 has a noticeable distance from the others.

Figure 3.27 shows the maximum vertical stress at a monitoring node on the back of the N9175-P1-155 undercut drift. The trends of developing the tensile stress (relaxation zone) from step 1 to 5 are presented under different SCNs. Here, again, SCN 2 and SCN 3 give close results, while SCN 1 is distinctively following a different path and failed to predict any tensile stress on the back of the drift. The results of the MCS is significant because, based on the results of SCN 1, the magnitude of induced tensile stress on the back of the monitoring drift is not only zero, but it also is under around 2 MPa compressive stress which is completely wrong. The other two SCNs show the induced tensile stress close to 1 MPa. (It should be noted that in Abaqus, unlike in rock mechanics, compressive stress has a negative sign and tensile stress has a positive sign).



**Figure 3.27** MCS on vertical stress at a monitoring node



**Figure 3.28** MCS: active yield flag at the monitoring node

Finally, the ability of each scenario to predict the yielding zones had been tests. As can be seen from figure 3.28, SCN 2 and SCN 3 have very close predictions; however, SCN 1 fails to predict any yielding at the same monitoring point.

The central processing unit (CPU) time for the first iteration in step 1 of the simulation for each scenario is presented in table 3.9. As as the mesh density increases, the calculation time increases significantly.

**Table 3.9** CPU time for the first iteration\*

| Mesh Scenario | CPU Time (Min) |
|---------------|----------------|
| SCN 1         | 3.3            |
| SCN 2         | 22             |
| SCN 3         | 86.2           |

\*Referring to table 3.9, an iteration is an attempt to find an equilibrium solution in an increment. In nonlinear analysis, the total load applied in a step is divided into smaller increments so that the nonlinear solution path can be developed. If the model is not at equilibrium at the end of each iteration, Abaqus will take another iteration attempt until it reaches equilibrium. Here the CPU time for the first iteration in step 1 of each meshing scenario is presented.

Based on the MCS results, the best meshing scenario is SCN 2. In fact, the difference between the displacement results obtained from SCN 2's meshing scenario and the solution obtained from the most refined mesh scenario, SCN 3, is approximately 5%, while the calculation time in SCN2 is reduced significantly (approximately by 75%).

### 3.4.4 Defining initial stress state (geostatic step)

Defining the pre-mining state of stress is an important step in geomechanical modeling. Underground structures are subjected to initial stresses prior to mining. Redistribution of these stresses due to the mining activities causes the development of mining-induced stresses which ultimately can lead to deformation and failure of the ground.

The vertical component of in-situ stress ( $\sigma_v$ ) was considered the minor principal stress (in both the host rock and A154 South orebody) and is calculated using equation (3.12).

$$\sigma_v = \gamma \cdot H \quad (3.12)$$

where  $\gamma$  is the average unit weight of the overburden rocks and  $H$  is the depth.

A heterogeneity stress field was assumed in the host rock (granite) and in the A154 South Kimberlite pipe. It was assumed that the maximum principal stresses ( $\sigma_{Hmax}$ ) are perpendicular to the strike of the stopes and the intermediate principal stresses ( $\sigma_{Hmin}$ ) are aligned with the strike of the stopes. Equations (3.13) and (3.14) are used to calculate the horizontal stress components:

$$\sigma_{Hmax} = k_{max} \cdot \sigma_v \text{ where } k_{max} = 1.5 \quad (3.13)$$

$$\sigma_{Hmin} = k_{min} \cdot \sigma_v \text{ where } k_{min} = 1.2 \quad (3.14)$$

where  $k$  is the ratio between horizontal and vertical in-situ stress.

However, the stress field for the A154 North pipe is different. Due to the geological history of the formation of this volcanic Kimberlite pipe and based on field observations (i.e. presence of water in the contact between granite and Kimberlite), it was concluded that the stress transfer from the host rock to the orebody cannot take place. Moreover, the observed separation between granite and the A154 North Kimberlite pipe, as shown in figure 3.30, supports this hypothesis. Consequently, the stress regime inside the A154 North Kimberlite

pipe is completely different from the one inside the granite and the other pipe. The  $k$  value inside the A154 North Kimberlite pipe has been estimated using equation (3.15) proposed by Terzaghi and Richart (1952):

$$k = \frac{\nu}{1-\nu} \quad (3.15)$$

where  $\nu$  is the Poisson's ratio of the rock. For the design purpose, the value of  $\nu$  for this pipe is assumed to be 0.3; therefore, the  $k$  value for the inside of the orebody is 0.43.

As illustrated in figure 3.29, the magnitude of the maximum in-situ principal stress in the model is estimated to be 31.2 MPa by the FE model. This value can be verified using equations (3.12) and (3.13) as follows (assuming  $0.026 \text{ MN/m}^3$  as the average unit weight of the overburden rocks):

$$\sigma_{Hmax} = k_{max}\sigma_v = 1.5 \times 0.026 \times H = 1.5 \times 0.026 \times 800 = 31.2 \text{ MPa}$$

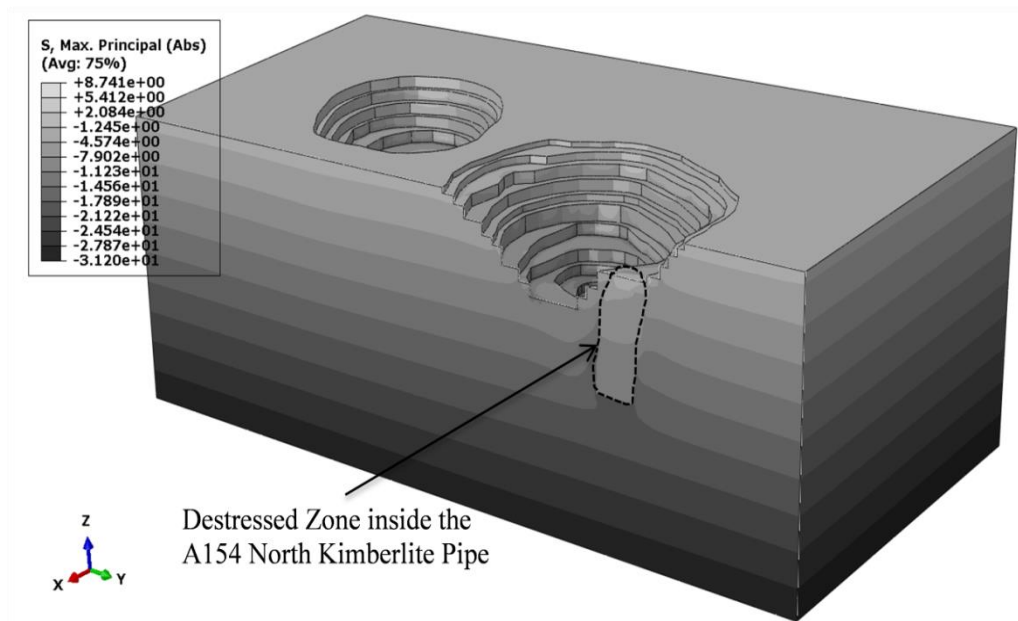


**Figure 3.29** Initial state of stress as simulated in step 1 (geostatic step)

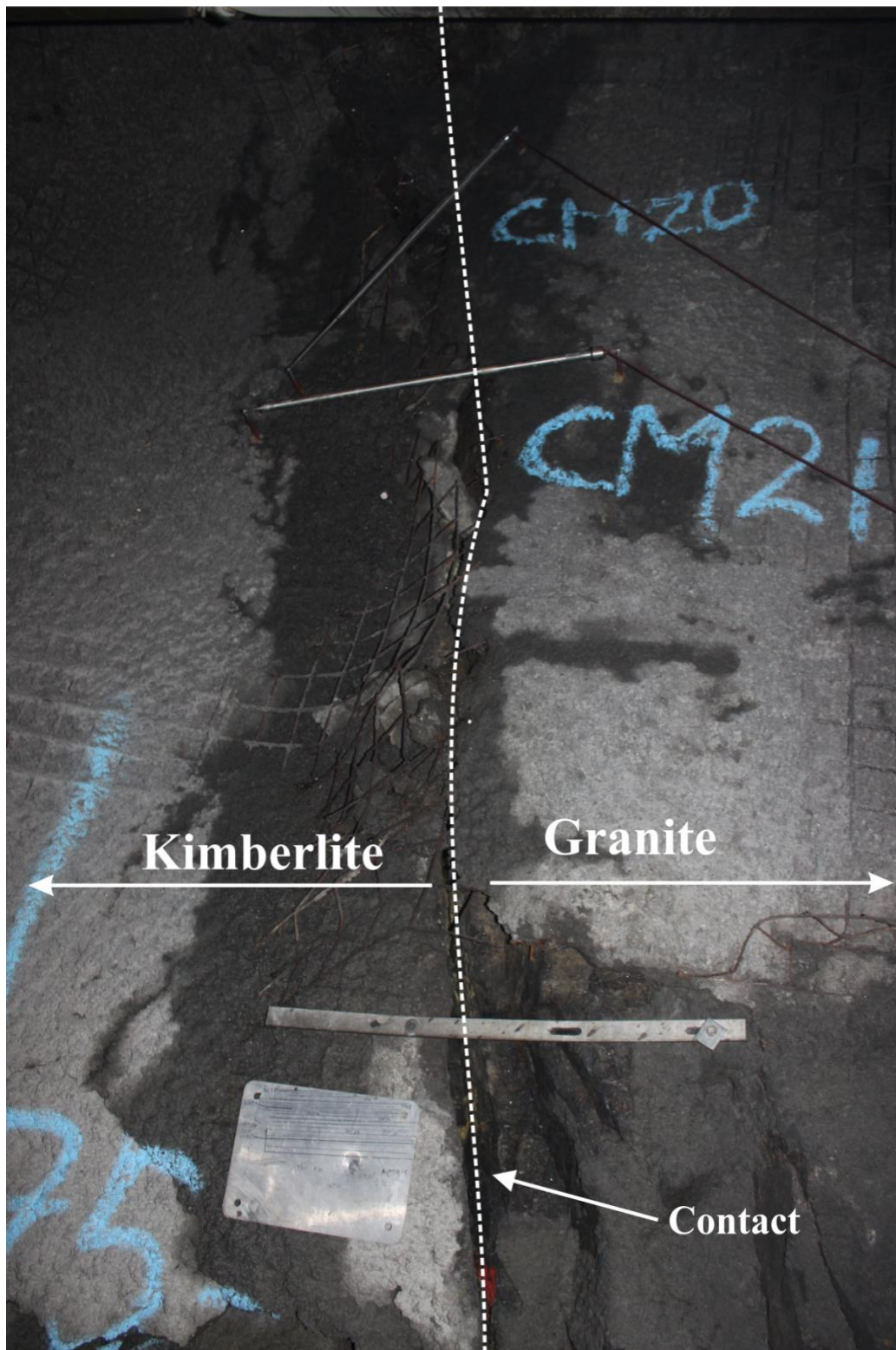


**Figure 3.30** Contact between granite and the A154 North Kimberlite Pipe at mine level N9275

### **3.4.5 Simulation steps**

The developed numerical model has 123 simulation steps. Throughout these simulation steps the mining and backfilling of the drifts and stopes, in both Kimberlite pipes, are simulated in the model step-by-step. Therefore, two mining methods, BHS and SLR, are simulated simultaneously. Consequently, the developed FE model simulates the complete stress-strain path through the entire excavation and backfilling simulation steps.

Step 1 is the geostatic step, which is basically for calculating the initial state of stress before starting the excavation of the underground openings. Step 2 is the excavation of all main haulage drifts and ramps. Mining starts from mine level N9175 in the North pipe and S9125 in the South pipe from step 3 to step 123 of the simulation. The sequences of the excavation/backfilling in the North pipe and the extraction in the South pipe are defined according to the mine production plan; however, some simplifications in the shape of the stopes have been made. The sequence of stope mining and the corresponding simulation steps for mining Block A and B are shown in figures 3.31 and 3.32, respectively. As shown in figure 3.32, mining in Block B starts from step 34, with the excavation of the N9050-P1-95 undercut drift. Referring to these two figures, P stands for primary stopes and S stands for secondary stopes. There are two kinds of Primaries and secondaries denoted as: (i) P1 and P2 and (ii) S1 and S2 respectively. For example in mining Block A, operation starts with excavation of all primary stopes (P1 and P2) from lower level of N9175, and goes upward to N9225. After all primary stopes have been excavated and backfilled, excavation of the secondary stopes will be initiated from the N9175 level, according to the mining sequence shown in this figure. Meanwhile the excavation of the primary stopes to N9250 will be continued. Same mechanism will be followed for Mining Block B.

SLR mining in the A154 South pipe is simulated for the stopes located between mine levels S9050 and S9125. In steps 2 and 3, the bottom of the pit has been set at S9125. The sequence of the mining and the corresponding simulation steps for each mining level, S9100, S9075 and S9050, are shown in figures 3.33, 3.34 and

3.35, respectively. For example, referring to figure 3.33, excavation of the production and slot drifts in level S9100 are being done through steps 5 to 13. The first SLR stopes in the model is excavated in step 24 with the excavation of SLR9100-970-Block 1 starting from the far Kimberlite contact as shown in figure 3.33 in a retreat manner. Same mechanism will be followed for S9075 and S9050.

The defined simulation steps in Abaqus code language can be found in Appendix D.

|    |    |    |       |       |       |     |     |     |     |     |     |     |     |     |     |     |     |     |     |     |     |       |    |       |    |       |    |    |    |       |
|----|----|----|-------|-------|-------|-----|-----|-----|-----|-----|-----|-----|-----|-----|-----|-----|-----|-----|-----|-----|-----|-------|----|-------|----|-------|----|----|----|-------|
| P1 | S2 | P2 | S1    | P1    | S2    | P2  | S1  | P1  | S2  | P2  | S1  | P1  | S2  | P2  | S1  | P1  | S2  | P2  | S1  | P1  | S2  | P2    |    |       |    |       |    |    |    |       |
| 65 | 73 | 80 | 88    | 95    | 103   | 110 | 118 | 125 | 133 | 140 | 148 | 155 | 163 | 170 | 178 | 185 | 193 | 200 | 208 | 215 | 223 | 230   |    |       |    |       |    |    |    |       |
|    |    |    |       |       |       | 75  | 97  | 71  | 108 | 75  | 98  | 70  | 109 | 76  | 96  | 71  | 110 | 77  | 95  | 72  | 96  | N9275 |    |       |    |       |    |    |    |       |
|    |    |    |       |       | Stope | 80  | 98  | 74  | 109 | 78  | 99  | 72  | 110 | 79  | 100 | 73  | 111 | 81  | 101 | 75  | 97  |       |    |       |    |       |    |    |    |       |
|    |    |    | 83    | 33    | 93    | 46  | 83  | 34  | 94  | 47  | 81  | 30  | 95  | 48  | 82  | 31  | 96  | 49  | 84  | 32  | 53  | N9250 |    |       |    |       |    |    |    |       |
|    |    |    | Stope | 83    | 44    | 99  | 53  | 87  | 41  | 100 | 50  | 85  | 39  | 101 | 51  | 86  | 40  | 102 | 52  | 88  | 34  | 71    |    |       |    |       |    |    |    |       |
|    |    |    |       | 89    | 103   |     | 93  | 45  | 104 | 54  | 94  | 42  | 105 | 55  | 91  | 43  | 106 | 56  |     |     |     |       |    |       |    |       |    |    |    |       |
|    |    |    |       | 92    | 49    | 107 | 57  | 96  | 48  | 108 | 58  | 97  | 46  | 109 | 59  | 95  | 47  | 110 | 60  | 90  | 36  |       |    |       |    |       |    |    |    |       |
|    |    |    |       | 36    | 66    | 13  | 88  | 31  | 65  | 16  | 87  | 33  | 67  | 15  | 90  | 33  | 68  | 14  | 89  | 35  | 69  | 28    | 50 | N9225 |    |       |    |    |    |       |
|    |    |    |       | Stope | 40    | 75  | 22  | 90  | 35  | 73  | 20  | 91  | 34  | 72  | 19  | 92  | 41  | 74  | 23  | 93  | 42  | 76    | 31 | 51    |    |       |    |    |    |       |
|    |    |    |       |       | 43    | 81  | 28  | 94  | 37  | 77  | 26  | 95  | 36  | 78  | 25  | 96  | 44  | 79  | 27  | 97  | 45  |       |    |       |    |       |    |    |    |       |
|    |    |    |       |       |       |     |     | 98  | 39  | 82  | 32  | 99  | 38  | 83  | 29  | 100 | 46  | 84  | 30  | 101 | 47  | 80    | 33 |       |    |       |    |    |    |       |
|    |    |    |       |       | 44    | 29  | 57  | 4   | 78  | 22  | 56  | 4   | 78  | 23  | 55  | 4   | 79  | 24  | 58  | 4   | 79  | 33    | 59 | 18    | 42 | N9200 |    |    |    |       |
|    |    |    |       |       | Stope | 45  | 35  | 64  | 7   | 79  | 25  | 62  | 6   | 80  | 27  | 61  | 5   | 81  | 26  | 63  | 8   | 82    | 34 | 65    | 21 | 43    |    |    |    |       |
|    |    |    |       |       |       |     |     | 69  | 11  | 83  | 29  | 67  | 10  | 84  | 30  | 66  | 9   | 85  | 28  | 68  | 12  | 86    |    |       |    |       |    |    |    |       |
|    |    |    |       |       |       |     |     |     | 74  | 15  | 87  | 33  | 72  | 14  | 88  | 31  | 71  | 13  | 89  | 32  | 73  | 16    | 90 | 36    | 70 | 24    |    |    |    |       |
|    |    |    |       |       |       |     |     |     |     |     |     |     |     | 18  | 88  | 31  | 71  | 17  | 89  | 32  | 73  | 16    | 90 | 36    | 70 | 24    |    |    |    |       |
|    |    |    |       |       |       |     |     |     | 43  | 28  | 53  | 3   | 76  | 19  | 51  | 3   | 76  | 21  | 50  | 3   | 77  | 20    | 52 | 3     | 77 | 30    | 54 | 17 | 41 | N9175 |

**START**

| Block "A" Stope Sequence: |      |     |    |  |    |      |     |    |  |    |      |     |    |  |    |      |     |    |  |    |      |     |    |  |    |      |     |    |
|---------------------------|------|-----|----|--|----|------|-----|----|--|----|------|-----|----|--|----|------|-----|----|--|----|------|-----|----|--|----|------|-----|----|
| 1                         | 9175 | 155 | P1 |  | 11 | 9175 | 110 | P2 |  | 21 | 9175 | 223 | S2 |  | 31 | 9175 | 148 | S1 |  | 41 | 9200 | 178 | S1 |  | 51 | 9225 | 178 | S1 |
| 2                         | 9175 | 125 | P1 |  | 12 | 9175 | 170 | P2 |  | 22 | 9225 | 155 | P1 |  | 32 | 9175 | 118 | S1 |  | 42 | 9250 | 125 | P1 |  | 52 | 9250 | 223 | S2 |
| 3                         | 9175 | 95  | P1 |  | 13 | 9200 | 215 | P1 |  | 23 | 9225 | 185 | P1 |  | 33 | 9175 | 178 | S1 |  | 43 | 9200 | 88  | S1 |  | 53 | 9225 | 88  | S1 |
| 4                         | 9175 | 185 | P1 |  | 14 | 9175 | 80  | P2 |  | 24 | 9225 | 215 | P1 |  | 34 | 9175 | 88  | S1 |  | 44 | 9250 | 200 | P2 |  | 54 | 9225 | 208 | S1 |
| 5                         | 9200 | 155 | P1 |  | 15 | 9200 | 140 | P2 |  | 25 | 9225 | 125 | P1 |  | 35 | 9175 | 208 | S1 |  | 45 | 9200 | 208 | S1 |  | 55 | 9250 | 148 | S1 |
| 6                         | 9200 | 125 | P1 |  | 16 | 9200 | 110 | P2 |  | 26 | 9225 | 95  | P1 |  | 36 | 9200 | 148 | S1 |  | 46 | 9250 | 140 | P2 |  | 56 | 9250 | 118 | S1 |
| 7                         | 9200 | 95  | P1 |  | 17 | 9175 | 200 | P2 |  | 27 | 9225 | 140 | P2 |  | 37 | 9225 | 223 | S2 |  | 47 | 9250 | 170 | P2 |  | 57 | 9250 | 178 | S1 |
| 8                         | 9200 | 185 | P1 |  | 18 | 9200 | 170 | P2 |  | 28 | 9225 | 170 | P2 |  | 38 | 9250 | 155 | P1 |  | 48 | 9250 | 200 | P2 |  | 58 | 9250 | 208 | S1 |
| 9                         | 9175 | 215 | P1 |  | 19 | 9200 | 200 | P2 |  | 29 | 9225 | 110 | P2 |  | 39 | 9200 | 118 | S1 |  | 49 | 9225 | 148 | S1 |  |    |      |     |    |
| 10                        | 9175 | 140 | P2 |  | 20 | 9200 | 80  | P2 |  | 30 | 9200 | 223 | S2 |  | 40 | 9250 | 185 | P1 |  | 50 | 9225 | 118 | S1 |  |    |      |     |    |

Figure 3.31 Mining Block A sequence and simulation steps\*

\*Note: P stands for primary stopes and S stands for secondary stopes. There are two kinds of Primaries and secondaries denoted as: (i) P1 and P2 and (ii) S1 and S2 respectively. For example in mining Block A, operation starts with excavation of all primary stopes (P1 and P2) from lower level of N9175, and goes upward to N9225. After all primary stopes have been excavated and backfilled, excavation of the secondary stopes will be initiated from the N9175 level, according to the mining sequence shown in this figure. Meanwhile the excavation of the primary stopes to N9250 will be continued.

| S1 | P1 | S2  | P2  | S1  | P1  | S2  | P2  | S1  | P1  | S2  | P2  | S1  | P1  | S2  | P2  | S1  | P1  | S2  | P2  | S1  | P1  | S2          | P2          |
|----|----|-----|-----|-----|-----|-----|-----|-----|-----|-----|-----|-----|-----|-----|-----|-----|-----|-----|-----|-----|-----|-------------|-------------|
| 58 | 65 | 73  | 80  | 88  | 95  | 103 | 110 | 118 | 125 | 133 | 140 | 148 | 155 | 163 | 170 | 178 | 185 | 193 | 200 | 208 | 215 | 223         | 230         |
|    |    | 116 | 90  | 112 | 72  | 117 | 91  | 114 | 73  | 118 | 92  | 115 | 74  | 119 | 94  | 115 | 75  | 120 | 89  | 97  | 76  | N9150 Level |             |
|    |    | 117 | 97  | 114 | 85  | 118 | 93  | 115 | 83  | 119 | 96  | 116 | 84  | 122 | 98  | 120 | 82  | 121 | 94  | 108 | 95  |             |             |
|    |    | 117 | 99  | 114 | 87  | 118 | 100 | 115 | 88  | 119 | 101 | 116 | 89  | 122 | 102 | 120 | 86  | 121 | 94  | 108 | 76  |             |             |
|    |    | 117 | 103 | 114 | 90  | 118 | 104 | 115 | 91  | 119 | 105 | 116 | 92  | 122 | 106 | 120 | 86  | 121 | 94  | 108 | 76  |             |             |
|    |    | 62  | 113 | 80  | 105 | 60  | 114 | 81  | 106 | 61  | 115 | 82  | 107 | 63  | 115 | 83  | 108 | 64  | 105 | 81  | 97  | N9125 Level |             |
|    |    | 75  | 115 | 83  | 106 | 73  | 116 | 85  | 107 | 77  | 117 | 87  | 108 | 71  | 118 | 88  | 109 | 74  | 119 | 84  | 98  |             |             |
|    |    | 75  | 111 | 76  | 116 | 89  | 113 | 78  | 117 | 90  | 114 | 82  | 118 | 91  | 110 | 79  | 119 | 84  | 98  | 98  |     |             |             |
|    |    | 75  | 115 | 86  | 112 | 80  | 116 | 92  | 113 | 81  | 117 | 93  | 114 | 82  | 118 | 91  | 110 | 79  | 119 | 84  | 98  |             |             |
|    |    | 47  | 99  | 68  | 89  | 44  | 103 | 69  | 94  | 45  | 104 | 70  | 95  | 46  | 104 | 70  | 95  | 52  | 102 | 68  | 90  | N9100 Level |             |
|    |    | 59  | 105 | 75  | 92  | 63  | 106 | 71  | 95  | 62  | 107 | 72  | 96  | 60  | 108 | 73  | 97  | 61  | 104 | 74  | 94  |             |             |
|    |    | 59  | 93  | 75  | 93  | 67  | 110 | 76  | 100 | 65  | 112 | 77  | 101 | 64  | 113 | 78  | 99  | 66  | 104 | 74  | 94  |             |             |
|    |    | 59  | 109 | 75  | 98  | 70  | 111 | 79  | 102 | 68  | 112 | 80  | 103 | 69  | 113 | 81  | 99  | 66  | 104 | 74  | 94  |             |             |
|    |    | 67  | 39  | 93  | 55  | 81  | 40  | 92  | 54  | 81  | 41  | 94  | 56  | 82  | 42  | 91  | 57  | 82  | 43  | 90  | 58  | 66          | N9075 Level |
|    |    | 78  | 48  | 94  | 60  | 82  | 47  | 95  | 61  | 83  | 49  | 96  | 59  | 84  | 50  | 97  | 62  | 85  | 51  | 93  | 63  | 77          |             |
|    |    | 78  | 98  | 64  | 86  | 52  | 99  | 66  | 87  | 53  | 100 | 67  | 88  | 54  | 101 | 68  | 89  | 52  | 93  | 63  | 77  |             |             |
|    |    | 67  | 35  | 93  | 54  | 64  | 34  | 92  | 58  | 79  | 36  | 94  | 55  | 80  | 37  | 91  | 53  | 80  | 38  | 90  | 52  | 65          | N9050 Level |

START

| Block "B" Stope Sequence: |      |     |    |  |    |      |     |    |  |    |      |     |    |  |    |      |     |    |  |    |      |     |    |    |      |     |    |
|---------------------------|------|-----|----|--|----|------|-----|----|--|----|------|-----|----|--|----|------|-----|----|--|----|------|-----|----|----|------|-----|----|
| 1                         | 9050 | 95  | P1 |  | 11 | 9075 | 155 | P1 |  | 21 | 9100 | 140 | P2 |  | 31 | 9125 | 170 | P2 |  | 41 | 9075 | 88  | S1 | 51 | 9100 | 133 | S2 |
| 2                         | 9050 | 65  | P1 |  | 12 | 9075 | 110 | P2 |  | 22 | 9125 | 95  | P1 |  | 32 | 9050 | 118 | S1 |  | 42 | 9075 | 148 | S1 | 52 | 9100 | 73  | S2 |
| 3                         | 9050 | 125 | P1 |  | 13 | 9075 | 80  | P2 |  | 23 | 9125 | 125 | P1 |  | 33 | 9050 | 88  | S1 |  | 43 | 9075 | 103 | S2 | 53 | 9100 | 163 | S2 |
| 4                         | 9050 | 155 | P1 |  | 14 | 9075 | 140 | P2 |  | 24 | 9125 | 185 | P1 |  | 34 | 9050 | 148 | S1 |  | 44 | 9075 | 133 | S2 | 54 | 9125 | 148 | S1 |
| 5                         | 9050 | 80  | P2 |  | 15 | 9100 | 95  | P1 |  | 25 | 9125 | 155 | P1 |  | 35 | 9050 | 58  | S1 |  | 45 | 9075 | 73  | S2 | 55 | 9125 | 118 | S1 |
| 6                         | 9050 | 110 | P2 |  | 16 | 9100 | 125 | P1 |  | 26 | 9125 | 215 | P1 |  | 36 | 9050 | 103 | S2 |  | 46 | 9075 | 163 | S2 | 56 | 9125 | 178 | S1 |
| 7                         | 9050 | 140 | P2 |  | 17 | 9100 | 65  | P1 |  | 27 | 9125 | 110 | P2 |  | 37 | 9050 | 133 | S2 |  | 47 | 9100 | 118 | S1 | 57 | 9125 | 88  | S1 |
| 8                         | 9075 | 95  | P1 |  | 18 | 9100 | 155 | P1 |  | 28 | 9125 | 140 | P2 |  | 38 | 9050 | 73  | S2 |  | 48 | 9100 | 88  | S1 | 58 | 9125 | 208 | S1 |
| 9                         | 9075 | 65  | P1 |  | 19 | 9100 | 110 | P2 |  | 29 | 9125 | 80  | P2 |  | 39 | 9050 | 163 | S2 |  | 49 | 9100 | 148 | S1 | 59 | 9125 | 133 | S2 |
| 10                        | 9075 | 125 | P1 |  | 20 | 9100 | 80  | P2 |  | 30 | 9125 | 200 | P2 |  | 40 | 9075 | 118 | S1 |  | 50 | 9100 | 103 | S2 | 60 | 9125 | 163 | S2 |
|                           |      |     |    |  |    |      |     |    |  |    |      |     |    |  |    |      |     |    |  |    |      |     |    | 61 | 9125 | 73  | S2 |

Figure 3.32 Mining Block B sequence and simulation steps\*

\*Note: Mining at Block B starts at step 34 of the simulation model with excavation of the N9050-P1-95 undercut drift. It will end at step 122 with the excavation of Stope-N9150-S2-163. This stope will be backfilled at step 123 of the simulation model. Same mining mechanism as explained in figure 3.31 will be followed.

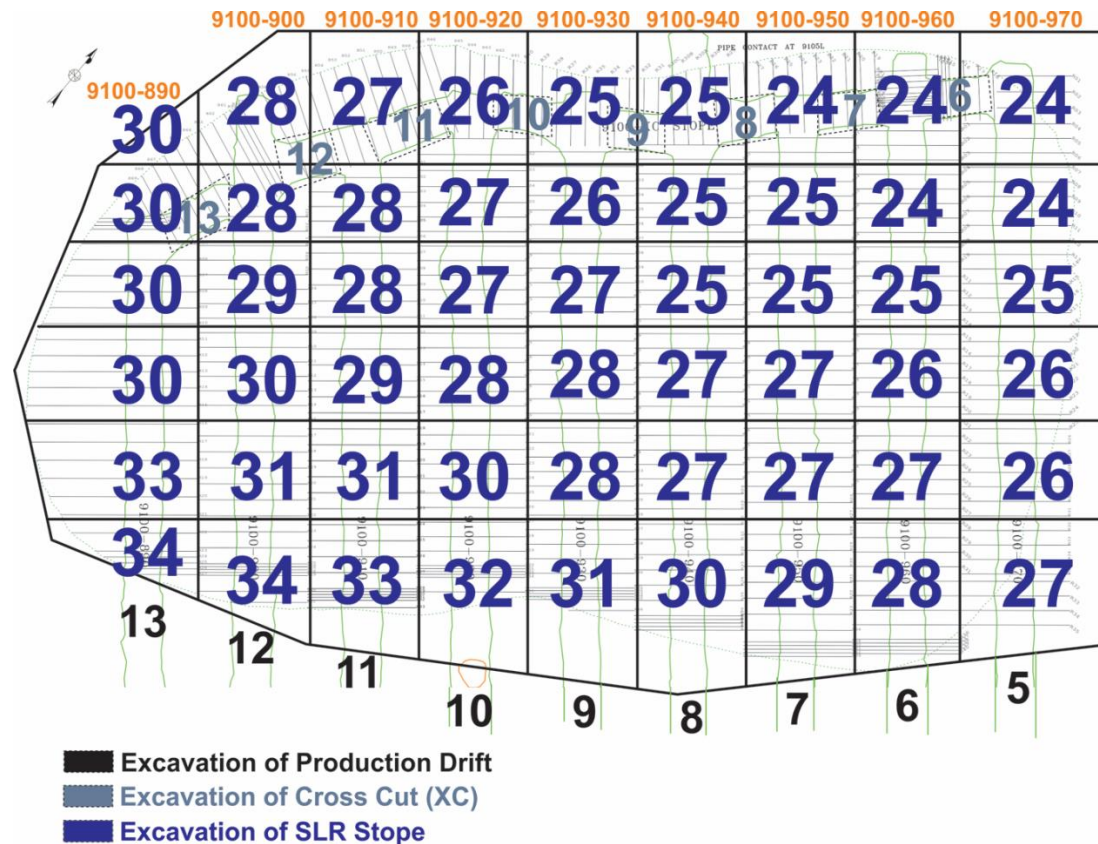


**Figure 3.33** Sequence of mining and simulation steps for mine level S9100 of the A154 South pipe\* (using SLR)

*\*Note: excavation of the production and slot drifts in level S9100 are being done through steps 5 to 13. The first SLR stopes in the model is excavated in step 24 with the excavation of SLR9100-970-Block 1 starting from the far Kimberlite contact as shown in this figure in a retreat manner.*

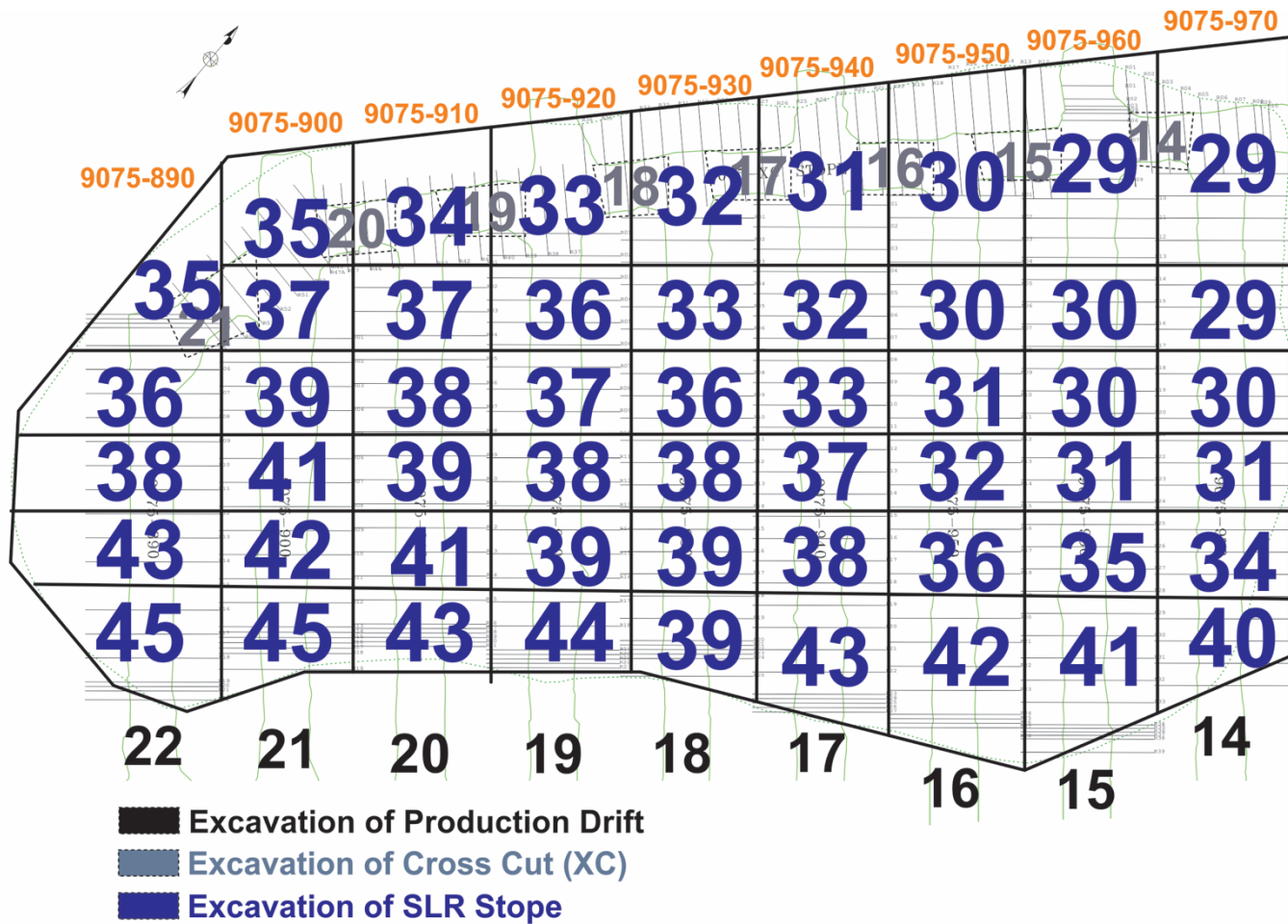


Figure 3.34 Sequence of mining and simulation steps for mine level S9075 of the A154 South pipe (using SLR)

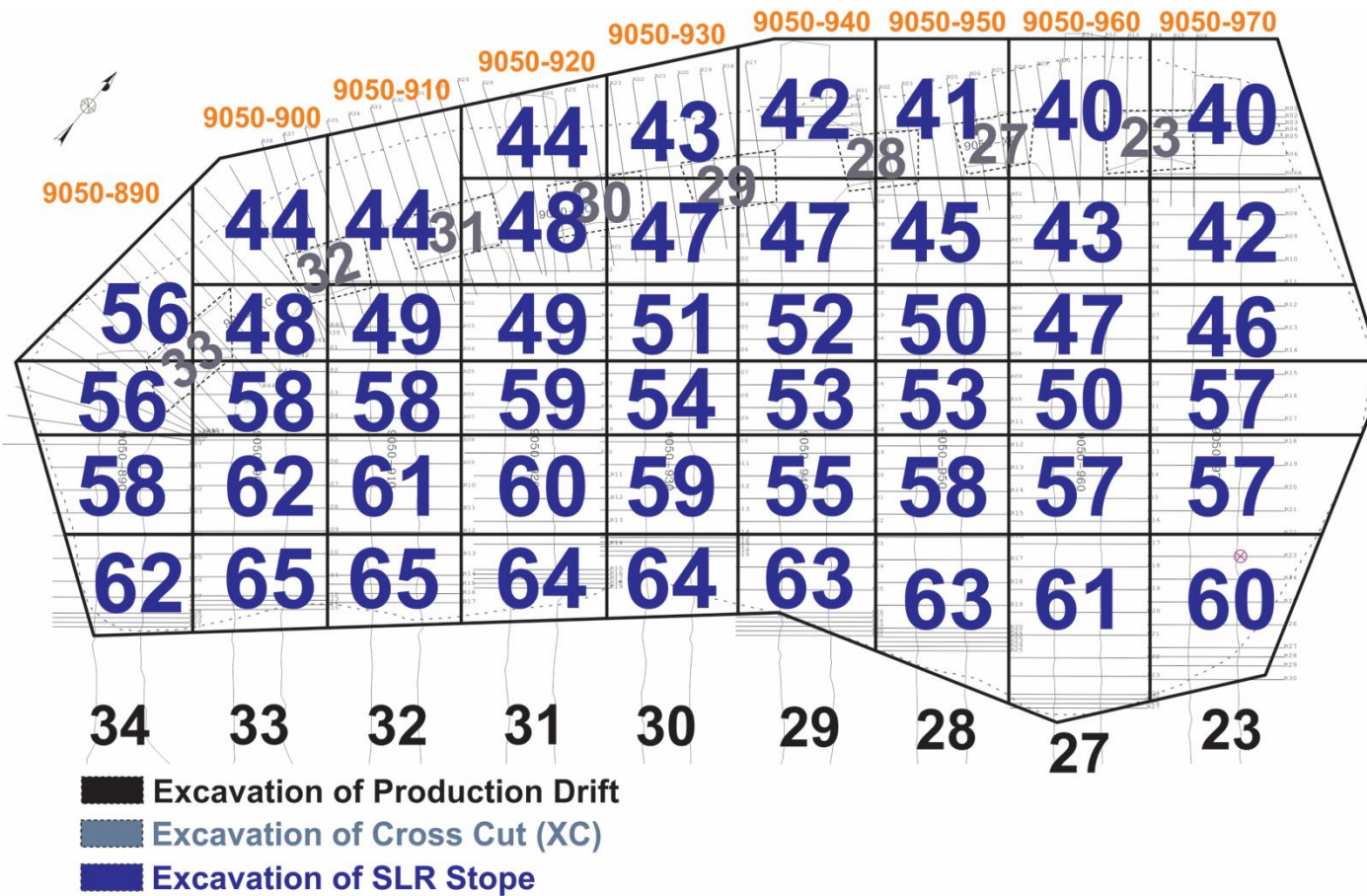


Figure 3.35 Sequence of mining and simulation steps for mine level S9050 of the A154 South pipe (using SLR)

### 3.4.6 Running the Model

The Hungabee supercomputer located at University of Alberta was used to run the developed FE model. Access to this high performance computing resource was provided by WestGrid and Compute/Calcul Canada. The computer specification and calculation time are presented in table 3.10.

**Table 3.10** Cost and Time of Calculations

|  |         |
|--|---------|
| <b>CPUs (Cores)</b>                            | 48      |
| <b>RAM per core (GB)</b>                       | 16.380  |
| <b>RAM in Total (GB)</b>                       | 786.240 |
| <b>Size of Output File (GB) (Just the ODB)</b> | 730     |
| <b>First Iteration Time (Min.)</b>             | 22      |

### 3.5 Summary and conclusion

In this chapter, the main objective was to develop an integrated engineering methodology to estimate the in-situ and mining-induced stress regimes in the host rock and orebody using the FE analysis method. The methodology utilized the commercially available FE code called Abaqus.

A case study of Diavik Diamond Mine was used to illustrate the estimation procedure and to implement the proposed methodology. Five rock types of Kimberlite samples were collected from the mine site to estimate their elastoplastic strength properties in the laboratory. Subsequently, a methodology has been proposed to obtain the modeling parameters for the rock mass strength based on the laboratory test results.

A full realistic 3D elastoplastic FE model of the mine has been constructed. This FE analysis model will be used to determine the in-situ and mining-induced stress regime at the case study mine.

The results of this analysis will be presented in the subsequent chapters focusing on the direct products of the mining-induced stress. These important products include: (i) mining-induced rockbursts (chapter 4); (ii) mining-induced surface subsidence (chapter 5); and (iii) yielding and relaxation zones around the excavated stopes (chapter 6). The results of the developed FE model are verified and validated in chapter 7, using actual ground movement data from the field.

## **CHAPTER 4: EVALUATION OF MINING-INDUCED ENERGY AND ROCKBURST PREDICTION USING THE FINITE ELEMENT ANALYSIS MODEL**

*Rockburst is an instantaneous and violent failure of rock which occurs when a volume of rock is strained beyond its elastic limit. It poses a serious threat to the safety of underground personnel. In this chapter, a review of current state-of-the-art methods of rockburst prediction is presented; then, a methodology is proposed to evaluate the extent and magnitude of the mining-induced strain energy and its accumulation in a rock mass to predict the rockburst potentials in an underground mine.*

## 4.1 Introduction

Rockburst is an instantaneous and violent failure of rock which occurs when a volume of rock is strained beyond its elastic limit. According to the Mine Safety and Health Administration (1984), a rockburst can be defined as “a sudden and violent failure of a large volume of overstressed rock, resulting in the instantaneous release of large amounts of accumulated energy”.

Some researchers (Ortlepp and Stacy, 1994; Ortlepp, 1997) classified rockburst into five categories: (i) strainburst; (ii) buckling; (iii) face crush or pillar burst; (iv) shear rupture; and (v) fault-slip burst. However, other researchers (Blake and Hedley, 2009; Kaiser and Cai, 2012; Mazaire and Konicek 2015) group buckling into the strainburst type of rockburst and consider shear ruptures as fault-slip rockbursts. In general, rockbursts are classified to three main groups: (i) strainburst; (ii) pillar burst; and (iii) fault-slip burst (figure 4.1).

Strainbursts are the most common rockburst type and are caused by local high-stress concentrations at the edge of underground openings. According to Kaiser and Cai (2012), from a loading point of view, two conditions must be met in order for a strainburst to occur: (i) first, in the skin of the excavation, a concentration of the tangential stress (the maximum principal stress) must exist; and (ii) second, the stiffness of the loading system must be soft. If the loading system is softer than the pillar stiffness, the rock fails in a violent manner.

Pillar bursts occur when the mining-induced stress on a pillar exceeds its strength. The main characteristic of a pillar burst is a violent failure in the pillar core which can even cause the complete collapse of the pillar. Consequently, when the pillar fails, a large amount of strain energy stored in the rock mass will be released violently.

Finally, a fault-slip burst occurs when the mining-induced shear stress along a geological structure exceeds the normal stress acting on the structure. In some cases, the reduction of the normal stress acting on a pre-existing fault, as a result of nearby stoping, can cause a fault-slip burst.

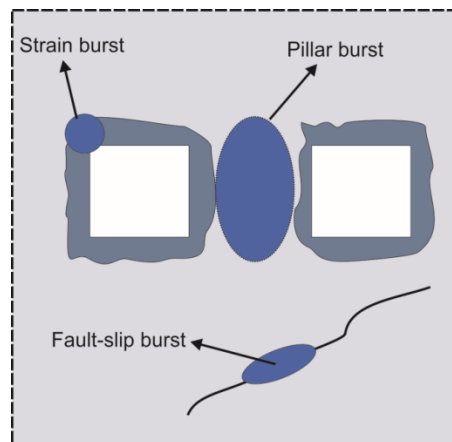


**Figure 4.1** Schematic representation of rockburst potentials (after Castro et al., 2012)

According to the studies carried out by Park (1995), Wang and Park (2001), Kwasneiwski and Wang (1999) and Miao et al. (2016), the occurrence of rockburst depends on two main factors: (i) the property of the rock mass in storing the strain energy; and (ii) the environment for creating and storing high stress and strain energy in the rock system. This means for a rockburst to occur, the rock must have the ability to store a considerable amount of strain energy which could be released violently at failure and there must be an environment for stress concentration and energy accumulation (Wang and Park, 2001). Examples of environmental factors include in-situ stress state and loading system stiffness, which is governed by the geometry of underground openings (for example, stope and pillar dimensions and spans), and mining sequence.

In this chapter, a review of current state-of-the-art methods for rockburst prediction is presented. Then, a methodology is proposed to assess the extent and magnitude of the strain energy distribution and its accumulation in a rock mass to predict the potential mining-induced rockbursts.

## 4.2 Review of rockburst prediction criteria

### 4.2.1 Strain energy storage index

In the UCS test, a rock specimen deforms elastically and plastically. In the meantime, it stores certain amounts of strain energy. Studies have shown that if the load is removed from the rock specimen prior to its peak strength

(approximately 70 to 80% of its UCS), the elastic deformation is reversible, while, as expected, the plastic deformation is permanent (Kidybiski, 1981; Kwasniewski et al., 1994). This will generate a hysteresis loop as shown in figure 4.2. Using this hysteresis loop, the energy accumulation in the rock specimens can be examined and quantified.

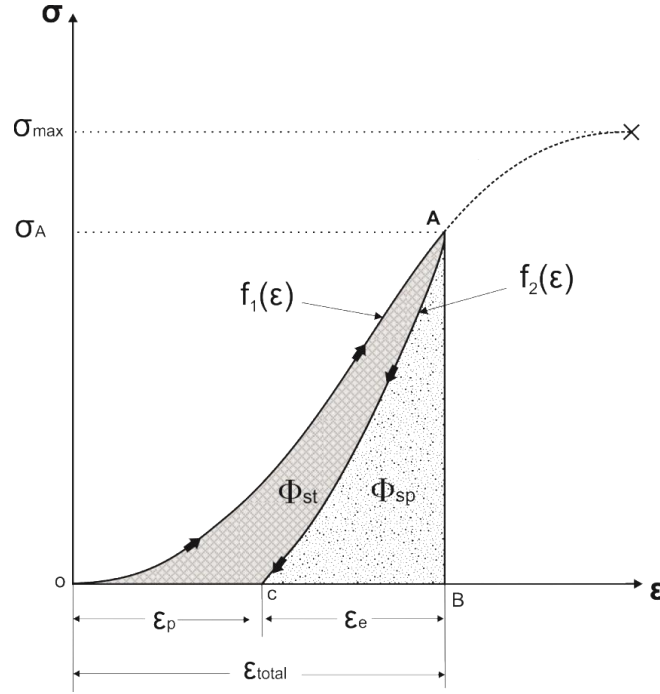


**Figure 4.2** Typical UCS hysteresis looping test curve (after Kwasniewski et al., 1994)

From figure 4.2,  $\phi_{st}$  is dissipated energy in creation of the plastic deformation and can be calculated using equation (4.1).  $\phi_{sp}$  is the elastic energy stored in the rock through loading upon to  $\sigma_A$  (70 to 80% of the UCS) and unloading, and can be calculated using equation (4.3).  $\sigma_c$  is the maximum strength of the rock under the UCS test. Referring to figure 4.2:

$$\phi_{st} = \phi_C - \phi_{sp} \quad (4.1)$$

where

$$\phi_C = \int_0^{\epsilon_{total}} f_1(\epsilon) d\epsilon \quad (4.2)$$

$$\phi_{sp} = \int_{\epsilon_p}^{\epsilon_{total}} f_2(\epsilon) d\epsilon \quad (4.3)$$

According to Kwasniewski et al. (1994) the ratio of elastic energy to dissipated energy ( $F$ ) can be used as an index of strain energy storage in the rock under compression.

$$F = \frac{\phi_{sp}}{\phi_{st}} \quad (4.4)$$

#### 4.2.2 Elastic strain energy density criterion

The stored elastic strain energy per unit volume of the rock is called the elastic strain energy density (SED). The elastic SED is an important factor to identify the potential for rockburst phenomenon in an underground mine (Jaeger et al., 2008).

For a rock specimen under the UCS test, using the principle of conservation of energy and the linear elasticity theory, the storage elastic SED can be calculated using equation (4.5).

$$SED = \frac{\sigma_c^2}{2E_s} \quad (4.5)$$

where  $\sigma_c$  is the UCS and  $E$  is the Young's modulus in the unloading curve.

According to the study by Miao et al. (2016), based on the value of the SED, the rockburst intensity in a rock mass can be classified into four groups. The result of this rating system is presented in table 4.1.

**Table 4.1** Rockburst hazard rating system proposed by Miao et al. (2016)

| <b><i>SED</i> (kJ / m<sup>3</sup>)</b> | <b>Rockburst Hazard</b> |
|--|-------------------------|
| $SED < 40$                             | Low                     |
| $40 \leq SED < 100$                    | Moderate                |
| $100 \leq SED < 200$                   | Strong                  |
| $SED \geq 200$                         | Extra-Strong            |

### 4.2.3 Rock brittleness coefficient

Rock brittleness can be assessed based on the ratio of UCS to tensile strength of a rock specimen. This ratio is called the rock brittleness coefficient ( $B$ ) and can be estimated using equation (4.6).

$$B = \frac{\sigma_c}{\sigma_T} \quad (4.6)$$

where  $\sigma_c$  is the UCS of the rock and  $\sigma_t$  is the tensile strength of the rock.

Based on the experimental and in-situ investigations done by Qio and in 1998 (as reported in Cai, 2015) the rockburst tendency can be estimated using  $B$  as presented in table 4.2.

**Table 4.2** Rockburst tendency prediction using the rock brittleness coefficient

| Rock brittleness coefficient ( $B$ ) | Rockburst tendency |
|--------------------------------------|--------------------|
| $B > 40$                             | No rockburst       |
| $26.7 < B \leq 40$                   | Weak               |
| $14.5 < B \leq 26.7$                 | Strong             |
| $B \leq 14.5$                        | Violent            |

It should be considered that both  $B$  and the storage elastic SED criterion only assess the tendency of the rockburst based on the strength property of the rock. However, as discussed in the introduction of this chapter, in the prediction of rockbursts, there are two factors that must be considered: the strength properties of the rock and the environment. The two prediction methods presented below consider these two factors simultaneously.

### 4.2.4 Criterion of tangential stress

This method considers the strength property of the rock and induced tangential stress (environmental factor) in the rock mass. Therefore, both conditions required for a rockburst to occur can be evaluated. The tangential stress ( $T_s$ ) criterion can be estimated using equation (4.7) below:

$$T_s = \frac{\sigma_\theta}{\sigma_c} \quad (4.7)$$

where,  $\sigma_c$  is the UCS of the rock and  $\sigma_\theta$  is the tangential stress around the underground opening (i.e. stopes, drifts, etc.). According to Wang and Park (2001), the rockburst tendency can be evaluated using  $T_s$  criterion as presented in table 4.3.

**Table 4.3** Rockburst tendency prediction using the tangential stress criterion (Wang and Park, 2001)

| Tangential Stress Criterion ( $T_s$ ) | Rockburst tendency |
|---------------------------------------|--------------------|
| $T_s < 0.3$                           | No rockburst       |
| $0.3 \leq T_s < 0.5$                  | Weak               |
| $0.5 \leq T_s < 0.7$                  | Strong             |
| $T_s \geq 0.7$                        | Violent            |

#### 4.2.5 Energy-based burst potential index

Mitri et al. (1999) developed an energy-based burst potential index (BPI). The basic assumption in this method is that violent failure (rockburst) will occur when the energy stored in the rock mass exceeds the critical energy value ( $e_c$ ). The  $e_c$  is the maximum capacity of the rock to store energy, and it can be obtained from the UCS test or from the UCS hysteresis looping test curve with equation (4.5). Therefore, the BPI can be defined as:

$$BPI = \frac{ESR}{e_c} \times 100\% \quad (4.8)$$

where  $ESR$  is the energy storage density (also called the energy storage rate) ( $\text{kJ/m}^3$ ) in the rock mass and  $e_c$  is the critical (maximum) SED ( $\text{kJ/m}^3$ ) of the rock. The larger the value of the BPI, the higher the probability of a rockburst occurring. The value of  $e_c$  can be calculated either from equation (4.5) or it can be approximated using the following equation:

$$e_c = \frac{\sigma_c^2}{E} \quad (4.9)$$

where  $\sigma_c$  is the UCS and  $E$  is the Young's modulus in the UCS test. It should be noted that estimating  $e_c$  using equation (4.9) is a conservative approach, because the energy dissipated by fracturing and plastic deformations is neglected. However, in the absence of the detailed UCS hysteresis looping stress-strain curve, it is a close approximation.

### 4.3 Methodology

To analyze the potential for rockbursts in a mine, two main parameters must be evaluated:

- 1) The rock mass strength properties to store and accumulate the strain energy.
- 2) The environment required to induce zones of high concentration stresses. In addition, loading system characteristics, such as stiffness of the loading system, has an important role on the type of failure.

In this research, a methodology is proposed combining the FE analysis model and conventional criteria to evaluate the potential rockburst in an underground mine. The flowchart of the proposed methodology is shown in figure 4.3. The main objective of this methodology is to analyze the two abovementioned parameters simultaneously to effectively predict possible rockburst zones in an underground mine.

A case study of Diavik Diamond Mine has been used to implement the proposed methodology. Site investigations have been conducted by traveling several times to the mine site and gathering essential data such as in-situ stress states, mining methods, the geometry of underground openings, mining and stoping sequences and rock mass classification. Kimberlite samples from both pipes have been collected for rock mechanics laboratory tests (UCS,  $E$ ,  $\nu$ ,  $\sigma_t$ ,  $C$  and  $\phi$ ). Finally, based on the results of the numerical model, two rockburst criteria ( $T_s$  and BPI) have been used to assess the rockburst tendency in the understudy domain.

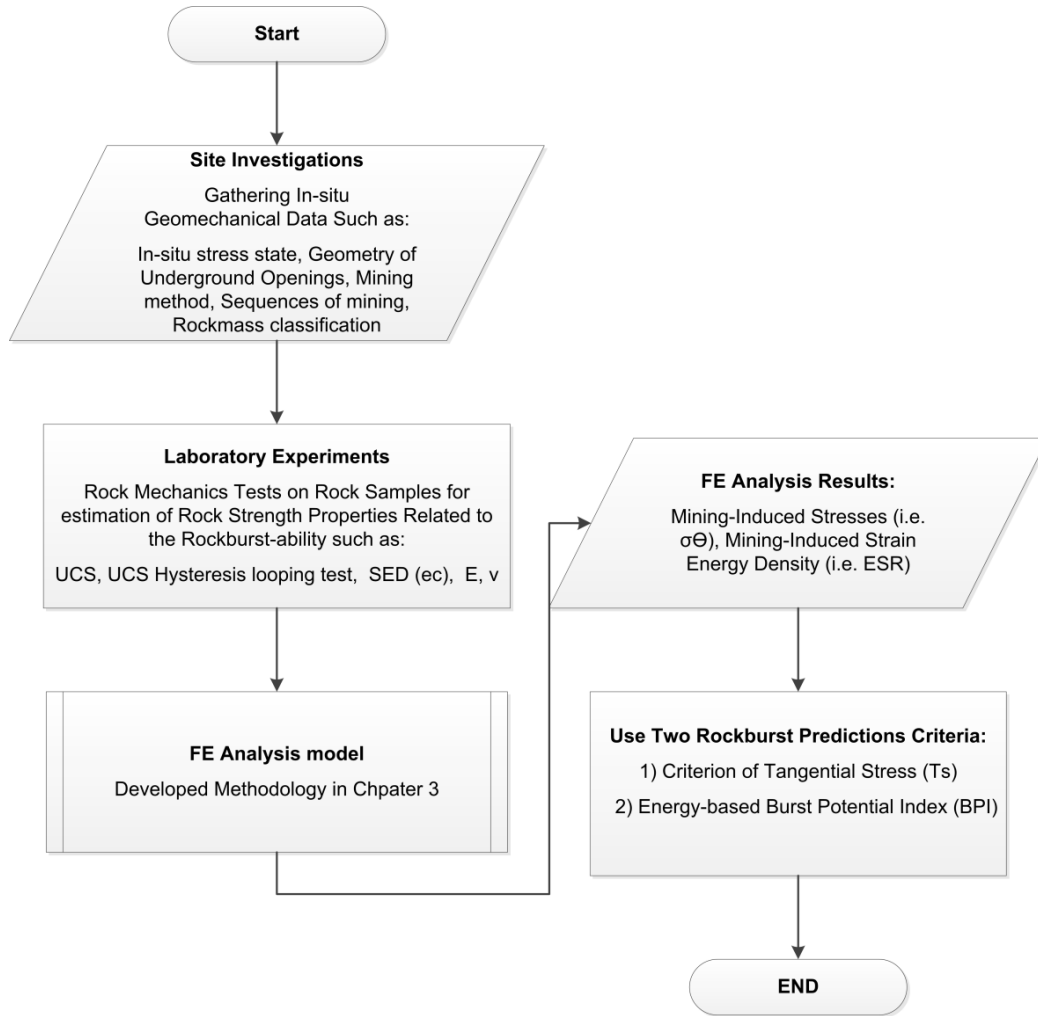


**Figure 4.3** Proposed methodology for rockburst prediction

Three major domains have been studied: (i) the host rock (granite); (ii) the orebody (Kimberlite); and (iii) the sill pillar at the A154 North Kimberlite pipe. The results of the FE analysis are presented in the following sections.

#### 4.4 Results and discussions

A full 3D elastoplastic FE model was constructed as presented in chapter 3. Using the proposed methodology in section 4.3, the potential for rockbursts were evaluated in the following domains:

- Granite (host rock): Three main zones were identified and evaluated.

- Kimberlite (orebody): Some rockburst potentials were identified in the A154 North pipe in Mining Block B between mining levels N9050 and N9150.
- Sill pillar in the A154 North pipe located between mining levels N9150 and N9175.

#### 4.4.1 Rockburst potentials in granite

In order to evaluate the rockburst potentials in the host rock (granite), it is necessary to estimate the  $e_c$  for this rock type. Since no UCS hysteresis looping test data were available, equation (4.9) was used to estimate this value. The result of the estimation is presented in table 4.4. The UCS and the Young's modulus for the granite are based on values reported in the literature and the geomechanical reports available from Diavik Diamond Mine (Yip and Thomson, 2015).

**Table 4.4** Estimation of the critical strain energy for granite

| UCS (MPa) | E (GPa) | $e_c$ (kJ/m <sup>3</sup> ) |
|-----------|---------|----------------------------|
| 130       | 21      | 402.38                     |

The value of the energy storage density (ESR) is computed using the developed FE model. Based on the calculated ESR and using equation (4.8), the BPI was estimated for each identified zone. In addition, in each step of the FE analysis, mining-induced stresses and displacements were computed. Therefore,  $T_s$  was used to evaluate the rockburst tendency in the understudy domain. Based on the results of the FE model, the rockburst potentials were identified in three main zones: Zone 1, 2 and 3. All these zones are located at the bottom of the pit, in the granite-Kimberlite contact at the A154 South pipe (figure 4.4).

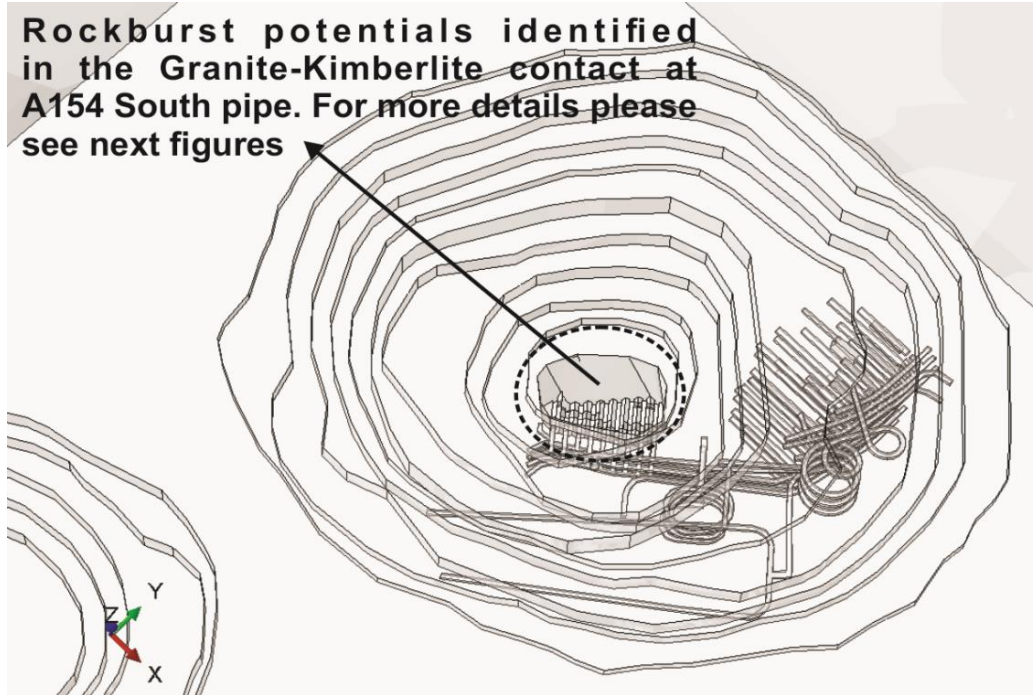


**Figure 4.4** Identified zones of rockburst potentials in the granite-Kimberlite contact at the A154 South pipe

#### 4.4.1.1. Potential rockbursting in Zone 1

For this zone, four monitoring nodes, shown in figure 4.5, were defined to analyze the development of the ESR throughout the simulation steps. The depth of each monitoring point from the surface and from the bottom of the pit are presented in table 4.5.

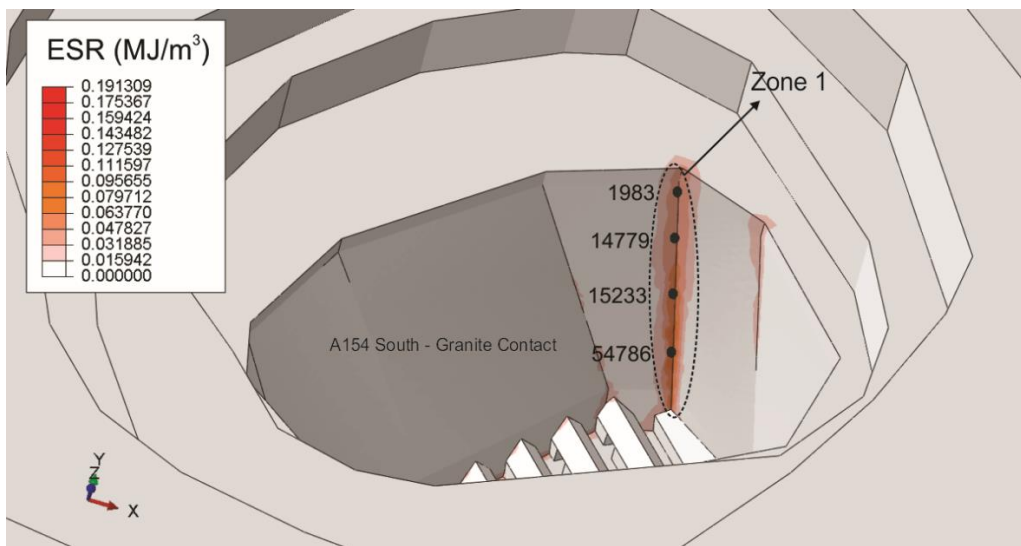


**Figure 4.5** Rockburst potential Zone 1 and monitored points

**Table 4.5** Depth of each monitoring point in Zone 1

| Monitoring Point No. | Depth from surface (m) | Depth from pit bottom (m) |
|----------------------|------------------------|---------------------------|
| 1983                 | 266                    | 6                         |
| 14779                | 288                    | 28                        |
| 15233                | 307                    | 47                        |
| 54786                | 329                    | 69                        |

The mining-induced ESR in each simulation step was computed, and the results are illustrated in figure 4.6. Based on the calculated ESR and using equation (4.8), the BPI was estimated for each monitoring point throughout the simulation steps and the results are presented in figure 4.7. The maximum induced tangential stress around underground openings was calculated using the FE model. Furthermore, the Tangential Stress Criterion ( $T_s$ ) was used to evaluate the rockburst tendency in Zone 1. The results are presented in figure 4.8.

Based on the results of the FE model, the type of potential rockburst in this zone will be strainburst.

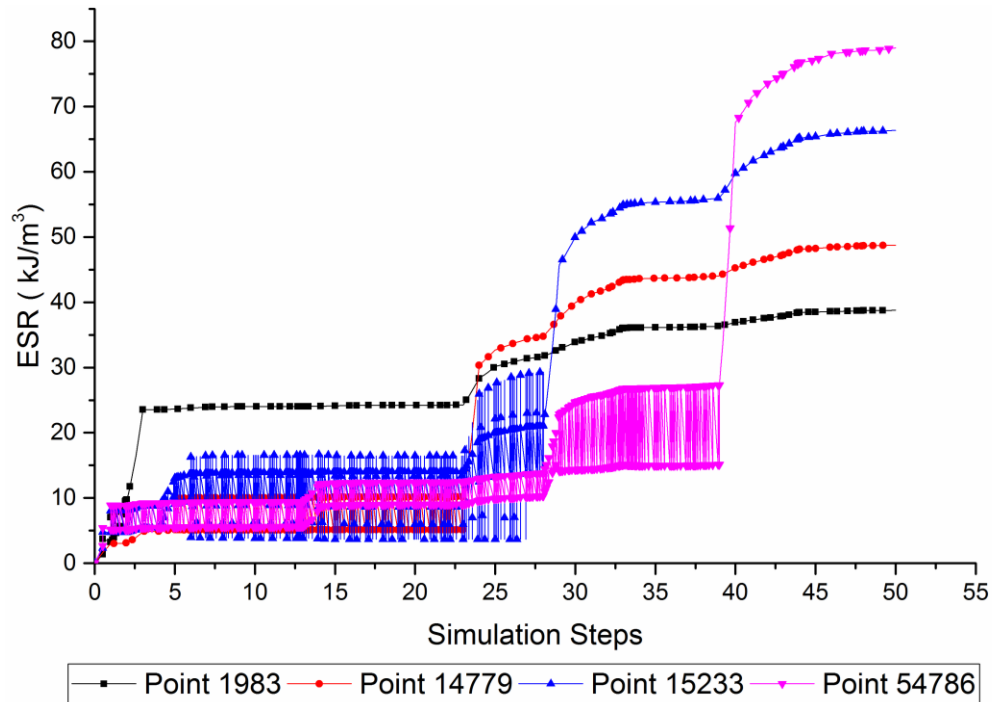


**Figure 4.6** Energy storage density at the monitoring points in Zone 1 throughout the simulation

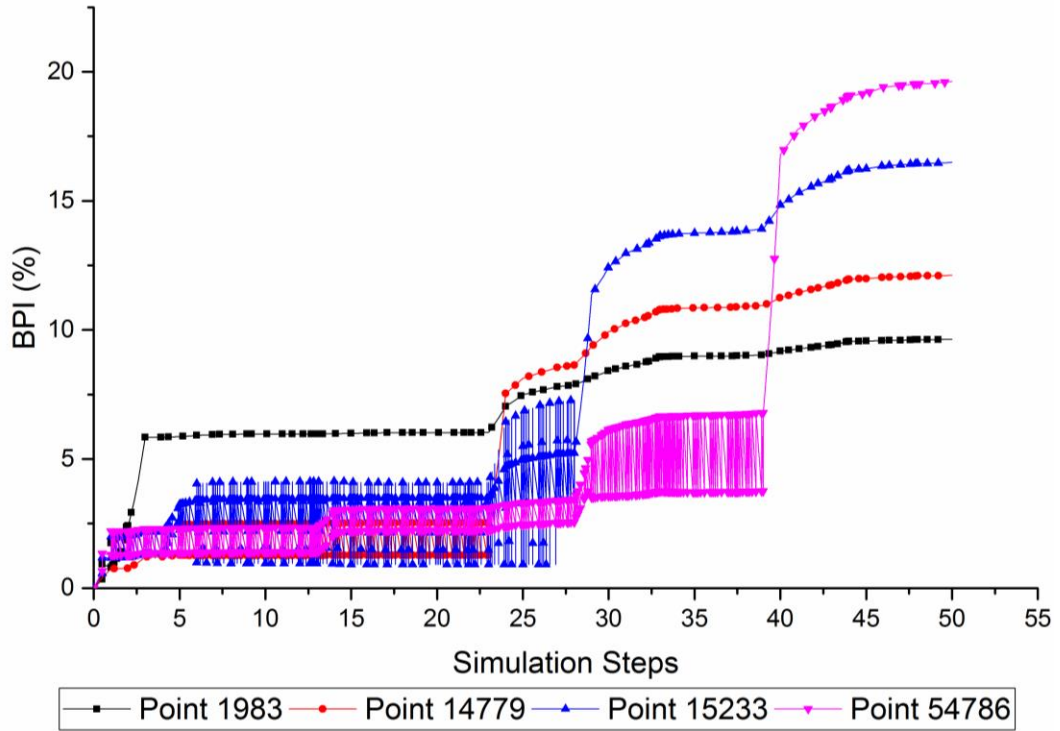


Figure 4.7 Burst potential index at the monitoring points at Zone 1 throughout the simulation steps

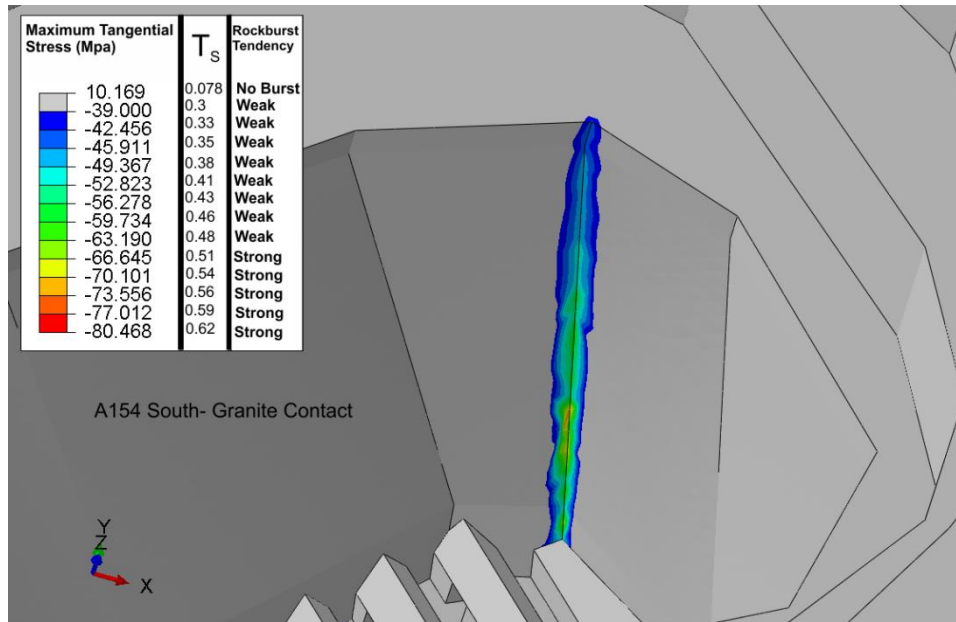
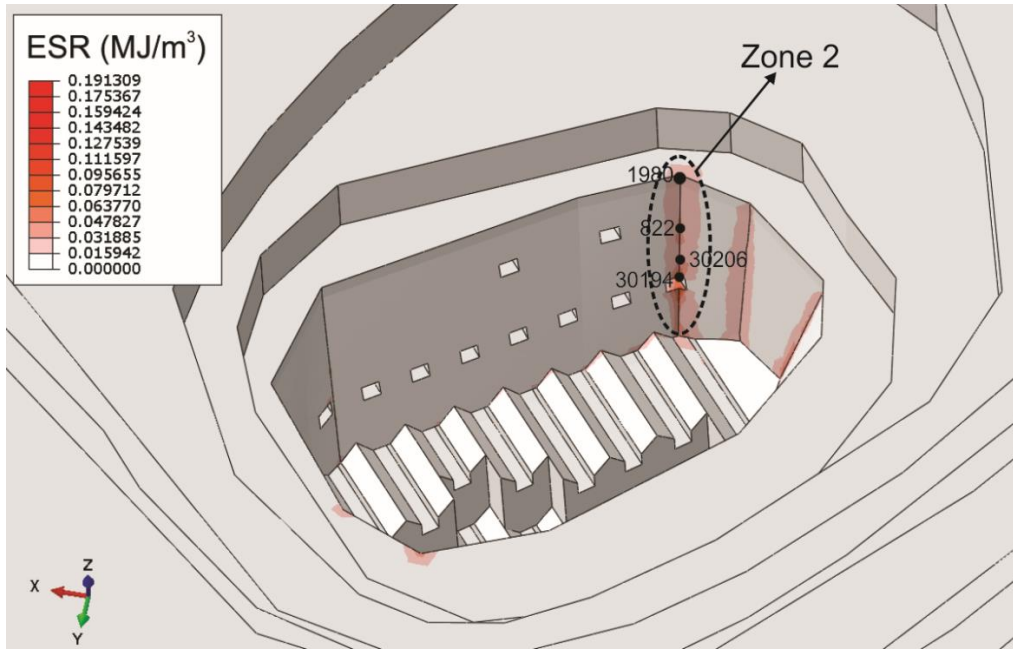


Figure 4.8 Rockburst tendency evaluation based on the tangential stress criterion

#### 4.4.1.2. Potential rockbursting in Zone 2

Four monitoring nodes (figure 4.9) were defined to analyze the development of the ESR throughout the simulation steps. The depth of each monitoring point from the surface and from the bottom of the pit are presented in table 4.6.



**Figure 4.9** Rockburst potential Zone 2 and monitored points

**Table 4.6** Depth of each monitoring point in Zone 2

| Monitoring Point No. | Depth from surface (m) | Depth bottom of the pit (m) |
|----------------------|------------------------|-----------------------------|
| 1980                 | 260                    | 0                           |
| 822                  | 284                    | 24                          |
| 30206                | 297                    | 37                          |
| 30194                | 304                    | 44                          |

The mining-induced ESR in each simulation step was computed, and the results are illustrated in figure 4.10. Based on the calculated ESR and using equation (4.8), the BPI was estimated for each monitoring point throughout the simulation, and the results are presented in figure 4.11.

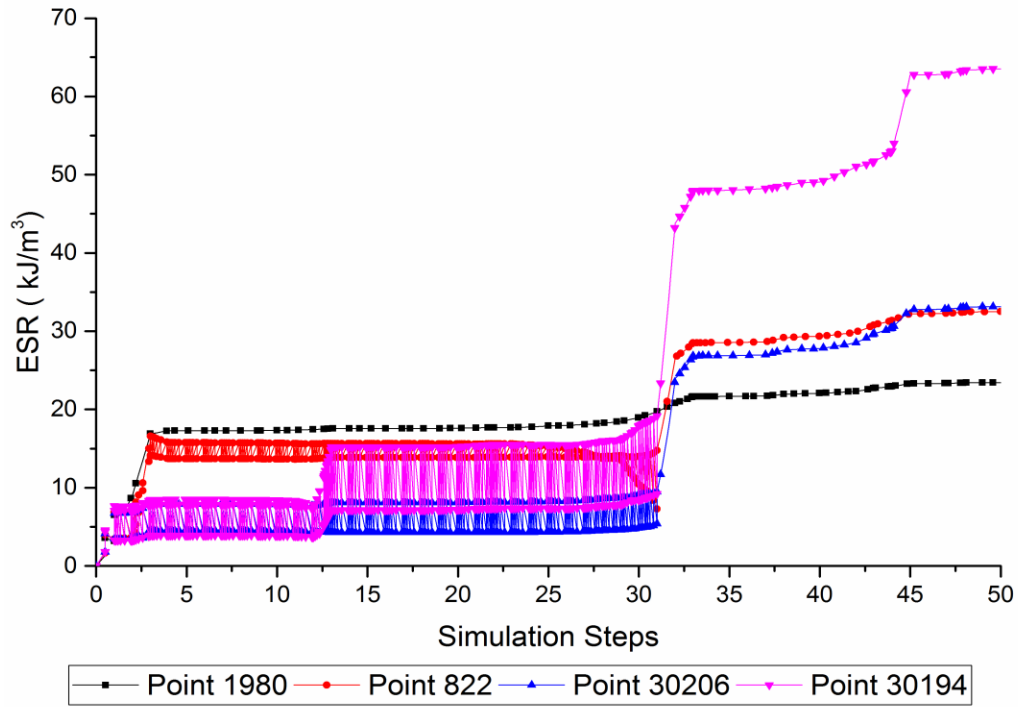


**Figure 4.10** Energy storage rate at the monitoring points in Zone 2 throughout the simulation

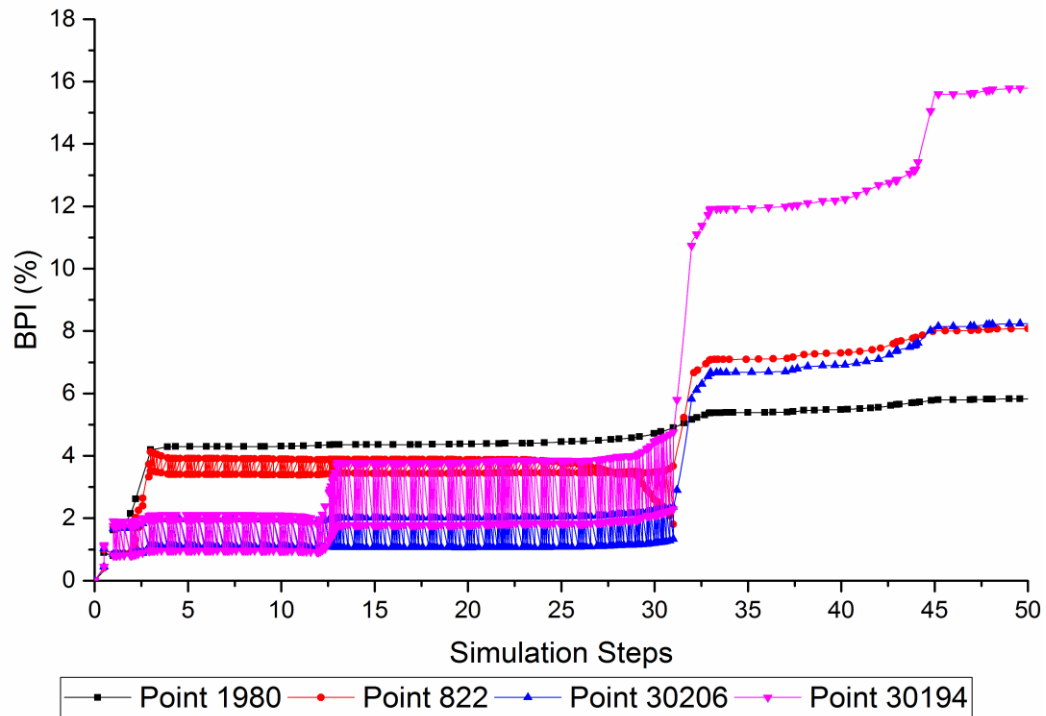


**Figure 4.11** Burst potential index at the monitoring points in Zone 1 throughout the simulation

The maximum induced tangential stress around underground openings was calculated using the FE model.  $T_s$  was used to evaluate the rockburst tendency in one 2, and the results are presented in figure 4.12.

Based on the results of the FE model, the type of potential rockburst in this zone will also be "Strainburst". As seen in figure 4.12, there is a weak to strong rockburst tendency on the back and even on the floor of the S9100-890 drifts.

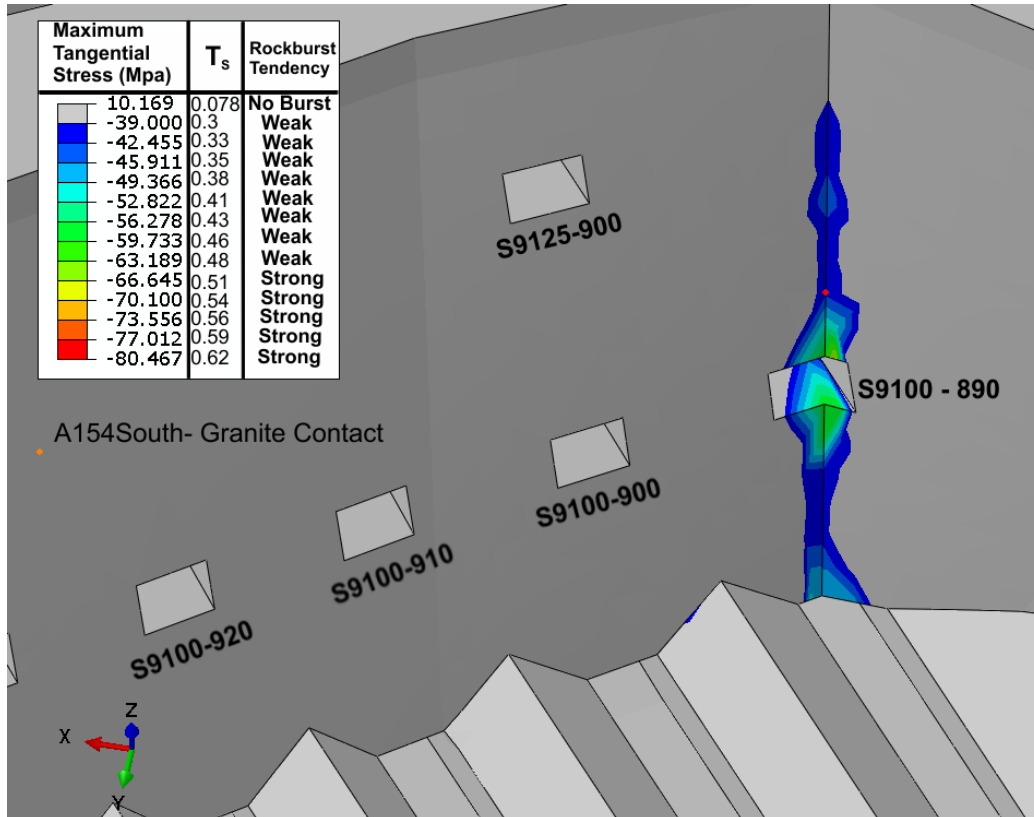


**Figure 4.12** Rockburst tendency evaluation based on the tangential stress criterion at the A154 South-granite contact in Zone 2

#### 4.4.1.3. Potential rockbursting in Zone 3

For this zone, only one monitoring node (figure 4.13) was defined to analyze the development of the ESR throughout the simulation. The depth of the monitored node from the surface is 318 m and from the bottom of the pit, 58 m.

The mining-induced ESR in each simulation step was computed, and the results are illustrated in figure 4.14. Based on the calculated ESR and using equation

(4.8), the BPI was estimated for each monitoring point throughout the simulation, and the results are presented in figure 4.15.

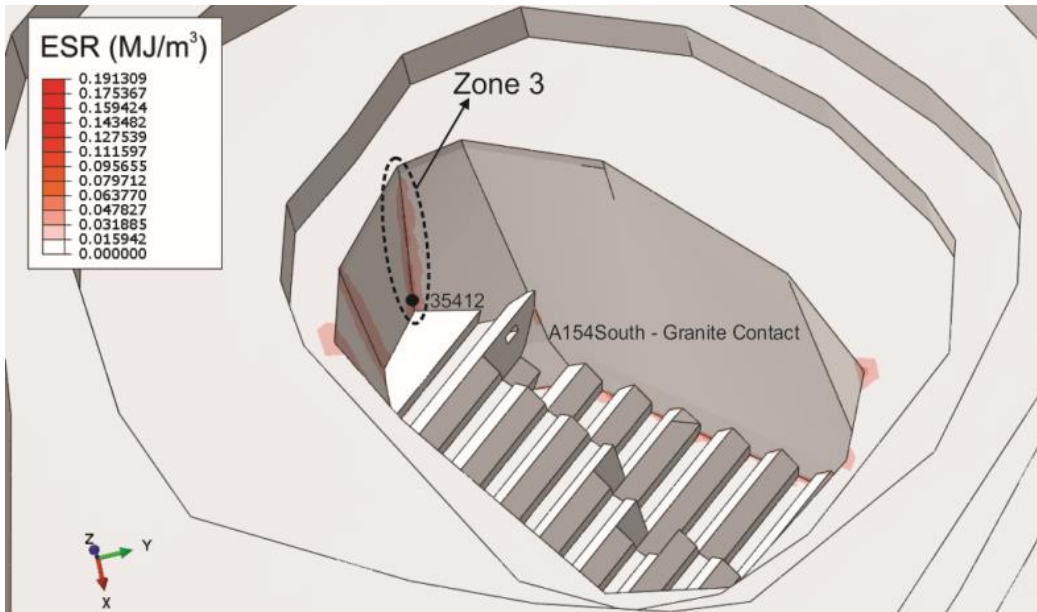


Figure 4.13 Rockburst potential in Zone 3 and monitored points

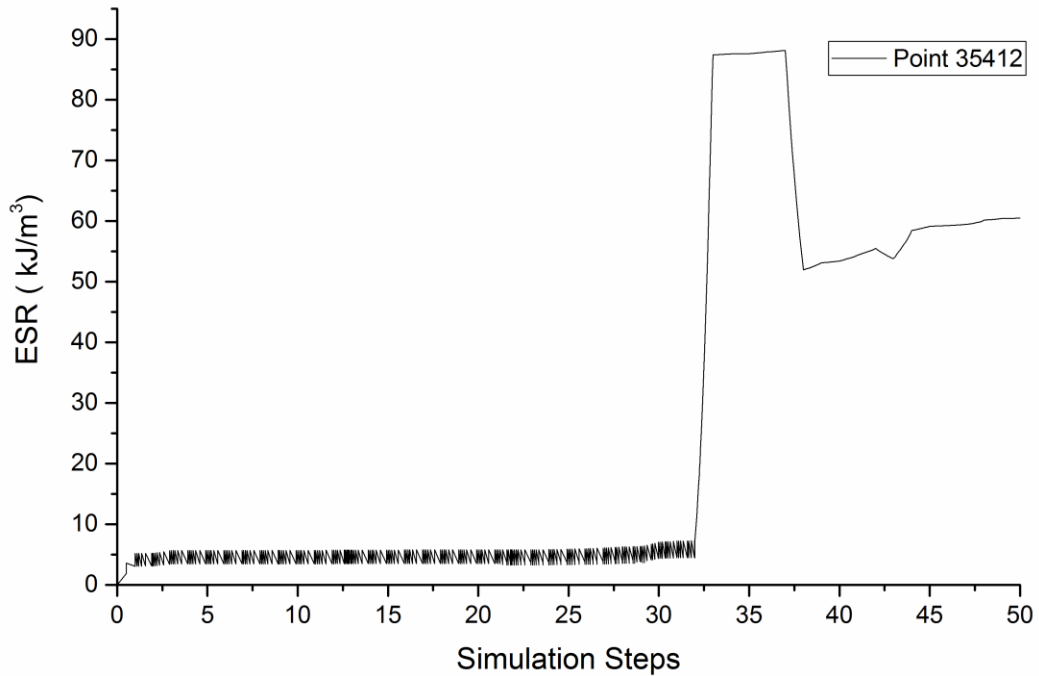
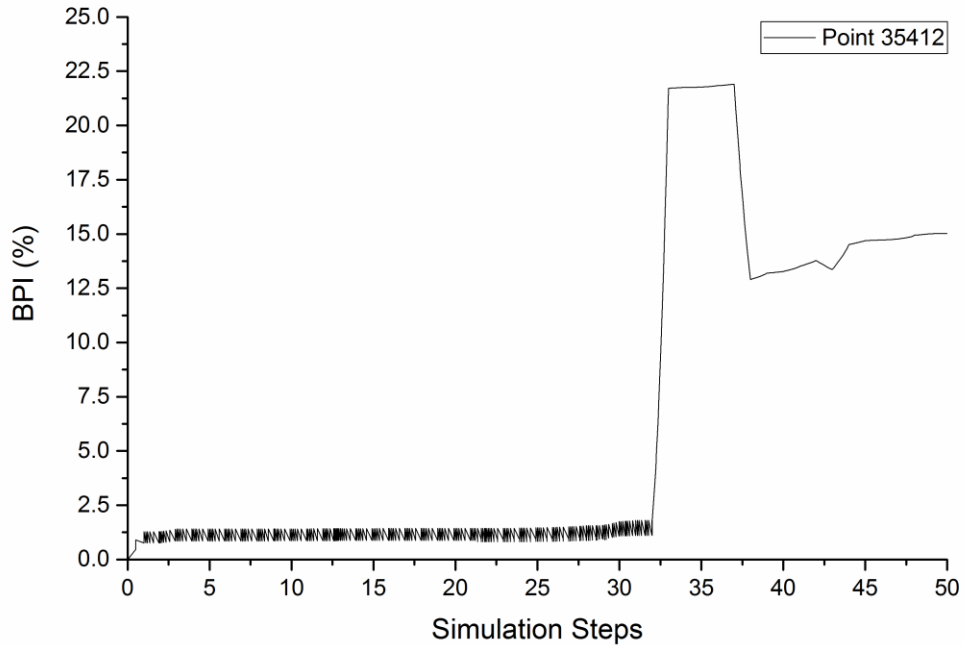
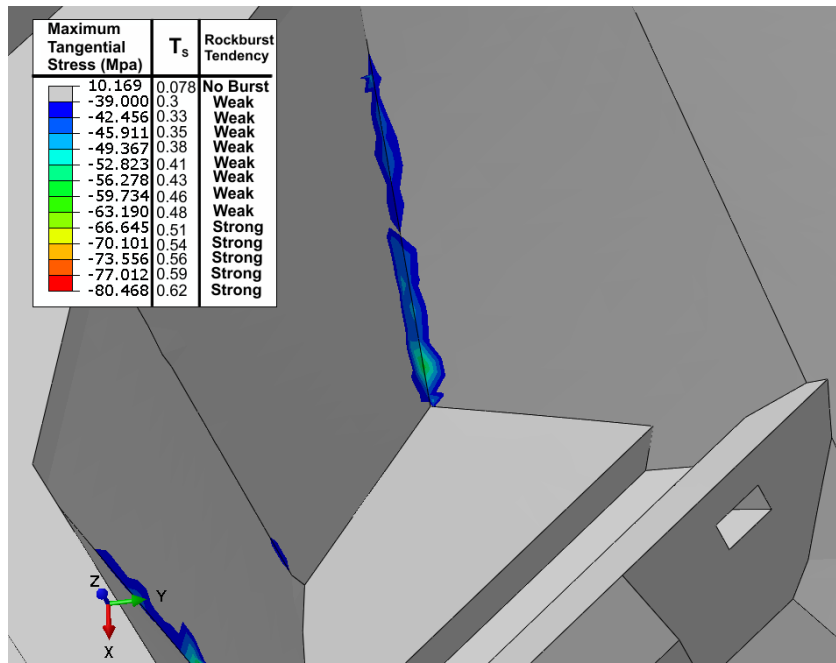


Figure 4.14 Energy storage rate at the monitoring points in Zone 3 throughout the simulation steps



**Figure 4.15** Burst potential index (BPI) in the monitoring point at zone 3

The maximum induced tangential stress around underground openings was calculated using the FE model.  $T_s$  was used to evaluate the rockburst tendency in Zone 3, and the results are presented in figure 4.16.



**Figure 4.16** Rockburst tendency evaluation based on the tangential stress criterion at the A154 South-granite contact in Zone 3

From figures 4.14 and 4.15, it can be concluded that after step 31 (excavation of the SLRS9100C890 mining block), conditions favorable for a strainburst are building up. There is a significant jump in the amount of the storage energy at this monitoring point.

#### 4.4.2 Potential rockbursting in the Kimberlite pipes

The values of the critical energy “ $e_c$  for both pipes were estimated using UCS hysteresis looping tests by Leveille (2015) and Leveille et al. (2016) at the University of Alberta Rock Mechanics Laboratory Facility (Table 4.7). Using the developed FE model, the ESR in both Kimberlite pipes were computed.

**Table 4.7** Average critical energy values for both Kimberlite pipes (from Leveille, 2015; Leveille et al., 2016)

| Kimberlite Pipe | Average Critical Energy Value<br>(kJ/m <sup>3</sup> ) |
|-----------------|---|
| A154 North      | 119.7   |
| A154 South      | 91.5  |

In addition, as presented in chapter 3, the UCS test was performed on Kimberlite samples from both pipes. The average values for both pipes are presented in table 4.8.

**Table 4.8** Average UCS values estimated from laboratory tests on Kimberlite samples

| Kimberlite Pipe | UCS (MPa) |
|-----------------|-----------|
| A154 North      | 79        |
| A154 South      | 66        |

The rockburst potentials are analyzed in two Kimberlite pipes: A154 North and A154 South. Like the granite domain, two rockburst criteria ( $T_s$  and BPI) were used to assess the rockburst tendency in both Kimberlite pipes. The results are presented in the following sections.

#### 4.4.2.1. Potential rockbursting in the A154 North Kimberlite pipe

According to the FE model results, the rockburst potential are identified in Mining Block B, located between mining levels N9050 and N9150. The results are illustrated in figure 4.17. It is predicted that the type of rockburst will be strainburst.

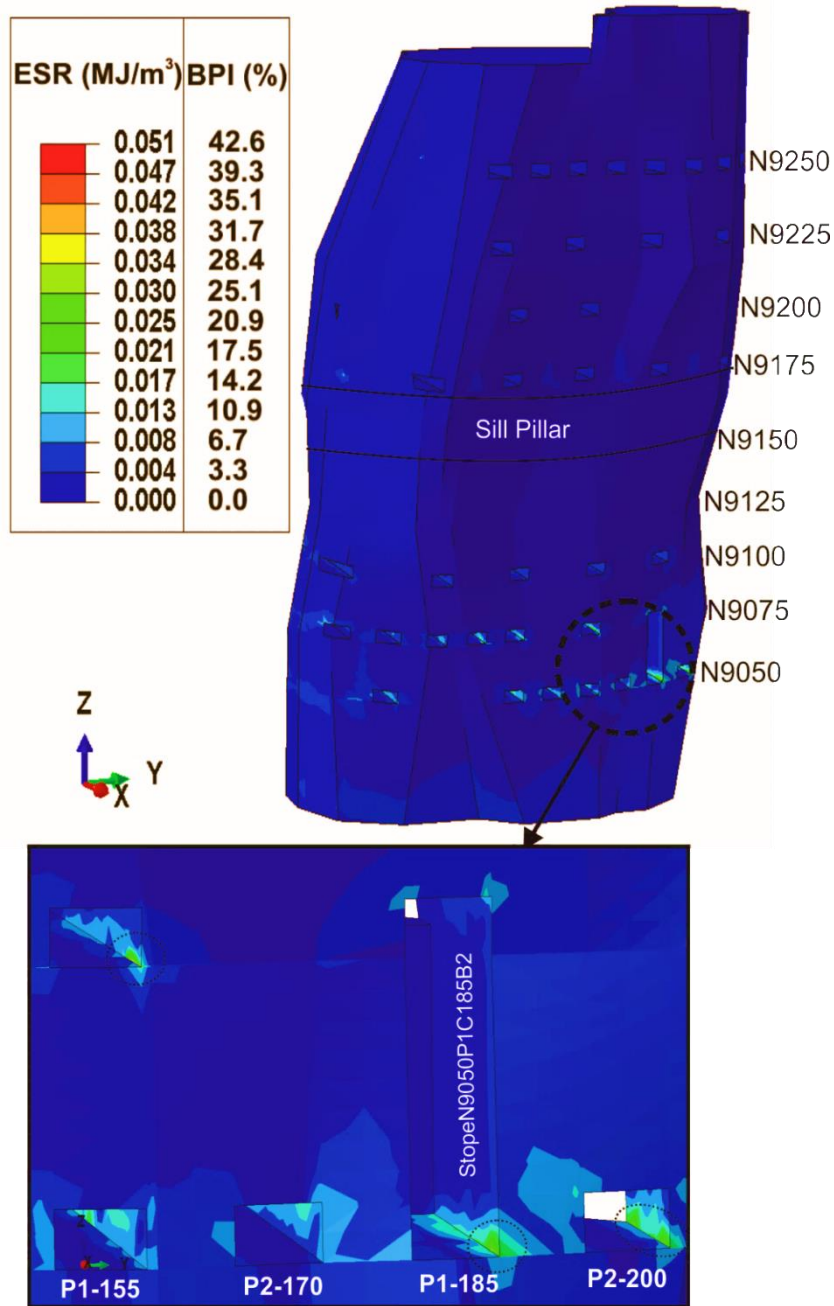


**Figure 4.17** Estimation of the burst potential index and energy storage density in the A154 North Kimberlite pipe

The maximum induced tangential stress distribution around the A154 North Kimberlite pipe was computed using the FE model.  $T_s$  was used to evaluate the rockburst tendency in this pipe, and the results are presented in figure 4.18.

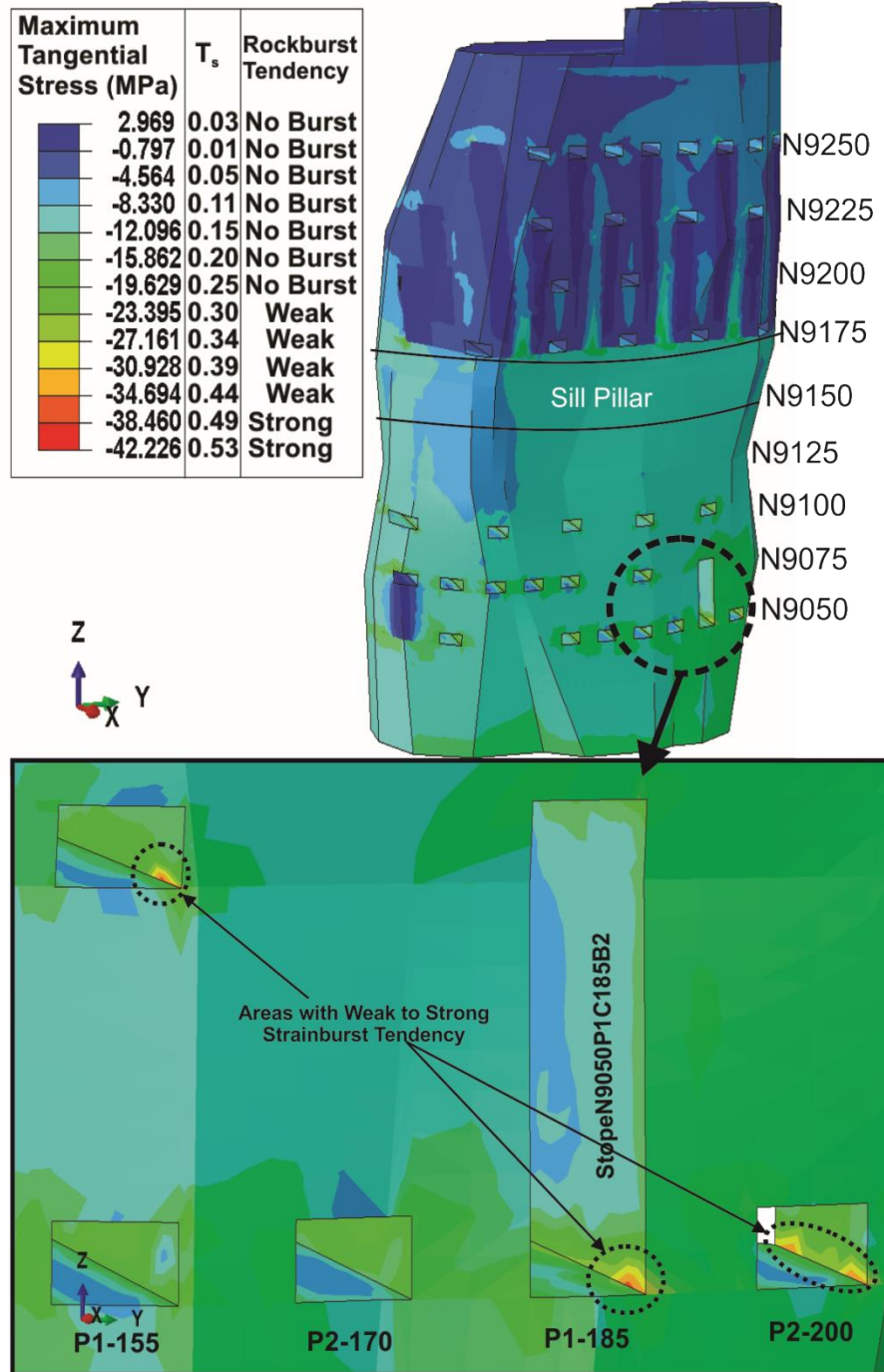


**Figure 4.18** Maximum tangential stress distribution and estimated rockburst tendency for the A154 North Kimberlite pipe

Based on the results illustrated in figure (4.17) and (4.18), there is no significant potential for pillar bursting throughout the North pipe. However, there is a clear linkage between mining depth and increasing the potential for strainbursts.

Both criteria agree that Mining Zone A, located between mining levels 9175 to 9290, have no rockburst tendency. However, as expected, this is not the case for Mining Zone B. As the mining advances to deeper depths, in-situ stresses increase; therefore, the potential for rockbursts also increases.

#### 4.4.2.2. Potential rockbursting in the A154 South Kimberlite pipe

Using the BPI, some potential rockbursts were identified in the Kimberlite-granite contact on the Kimberlite side (figure 4.19). However, as mentioned in chapter 3, the mining method in the A154 South pipe is SLR, which is a sublevel block-caving method. Therefore, these blocks will be excavated quickly from the lower levels.

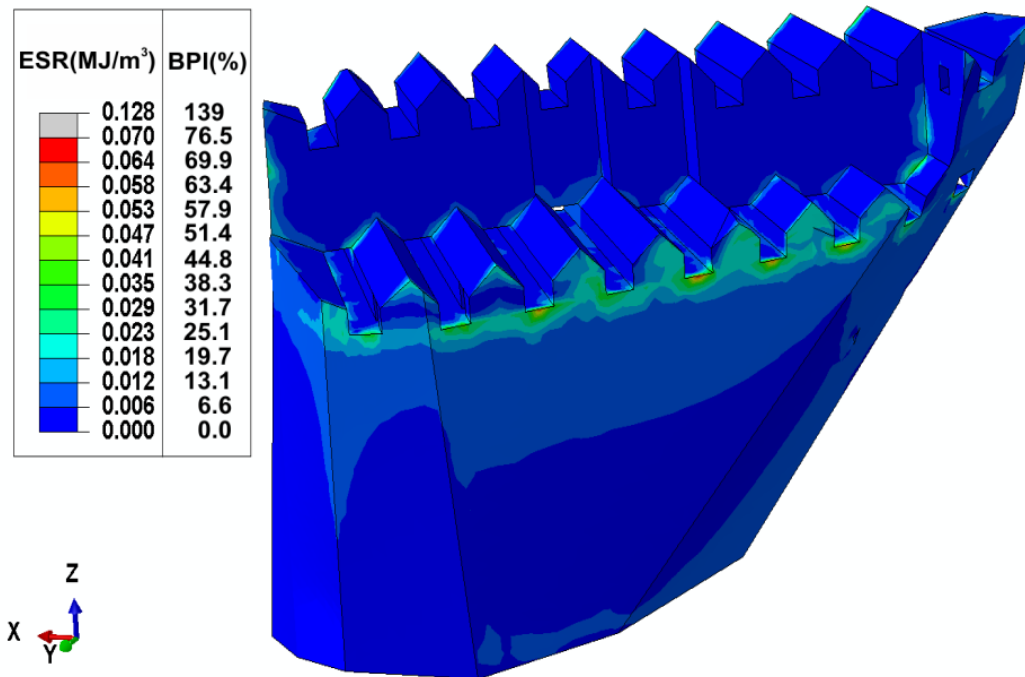


**Figure 4.19** Estimation of the burst potential index and energy storage density at the A154 South Kimberlite pipe

However, using  $T_s$ , some significant zones of potential rockburst were identified. In fact, according to this criterion, the rockburst tendency will be violent in these areas. The results are illustrated in figure 4.20 and will be verified in chapter 7.

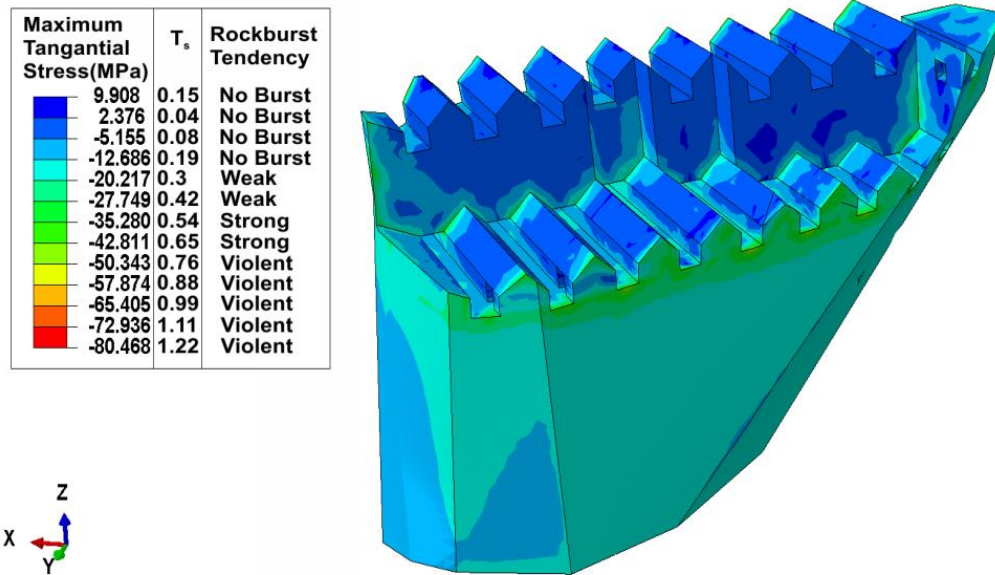


**Figure 4.20** Maximum tangential stress distribution and estimated rockburst tendency for the A154 South Kimberlite pipe

#### 4.4.3 Rockburst potentials in the sill pillar

As shown in figures 4.17 and 4.18, the sill pillar is in the A154 North Kimberlite pipe, located between mining levels N9150 and N9175. The ESR at the end of step 55 of the simulation is shown in figure 4.21. It should be noted that in step 55, mining at Block B has not reached the sill pillar yet; therefore, there is no significant mining-induced stress concentration in this pillar yet. However, zones under the influence of the mining-induced stresses from Mining Block A are clearly recognizable in figure 4.24.

To show the variation of the energy storage and BPI throughout the simulation, a circumferential path (shown in figure 4.21) is defined along the pillars' longitudinal axis. The results are shown in figures 4.22 and 4.23. Based on the FE analyses, the portion of the pillar located on the right side of the pillar normal axis, has more rockburst tendency.

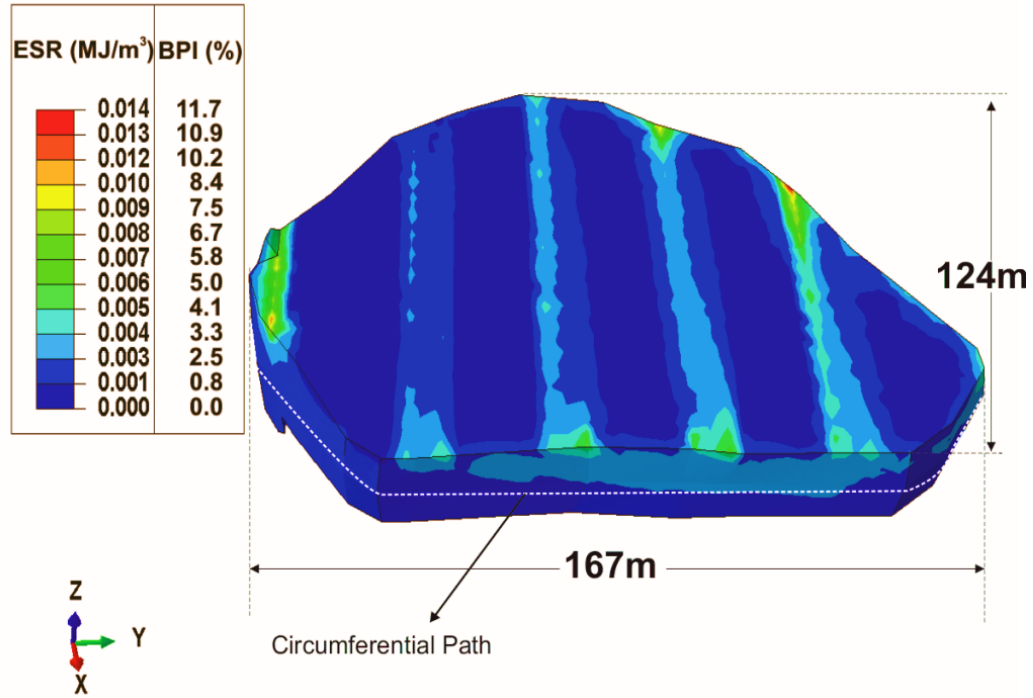


Figure 4.21 Estimation of the burst potential index and energy storage density in the sill pillar

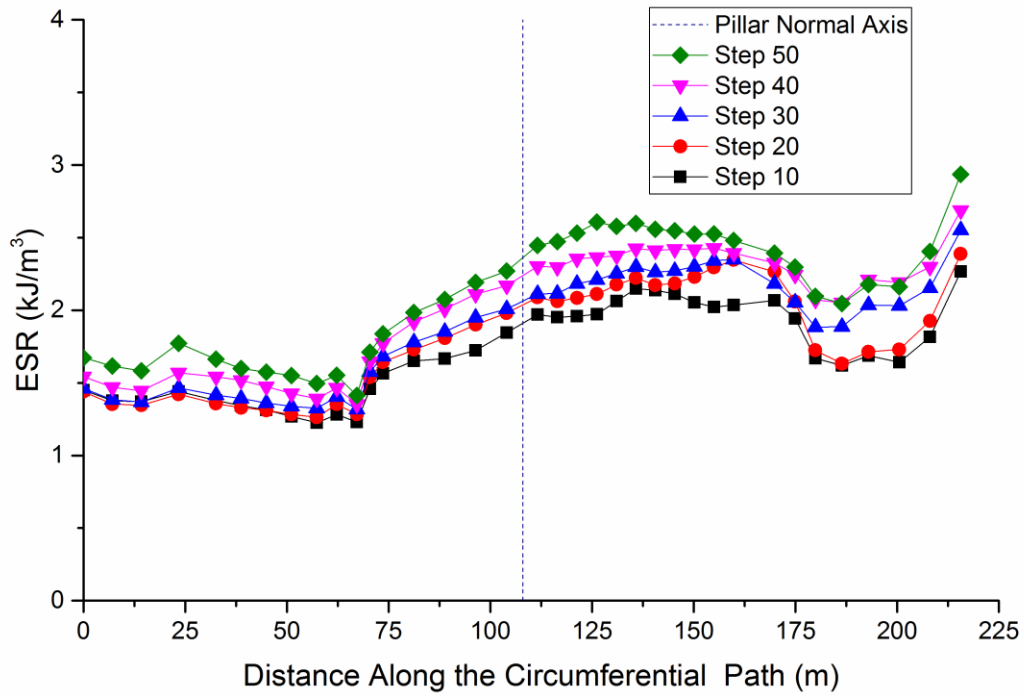
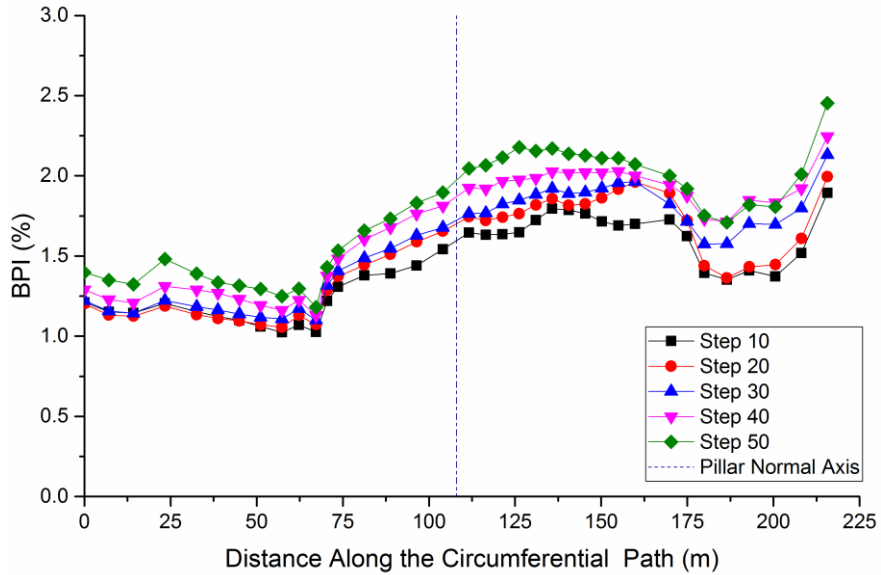
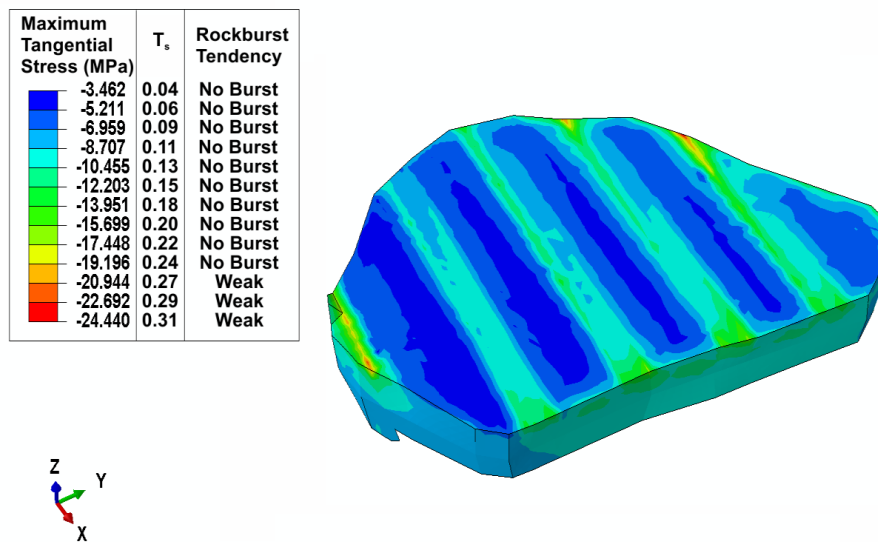


Figure 4.22 Variation of the energy storage rate along the circumferential path



**Figure 4.23** Variation of the burst potential index along the circumferential path

The maximum induced tangential stress distribution around the sill pillar was computed using the FE model.  $T_s$  is used to evaluate the rockburst tendency in this pillar, and the results are presented in figure 4.24. As can be seen, there is no significant rockburst tendency yet in this pillar. However, it should be considered that the results are based on Step 55 of the simulation. It is expected that the situation will change when mining in Block B reaches the lower level of the sill pillar (mining level N9150).



**Figure 4.24** Maximum tangential stress distribution and estimated rockburst tendency in the sill pillar

#### **4.5 Summary and conclusion**

The FE analysis model and the methodology developed in chapter 3 were used as the basis of a methodology, developed in this chapter, for predicting the rockburst tendency in an underground mine. Both conventional and numerical methods have been combined to estimate the rockburst potentials in a real case study mine.

The advantages of the proposed methodology presented in this chapter are as follows:

- It accounts for both mining-induced stresses (which is the environmental factor) and the strength characteristics of the rock (which is the physical properties of the rock).
- The impact of the in-situ stress state, mining methods, geometry of the underground openings and mining sequence are also considered in this method (with help of the FE analysis model).
- A full 3D analysis model of the mine is a powerful design tool to study the stiffness of the loading system (also called mine stiffness) as one of the important factors influencing the failure of the rock mass. The mine stiffness is controlled by the dimension and size of the pillars, span between the pillars, mining sequence and strength properties of the pillar. Most of these factors are taken into consideration in the developed methodology. Therefore, a sensitivity study can be performed, using the developed FE model, to assess the impact of each one of these parameters (separately or combined) on the mine stiffness and consequently revise these design parameters in real life.
- Utilizing the proposed methodology, potentially hazardous areas can be identified. The methodology can also assist in the planning and design of underground openings such that the high stresses and energy release induced by mining can be minimized.

## **CHAPTER 5: PREDICTION OF MINING-INDUCED SURFACE SUBSIDENCE AND GROUND MOVEMENTS AT DIAVIK DIAMOND MINE USING A FULL 3D ELASTOPLASTIC FINITE ELEMENT MODEL**

*Prediction of the surface subsidence profile and its magnitude is a critical task for rock mechanics engineers, and it is crucial for planning underground mining operations. In this chapter, the forecast capacity of a numerical model to predict mining-induced surface subsidence and ground movement in a case study is investigated. A full three dimensional elastoplastic finite element model of Diavik Diamond Mine was developed to predict surface-induced ground movement due to underground blasthole stopping activities. The developed model was calibrated using two extensometers installed on the back of two secondary undercut drifts in one of the Kimberlite pipes. The results of the calibrated model are verified using pit surface prism monitoring system data. The comparison between the predicted results of the finite element model and monitoring data showed that the predictive capacity of the numerical model is a valuable tool for stability and design analysis of underground mines.*

## 5.1 Introduction

Subsidence is the downward settlement of the ground surface. Mining-induced surface subsidence is a phenomenon that occurs due to the underground extraction of an orebody. Open pit and underground mining operations cause stress redistribution; consequently, this causes some induced displacements on the ground surface.

According to the elasticity theory, any excavation at any depth and extend can cause movement on the ground surface. This means that all underground mining methods can cause surface subsidence. According to Pariseau (2007), the most common reasons of surface subsidence are:

- Redistribution of the stresses due to mining activities
- De-watering of the ground during mining activities which cause lowering of the groundwater tables

Prediction of the surface subsidence profile and its magnitude is a critical task for rock mechanics engineers, and it is crucial for planning underground mining operations. A comprehensive review of the methods to determine mining-induced surface subsidence is given by Brady and Brown (2004). Several empirical, numerical, observational, graphical and physical methods to predict subsidence parameters have been developed by scholars such as Berry (1963), Jennings et al. (1965), Brauner (1973), Hoek (1974), the National Coal Board (1975), Dunrud (1976), Brown and Ferguson (1979), Laubcher (1994), Bétournay (1995), Unlu et al. (2013) and Yang and Xia (2013).

To meet the objective of this paper, FE model is used for numerical analysis due to its recognition as a tool to solve rock mechanics and geomechanical problems. It has the ability to deal with material heterogeneity, non-linearity, complex-boundary conditions, in-situ stresses and gravity.

To predict the induced surface subsidence due to underground mining activity at Diavik Diamond Mine, a full 3D elastoplastic FE model was established. The initial results of the model were calibrated using two underground calibration points. Finally, the calibrated model was used to predict the induced settlement profile for the surface of the N9290 bench located in the A154 pit at Diavik Mine. Results of the developed FE model were verified by comparing the outputs of the constructed FE model with available pit monitoring data.

## **5.2 Diavik Diamond Mine**

Diavik Diamond Mine is located on a 20 square kilometer island in the lake Lac de Gras, approximately 300 kilometers northeast of Yellowknife, capital city of the Northwest Territories. Diavik reserves are contained in four diamond bearing kimberlite pipes, named as A154 North, A154 South, A148 and A21. The host rock is granite. All four pipes were located under the waters of Lac de Gras. To enable open pit mining to be conducted, first the water was removed and dikes were constructed to drain the water and prepare the surface for the open pit mining.

### **5.2.1 Mining Method**

Extraction of the ore at Diavik began with open pit mining. In late 2012, the transition from open pit to underground mining had been completed and Diavik became an underground mine. Two underground mining methods, sublevel longhole retreat (SLR) and blasthole stoping (BHS), were used. A154 South and A418 pipes are mined by SLR. BHS is used in A154 North pipe. The research area of this paper is focused on A154 North Pipe.

In BHS (Figure 5.1), generally, the work involves two sublevels and certain amount of preparation of the stope before the actual production can proceed. One sublevel is used for drilling, which is called overcut (Or drilling access), and another sublevel is used for the production, which is called undercut. According

to Hustrulid (2001), BHS method is the best option when the ore body has the following characteristics:

- The dip of ore body is steep. (which is the case in most underground Canadian Diamond Mines)
- Ore and host rock are competent. (In diamond mines the host rock is often granite)
- Ore boundaries are regular.
- Strong hanging-wall and Foot-wall.

Mining in BHS is performed in a Primary/Secondary manner. First the primary stopes are excavated. After the primary stopes completely excavated and backfilled, excavation of the secondary stopes will be initiated. Finally, after completion of mining of one level, the operation moves to the next mining level.

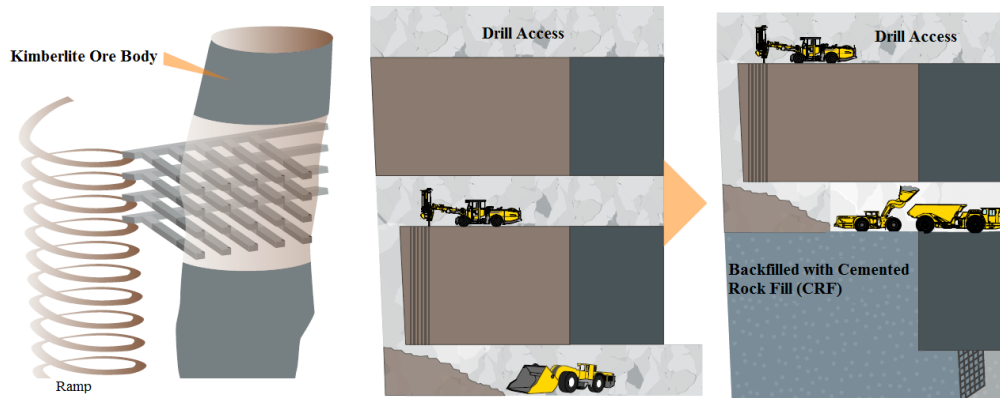


**Figure 5.1** Blasthole Stopping Method (After Diavik Diamond Mine fact book 2012)

The planned blasthole stopes in Diavik include primary and secondary stopes. All stopes have 7.5m width, the strike length approximately 100m, and height approximately 30m sill to sill. Cemented rock-fill (CRF) is being used to backfill the stopes. The dimensions of each undercut/overcut are 7.5m width by 5m height.

## 5.3 Methodology

### 5.3.1 Model geometry

A full three dimensional finite element analysis model of the mine, as shown in figure 5.2, is constructed using Abaqus (Dassault Systems Simulia Corp.) Two simple representative geometries of the open pits, A154 and A148, are included in the model. The analysis domain dimensions are 2.2Km by 2.2Km and maximum depth of the model is 800m. The domain dimensions are sufficient to eliminate the influence of the boundaries on the model. On the vertical boundary of the model, horizontal restraints (on both X and Y directions) are applied. Encastre boundary conditions are applied at the bottom of the model (Encastre means completely fixed in all directions).

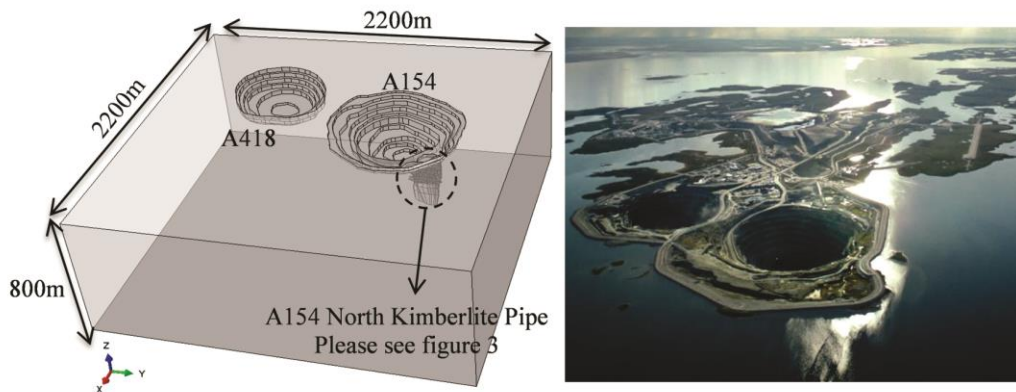


**Figure 5.2** Full 3D model of the mine in Abaqus

To accurately calculate the initial state of the stresses, both open pits are included in the model. This allows the model to calculate the initial geostatic state of the stresses in the first step of the simulation. Moreover, including both pits allows the model to account for the zone of influence of these pits on the induced stresses.

For this analysis, only the geometry of the A154 North Kimberlite pipe with all of its BHS primary and secondary stopes located between mining levels N9175 and N9275 have been introduced into the model, as shown in figure 5.3. The A154N

Kimberlite pipe is located under the N9290 pit bench; therefore, some road profile preparation, as shown in figure 5.4, had been done during the open pit operations. These CRF and URF structures, located at the surface crown pillar, were also included in the model.

A 3D model of Mining Block A in Diavik Diamond Mine is shown in figure 5.5a. Mining Block A is located between mine elevations N9175 m and N9275 m. As shown in figure 5.5b, each BHS stope is divided into three mining blocks. However, in some cases, stopes are divided into two or four mining blocks. Each mining block has a strike length of less than 50 m.

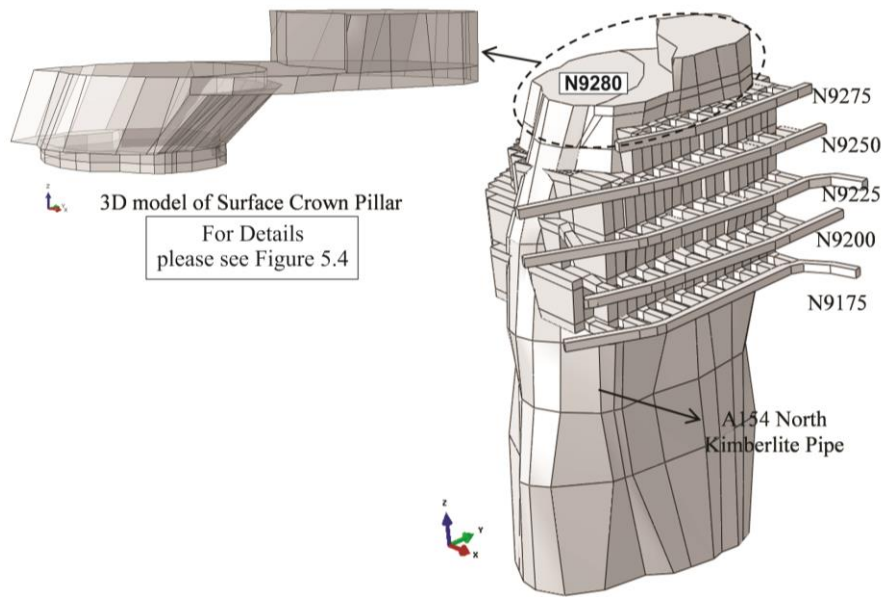


**Figure 5.3** 3D geometry of the A154N Kimberlite pipe created in abaqus

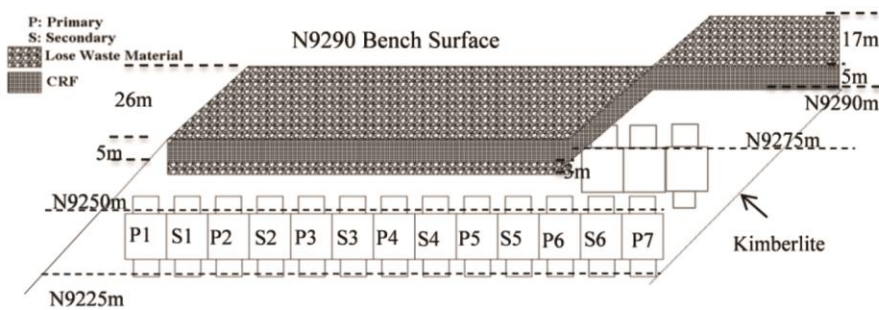


**Figure 5.4** The A154 North Kimberlite surface crown pillar at mine elevation N9225 m to N9290 m

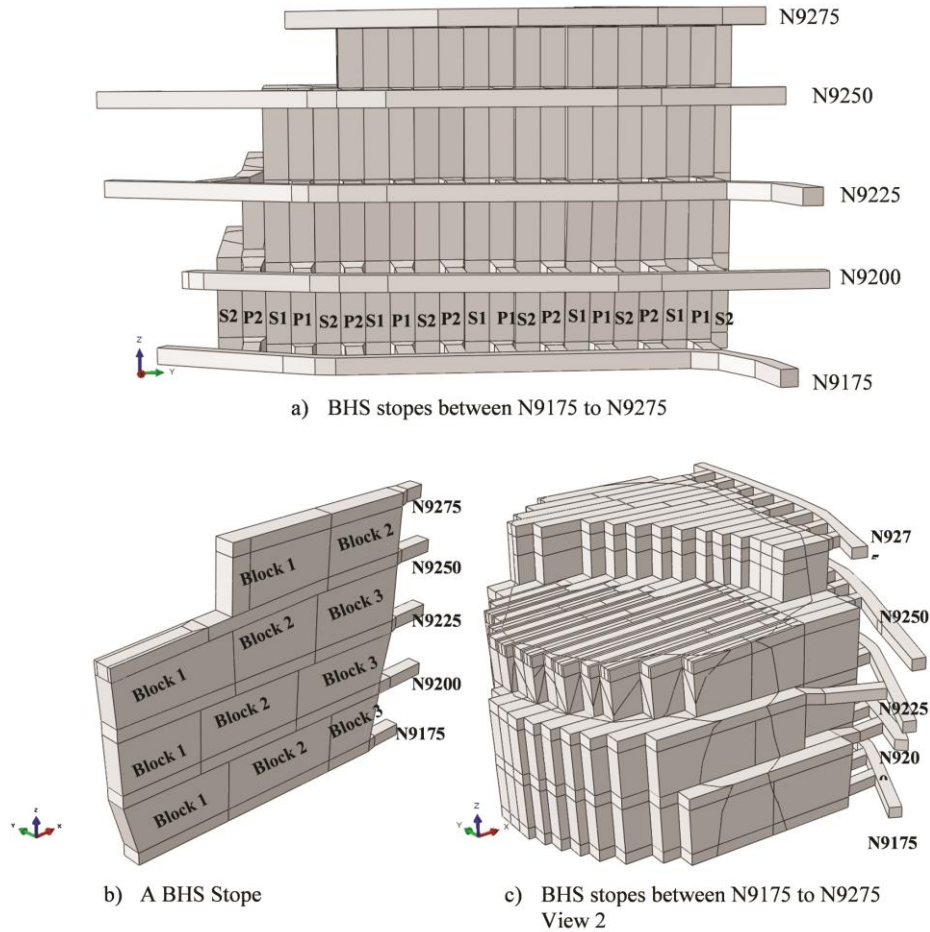


**Figure 5.5** 3D geometries of blasthole stopes created in Abaqus

### 5.3.2 Finite element mesh

10-node quadratic tetrahedron element (C3D10) is used to discretize the analysis domain. A mesh convergence study (MCS) is performed to make sure that a sufficient refined mesh has been used. As the density of the mesh increases the accuracy of the results improves as well. However, as the mesh is refined, the computer resources and calculation time required to run the simulation model increases. The main objective of the MCS is to reach to a meshing scenario when furthered mesh refinement produces a negligible change in the results.

Initially, three meshing scenarios are defined, as presented in the table 5.1. The density of the mesh increases from SCN 1 to SCN 3. In all three scenarios mesh density varies throughout the analysis domain. A fine mesh is used around the underground drifts and stopes, while a coarse mesh is used elsewhere.

**Table 5.1** Mesh Scenarios used to perform a Mesh Convergence Study (MCS)

| Scenario | Total Number of Elements | Total Number of Nodes | Number of Variables (Degree of Freedom) |
|----------|--------------------------|-----------------------|---|
| SCN 1    | 336,976                  | 461,749               | 1,385,247                               |
| SCN 2    | 776,794                  | 1,049,925             | 3,149,775                               |
| SCN 3    | 1,191,304                | 1,601,279             | 4,803,837                               |

All three scenarios have been tested for the first 5 simulation steps out of actual 95 simulation steps. The goal was to find a best acceptable arrangement between the accuracy of the results and the cost of finite element simulation. Here cost refers to calculation time and required computer resources.

Figure 5.6 shows the maximum magnitude of displacement generated in the first 5 simulation steps of the model under different meshing scenarios. As it can be seen, SCN2 and SCN3 graph results are almost overlapping each other, while SCN 1 has a noticeable distance from the others.

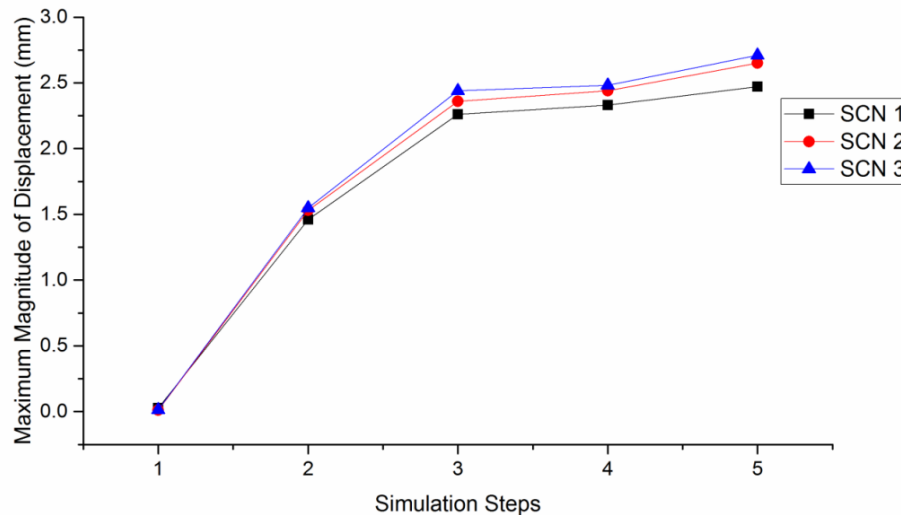
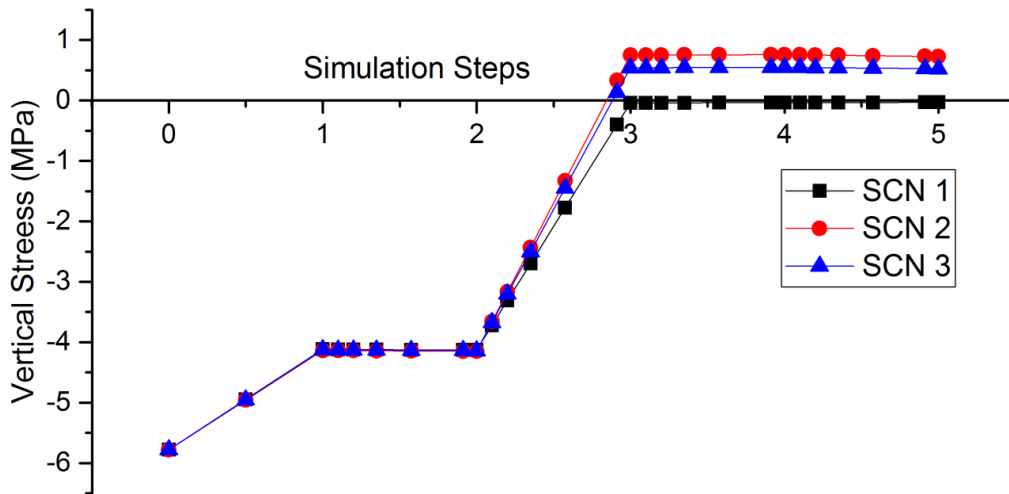
**Figure 6** Mesh Convergence Study on Maximum Displacement

Figure 5.7 shows the maximum vertical stress at a monitoring node on the back of undercut drift located at level N9175. As it can be seen the trends of developing the tensile stress from step 1 to 5 are presented under different meshing scenarios. Here again, SCN 2 and SCN 3 giving close results, while SCN 1 is distinctively

following different path. It is significant, because based on the results of SCN 1 the magnitude of induced tensile stress on the back of the monitoring drift is close to zero, while the other two scenarios showing the induced tensile stress close to 1 MPa. (It should be noted that in Abaqus, unlike in rock mechanics, compressive stress has negative sign and tensile stress has positive sign).



**Figure 5.7** MCS on Vertical Stress at a monitoring node at the back of N9175 Undercut drift

The CPU time for the first iteration in the step 1 of simulation model is presented in table 5.2. As it can be seen as the mesh density increases the calculation time increases significantly.

**Table 5.2** CPU Time for the First Iteration\*

| Mesh Scenario | CPU Time (Min) |
|---------------|----------------|
| SCN 1         | 4.45           |
| SCN 2         | 19.62          |
| SCN 3         | 94.55          |

\*Note: An “iteration” is an attempt to find an equilibrium solution in an increment. In non-linear analysis the total load applied in a step is divided into smaller increments so that the nonlinear solution path can be developed. If the model is not at equilibrium at the end of each iteration, Abaqus will take another iteration until it reaches to equilibrium. Here the CPU time for the first iteration in step 1 of each meshing scenario is presented.

Based on the MCS results the best meshing scenario is SCN 2. In fact, the difference between the displacement results obtained from SCN 2 meshing scenario and the solution obtained from the most refined mesh scenario, SCN 3, is approximately 2%; while, the calculation time in SCN2 is reduced significantly (Approx. by 79%).

### 5.3.3 Constitutive model and material properties

The behavior of the rock was assumed to be governed by an elastoplastic constitutive relation based on the elasticity theory and the Mohr-Coulomb plasticity criterion. The Mohr-Coulomb failure criterion is the combination of the coulomb failure criterion presented by Coulomb (1773) and Mohr (1990) criterion. The basic assumption in this model is that failure is govern by the maximum shear stress and that this shear failure depends on the normal stress. The Mohr's circles can be plotted for states of principal maximum and minimum stresses (Figure 8). The Mohr-Coulomb failure criterion is the best straight (linear) envelope that touches the Mohr's circles. The equation of this linear envelope can be written as:

$$\tau_p = C + \sigma_n \tan\phi \quad (5.1)$$

Where  $\sigma_1$  and  $\sigma_3$ , shown in figure 5.8, are the maximum and minimum principal stresses, respectively;  $\tau_p$  is the peak shear stress or shear strength,  $\sigma_n$  is the normal stress,  $C$  is the cohesion of the rock materials, and  $\phi$  is the angle of friction.

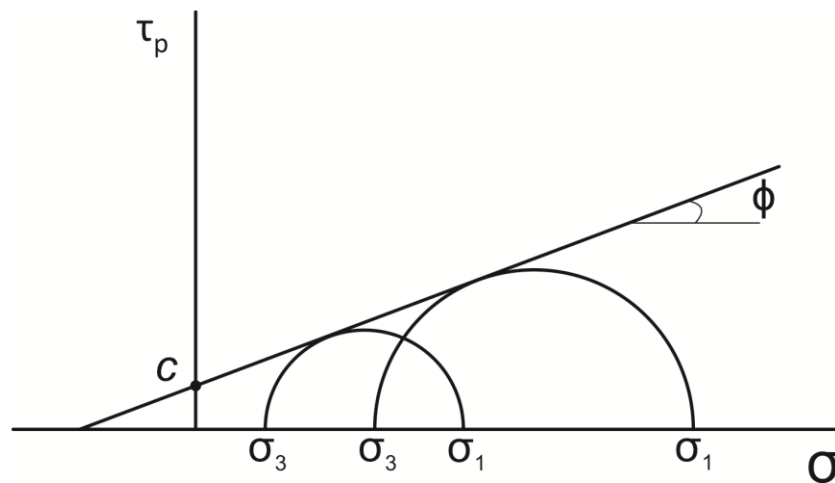


**Figure 5.8** The Mohr-Coulomb Failure Criterion

Rock mass properties for the Kimberlite were estimated based on the average RMR systems value and the generalized Hoek-Brown criterion (1995) as shown in figure 5.9. However, since Abaqus uses the Mohr-Coulomb failure criterion, the estimated Hoek-Brown parameters must be converted to the Mohr-Coulomb parameters. For this purpose, RocLab software (Rocscience Inc.), which was developed by Hoek et al. (2002), was used to assess the Mohr-Coulomb failure criterion parameters.

The material properties used in the model are presented in table 5.3. For granite and CRF, typical values found in the literature (Hassani and Archibald 1998; Zhang and Mitri 2008) were used. It was assumed that the URF materials are perfectly elastic.

**Table 5.3** Material properties

| Material   | Unit weight ( $\gamma$ )<br>MN/m <sup>3</sup> | Elastic modulus (GPa) | Poisson's ratio ( $\nu$ ) | Cohesion (MPa) | Friction angle ( $\phi$ ) <sup>o</sup> | UCS (MPa) | Tensile strength (MPa) |
|------------|---|-----------------------|---------------------------|----------------|--|-----------|------------------------|
| Granite    | 0.026   | 21                    | 0.3                       | 9.3            | 45                                     | 130       | 0                      |
| Kimberlite | 0.026   | 15                    | 0.3                       | 2.3            | 42                                     | 60        | 0                      |
| CRF        | 0.022   | 2                     | 0.3                       | 1.3            | 35                                     | 1.5       | 0.2                    |
| URF        | 0.026   | 2                     | 0.3                       | 0              | 0                                      | 0         | 0                      |

#### 5.3.4 Simulation steps

The developed numerical model has 95 simulation steps. Throughout these simulation steps the mining and backfilling of the drifts and stopes are simulating in the model step-by-step. Step one is the geostatic step, which basically is for calculation of the initial state of stress before starting the excavation of the underground openings. Step two is the excavation of five main haulage drifts between N9175 and N9250 mine levels. Mining is started from mine level N9175, through steps 3 to step 95 of simulation, and progressed upward to N9275 mine level. Simulation steps are matched to the last date of available surface monitoring data points (i.e. January 31, 2016), which are used to verify the

results. The sequence of stope mining and the simulation steps are shown in figure 5.10.

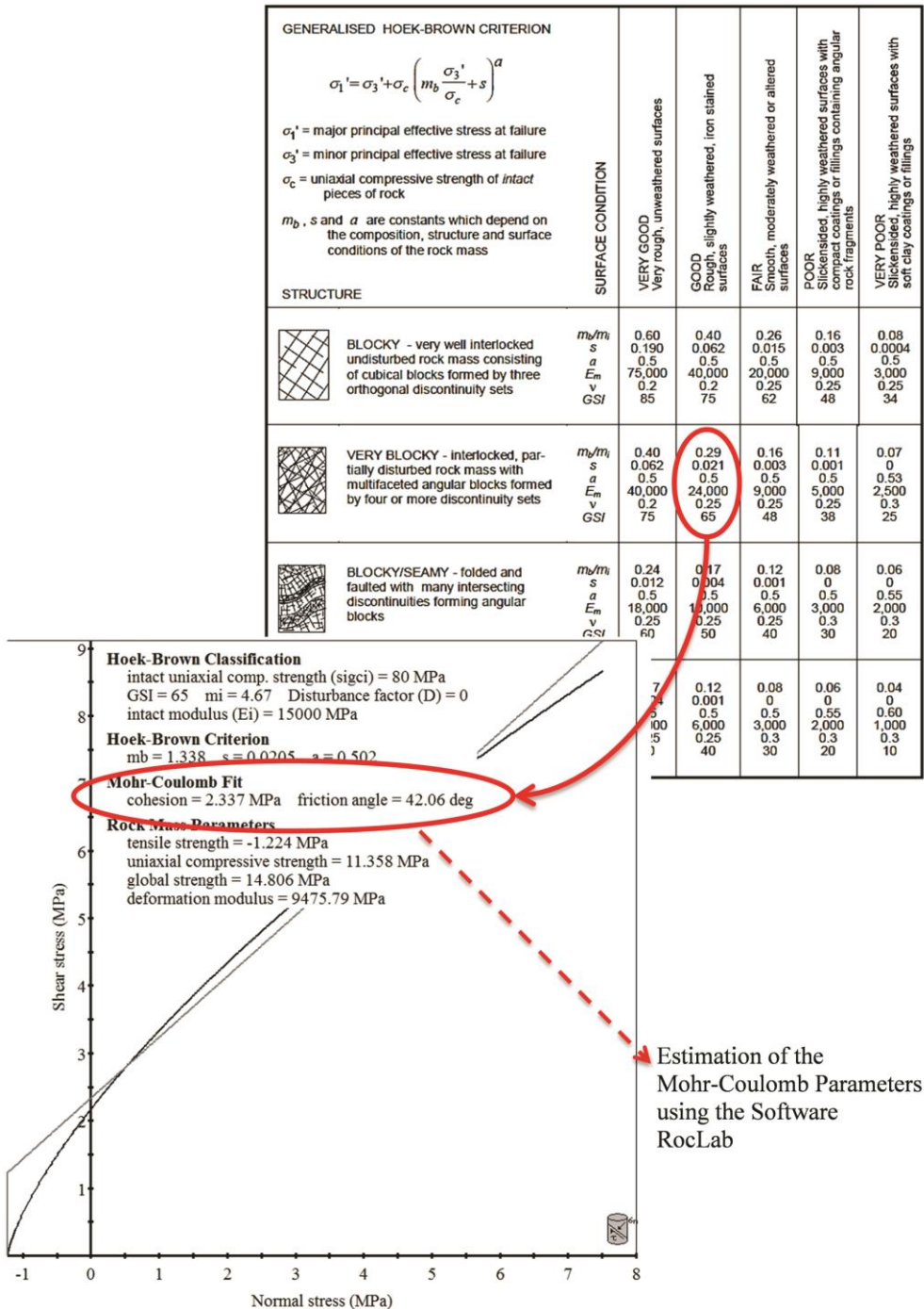


Figure 5.9 Estimation of the Mohr-Coulomb parameters (Hoek et al. 1995) for Kimberlite using RocLab software



$$\sigma_{hmax} = k_{max} \cdot \sigma_v \text{ where } k_{max} = 1.5 \quad (5.3)$$

$$\sigma_{hmin} = k_{min} \cdot \sigma_v \text{ where } k_{min} = 1.2 \quad (5.4)$$

Where  $k$  is the ratio between horizontal to vertical in-situ stresses.

Because of the geological history of the formation of the volcanic Kimberlite pipes and based on the field observations (i.e. presence of water in the contact between granite and Kimberlite) it is concluded that the stress transfer from the host rock to the orebody cannot take place. Moreover, the observed separation between Granite and A154 North Kimberlite pipe, as shown in chapter 3, supports this hypothesis. Therefore stress regime inside the Kimberlite pipe is completely different from the one inside the Granite. The  $k$  value inside the Kimberlite ore body, has been estimated using the equation (5.5) proposed by Terzaghi and Richart (1952).

$$k = \frac{\nu}{1-\nu} \quad (5.5)$$

Where  $\nu$  is the poisson's ratio of the rock. The Poisson's ratio for the Kimberlite is assumed to be 0.3 therefore the  $k$  value for the inside of the orebody is 0.43.

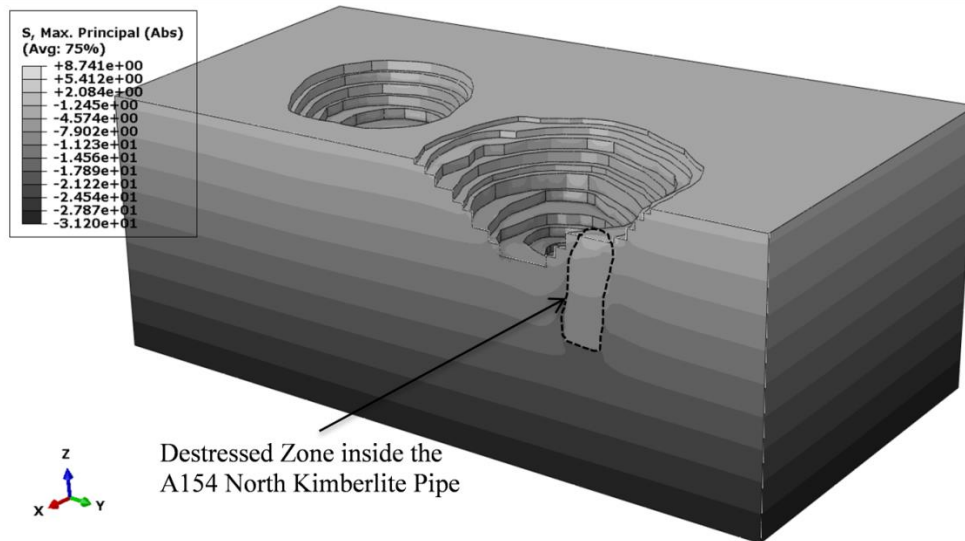


**Figure 5.11** Initial State of Stress- Simulated in Step one (Geostatic Step)

As it is illustrated in figure 5.11, the magnitude of the maximum in-situ principal stress in the model is estimated to be 31.2 MPa. This value can be verified using equations (5.2) and (5.3) as follows:

Assuming  $0.026 \text{ MN/m}^3$  as average unit weight of the overburden rocks:

$$\sigma_{H_{\max}} = k_{\max} \sigma_v = 1.5 \times 0.026 \times H = 1.5 \times 0.026 \times 800 = 31.2 \text{ MPa}$$

#### 5.4 Calibration of the finite element model

The developed FE model was calibrated using two extensometers installed on the back of the N9175-118 and N9175-148 secondary undercut drifts. To calibrate the model, the preliminary results of the FE model were compared with the results of the underground monitoring data points. Figure 5.12 illustrates the data from the multi-point vibrating wire inline extensometers installed at the N9175-118 secondary undercut drift. Data are available from October 07, 2013 (the day it was installed), to September 17, 2014 (the day it was lost due to blasting of Stope Block 2).

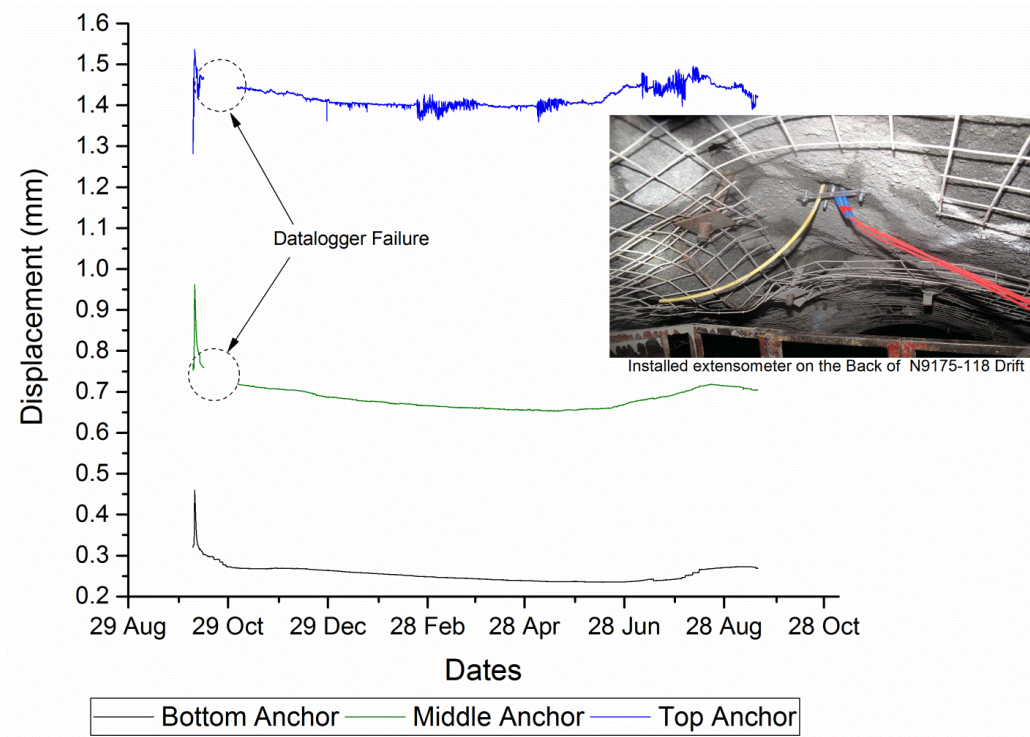


**Figure 5.12** Ground movement extensometer data measured at N9175- S118's undercut

According to figure 5.12, the average displacement on the back of the N9175-S118 undercut drift, before stopping initiated (before June 28, 2014) is approximately 0.05 mm, and during stopping (June 28 to September 28, 2014), it is close to 0.1 mm. These data were compared with the results of the FE model. As can be seen in figure 5.13, at step 80 of the initial model, the direction of displacement is temporary changed upward. The reason for this phenomenon is that, in this step in the model, the excavation of the N9200-S118 overcut is initiated, while in reality (figure 5.12) this behavior was not observed. However, the behaviors of the remaining mining activities were predicted close to the reality. When Stope Block 1 is excavated, the maximum displacement is approximately 0.125 mm which is close with the observed data. In order to calibrate the model and fix this problem (shown in step 80), it was decided to revise the simulation steps in order to meet the observed behavior. The results from the initial model and the calibrated model are shown in figure 5.13. As can be seen, the results are improved in the calibrated model.

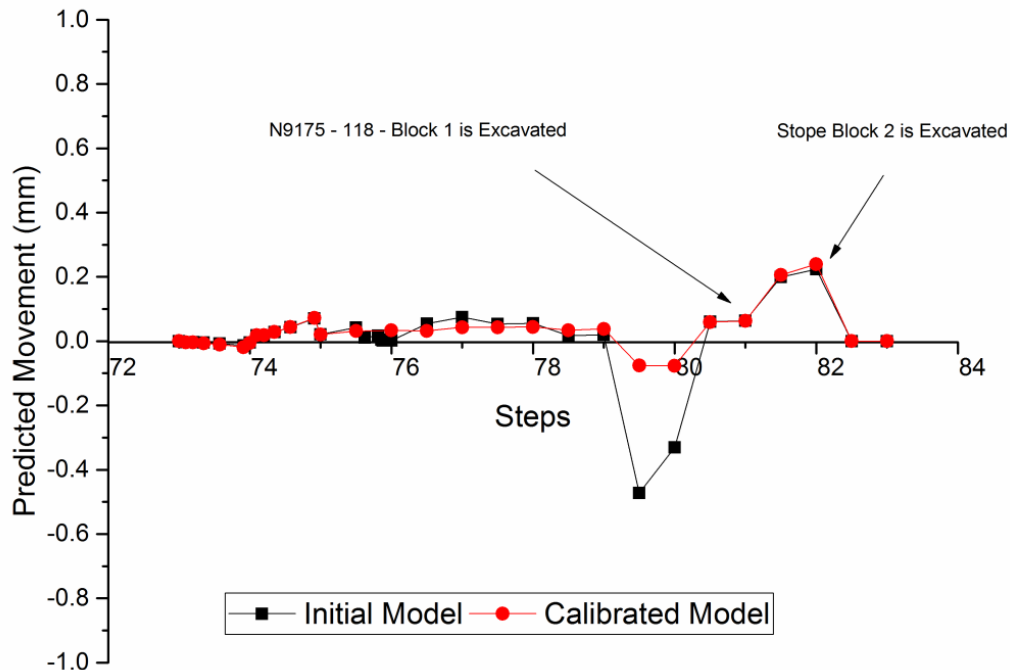


**Figure 5.13** Movements of the calibration point on the back of the N9175-118 drift

The second monitoring point is located on the back of the N9175-148 undercut drift. It is used to calibrate the model. The available data for this point are shown in figure 5.14. As seen from this figure, the displacements are close to zero (almost flat line), and the extensometer was lost due to the blasting of N9175-118-Block 2 on July 15, 2014. However, the model was calibrated using the available data. A similar procedure has been used to calibrate the results of the FE model using this data point.

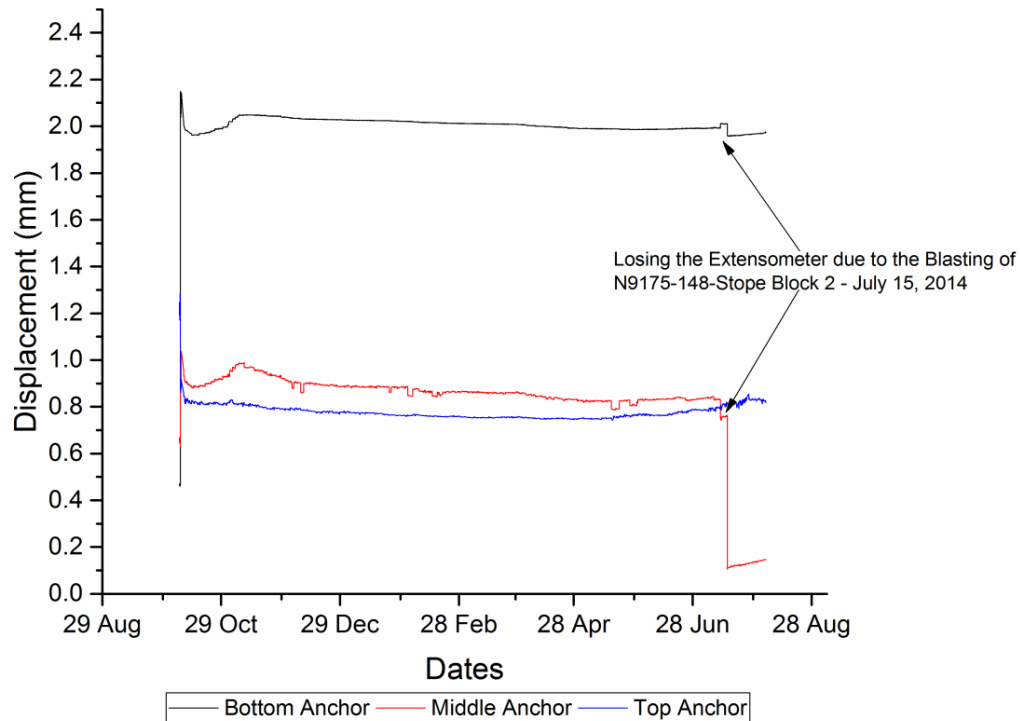


**Figure 5.14** Ground movement extensometer data measured at the N9175- S148 undercut

A comparison between the initial model and the calibrated model results are shown in figure 5.15. As seen in figure 5.15, the displacements throughout the simulation in the calibrated model are close to zero, which matches the observed data.

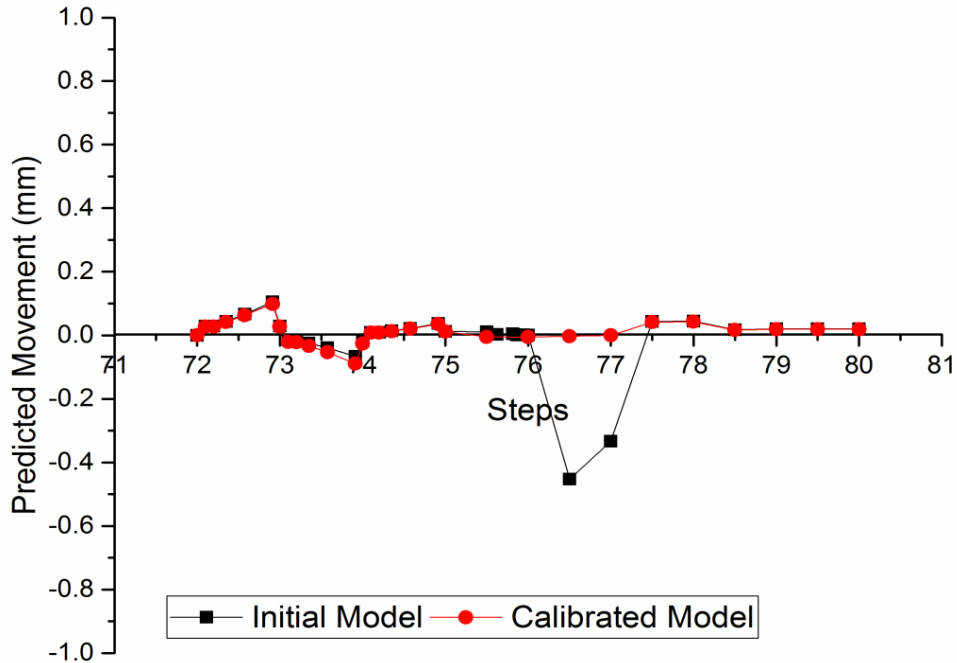


**Figure 5.15** Movements of the calibration point on the back of the N9175-118 drift

## 5.5 Results and discussion

The objective of this chapter was to develop a realistic numerical model which can be used as a prediction tool to estimate mining-induced surface subsidence. In the following sections, the results of the calibrated numerical model are presented, and the results are verified using available pit monitoring data.

### 5.5.1 Surface bench settlement

The FE model results show the development of downward surface settlement of up to 19 mm on the surface bench at the A154 pit. Figure 5.16 illustrates the predicted settlements. A monitoring nodes path is defined on the surface of the bench on the FE model, as shown in figure 5.16.

The surface movement developments along the monitoring nodes path in different simulation steps are shown in figure 5.17. As predicted, in step 1 of the simulation, the movement on the bench is close to zero due to the use of the

geostatic step to simulate the initial stress state before underground mining commences.

As the mining direction goes upward, the amount of the displacement on the surface increases. The significant jump in ground movements occurred after step 90 of the simulation, when mining of the stopes located between N9275 and N9250 is initiated. The magnitude of the displacement jumped from 13.46 mm in step 90 to 19.37 mm in step 95 (approximately by 44%).

In figure 5.18, the numerical prediction of the surface subsidence matches well with the Gaussian distribution. This concept was first proposed by Peck (1969) for calculating the surface subsidence profile due to tunneling in soft ground. However, it is not generally applied for mining-induced surface subsidence.

According to the FE analysis model, there is no yielding, and the plastic strain level on the surface is zero.

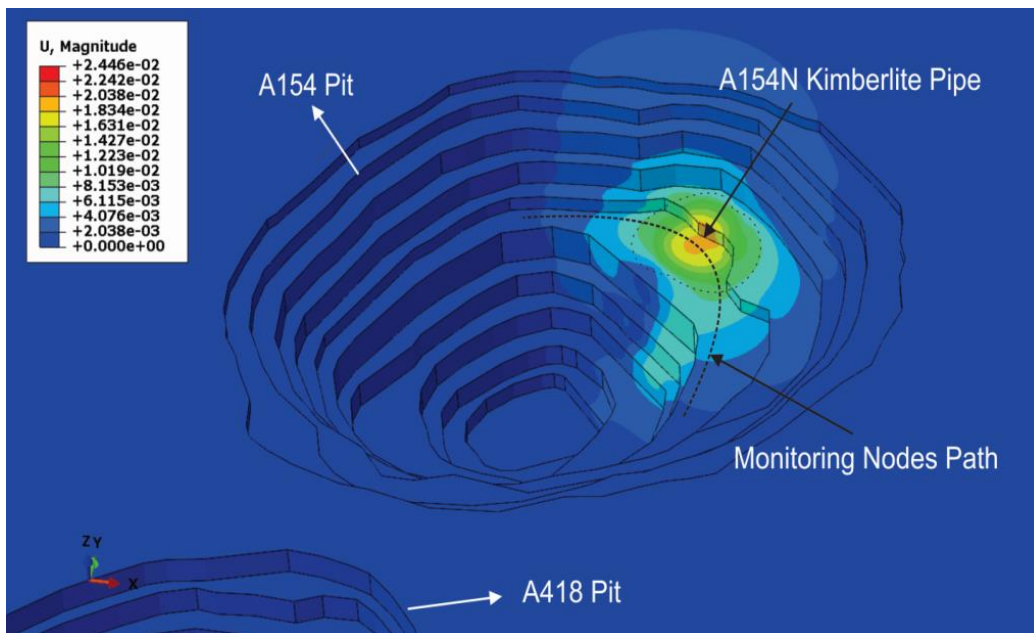


**Figure 5.16** Displacement on the pit surface predicted by the finite element model

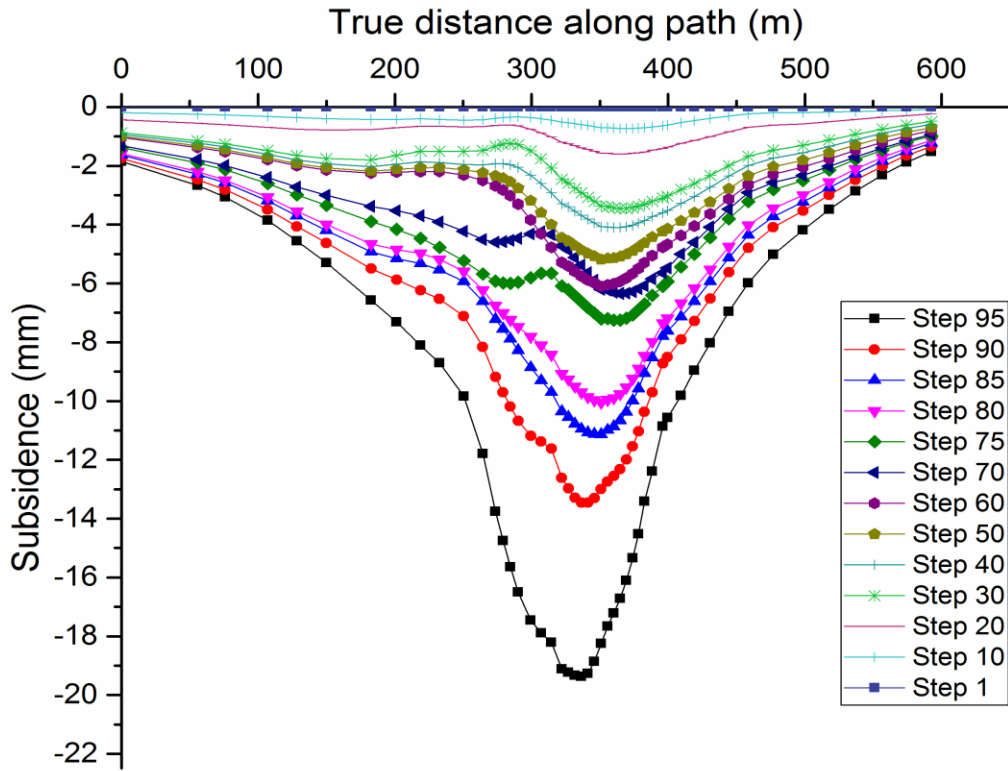


**Figure 5.17** Predicted surface subsidence along the monitoring nodes path in different simulation steps

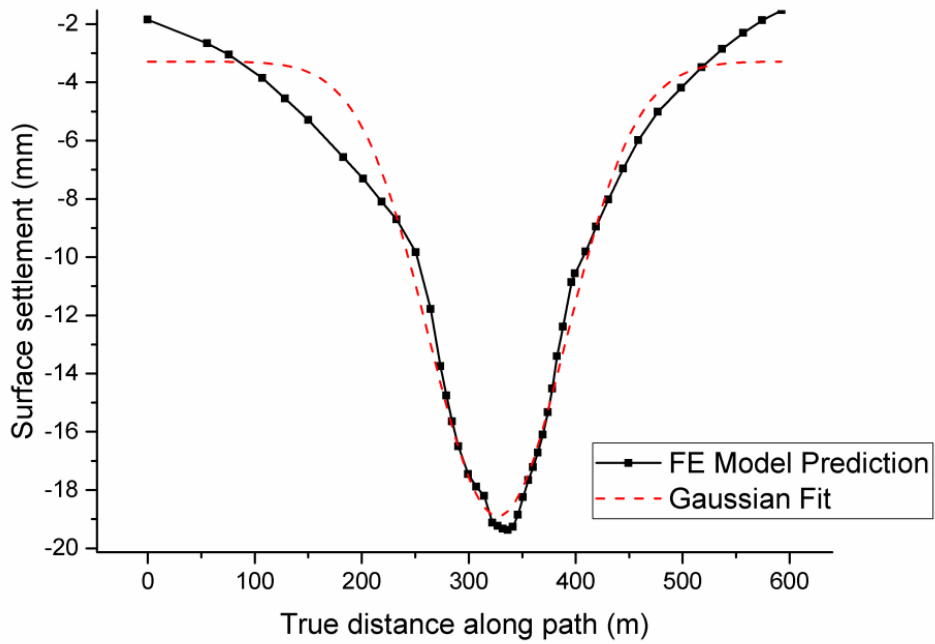


**Figure 5.18** Curve fitting of the numerical predictions

The cross section of the modeled BHS mining method is shown in figure 5.19. From this figure, the maximum induced movement in the model is 24.4 mm and is located between mine levels N9250 and N9225. The concentration of the induced movement is in the middle of the Mining Block A operation zone.

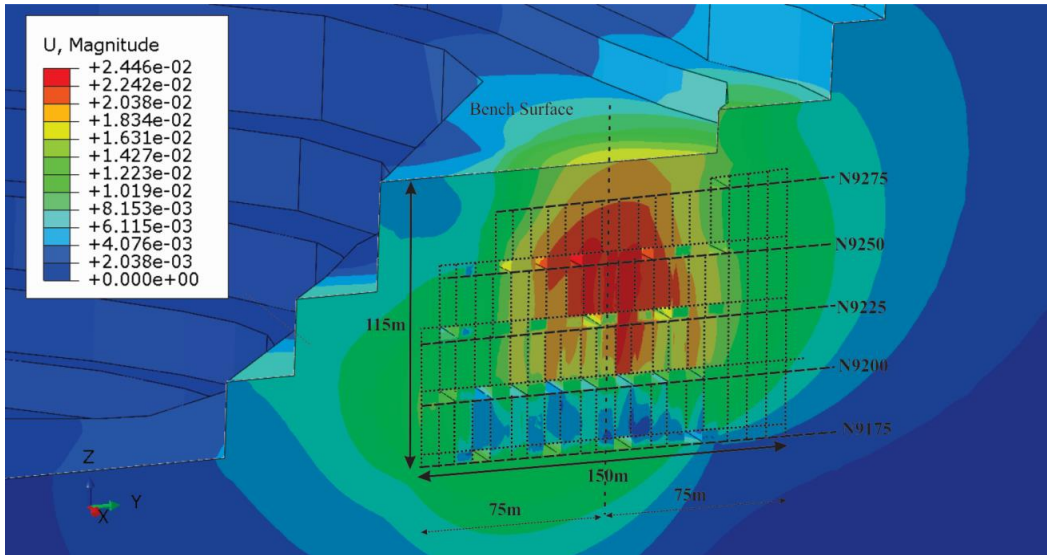


**Figure 5.19** Cross section of BHS mining and induced movements. Mining Block A is located at the A154 North pipe between mine levels N9175 and N9275

### 5.5.2 Verification of the results

The results of the calibrated model were compared and verified using pit movement monitoring prisms data. Figure 5.20 shows the locations of the monitoring prisms used to verify the results of the FE model. Monitoring Zone 1 consists of two prisms (i.e. CRF-S01 and CRF-S02). Monitoring Zone 2 consists of two prisms (i.e. CRF-N01 and CRF-N02). Two other prisms (280-10 and 280-12) are installed within 30 m of each other along the bench crest.

Figure 5.21 shows the comparison between the FE model movement prediction and the data from the installed prisms in Monitoring Zone 1. The maximum movements read from the CRF-S01 and CRF-S02 prisms were 15.59 mm and 15.2 mm, respectively, while the FE model predicted maximum movement of

15.78 mm for this location. The maximum relative error of prediction of the subsidence for this location is 2.5%.

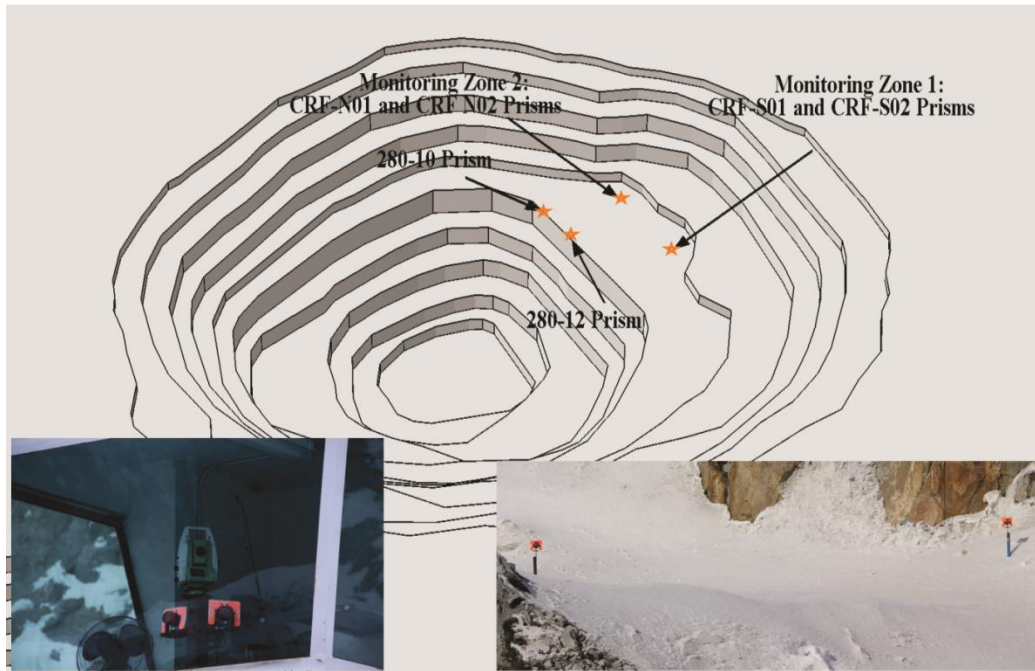


**Figure 5.20** Location of the monitoring prisms on the bench used for finite element model verification

The comparison between the FE model results and the available data from the prisms in Monitoring Zone 2 are presented in figure 5.22. The maximum surface settlement read from CRF-N01 and CRF-N02 are 9.3 mm and 9.7 mm, respectively. The maximum subsidence predicted by the FE model for this location is 10.18 mm. This brings the maximum relative error of prediction to 7% for this location.

Figures 5.23 and 5.24 illustrate the comparisons between the FE model predictions and actual movement at the locations of the 280-10 and 280-12 prisms, respectively. The maximum surface settlement at the 280-10 prism is 5.8 mm, and the FE model prediction for this location is 5 mm. The actual movement at the 280-12 prism is 3.6 mm, and the predicted movement for this location is 3.3 mm.

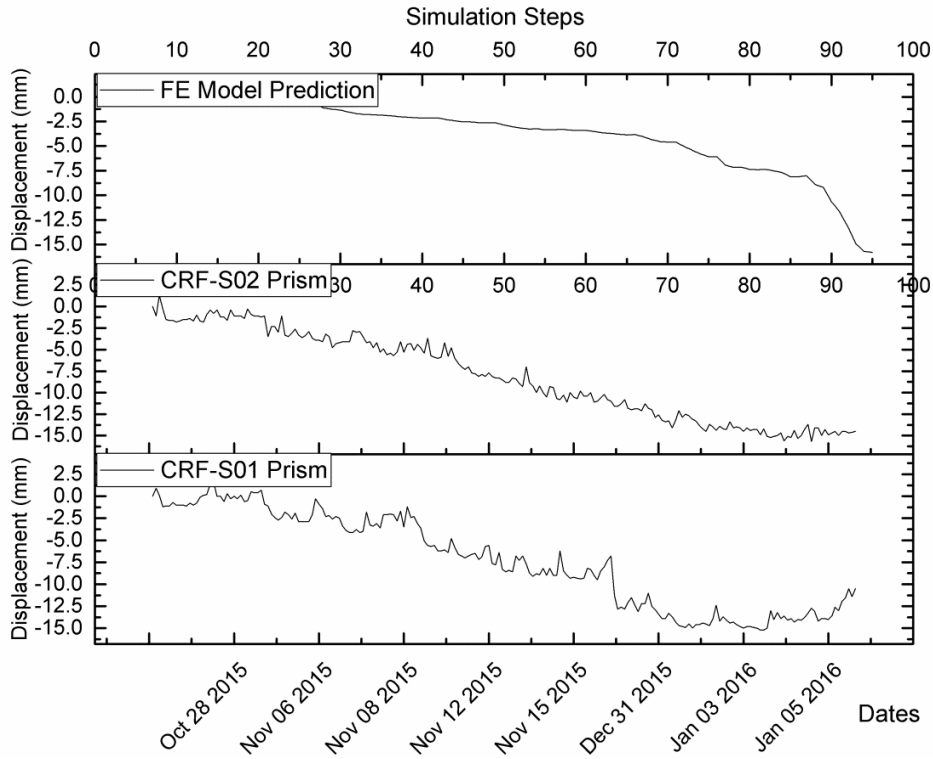


Figure 5.21 Comparison of the magnitude of displacement for Monitoring Zone 1

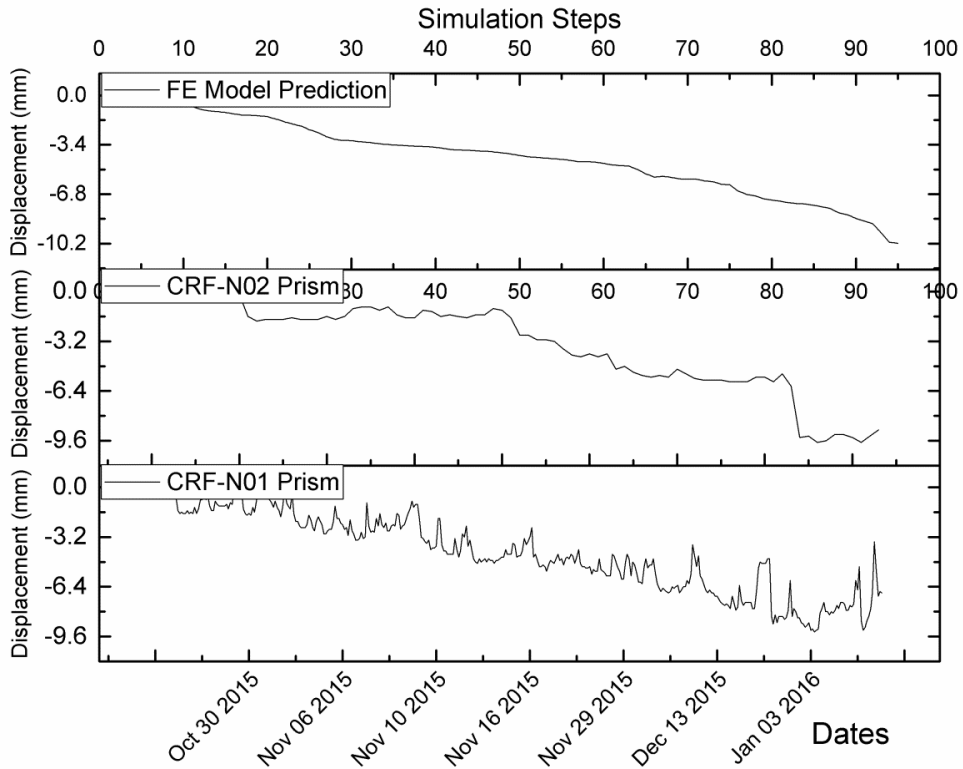


Figure 5.22 Comparison of the magnitude of displacement for Monitoring Zone 2

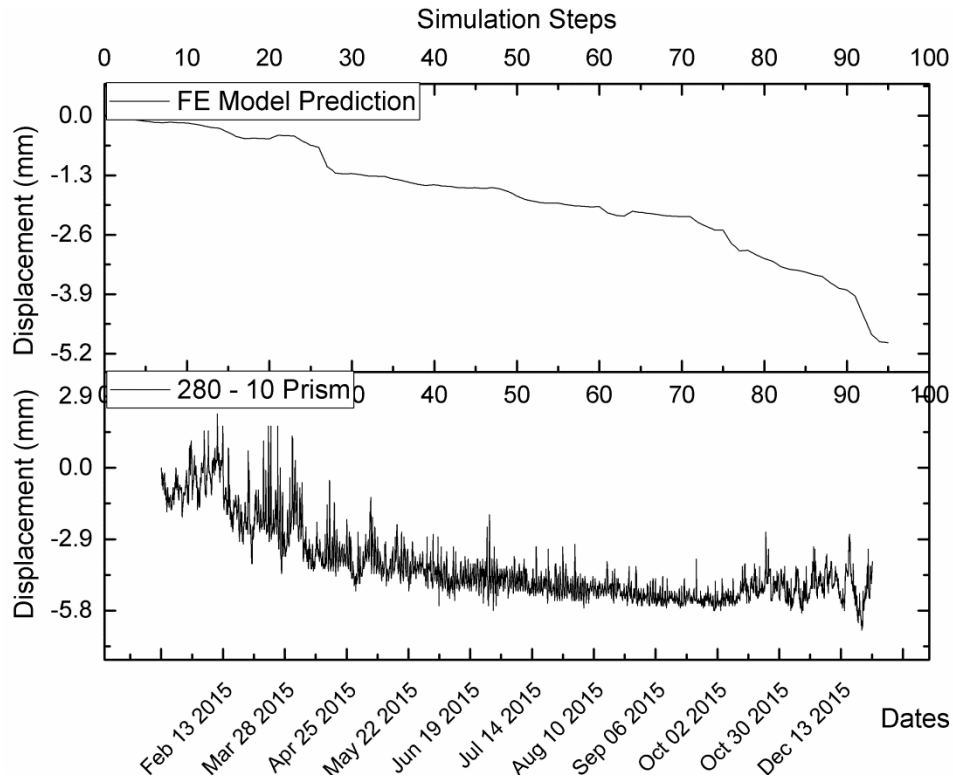


Figure 5.23 Comparison of the magnitude of displacement of the 280-10 prism

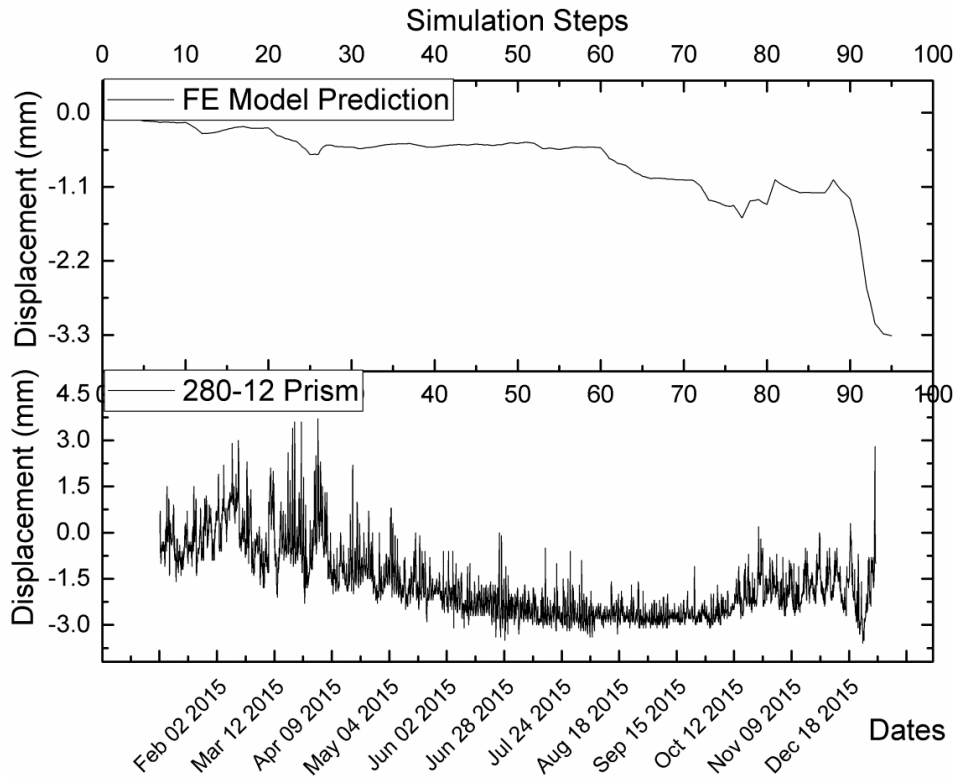


Figure 5.24 Comparison of the magnitude of displacement of the 280-12 prism

Comparisons between the actual ground monitoring data and the FE model results are summarized in table 5.4.

**Table 5.4** Comparison between finite element model results and the measured data

| Locations of the Prisms                                  | Measured<br>Data<br>(mm) | FE Model<br>Prediction<br>(mm) | Relative<br>Error<br>(%) |
|--|--------------------------|--------------------------------|--------------------------|
| <b>Mining Zone 1 (Average between CRF-S01 &amp; S02)</b> | 15.39                    | 15.78                          | 2.5                      |
| <b>Mining Zone 2 (Average between CRF-N01 &amp; N02)</b> | 9.5                      | 10.18                          | 7.2                      |
| <b>280-10 Prism</b>                                      | 5.8                      | 5                              | 13.8                     |
| <b>280-12 Prism</b>                                      | 3.6                      | 3.3                            | 8.3                      |

## 5.6 Conclusion

In this study, a full 3D elastoplastic FE model of Diavik Diamond Mine was constructed. The main objective of the paper was to predict the mining-induced surface subsidence and induced settlements due to underground mining activities in the A154 North Kimberlite pipe.

In order to obtain reliable results, the developed FE model was calibrated with two extensometers installed on the back of two secondary undercut drifts located at the A154 North Kimberlite pipe at mining level N9175. The results of the calibrated model were verified using ground monitoring field data (prisms monitoring systems) from the pit surface.

It was shown that the numerical predictions of the mining-induced surface subsidence, due to the BHS mining method, matched well with the Gaussian distribution. However, further investigations are needed to confirm the generalizability of these findings.

The model results predicted a maximum 19.37 mm surface subsidence until the last defined mining stage in the model (which matched the last day of available surface monitoring data points, i.e. January 31, 2016). However, the results

showed a significant increase (approximately by 44%) in the amount of induced settlements on the surface as mining activities reached near surface ground levels (N9275 and N9250). This raises considerable concern regarding the recovery of the surface crown pillar (located between mine levels N9290 and N9275) at later stages of the mining operation. Further numerical analyses are ongoing using a larger and more realistic scale of the mine to predict the state of the surface crown and sill pillars at later stages of the mining operation.

Overall, the FE model predictions of surface-induced settlements are in good agreement with the real measured data.

## CHAPTER 6: STOPE STABILITY ASSESSMENT, YIELDING AND RELAXATION ZONES, AND SENSITIVITY ANALYSIS USING THE FINITE ELEMENT MODEL

*Predicting the stability of open stopes can be a challenging task for underground mine engineers. For decades, the stability graph method has been used as the first step of open stope design around the world. However, there are some shortcomings with this method. For instance, the stability graph method does not account for the relaxation zones around the stopes. Another limitation of the stability graph is that this method cannot to be used to evaluate the stability of stopes with high walls made of backfill materials. However, there are several analytical and numerical methods that can be used to overcome these limitations. In this chapter, both empirical and numerical methods have been used to assess the stability of an open stope located between mine levels N9225 and N9250 at Diavik Diamond Mine. It was shown that the numerical methods can be used as complementary methods along with other analytical and empirical methods to assess the stability of open stopes. A three dimensional elastoplastic finite element model was constructed using Abaqus software. In this chapter a sensitivity analysis was performed to investigate the impact of the stress ratio ( $k$ ) on the extent of the yielding and relaxation zones around the hanging wall and foot wall of the understudy stope.*

## 6.1 Introduction

The assessment of the stability of open stopes is one of the critical stages in the underground mine design process. For decades, the stability graph method has been used as the first step of open stope designs around the world. The stability graph method originally developed by Mathews et al. (1981) is simple and is much faster than 3D numerical modeling. This method has proven its reliability in open stope design over many years of application. However, there are some limitations with this method. First, the stability graph method does not account for the relaxation zones around the stopes. The stress factor in this method is based only on induced compressive stress, while the relaxation zones can cause instability and dilution in many open stopes. Moreover, this method cannot be used to assess the stability of stope surfaces made of backfill materials. This is vital in assessing the stability of secondary stopes developed using the BHS method. One way to better evaluate the state of induced stress around open stopes is the use of numerical models as complementary methods along with analytical and empirical methods.

Throughout this chapter, the stability of the proposed stope was evaluated using the following three steps:

First, using the modified Mathews stability graph proposed by Hadjigeorgiou et al. (1995), the stability of the proposed stope was investigated as a single mining block. In reality, the stope strike length would be divided into three mining blocks, with a strike length of less than 50 m for each block. The software packages used to estimate the *A*, *B* and *C* stability factors (i.e. stress, joint orientation and gravity adjustment factors, respectively) included Geomechanical Design Analysis (GDA; DIAS Engineering Inc., 2000) and DIPS 7.0 (Rocscience Inc., 2016).

Next, to better understand the stress distribution around the stope blocks, a full 3D elastoplastic numerical model was constructed using Abaqus (ABAQUS/Standard Dassault Systemes Inc., 2012). The numerical model provides more in depth

details regarding the displacement, yielding and failure zones around the proposed open stope. In addition, using this model, it is possible to predict the zone of relaxation around the surfaces of the hanging wall and foot wall of each mining block.

Finally, using the developed FE model, a sensitivity analysis was performed to investigate the impact of the horizontal stress to vertical stress ratio ( $k$  value) on the propagation of the relaxation and yielding zones around underground openings.

### **6.1.1 Case study: Diavik Diamond Mine**

The Diavik Diamond Mine is located approximately 300 kilometers northeast of Yellowknife, Northwest Territories in Canada. Diavik reserves are contained in four kimberlite pipes, named as A154 North, A154 South, A148 and A21. The host rock is granite. All four pipes located under the waters of Lake Lac de Gras. The underground mining methods for the A154 North, A154 South, and A418 kimberlite pipes are Sublevel Longhole Retreat (SLR) and Blasthole Stopping (BHS). The SLR is used in the A154 South and A418 pipes. BHS is used in the A154 North pipe. The planned blasthole stopes will include primary and secondary stopes. All stopes have 7.5m width, the strike length approximately 100m, and height approximately 30m sill to sill. Cemented rockfill (CRF) is to be used to backfill the stopes.

### **6.1.2 Problem definition and objectives**

The major area of concern in this case study was the assessment of the stability of a stope located at the A154 North pipe between mine levels N9225 and N9250. The understudy stope is 7.5 m wide, 30 m high and the strike length of the stope is approximately 114 m. As mentioned previously, the stope is divided into three excavation blocks, and the strike length of each block is less than 50 m. After excavation of each block, the empty stope block is backfilled immediately and excavation of the next block will be initiated.

In summary, the main objectives of this paper are: (i) to assess the stability of the proposed stope using the empirical and numerical methods; and (ii) to investigate the impact of the horizontal to vertical stress ratio on the development of yielding and relaxation zones around an underground opening.

## 6.2 Overview of the stability graph method

The stability graph method for open stope design was initially introduced by Mathews et al. (1981) almost three decades ago. The method was modified and calibrated by Potvin (1988) and then Nickelson (1992). The Mathews stability graph method was updated by Hadjigeorgiou et al. (1995) and Stewart and Forsyth (1995). Today, the extended version of the method, given by Truman et al. (2000) and Mawdesley et al. (2001), is based on more than 400 case histories collected from underground hard rock mines. A comprehensive review by Suorineni (2010) shows that there are some shortcomings with this method, such as the need for factors that account for the stope stand-up time and blast damage. In addition, this method does not have procedures for determining the stability of stope surfaces made of backfill. Moreover, the stress factor does not account for the zones of relaxation and tension around the open stope.

The design procedure using the stability graph is based on the calculation of two parameters:  $N'$ , the modified stability number, and  $S$ , the shape factor (also called the hydraulic radius, HR). Using these two parameters and the proposed graph, it is possible to estimate the stability of the understudy stope.

$N'$  represents the ability of the rock to stand up without support under a given stress condition and is defined by Potvin (1988) as:

$$N' = Q' \times A \times B \times C \quad (6.1)$$

where  $Q'$  is the modified tunneling quality index introduced by Barton et al. (1974),  $A$  is the stress factor,  $B$  is the joint orientation factor and  $C$  is the gravity adjustment factor.

HR, or  $S$ , accounts for the influence of the shape and size of the stope surface and is calculated using equation (6.2).

$$S = \frac{\text{Area of the given stope surface}}{\text{perimeter of the stope surface}} \quad (6.2)$$

### 6.3 Stability assessment using the stability graph method

The Mathews stability graph was used to determine the stability of the proposed stope. The first step was the determination of  $N'$  and  $S$  for the stope surface. Four stope surfaces were investigated: the hanging wall, foot wall, back (or roof) and vertical end-walls.

In the following sections, the modified tunneling quality index,  $Q'$ , was estimated based on the rock mass quality data, and the results are presented in table 6.1. The dimensions of the proposed stope block are presented in table 6.2. Based on the proposed dimensions, the estimated  $S$  value is shown in table 6.3. Finally, the other stability factors (i.e.  $A$ ,  $B$  and  $C$ ) were determined.

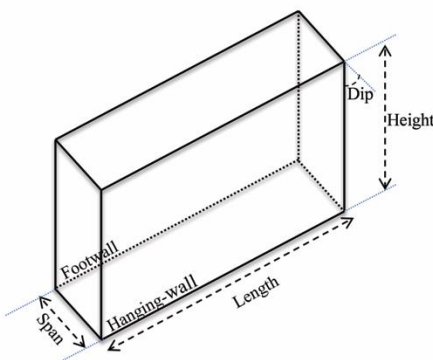
As seen from table 6.1, two different values of  $Q'$  were estimated along the length of the stope. Therefore, the stope strike length was divided into two portions: 0 to 30 m and 30 to 114 m. Consequently, two different  $N'$  values were calculated for the hanging wall and foot wall.

**Table 6.1** Value of the modified tunneling quality index

| Stope surfaces   | $Q'$ |
|--|------|
| Back   | 5.3  |
| Vertical end-walls   | 63   |
| Hanging wall and foot wall for section 1 (0-30m of the stope length)   | 2.7  |
| Hanging wall and foot wall for section 2 (30-114m of the stope length) | 8.9  |

**Table 6.2** Proposed stope dimensions

| Stope Dimension | Low | High |
|-----------------|-----|------|
| Length (m)      | 40  | 60   |
| Height (m)      | 30  | 30   |
| Span (m)        | 7.5 | 7.5  |
| Dip (°)         | 90  | 90   |


**Table 6.3** Calculated shape factor

| Stope surface      | Area (m <sup>2</sup> ) |      | Perimeter (m) |      | Shape factor S (m) |      |
|--------------------|------------------------|------|---------------|------|--------------------|------|
|                    | Low                    | High | Low           | High | Low                | High |
| Hanging wall       | 1200                   | 1800 | 140           | 180  | 8.57               | 10   |
| Foot wall          | 1200                   | 1800 | 140           | 180  | 8.57               | 10   |
| Vertical end-walls | 225                    | 225  | 75            | 75   | 3                  | 3    |
| Back               | 300                    | 450  | 95            | 135  | 3.16               | 3.33 |

### 6.3.1 Stress factor (*A*)

The vertical stress was determined based on the average unit weight of the overburden rock ( $\gamma = 0.026 \text{ MN/m}^3$ ). The depth of the stope is approximately 50 m. Using equation (6.3), the vertical stress was estimated to be 1.3 MPa.

$$\sigma_v = \gamma \cdot H = 0.026 \times 50 = 1.3 \text{ MPa} \quad (6.3)$$

The UCS of the Kimberlite for this area was estimated to be 66 MPa. Therefore, based on the calculated vertical stress ( $\sigma_v$ ), the value of the UCS ( $\sigma_c$ ) and figure 6.1, the rock stress factor *A* for all stope surfaces will be 1.

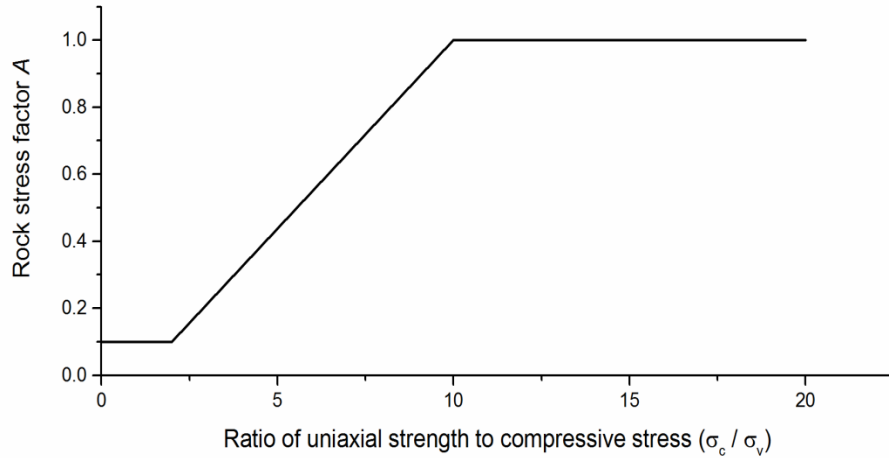


Figure 6.1 Rock stress factor for different values of  $\sigma_c/\sigma_v$  (after Mathews et al., 1981)

### 6.3.2 Joint orientation factor (B)

Based on the site characterization data available for this stope, principal joints sets were defined. The dominant structure sets were determined using DIPS 7.0, and the results are illustrated in figure 6.2. Using the GDA software, the estimated joint orientation factors are presented in table 6.4.

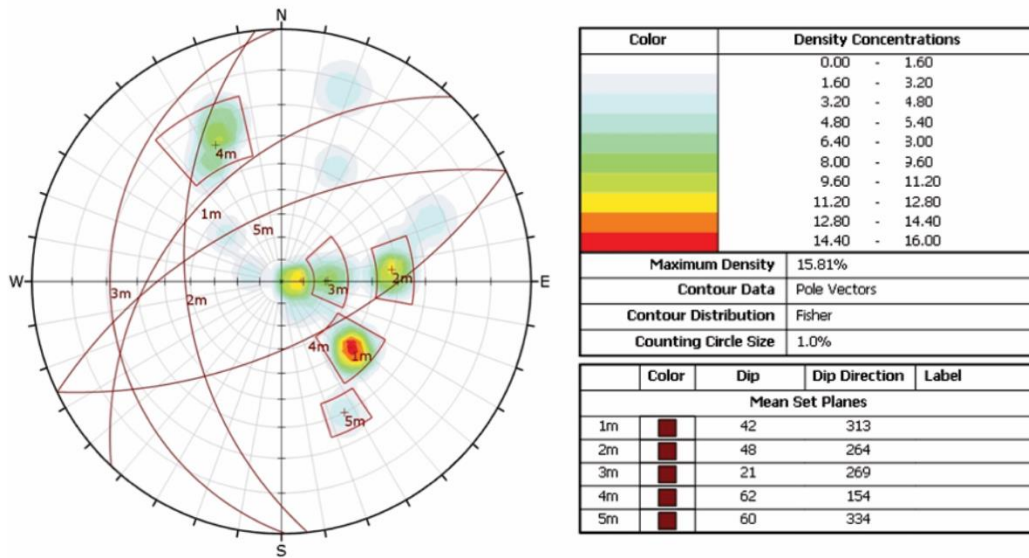


Figure 6.2 The dominant structure sets

**Table 6.4** Joint orientation factor

| Stope surface      | Factor B |
|--------------------|----------|
| Hanging wall       | 0.40     |
| Foot wall          | 0.33     |
| Vertical end-walls | 0.38     |
| Back               | 0.2      |

### 6.3.3 Gravity adjustment factor (C)

This value of the gravity adjustment factor (*C*) can be estimated using equation (6.4), based on the inclination of each stope surface ( $\alpha$ ). The results are presented in table 6.5 below.

$$\text{Factor } C \text{ for gravity fall and slabbing} = 8 - 6\text{COS}(\alpha) \quad (6.4)$$

**Table 6.5** Gravity adjustment factor

| Stope surface      | Inclination ( $\alpha^{\circ}$ ) | Factor C |
|--------------------|----------------------------------|----------|
| Hanging wall       | 90                               | 8        |
| Foot wall          | 90                               | 8        |
| Vertical end-walls | 90                               | 8        |
| Back               | 0                                | 2        |

## 6.4 Results of the assessment using the stability graph

### 6.4.1 Results for the first section (0 to 30 m of the stope length)

All of the stability parameters estimated for the first section of the stope length (0 to 30 m) are presented in table 6.6.

**Table 6.6** Stability parameters for section 1 (0 to 30 m)

| Stope Surface      | Q'  | A | B    | C | N'     | S (m) |      |
|--------------------|-----|---|------|---|--------|-------|------|
|                    |     |   |      |   |        | Low   | High |
| Hanging wall       | 2.7 | 1 | 0.4  | 8 | 8.66   | 8.57  | 10   |
| Foot wall          | 2.7 | 1 | 0.33 | 8 | 7.17   | 8.57  | 10   |
| Vertical end-walls | 63  | 1 | 0.38 | 8 | 190.39 | 3     | 3    |
| Back               | 5.3 | 1 | 0.20 | 2 | 2.12   | 3.16  | 3.33 |

Based on the results presented in table 6.6 and using GDA software and the stability graph, the stabilities of the planned stope surfaces are shown in figure 6.3. From figure 6.3, the stope vertical end-walls are in the stable zone. The stope back is on the unsupported transition zone boundary. The stope sidewalls are unstable. The sensitivity analysis for 40 to 60 m length of each stope, revealed that as the length of the stope increases the stability of the hanging wall and foot wall decrease. Initially, with a 40 m stope length, they are in the stable with support zone. But, as the length of the stope increases to 60 m, they moved to the caving zone. In other words, with a 60 m strike length, they are not stable even with support.

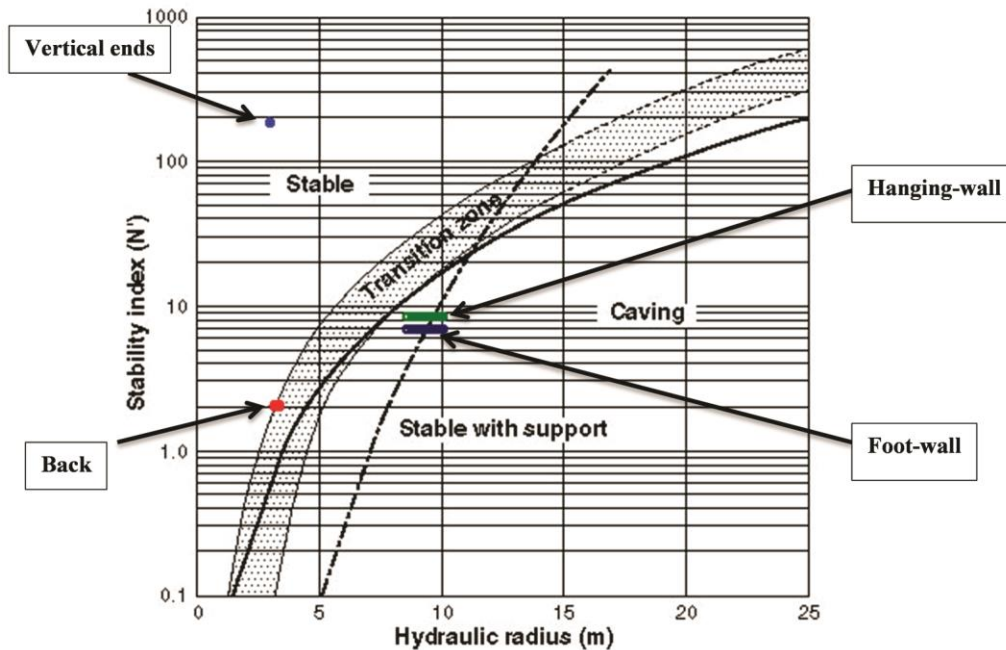


**Figure 6.3** Stability assessment using Mathews stability graph for section 1 using GDA software

#### 6.4.2 Stability assessment for the second section (30 to 114 m of the stope length)

All of the Mathews stability parameters estimated for this section of the stope (30 to 114 m) are presented in table 6.7. The hanging wall and foot wall in this portion of the stope have higher modified tunnelling quality index  $Q'$  values than section 1. Consequently, a larger  $N'$  value has been estimated.

**Table 6.7** Stability parameters for section 2 (30 to 114 m)

| Stope Surface      | $Q'$ | $A$ | $B$  | $C$ | $N'$   | $S$ (m) |      |
|--------------------|------|-----|------|-----|--------|---------|------|
|                    |      |     |      |     |        | Low     | High |
| Hanging wall       | 8.9  | 1   | 0.4  | 8   | 28.54  | 8.57    | 10   |
| Foot wall          | 8.9  | 1   | 0.33 | 8   | 23.62  | 8.57    | 10   |
| Vertical end-walls | 63   | 1   | 0.38 | 8   | 190.39 | 3       | 3    |
| Back               | 5.3  | 1   | 0.20 | 2   | 2.12   | 3.16    | 3.33 |

Based on the results presented in table 6.7 and using the stability graph, the stabilities of the planned stope surfaces are estimated in figure 6.4.

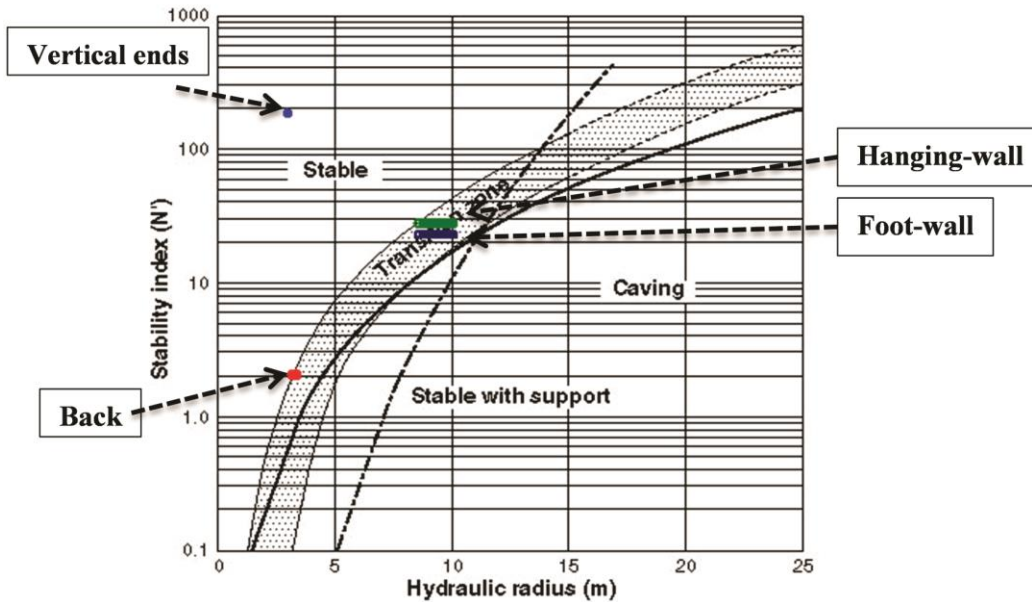


**Figure 6.4** Stability assessment using Mathews stability graph for section 2 using GDA software

As can be seen from figure 6.4, the stope vertical end-walls are in the stable zone. The stope back is on the boundary of the transition zone between stable without support and stable with support. The stope sidewalls are at the same transition zone. However, the stability of the sidewalls has improved in this section.

## **6.5 Overview of the numerical approach: finite element method**

In the last three decades, numerical methods have become popular, due to rapid advancements in computer technology. The suitability of these methods for analysis and design of very complex geotechnical problems is another reason for their popularity. Many conventional methods in rock mechanics are applicable to situations similar to the ones for which they were developed; however, there are many design problems for which no past experience is available. FEM is a well-recognized numerical method which can be used for rock mechanics and geomechanical problems. It has the ability to deal with material heterogeneity, non-linearity, complex-boundary conditions, in-situ stresses and gravity.

A full 3D elastoplastic FE model was developed to assess the stability of the primary and secondary stopes located between mine levels N9175 to N9275 at the Diavik Diamond Mine. The FE software Abaqus (by Dassault Systems) was used to generate the FE model. In the generated model, some geometries such as the open pits were simplified such that the effective influence of the extracted pits on the in-situ stress distribution field could be captured. However, the geometries of the Kimberlite pipe, undercut and overcut drifts, and the stope blocks are more representative of the actual structures.

### **6.5.1 Numerical model**

A full 3D geometric representation of the mine, which is shown in figure 6.5, was created based on the input data provided by Diavik Diamond Mine. The FE model presented in this chapter was also used to predict possible subsidence on the surface due to underground mining activities. The results of these stability assessments were presented in chapter 5. To accurately calculate the initial state of the stresses and to account for the zone of influence of the open pits, both A418 and A154 pits are included in the model. This allows the software to calculate the true initial state of the stresses accordingly in the first step of the simulation.

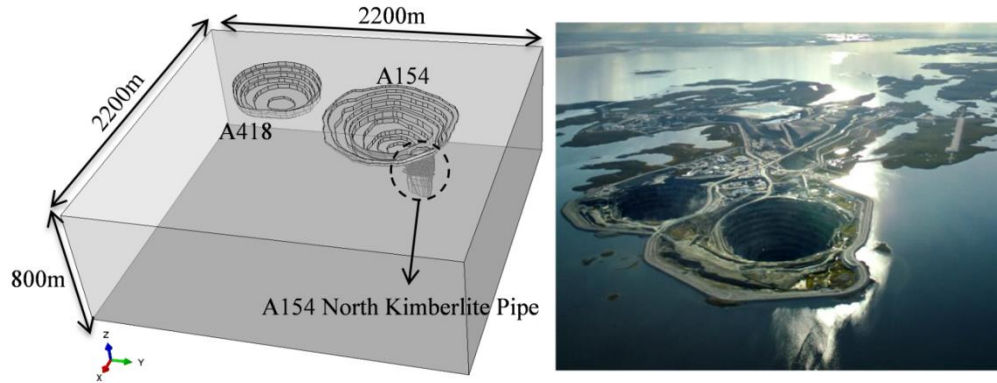


**Figure 6.5** Full 3D model of the mine in Abaqus (left) and aerial view of the mine

In this study, the main focus is only on one stope: N9225-P1-185. Therefore, only the A154 North Kimberlite pipe and Mining Block A, located between mine levels N9175 and N9275 constructed via BHS, are included in the model. Figure 6.6 shows the simplified model used for FE analysis in this chapter.

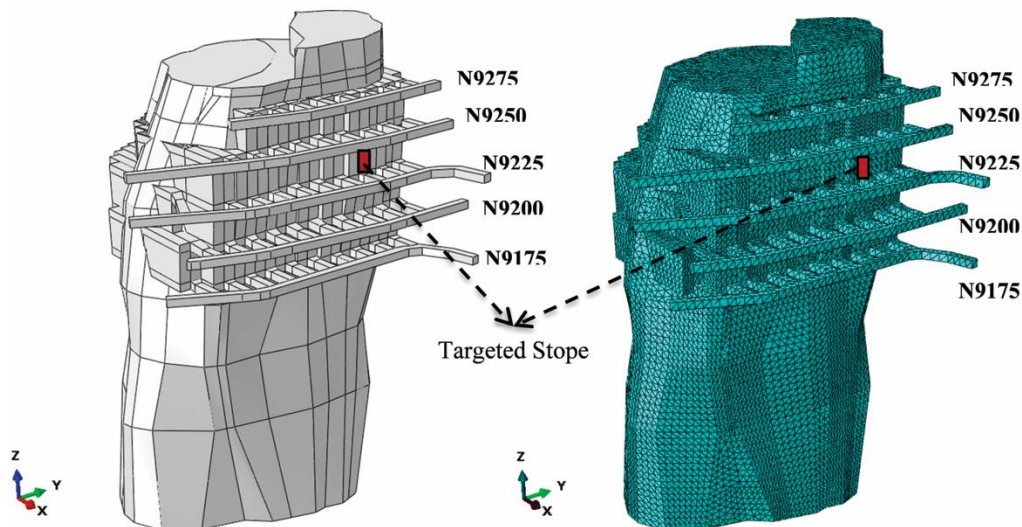


**Figure 6.6** Simplified model of the A154 North Kimberlite pipe and Mining Block A

In order to follow the exact sequence of mining, all primary and secondary stopes located at Mining Block A have been included in the model (figure 6.6). The geometry and the FE mesh of the P1-185 stopes between mine levels N9175 and N9275 in the model are illustrated in figure 6.7. The target stope is located

between mine levels N9225 and N9250. The stope is divided into three excavation blocks.

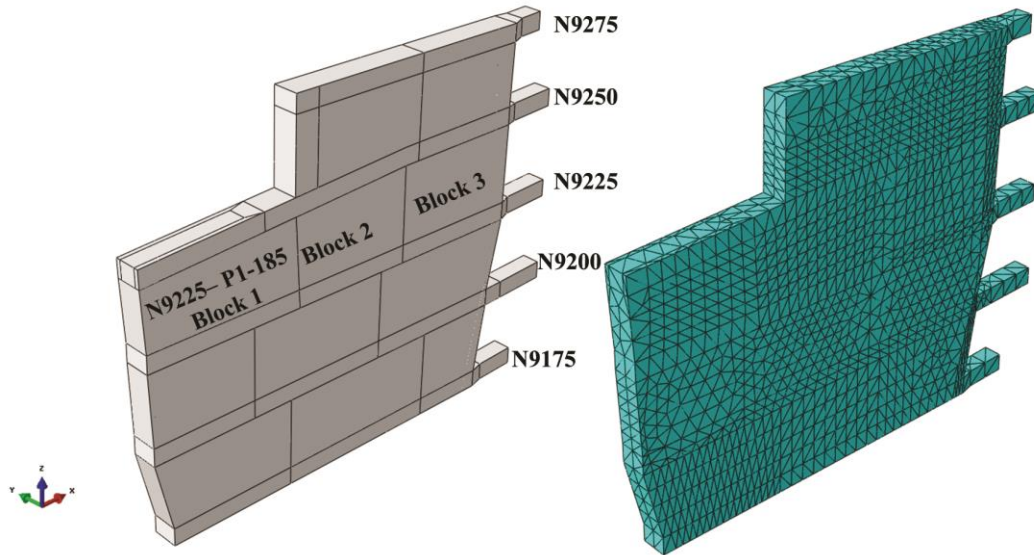


**Figure 6.7** Targeted stope P1-185 is located between mine levels N9225 and N9250

### 6.5.2 Input data assumptions and defining elements

The behavior of the rock was assumed to be governed by an elastic-plastic constitutive relation based on the elasticity theory and the Mohr-Coulomb plasticity criterion. Based on previous studies in Diavik Mine, the ratio of the horizontal stress to the vertical stress ( $k$ ) is assumed to be 1 in this model. The material properties used for the modeling is shown in table 6.8. The model has 776,794 quadratic tetrahedron elements (type C3D10), which creates 3,149,775 variables (including all degrees of freedom).

**Table 6.8** Material properties

| Material   | Unit weight $\gamma$<br>(MN/m <sup>3</sup> ) | Elastic modulus<br>(GPa) | Poisson's ratio ( $\nu$ ) | Cohesion<br>(MPa) | Friction angle<br>( $\phi$ ) <sup>o</sup> | UCS<br>(MPa) | Tensile strength<br>(MPa) |
|------------|--|--------------------------|---------------------------|-------------------|---|--------------|---------------------------|
| Granite    | 0.026  | 21                       | 0.3                       | 9.3               | 45  | 130          | 0                         |
| Kimberlite | 0.026  | 15                       | 0.3                       | 1.4               | 42  | 66           | 0                         |
| CRF        | 0.022  | 2                        | 0.3                       | 1.3               | 35  | 1.5          | 0.2                       |

### 6.5.3 Simulation steps

The excavation and backfilling procedures for the drifts and stopes are introduced to the model step by step. Consequently, the numerical model has 70 simulation steps. Step one is the geostatic step, which calculates the initial state of stress before starting the underground opening excavation. Step two is the excavation of five main haulage drifts between mine levels N9175 and N9275. Mining starts at mine level N9175 and goes upward to N9250, through steps 3 to 70 of the simulation. The stope mining sequence and corresponding simulation steps are shown in figure 6.8.

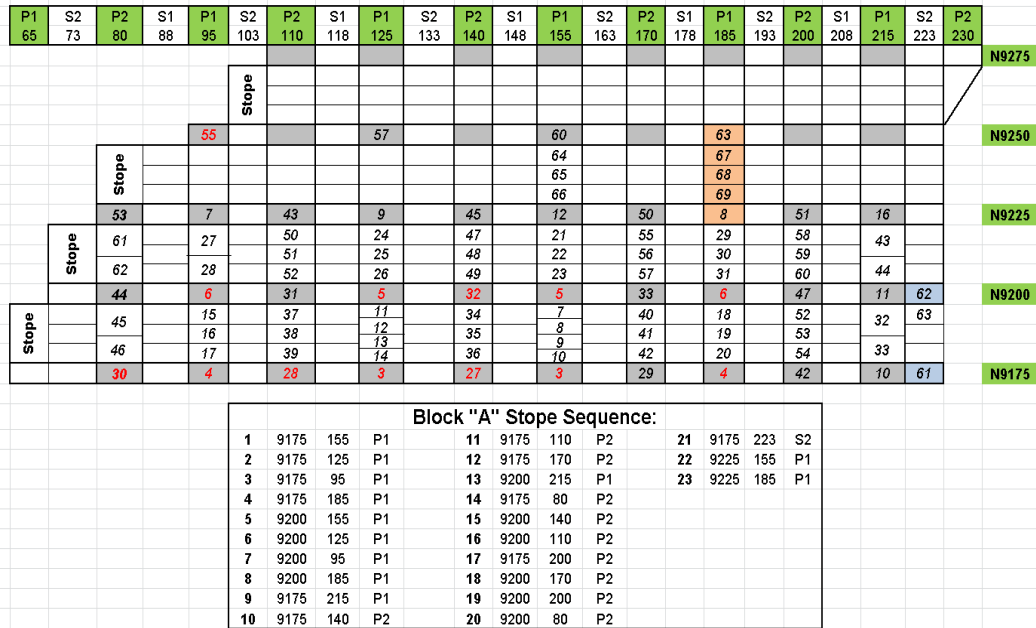


Figure 6.8 Mining sequence and simulation steps

The stope geometry is divided into three mining blocks. In step 67, block one of the targeted stope is excavated; step 68 is the backfilling of block one and excavation of block two of this stope; step 69 is the backfilling of block two and excavation of block 3; and step 70 is the backfilling of block 3.

### 6.6 Results of the stability assessments using the numerical model

During this study, the stability of each mining block of a targeted stope was investigated. The main areas of interest were the stability of the hanging wall, foot

wall, vertical end-walls and the back of each excavation block of the targeted stope. To assess the stability of the understudy stope, two criteria were used: (i) yielding zones; and (ii) relaxation zones.

### 6.6.1 Yielding zones

In this study, it was assumed that the behavior of the rock is elastoplastic. The Mohr-Coulomb yield function with non-associated flow rule was used. In geomechanics problems, the yielding zones can have great impact on the developing instability. Based on the results of the FE model, there were no significant yielding zones around each stope block, except around the Kimberlite vertical wall of Block 2 shown in figure 6.9.

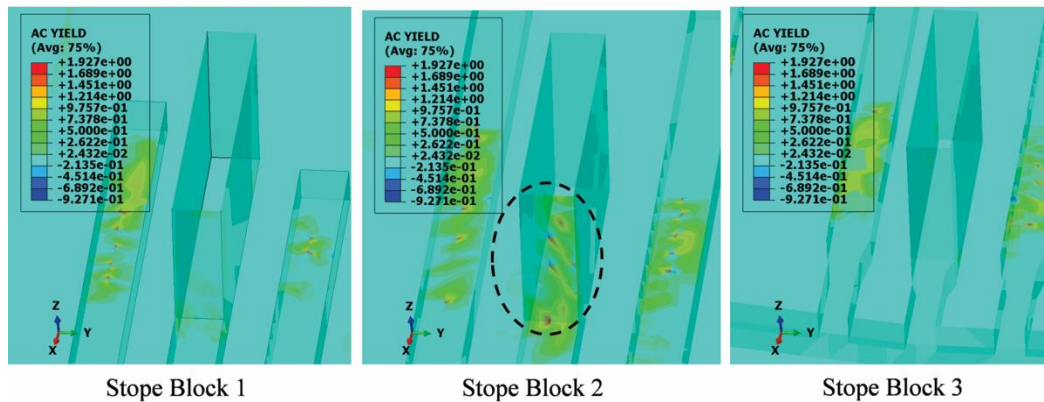


Figure 6.9 Yielding zones around each stope block

### 6.6.2 Relaxation zones

One of the important factors that can influence the stability of an underground opening is the relaxation zone or tensile stress zone. According to Potvin (1988), because there is no confinement around this zone, individual rock blocks have more freedom to move. Therefore, under the influence of the gravitational forces, there is a high potential for instability and unplanned dilution. The relaxation zones around each stope block are shown in figure 6.10. A significant development of the relaxation zone around Block 3 is illustrated in figure 6.11.

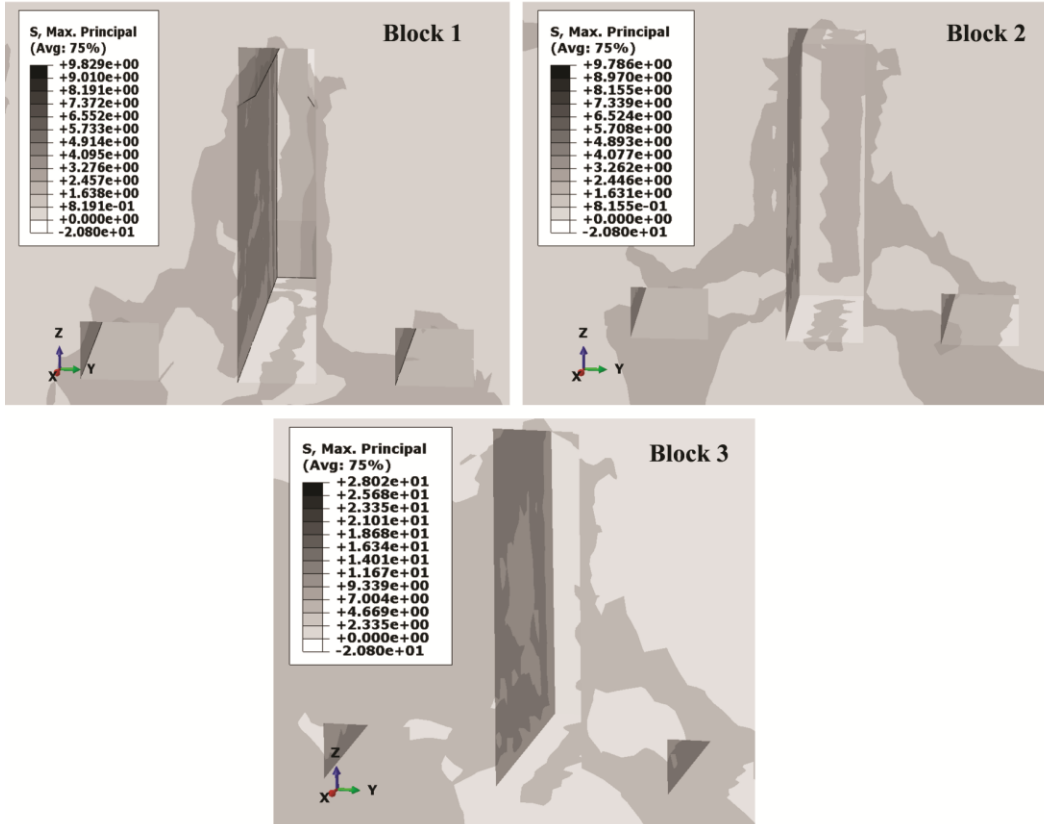


Figure 6.10 Relaxation zones around each stope block

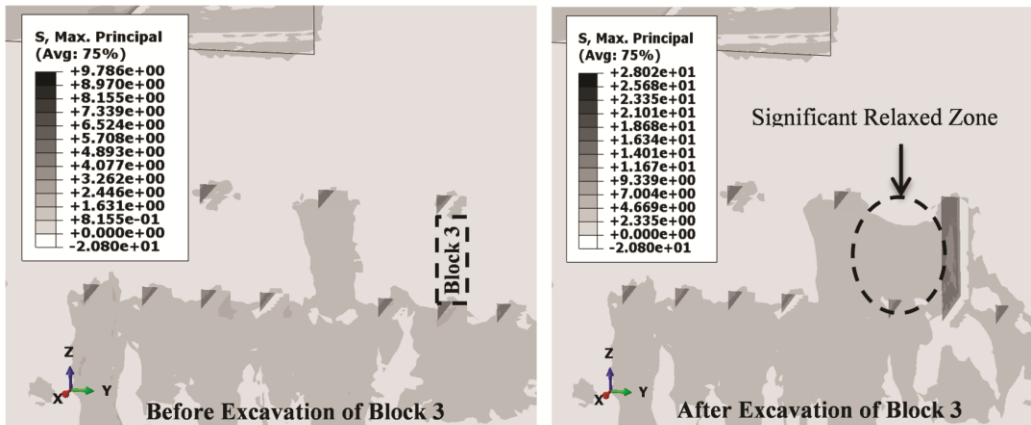


Figure 6.11 Development of the relaxed zone after the excavation of Stope Block 3

## 6.7 Sensitivity analysis

To investigate the effect of the  $k$  value (i.e. the ratio of the horizontal stress to vertical stress) on the stability of the open stope, a sensitivity analysis was performed. Seven heterogeneous stress regimes with different  $k$  values ranging from 0.33 to 1.6 were assumed. In this study, the influence of the stress regime on the relaxation zone and yielding zones were quantified. The main model was simplified and concentrated only on the targeted stope.

### 6.7.1 Yielding zone

The extent of the yielding zones around Block 1 of the understudy stope, under different  $k$  value situations, are illustrated in figure 6.12. Five different in-situ stress regimes were investigated. As the  $k$  value increases, the yielding zones around the opening extend significantly. When the  $k$  value is 2, the yielding zone reaches the N9290 bench surface.

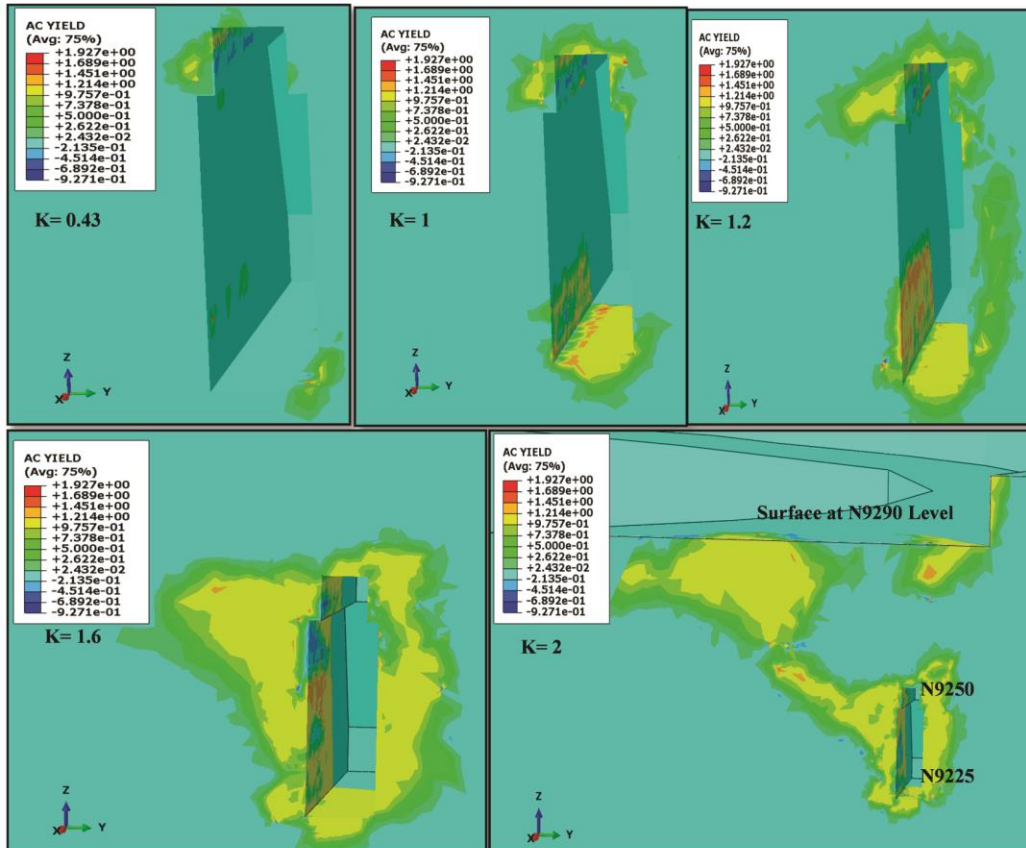


Figure 6.12 The extent of the yielding zones around Block 1 with different  $k$  values

### 6.7.2 Relaxation zones

To investigate the impact of the stress regime on the relaxation zone, seven different stress regimes were examined. The average relaxation depth around Stope Block 2 was recorded under different stress regimes. The results are presented in figures 6.13 and 6.14.

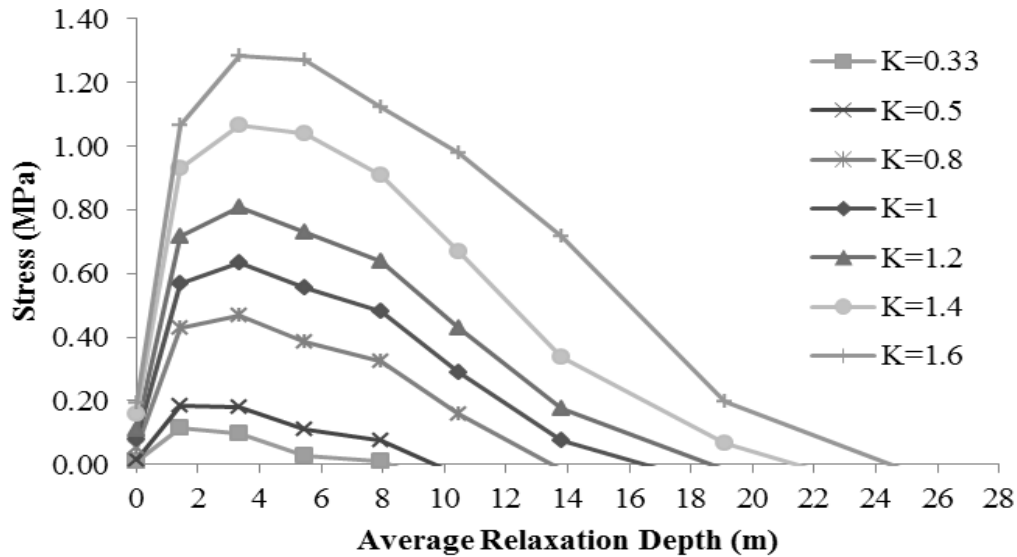


Figure 6.13 Average relaxation depth for different stress regimes

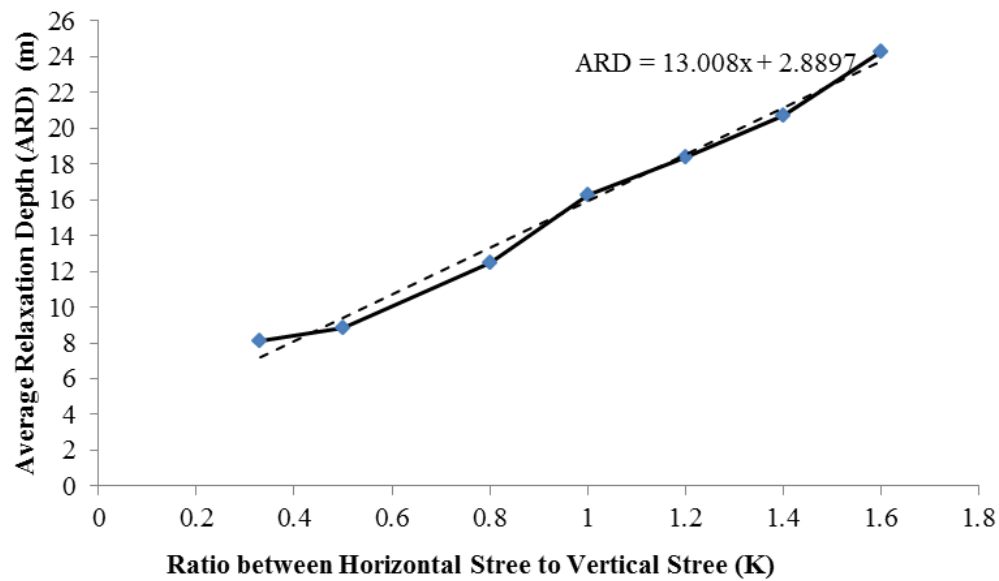


Figure 6.14 Average relaxation depth for different stress regimes

## 6.8 Discussion and conclusions

Throughout this chapter, two underground stability assessment methods (one empirical and one numerical) were presented. The main objective was to estimate the stability of a targeted stope located between mine levels N9250 and N9225 at Diavik Mine. A sensitivity analysis was also performed to investigate the effect of the stress ratio,  $k$ , on the development of the relaxation zones and the yielding zones around the underground stope walls. Overall, the following conclusions can be drawn from this study:

- The numerical model provides a better understanding of the stress distribution around the stope side walls. Particularly, the de-stressed area around the hanging wall and foot wall of each stope block can be estimated accurately. Having a better understanding of this de-stressed area can help identify possible zones of tensile stress. For instance, the depth of the relaxation zone can be easily identified in the numerical model. In addition, it can provide assistance when correcting the ground support design parameters (i.e. the length of the rock bolts or cable bolts).
- Based on the results of this study, the  $k$  value has a significant impact on the development and propagation of the relaxation and yielding zones around underground openings.
- Since the  $k$  value is an uncertain parameter in most underground mines, results of this sensitivity analysis can be used to further the risk analysis associated with the stability of the stope.

The numerical model generated in this study was based on the assumption that the rock mass is continuous. By introducing the discontinuities and joint sets into the model, more accurate results can be obtained.

## CHAPTER 7: VERIFICATION, VALIDATION AND DISCUSSION OF THE RESULTS

*In this chapter, the developed finite element model code is verified through a process referred to as numerical algorithm verification. In addition, the finite element model is validated by comparing the model results to actual field data and site observations. The main objective is to find the answers to the following two questions:*

- *Did I build the model right? (Verification process)*
- *Did I build the right model? (Validation process)*

## 7.1 Introduction

Model verification and validation (V&V) is an effective methodology to develop reliable geomechanics numerical models to make engineering predictions with quantified confidence. Quantifying the reliability and predictive accuracy of the FE model calculations provides underground designers with essential information to make high-consequence decisions (Thacker et al., 2004).

The U.S. Department of Defence (DoD) Modeling and Simulation Office (DoD, 2009) defines V&V of a model as follows:

- “Verification is the process of determining that a model or simulation implementation accurately represents the developer’s conceptual description and specifications of the model.” (DoD, 2009)

In other words, verification answers this question: Did I build the model right?

- “Validation is the process of determining the degree to which a model or simulation is an accurate representation of the real world from the perspective of the intended uses of the model.” (DoD, 2009)

In other words, validation answers this question: Did I build the right model?

Overall, the objective of the FE model V&V process is to quantify the level of agreement between the actual field data and the FE model prediction, and the model’s level of accuracy. To ensure that a valid model and a reliable simulation exist, V&V of the model and the results of the simulation must be completed (Cook and Skinner, 2005).

In this chapter, the developed FE model code is verified through numerical algorithm verification. Part of the process of verification (called calculation verification) was conducted in chapter 3 through the mesh convergence study. In addition, the FE model is validated by comparing the FE model results to actual field data and site observations.

## 7.2 Verification

The verification process can be classified into two distinct parts: (i) code verification; and (ii) calculation verification.

The purpose of code verification is to confirm that the utilized software (i.e. Abaqus) is working as intended and to verify the correctness of the numerical algorithms that are implemented in the code (Thacker et al., 2004). This process is also called numerical algorithm verification. One way to conduct code verification is to compare the FE model results with the known analytical solution. However, this approach is not always possible, because there are many geomechanical problems where there is no analytical solution.

The purpose of calculation verification is to estimate the numerical accuracy of a given solution to the governing equation. The objective is to quantify the error of a numerical simulation by conducting the (mesh) convergence study for the particular FE model under study. This activity was done in chapter 3 (please refer to section 3.4.3 regarding the mesh convergence study).

### 7.2.1 Pre-mining state of stress

The analytical method of specifying the in-situ state of stress at a point in a rock mass is shown in figure 7.1. The Cartesian global reference axis is established by orienting the x, y and z axes toward the mine north, mine east and vertically downwards, respectively.

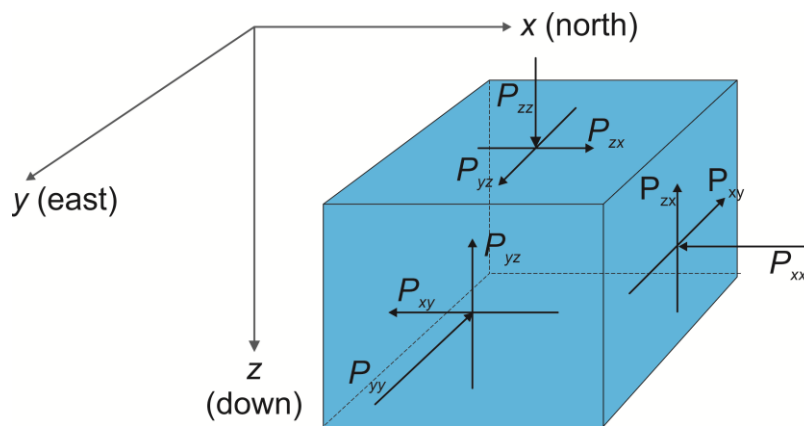


**Figure 7.1** Method of specifying the in-situ state of stress relative to a set of global references axes (after Brady and Brown, 2004)

The ambient stress components are denoted as  $P_{xx}$ ,  $P_{yy}$ ,  $P_{zz}$ ,  $P_{xy}$ ,  $P_{yz}$  and  $P_{zx}$ . Discussion on the calculation of all components of the stresses are beyond the scope of this chapter; however, the vertical normal stress,  $P_{zz}$ , can be calculated using equation (7.1):

$$P_{zz} = \gamma z \quad (7.1)$$

where  $\gamma$  is the unit weight of the rock and  $z$  is the depth below ground surface.

In order to verify the FE model, the results of the FE model solution for the calculation of the vertical in-situ stress for 15 monitoring points in granite with an average unit weight of  $0.026 \frac{\text{MN}}{\text{m}^3}$  are compared with equation (7.1). As presented in table 7.1, the relative error between the FE model solution and the analytical solution is less than 0.7%.

**Table 7.1** Comparison of the analytical and finite element model solutions

| Monitoring Point | Depth (m) | In-situ Vertical Stress (MPa) |                     | Error (%) |
|------------------|-----------|-------------------------------|---------------------|-----------|
|                  |           | FE Model                      | Analytical Solution |           |
| 1                | 0.00      | 0.00                          | 0.00                | 0.00      |
| 2                | -57.14    | 1.50                          | 1.49                | 0.70      |
| 3                | -114.29   | 2.99                          | 2.97                | 0.68      |
| 4                | -171.43   | 4.48                          | 4.46                | 0.61      |
| 5                | -228.57   | 5.98                          | 5.94                | 0.55      |
| 6                | -285.71   | 7.46                          | 7.43                | 0.49      |
| 7                | -342.86   | 8.95                          | 8.91                | 0.42      |
| 8                | -400.00   | 10.44                         | 10.40               | 0.35      |
| 9                | -457.14   | 11.92                         | 11.89               | 0.27      |
| 10               | -514.29   | 13.40                         | 13.37               | 0.20      |
| 11               | -571.43   | 14.88                         | 14.86               | 0.12      |
| 12               | -628.57   | 16.35                         | 16.34               | 0.05      |
| 13               | -685.71   | 17.83                         | 17.83               | 0.00      |
| 14               | -742.86   | 19.30                         | 19.31               | -0.08     |
| 15               | -800.00   | 20.77                         | 20.80               | -0.12     |

The results of verification are illustrated in figure 7.1. As can be seen from this figure, both solutions almost match.

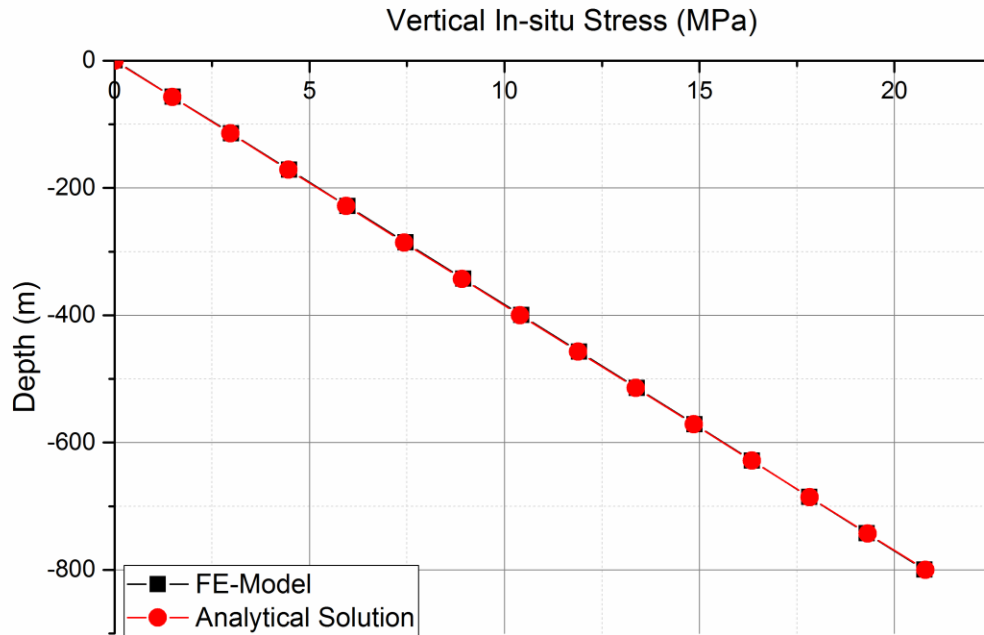


**Figure 7.2** Compression of the analytical and finite element model solutions

### 7.3 Discussion and validation of the finite element model results

In this section, the results of the FE model are validated using actual measurements and observations. In some cases, due to a lack of measured data, the results were validated based only on the observations (for instance, checking the predicted failure in the model and the actual failure in reality).

The main objective in this section is to check the range of accuracy (agreement) between the FE model results and the actual measured data. An acceptable range of accuracy is the amount of accuracy that is required for a model to be valid for its intended purpose and is usually specified for each model variable of interest as a range for the difference between that model variable and the corresponding system variable (Sargent, 2013).

### 7.3.1 Surface subsidence at the N9280 bench: discussion and validation of the results

As shown in chapter 5, the simplified FE model predicted a maximum displacement of 15.78 mm until the end of January 2016. It was shown that the average relative error between the FE model predictions and actual measured data was 7.95%. However, the model presented in chapter 5 was a smaller scale model of the main FE model.

In this section, the results of the main FE model are validated using the updated data. The last data point is dated June 03, 2016. This date corresponds to step 93 of the main FE model. The FE model predicted the development of downward surface settlement (up to 36.58 mm) in the N9280 bench surface. In addition, the model predicted the wall failure at the bottom of the pit, which will be discussed in the next chapter. Both of these predictions are shown in figure 7.3. A monitoring nodes path was defined in the FE model, as done previously.

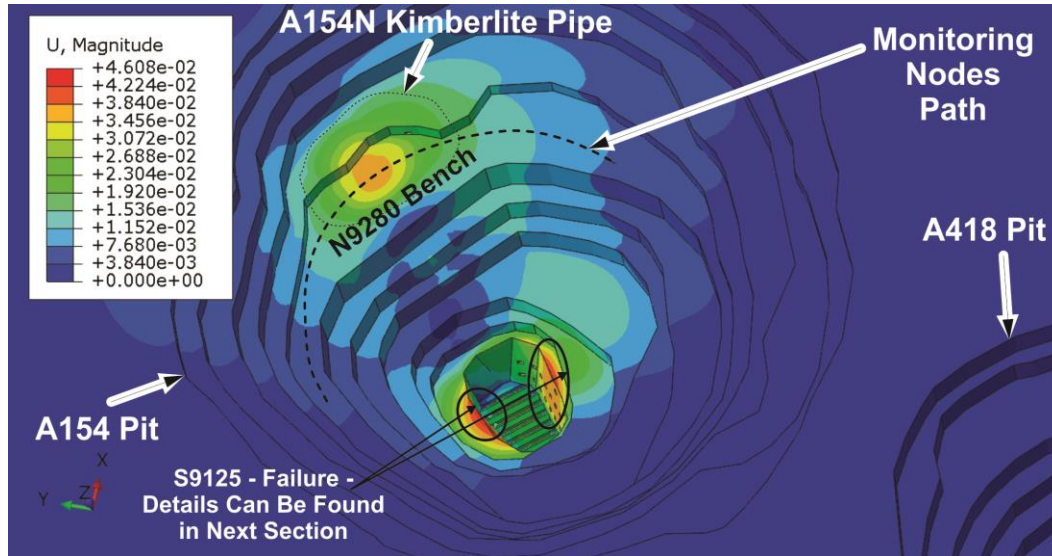


**Figure 7.3** Surface subsidence displacements calculated by the finite element model for the N9280 bench

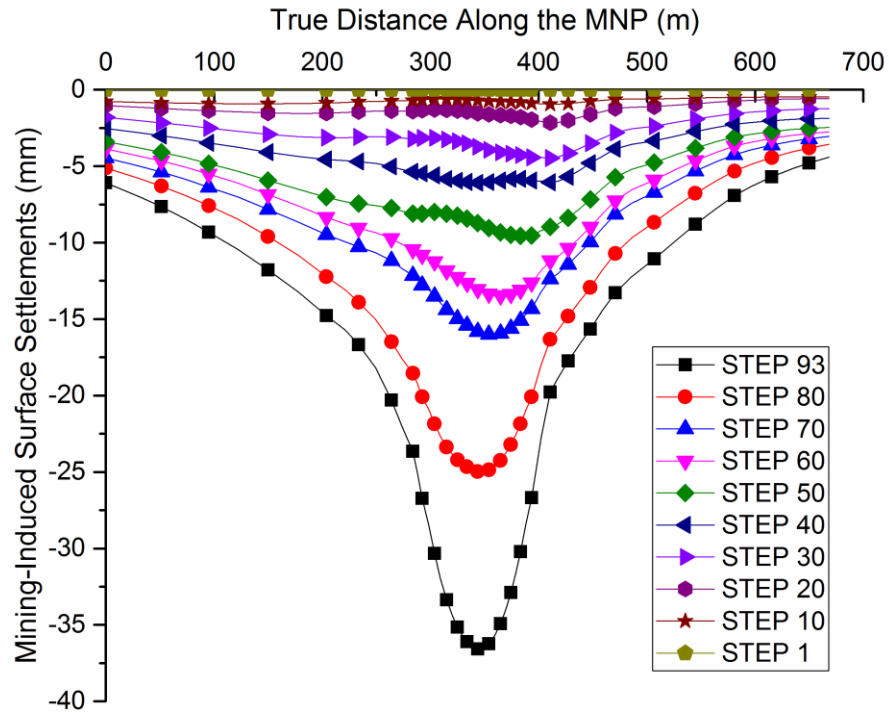


Figure 7.4 Mining-induced surface subsidence growth throughout the finite element model simulation

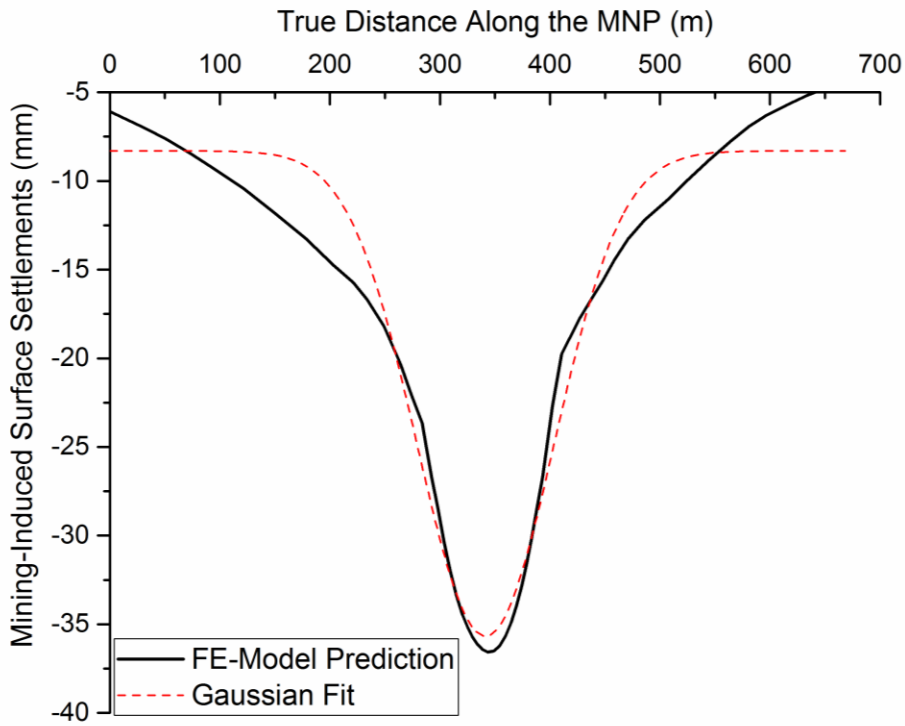


Figure 7.5 Curve fitting of the finite element model results for N9280's mining-induced surface subsidence

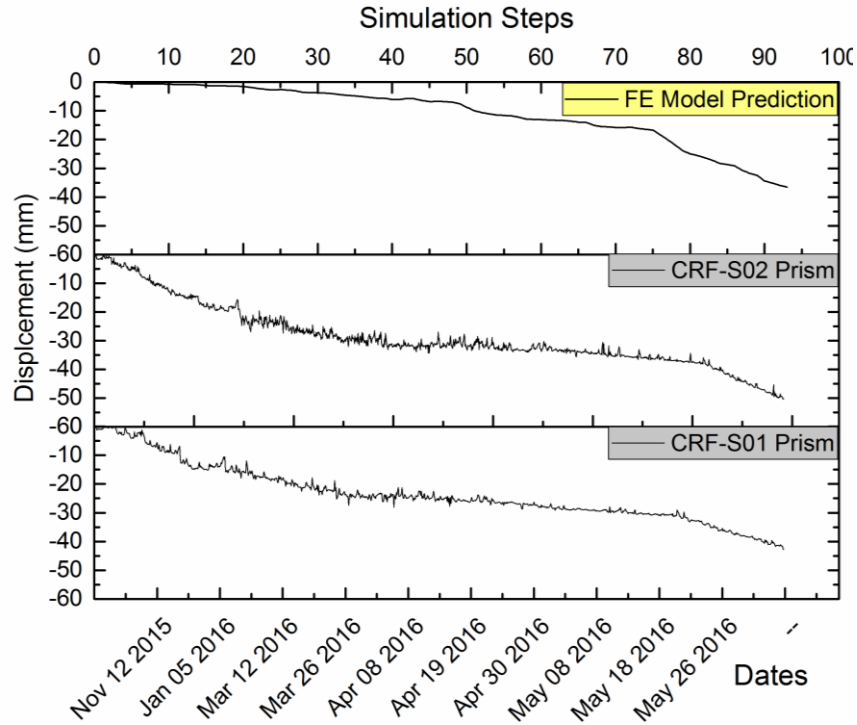
The FE model results are compared with the pit movement monitoring prisms. The location of the monitoring prisms is shown in chapter 5.

Figure 7.6 shows the comparison between the FE model predictions and the measured data from the installed monitoring prisms at Monitoring Zone 1. In this location, two prisms (CRF-SO1 and CRF-SO2) are installed with a distance of 6 m in between. The maximum average movement measured from these two prisms is 46.7 mm, while the FE model predicted 36.6 mm of settlement for this location. This brings the average relative error of the FE model prediction to 21%.

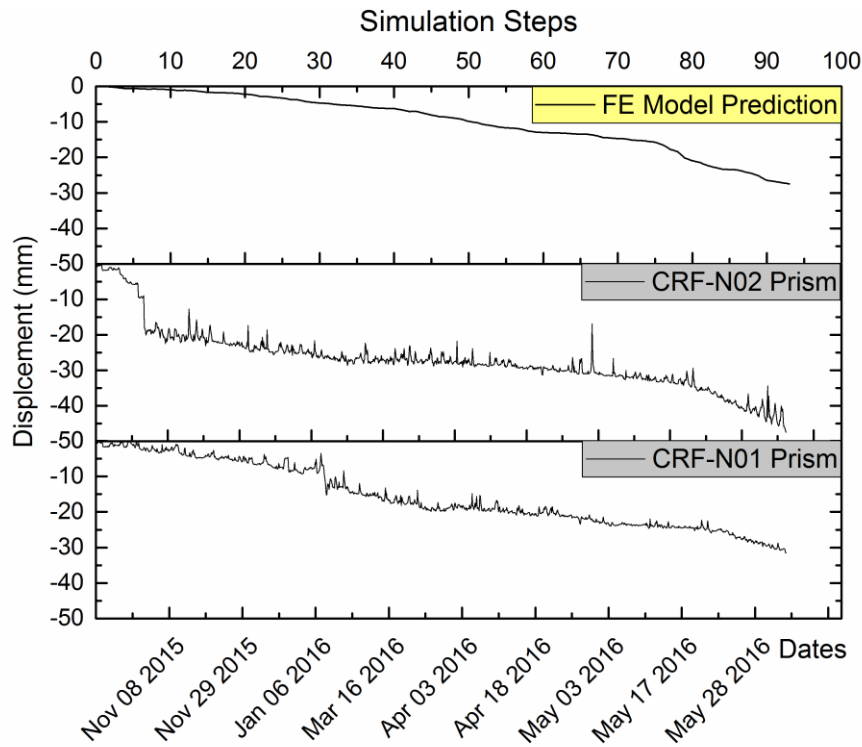
Figure 7.7 shows the comparison between the FE model predictions and the measured data from the installed monitoring prisms at Monitoring Zone 2. In this location, two prisms (CRF-NO1 and CRF-NO2) are installed also with a distance of 6 m in between. The maximum average movement measured from these two prisms is 39.55 mm, while the FE model predicted 27.46 mm of settlement for this location. This brings the average relative error of the FE model predictions to 30.6%.

Figure 7.8 and 7.9 illustrate the comparison between the FE model predictions and the actual measured settlements at the 280-10 and 280-12 prisms, respectively. The maximum surface movement reading by the 280-10 prism is 9.4 mm, and the FE model predicted 10.51 mm. The relative error of the prediction is 11.8%. The maximum surface movement reading by the 280-12 prism is 6.5 mm, and the FE model predicted 6.8 mm, a relative error of prediction of 4.6%.

The comparisons between the FE model results and the actual measured ground settlement data are summarized in table 7.2. The average relative error of prediction for the surface subsidence for this area is 17%. This is a significant jump in the accuracy of the predictions compared to the previous model which had a relative error of prediction of 7.9%. However, the FE model results are still in an acceptable range of accuracy.



**Figure 7.6** Comparison of monitored displacements at Monitoring Zone 1 versus the finite element model's calculated values



**Figure 7.7** Comparison of monitored displacements at Monitoring Zone 2 versus the finite element model's calculated values

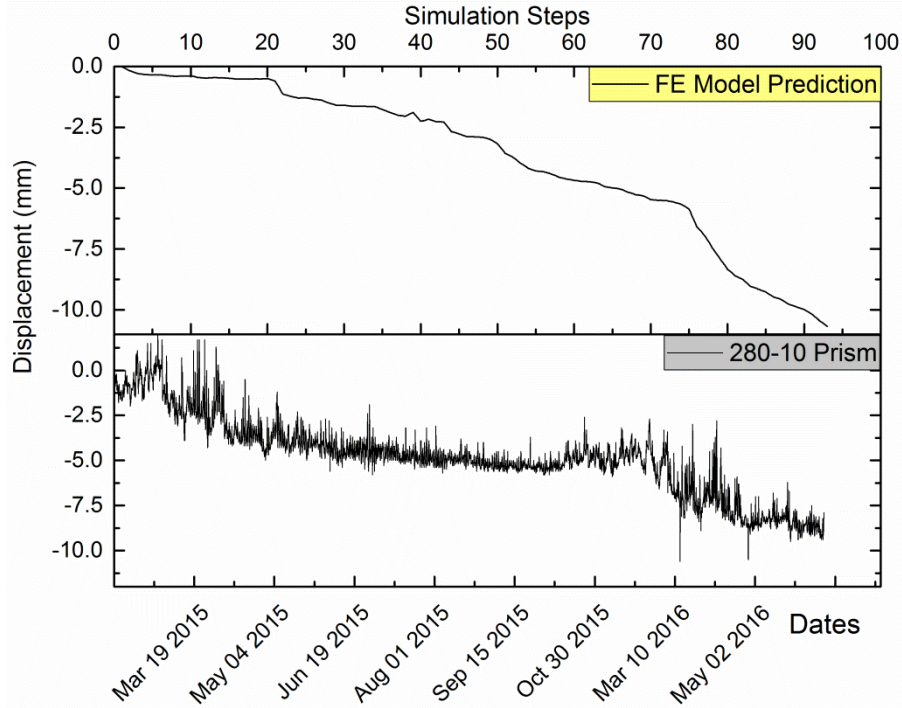


**Figure 7.8** Comparison of monitored displacements of the 280-10 prism and the finite element model's calculated values

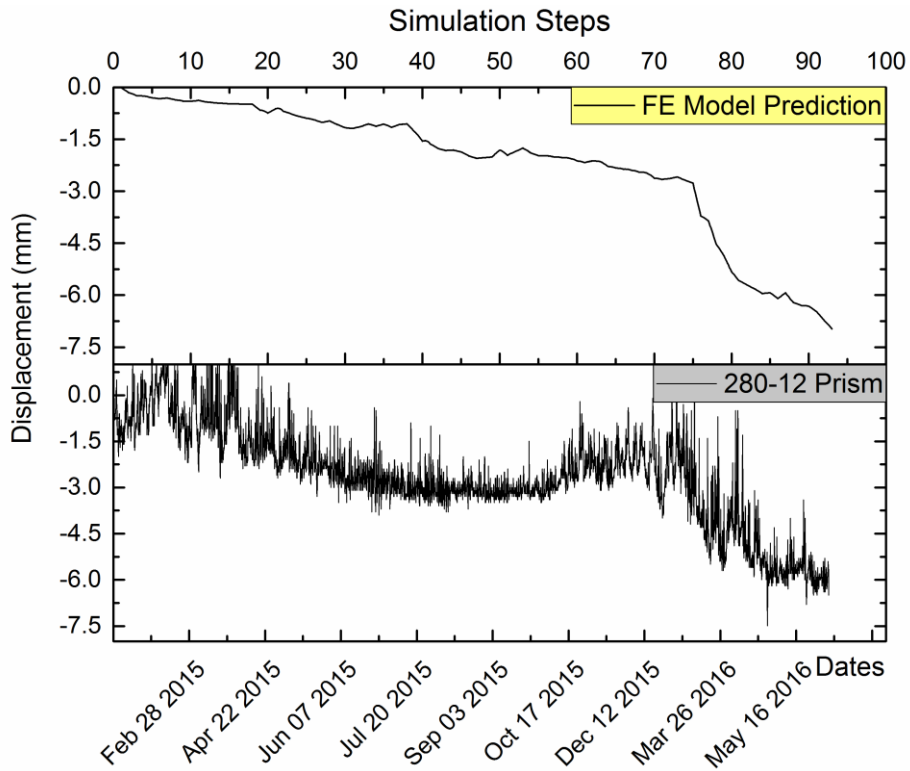


**Figure 7.9** Comparison of monitored displacements of the 280-12 prism and the finite element model's calculated values

**Table 7.2** Comparison between the measured data and the finite element model's calculations

| <b>Locations of the Prisms</b>              | <b>Measured Data (mm)</b> | <b>FE Model Prediction (mm)</b> | <b>Relative Error (%)</b> |
|---|---------------------------|---------------------------------|---------------------------|
| Mining Zone 1 (Average between CRF-S01&S02) | 46.7                      | 36.58                           | 21                        |
| Mining Zone 2 (Average between CRF-N01&N02) | 39.55                     | 27.46                           | 30.6                      |
| 280-10 Prism                                | 9.4                       | 10.51                           | 11.8                      |
| 280-12 Prism                                | 6.5                       | 6.8                             | 4.6                       |
| <b>Average Relative Error (%)</b>           |                           |                                 | <b>17</b>                 |

### 7.3.2 S9125 South wall movements and failure: Bottom of the pit

The FE model predicted mining-induced surface subsidence due to the SLR mining method used in the A154 South pipe. As discussed in chapter 3, this mining method can be classified as a sublevel block caving method. When the orebody is vertical, which is the case in Diavik Mine, and has a well-defined cut-off between it and the surrounding host rock, in this case granite, the cave will be expected to propagate vertically to the surface. This is confirmed by the developed FE model, as shown in figure 7.10. The extent of the mining-induced subsidence will depend on a number of features of the orebody, host rock, the local geology and the mine topography. These factors are summarized by Brown (2003): (i) the strength of the orebody; (ii) the strength of the host rock; (iii) the strength of the overburden or cap rock; (iv) the dip of the orebody; (v) the shape of the orebody in plan; (vi) the presence of major structural features such as faults and dikes intersecting the orebody; (vii) the in-situ stress field and the depth of the mine; (viii) open pit mining and the slope of the pit; (ix) backfilling of the excavated stopes; and (x) nearby underground excavations. All of these factors are included in the developed FE model. However, there is no major structural features and dikes that intersect the orebody. Figure 7.10 illustrates the results of the FE model calculations regarding mining-induced surface subsidence in the mine domain.

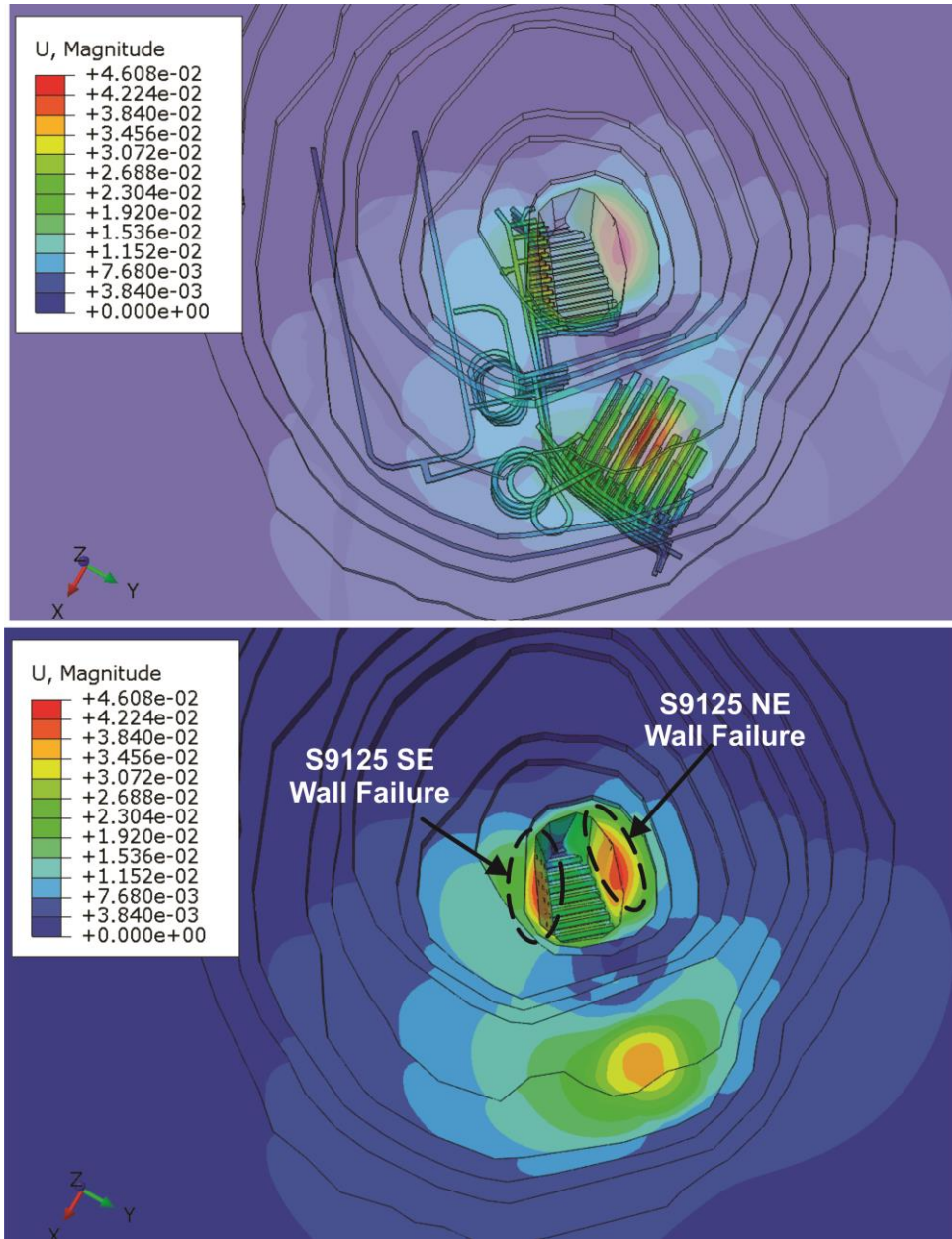


**Figure 7.10** Surface settlements predicted by the finite element model for the S9125 South and North wall failure

The magnitude and direction of the the displacements induced in the rock mass around the caved zone at the bottom of the pit are shown in figure 7.11. In addition, the extent of the disturbance zone is shown in this figure. Three key features calculated by the FE model and shown in this figure are (definitions are from Brady and Brown, 2004): (i) the angle of break ( $\alpha$ , also called the angle of subsidence) is the angle made with the horizontal at a mining level by a straight

line (red lines in the figure) drawn from the undercut level to the surface disturbance; (ii) the subsidence zone is defined by the angle of break as shown in figure 7.11. Large-scale or macro-deformations will occur in this zone; and (iii) the zone of influence, which is the zone of disturbance outside of a subsidence zone. Small-scale or micro-deformations will occur in this zone. It must be noted that, although the deformations occurring within this zone is small in comparison with the ones occurring within the subsidence zone, depending on the geological features of the site, these deformations can be large enough to damage underground excavation and even the mine infrastructure located in the zone of influence.

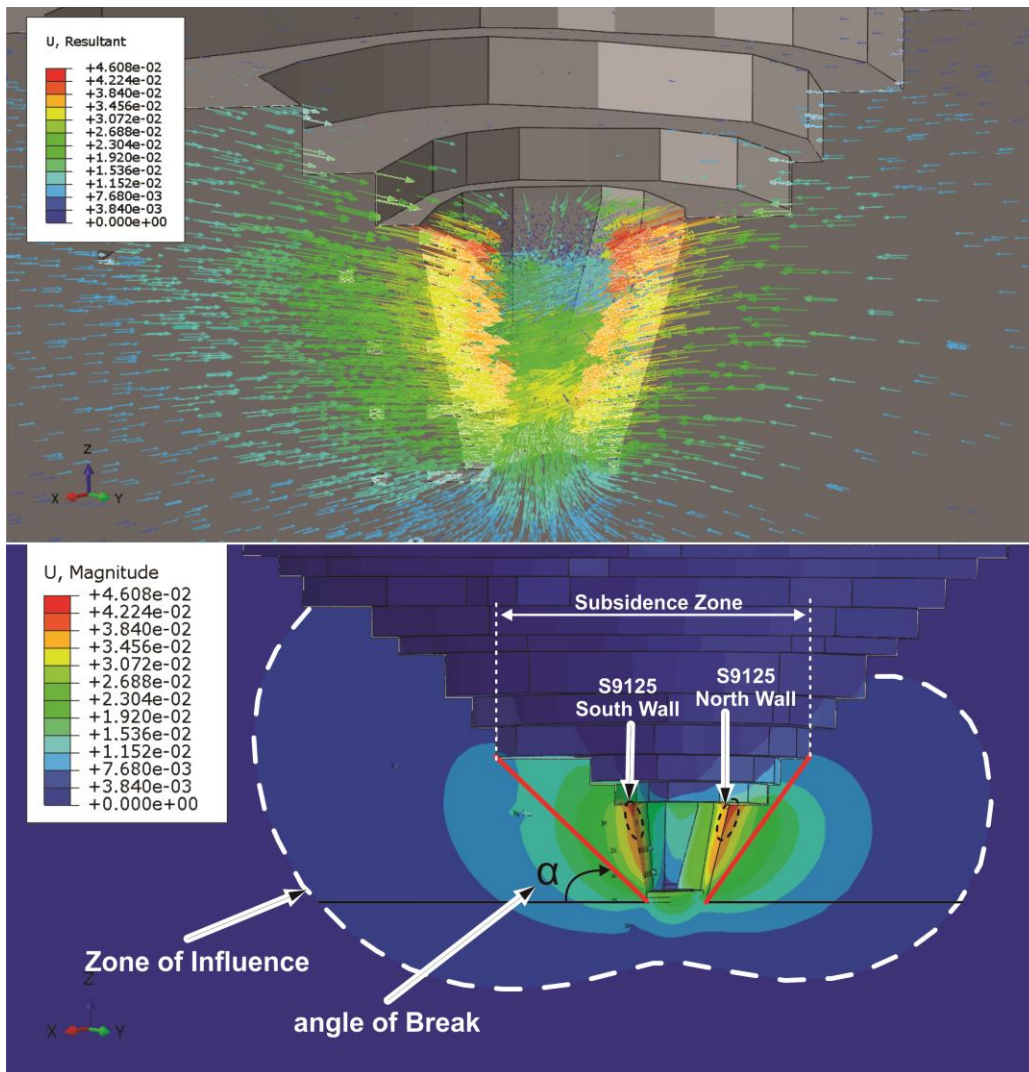


**Figure 7.11** The extent of the mining-induced surface subsidence predicted by the finite element model

As it shown in figures 7.10 and 7.11, the FE model predicted large displacements on both the S9125 South and North walls. At the time of writing this thesis, one of these predictions has been confirmed.

The FE model's prediction of the mining-induced movements on the S125 Southeast wall was immediately marked as a possible failure zone. This decision was based on the development of major cracks on the walls of the S9125-920 drift. To closely monitor the movements of this wall, two crack meters (CMs) were installed, as shown in figure 7.12. Measured data from these CMs are presented in figure 7.13. Figure 7.14 shows the measured data from the S9125 prisms before failure of the S9125 South wall.

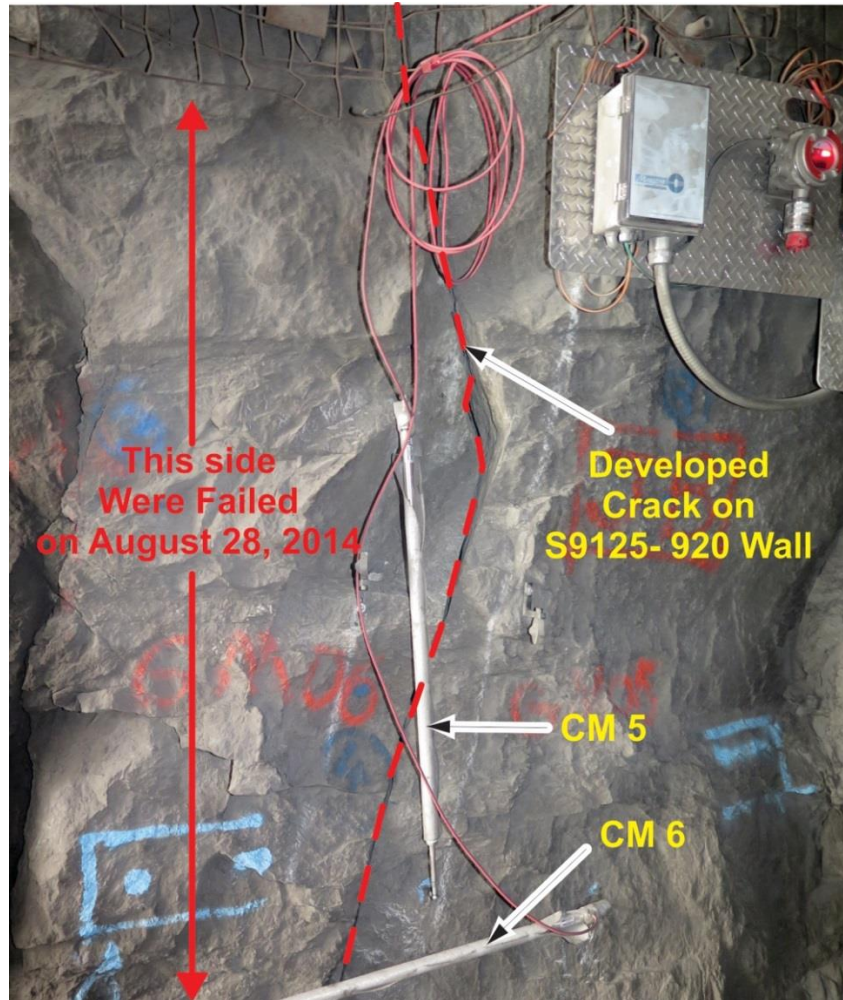


**Figure 7.12** Crack meters installed in the S9125-920 drift by the mine (courtesy of Diavik Diamond Mine)

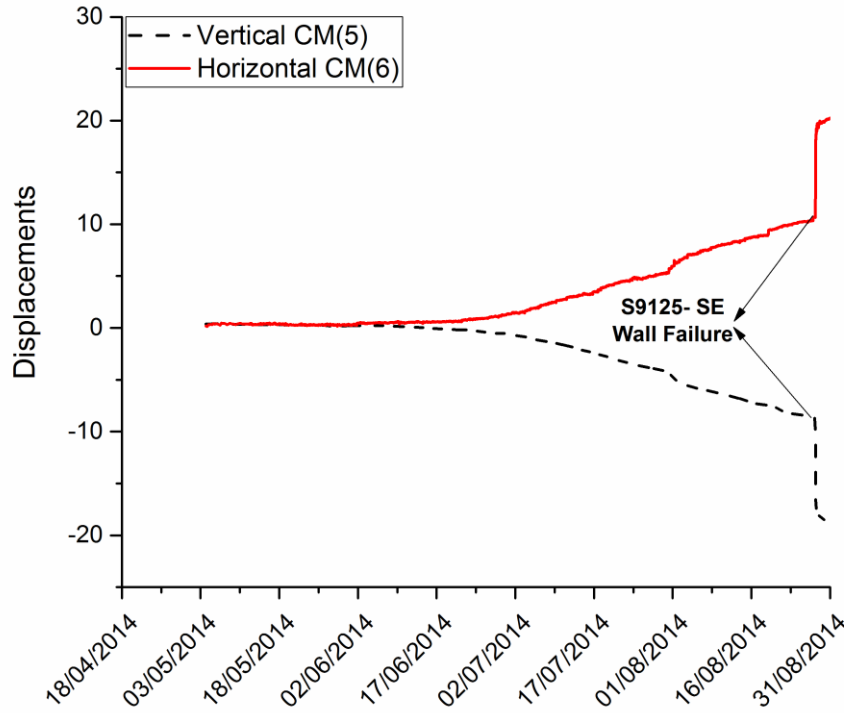


**Figure 7.13** Measured displacements along the horizontal and vertical crack meters (CM 6 and CM5, respectively)

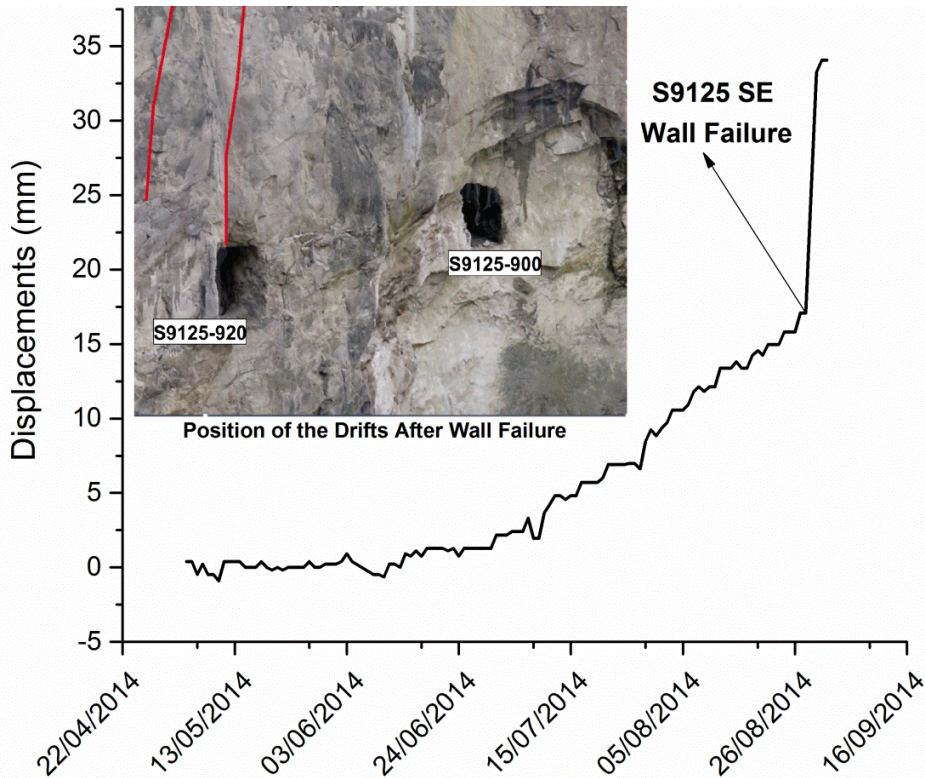


**Figure 7.14** The S9125 South wall failure (from the S9125 prisms data; photo courtesy of Diavik Diamond Mine)

### 7.3.3 Fall of ground at the N9225-118 drift

On August 29, 2015, the fall of ground was discovered at the N9225-118 drift. The fall occurred on the granite/Kimberlite contact in the back (roof) of the N9225-118 level entry, as shown in figure 7.15. The N9225-118 level entry was barricaded and the level evacuated. Figure 7.15 shows the FE model predictions for this drift at the same location (Kimberlite/granite contact). The model predicted yielding zones around the drift as well as around its back.

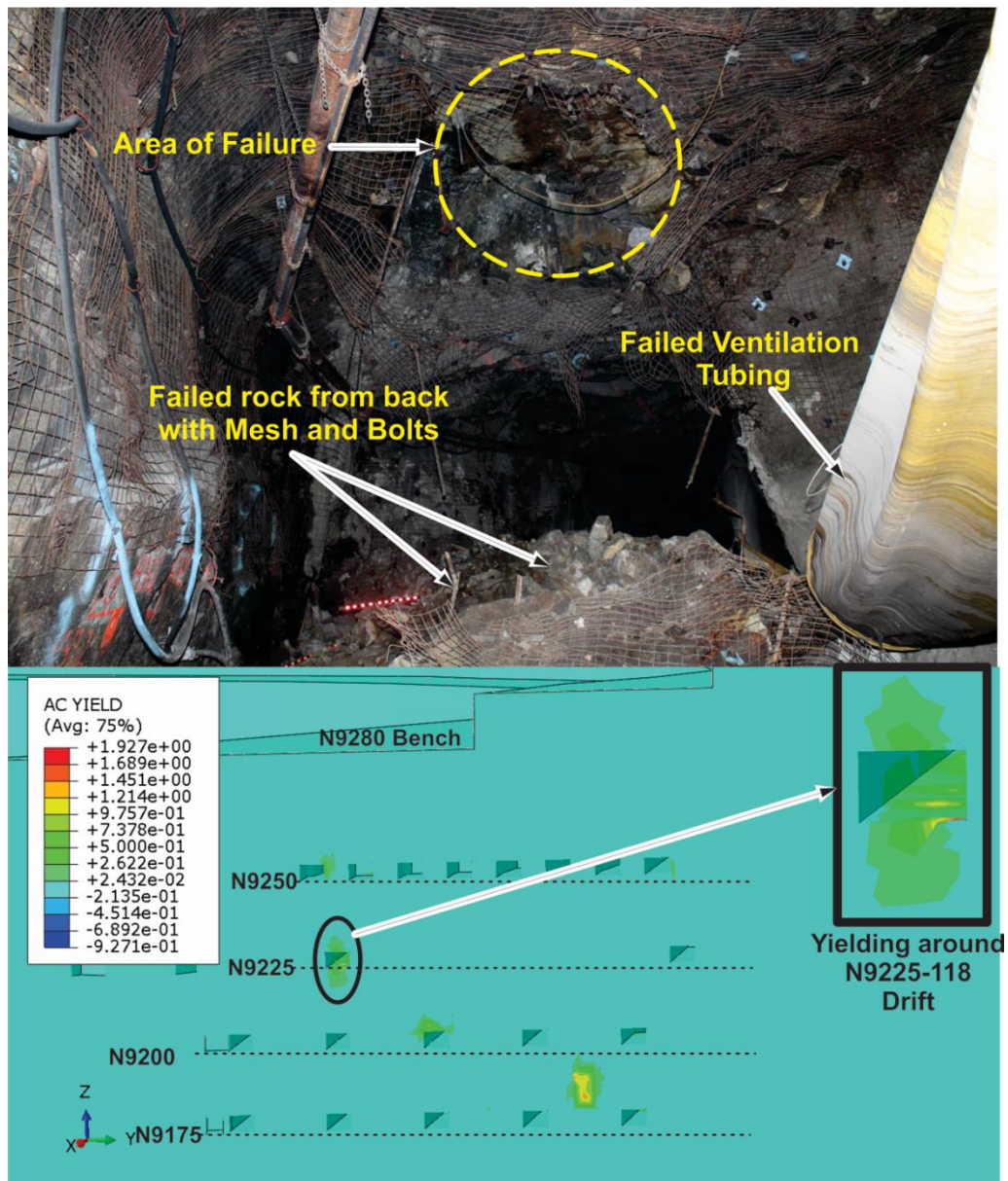


**Figure 7.15** fall of ground at the N9225-118 drift and the finite element model predictions for this drift (photo courtesy of Diavik Diamond Mine)

### 7.3.4 Rockburst failure incident at the S9050-940 drift and finite element model prediction

Ground failure occurred on December 14, 2013, at 3:30 pm at the A154 South Kimberlite pipe. Eight tons of Kimberlite caved in, and 12 bolts failed. Significant zones of potential rockburst were identified using the FE model, as discussed in chapter 4 and shown in figure 7.16. The geometry of the A154 South Kimberlite pipe shown in figure 7.16 corresponds to the date of the incident (step 55 of the FE simulation model). The FE model predicted a strong rockburst tendency for this drift due to the concentration of the stresses on the back of this drift.

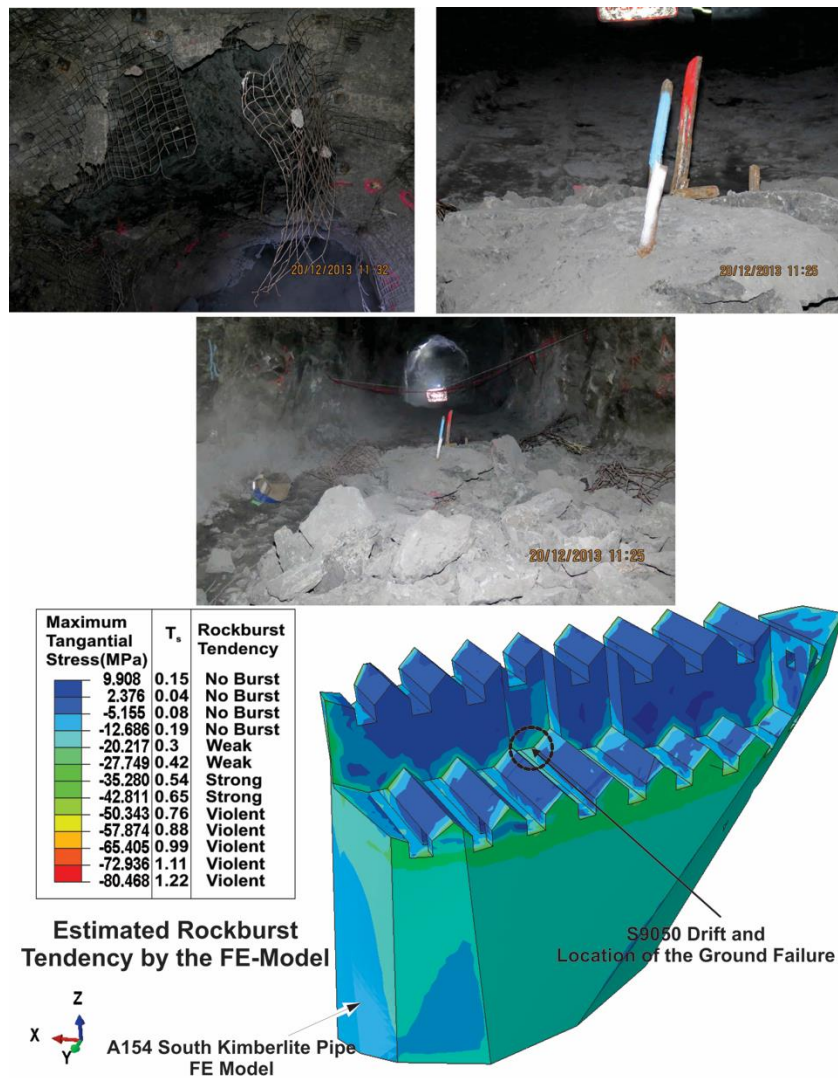


Figure 7.16 Ground failure at S9050 SLR (A154 South) and the finite element model predictions (photo courtesy of Diavik Diamond Mine)

#### **7.4 Summary and conclusion**

Throughout this chapter, the developed FE model code was verified through numerical algorithm verification. In addition, the FE model results were validated by comparison to actual field data and site observations to quantify the accuracy and precision of the FE model results. It was concluded that the model is in a good agreement with the actual conditions of the mine. In addition, not only did the model successfully forecast the possible yielding, failure and subsidence zones, but it also identified the stable areas of the mine as well.

It must be noted that, due to the nature of rock, full validation of numerical models in geomechanics is impossible. One reason for this is that natural systems are not closed systems. This means there are many uncertainties and variables that either there is no means to capture them or including them into the model will increase the complexity of the model such that the calculation costs would be unaffordable.

In conclusion, the comparison between the predicted results of the developed FE model and actual monitoring data and site observations showed that the predictive capacity of the developed FE model is a valuable tool for stability and design analysis in underground mines.

## **CHAPTER 8: SUMMARY, CONCLUSIONS AND RECOMMENDATIONS**

*This chapter presents the thesis summary and research conclusions. The significance and contributions of this research are discussed. In addition, this chapter contains recommendations for future work in the determination of in-situ and mining-induced stress in underground mines.*

### **8.1 Summary of the research**

One of the essential components of the underground excavation design process, which directly influences the performance and stability of underground constructions, is knowledge of the in-situ and mining-induced stress. Knowing the magnitudes and directions of these stresses can help us determine the suitable shapes and orientations of the tunnels (drifts) and stopes. In addition, knowing the stress regime in the rock mass can predict the type of rock failure that may occur in the future and identify potential rockbursting zones. Furthermore, important direct products of mining-induced stress are surface subsidence and ground movements. Prediction of the mining-induced surface subsidence profile (i.e. zone of influence, zone of subsidence, angle of break) and its magnitude are critical tasks for rock engineers.

A comprehensive literature review of stress analysis methods and underground stability design has been presented in chapter 2. In summary, the major shortcomings revealed by the literature include: (i) it is difficult and costly to estimate the magnitude and direction of the pre-mining stresses by using direct measurement techniques; (ii) most of these techniques measure stress at a point in the rock mass, and this has been proven to be a measure with a wide scatter; and (iii) there is a need for an integrated engineering methodology which can be used as a predictive design tool to properly simulate the complete stress-strain path of the mine history throughout the mine domain.

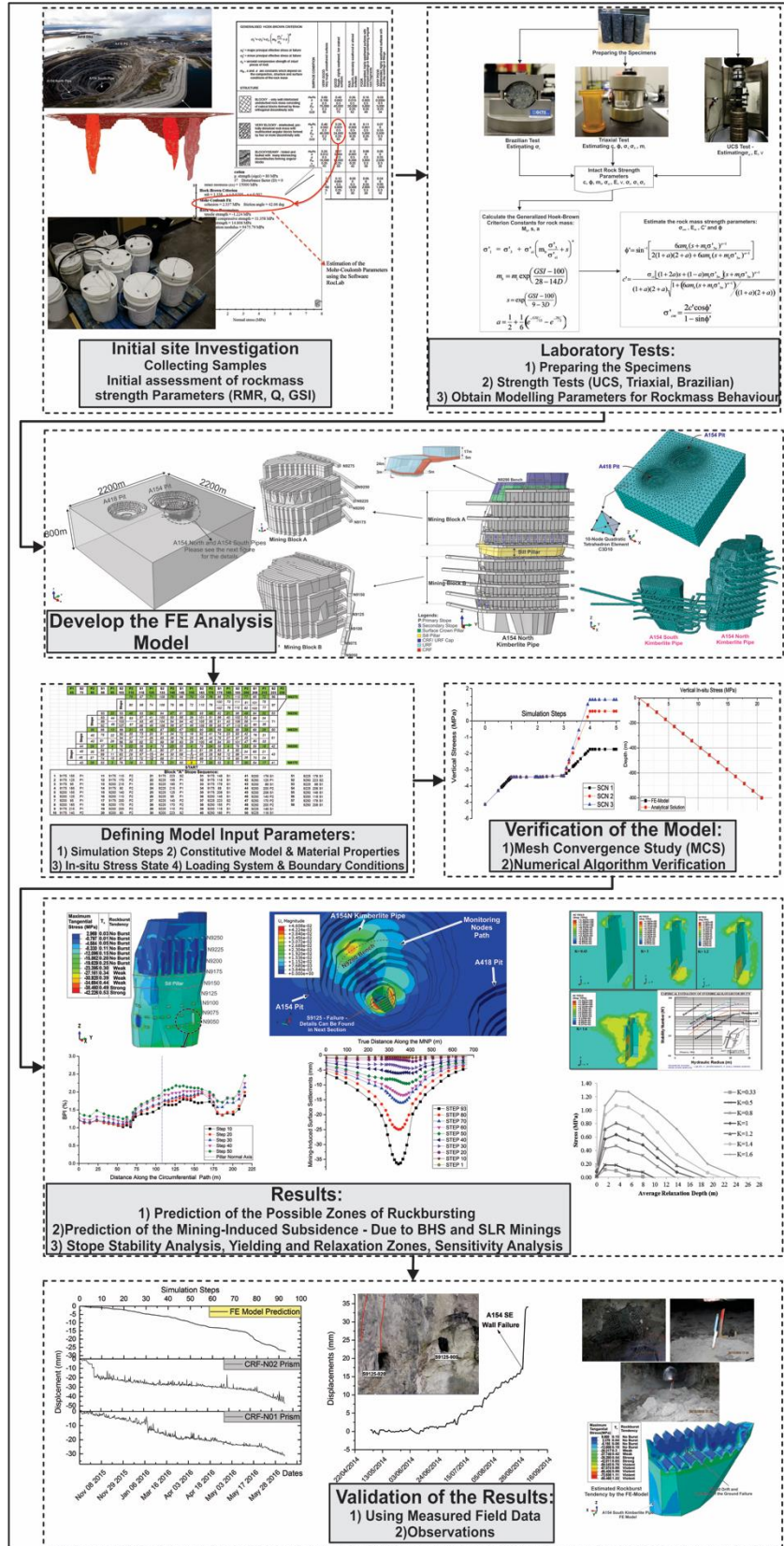


Figure 8.1 Visual summary of the research methodology

This research dissertation aimed to develop an integrated methodology which utilizes a combination of all the available methods reviewed in chapter 2 (the shaded boxes in figure 2.24) as needed, incorporating the advantages of the many methods available. Figure 8.1 illustrates this research methodology and the developed model. The development, implementation and verification of this engineering methodology have been conducted in four major stages: (i) initial site investigation, collecting rock samples, initial estimation of the rock mass (using Hoek-Brown criterion), gathering all data needed for building an accurate and realistic 3D geometry of the mine structures; (ii) implementing the FE model and the estimation of the modeling input parameters for rock mass properties through a series of rock mechanics laboratory tests (UCS, triaxial and Brazilian tests); (iii) conducting a series of analyses focusing on mining-induced energy and rockbursting, mining-induced surface subsidence, stope stability analysis, yielding and relaxation zones, and sensitivity analysis; and (iv) verification and validation of the FE model and results.

In this research, the main objective is to develop, implement and verify an integrated engineering methodology to estimate the in-situ and mining-induced stress regimes in the host rock and orebody using a realistic full 3D FE analysis model. The goal was to seek a detailed understanding of the stress (in-situ and mining-induced) distribution regimes in a mine as a function of mining methods. The methodology utilized the commercially available FE code called Abaqus.

A case study of Diavik Diamond Mine was used to illustrate the estimation procedure and to implement the proposed methodology. During this research, five Kimberlite sample rock types were collected from the mine site to estimate their elastoplastic strength properties in the laboratory. Consequently, a methodology has been proposed to obtain the modeling parameters for the rock mass strength based on the laboratory test results.

The developed FE model code was verified through a process referred to as numerical algorithm verification. Also, the FE model calculation was verified through a process called mesh convergence study.

The results of the FE model analysis are presented and discussed through chapters 4, 5 and 6, focusing on:

- 1) *Prediction of the mining-induced energy and rockbursting potentials:* A new approach is proposed to combine the developed full 3D elastoplastic FE analysis model and the available conventional criteria to evaluate the potential rockburst in an underground mine in its full scale.
- 2) *Prediction of the mining-induced subsidence:* It was shown that the numerical predictions of the mining-induced surface subsidence, due to the BHS mining method, matched well with the Gaussian distribution. However, further investigations are needed to confirm the generalizability of these findings.
- 3) *Stope stability assessment, yielding and relaxation zones, sensitivity analysis:* Two underground stability assessment methods (empirical and numerical methods) have been used. The main objective was to estimate the stability of the targeted stope located between mine levels N9225 and N9250 at Diavik Diamond Mine. Also, a sensitivity analysis was performed to investigate the effect of the stress ratio  $k$  on the development of yielding and relaxation zones around underground stope walls.

Finally, the developed FE model results were validated by comparing them to actual field data and site observations to quantify the accuracy and precision of the FE model results. The developed FE model not only successfully forecasted the possible yielding, failure and subsidence zones, but also it identified the stable areas of the mine as well. It is concluded that the model is in good agreement with the actual conditions of the mine.

## **8.2 Research conclusions**

Throughout this research, an integrated methodology has been developed, implemented and verified to estimate the in-situ and mining-induced stress as a function of different underground mining methods. A case study of the Diavik Diamond Mine has been used to implement the proposed methodology. All the research objectives outlined in Chapter 1 have been achieved throughout this study. Overall, the following conclusions were drawn from the implementation of the developed methodology:

- Throughout this study, a new approach was proposed to estimate the extent and magnitude of the mining-induced strain energy and its accumulation in a rock mass, using full 3D elastoplastic FE analysis model, to predict the rockburst potentials (chapter 4). In addition, the design capability of the developed FE model as a powerful design tool to study the stiffness of the loading system (also called mine stiffness) was discussed. Mine stiffness is an important factor influencing the failure of the rock mass; it can be used to predict potential rockbursting zones. The mine stiffness is controlled by the dimension and size of the pillars, span between pillars, mining sequence and strength properties of the pillar. Most of these factors are taken into consideration in the developed methodology. Therefore, a sensitivity study can be performed, using the developed FE model in this thesis, to assess the impact of each one of these parameters (separately or combined) on mine stiffness and consequently to revise these design parameters for actual mine projects.
- It was shown (chapter 5) that the numerical predictions of the mining-induced surface subsidence due to BHS matched well with the Gaussian distribution.
- It was shown (chapter 5) that a significant increase (approximately by 44%) to the amount of the induced settlements on the surface occurred as the mining activities reached near surface ground levels (mine levels

N9275 and N9250). This raised considerable concern about assessing the stability and recovery of the surface crown pillar at a late stage of the mining operation.

- Throughout this study (chapter 6), applications of both empirical and numerical methods in open stope stability assessments were presented. The Mathews stability graph method is simple and much faster than numerical modeling. It should be used as the first stage in the stope stability assessment. However, a reliable 3D numerical model can provide a more in-depth understanding of the induced stress distribution around the stope side walls. Particularly, when the stope surfaces are made by backfilled materials or when the geometry of the stope become complicated, and in the presence of uncertain parameters such as stress ratio  $k$ , using a numerical model should be considered as a complementary method along with other analytical and empirical methods.
- The numerical model provides a better understanding of the stress distribution around the stope side walls. Particularly, the de-stressed area around the hanging wall and foot wall of each stope block can be estimated accurately. Having a better understanding of this de-stressed area can identify possible tensile stress zones (or relaxation zones). For instance, the depth of a relaxation zone can be easily identified in the numerical model. It can provide assistance when correcting the ground support design parameters (i.e. the length of the rock bolts or cable bolts).
- The importance of the impact of the horizontal to vertical stress ratio,  $k$ , on the development of the yielding and relaxations zones around an underground opening has been investigated. Since the  $k$  value is uncertain in most underground mines, the results of this sensitivity analysis can be used to further the risk analysis associated with the stability of the stope.
- Throughout this study, it has been shown that the numerical models are most sensitive to: (i) geometry; (ii) meshing size; (iii) pre-mining stress

state; (iv) material properties; (v) simulation steps; and (vi) boundary conditions and loading systems.

- A comparison between the predicted results of the developed FE model in this research and the actual monitoring data and site observations showed that the predictive capacity of the developed FE model is a valuable tool for stability and design analysis in underground mines.
- Full validation of the geomechanics numerical models is impossible because geomechanical systems are not closed and have many variables and uncertainties associated with them. It is impossible to accurately capture and quantify the required input parameters, or even if it were possible, including them into the model will increase the cost of calculation significantly in an unaffordable way. However, these uncertainties are part of the everyday tasks for rock mechanics engineers. Most analytical methods are developed based on simple assumptions which sometimes are not even close to reality. In addition, most of the empirical methods in rock mechanics are applicable for a similar environment from which they were developed (for instance, an empirical method which was developed based on the work done on coal mines may not necessarily be applicable to an iron mine). The real valuable design tools for rock mechanics engineers, which allow them to overcome the associated uncertainties, are their engineering and scientific judgment.

### **8.3 Significance and contributions of the research**

The uniqueness of this research project is the development of a realistic full 3D FE model of a mine, with real input data which captures the true geometry of the underground features (i.e. drifts, stopes, etc.). In addition, for the first time, the generated model simulates the complete stress-strain path through the entire excavation and backfilling simulation steps in full 3D spaces. Consequently, at the beginning of each step of the simulation, the approximate true state of stress

and displacement from the previous step would be used as the new initial state of stress for that particular new step. This facilitates a better and more reliable prediction of the stress distribution, yielding and displacements in rock materials. The model has provided a detailed understanding of stress distribution and its variability over the mine domain.

The main contribution of this study is the development, implementation and application of an integrated methodology for the estimation of in-situ and mining-induced stress in the mine, providing a better understanding of the stress distribution regime in a mine and investigating the role of mining methods on the induced stress field. The outcomes of this research will enhance our knowledge of the effect of the stress ratio (horizontal to vertical stress) and stress heterogeneity regime on the stability of underground excavations and possible zones of failure.

Finally, the resultant methodology developed in this research can be used to assess the stability of surface crown pillars and sill pillars with respect to the mine stress (both in-situ and mining-induced) distribution regime. Recovery of the surface crown pillars and sill pillars is a common problem between underground mines. Identifying and quantifying the critical factors influencing their stability (factors like stress distribution regime around the excavations) for the safe and economic extraction of these pillars will make a significant contribution to the industry. Typically, most mining operations are driven by economics, thus improving ore extraction methods and increasing the percentage of ore pillar recovery will be critical to mine operators, as it will result in a significant increase in the overall production life of a mine.

In conclusion, having a better understanding of the stress regime distribution around underground excavations can improve the safety of the operation (both for personnel and equipment) and prevent catastrophic rock failures in underground environments.

#### **8.4 Recommendations for future work**

The FE model and methods developed in this study provided an engineering methodology to estimate the in-situ and mining-induced stress regimes which can be used in stability assessments for open stopes and for predicting rockbursting and surface subsidence in an underground hard rock mine. However, there is still a need for continued investigations into the use of this methodology in a mine environment. The following recommendations could improve the method and add to the body of knowledge in this research area:

- The numerical model generated in this study was based on the assumption that the rock mass is continuous. By introducing discontinuities, faults and joint sets into the model, more accurate results can be obtained. Furthermore, the effect of these discontinuities on the stability and release of excess energy in an underground mining environment should be examined.
- Including more realistic rock mass fracturing systems into the model requires proposing a new methodology based on hybrid methods (for instance, combining FE and discrete fracturing network (FEM/DFN) methods).

It is necessary that the magnitude of the rock mass strength be correctly specified. The rock mechanics tests revealed a large scatter in the strength of the rock types. Obviously more samples are needed to correct this variation. Therefore, a statistical analysis must be conducted to estimate the correct number of samples for each rock type. This way, the variations between the test results can be decreased, which leads to less uncertainties in the input parameters and increases the stability of the model predictions.

## **BIBLIOGRAPHY**

ABAQUS/Standard User's Manual, Dassault Systemes Simulia Corp, 2015.

Adeeb S., (2010). Introduction to Finite Element Analysis, Course notes, University of Alberta.

ASTM D3967-08 (2008). Standard Test Method for Splitting Tensile Strength of Intact Rock Core Specimens.

ASTM D4543-08 (2008). Standard Practices for Preparing Rock Core as Cylindrical Test Specimens and Verifying Conformance to Dimensional and Shape Tolerances.

ASTM D4623-08 (2008). Standard Test Method for Determination of In Situ Stress in Rock Mass by Overcoring Method—USBM Borehole Deformation Gauge1.

ASTM D4729-08 (2008). Standard Test Method for In Situ Stress and Modulus of Deformation Using Flatjack Method

ASTM D7012-13 (2013). Standard Test Methods for Compressive Strength and Elastic Moduli of Intact Rock Core Specimens under Varying States of Stress and Temperatures.

Aydan, ö. (2014). Methods of In-situ Stress Measurements and its Applications to Turkey. *Yer mühendisliği*, No. 2, 46-51.

Aydan, ö. and Kawamoto, T. (1997) The general characteristics of the stress state in the various parts of the earth's crust. In Sugawara, K., and Obara, Y. (Eds.). *Rock Stress, Proc. Int. Symp.*, Kumamoto, Balkema: Rotterdam, 369–73.

Barton N.R, (1974). A review of the shear strength of filled discontinuities in rock. Oslo: Norwegian Geotech. Inst. Publ. No. 105.

Barton N., Lien R., Lunde J., (1974) Engineering classification of rock masses for the design of tunnel support, *Rock. Mech.* Vol. 6. pp. 189-232.

Beer G., Meek J., (1982). Design curves for roofs and hanging-walls in bedded rock based on “voussoir” beam and plate solutions. *Trans. Inst. Min. Metall Vol.* 91:A18-A22.

Berry D. S. (1963). Ground movement considered as an elastic phenomenon. *The Mining Engineer*, 37: 28–41.

Bétournay M.C. (1995). The stability of shallow stopes of hard rock mine, PhD Thesis, McGill University.

Bieniawski Z.T., (1973). Engineering classification of Jointed rock masses. Trans. S. Afr. Inst. Civ. Engrs Vol 15, pp 335-344.

Bieniawski, Z.T. (1974) Geomechanics classification of rock masses and its application in tunneling, in Proc. 3rd. Cong. *ISRM*, Denver, Vol.2A, pp. 27-32.

Bienawski, Z.T., (1976) Rock mass classification in rock engineering. In exploration for rock engineering Proc. Symp., Cape Town: Balkema, (ed. Bienaski Z.T.). Vol 1, pp. 97-106.

Bienawski Z.T., (1989). Engineering Rock Mass Classifications: A Complete Manual for Engineers and Geologists in Mining, Civil, and Petroleum Engineering, John Wiley & Sons, Pages 272.

Bieniawski, Z.T., (1993) Classification of rock masses for engineering: The RMR system and future trends, *In: Hudson, J.A., ed., Comprehensive Rock Engineering, Volume 3: Oxford ; New York, Pergamon Press, p. 553-573.*

Blake, W. and Hedley (2009). *Rockbursts: Case studies from North American Hard-Rock Mines*. Society of Mining, Metallurgy, and Exploration Inc., Colorado, USA.

Bobet A, Fakhimi A, Johnson S, Morris J, Tonon F and Ronald Yeung M, (2009). "Numerical Models in Discontinuous media: Review of advances for rock mechanics applications". *Journal of Geotechnical and Geoenvironmental Engineering, ASCE, November, 1547*

Brady, B., and Brown, E. (2004) *Rock mechanics for underground mining*, Kluwer Academic Publishers, pp 628.

Brauner G. (1973). Subsidence due to underground mining: I - Theory and practices in predicting surface deformation, US Bureau of Mines Information Circular, No 8571.

Brown E.T., (1970). Strength of models of rock with intermittent joints. *J. Soil Mech. Found Div., ASCE vol 96, SM6, pp. 1935-1949.*

Brown E.T., and Ferguson G.A. (1979). Progressive hangingwall caving at Gath's mine, Rhodesia. *Transactions of the Institution of Mining and Metallurgy, Section A: Mining Industry, 88:92-105.*

Brown, E. T. (2003). *Block Caving Geomechanics*. Julius Kruttschnitt Mineral Research Centre: Brisbane

Cai, M. (2015). *Prediction and prevention of rockburst in metal mines – A case study of Sanshandao gold mine*. Journal of Rock Mechanics and Geotechnical Engineering, 1-8.

Castro, L. M., Bewick, R. P., and Carter, T. G. (2012). *An overview of numerical modelling applied to deep mining*. In: Innovative Numerical Modelling in Geomechanics, Azevedo R. (Ed.), CRC Press, London, pp.393-414.

Christiansson R., Hudson J.A., (2003). ISRM Suggested Methods for rock stress estimation – Part 4: Quality control of rock stress estimation. International Journal of Rock Mechanics & Mining Sciences 40, 1021-1025.

Cook D.A., and Skinner J.M. (2005). How to Perform Credible Verification, Validation and Accreditation for Modeling and Simulation. In Special Systems & Software Technology Conference, Issue, Cross Talk The Journal of Defense Software Engineering, Vol (18) pp. 20-24.

Cook R.D, Malkus D.S, Plesha M.E, Witt R.J, (2001). Concepts and applications of finite element analysis. Fourth Edition, John Wiley and Sons Inc.

Coulomb C.A, (1773), Application of the rules of maxima and minima to some problems of statics related to architecture, Acad. Roy. Sci. Mem. Math. Phys., Vol. 7, pp 343-382.

Deer, D.U., Hendron, A.J., Patton, F.D. and Cording, E.J. (1967). Design of surface and near surface construction in rock. In C. Fairhurst (ed.) *Failure and breakage of rock, proc. 8th U.S. symp. Rock mech.*, 237-302. New York: Soc. Min.Engrs, Am. Inst. Min. Metall. Petrolm Engrs.

Diavik Dialogue, (2011), Diavik Diamond Mine Inc., Volume 14, 4<sup>th</sup> quarter, pp:1-8.

Diavik Diamond Mine (2012). Fact Book, RioTinto.

DIAS Engineering Inc., 2000. *GDA 1.0 Geomechanical Design Analysis Software*, User's Guide, Sudbury. ON, Canada.

Diederichs M.S, Kaiser P.K, (1999). Stability of large excavations in laminated hard rock masses; the voussoir analogue revisited, International Journal of Rock Mechanics and Mining Science Vol 36, pp. 97-117.

*DIPS 7.0*. (2016). Rocscience Inc, Toronto, ON, Canada

DoD Modeling and Simulation (M&S) Verification, Validation, and Accreditation (VV&A), (, 2009). DoD Instruction 5000.61, December 9

Dunrud C.R. (1976). Some engineering geologic factors controlling coal mine subsidence in Utah and Colorado, U.S Department of the Interior Geological Survey, Washington.

Evans W.H., (1941). The strength of undermined strata. *Trans. Inst. Min. Metall.* Vol 50., pp. 475-500.

Feng X.T. and Hudson J.A. (2011). *Rock Engineering Design*, Leiden: CRC Press/Balkema, pp 464.

Goodman R. (1989). *Introduction to rock mechanics*, 2<sup>nd</sup> ed. John Wiley & sons, New York.

Goricki, A. (2003). *Classification of Rock Mass Behaviour based on a Hierarchical Rock Mass Characterisation for the Design of Underground Structures*. Doctoral Thesis, Institute for Rock Mechanics and Tunnelling, Graz, University of Technology

Grimstad, E. and Barton, N. (1993). Updating the Q-System for NMT. *Proc. int. symp. on sprayed concrete - modern use of wet mix sprayed concrete for underground support*, Fagernes. 46-66. Oslo: Norwegian Concrete Assn.

Grimstad E., Kankes K., Bhasin R., Magnussen A., Kaynia A., (2002). Rock mass quality Q used in designing reinforced ribs of sprayed concrete and energy absorption. In proceeding: *International Symposium on Sprayed concrete*. Davos. pp. 134-142.

Hadjigeorgiou J., Leclair J. G., Potvin Y., (1995)., An updated of the stability graph method for open stope desing. 97<sup>th</sup> CIM-AGM, Rock Mechanics and Strata Control Session, Halifax, Nova Scotia.

Haimson B.C., Cornet F.H, (2003). ISRM Suggested Methods for rock stress estimation – Part 3: hydraulic fracturing (HF) and/or hydraulic testing of pre-existing fractures (HTPF), *International Journal of Rock Mechanics & Mining Sciences* 40, 1011-1020.

Hassani F., Archibald J. (1998). *Mine Backfill 1998.*, Canadian Institute of Mining & Metallurgy (CIM) Special vol. 48 on CD ROM.

Heidbach, O., Tingay, M., Barth, A., Reinecker, J., Kurfes, D. and Müller, B., *The World Stress Map database release 2008* doi:10.1594/GFZ.WSM.Rel2008, 2008.

Hoek E., (1968). “*Brittle failure of rock*” in *Rock mechanics in Engineering Practice* (eds. Stagg K.G, and Zienkiewicz O.C.) pp. 99-124. London, Wiley.

Hoek E. (1974). Progressive caving induced by mining an inclined orebody, Transactions of the Institution of Mining and Metallurgy, Section A: Mining Industry, 83:133-139.

Hoek E., (1994). Strength of rock masses. ISRM New Journal, 2(2). pp. 4-16.

Hoek, E., Brown, E.T, (1980a). Empirical strength criterion for rock masses. J. Geotech. Engng Div., ASCE 106 (GT9), pp. 1013-1035.

Hoek R., Brown E.T, (1980b). Underground Excavations in Rock, London, The institution of mining & metallurgy, Pages 527.

Hoek, E. and Brown, E.T. (1997). *Practical estimated of rock mass strength*. International Journal of Rock Mechanics and Mining Sciences, Vol 34, No 8, pp. 1165-1186.

Hoek E., Carranza T., Corkum B., (2002)., Hoek-Brown failure criterion-2002 Edition, Proc. NARMS-TAC Conference Processing, Toronto, pp 267-273.

Hoek, E., Carter, T.G., and Diederichs, M.S. (2013). Quantification of the Geological Strength Index Chart. In 47<sup>th</sup> US Rock Mechanics/Geomechanics Symposium, San Francisco, CA, USA.

Hoek, E. and Franklin, J.A. (1968). *A simple triaxial cell for field and laboratory testing of rock*. Trans. Instn. Min. Metall. 77, A22-26.

Hoek E., Kaiser P.K, and Bawden W.F., (1995). Support of underground excavations in hard rock. Rotterdam, Balkama, Pages 230.

Hoek E., Marinos P., (2007)., A brief history of the development of the Hoek-Brown failure criterion, Soils and Rocks, No. 2.

Hudson J.A, Cornet F.H, Christiansson R, (2003). "ISRM Suggested Methods for rock stress estimation – Part 1: Strategy for rock stress estimation. International Journal of Rock Mechanics & Mining Sciences 40, 991-998.

Hudson J.A. (1993). Comprehensive Rock Engineering: Principles, Practice & Projects. Pergamon Press.

Hudson J., Feng X., (2007). Updated flowcharts for rock mechanics modelling and rock engineering design., International Journal of Rock Mechanics & Mining Sciences 44, 174–195.

Hudson J.A and Feng X.T. (2010). Specifying the information required for rock mechanics modelling and rock engineering design, International Journal of Rock Mechanics & Mining Sciences, 47: 179–194.

Hudson J.A, Harrison J.P, (1997). Engineering rock mechanics: An introduction to the principles, Imperial College of Science, Technology and Medicine, University of London, UK, Pergamon, Elsevier Science Ltd.

Hustrulid, W.A and Bullock, R.L. (2001). Underground mining method: engineering fundamentals and international case studies. Society of Mining, Metallurgy, and Exploration (SME), USA.

Hutchinson, J.D., Diederichs, M.S (1996). Cablebolting in underground mines, BiTech Publishers Ltd., Richmond, Canada, pages 401.

ISRM (1978). *Suggested methods for determining tensile strength of rock materials*. International Journal of Rock Mechanics, Mining Science & Geomech. Vol. 15. Pp 99-103.

Jaeger, J. C., Cook, N. G. W., and Zimmerman, R. W. (2008). Fundamentals of Rock Mechanics. Fourth Edition, Blackwell Publishing Ltd., UK.

Jennings, J. E., Brink, A. B. A., Louw, A. and Gowan, G. D. (1965). Sinkholes and subsidences in the transvaal dolomites of South Africa. In proceeding, 6<sup>th</sup> International Conference on Soil Mechanics and Foundation Engineering, Montreal, pp. 51–54.

Jing L, (2003). A review to techniques, advances and outstanding issues in numerical modeling for rock mechanics and rock engineering. International Journal of Rock Mechanics & Mining Science 40 283-353.

Jing L, Hudson J.A, (2002). Numerical Methods in Rock Mechanics. International Journal of Rock Mechanics & Mining Science 39 409-427.

Kaiser, P. K. and Cai, M. (2012). *Design of rock support system under rockburst condition*. Journal of Rock Mechanics and Geotechnical Engineering, 4(3), 215-227.

Kim K., Franklin J.A. (1987). Suggested Methods for Rock Stress Determination, Journal of Rock Mechanics & Mining Sciences & Geomechanics, Abstracts, Volume 24, Issue 1: 55-73.

Kidybiski, A. (1981). *Bursting liability indices of coal*. International Journal of Rock Mechanics and Mining Sciences & Geomechanics. 18 (4) :295 -304.

Kirsch G., (1889). Die theorie der Elastizitat und die Bedurfnisse der festigkeitslehre, ueit. Deut. Ing, Vol 42(28), pp. 797-807.

Kwasniewski, M. and Wang, J. A. (1999). *Three-dimensional numerical modelling and study of mine tremors associated with coal mining in the vicinity of*

*major faults*, Publications of the Institute of Geophysics, Polish Academy of Sciences, M-22 (310), 351-364.

Kwasniewski, M., Szutkowski, I., and Wang J. A. (1994). *Study of ability of coal from seam 510 for storing elastic energy in the aspect of assessment of hazard in Porabka-Klimontow Colliery*. Sci. Rept. Silesian Technical University.

Laubscher, D. H. (1994). Cave mining – the state of the art. *Journal of the South Africa Institute of Mining and Metallurgy* ; 94(10): 279–93.

Lauffer H., (1958). Gebirgsklassifizierung für den Stollenbau, *Geol. Bauwesen* Vol 24(1), pp 46-51.

Leveille P. (2015). Rockbursting properties of Kimberlite – Diavik Diamond Mine Case Study. Master of Science Thesis, University of Alberta.

Leveille, P., Sepehri, M., Apel, D. (2016). *Rockbursting potential of Kimberlite: A Case Study Diavik Diamond Mine*. University of Alberta. (A journal article in Submission Process).

Liu G.R, Quek S.S, *Finite Element Method a practical course*, Butterworth-Heinemann publication, 2003

Martin C.D, Chandler N.A, (1993). Stress heterogeneity and geological structures. *International Journal of Rock Mechanics & Mining Sciences* Vol 30, No.7: 993-999.

Martin C.D., Tannant D.D., Yazici S., Kaiser P.K., 1999. *Stress path and instability around mine openings*, 9<sup>th</sup> ISRM congress, Paris, 25-28.

Mathews K.E., Hoek E., Wyllie D.C., Stewart S.B.V., (1981). Prediction of stable excavation spans for mining at depths below 1000m in hard rock, CANMET Report DSS Serial No. OSQ80-00081.

Mawdesley C., Trueman R., and Whiten W., (2001). Extending the Mathews stability graph for open-stope design, *Trans. Instn Min. Metall (Sect. A: Min. technol)* 110, A27-A39.

Mazaira, A. and Konicek, P. (2015). *Intense rockburst impacts in deep underground construction and their prevention*. *Canadian Geotechnical Journal*, 53, 1426-1439.

Miao, S., Cai, M., Guo, Q. and Huang Z. (2016). *Rock burst prediction based on in-situ and energy accumulation theory*. *International Journal of Rock Mechanics & Mining Sciences*, 83, 86-94.

Mine Safety and Health Administration, (1984). *Hearing on Proposed Standards for Ground Control Metal/Nonmetal Mines*, United States Department of Labor, Spokane, WA, June.

Mitri, H.S., Hughes, R., and Zhang, Y. (2011). New Rock Stress Factor for the Stability Graph Method. *International Journal of Rock Mechanics and Mining Sciences*, 48, 141-145.

Mitri, H. S., Tang, B., and Simon, R. (1999). *FE Modelling of mining-induced energy released and storage rates*. *The Journal of South African Institute of Mining and Metallurgy*, 99(2), 103-110

Morh O., (1900) Welche umstände bedingen die Elastizitätsgrenze und den Bruch eines Materials? *Zeitschrift des verienes deutscher Ingenieure*, Vol. 44, pp. 1524-1530.

National Coal Board (1975). *Subsidence Engineers Handbook*, National Coal Board Mining Department, UK, London.

Nickson, S.D., (1992). *Cable support guidelines for underground hard rock mine operations*, Master of Applied Science thesis, Department of Mining and Mineral Process Engineering, University of British Columbia.

Obert L., Duvall W.I, (1967). *Rock mechanics and the design of structures in rock*, John Wiley and Sons, Pages 650.

Ortleep, W. D. and Stacey T. R., (1994). *Rockburst mechanisms in tunnels and shafts*, *Tunnelling and Underground Space Technology*, Vol. 9, No .1, pp. 59-65.

Ortleep, W. D. (1997). *Rock fracture and rockbursts : an illustrative study*. The south African Institute of Mining and Metallurgy, Johannesburg.

Pacher F. (1975). *The Development of the New Austrian Tunneling Method and the Main Features in Design Work and Construction*, In Proc. 16<sup>th</sup> Sympo. On Rock Mechanics, Minneapolis, Minnesota, pp:223-232.

Pahl, G. and W. Beitz (1984), *Engineering Design*. London, The Design Council. Springer Verlag, London.

Pande G.N., Beer G., (1990). Williams J.R, *Numerical Methods in Rock Mechanics*, John Wiley & Sons Ltd, England.

Pariseau, W.G. (2007). *Design analysis in rock mechanics*, Taylor & Francis/Balkema,

Park, H. D. (1995). Tensile rock strength and related behavior revealed by hoop tests, PhD Thesis, University of London.

Peck R.B., (1969). Advantages and limitations of the observational methods in applied soil mechanics.

Peck R. B., (1969). Deep excavations and tunnelling in soft ground. in Proceedings, 7<sup>th</sup> International Conference on Soil Mechanics and Foundation Engineering, Mexico city., 225-290.

Potvin, Y., (1988). Empirical open stope design in Canada, Ph.D. thesis, Department of Mining and Mineral Process Engineering, University of British Columbia.

Potvin Y., Hadjigeorgiou J., (2001). “*The stability graph method for open-stope design*” in Underground mining methods (eds. Hustrulid W., Bullock R.L) Society of Mining, Metallurgy, and Exploration (SME, pp. 513-520.

Qiao, C. S., Tian, Y. Z. (1998). *Study of possibility of rockburst in Don-gua-shan Copper Mine*. Chinese Journal of Rock Mechanics and Engineering. 17, 917-921.

Rabcewicz, L.V. (1964). The New Austrian Tunnelling Method. Water Power, 16, November, pp:453-515.

ROCLAB (2002). User’s Manual, Rocscience INC.

Sargent R.G. (2013). Verification and Validation of Simulation Models. Journal of Simulation, February, Volume 7, 1, pp. 12-24.

Sheory P.R., (1994). A theory for in situ stresses in isotropic and transversely isotropic rock. International Journal of Rock Mechanics & Mining Sciences & Geomechanics. 31 (1), 23-34

Singh R, Ghose A. (2006). Engineering Rock Structures in Mining and Civil construction, Taylor & Francis, London.

Singiresu S.R, (2004). The Finite Element Method in Engineering, Fourth Edition. Elsevier Science & Technology Books, December.

Sjboerg J., Christiansson R., Hudson J.A., (2003). ISRM Suggested Methods for rock stress estimation – Part 2: Overcoring methods, International Journal of Rock Mechanics & Mining Sciences 40, 999-1010.

Sofianos, A. I., (1996). Analysis and design of an underground hard rock voussoir beam roof, Int. J. Rock Mech. Min. Sci. & Gemech. Abstr. Vol 33. No.2, pp. 153-166.

Steward S. B. V., Forsyth W. W., (1995). The Mathews method for open stop design, CIM Bull. 88, 45-53.

Spross, J. (2014). A Critical Review of the Observational Methods, Licentiate Thesis, KTH Royal Institute of Technology, Stockholm, Sweden.

Suorineni F.T., (2010). The stability graph after three decades in use: Experience and the way forward, International journal of mining, Reclamation and Environment, Vol. 24, No.4, 307-339.

Suorineni, F.T., Tannant, D.D., and Kaiser, P.K. (2001). Likelihood Statistic for interpretation of the stability graph for open stope design, International Journal of Rock Mechanics & Mineral Science, 36 (7):891-906.

Taherynia M. H., Agha S., and Fahimifar A., (2016). *In-Situ Stress State and Tectonic Regime in Different Depths of Earth Crust*. Geotech. Geol. Eng., Springer, 34 :679-687.

Terzaghi, K. 1946. Rock defects and loads on tunnel supports. In *Rock tunneling with steel supports*, (eds R. V. Proctor and T.L. White) 1, 17-99. .

Terzaghi K., Peck R.B., (1948). Soil mechanics in engineering practice, John Wiley and Sons.

Terzaghi K., Richart F.E., (1952). Stress in rock about cavities. Geotechnique 3, 57-90.

Thacker, B.H., Doebling, S.W., Hemez, F.M., Anderson, M.C., Pepin J.E., Rodriguez E.R. (2004). Concepts of Model Verification and Validation. LosAlamos National Laboratory, California, USA.

Thompson P.M, Chandler N.A. (2004). In situ Rock Stress determinations in deep boreholes at the Underground Research Laboratory. International Journal of Rock Mechanics & Mining Sciences 41: 1305-1316.

Trueman R., Mikula P., Mawdesley C., Haries N., (2000)., Experience in Australia with the application of the Mathews method of open stope desing. CIM Bull. 93. 162-167.

Unlu T., Akcin H., and Yilmaz O. (2013). An integrated approach for the prediction of subsidence for coal mining basins, Engineering Geology, 166:186-203.

Wang J., Milne D., Wegner L., Reeves M., 2006. *Numerical evaluation of the effects of stress and excavation surface geometry on the zone of relaxation around open stope hanging walls*. International Journal of Rock Mechanics and Mining Sciences 44, 289-298.

Wang, J. A. and Park, H. D. (2001). *Comprehensive prediction of rockburst based on analysis of strain energy in rocks*. Tunnelling and Underground Space Technology, 16 (2001) 29-57.

Whitney H.T, Butter G.L., (1983). The new Austrian tunneling method A rock mechanics philosophy, 24<sup>th</sup> U.S.Symposium on rock mechanics.

Wickham, G.E., Tiedemann, H.R. and Skinner, E.H. (1972). Support determination based on geologic predictions. In K.S. Lane and L.A. Garfield (Eds.), *Proc. North American rapid excav. tunneling conf.*, Chicago, 43-64. New York: Soc. Min. Engrs, Am. Inst. Min. Metall. Petrolm Engrs.

Wikel, K. (2011). *Geomechanics: Bridging the Gap from Geophysics to Engineering in Unconventional Reservoirs*. Canadian Society of Exploration Geophysicists RECORDER, Vol. 36, No. 05, pp:36-44.

Wiles, T. D. (2006). *Reliability of numerical modelling predictions*. International Journal of Rock Mechanics & Mining Sciences 43, 454-472.

Yang, W., and Xia, X. (2013). Prediction of mining subsidence under thin bedrocks and thick unconsolidated layers based on field measurement and artificial neural networks, Computers & Geosciences, 52: 199-203.

Yip, C. G., and Thompson, K. S. (2015). Diavik Diamond Mine – Technical Report NI43-101. Diavik Diamond Mine Corporation, Yellowknife, Canada

Zhang Y., Mitri H.(2008). Elastoplastic stability analysis of mine haulage drift in the vicinity of mined stopes. International Journal of Rock Mechanics & Mining Sciences. 45: 547 -593

## **Appendix A: Rock Mechanics Laboratory Tests Results**

*This Appendix contains the results of the rock mechanics tests conducted during this research. These are included the Uniaxial Compressive Strength (UCS), Brazilian, and Triaxial compressive strength tests.*

### A.1 Uniaxial Compressive Strength Test Results

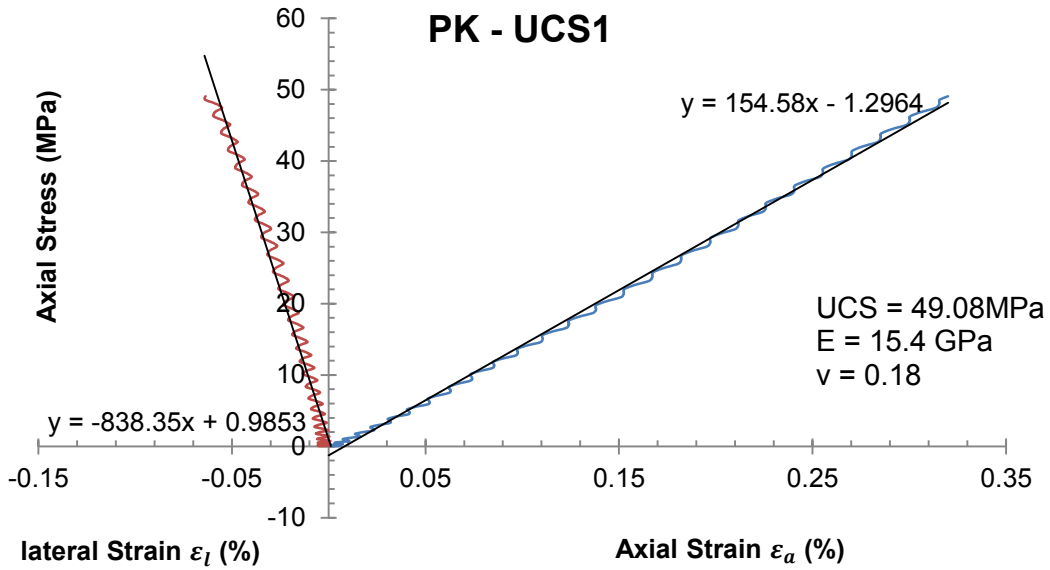


Figure A-1 Sample No. PK - UCS 1

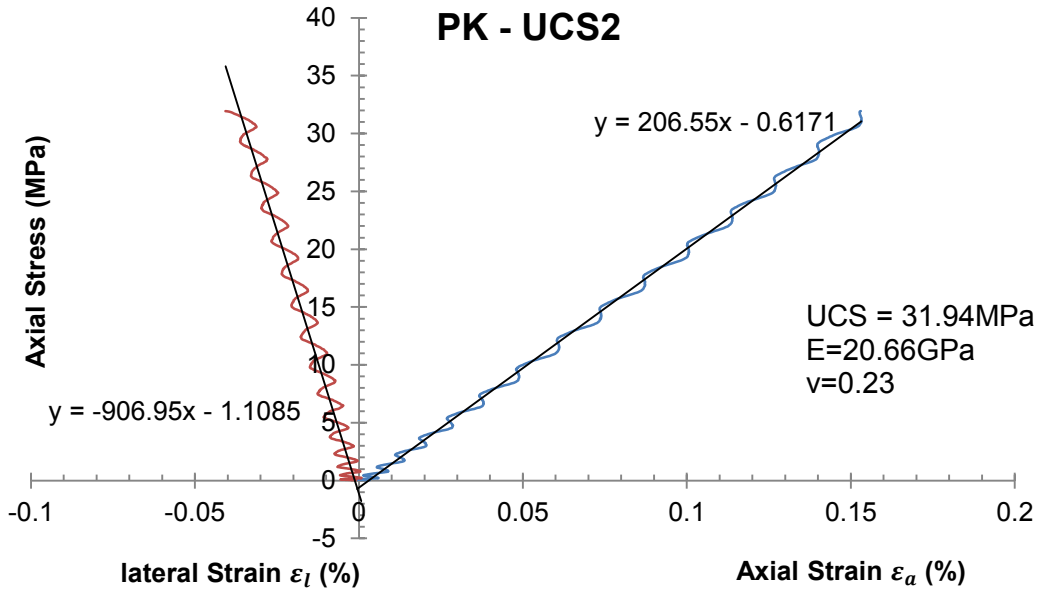


Figure A-2 Sample No. PK - UCS 2

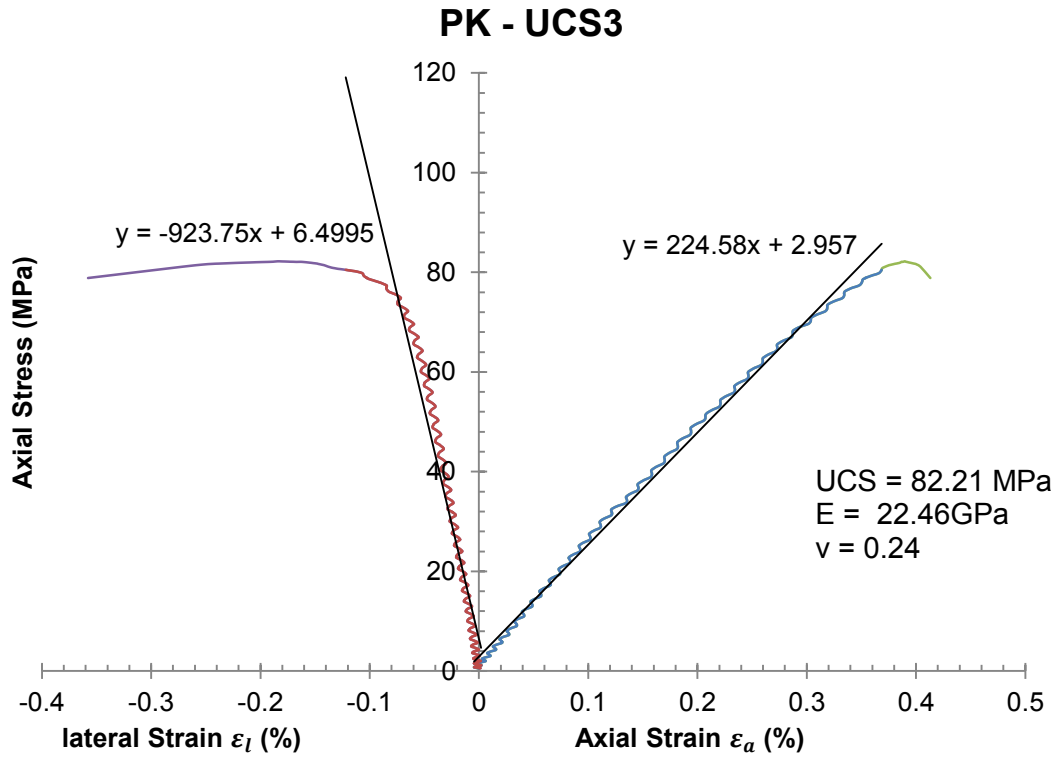


Figure A-3 Sample No. PK - UCS 3

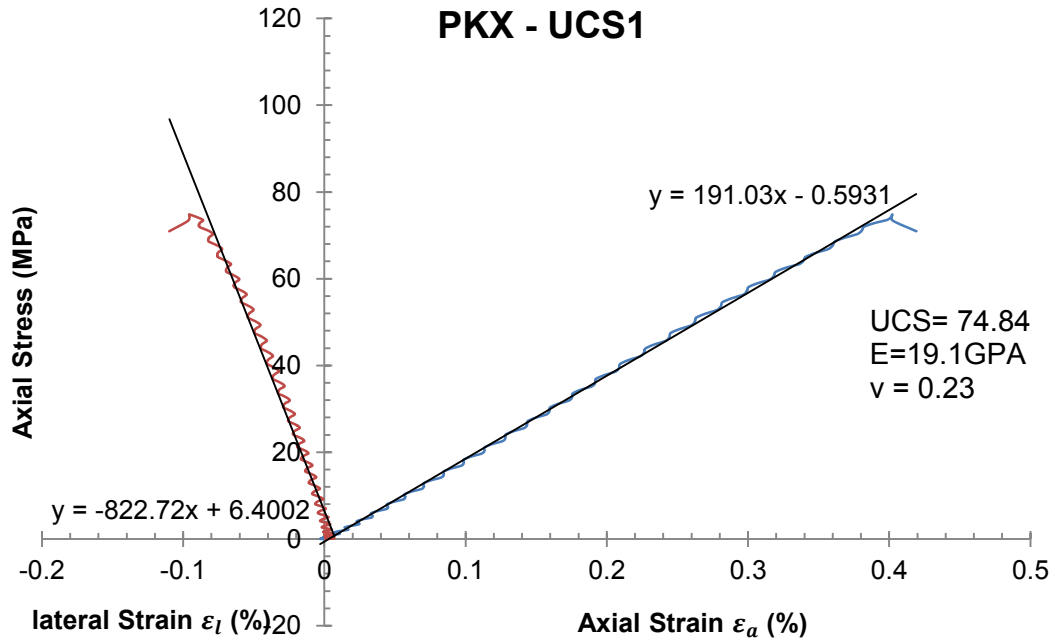


Figure A-4 Sample No. PKX-UCS 1

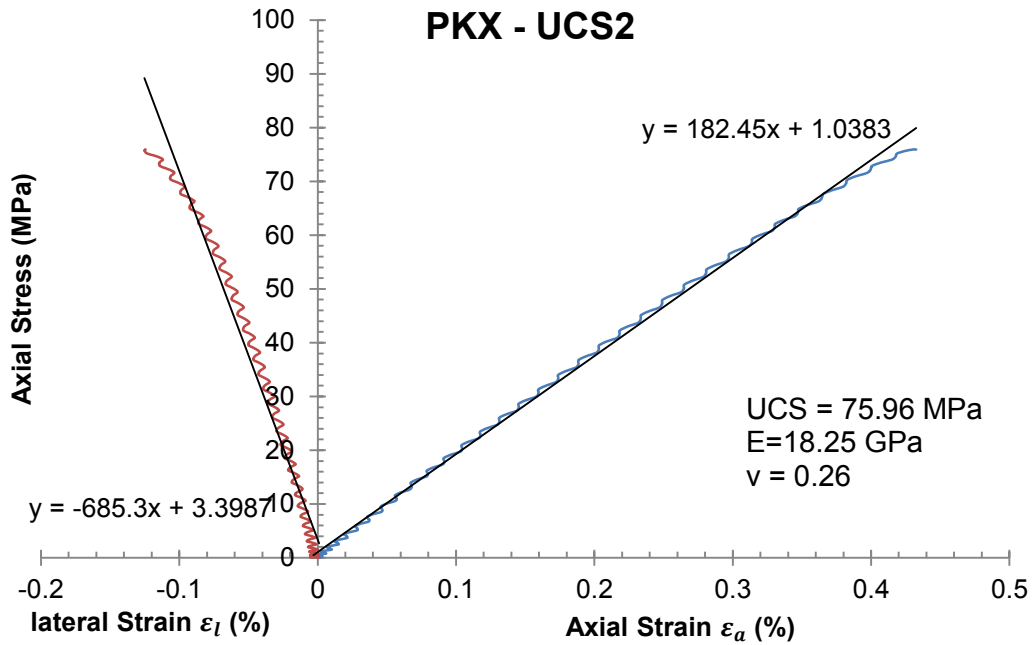


Figure A-5 Sample No. PKX-UCS 2

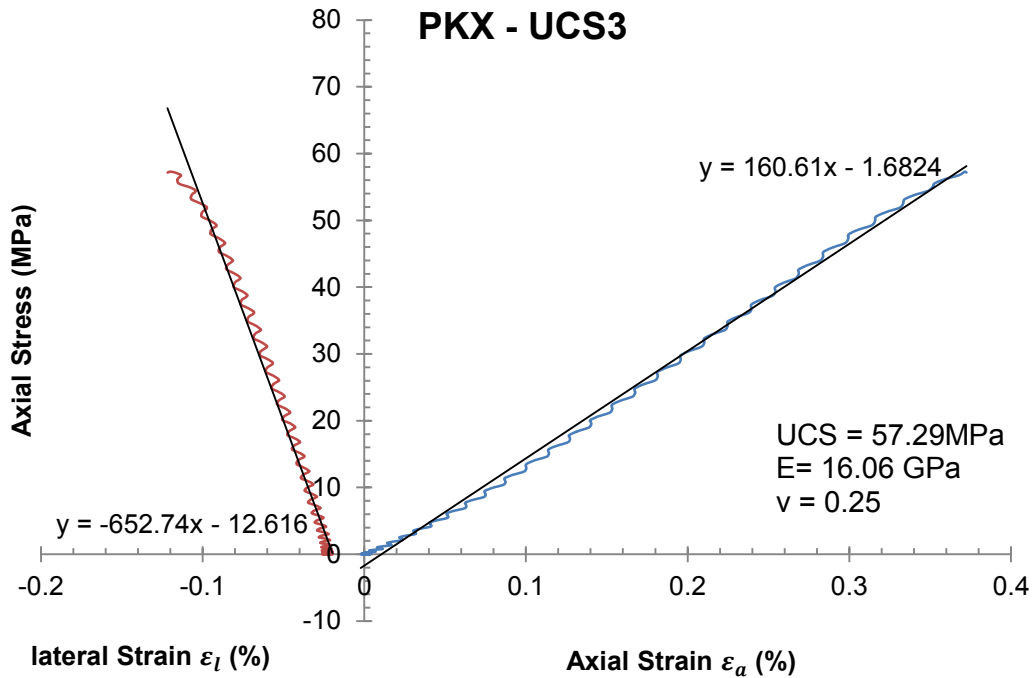


Figure A-6 Sample No. PKX-UCS3

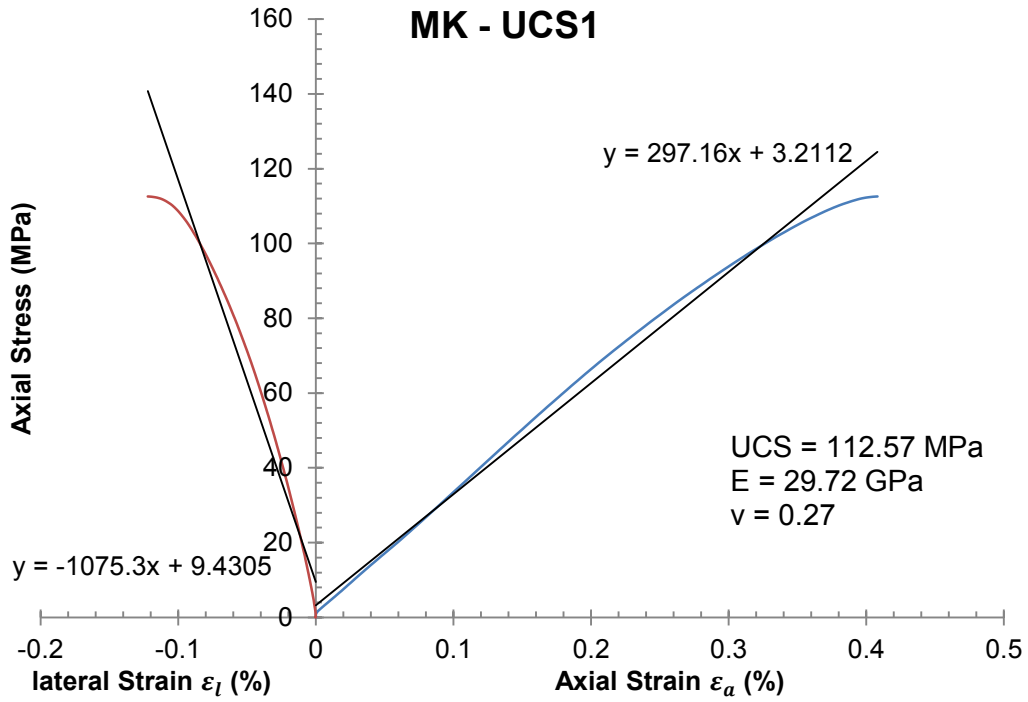


Figure A-7 Sample No. MK-UCS1

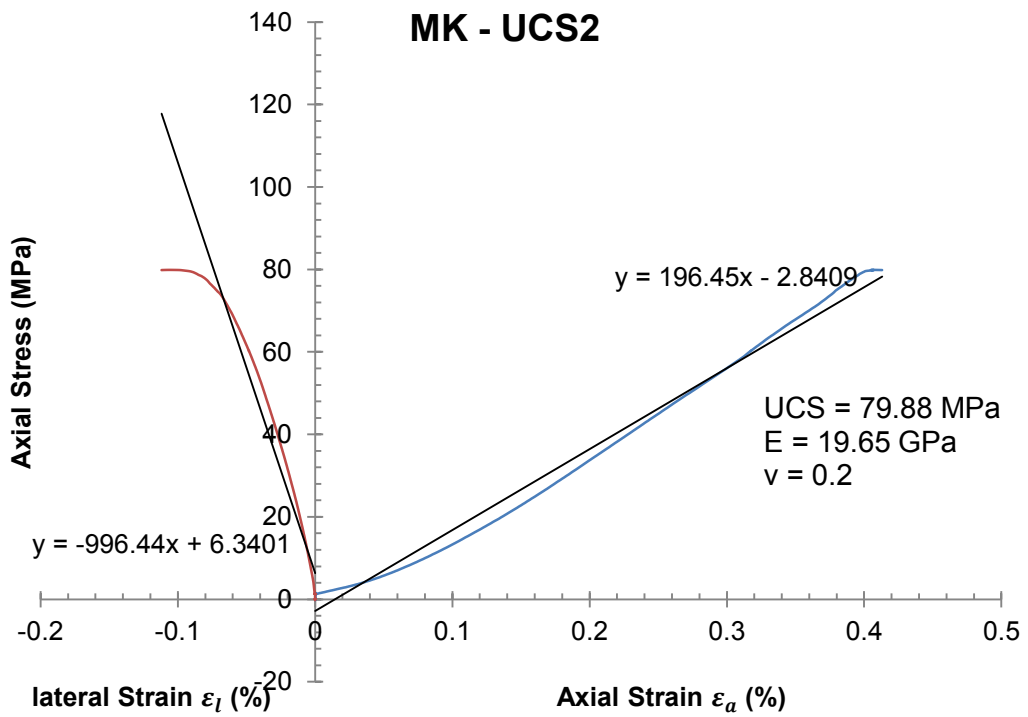


Figure A-8 Sample No. MK-UCS2

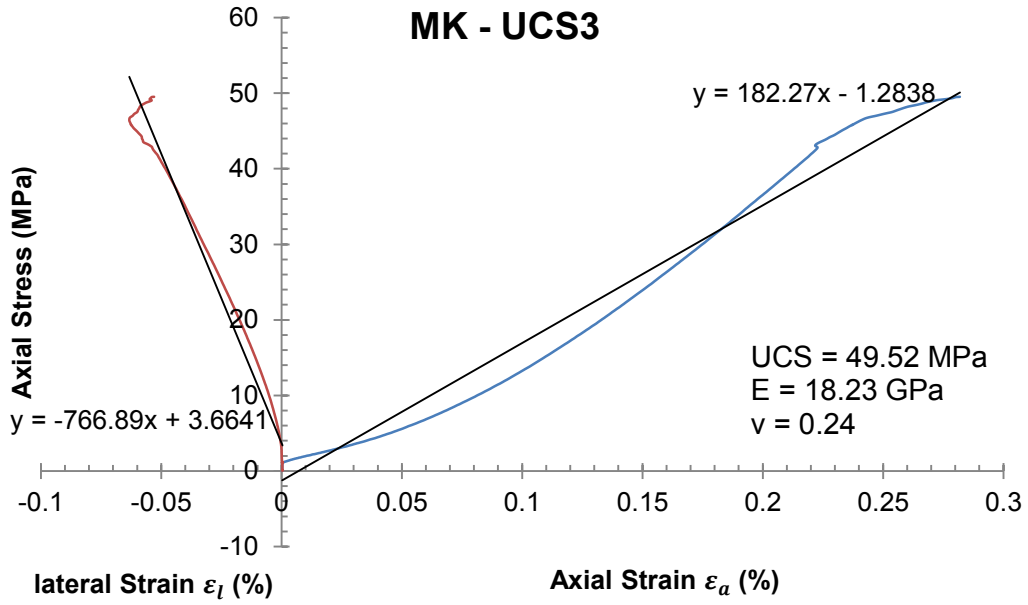


Figure A-9 Sample No. MK-UCS3

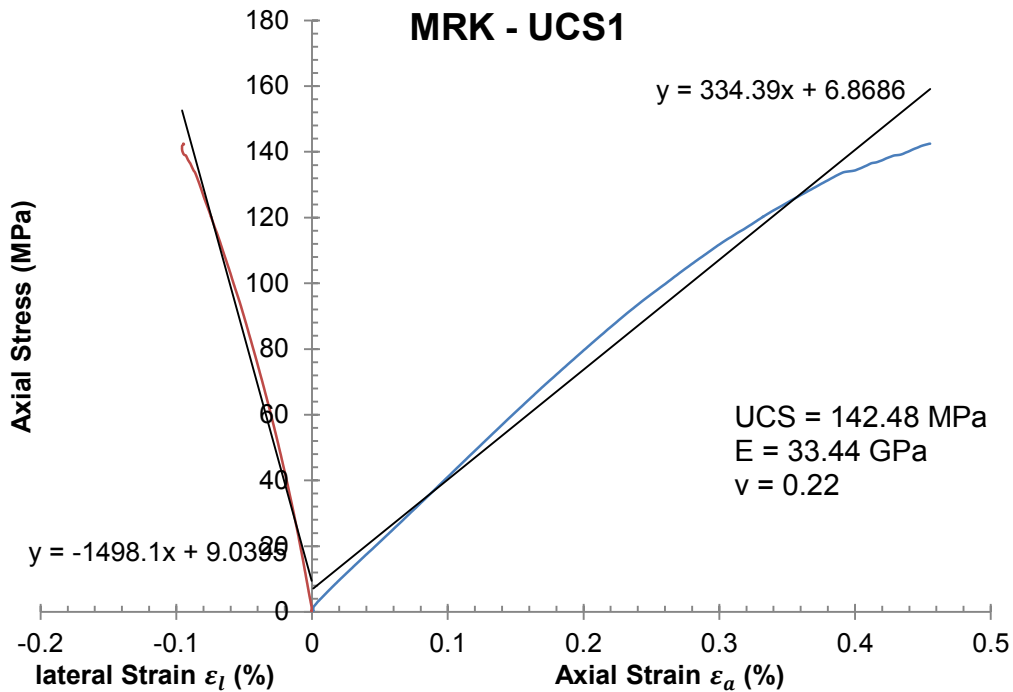


Figure A-10 Sample No. MRK-UCS1

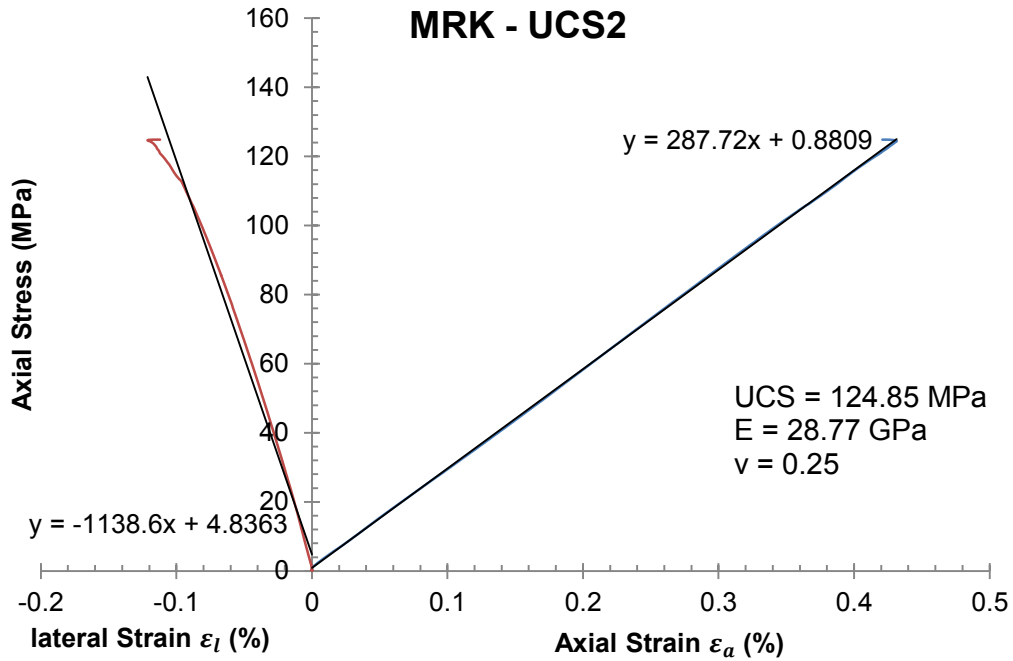


Figure A-11 Sample No. MRK-UCS2

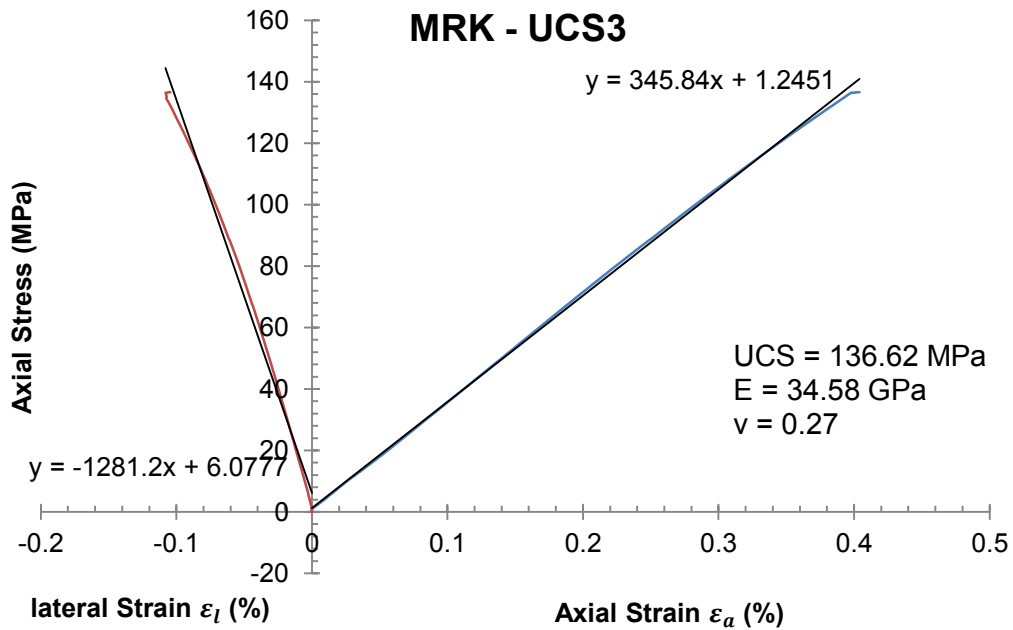


Figure A- 12 Sample No. MRK-UCS3

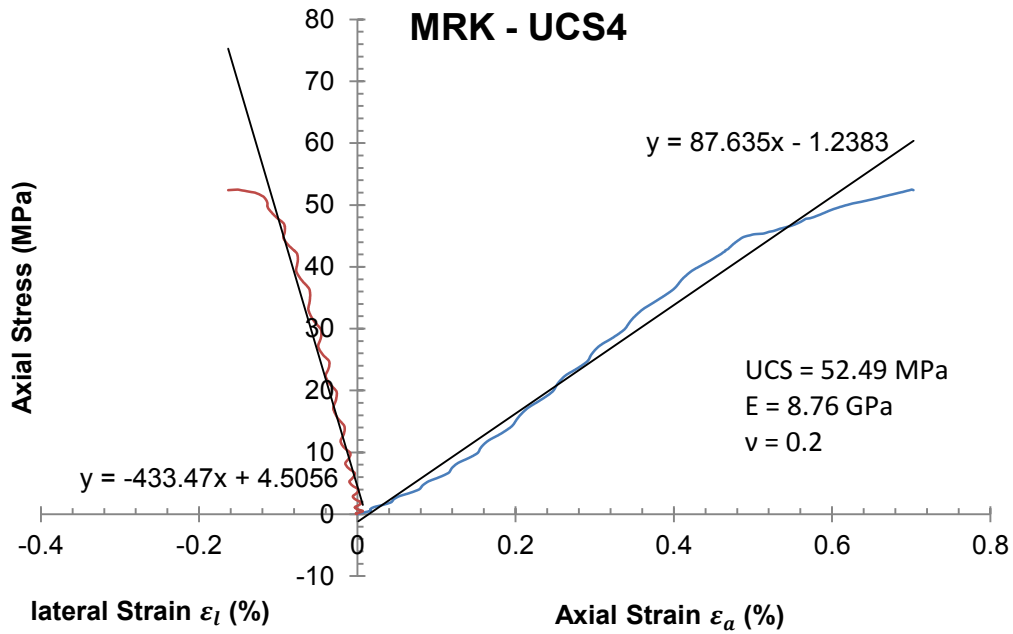


Figure A-13 Sample No. MRK-UCS4

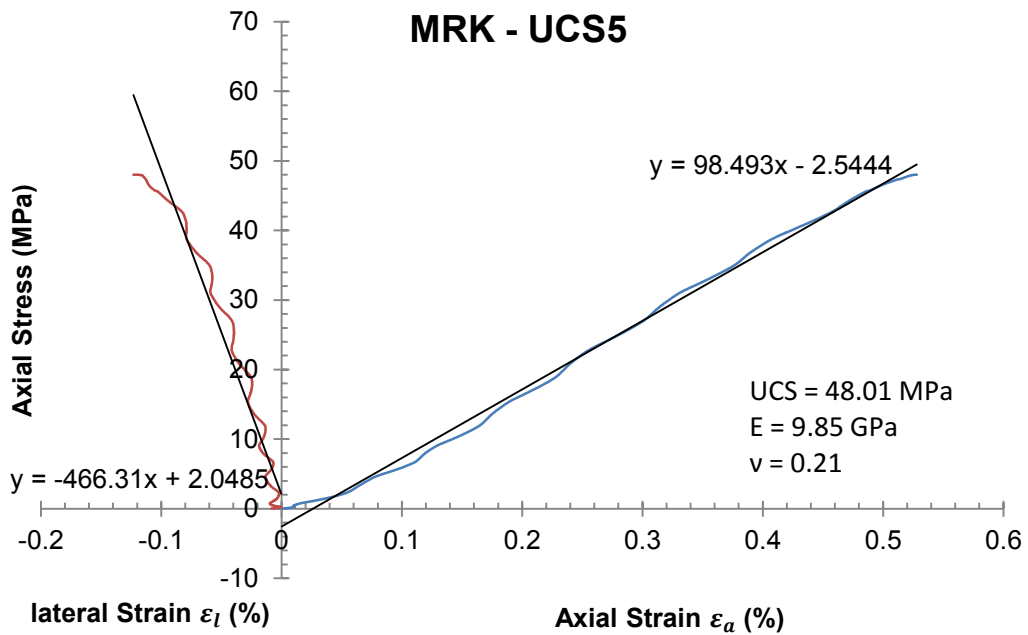


Figure A-14 Sample No. MRK-UCS5

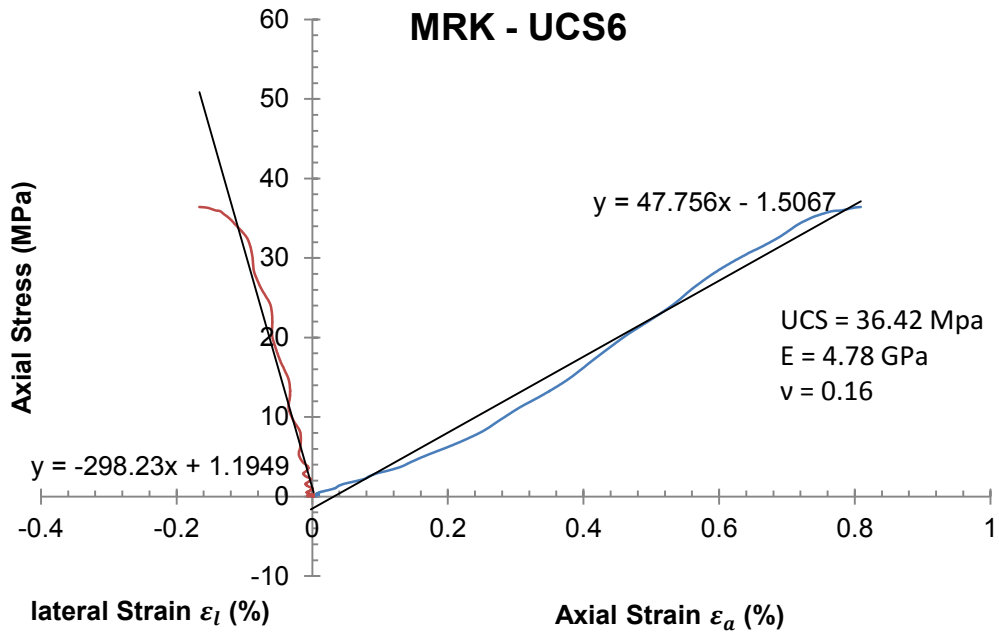


Figure A-15 Sample No. MRK-UCS6

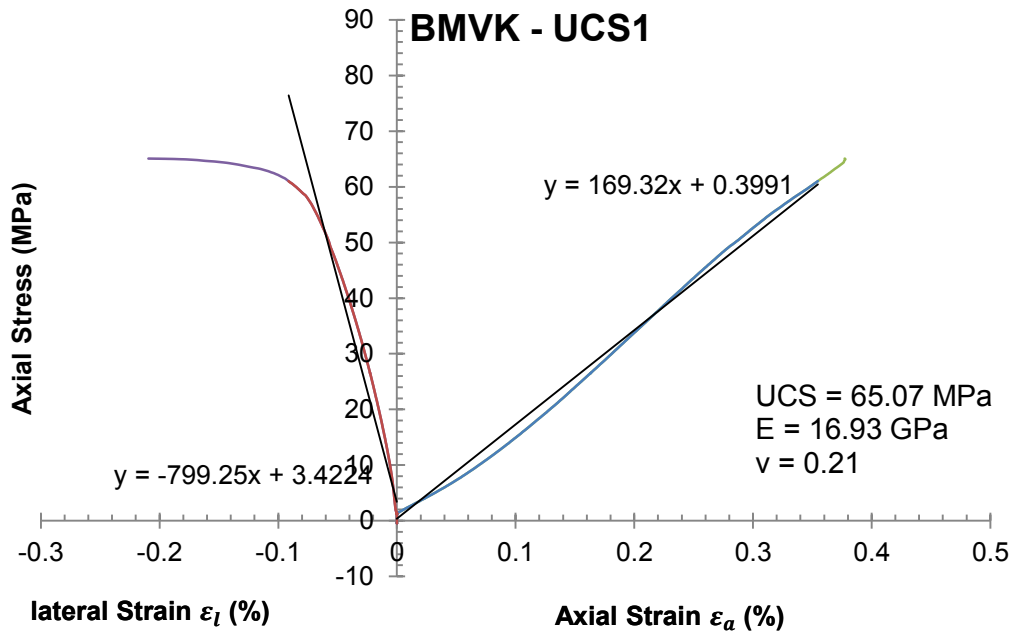


Figure A-16 Sample No. BMVK-UCS1

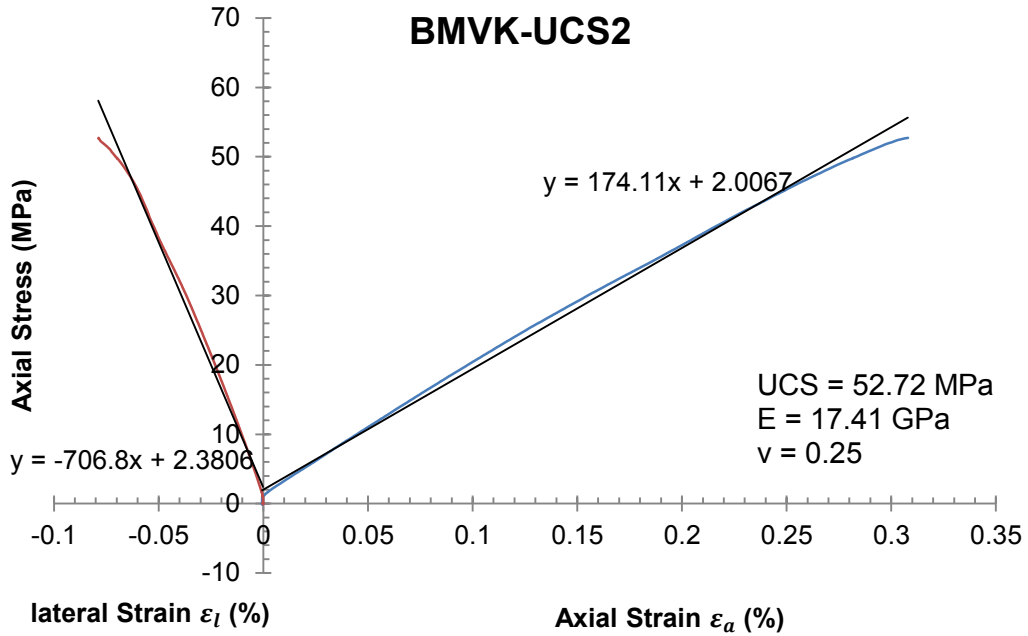


Figure A-17 Sample No. BMVK-UCS2

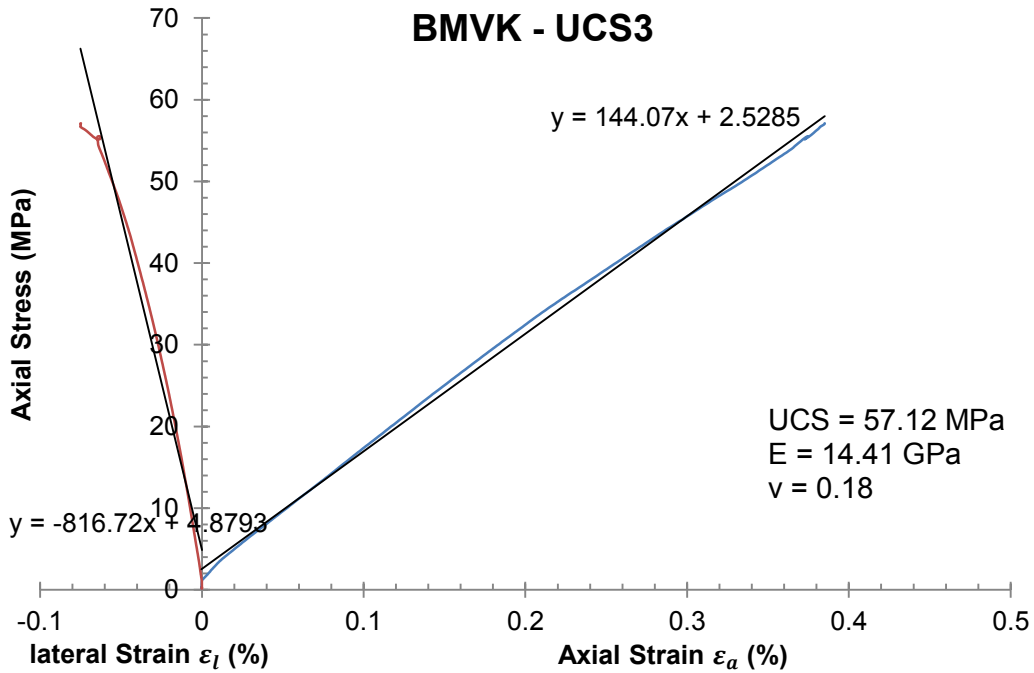


Figure A-18 Sample No. BMVK-UCS3

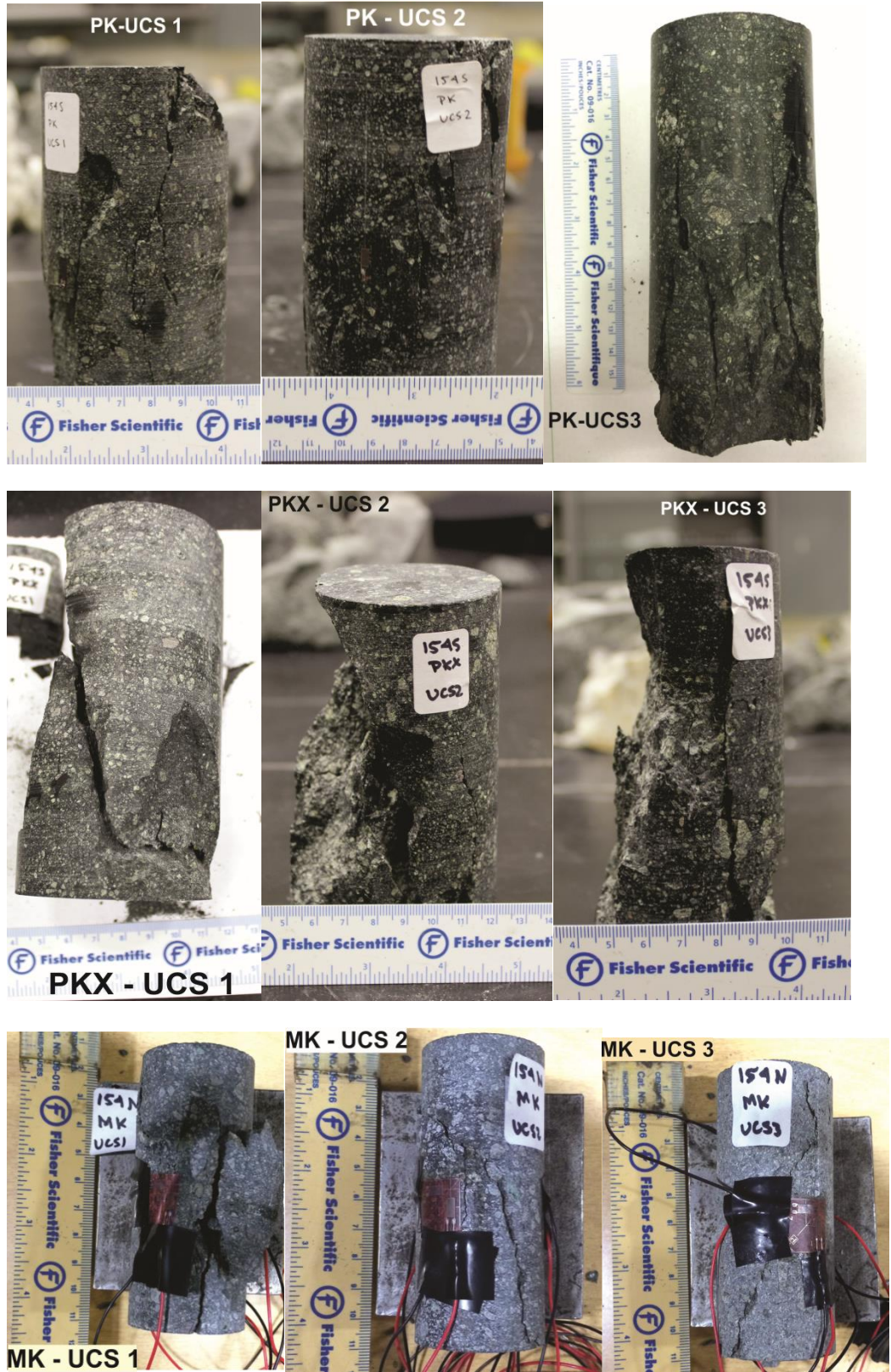


Figure A-19 Uniaxial Compressive Strength Tests Results - Failure Modes for PK, PKX and MK Rock Types



**Figure A-20** Uniaxial Compressive Strength Tests Results - Failure Modes for BMVK and MRK Rock Types

### A.2 Brazilian Test

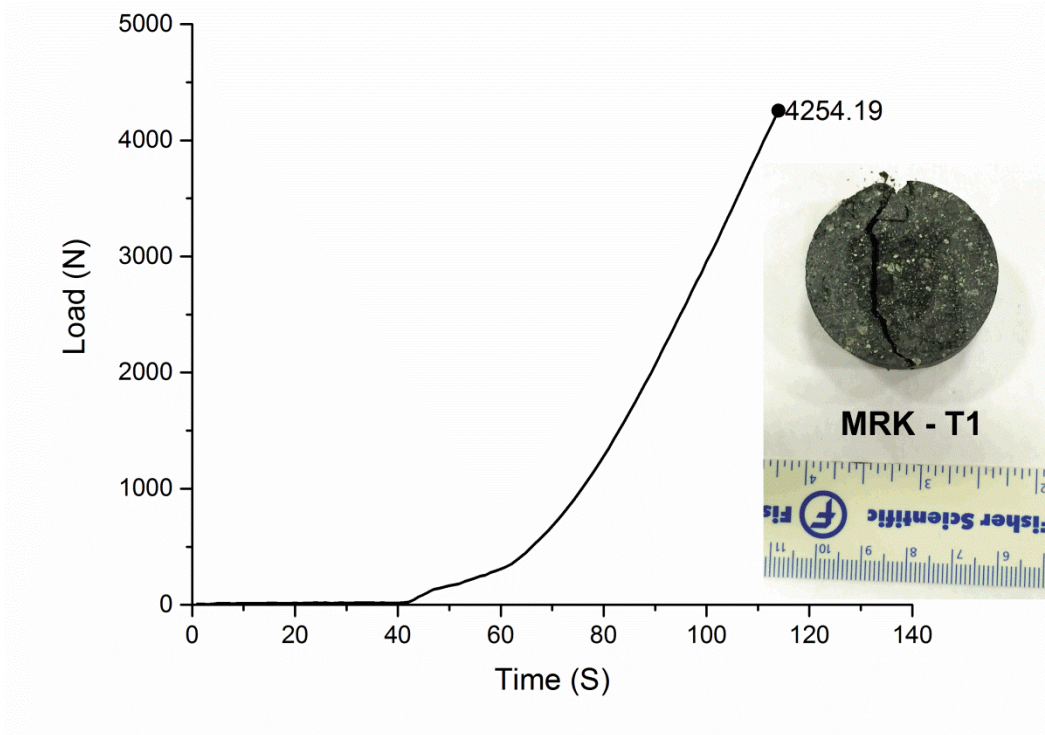


Figure A-21 Brazilian Test - Sample No. MRK - T1

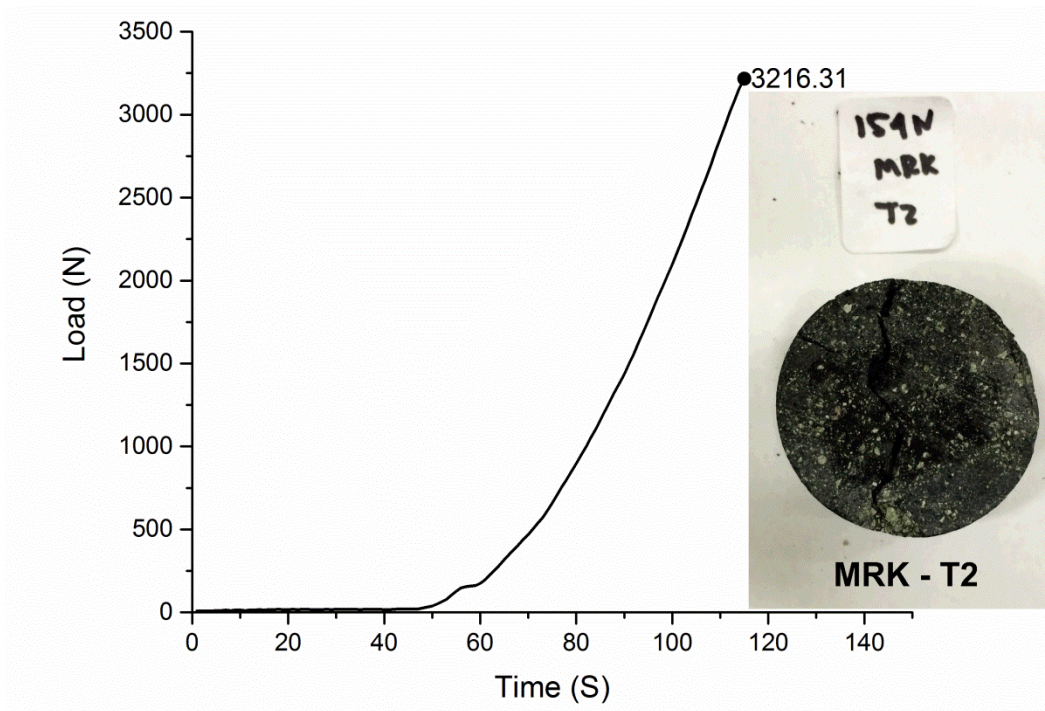


Figure A-22 Brazilian Test - Sample No. MRK - T2

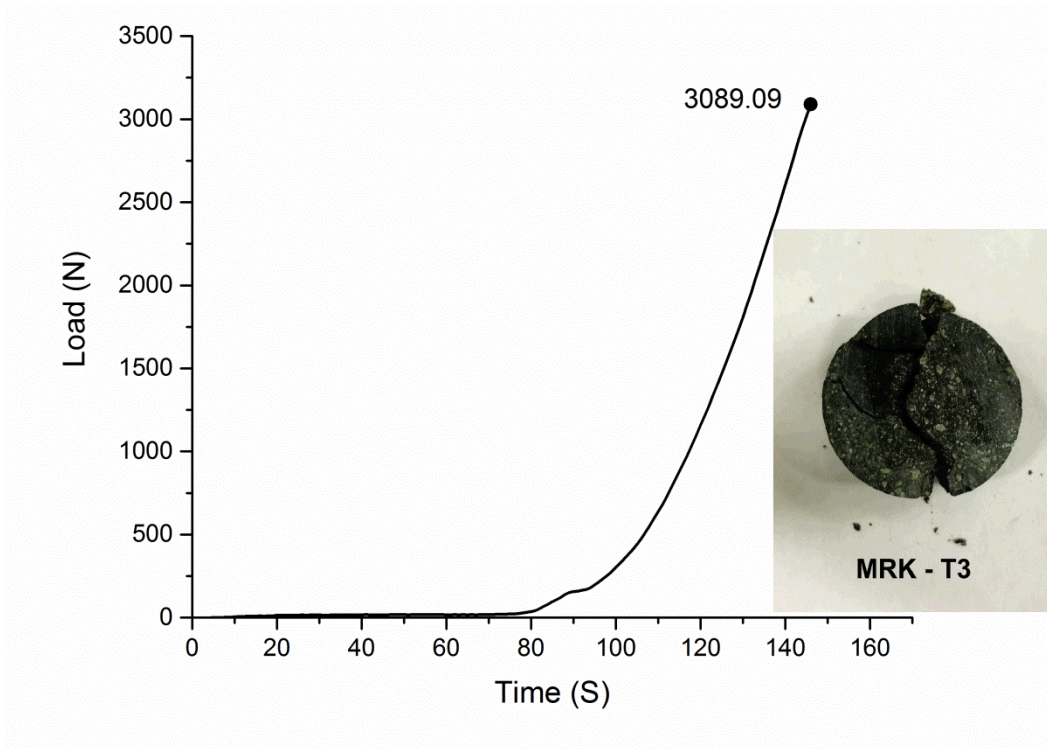


Figure A-23 Brazilian Test - Sample No. MRK - T3

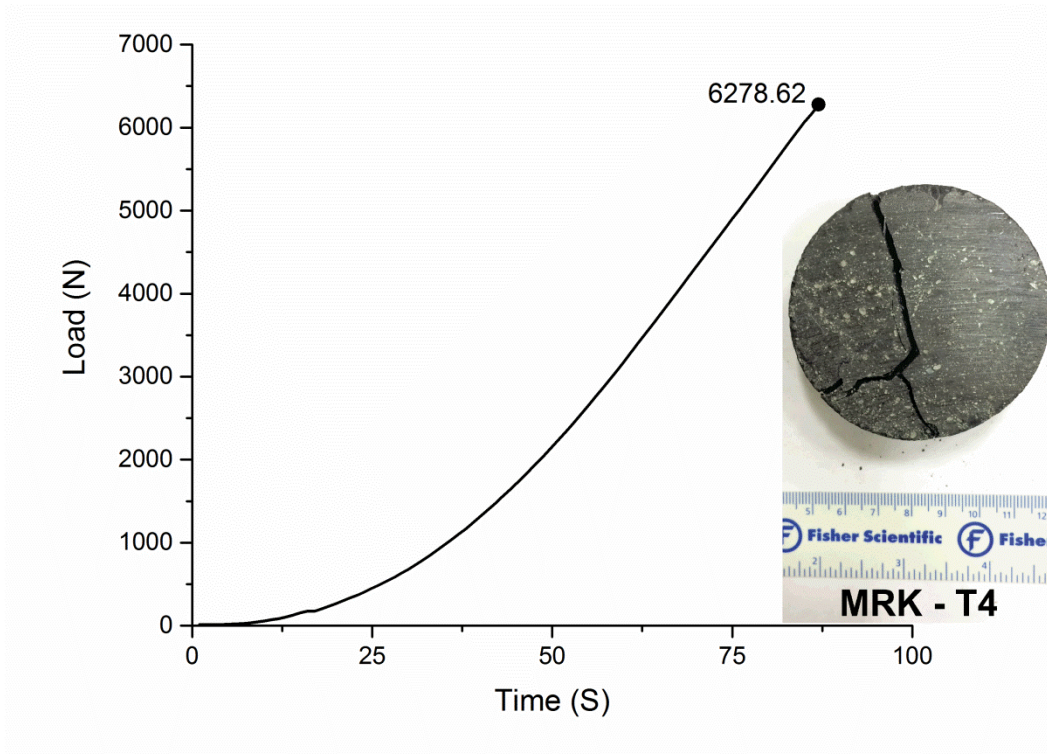


Figure A-24 Brazilian Test - Sample No. MRK - T4

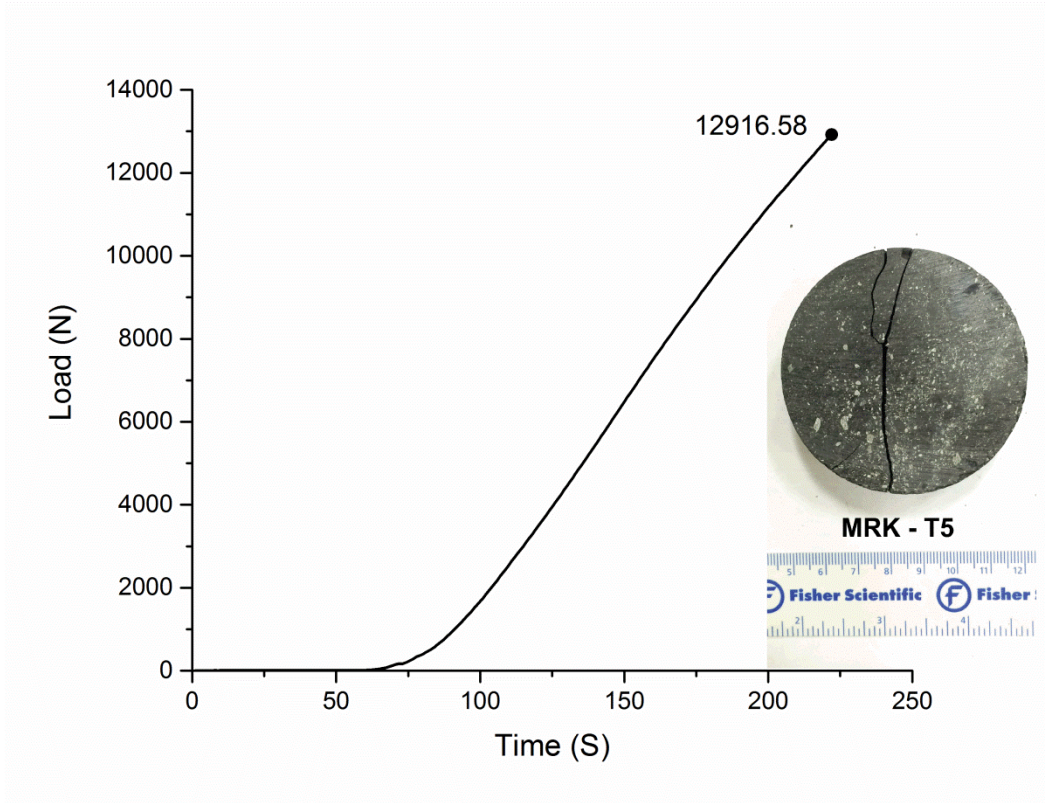


Figure A-25 Brazilian Test - Sample No. MRK - T5

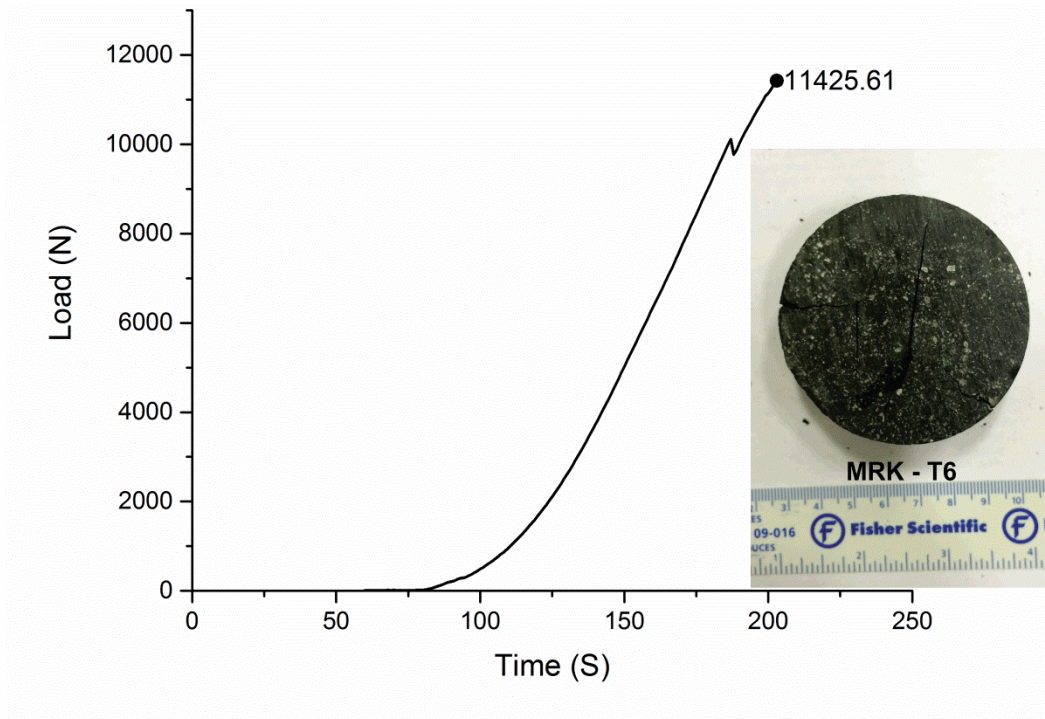


Figure A-26 Brazilian Test - Sample No. MRK - T6

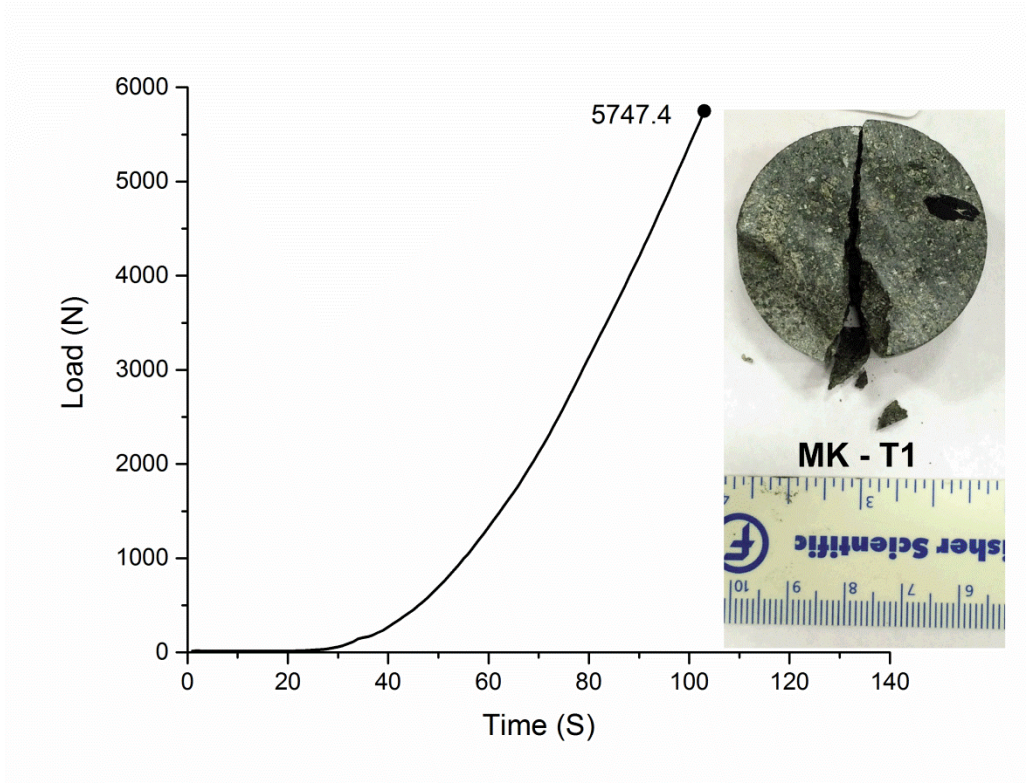


Figure A-27 Brazilian Test - Sample No. MK – T1

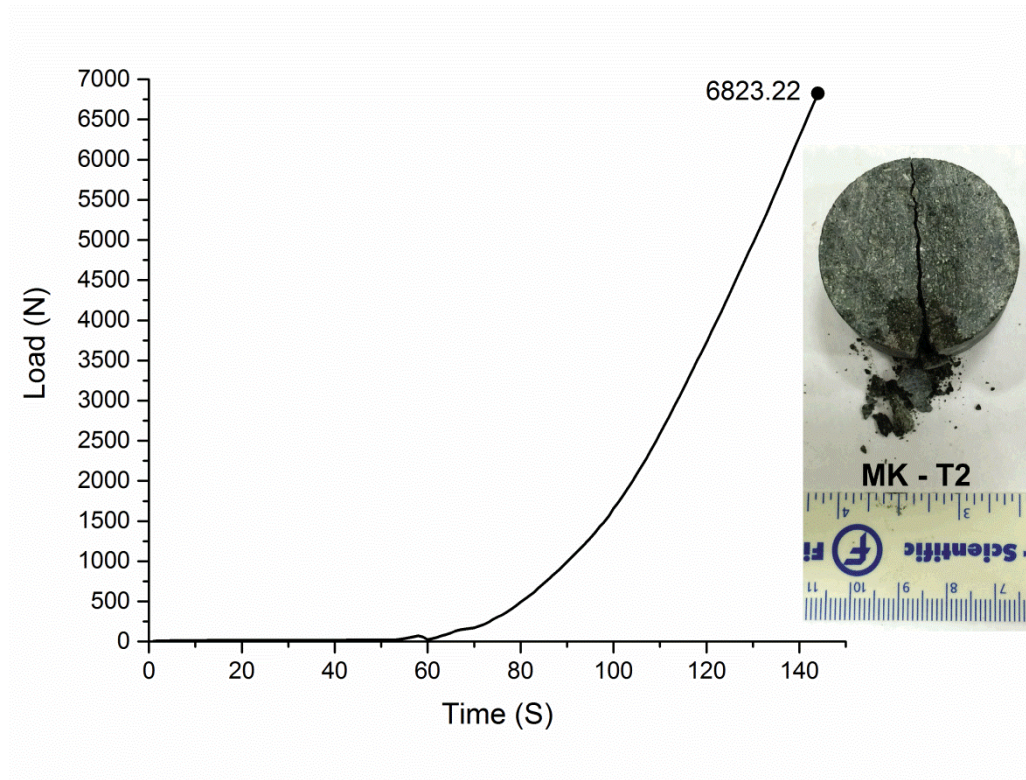


Figure A-28 Brazilian Test - Sample No. MK – T2

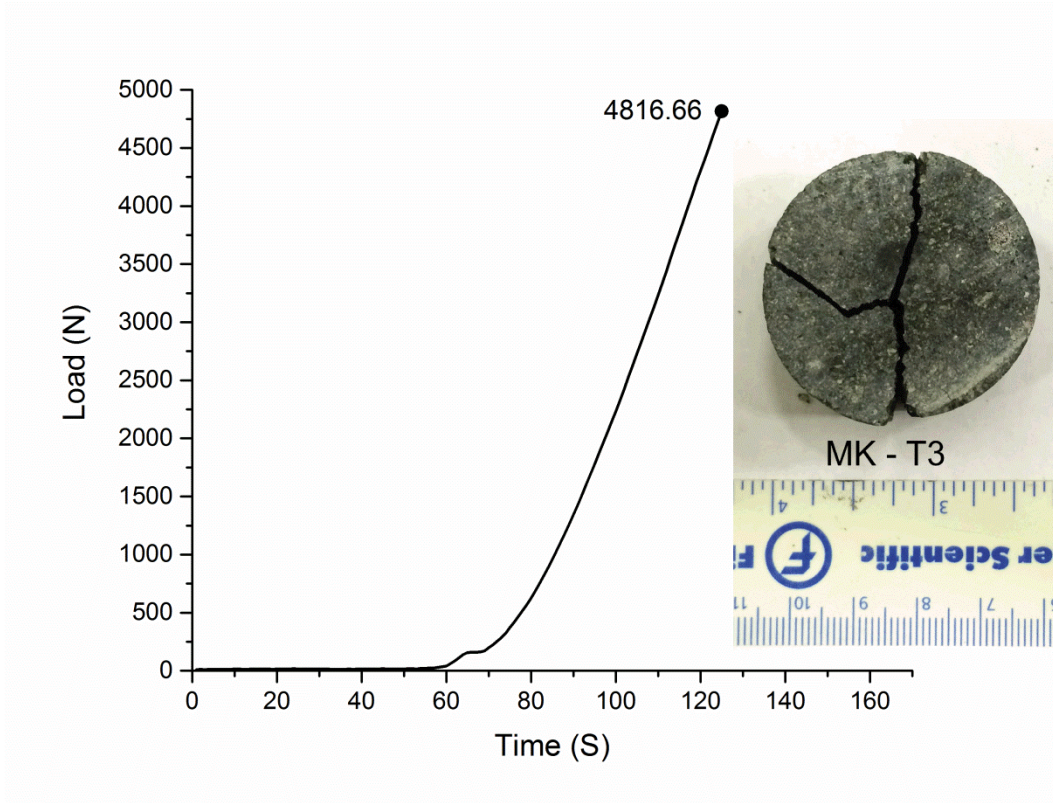


Figure A-29 Brazilian Test - Sample No. MK – T3

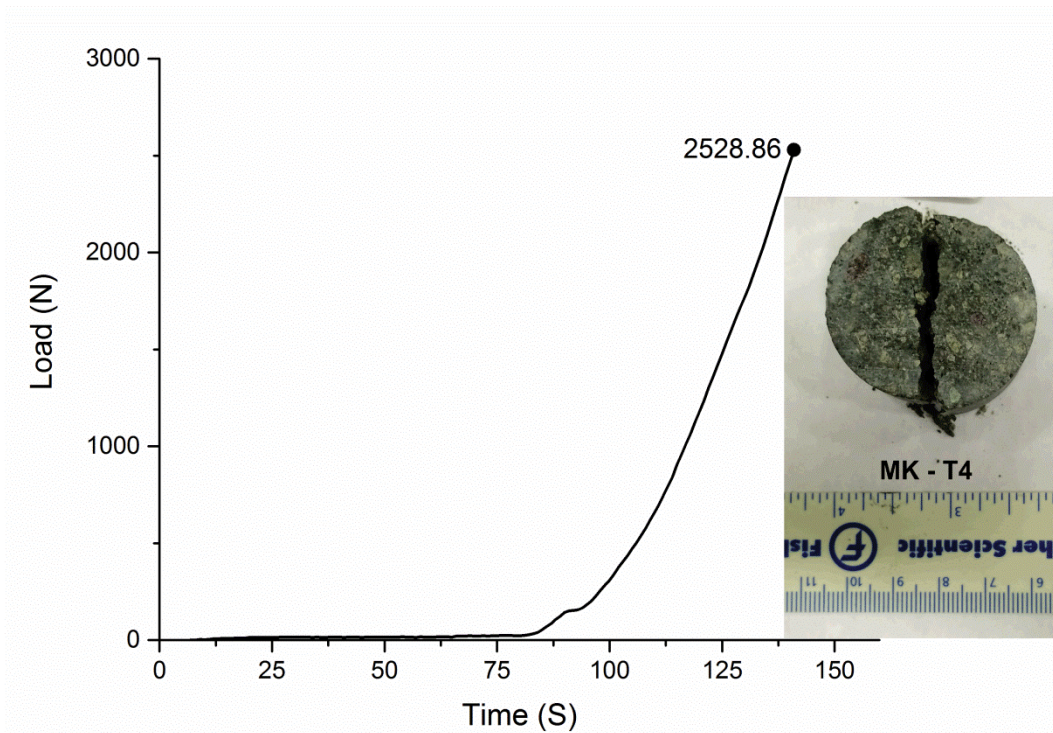


Figure A-30 Brazilian Test - Sample No. MK – T4

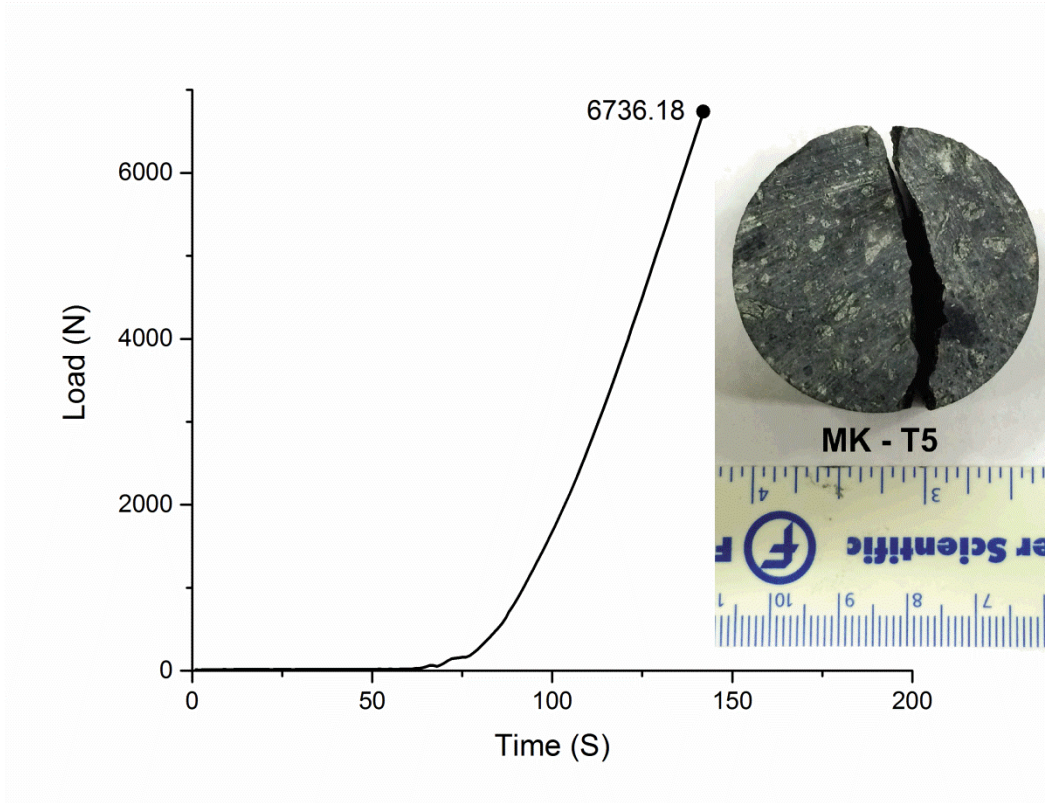


Figure A-31 Brazilian Test - Sample No. MK – T5

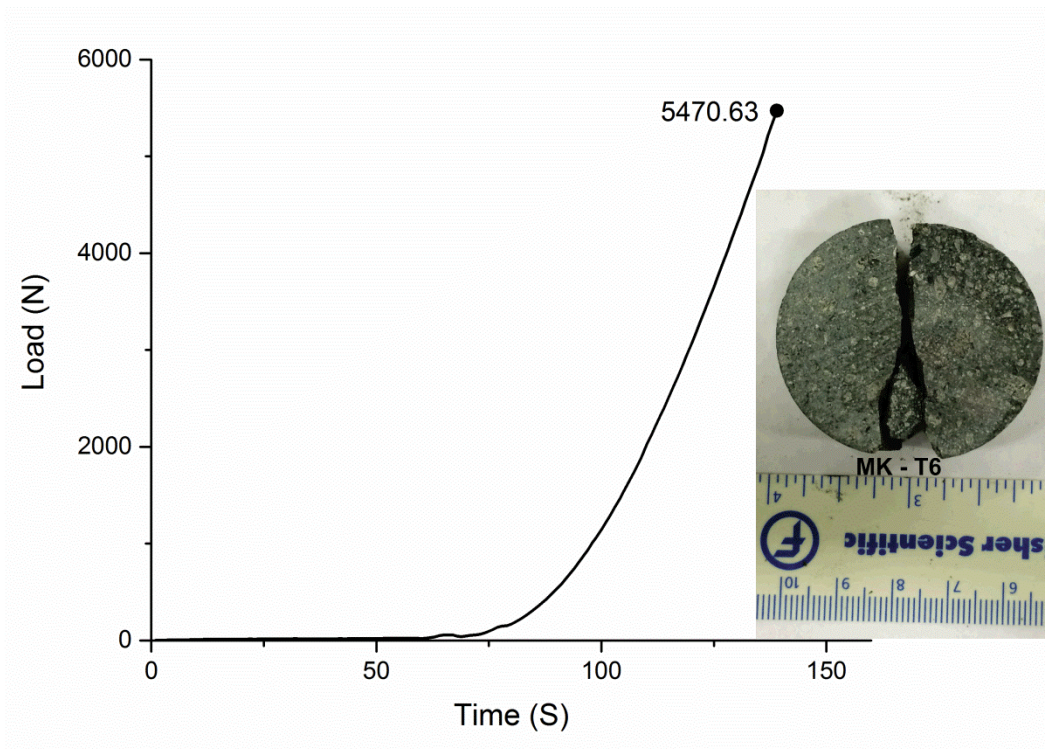


Figure A-32 Brazilian Test - Sample No. MK – T6

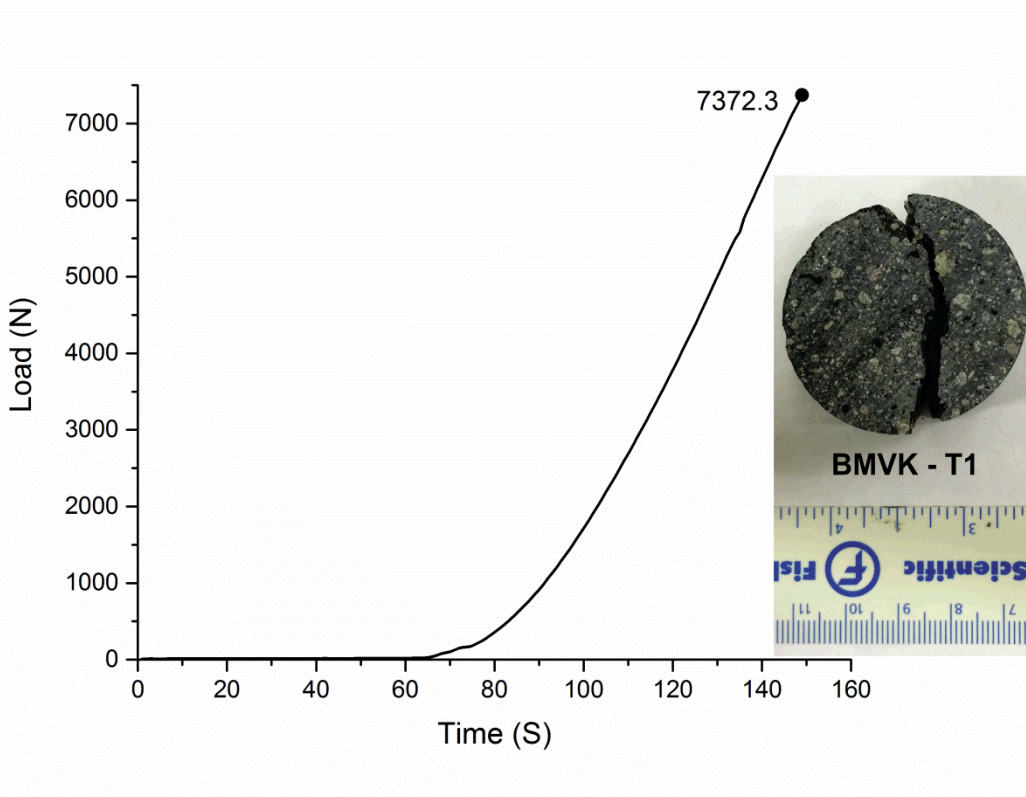


Figure A-33 Brazilian Test - Sample No. BMVK – T1

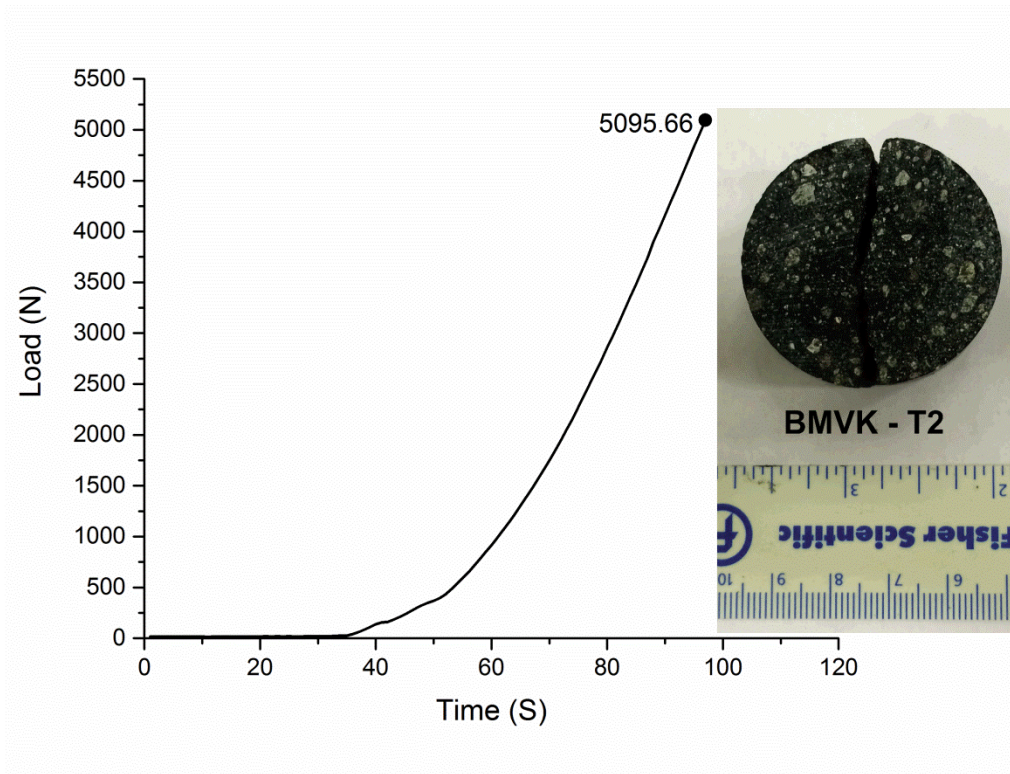


Figure A-34 Brazilian Test - Sample No. BMVK – T2

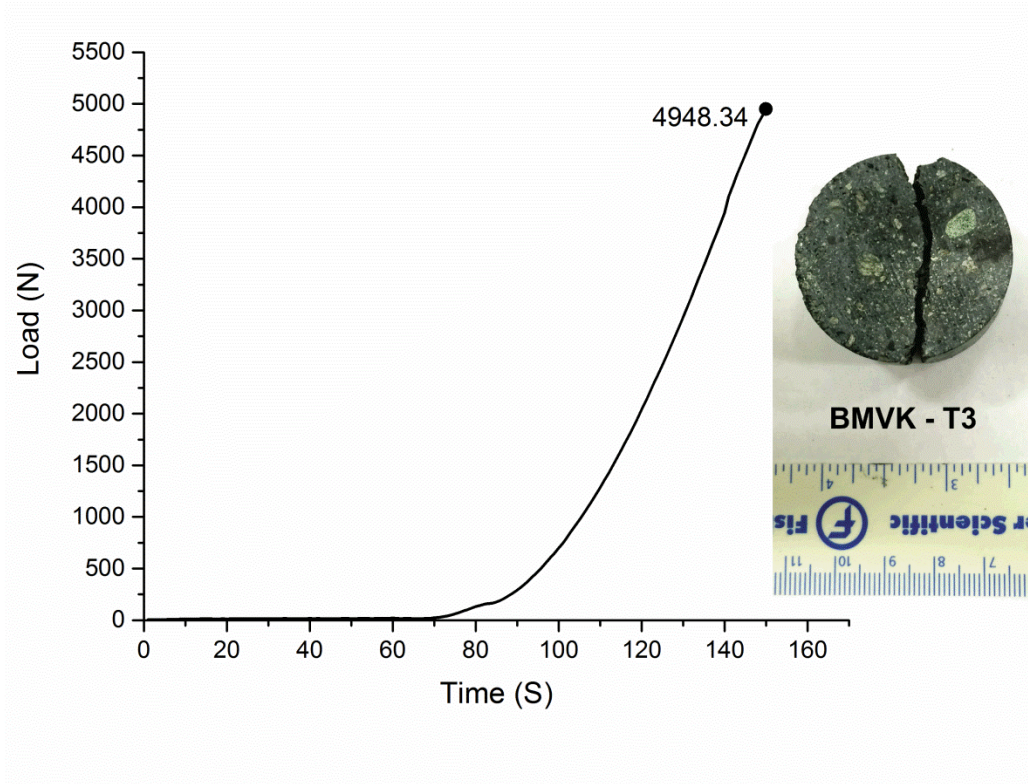


Figure A-35 Brazilian Test - Sample No. BMVK – T3

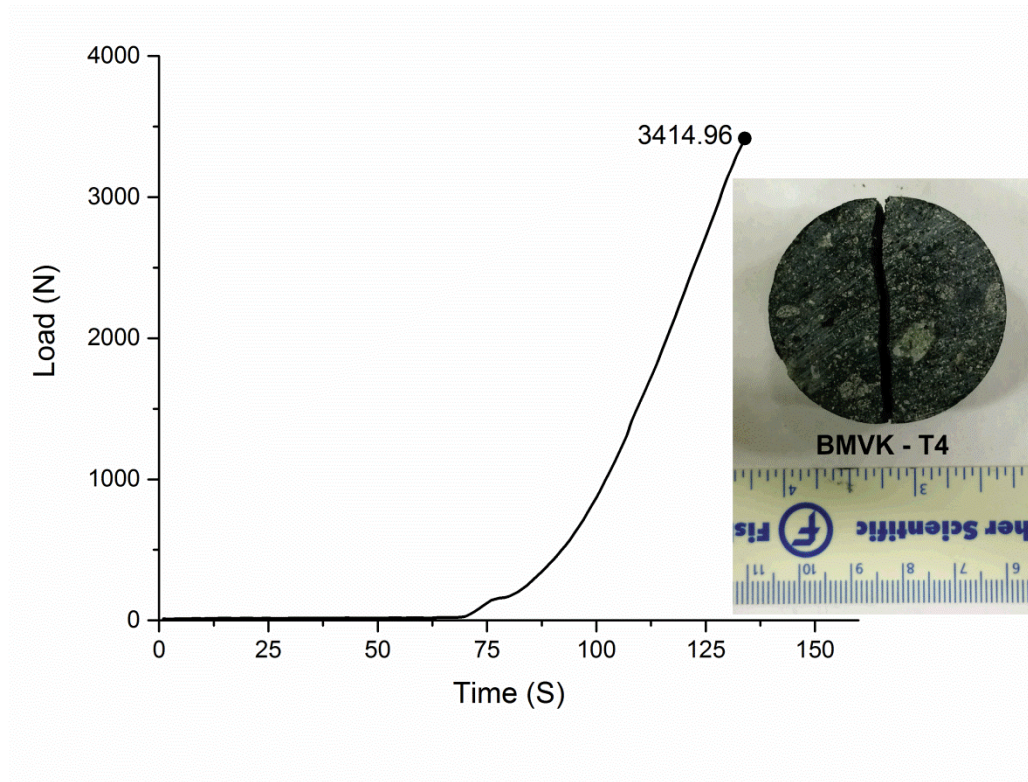


Figure A-36 Brazilian Test - Sample No. BMVK – T4

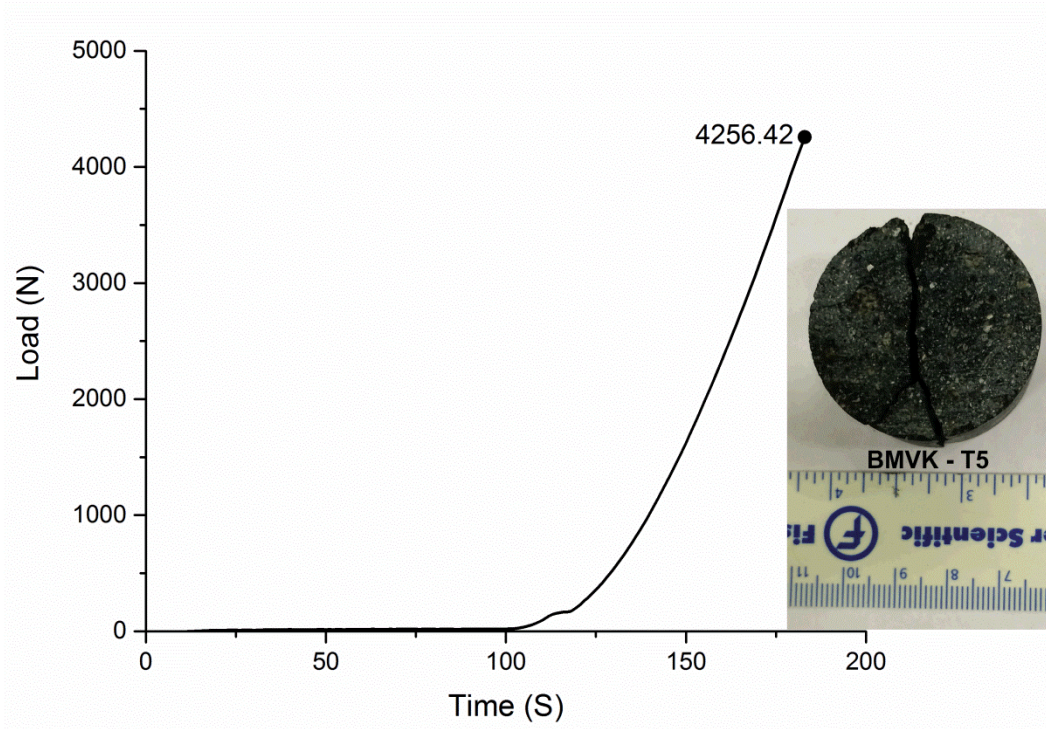


Figure A-37 Brazilian Test - Sample No. BMVK – T5

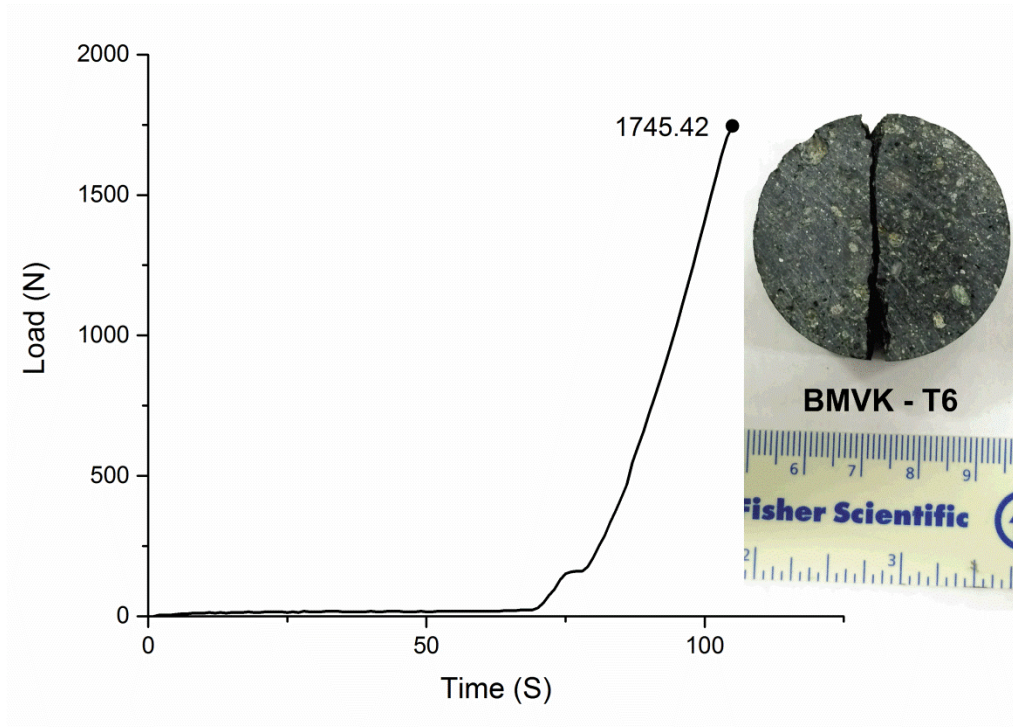


Figure A-38 Brazilian Test - Sample No. BMVK – T6

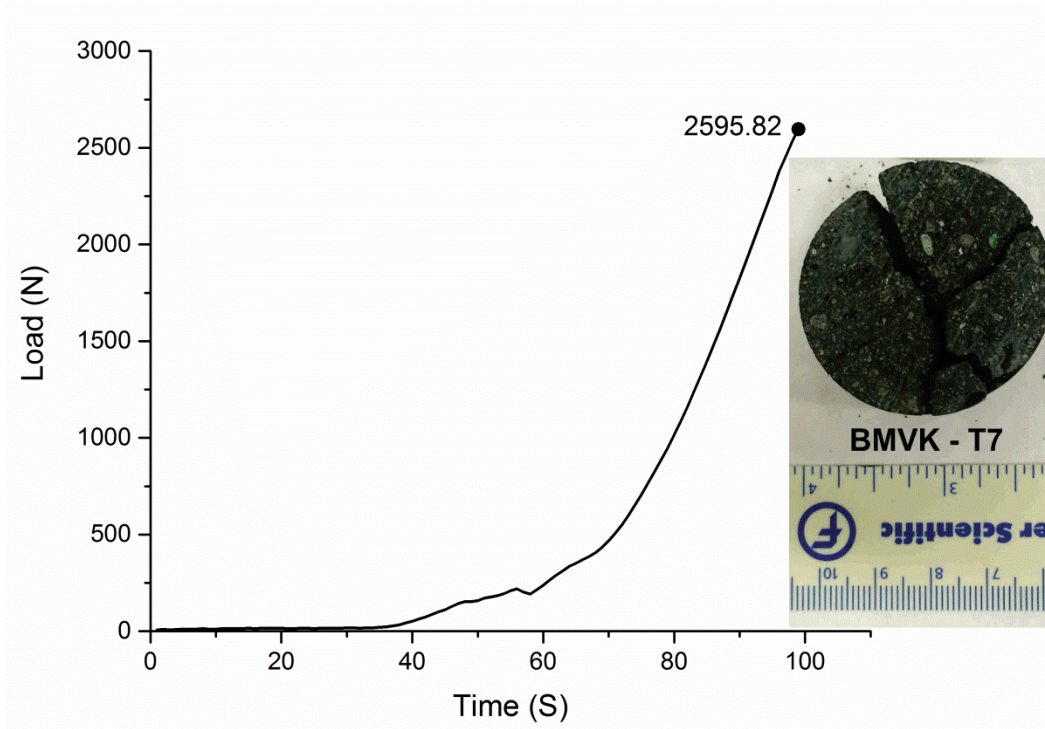


Figure A-39 Brazilian Test - Sample No. BMVK – T7

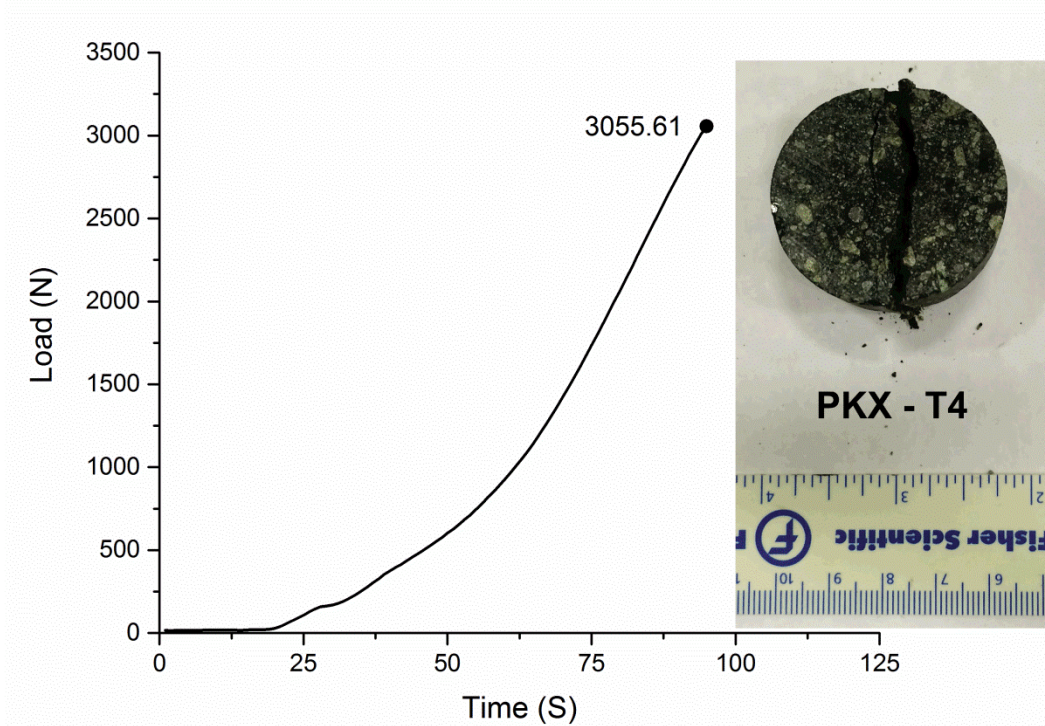


Figure A-40 Brazilian Test - Sample No. PKX – T4

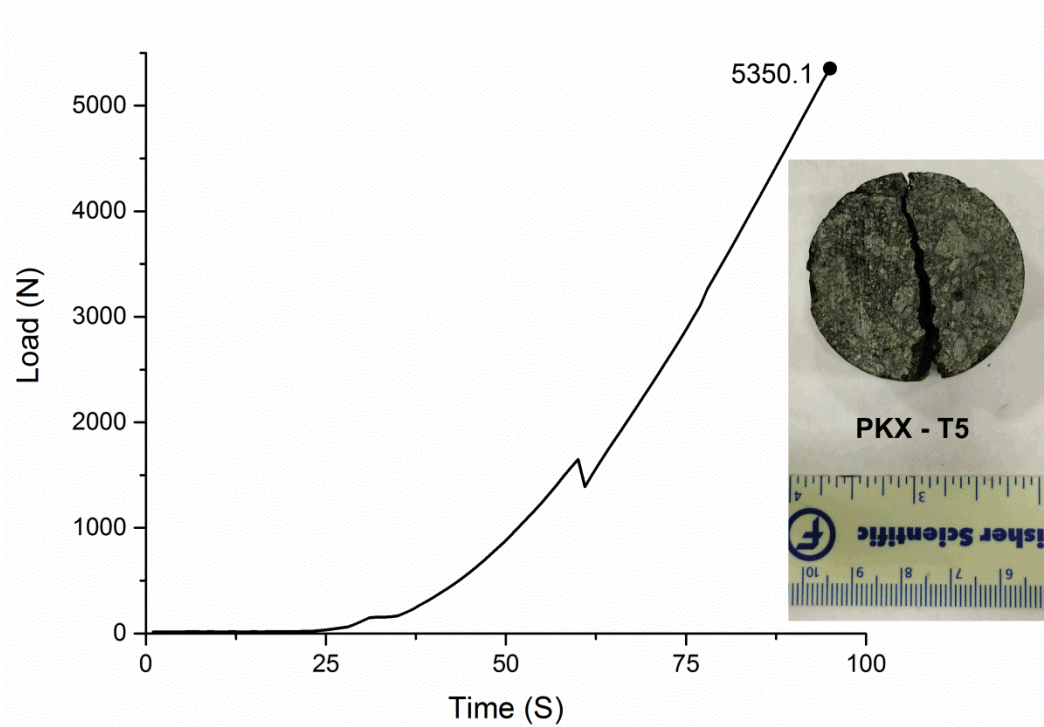


Figure A-41 Brazilian Test - Sample No. PKX – T5

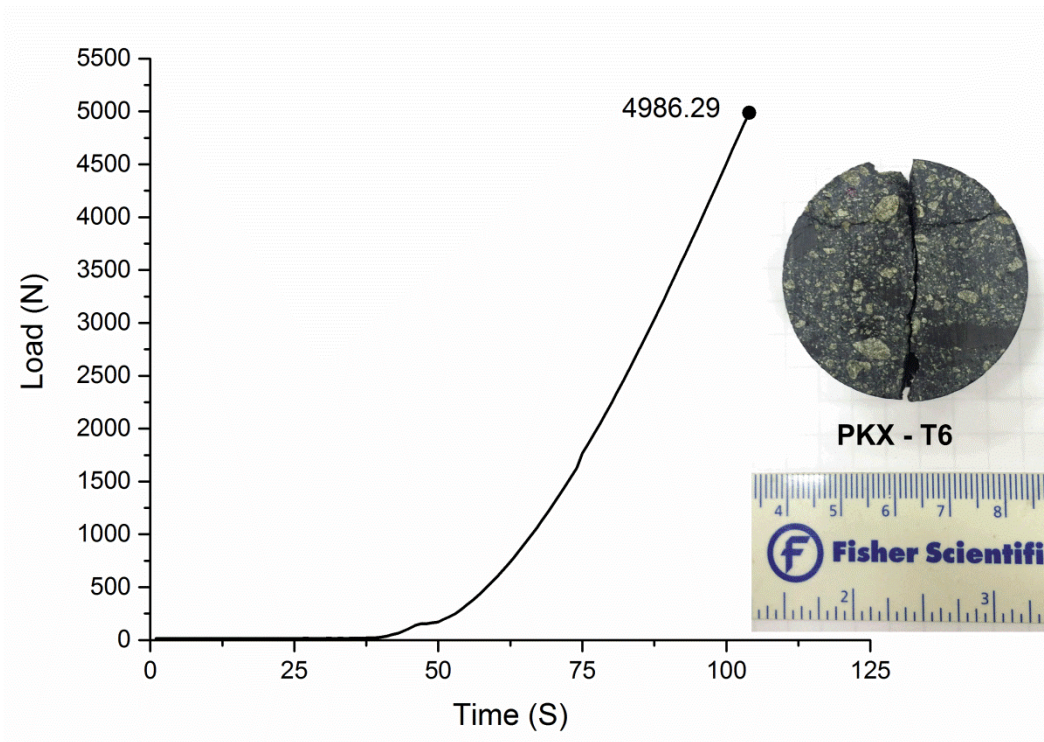


Figure A-42 Brazilian Test - Sample No. PKX – T6

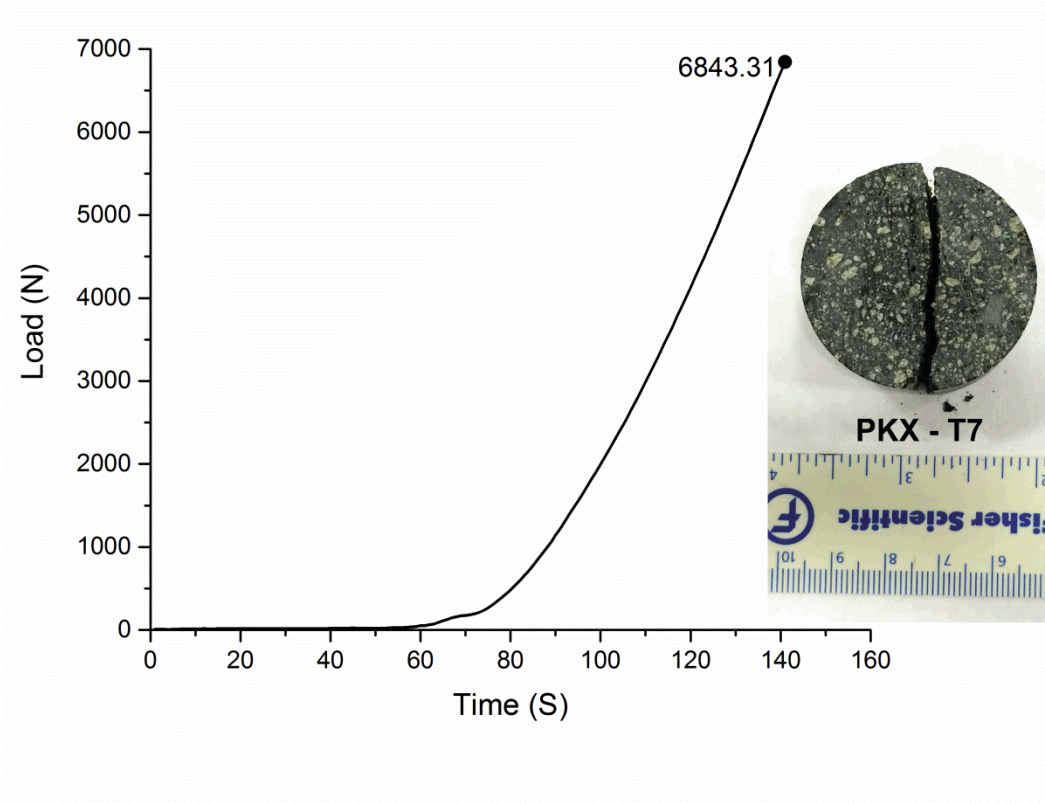


Figure A-43 Brazilian Test - Sample No. PKX – T7

## A.3 Triaxial Test Results

### A.3.1 PK Kimberlite Rock Type

Six cores specimens were prepared for the test. Since it was the first the Hoek's Cell were used and the performance, bearing capacity and behaviour of the Cell were unknown, the confinement pressures were started from 4 MPa and it was gradually increased to 25 MPa.

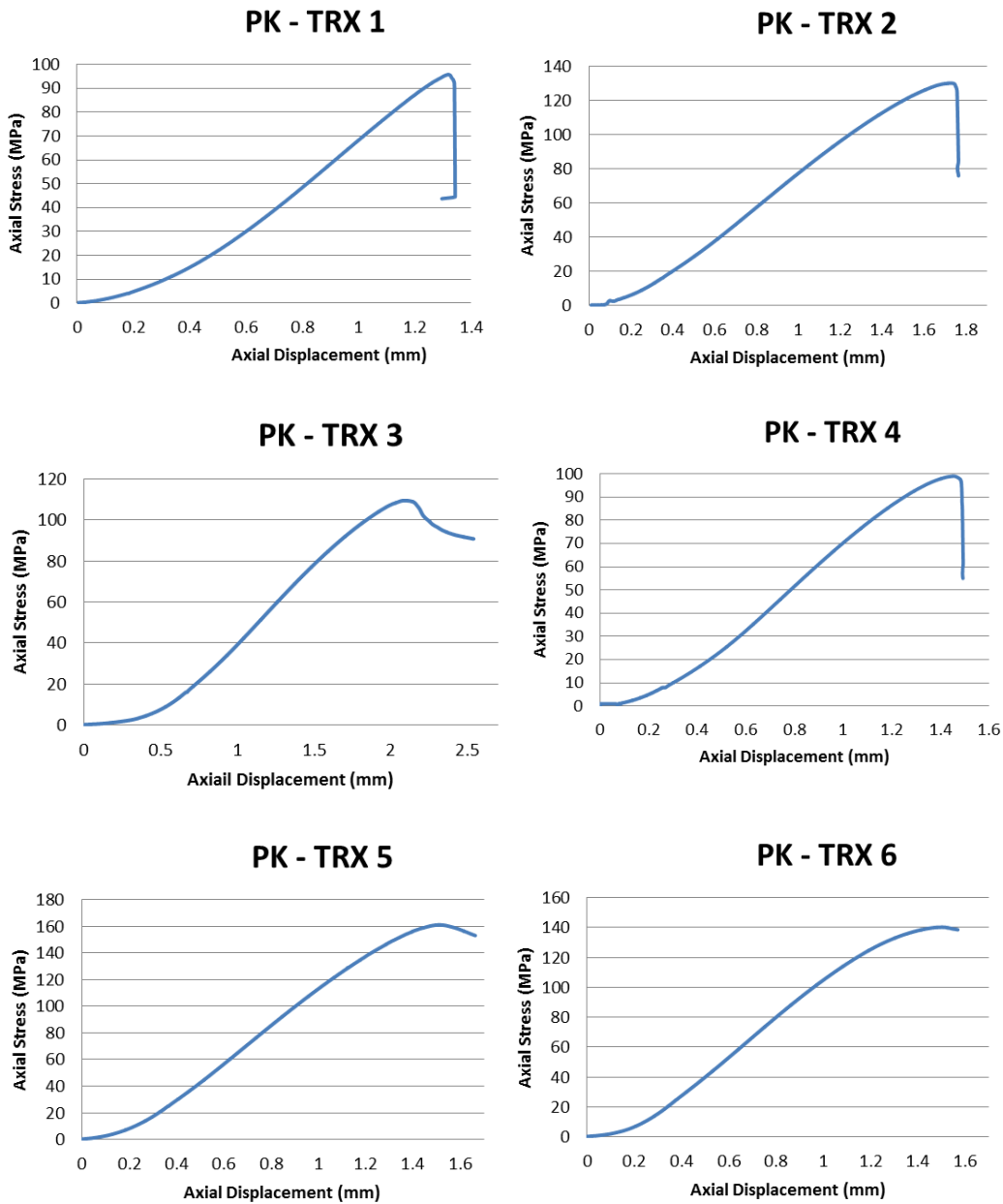


Figure A.44 Axial Stress vs Piston Displacement for Each Specimen – Rock Type PK

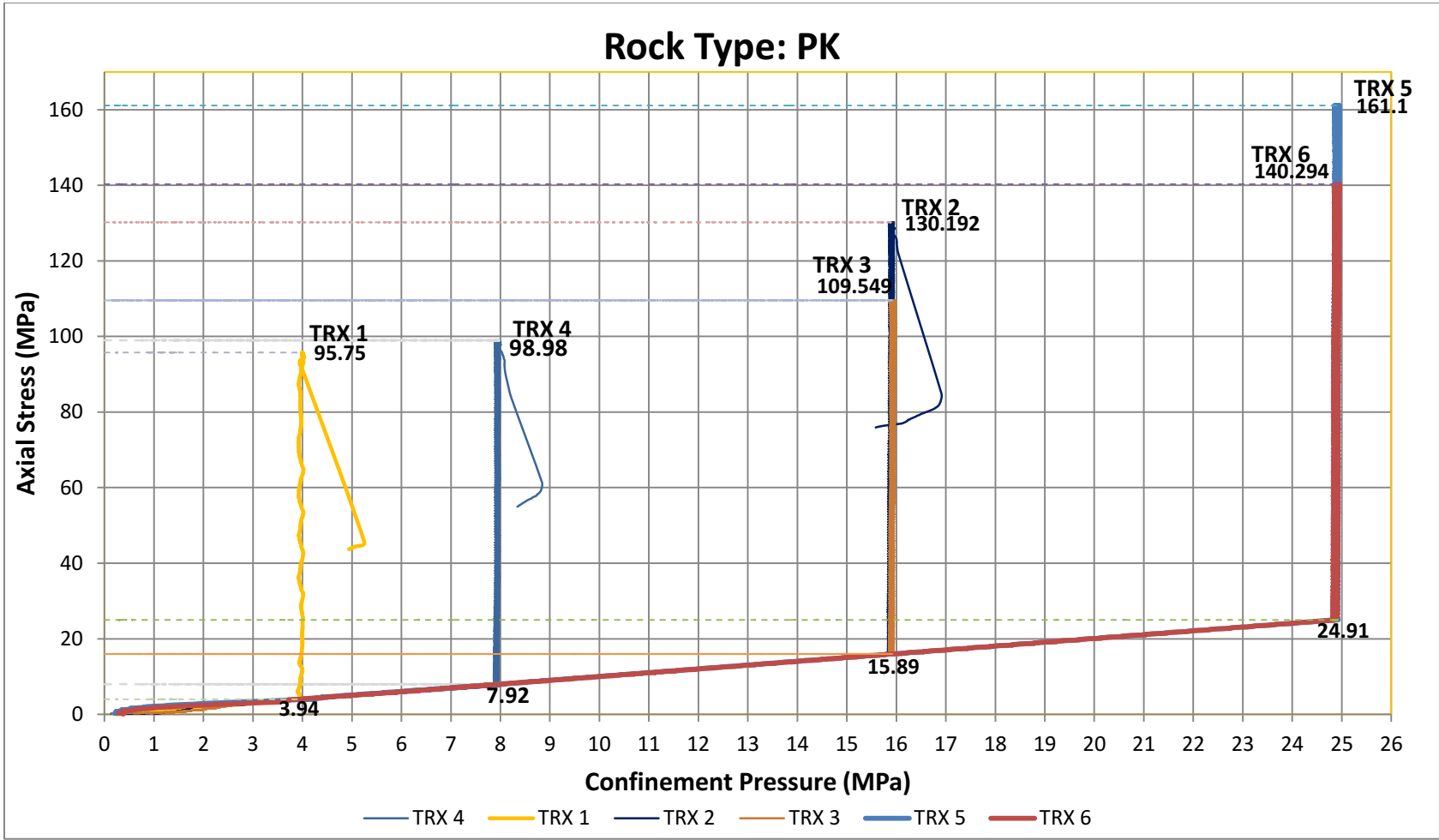
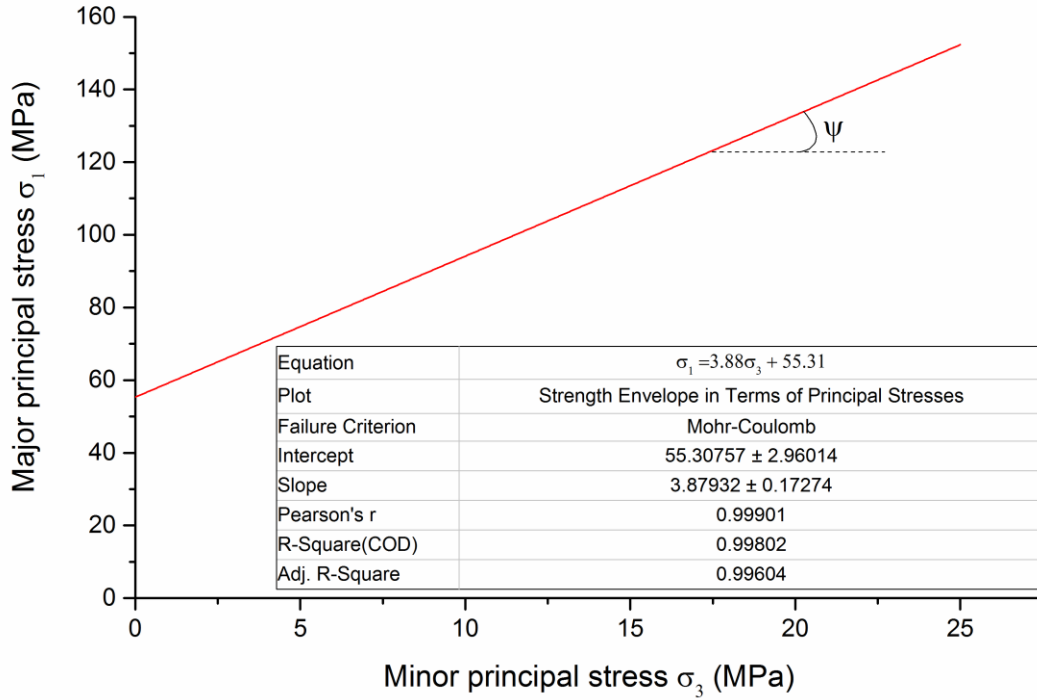
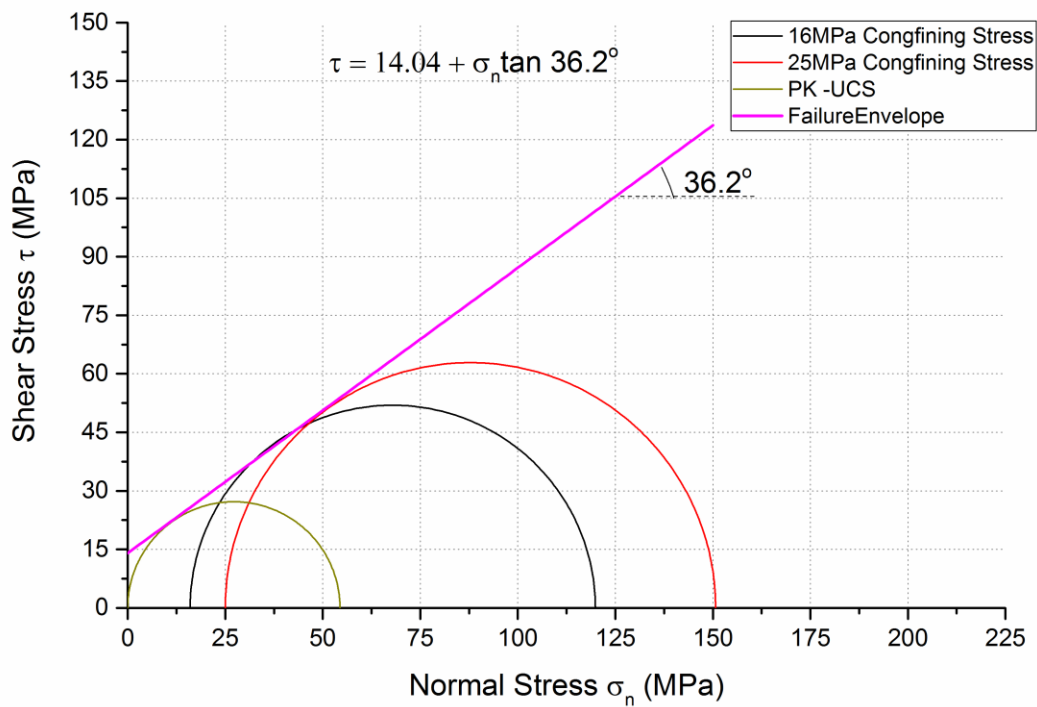


Figure A.45 Axial Stress vs. Confinement Pressure for Each Specimen - Rock Type: PK



**Figure A.46** The linear relationship between the major and minor principal stresses for PK Kimberlite



**Figure A.47** Mohr-Coulomb failure envelope for intact PK Kimberlite (based on the Average Acceptable data)

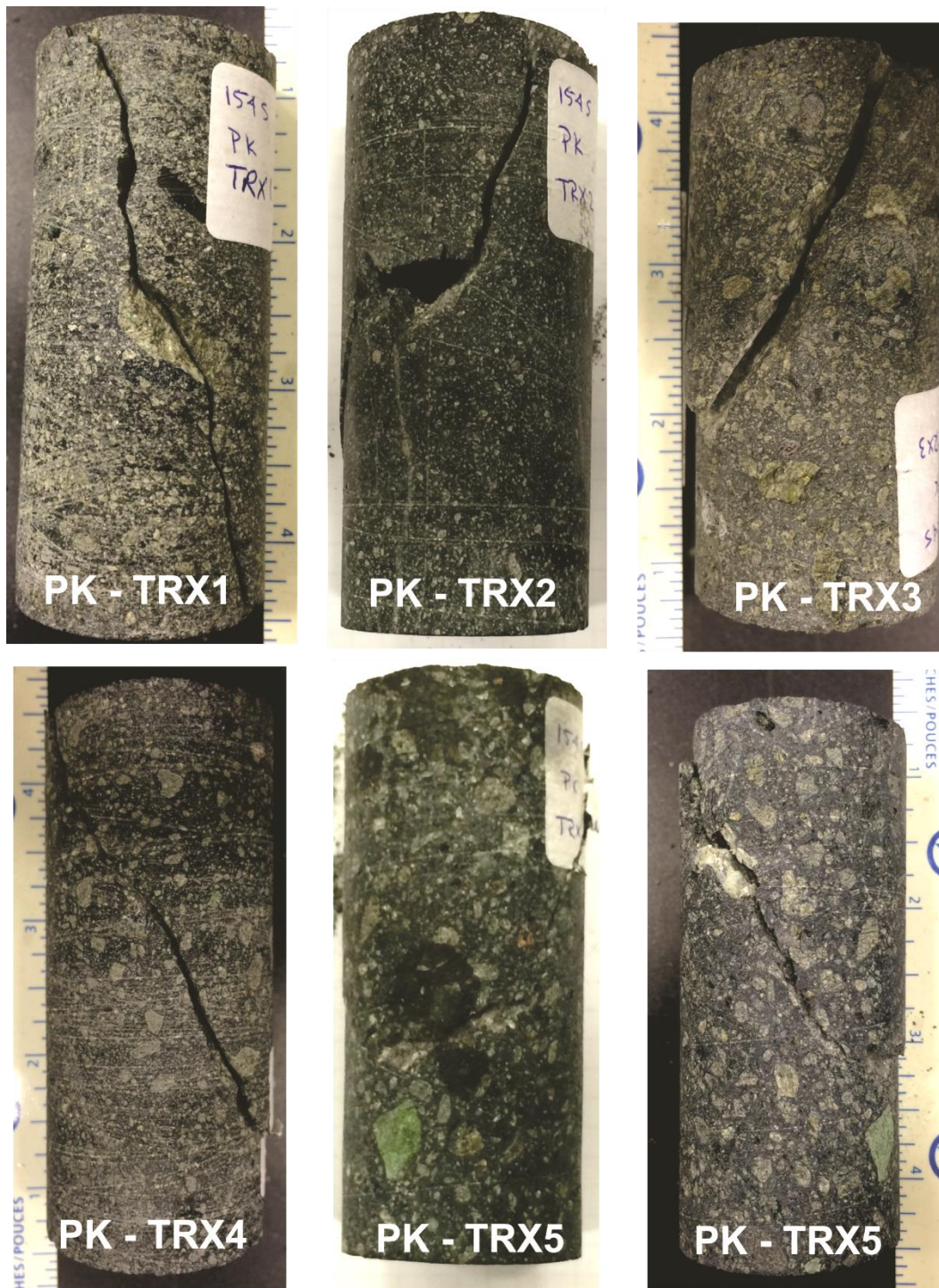
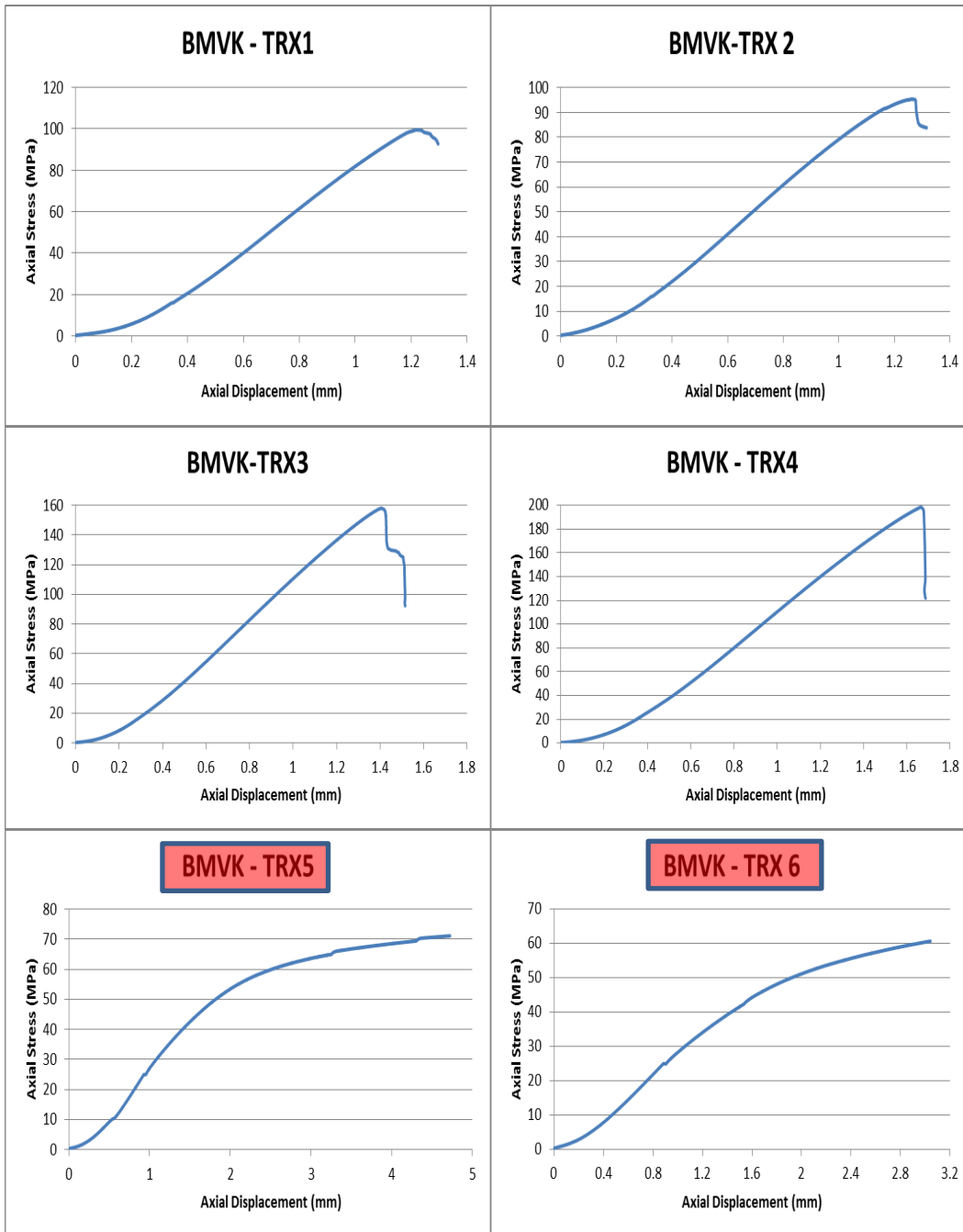


**Figure A.48** Failure Mode of Each Core Specimen - PK Kimberlite - Triaxial Test

### A.3.2 BMVK Kimberlite Rock Type

6 core samples have been provided for the test. Two confinement pressures are used: 16 MPa and 25 MPa. However, based on the mode of failure and available data the test results for TRX -5 and TRX – 6 are discarded.



**TRX 5 and TRX 6 are Discarded Results**

**Figure A.49** Axial Stress vs Piston Displacement for Each Sample – Rock Type BMVK

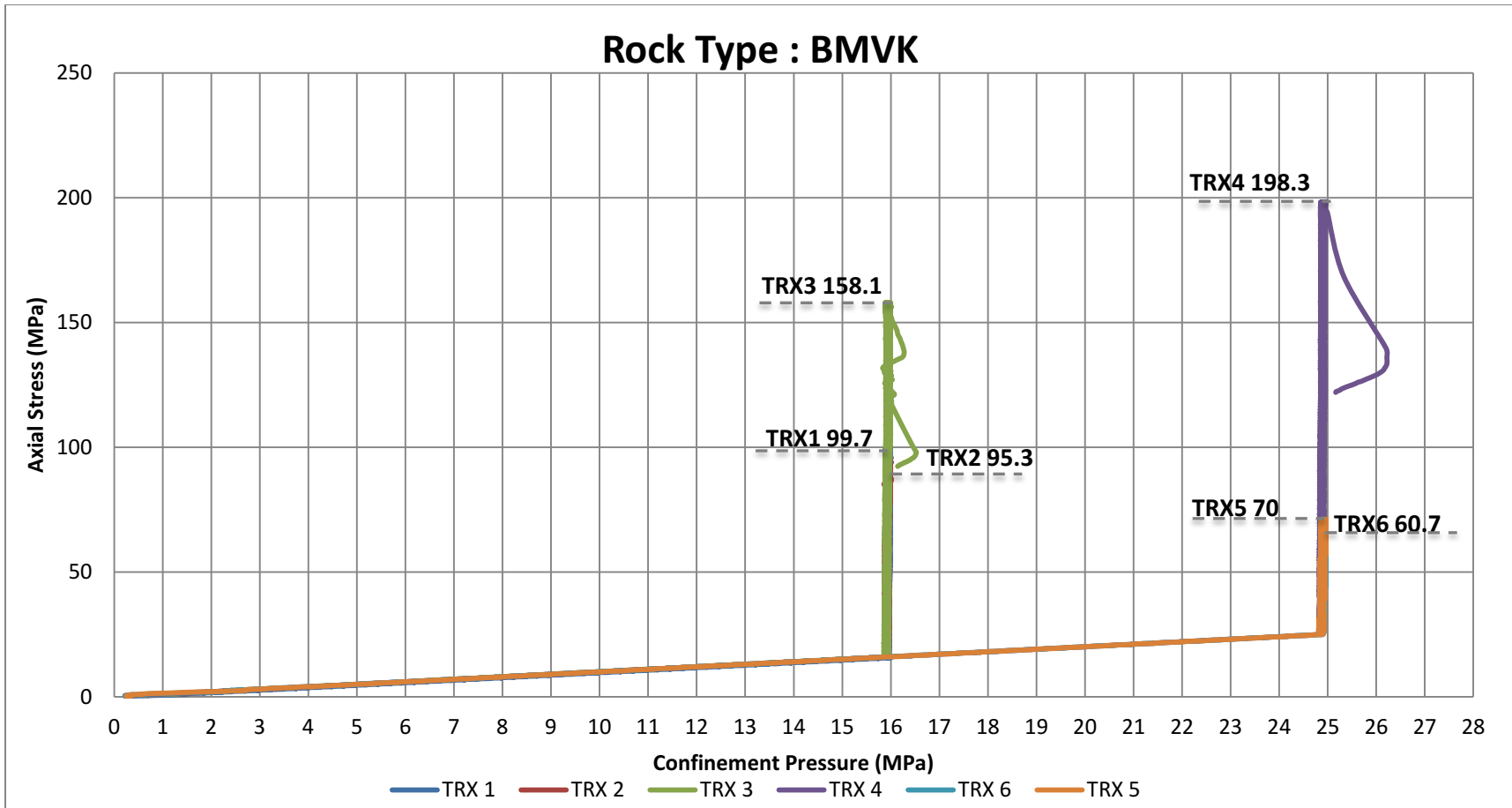


**Figure A.50** Axial Stress vs. Confinement Pressure for Each Specimen - Rock Type: BMVK

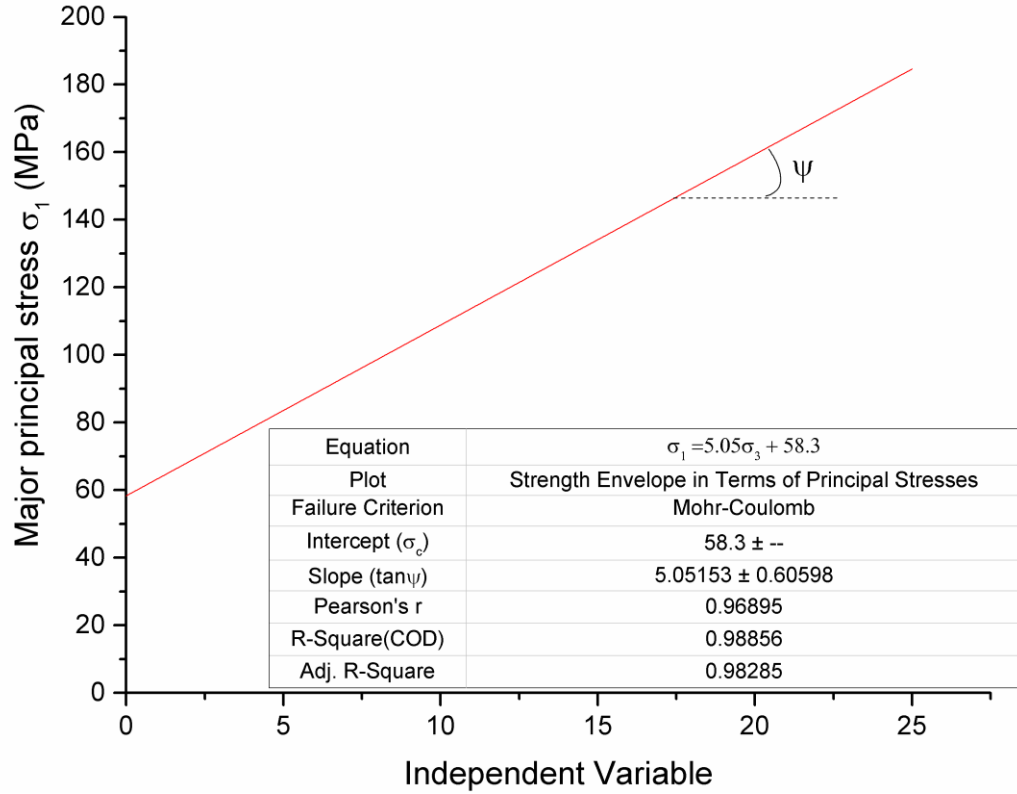


**Figure A.51** The linear relationship between the major and minor principal stresses for BMVK Kimberlite

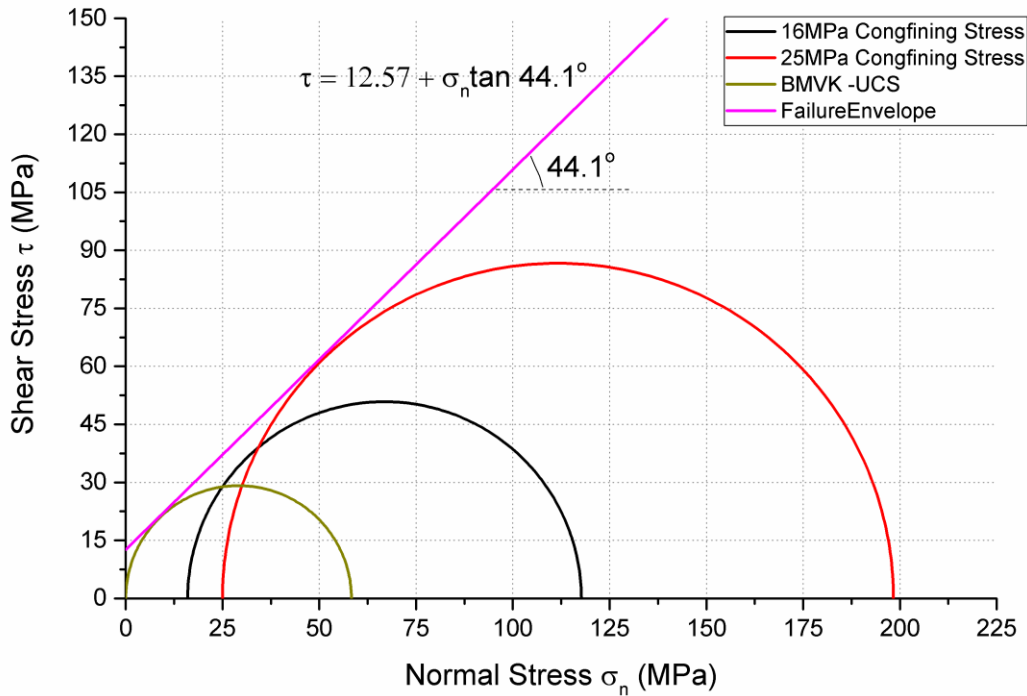


**Figure A.52** Mohr-Coulomb failure envelope for intact BMVK Kimberlite (based on the Average Acceptable data)

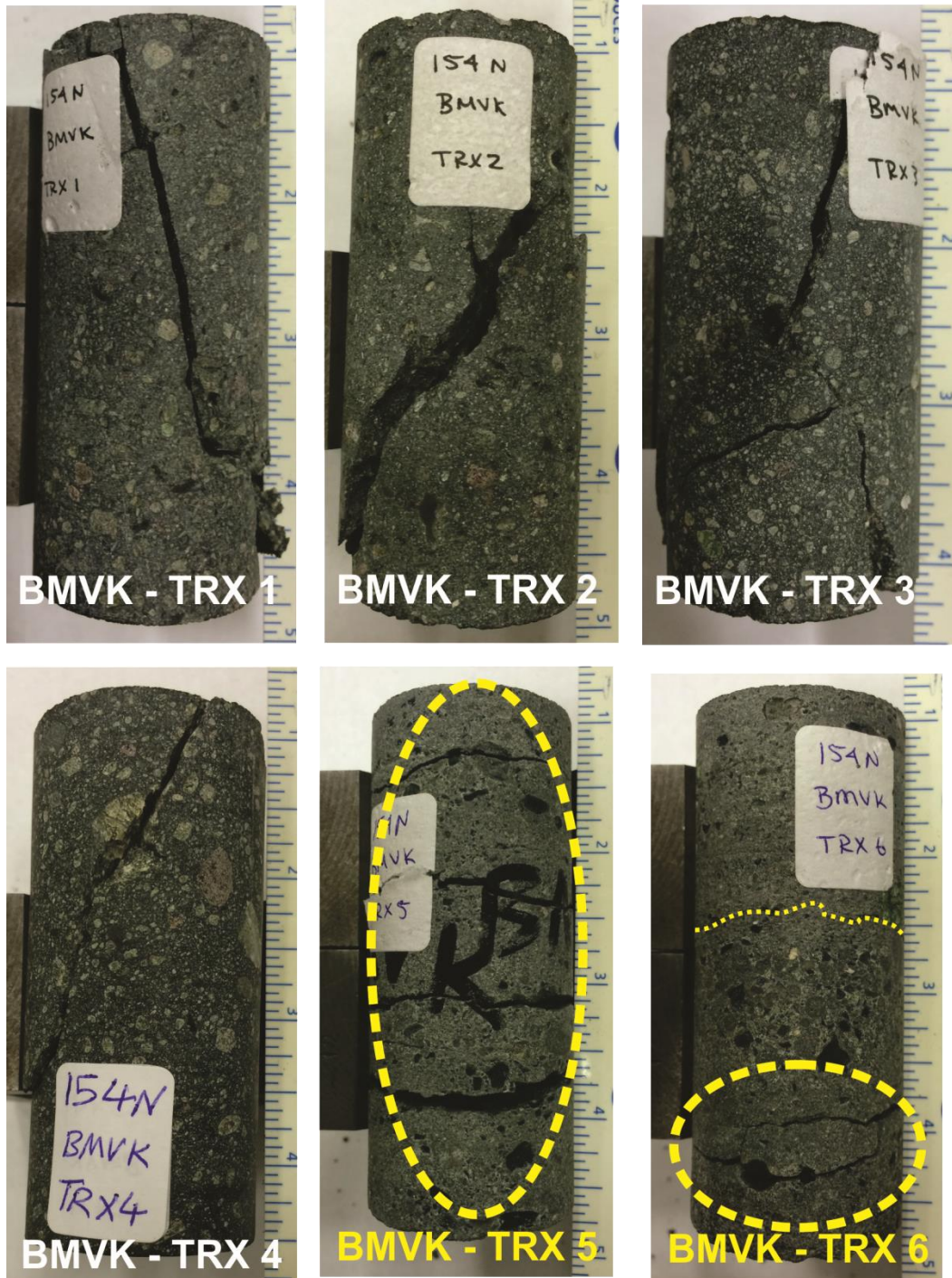


**Figure A.53** Failure Mode of Each Core Specimen - BMVK Kimberlite - Triaxial Test

### A.3.3 MRK Kimberlite Rock Type

Only three conducted tests results were acceptable. TRX B1, B3 and B6.

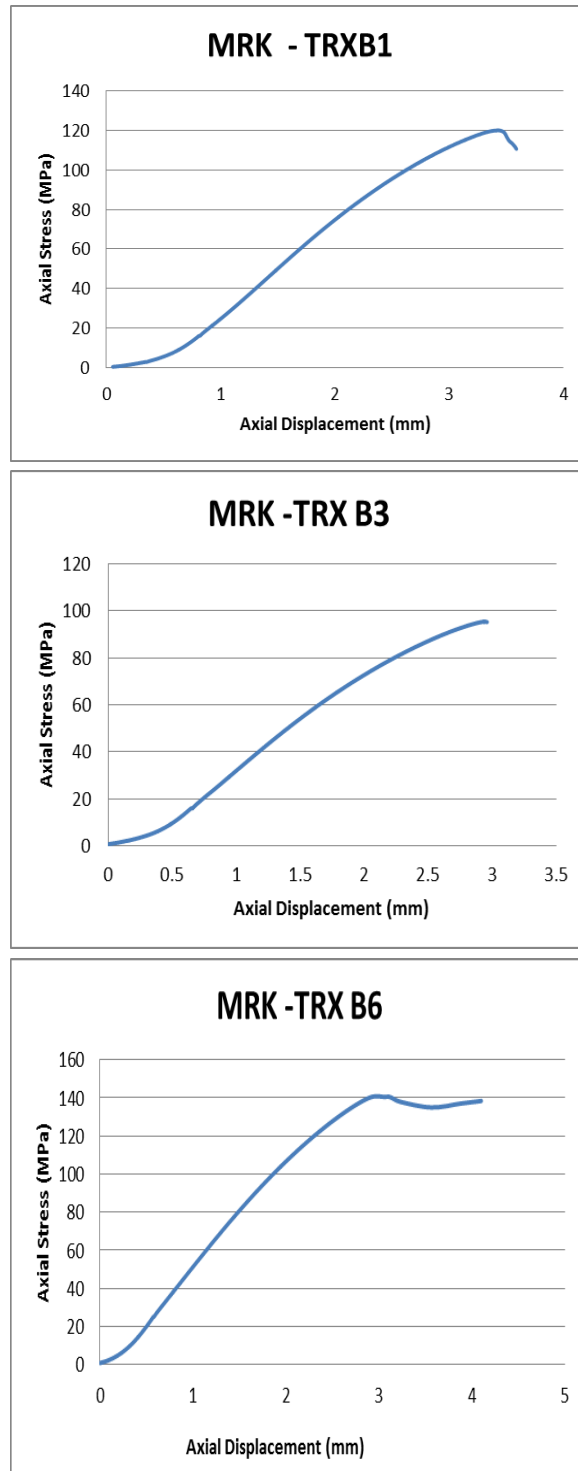


Figure A.54 Axial Stress vs Piston Displacement for Each Sample – Rock Type MRK

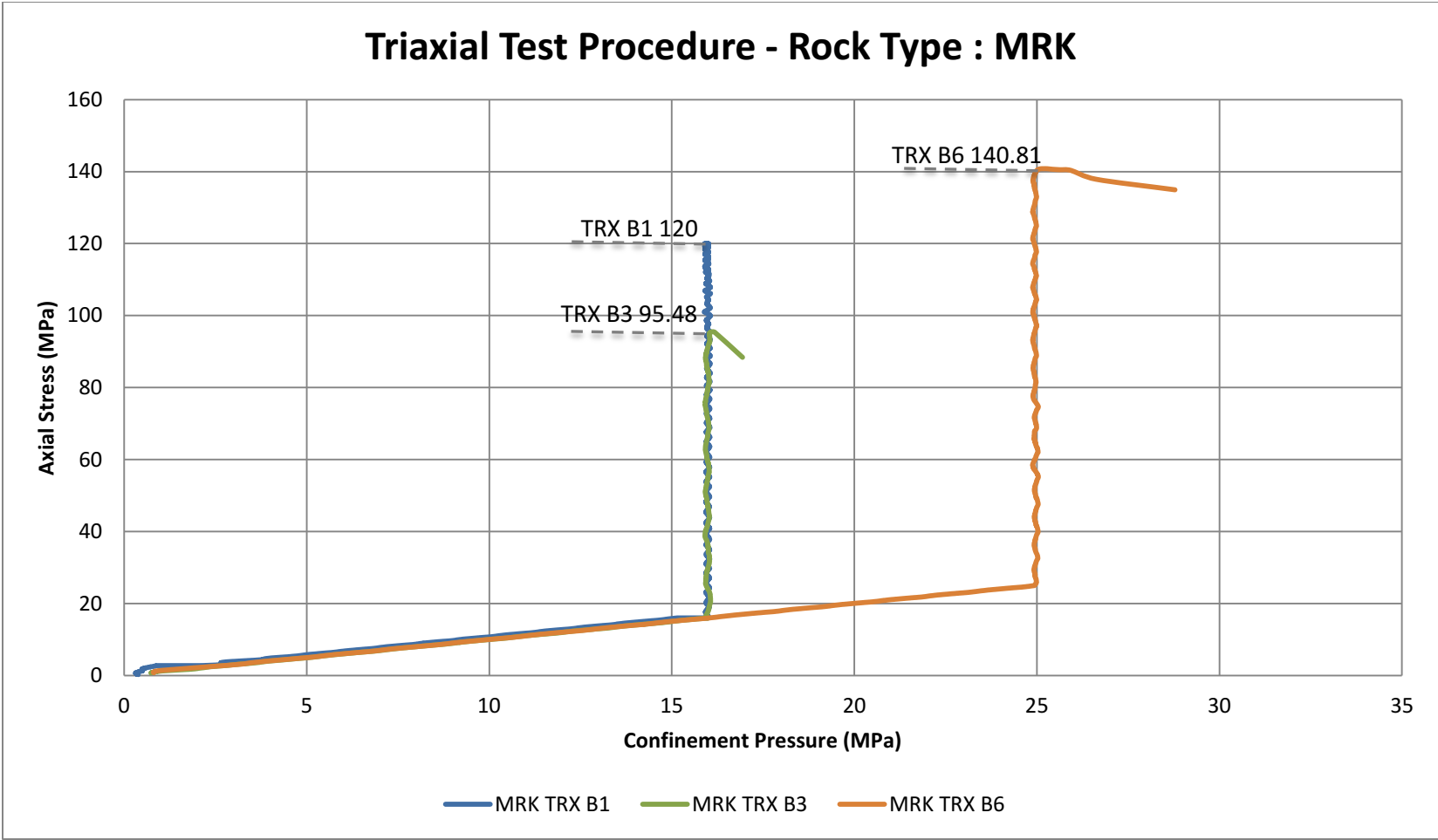


Figure A.55

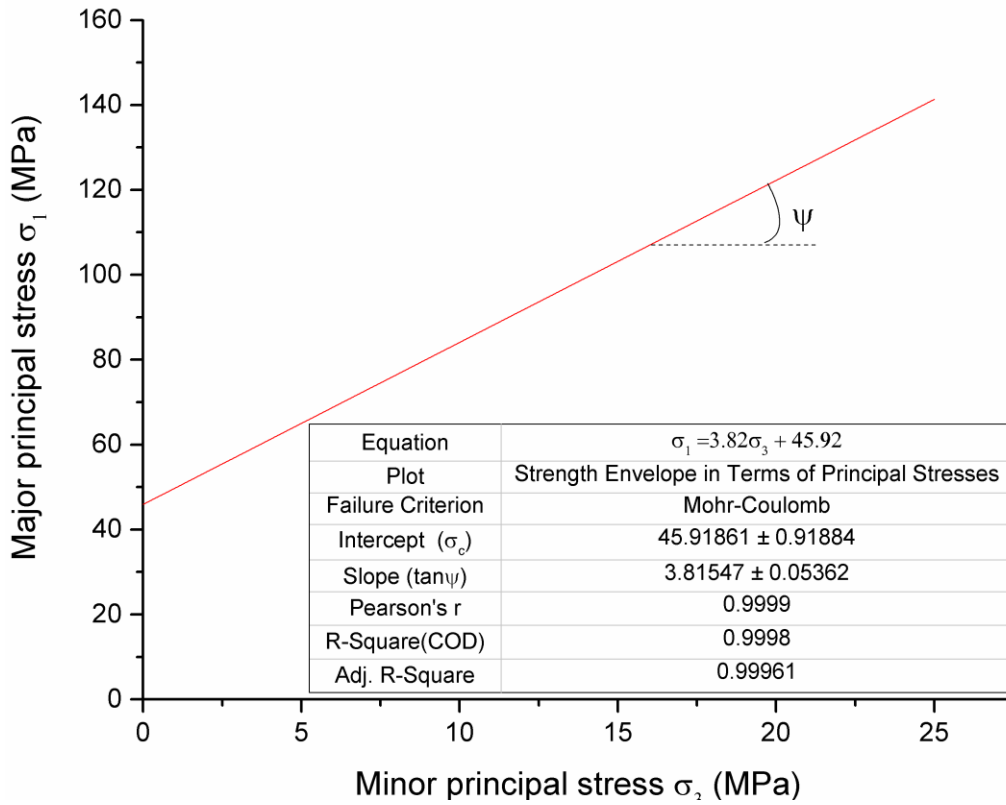


Figure a.56 The linear relationship between the major and minor principal stresses for MRK Kimberlite

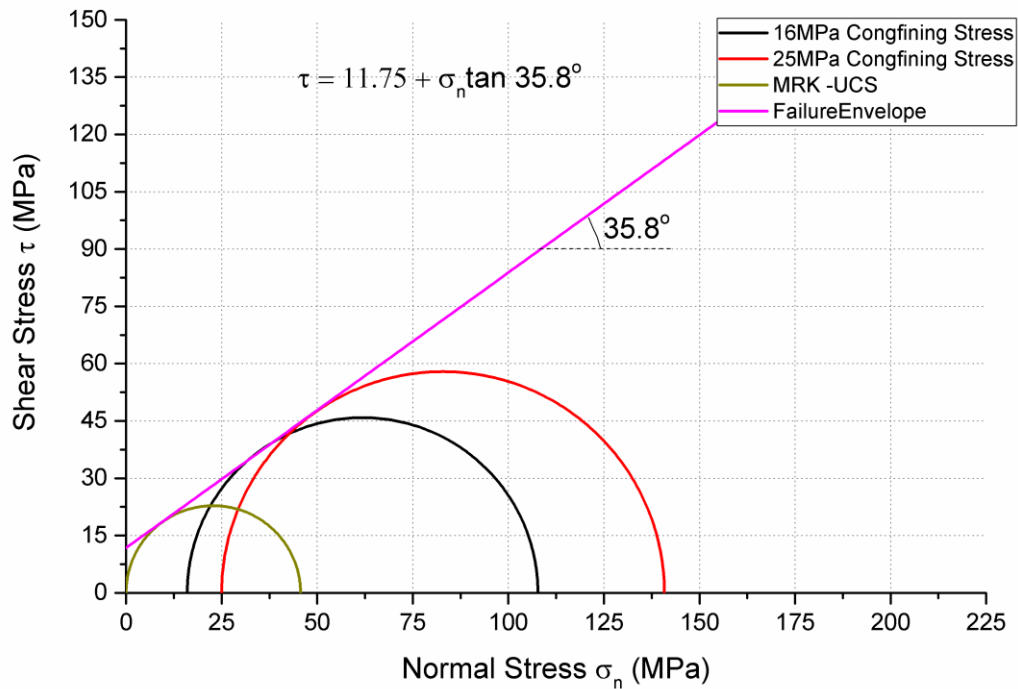


Figure A.57 Mohr-Coulomb failure envelope for intact MRK Kimberlite (based on the Average Acceptable data)



Figure A.58 Failure Mode of Each Core Specimen - MRK Kimberlite - Triaxial Test

### A.3.4 MK Kimberlite Rock Type

Four of the conducted tests results were acceptable (TRX 2, 4, 5, and 6).

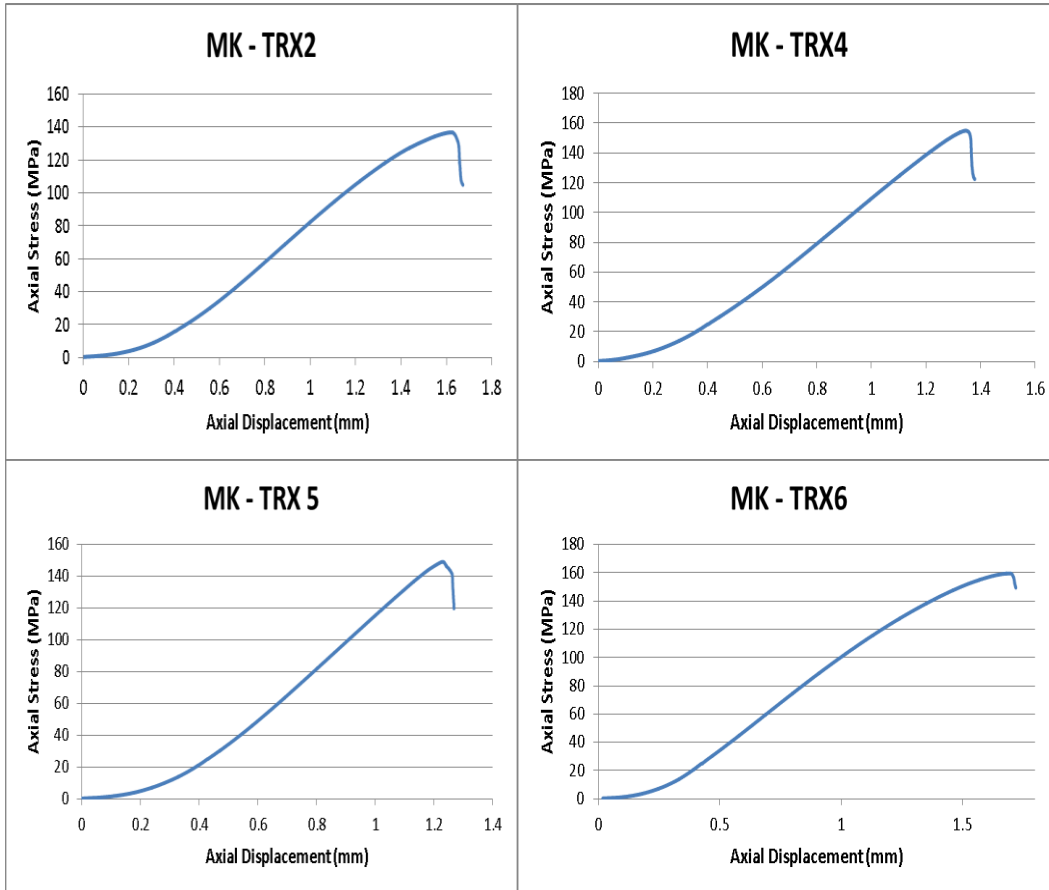
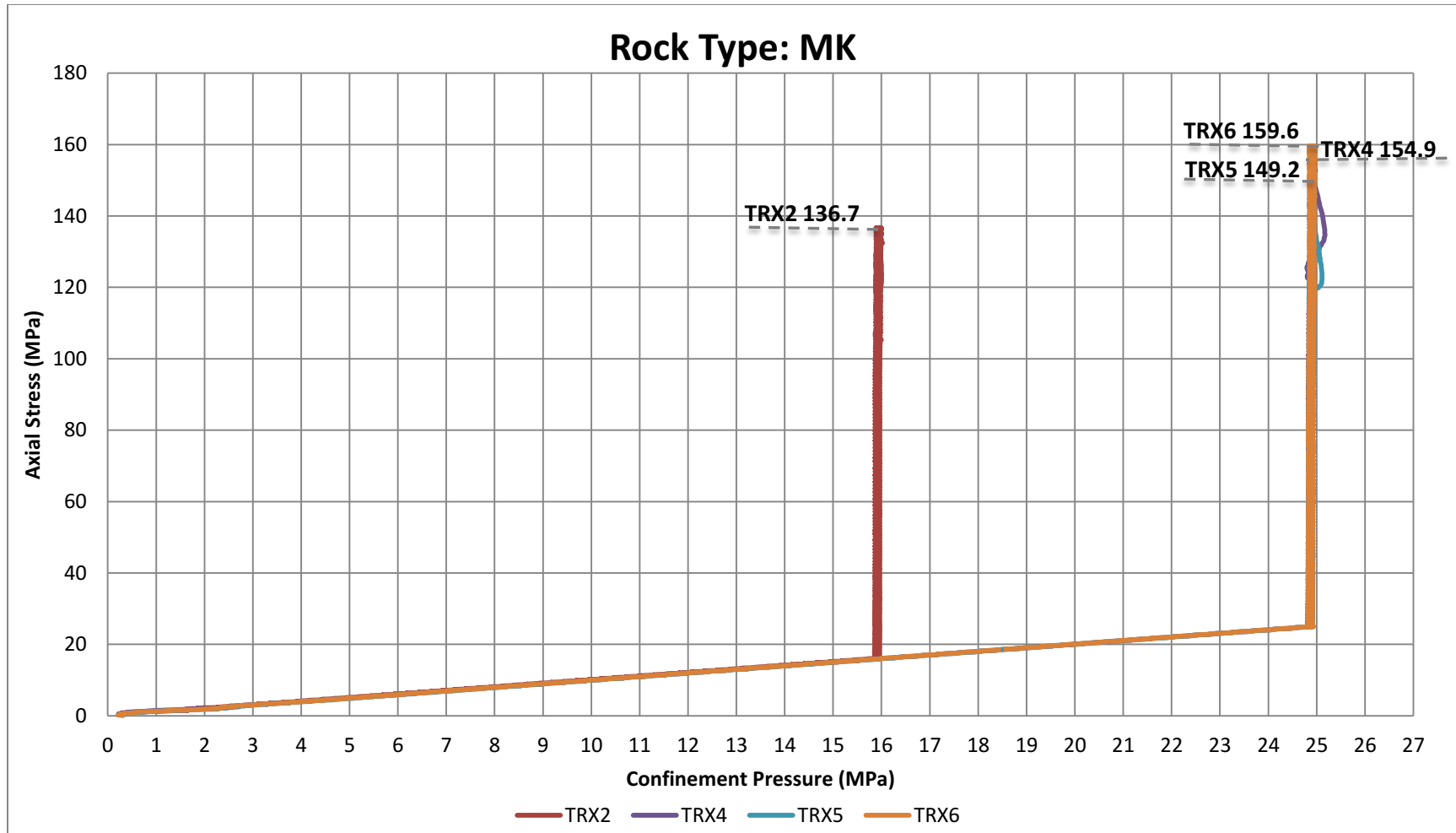


Figure A.59 Axial Stress vs Piston Displacement for Each Sample – Rock Type MK



**Figure A.60** Axial Stress vs. Confinement Pressure for Each Specimen - Rock Type: MK

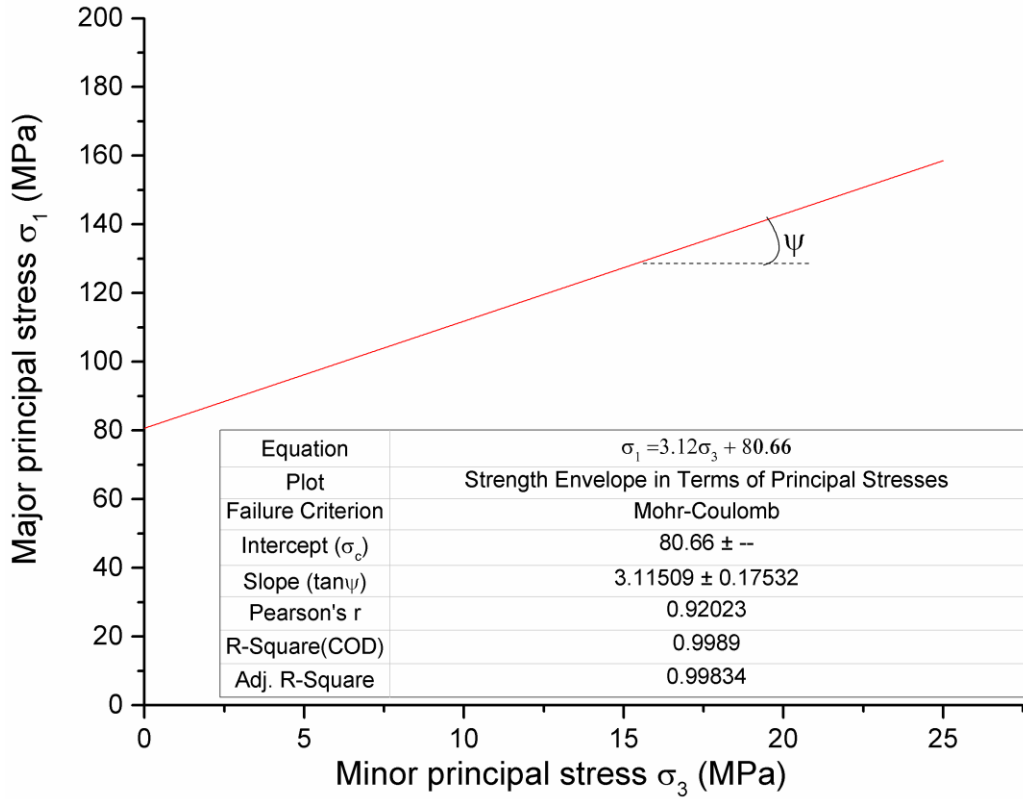


Figure A.61 The linear relationship between the major and minor principal stresses for MRK Kimberlite

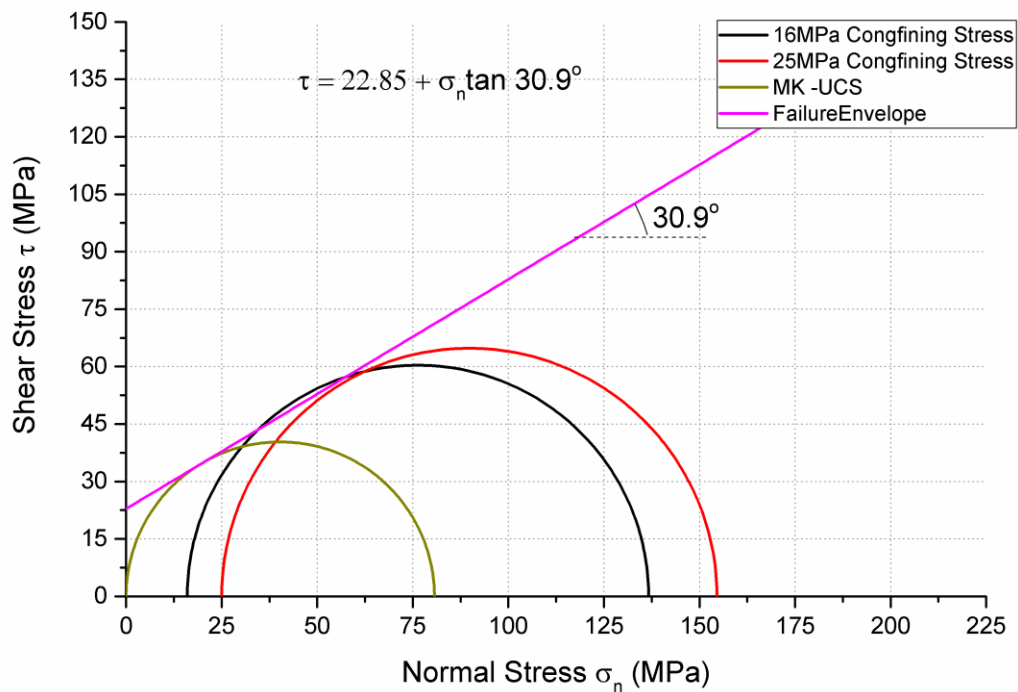


Figure A.62 Mohr-Coulomb failure envelope for intact MRK Kimberlite (based on the Average Acceptable data)

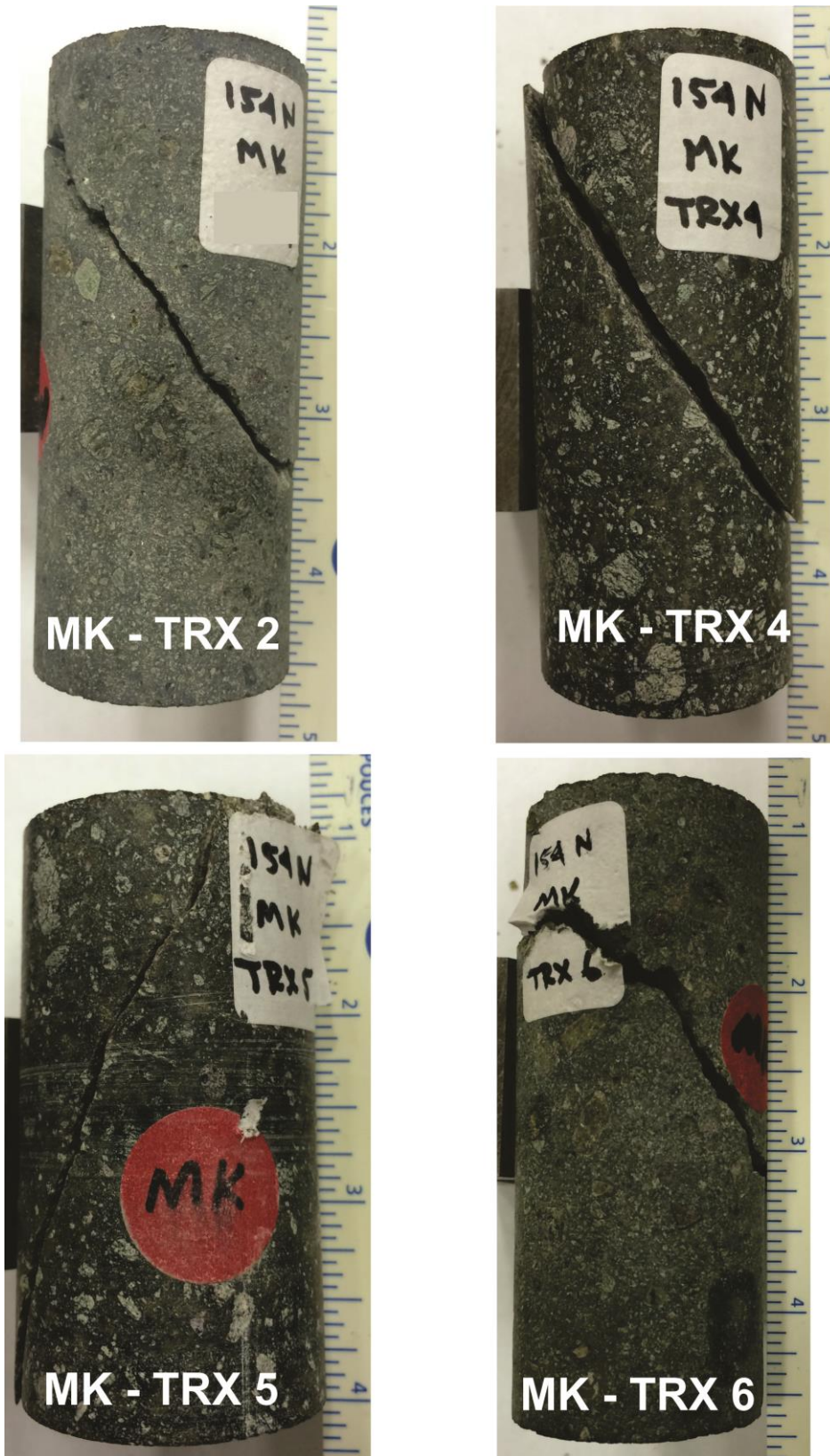
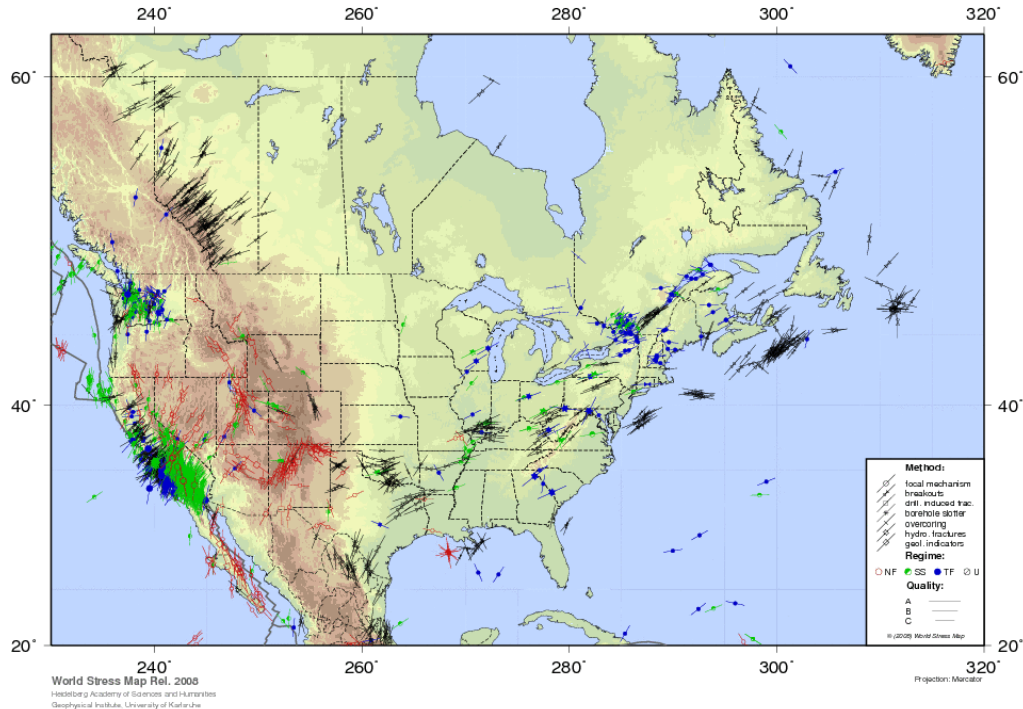


Figure A.63 Failure Mode of Each Core Specimen - MRK Kimberlite - Triaxial Test

## Appendix B: WORLD STRESS MAP

World Stress Map (WSM) is a global database of tectonic stress of the earth's crust from a wide range of stress indicators. This project originally began in 1986 as part of the International Lithosphere Program (ILP).

Figures B-1 and B-2, respectively, show the stress map for North America and the World Stress Map displaying the orientations of the maximum horizontal stress.



**Figure B-1** North America Stress Map (Heidbach et al. 2008)

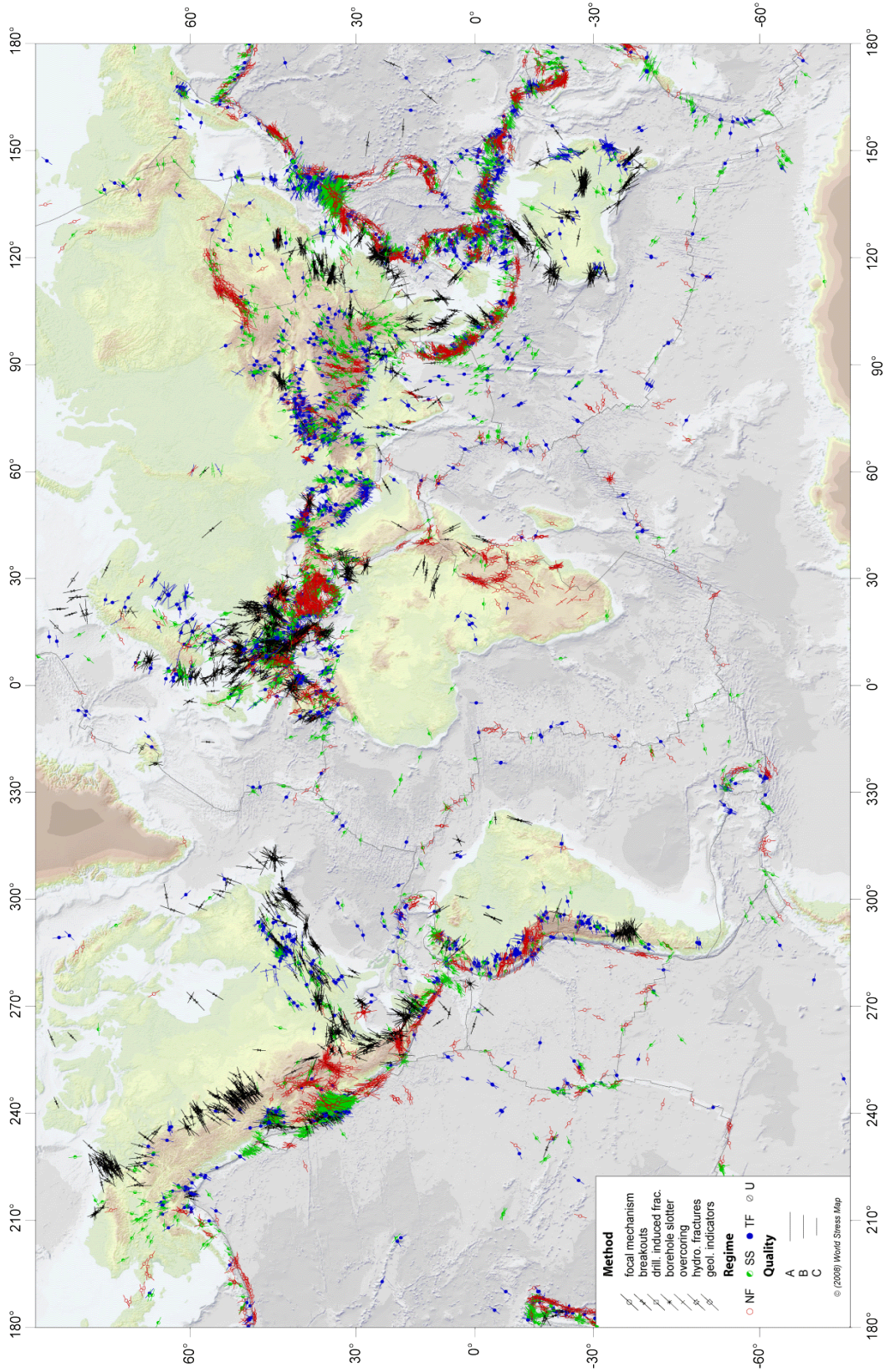


Figure B-2 World Stress Map (Heidbach et al. 2008)

# Appendix C: The Support Chart Based on the Tunnelling Quality Index Q

Table D-1 The Value of ESR proposed by Barton et al., (1974)

| Excavation Category  | ESR |
|--|-----|
| A Temporary mine opening   | 3-5 |
| B Permanent mine opening, water tunnels for hydropower (excluding high pressure penstocks), pilot tunnels, drifts and headings for large excavations | 1.6 |
| C Storage rooms, water treatment plants, minor road and railway tunnels, surge chambers, access tunnels  | 1.3 |
| D Power stations, major road and railway tunnels, civil defence chambers, portal intersections   | 1.0 |
| E Underground nuclear power stations, railway stations, sports and public facilities, factories  | 0.8 |

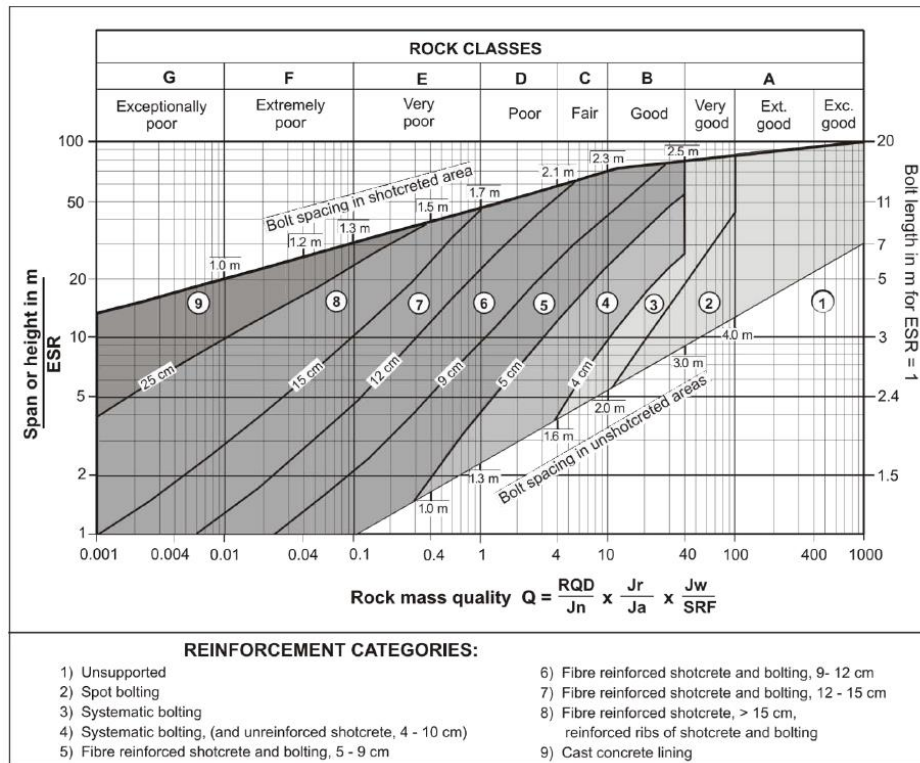


Figure D-1 Estimation of Support parameters based on tunnelling quality index Q (After Grimstad and Barton 1993, From Palmstrom and Broch, 2006)

## **Appendix D: ABAQUS CODE – SIMULATION STEPS**

*This Appendix contains the 123 simulation steps written in Abaqus code*

```

** STEP: Step-1
**
*Step, name=Step-1, nlgeom=YES, inc=200,
unsymm=YES
Geostatic - Initial State Stress
*Geostatic, utol
0.5, 1., 1e-05, 1.
**
** LOADS
**
** Name: Load-1  Type: Gravity
*Dload
, GRAV, 1., 0., 0., -1.
**
** OUTPUT REQUESTS
**
*Restart, write, frequency=0
**
** FIELD OUTPUT: F-Output-2
**
*Output, field
*Element Output, directions=YES
ELEDEN, ELEN, ENER, PEEQMAX, PEEQT
*Contact Output
EFENRRTR, ENRRT
**
** FIELD OUTPUT: F-Output-1
**
*Output, field, variable=PRESELECT
**
** HISTORY OUTPUT: H-Output-1
**
*Output, history, variable=PRESELECT
*End Step
** -----
-
**
** STEP: Step-2
**
*Step, name=Step-2, nlgeom=YES, inc=200,
unsymm=YES
Excavation of the MainDrifts & A154SCAP
*Static
0.1, 1., 1e-07, 1.
*CONTROLS, ANALYSIS=DISCONTINUOUS
*MODEL CHANGE, REMOVE
FEMDDM-1.MAINDRFS, FEMDDM-1.A154SCAP
**
** OUTPUT REQUESTS
**
*Restart, write, frequency=0
**
** FIELD OUTPUT: F-Output-2
**
*Output, field
*Element Output, directions=YES
ELEDEN, ELEN, ENER, PEEQMAX, PEEQT
*Contact Output
EFENRRTR, ENRRT
**
** FIELD OUTPUT: F-Output-1
**
*Output, field, variable=PRESELECT
**
** HISTORY OUTPUT: H-Output-1
**
*Output, history, variable=PRESELECT
*End Step
** -----
-
**
** STEP: Step-3
**
*Step, name=Step-3, nlgeom=YES, inc=200,
unsymm=YES
Excavation of the N9175P1C155UC and
N9175P1C125UC
*Static
0.1, 1., 1e-07, 1.
*CONTROLS, ANALYSIS=DISCONTINUOUS
*MODEL CHANGE, REMOVE
FEMDDM-1.N9175P1C155UC, FEMDDM-
1.N9175P1C125UC, FEMDDM-1.N9175P1C95UC,
FEMDDM-1.N9175P1C185UC, FEMDDM-
1.S9125ALL
**
** OUTPUT REQUESTS
**
*Restart, write, frequency=0
**
** FIELD OUTPUT: F-Output-2
**
*Output, field
*Element Output, directions=YES
ELEDEN, ELEN, ENER, PEEQMAX, PEEQT
*Contact Output
EFENRRTR, ENRRT
**
** FIELD OUTPUT: F-Output-1
**
*Output, field, variable=PRESELECT
**
** HISTORY OUTPUT: H-Output-1
**
*Output, history, variable=PRESELECT
*End Step
** -----
-
**
** STEP: Step-4
**
*Step, name=Step-4, nlgeom=YES, inc=200,
unsymm=YES
Excavation of the N9175P1C95 AND N9175P1C185
*Static
0.1, 1., 1e-07, 1.
*CONTROLS, ANALYSIS=DISCONTINUOUS
*MODEL CHANGE, REMOVE
FEMDDM-1.N9200P1C155UC, FEMDDM-
1.N9200P1C125UC, FEMDDM-1.N9200P1C95UC,
FEMDDM-1.N9200P1C185UC, FEMDDM-
1.S9125ACCESSDRFS
**
** OUTPUT REQUESTS
**
*Restart, write, frequency=0
**
** FIELD OUTPUT: F-Output-2
**
*Output, field
*Element Output, directions=YES
ELEDEN, ELEN, ENER, PEEQMAX, PEEQT
*Contact Output
EFENRRTR, ENRRT
**
** FIELD OUTPUT: F-Output-1
**
*Output, field, variable=PRESELECT
**
** HISTORY OUTPUT: H-Output-1

```

```

**
*Output, history, variable=PRESELECT
*End Step
** -----
-
**
** STEP: Step-5
**
*Step, name=Step-5, nlgeom=YES, inc=200,
unsymm=YES
Excavation of the N9175P1C155 AND
S9100C970DRF
*Static
0.1, 1., 1e-07, 1.
*CONTROLS,ANALYSIS=DISCONTINUOUS
*MODEL CHANGE, REMOVE
FEMDDM-1.STOPEN9175P1C155B1, FEMDDM-
1.S9100C970DRF
**
** OUTPUT REQUESTS
**
*Restart, write, frequency=0
**
** FIELD OUTPUT: F-Output-2
**
*Output, field
*Element Output, directions=YES
ELEDEN, ELEN, ENER, PEEQMAX, PEEQT
*Contact Output
EFENRRTR, ENRRT
**
** FIELD OUTPUT: F-Output-1
**
*Output, field, variable=PRESELECT
**
** HISTORY OUTPUT: H-Output-1
**
*Output, history, variable=PRESELECT
*End Step
** -----
-
**
** STEP: Step-6
**
*Step, name=Step-6, nlgeom=YES, inc=200,
unsymm=YES
Excavation of the STOPEN9175P1C125B1,
S9100C960DRF AND S9100XC970T960 -
BACKFILLING STOPEN9175P1C155
*Static
0.1, 1., 1e-07, 1.
*CONTROLS,ANALYSIS=DISCONTINUOUS
*MODEL CHANGE, ADD
FEMDDM-1.STOPEN9175P1C155B1, FEMDDM-
1.N9175P1C155UCB1
*FIELD
FEMDDM-1.STOPEN9175P1C155BACKFILL1, 1.0
*MODEL CHANGE, REMOVE
FEMDDM-1.STOPEN9175P1C125B1, FEMDDM-
1.S9100C960DRF, FEMDDM-1.S9100XC970T960
**
** OUTPUT REQUESTS
**
*Restart, write, frequency=0
**
** FIELD OUTPUT: F-Output-2
**
*Output, field
*Element Output, directions=YES
ELEDEN, ELEN, ENER, PEEQMAX, PEEQT
**
*Contact Output
EFENRRTR, ENRRT
**
** FIELD OUTPUT: F-Output-1
**
*Output, field, variable=PRESELECT
**
** HISTORY OUTPUT: H-Output-1
**
*Output, history, variable=PRESELECT
*End Step
** -----
-
**
** STEP: Step-7
**
*Step, name=Step-7, nlgeom=YES, inc=200,
unsymm=YES
Excavation of the STOPEN9175P1C95B1,
S9100C950DRF, S9100XC960T950 - BACKFILLING
STOPEN9175P1C125B1
*Static
0.1, 1., 1e-07, 1.
*CONTROLS,ANALYSIS=DISCONTINUOUS
*MODEL CHANGE, ADD
FEMDDM-1.STOPEN9175P1C125B1, FEMDDM-
1.N9175P1C125UCB1
*FIELD
FEMDDM-1.STOPEN9175P1C125BACKFILL1, 1.0
*MODEL CHANGE, REMOVE
FEMDDM-1.STOPEN9175P1C95B1, FEMDDM-
1.SLR9100C950DRF, FEMDDM-1.S9100XC960T950
**
** OUTPUT REQUESTS
**
*Restart, write, frequency=0
**
** FIELD OUTPUT: F-Output-2
**
*Output, field
*Element Output, directions=YES
ELEDEN, ELEN, ENER, PEEQMAX, PEEQT
*Contact Output
EFENRRTR, ENRRT
**
** FIELD OUTPUT: F-Output-1
**
*Output, field, variable=PRESELECT
**
** HISTORY OUTPUT: H-Output-1
**
*Output, history, variable=PRESELECT
*End Step
** -----
-
**
** STEP: Step-8
**
*Step, name=Step-8, nlgeom=YES, inc=200,
unsymm=YES
Excavation of the STOPEN9175P1C185B1,
S9100C940DRF, S9100XC950T940 - BACKFILLING
STOPEN9175P1C95B1
*Static
0.1, 1., 1e-07, 1.
*CONTROLS,ANALYSIS=DISCONTINUOUS
*MODEL CHANGE, ADD
FEMDDM-1.STOPEN9175P1C95B1, FEMDDM-
1.N9175P1C95UCB1
*FIELD

```

```

FEMDDM-1.STOPEN9175P1C95BACKFILL1, 1.0
*MODEL CHANGE, REMOVE
FEMDDM-1.STOPEN9175P1C185B1, FEMDDM-
1.S9100C940DRF, FEMDDM-1.S9100XC950T940
**
** OUTPUT REQUESTS
**
*Restart, write, frequency=0
**
** FIELD OUTPUT: F-Output-2
**
*Output, field
*Element Output, directions=YES
ELEDEN, ELEN, ENER, PEEQMAX, PEEQT
*Contact Output
EFENRRTR, ENRRT
**
** FIELD OUTPUT: F-Output-1
**
*Output, field, variable=PRESELECT
**
** HISTORY OUTPUT: H-Output-1
**
*Output, history, variable=PRESELECT
*End Step
** -----
-
**
** STEP: Step-9
**
*Step, name=Step-9, nlgeom=YES, inc=200,
unsymm=YES
Excavation of the STOPEN9175P1C155B2,
S9100C930DRF, S9100XC940T930 - BACKFILLING
STOPEN9175P1C185B1
*Static
0.1, 1., 1e-07, 1.
*CONTROLS, ANALYSIS=DISCONTINUOUS
*MODEL CHANGE, ADD
FEMDDM-1.STOPEN9175P1C185B1, FEMDDM-
1.N9175P1C185UCB1
*FIELD
FEMDDM-1.STOPEN9175P1C185BACKFILL1, 1.0
*MODEL CHANGE, REMOVE
FEMDDM-1.STOPEN9175P1C155B2, FEMDDM-
1.S9100C930DRF, FEMDDM-1.S9100XC940T930
**
** OUTPUT REQUESTS
**
*Restart, write, frequency=0
**
** FIELD OUTPUT: F-Output-2
**
*Output, field
*Element Output, directions=YES
ELEDEN, ELEN, ENER, PEEQMAX, PEEQT
*Contact Output
EFENRRTR, ENRRT
**
** FIELD OUTPUT: F-Output-1
**
*Output, field, variable=PRESELECT
**
** HISTORY OUTPUT: H-Output-1
**
*Output, history, variable=PRESELECT
*End Step
** -----
-
**
** STEP: Step-10
**
*Step, name=Step-10, nlgeom=YES, inc=200,
unsymm=YES
Excavation of the STOPEN9175P1C125B2,
S9100C920DRF, S9100XC930T920 - BACKFILLING
STOPEN9175P1C155B2
*Static
0.1, 1., 1e-07, 1.
*CONTROLS, ANALYSIS=DISCONTINUOUS
*MODEL CHANGE, ADD
FEMDDM-1.STOPEN9175P1C155B2, FEMDDM-
1.N9175P1C155UCB2
*FIELD
FEMDDM-1.STOPEN9175P1C155BACKFILL2, 1.0
*MODEL CHANGE, REMOVE
FEMDDM-1.STOPEN9175P1C125B2, FEMDDM-
1.S9100C920DRF, FEMDDM-1.S9100XC930T920
**
** OUTPUT REQUESTS
**
*Restart, write, frequency=0
**
** FIELD OUTPUT: F-Output-2
**
*Output, field
*Element Output, directions=YES
ELEDEN, ELEN, ENER, PEEQMAX, PEEQT
*Contact Output
EFENRRTR, ENRRT
**
** FIELD OUTPUT: F-Output-1
**
*Output, field, variable=PRESELECT
**
** HISTORY OUTPUT: H-Output-1
**
*Output, history, variable=PRESELECT
*End Step
** -----
-
**
** STEP: Step-11
**
*Step, name=Step-11, nlgeom=YES, inc=200,
unsymm=YES
Excavation of the STOPEN9175P1C95B2,
S9100C910DRF, S9100XC920T910 - BACKFILLING
STOPEN9175P1C125B2
*Static
0.1, 1., 1e-07, 1.
*CONTROLS, ANALYSIS=DISCONTINUOUS
*MODEL CHANGE, ADD
FEMDDM-1.STOPEN9175P1C125B2, FEMDDM-
1.N9175P1C125UCB2
*FIELD
FEMDDM-1.STOPEN9175P1C125BACKFILL2, 1.0
*MODEL CHANGE, REMOVE
FEMDDM-1.STOPEN9175P1C95B2, FEMDDM-
1.S9100C910DRF, FEMDDM-1.S9100XC920T910
**
** OUTPUT REQUESTS
**
*Restart, write, frequency=0
**
** FIELD OUTPUT: F-Output-2
**
*Output, field
*Element Output, directions=YES
ELEDEN, ELEN, ENER, PEEQMAX, PEEQT

```

```

*Contact Output
EFENRRTR, ENRRT
**
** FIELD OUTPUT: F-Output-1
**
*Output, field, variable=PRESELECT
**
** HISTORY OUTPUT: H-Output-1
**
*Output, history, variable=PRESELECT
*End Step
** -----
-
**
** STEP: Step-12
**
*Step, name=Step-12, nlgeom=YES, inc=200,
unsymm=YES
Excavation of the STOPEN9175P1C185B2,
S9100C900DRF, S9100XC910T900 - BACKFILLING
STOPEN9175P1C95B2
*Static
0.1, 1., 1e-07, 1.
*CONTROLS,ANALYSIS=DISCONTINUOUS
*MODEL CHANGE, ADD
FEMDDM-1.STOPEN9175P1C95B2, FEMDDM-
1.N9175P1C95UCB2
*FIELD
FEMDDM-1.STOPEN9175P1C95BACKFILL2, 1.0
*MODEL CHANGE, REMOVE
FEMDDM-1.STOPEN9175P1C185B2, FEMDDM-
1.S9100C900DRF, FEMDDM-1.S9100XC910T900
**
** OUTPUT REQUESTS
**
*Restart, write, frequency=0
**
** FIELD OUTPUT: F-Output-2
**
*Output, field
*Element Output, directions=YES
ELEDEN, ELEN, ENER, PEEQMAX, PEEQT
*Contact Output
EFENRRTR, ENRRT
**
** FIELD OUTPUT: F-Output-1
**
*Output, field, variable=PRESELECT
**
** HISTORY OUTPUT: H-Output-1
**
*Output, history, variable=PRESELECT
*End Step
** -----
-
**
** STEP: Step-13
**
*Step, name=Step-13, nlgeom=YES, inc=200,
unsymm=YES
Excavation of the STOPEN9175P1C155B3,
S9100C890DRF, S9100XC900T890 - BACKFILLING
STOPEN9175P1C185B3
*Static
0.1, 1., 1e-07, 1.
*CONTROLS,ANALYSIS=DISCONTINUOUS
*MODEL CHANGE, ADD
FEMDDM-1.STOPEN9175P1C185B2, FEMDDM-
1.N9175P1C185UCB2
*FIELD
FEMDDM-1.STOPEN9175P1C185BACKFILL2, 1.0
*MODEL CHANGE, REMOVE
FEMDDM-1.STOPEN9175P1C155B3, FEMDDM-
1.S9100C890DRF, FEMDDM-1.S9100XC900T890
**
** OUTPUT REQUESTS
**
*Restart, write, frequency=0
**
** FIELD OUTPUT: F-Output-1
**
*Output, field, variable=PRESELECT
**
** HISTORY OUTPUT: H-Output-1
**
*Output, history, variable=PRESELECT
*End Step
** -----
-
**
** STEP: Step-14
**
*Step, name=Step-14, nlgeom=YES, inc=200,
unsymm=YES
Excavation of the STOPEN9175P1C125B3,
S9075C970DRF, S9075XC970T960,
N9225P1C185UC - BACKFILLING
STOPEN9175P1C155B3
*Static
0.1, 1., 1e-07, 1.
*CONTROLS,ANALYSIS=DISCONTINUOUS
*MODEL CHANGE, ADD
FEMDDM-1.STOPEN9175P1C155B3, FEMDDM-
1.N9175P1C155UCB3
*FIELD
FEMDDM-1.STOPEN9175P1C155BACKFILL3, 1.0
*MODEL CHANGE, REMOVE
FEMDDM-1.STOPEN9175P1C125B3, FEMDDM-
1.S9075C970DRF, FEMDDM-1.N9225P1C185UC
**
** OUTPUT REQUESTS
**
*Restart, write, frequency=0
**
** FIELD OUTPUT: F-Output-2
**
*Output, field
*Element Output, directions=YES
ELEDEN, ELEN, ENER, PEEQMAX, PEEQT
*Contact Output
EFENRRTR, ENRRT
**
** FIELD OUTPUT: F-Output-1
**
*Output, field, variable=PRESELECT
**
** HISTORY OUTPUT: H-Output-1
**
*Output, history, variable=PRESELECT
*End Step
** -----
-

```

```

**
** STEP: Step-15
**
*Step, name=Step-15, nlgeom=YES, inc=200,
unsymm=YES
Excavation of the STOPEN9175P1C95B3,
S9075C960DRF, S9075XC960T950,
N9225P1C155UC - BACKFILLING
STOPEN9175P1C125B3
*Static
0.1, 1., 1e-07, 1.
*CONTROLS, ANALYSIS=DISCONTINUOUS
*MODEL CHANGE, ADD
FEMDDM-1.STOPEN9175P1C125B3, FEMDDM-
1.N9175P1C125UCB3
*FIELD
FEMDDM-1.STOPEN9175P1C125BACKFILL3, 1.0
*MODEL CHANGE, REMOVE
FEMDDM-1.STOPEN9175P1C95B3, FEMDDM-
1.S9075C960DRF, FEMDDM-1.S9075XC960T950,
FEMDDM-1.N9225P1C155UC
**
** OUTPUT REQUESTS
**
*Restart, write, frequency=0
**
** FIELD OUTPUT: F-Output-2
**
*Output, field
*Element Output, directions=YES
ELEDEN, ELEN, ENER, PEEQMAX, PEEQT
*Contact Output
EFENRRTR, ENRRT
**
** FIELD OUTPUT: F-Output-1
**
*Output, field, variable=PRESELECT
**
** HISTORY OUTPUT: H-Output-1
**
*Output, history, variable=PRESELECT
*End Step
** -----
-
**
** STEP: Step-16
**
*Step, name=Step-16, nlgeom=YES, inc=200,
unsymm=YES
Excavation of the STOPEN9175P1C185B3,
S9075C950DRF, S9075XC950T940,
N9225P1C125UC - BACKFILLING
STOPEN9175P1C95B3
*Static
0.1, 1., 1e-07, 1.
*CONTROLS, ANALYSIS=DISCONTINUOUS
*MODEL CHANGE, ADD
FEMDDM-1.STOPEN9175P1C95B3, FEMDDM-
1.N9175P1C95UCB3
*FIELD
FEMDDM-1.STOPEN9175P1C95BACKFILL3, 1.0
*MODEL CHANGE, REMOVE
FEMDDM-1.STOPEN9175P1C185B3, FEMDDM-
1.S9075C950DRF, FEMDDM-1.S9075XC950T940,
FEMDDM-1.N9225P1C125UC
**
** OUTPUT REQUESTS
**
*Restart, write, frequency=0
**
** FIELD OUTPUT: F-Output-2
**
*Output, field
*Element Output, directions=YES
ELEDEN, ELEN, ENER, PEEQMAX, PEEQT
*Contact Output
EFENRRTR, ENRRT
**
** FIELD OUTPUT: F-Output-1
**
*Output, field, variable=PRESELECT
**
** HISTORY OUTPUT: H-Output-1
**
*Output, history, variable=PRESELECT
*End Step
** -----
-
**
** STEP: Step-17
**
*Step, name=Step-17, nlgeom=YES, inc=200,
unsymm=YES
Excavation of the STOPEN9175P1C155B4,
S9075C940DRF, S9075XC940T930,
N9175P1C215UC - BACKFILLING
STOPEN9175P1C185B3
*Static
0.1, 1., 1e-07, 1.
*CONTROLS, ANALYSIS=DISCONTINUOUS
*MODEL CHANGE, ADD
FEMDDM-1.STOPEN9175P1C185B3, FEMDDM-
1.N9175P1C185UCB3
*FIELD
FEMDDM-1.STOPEN9175P1C185BACKFILL3, 1.0
*MODEL CHANGE, REMOVE
FEMDDM-1.STOPEN9175P1C155B4, FEMDDM-
1.S9075C940DRF, FEMDDM-1.S9075XC940T930,
FEMDDM-1.N9175P1C215UC
**
** OUTPUT REQUESTS
**
*Restart, write, frequency=0
**
** FIELD OUTPUT: F-Output-2
**
*Output, field
*Element Output, directions=YES
ELEDEN, ELEN, ENER, PEEQMAX, PEEQT
*Contact Output
EFENRRTR, ENRRT
**
** FIELD OUTPUT: F-Output-1
**
*Output, field, variable=PRESELECT
**
** HISTORY OUTPUT: H-Output-1
**
*Output, history, variable=PRESELECT
*End Step
** -----
-
**
** STEP: Step-18
**
*Step, name=Step-18, nlgeom=YES, inc=200,
unsymm=YES
Excavation of the STOPEN9175P1C125B4,
S9075C930DRF, S9075XC930T920,

```

```

N9200P1C215UC - BACKFILLING
STOPEN9175P1C155B4
*Static
0.1, 1., 1e-07, 1.
*CONTROLS,ANALYSIS=DISCONTINUOUS
*MODEL CHANGE, ADD
FEMDDM-1.STOPEN9175P1C155B4, FEMDDM-
1.N9175P1C155UCB4
*FIELD
FEMDDM-1.STOPEN9175P1C155BACKFILL4, 1.0
*MODEL CHANGE, REMOVE
FEMDDM-1.STOPEN9175P1C125B4, FEMDDM-
1.S9075C930DRF, FEMDDM-1.S9075XC930T920,
FEMDDM-1.N9200P1C215UC
**
** OUTPUT REQUESTS
**
*Restart, write, frequency=0
**
** FIELD OUTPUT: F-Output-2
**
*Output, field
*Element Output, directions=YES
ELEDEN, ELEN, ENER, PEEQMAX, PEEQT
*Contact Output
EFENRRTR, ENRRT
**
** FIELD OUTPUT: F-Output-1
**
*Output, field, variable=PRESELECT
**
** HISTORY OUTPUT: H-Output-1
**
*Output, history, variable=PRESELECT
*End Step
** -----
-
**
** STEP: Step-19
**
*Step, name=Step-19, nlgeom=YES, inc=200,
unsymm=YES
Excavation of the STOPEN9200P1C155B1,
S9075C920DRF, S9075XC920T910,
N9175P2C110UC - BACKFILLING
STOPEN9175P1C125B4
*Static
0.1, 1., 1e-07, 1.
*CONTROLS,ANALYSIS=DISCONTINUOUS
*MODEL CHANGE, ADD
FEMDDM-1.STOPEN9175P1C125B4, FEMDDM-
1.N9175P1C125UCB4
*FIELD
FEMDDM-1.STOPEN9175P1C125BACKFILL4, 1.0
*MODEL CHANGE, REMOVE
FEMDDM-1.STOPEN9200P1C155B1, FEMDDM-
1.S9075C920DRF, FEMDDM-1.N9175P2C110UC
**
** OUTPUT REQUESTS
**
*Restart, write, frequency=0
**
** FIELD OUTPUT: F-Output-2
**
*Output, field
*Element Output, directions=YES
ELEDEN, ELEN, ENER, PEEQMAX, PEEQT
*Contact Output
EFENRRTR, ENRRT
**
** FIELD OUTPUT: F-Output-1
**
*Output, field, variable=PRESELECT
**
** HISTORY OUTPUT: H-Output-1
**
*Output, history, variable=PRESELECT
*End Step
** -----
-
**
** STEP: Step-20
**
*Step, name=Step-20, nlgeom=YES, inc=200,
unsymm=YES
Excavation of the STOPEN9200P1C125B1,
S9075C910DRF, S9075XC910T900,
N9175P2C170UC - BACKFILLING
STOPEN9200P1C155B1
*Static
0.1, 1., 1e-07, 1.
*CONTROLS,ANALYSIS=DISCONTINUOUS
*MODEL CHANGE, ADD
FEMDDM-1.STOPEN9200P1C155B1, FEMDDM-
1.N9200P1C155UCB1
*FIELD
FEMDDM-1.STOPEN9200P1C155BACKFILL1, 1.0
*MODEL CHANGE, REMOVE
FEMDDM-1.STOPEN9200P1C125B1, FEMDDM-
1.S9075C910DRF, FEMDDM-1.S9075XC910T900,
FEMDDM-1.N9175P2C170UC
**
** OUTPUT REQUESTS
**
*Restart, write, frequency=0
**
** FIELD OUTPUT: F-Output-2
**
*Output, field
*Element Output, directions=YES
ELEDEN, ELEN, ENER, PEEQMAX, PEEQT
*Contact Output
EFENRRTR, ENRRT
**
** FIELD OUTPUT: F-Output-1
**
*Output, field, variable=PRESELECT
**
** HISTORY OUTPUT: H-Output-1
**
*Output, history, variable=PRESELECT
*End Step
** -----
-
**
** STEP: Step-21
**
*Step, name=Step-21, nlgeom=YES, inc=200,
unsymm=YES
Excavation of the STOPEN9175P1C215B1,
S9075C900DRF, S9075XC900T890,
N9175P2C140UC - BACKFILLING
STOPEN9200P1C125B1
*Static
0.1, 1., 1e-07, 1.
*CONTROLS,ANALYSIS=DISCONTINUOUS
*MODEL CHANGE, ADD
FEMDDM-1.STOPEN9200P1C125B1, FEMDDM-
1.N9200P1C125UCB1
*FIELD

```

```

FEMDDM-1.STOPEN9200P1C125BACKFILL1, 1.0
*MODEL CHANGE, REMOVE
FEMDDM-1.STOPEN9175P1C215B1, FEMDDM-
1.S9075C900DRF, FEMDDM-1.S9075XC900T890,
FEMDDM-1.N9175P2C140UC, FEMDDM-
1.N9225P1C95UC
**
** OUTPUT REQUESTS
**
*Restart, write, frequency=0
**
** FIELD OUTPUT: F-Output-2
**
*Output, field
*Element Output, directions=YES
ELEDEN, ELEN, ENER, PEEQMAX, PEEQT
*Contact Output
EFENRRTR, ENRRT
**
** FIELD OUTPUT: F-Output-1
**
*Output, field, variable=PRESELECT
**
** HISTORY OUTPUT: H-Output-1
**
*Output, history, variable=PRESELECT
*End Step
** -----
-
**
** STEP: Step-22
**
*Step, name=Step-22, nlgeom=YES, inc=200,
unsymm=YES
Excavation of the STOPEN9200P1C95B1,
S9075C890DRF, N9200P2C110UC - BACKFILLING
STOPEN9175P1C215B1
*Static
0.1, 1., 1e-07, 1.
*CONTROLS, ANALYSIS=DISCONTINUOUS
*MODEL CHANGE, ADD
FEMDDM-1.STOPEN9175P1C215B1, FEMDDM-
1.N9175P1C215UCB1
*FIELD
FEMDDM-1.STOPEN9175P1C215BACKFILL1, 1.0
*MODEL CHANGE, REMOVE
FEMDDM-1.STOPEN9200P1C95B1, FEMDDM-
1.S9075C890DRF, FEMDDM-1.N9200P2C110UC
**
** OUTPUT REQUESTS
**
*Restart, write, frequency=0
**
** FIELD OUTPUT: F-Output-2
**
*Output, field
*Element Output, directions=YES
ELEDEN, ELEN, ENER, PEEQMAX, PEEQT
*Contact Output
EFENRRTR, ENRRT
**
** FIELD OUTPUT: F-Output-1
**
*Output, field, variable=PRESELECT
**
** HISTORY OUTPUT: H-Output-1
**
*Output, history, variable=PRESELECT
*End Step
** -----
-
**
** STEP: Step-24
**
*Step, name=Step-24, nlgeom=YES, inc=200,
unsymm=YES
Excavation of the STOPEN9175P1C215B2,
SLRS9100C970B1, SLRS9100C970B2,
SLRS9100C960B1, SLRS9100C960B2,
SLRS9100C970B2, , SLRS9100C950B1,
N9200P2C170UC - BACKFILLING
STOPEN9200P1C185B1
*Static
0.1, 1., 1e-07, 1.
*CONTROLS, ANALYSIS=DISCONTINUOUS
*MODEL CHANGE, ADD
FEMDDM-1.STOPEN9200P1C185B1, FEMDDM-
1.N9200P1C185UCB1
*FIELD
FEMDDM-1.STOPEN9200P1C185BACKFILL1, 1.0
*MODEL CHANGE, REMOVE
FEMDDM-1.STOPEN9175P1C215B2, FEMDDM-
1.SLRS9100C970B1, FEMDDM-1.SLRS9100C970B2,
FEMDDM-1.SLRS9100C960B1, FEMDDM-

```

```

1.SLRS9100C960B2, FEMDDM-1.SLRS9100C950B1,
FEMDDM-1.N9200P2C170UC
**
** OUTPUT REQUESTS
**
*Restart, write, frequency=0
**
** FIELD OUTPUT: F-Output-2
**
*Output, field
*Element Output, directions=YES
ELEDEN, ELEN, ENER, PEEQMAX, PEEQT
*Contact Output
EFENRRTR, ENRRT
**
** FIELD OUTPUT: F-Output-1
**
*Output, field, variable=PRESELECT
**
** HISTORY OUTPUT: H-Output-1
**
*Output, history, variable=PRESELECT
*End Step
** -----
-
**
** STEP: Step-25
**
*Step, name=Step-25, ngeom=YES, inc=200,
unsymm=YES
Excavation of the STOPEN9175P2C110B1,
STOPEN9200P1C155B2, SLRS9100C970B3,
SLRS9100C960B3, SLRS9100C950B2,
SLRS9100C950B3, SLRS9100C940B1,
SLRS9100C940B2, SLRS9100C940B3,
SLRS9100C930B1 - BACKFILLING
STOPEN9175P1C215B2
*Static
0.1, 1., 1e-07, 1.
*CONTROLS,ANALYSIS=DISCONTINUOUS
*MODEL CHANGE, ADD
FEMDDM-1.STOPEN9175P1C215B2, FEMDDM-
1.N9175P1C215UCB2
*FIELD
FEMDDM-1.STOPEN9175P1C215BACKFILL2, 1.0
*MODEL CHANGE, REMOVE
FEMDDM-1.STOPEN9175P2C110B1, FEMDDM-
1.STOPEN9200P1C155B2, FEMDDM-
1.SLRS9100C970B3, FEMDDM-1.SLRS9100C960B3,
FEMDDM-1.SLRS9100C950B2, FEMDDM-
1.SLRS9100C950B3, FEMDDM-1.SLRS9100C940B1
*MODEL CHANGE, REMOVE
FEMDDM-1.SLRS9100C940B2, FEMDDM-
1.SLRS9100C940B3, FEMDDM-1.SLRS9100C930B1
**
** OUTPUT REQUESTS
**
*Restart, write, frequency=0
**
** FIELD OUTPUT: F-Output-2
**
*Output, field
*Element Output, directions=YES
ELEDEN, ELEN, ENER, PEEQMAX, PEEQT
*Contact Output
EFENRRTR, ENRRT
**
** FIELD OUTPUT: F-Output-1
**
*Output, field, variable=PRESELECT
**
** HISTORY OUTPUT: H-Output-1
**
*Output, history, variable=PRESELECT
*End Step
** -----
-
**
** STEP: Step-26
**
*Step, name=Step-26, ngeom=YES, inc=200,
unsymm=YES
Excavation of the STOPEN9175P2C170B1,
STOPEN9200P1C125B2, SLRS9100C970B4,
SLRS9100C970B5, SLRS9100C960B4,
SLRS9100C930B2, SLRS9100C920B1 -
BACKFILLING STOPEN9175P2C110B1,
STOPEN9200P1C155B2
*Static
0.1, 1., 1e-07, 1.
*CONTROLS,ANALYSIS=DISCONTINUOUS
*MODEL CHANGE, ADD
FEMDDM-1.STOPEN9175P2C110B1, FEMDDM-
1.N9175P2C110UCB1, FEMDDM-
1.STOPEN9200P1C155B2, FEMDDM-
1.N9200P1C155UCB2
*FIELD
FEMDDM-1.STOPEN9175P2C110BACKFILL1, 1.0
FEMDDM-1.STOPEN9200P1C155BACKFILL2, 1.0
*MODEL CHANGE, REMOVE
FEMDDM-1.STOPEN9175P2C170B1, FEMDDM-
1.STOPEN9200P1C125B2, FEMDDM-
1.SLRS9100C970B4, FEMDDM-1.SLRS9100C970B5,
FEMDDM-1.SLRS9100C960B4, FEMDDM-
1.SLRS9100C930B2, FEMDDM-1.SLRS9100C920B1
**
** OUTPUT REQUESTS
**
*Restart, write, frequency=0
**
** FIELD OUTPUT: F-Output-2
**
*Output, field
*Element Output, directions=YES
ELEDEN, ELEN, ENER, PEEQMAX, PEEQT
*Contact Output
EFENRRTR, ENRRT
**
** FIELD OUTPUT: F-Output-1
**
*Output, field, variable=PRESELECT
**
** HISTORY OUTPUT: H-Output-1
**
*Output, history, variable=PRESELECT
*End Step
** -----
-
**
** STEP: Step-27
**
*Step, name=Step-27, ngeom=YES, inc=200,
unsymm=YES
Excavation of the STOPEN9200P1C185B1,
STOPEN9175P2C140B1, S9050C960DRF,
S9050XC960T950, SLRS9100C970B6,
SLRS9100C950B5, SLRS9100C940B5,
SLRS9100C950B4, SLRS9100C940B4,
SLRS9100C930B3, SLRS9100C920B2,B3,B4,

```

```

SLRS9100C910B1, - BACKFILLING
STOPEN9175P2C170B1, STOPEN9200P1C125B2
*Static
0.1, 1., 1e-07, 1.
*CONTROLS,ANALYSIS=DISCONTINUOUS
*MODEL CHANGE, ADD
FEMDDM-1.STOPEN9175P2C170B1, FEMDDM-
1.N9175P2C170UCB1, FEMDDM-
1.STOPEN9200P1C125B2, FEMDDM-
1.N9200P1C125UCB2
*FIELD
FEMDDM-1.STOPEN9175P2C170BACKFILL1, 1.0
FEMDDM-1.STOPEN9200P1C125BACKFILL2, 1.0
*MODEL CHANGE, REMOVE
FEMDDM-1.STOPEN9175P2C140B1, FEMDDM-
1.STOPEN9200P1C185B2, FEMDDM-
1.S9050C960DRF, FEMDDM-1.S9050XC960T950,
FEMDDM-1.SLRS9100C960B5, FEMDDM-
1.SLRS9100C970B6, FEMDDM-1.SLRS9100C950B4
*MODEL CHANGE, REMOVE
FEMDDM-1.SLRS9100C950B5, FEMDDM-
1.SLRS9100C940B4, FEMDDM-1.SLRS9100C940B5,
FEMDDM-1.SLRS9100C930B3, FEMDDM-
1.SLRS9100C920B2, FEMDDM-1.SLRS9100C920B3,
FEMDDM-1.SLRS9100C910B1
**
** OUTPUT REQUESTS
**
*Restart, write, frequency=0
**
** FIELD OUTPUT: F-Output-2
**
*Output, field
*Element Output, directions=YES
ELEDEN, ELEN, ENER, PEEQMAX, PEEQT
*Contact Output
EFENRRTR, ENRRT
**
** FIELD OUTPUT: F-Output-1
**
*Output, field, variable=PRESELECT
**
** HISTORY OUTPUT: H-Output-1
**
*Output, history, variable=PRESELECT
*End Step
** -----
-
**
** STEP: Step-29
**
*Step, name=Step-29, ngeom=YES, inc=200,
unsymm=YES
Excavation of the STOPEN9175P2C110B2,
STOPEN9200P1C155B3, S9050C940DRF,
S9050XC940T930, SLRS9100C950B6,
SLRS9100C910B4, SLRS9100C900B3,
SLRS9075C970B1,B2, SLRS9075C960B1,
N9200P2C80UC - BACKFILLING
STOPEN9175P2C170B2, STOPEN9200P1C95B2
*Static
0.1, 1., 1e-07, 1.
*CONTROLS,ANALYSIS=DISCONTINUOUS
*MODEL CHANGE, ADD
FEMDDM-1.STOPEN9175P2C170B2, FEMDDM-
1.N9175P2C170UCB2, FEMDDM-
1.STOPEN9200P1C95B2, FEMDDM-
1.N9200P1C95UCB2
*FIELD
FEMDDM-1.STOPEN9175P2C170BACKFILL2, 1.0
FEMDDM-1.STOPEN9200P1C95BACKFILL2, 1.0
*MODEL CHANGE, REMOVE
FEMDDM-1.STOPEN9175P2C110B2, FEMDDM-
1.STOPEN9200P1C155B3, FEMDDM-
1.S9050C940DRF, FEMDDM-1.SLRS9100C950B6,
FEMDDM-1.SLRS9100C910B4, FEMDDM-
1.SLRS9100C900B3
*MODEL CHANGE, REMOVE
FEMDDM-1.SLRS9075C970B1, FEMDDM-
1.SLRS9075C960B1, FEMDDM-1.SLRS9075C970B2,
FEMDDM-1.N9200P2C80UC
**
** OUTPUT REQUESTS

```

```

**
*Restart, write, frequency=0
**
** FIELD OUTPUT: F-Output-2
**
*Output, field
*Element Output, directions=YES
ELEDEN, ELEN, ENER, PEEQMAX, PEEQT
*Contact Output
EFENRRTR, ENRRT
**
** FIELD OUTPUT: F-Output-1
**
*Output, field, variable=PRESELECT
**
** HISTORY OUTPUT: H-Output-1
**
*Output, history, variable=PRESELECT
*End Step
** -----
-
**
** STEP: Step-30
**
*Step, name=Step-30, nlgeom=YES, inc=200,
unsymm=YES
Excavation of the
*Static
0.1, 1., 1e-07, 1.
*CONTROLS, ANALYSIS=DISCONTINUOUS
*MODEL CHANGE, ADD
FEMDDM-1.STOPEN9175P2C140B2, FEMDDM-
1.N9175P2C140UCB2, FEMDDM-
1.STOPEN9200P1C185B3, FEMDDM-
1.N9200P1C185UCB3
*FIELD
FEMDDM-1.STOPEN9175P2C140BACKFILL2, 1.0
FEMDDM-1.STOPEN9200P1C155BACKFILL3, 1.0
*MODEL CHANGE, REMOVE
FEMDDM-1.STOPEN9175P2C140B2, FEMDDM-
1.STOPEN9200P1C185B3, FEMDDM-
1.S9050C930DRF, FEMDDM-1.SLRS9100C940B6,
FEMDDM-1.SLRS9100C920B5, FEMDDM-
1.SLRS9100C900B4
*MODEL CHANGE, REMOVE
FEMDDM-1.SLRS9100C890B1, FEMDDM-
1.SLRS9100C890B3, FEMDDM-
1.SLRS9075C970B3, FEMDDM-
1.SLRS9075C960B2, FEMDDM-1.SLRS9075C960B3,
FEMDDM-1.N9225P1C215UC
*MODEL CHANGE, REMOVE
FEMDDM-1.SLRS9075C950B1, FEMDDM-
1.SLRS9075C950B2, FEMDDM-1.N9175P2C200UC,
FEMDDM-1.N9250P1C155UC
**
** OUTPUT REQUESTS
**
*Restart, write, frequency=0
**
** FIELD OUTPUT: F-Output-2
**
*Output, field
*Element Output, directions=YES
ELEDEN, ELEN, ENER, PEEQMAX, PEEQT
*Contact Output
EFENRRTR, ENRRT
**
** FIELD OUTPUT: F-Output-1
**
*Output, field, variable=PRESELECT
**
** HISTORY OUTPUT: H-Output-1
**
*Output, history, variable=PRESELECT
*End Step
** -----
-
**
** STEP: Step-31
**
*Step, name=Step-31, nlgeom=YES, inc=200,
unsymm=YES
Excavation of the
*Static
0.1, 1., 1e-07, 1.
*CONTROLS, ANALYSIS=DISCONTINUOUS
*MODEL CHANGE, ADD
FEMDDM-1.STOPEN9175P2C140B2, FEMDDM-
1.N9175P2C140UCB2, FEMDDM-
1.STOPEN9200P1C185B3, FEMDDM-
1.N9200P1C185UCB3
*FIELD
FEMDDM-1.STOPEN9175P2C140BACKFILL2, 1.0
FEMDDM-1.STOPEN9200P1C185BACKFILL3, 1.0
*MODEL CHANGE, REMOVE
FEMDDM-1.STOPEN9175P2C140B3, FEMDDM-
1.STOPEN9200P1C215B1, FEMDDM-
1.S9050C920DRF, FEMDDM-1.S9050XC920T910,
FEMDDM-1.SLRS9100C930B6
*MODEL CHANGE, REMOVE
FEMDDM-1.SLRS9100C910B5, FEMDDM-
1.SLRS9100C900B5, FEMDDM-1.SLRS9100C930B5
*MODEL CHANGE, REMOVE
FEMDDM-1.SLRS9100C890B3, FEMDDM-
1.SLRS9075C970B4, FEMDDM-1.SLRS9075C960B4,
FEMDDM-1.SLRS9075C950B3, FEMDDM-
1.SLRS9075C940B1, FEMDDM-1.N9250P1C185UC
**
** OUTPUT REQUESTS
**
*Restart, write, frequency=0
**
** FIELD OUTPUT: F-Output-2
**
*Output, field
*Element Output, directions=YES
ELEDEN, ELEN, ENER, PEEQMAX, PEEQT
*Contact Output
EFENRRTR, ENRRT
**
** FIELD OUTPUT: F-Output-1
**
*Output, field, variable=PRESELECT
**
** HISTORY OUTPUT: H-Output-1
**
*Output, history, variable=PRESELECT
*End Step
** -----
-
**

```

```

** STEP: Step-32
**
*Step, name=Step-32, ngeom=YES, inc=200,
unsymm=YES
Excavation of the
*Static
0.1, 1., 1e-07, 1.
*CONTROLS, ANALYSIS=DISCONTINUOUS
*MODEL CHANGE, ADD
FEMDDM-1.STOPEN9175P2C140B3, FEMDDM-
1.N9175P2C140UCB3, FEMDDM-
1.STOPEN9200P1C215B1, FEMDDM-
1.N9200P1C215UCB1
*FIELD
FEMDDM-1.STOPEN9175P2C140BACKFILL3, 1.0
FEMDDM-1.STOPEN9200P1C215BACKFILL1, 1.0
*MODEL CHANGE, REMOVE
FEMDDM-1.STOPEN9175P2C170B3, FEMDDM-
1.STOPEN9200P1C125B3, FEMDDM-
1.S9050C910DRF, FEMDDM-1.S9050XC910T900,
FEMDDM-1.SLRS9100C920B6, FEMDDM-
1.SLRS9100C890B4, FEMDDM-1.SLRS9075C950B4
*MODEL CHANGE, REMOVE
FEMDDM-1.SLRS9075C940B2, FEMDDM-
1.SLRS9075C930B1, FEMDDM-1.N9250P1C215UC
**
** OUTPUT REQUESTS
**
*Restart, write, frequency=0
**
** FIELD OUTPUT: F-Output-2
**
*Output, field
*Element Output, directions=YES
ELEDEN, ELEN, ENER, PEEQMAX, PEEQT
*Contact Output
EFENRRTR, ENRRT
**
** FIELD OUTPUT: F-Output-1
**
*Output, field, variable=PRESELECT
**
** HISTORY OUTPUT: H-Output-1
**
*Output, history, variable=PRESELECT
**
*End Step
** -----
-
**
** STEP: Step-33
**
*Step, name=Step-33, ngeom=YES, inc=200,
unsymm=YES
Excavation of the
*Static
0.1, 1., 1e-07, 1.
*CONTROLS, ANALYSIS=DISCONTINUOUS
*MODEL CHANGE, ADD
FEMDDM-1.STOPEN9175P2C170B3, FEMDDM-
1.N9175P2C170UCB3, FEMDDM-
1.STOPEN9200P1C125B3, FEMDDM-
1.N9200P1C125UCB3
*FIELD
FEMDDM-1.STOPEN9175P2C170BACKFILL3, 1.0
FEMDDM-1.STOPEN9200P1C125BACKFILL3, 1.0
*MODEL CHANGE, REMOVE
FEMDDM-1.STOPEN9175P2C110B3, FEMDDM-
1.STOPEN9200P1C215B2, FEMDDM-
1.S9050C900DRF, FEMDDM-1.S9050XC900T890,
FEMDDM-1.SLRS9100C890B5, FEMDDM-
1.SLRS9100C910B6, FEMDDM-1.SLRS9075C940B3
*MODEL CHANGE, REMOVE
FEMDDM-1.SLRS9075C930B2, FEMDDM-
1.SLRS9075C920B1, FEMDDM-1.N9225P2C170UC,
FEMDDM-1.N9250P1C95OC, FEMDDM-
1.N9225P2C140UC
**
** OUTPUT REQUESTS
**
*Restart, write, frequency=0
**
** FIELD OUTPUT: F-Output-2
**
*Output, field
*Element Output, directions=YES
ELEDEN, ELEN, ENER, PEEQMAX, PEEQT
*Contact Output
EFENRRTR, ENRRT
**
** FIELD OUTPUT: F-Output-1
**
*Output, field, variable=PRESELECT
**
** HISTORY OUTPUT: H-Output-1
**
*Output, history, variable=PRESELECT
**
*End Step
** -----
-
**
** STEP: Step-34
**
*Step, name=Step-34, ngeom=YES, inc=200,
unsymm=YES
Excavation of the
*Static
0.1, 1., 1e-07, 1.
*CONTROLS, ANALYSIS=DISCONTINUOUS
*MODEL CHANGE, ADD
FEMDDM-1.STOPEN9175P2C110B3, FEMDDM-
1.N9175P2C110UCB3, FEMDDM-
1.STOPEN9200P1C215B2, FEMDDM-
1.N9200P1C215UCB2
*FIELD
FEMDDM-1.STOPEN9175P2C110BACKFILL3, 1.0
FEMDDM-1.STOPEN9200P1C215BACKFILL2, 1.0
*MODEL CHANGE, REMOVE
FEMDDM-1.STOPEN9175P2C200B1, FEMDDM-
1.STOPEN9200P2C140B1, FEMDDM-
1.STOPEN9225P1C215B1, FEMDDM-
1.S9050C890DRF, FEMDDM-1.SLRS9100C900B6,
FEMDDM-1.SLRS9100C890B6
*MODEL CHANGE, REMOVE
FEMDDM-1.SLRS9075C970B5, FEMDDM-
1.SLRS9075C910B1, FEMDDM-1.N9050P1C95UC,
FEMDDM-1.N9250P1C125UC, FEMDDM-
1.N9225P2C110UC
**
** OUTPUT REQUESTS
**
*Restart, write, frequency=0
**
** FIELD OUTPUT: F-Output-2
**
*Output, field
*Element Output, directions=YES
ELEDEN, ELEN, ENER, PEEQMAX, PEEQT
*Contact Output
EFENRRTR, ENRRT

```

```

**
** FIELD OUTPUT: F-Output-1
**
*Output, field, variable=PRESELECT
**
** HISTORY OUTPUT: H-Output-1
**
*Output, history, variable=PRESELECT
*End Step
** -----
-
**
** STEP: Step-35
**
*Step, name=Step-35, nlgeom=YES, inc=200,
unsymm=YES
Excavation of the
*Static
0.1, 1., 1e-07, 1.
*CONTROLS, ANALYSIS=DISCONTINUOUS
*MODEL CHANGE, ADD
FEMDDM-1.STOPEN9175P2C200B1, FEMDDM-
1.N9175P2C200UCB1, FEMDDM-
1.STOPEN9200P2C140B1, FEMDDM-
1.N9200P2C140UCB1, FEMDDM-
1.STOPEN9225P1C215B1, FEMDDM-
1.N9225P1C215UCB1
*FIELD
FEMDDM-1.STOPEN9175P2C200BACKFILL1, 1.0
FEMDDM-1.STOPEN9200P2C140BACKFILL1, 1.0
FEMDDM-1.STOPEN9225P1C215BACKFILL1, 1.0
*MODEL CHANGE, REMOVE
FEMDDM-1.STOPEN9175P2C80B1, FEMDDM-
1.STOPEN9200P2C110B1, FEMDDM-
1.S9025C975DRF, FEMDDM-1.S9025XC975T960,
FEMDDM-1.SLRS9075C960B5, FEMDDM-
1.SLRS9075C900B1
*MODEL CHANGE, REMOVE
FEMDDM-1.SLRS9075C890B1, FEMDDM-
1.N9050P1C65UC, FEMDDM-1.N9225P2C200UC
**
** OUTPUT REQUESTS
**
*Restart, write, frequency=0
**
** FIELD OUTPUT: F-Output-2
**
*Output, field
*Element Output, directions=YES
ELEDEN, ELEN, ENER, PEEQMAX, PEEQT
*Contact Output
EFENRRTR, ENRRT
**
** FIELD OUTPUT: F-Output-1
**
*Output, field, variable=PRESELECT
**
** HISTORY OUTPUT: H-Output-1
**
*Output, history, variable=PRESELECT
*End Step
** -----
-
**
** STEP: Step-36
**
*Step, name=Step-36, nlgeom=YES, inc=200,
unsymm=YES
Excavation of the
*Static
0.1, 1., 1e-07, 1.
*CONTROLS, ANALYSIS=DISCONTINUOUS
*MODEL CHANGE, ADD
FEMDDM-1.STOPEN9175P2C200B2, FEMDDM-
1.N9175P2C200UCB2, FEMDDM-
1.STOPEN9200P2C140B2, FEMDDM-
1.N9200P2C140UCB2, FEMDDM-
1.STOPEN9225P1C215B2, FEMDDM-
1.N9225P1C215UCB2
*FIELD
FEMDDM-1.STOPEN9175P2C200BACKFILL2, 1.0
FEMDDM-1.STOPEN9200P2C140BACKFILL2, 1.0
FEMDDM-1.STOPEN9225P1C215BACKFILL2, 1.0
*MODEL CHANGE, REMOVE
FEMDDM-1.STOPEN9175P2C80B2, FEMDDM-
1.STOPEN9200P2C110B2, FEMDDM-
1.S9025C950DRF, FEMDDM-1.S9025XC950T935,
FEMDDM-1.SLRS9075C940B4, FEMDDM-
1.SLRS9075C920B3

```

```

*MODEL CHANGE, REMOVE
FEMDDM-1.SLRS9075C910B2, FEMDDM-
1.SLRS9075C900B2, FEMDDM-1.N9050P1C155UC
**
** OUTPUT REQUESTS
**
*Restart, write, frequency=0
**
** FIELD OUTPUT: F-Output-2
**
*Output, field
*Element Output, directions=YES
ELEDEN, ELEN, ENER, PEEQMAX, PEEQT
*Contact Output
EFENRRTR, ENRRT
**
** FIELD OUTPUT: F-Output-1
**
*Output, field, variable=PRESELECT
**
** HISTORY OUTPUT: H-Output-1
**
*Output, history, variable=PRESELECT
*End Step
** -----
-
**
** STEP: Step-38
**
*Step, name=Step-38, nlgeom=YES, inc=200,
unsymm=YES
Excavation of the
*Static
0.1, 1., 1e-07, 1.
*CONTROLS, ANALYSIS=DISCONTINUOUS
*MODEL CHANGE, ADD
FEMDDM-1.STOPEN9175P2C80B2, FEMDDM-
1.N9175P2C80UCB2, FEMDDM-
1.STOPEN9200P2C110B2, FEMDDM-
1.N9200P2C110UCB2
*FIELD
FEMDDM-1.STOPEN9175P2C80BACKFILL2, 1.0
FEMDDM-1.STOPEN9200P2C110BACKFILL2, 1.0
*MODEL CHANGE, REMOVE
FEMDDM-1.STOPEN9200P2C140B3, FEMDDM-
1.S9025C935DRF, FEMDDM-1.S9025XC935T920,
FEMDDM-1.SLRS9075C940B5, FEMDDM-
1.SLRS9075C930B4
*MODEL CHANGE, REMOVE
FEMDDM-1.SLRS9075C920B4, FEMDDM-
1.SLRS9075C910B3, FEMDDM-1.SLRS9075C890B3,
FEMDDM-1.N9050P1C185UC
**
** OUTPUT REQUESTS
**
*Restart, write, frequency=0
**
** FIELD OUTPUT: F-Output-2
**
*Output, field
*Element Output, directions=YES
ELEDEN, ELEN, ENER, PEEQMAX, PEEQT
*Contact Output
EFENRRTR, ENRRT
**
** FIELD OUTPUT: F-Output-1
**
*Output, field, variable=PRESELECT
**
** HISTORY OUTPUT: H-Output-1
**
*Output, history, variable=PRESELECT
*End Step
** -----
-
**
** STEP: Step-39
**
*Step, name=Step-39, nlgeom=YES, inc=200,
unsymm=YES
Excavation of the
*Static
0.1, 1., 1e-07, 1.
*CONTROLS, ANALYSIS=DISCONTINUOUS
*MODEL CHANGE, ADD
FEMDDM-1.STOPEN9200P2C140B3, FEMDDM-
1.N9200P2C140UCB3
*FIELD
FEMDDM-1.STOPEN9200P2C140BACKFILL3, 1.0
*MODEL CHANGE, REMOVE
FEMDDM-1.STOPEN9200P2C110B3, FEMDDM-
1.STOPEN9225P1C155B1, FEMDDM-
1.S9025C920DRF, FEMDDM-1.S9025XC920T910,
FEMDDM-1.SLRS9075C930B5, FEMDDM-
1.SLRS9075C930B6
*MODEL CHANGE, REMOVE
FEMDDM-1.SLRS9075C920B5, FEMDDM-
1.SLRS9075C910B4, FEMDDM-1.SLRS9075C900B3,
FEMDDM-1.N9075P1C65UC
**
** OUTPUT REQUESTS
**
*Restart, write, frequency=0
**
** FIELD OUTPUT: F-Output-2
**
*Output, field
*Element Output, directions=YES
ELEDEN, ELEN, ENER, PEEQMAX, PEEQT
*Contact Output
EFENRRTR, ENRRT
**
** FIELD OUTPUT: F-Output-1
**
*Output, field, variable=PRESELECT
**
** HISTORY OUTPUT: H-Output-1
**
*Output, history, variable=PRESELECT
*End Step
** -----
-
**
** STEP: Step-40
**
*Step, name=Step-40, nlgeom=YES, inc=200,
unsymm=YES
Excavation of the
*Static
0.1, 1., 1e-07, 1.
*CONTROLS, ANALYSIS=DISCONTINUOUS
*MODEL CHANGE, ADD
FEMDDM-1.STOPEN9200P2C110B3, FEMDDM-
1.N9200P2C110UCB3, FEMDDM-
1.STOPEN9225P1C155B1, FEMDDM-
1.N9225P1C155UCB1, FEMDDM-
1.N9250P1C155UCB1
*FIELD
FEMDDM-1.STOPEN9200P2C110BACKFILL3, 1.0
FEMDDM-1.STOPEN9225P1C155BACKFILL1, 1.0

```

```

*MODEL CHANGE, REMOVE
FEMDDM-1.STOPEN9200P2C80B1, FEMDDM-
1.STOPEN9225P1C185B1, FEMDDM-
1.S9025C910DRF, FEMDDM-1.SLRS9075C970B6,
FEMDDM-1.SLRS9050C970B1, FEMDDM-
1.N9075P1C95UC
*MODEL CHANGE, REMOVE
FEMDDM-1.S9075XC970T960, FEMDDM-
1.SLRS9050C960B1
**
** OUTPUT REQUESTS
**
*Restart, write, frequency=0
**
** FIELD OUTPUT: F-Output-2
**
*Output, field
*Element Output, directions=YES
ELEDEN, ELEN, ENER, PEEQMAX, PEEQT
*Contact Output
EFENRRTR, ENRRT
**
** FIELD OUTPUT: F-Output-1
**
*Output, field, variable=PRESELECT
**
** HISTORY OUTPUT: H-Output-1
**
*Output, history, variable=PRESELECT
*End Step
** -----
-
**
** STEP: Step-41
**
*Step, name=Step-41, nlgeom=YES, inc=200,
unsymm=YES
Excavation of the
*Static
0.1, 1., 1e-07, 1.
*CONTROLS,ANALYSIS=DISCONTINUOUS
*MODEL CHANGE, ADD
FEMDDM-1.STOPEN9200P2C80B1, FEMDDM-
1.N9200P2C80UCB1, FEMDDM-
1.STOPEN9225P1C185B1, FEMDDM-
1.N9225P1C185UCB1, FEMDDM-
1.N9250P1C185UCB1
*FIELD
FEMDDM-1.STOPEN9200P2C80BACKFILL1, 1.0
FEMDDM-1.STOPEN9225P1C185BACKFILL1, 1.0
*MODEL CHANGE, REMOVE
FEMDDM-1.STOPEN9200P2C170B1, FEMDDM-
1.STOPEN9225P1C125B1, FEMDDM-
1.SLRS9075C960B6, FEMDDM-1.SLRS9075C910B5,
FEMDDM-1.SLRS9075C900B4
*MODEL CHANGE, REMOVE
FEMDDM-1.SLRS9050C950B1, FEMDDM-
1.N9075P1C125UC, FEMDDM-1.N9175S2C223UC,
FEMDDM-1.N9200P2C200UC
**
** OUTPUT REQUESTS
**
*Restart, write, frequency=0
**
** FIELD OUTPUT: F-Output-2
**
*Output, field
*Element Output, directions=YES
ELEDEN, ELEN, ENER, PEEQMAX, PEEQT
*Contact Output
EFENRRTR, ENRRT
**
** FIELD OUTPUT: F-Output-1
**
*Output, field, variable=PRESELECT
**
** HISTORY OUTPUT: H-Output-1
**
*Output, history, variable=PRESELECT
*End Step
** -----
-
**
** STEP: Step-42
**
*Step, name=Step-42, nlgeom=YES, inc=200,
unsymm=YES
Excavation of the
*Static
0.1, 1., 1e-07, 1.
*CONTROLS,ANALYSIS=DISCONTINUOUS
*MODEL CHANGE, ADD
FEMDDM-1.STOPEN9200P2C170B1, FEMDDM-
1.N9200P2C170UCB1, FEMDDM-
1.STOPEN9225P1C125B1, FEMDDM-
1.N9225P1C125UCB1, FEMDDM-
1.N9250P1C125UCB1
*FIELD
FEMDDM-1.STOPEN9200P2C170BACKFILL1, 1.0
FEMDDM-1.STOPEN9225P1C125BACKFILL1, 1.0
*MODEL CHANGE, REMOVE
FEMDDM-1.STOPEN9200P2C200B1, FEMDDM-
1.STOPEN9225P1C155B2, FEMDDM-
1.SLRS9075C950B6, FEMDDM-1.SLRS9075C900B5,
FEMDDM-1.SLRS9050C970B2
*MODEL CHANGE, REMOVE
FEMDDM-1.SLRS9050C940B1, FEMDDM-
1.N9075P1C155UC, FEMDDM-1.N9200S2C223UC
**
** OUTPUT REQUESTS
**
*Restart, write, frequency=0
**
** FIELD OUTPUT: F-Output-2
**
*Output, field
*Element Output, directions=YES
ELEDEN, ELEN, ENER, PEEQMAX, PEEQT
*Contact Output
EFENRRTR, ENRRT
**
** FIELD OUTPUT: F-Output-1
**
*Output, field, variable=PRESELECT
**
** HISTORY OUTPUT: H-Output-1
**
*Output, history, variable=PRESELECT
*End Step
** -----
-
**
** STEP: Step-43
**
*Step, name=Step-43, nlgeom=YES, inc=200,
unsymm=YES
Excavation of the
*Static
0.1, 1., 1e-07, 1.
*CONTROLS,ANALYSIS=DISCONTINUOUS

```

```

*MODEL CHANGE, ADD
FEMDDM-1.STOPEN9200P2C200B1, FEMDDM-
1.N9200P2C200UCB1, FEMDDM-
1.STOPEN9225P1C155B2, FEMDDM-
1.N9225P1C155UCB2, FEMDDM-
1.N9250P1C155UCB2
*FIELD
FEMDDM-1.STOPEN9200P2C200BACKFILL1, 1.0
FEMDDM-1.STOPEN9225P1C155BACKFILL2, 1.0
*MODEL CHANGE, REMOVE
FEMDDM-1.STOPEN9175S2C223B1, FEMDDM-
1.STOPEN9200P2C80B2, FEMDDM-
1.STOPEN9225P1C185B2, FEMDDM-
1.SLRS9075C910B6, FEMDDM-1.SLRS9075C890B4
*MODEL CHANGE, REMOVE
FEMDDM-1.SLRS9050C960B2, FEMDDM-
1.SLRS9050C930B1, FEMDDM-1.N9075P1C185UC,
FEMDDM-1.N9175S2C73UC, FEMDDM-
1.SLRS9075C940B6
**
** OUTPUT REQUESTS
**
*Restart, write, frequency=0
**
** FIELD OUTPUT: F-Output-2
**
*Output, field
*Element Output, directions=YES
ELEDEN, ELEN, ENER, PEEQMAX, PEEQT
*Contact Output
EFENRRTR, ENRRT
**
** FIELD OUTPUT: F-Output-1
**
*Output, field, variable=PRESELECT
**
** HISTORY OUTPUT: H-Output-1
**
*Output, history, variable=PRESELECT
*End Step
** -----
-
**
** STEP: Step-44
**
*Step, name=Step-44, nlgeom=YES, inc=200,
unsymm=YES
Excavation of the
*Static
0.1, 1., 1e-07, 1.
*CONTROLS, ANALYSIS=DISCONTINUOUS
*MODEL CHANGE, ADD
FEMDDM-1.STOPEN9175S2C223B1, FEMDDM-
1.N9175S2C223UC, FEMDDM-
1.STOPEN9200P2C80B2, FEMDDM-
1.N9200P2C80UCB2, FEMDDM-
1.N9225P2C80OCB1
*MODEL CHANGE, ADD
FEMDDM-1.STOPEN9225P1C185B2, FEMDDM-
1.N9225P1C185UCB2
*FIELD
FEMDDM-1.STOPEN9175S2C223BACKFILL1, 1.0
FEMDDM-1.STOPEN9200P2C80BACKFILL2, 1.0
FEMDDM-1.STOPEN9225P1C185BACKFILL2, 1.0
*MODEL CHANGE, REMOVE
FEMDDM-1.STOPEN9200P2C170B2, FEMDDM-
1.STOPEN9225P1C95B1, FEMDDM-
1.N9225P1C95UCB1, FEMDDM-
1.N9250P1C95OCB1
*FIELD
FEMDDM-1.STOPEN9200P2C170BACKFILL2, 1.0
FEMDDM-1.STOPEN9225P1C95BACKFILL1, 1.0
*MODEL CHANGE, REMOVE
FEMDDM-1.STOPEN9175S2C73B1, FEMDDM-
1.STOPEN9200P2C200B2, FEMDDM-
1.STOPEN9225P1C125B2, FEMDDM-
1.SLRS9075C900B6
*MODEL CHANGE, REMOVE
FEMDDM-1.SLRS9075C890B5, FEMDDM-
1.SLRS9050C950B2, FEMDDM-1.N9100P1C125UC
**
** OUTPUT REQUESTS
**
*Restart, write, frequency=0
**
** FIELD OUTPUT: F-Output-2
**
*Output, field
*Element Output, directions=YES
ELEDEN, ELEN, ENER, PEEQMAX, PEEQT
*Contact Output
EFENRRTR, ENRRT
**
** FIELD OUTPUT: F-Output-1
**
*Output, field, variable=PRESELECT
**
FEMDDM-1.SLRS9050C900B1, FEMDDM-
1.SLRS9050C920B1, FEMDDM-1.N9100P1C95UC,
FEMDDM-1.N9200S2C73OC, FEMDDM-
1.S9075XC920T910
**
** OUTPUT REQUESTS
**
*Restart, write, frequency=0
**
** FIELD OUTPUT: F-Output-2
**
*Output, field
*Element Output, directions=YES
ELEDEN, ELEN, ENER, PEEQMAX, PEEQT
*Contact Output
EFENRRTR, ENRRT
**
** FIELD OUTPUT: F-Output-1
**
*Output, field, variable=PRESELECT
**
** HISTORY OUTPUT: H-Output-1
**
*Output, history, variable=PRESELECT
*End Step
** -----
-
**
** STEP: Step-45
**
*Step, name=Step-45, nlgeom=YES, inc=200,
unsymm=YES
Excavation of the
*Static
0.1, 1., 1e-07, 1.
*CONTROLS, ANALYSIS=DISCONTINUOUS
*MODEL CHANGE, ADD
FEMDDM-1.STOPEN9200P2C170B2, FEMDDM-
1.N9200P2C170UCB2, FEMDDM-
1.STOPEN9225P1C95B1, FEMDDM-
1.N9225P1C95UCB1, FEMDDM-
1.N9250P1C95OCB1
*FIELD
FEMDDM-1.STOPEN9200P2C170BACKFILL2, 1.0
FEMDDM-1.STOPEN9225P1C95BACKFILL1, 1.0
*MODEL CHANGE, REMOVE
FEMDDM-1.STOPEN9175S2C73B1, FEMDDM-
1.STOPEN9200P2C200B2, FEMDDM-
1.STOPEN9225P1C125B2, FEMDDM-
1.SLRS9075C900B6
*MODEL CHANGE, REMOVE
FEMDDM-1.SLRS9075C890B5, FEMDDM-
1.SLRS9050C950B2, FEMDDM-1.N9100P1C125UC
**
** OUTPUT REQUESTS
**
*Restart, write, frequency=0
**
** FIELD OUTPUT: F-Output-2
**
*Output, field
*Element Output, directions=YES
ELEDEN, ELEN, ENER, PEEQMAX, PEEQT
*Contact Output
EFENRRTR, ENRRT
**
** FIELD OUTPUT: F-Output-1
**
*Output, field, variable=PRESELECT
**

```

```

** HISTORY OUTPUT: H-Output-1
**
*Output, history, variable=PRESELECT
*End Step
** -----
-
**
** STEP: Step-46
**
*Step, name=Step-46, nlgeom=YES, inc=200,
unsymm=YES
Excavation of the
*Static
0.1, 1., 1e-07, 1.
*CONTROLS,ANALYSIS=DISCONTINUOUS
*MODEL CHANGE, ADD
FEMDDM-1.STOPEN9175S2C73B1, FEMDDM-
1.N9175S2C73UCB1, FEMDDM-
1.STOPEN9200P2C200B2, FEMDDM-
1.N9200P2C200UCB2, FEMDDM-
1.STOPEN9225P1C125B2, FEMDDM-
1.N9225P1C125UCB2, FEMDDM-
1.N9250P1C125UCB2
*FIELD
FEMDDM-1.STOPEN9175S2C73BACKFILL1, 1.0
FEMDDM-1.STOPEN9200P2C200BACKFILL2, 1.0
FEMDDM-1.STOPEN9225P1C95BACKFILL1, 1.0
*MODEL CHANGE, REMOVE
FEMDDM-1.STOPEN9175S2C73B2, FEMDDM-
1.STOPEN9200P2C170B3, FEMDDM-
1.STOPEN9225P1C155B3, FEMDDM-
1.SLRS9050C970B3, FEMDDM-1.N9100P1C155UC
*MODEL CHANGE, REMOVE
FEMDDM-1.N9250P2C110UC
**
** OUTPUT REQUESTS
**
*Restart, write, frequency=0
**
** FIELD OUTPUT: F-Output-2
**
*Output, field
*Element Output, directions=YES
ELEDEN, ELEN, ENER, PEEQMAX, PEEQT
*Contact Output
EFENRRTR, ENRRT
**
** FIELD OUTPUT: F-Output-1
**
*Output, field, variable=PRESELECT
**
** HISTORY OUTPUT: H-Output-1
**
*Output, history, variable=PRESELECT
*End Step
** -----
-
**
** STEP: Step-48
**
*Step, name=Step-48, nlgeom=YES, inc=200,
unsymm=YES
Excavation of the
*Static
0.1, 1., 1e-07, 1.
*CONTROLS,ANALYSIS=DISCONTINUOUS
*MODEL CHANGE, ADD
FEMDDM-1.STOPEN9050P1C95B1, FEMDDM-
1.N9050P1C95UCB1, FEMDDM-
1.STOPEN9200P2C200B3, FEMDDM-
1.N9200P2C200UCB3, FEMDDM-
1.STOPEN9225P1C185B3, FEMDDM-
1.N9225P1C185UCB3
*FIELD
FEMDDM-1.STOPEN9050P1C95BACKFILL1, 1.0
FEMDDM-1.STOPEN9200P2C200BACKFILL3, 1.0
FEMDDM-1.STOPEN9225P1C185BACKFILL3, 1.0
*MODEL CHANGE, REMOVE
FEMDDM-1.STOPEN9050P1C65B1, FEMDDM-
1.STOPEN9225P1C125B3, FEMDDM-
1.SLRS9050C920B2, FEMDDM-1.SLRS9050C900B2,
FEMDDM-1.N9250P2C170UC
**
** OUTPUT REQUESTS
**
*Restart, write, frequency=0
FEMDDM-1.STOPEN9200P2C170B3, FEMDDM-
1.N9200P2C170UCB3
*MODEL CHANGE, ADD
FEMDDM-1.STOPEN9225P1C155B3, FEMDDM-
1.N9225P1C155UCB3
*FIELD
FEMDDM-1.STOPEN9175S2C73BACKFILL2, 1.0
FEMDDM-1.STOPEN9200P2C170BACKFILL3, 1.0
FEMDDM-1.STOPEN9225P1C155BACKFILL3, 1.0
*MODEL CHANGE, REMOVE
FEMDDM-1.STOPEN9050P1C95B1, FEMDDM-
1.STOPEN9200P2C200B3, FEMDDM-
1.STOPEN9225P1C185B3, FEMDDM-
1.SLRS9050C960B3
*MODEL CHANGE, REMOVE
FEMDDM-1.SLRS9050C940B2, FEMDDM-
1.SLRS9050C930B2, FEMDDM-1.N9100P1C65UC,
FEMDDM-1.N9250P2C140UC
**
** OUTPUT REQUESTS
**
*Restart, write, frequency=0
**
** FIELD OUTPUT: F-Output-2
**
*Output, field
*Element Output, directions=YES
ELEDEN, ELEN, ENER, PEEQMAX, PEEQT
*Contact Output
EFENRRTR, ENRRT
**
** FIELD OUTPUT: F-Output-1
**
*Output, field, variable=PRESELECT
**
** HISTORY OUTPUT: H-Output-1
**
*Output, history, variable=PRESELECT
*End Step
** -----
-
**
** STEP: Step-47
**
*Step, name=Step-47, nlgeom=YES, inc=200,
unsymm=YES
Excavation of the
*Static
0.1, 1., 1e-07, 1.
*CONTROLS,ANALYSIS=DISCONTINUOUS
*MODEL CHANGE, ADD
FEMDDM-1.STOPEN9175S2C73B2, FEMDDM-
1.N9175S2C73UCB2, FEMDDM-1.N9200S2C73OC,

```

```

**
** FIELD OUTPUT: F-Output-2
**
*Output, field
*Element Output, directions=YES
ELEDEN, ELEN, ENER, PEEQMAX, PEEQT
*Contact Output
EFENRRTR, ENRRT
**
** FIELD OUTPUT: F-Output-1
**
*Output, field, variable=PRESELECT
**
** HISTORY OUTPUT: H-Output-1
**
*Output, history, variable=PRESELECT
*End Step
** -----
-
**
** STEP: Step-49
**
*Step, name=Step-49, nlgeom=YES, inc=200,
unsymm=YES
Excavation of the
*Static
0.1, 1., 1e-07, 1.
*CONTROLS, ANALYSIS=DISCONTINUOUS
*MODEL CHANGE, ADD
FEMDDM-1.STOPEN9050P1C65B1, FEMDDM-
1.N9050P1C65UCB1, FEMDDM-
1.STOPEN9225P1C125B3, FEMDDM-
1.N9225P1C125UCB3
*FIELD
FEMDDM-1.STOPEN9050P1C65BACKFILL1, 1.0
FEMDDM-1.STOPEN9225P1C125BACKFILL3, 1.0
*MODEL CHANGE, REMOVE
FEMDDM-1.STOPEN9050P1C125B1, FEMDDM-
1.STOPEN9225P1C95B2, FEMDDM-
1.SLRS9050C910B2, FEMDDM-1.SLRS9050C920B3,
FEMDDM-1.N9250P2C200UC
**
** OUTPUT REQUESTS
**
*Restart, write, frequency=0
**
** FIELD OUTPUT: F-Output-2
**
*Output, field
*Element Output, directions=YES
ELEDEN, ELEN, ENER, PEEQMAX, PEEQT
*Contact Output
EFENRRTR, ENRRT
**
** FIELD OUTPUT: F-Output-1
**
*Output, field, variable=PRESELECT
**
** HISTORY OUTPUT: H-Output-1
**
*Output, history, variable=PRESELECT
*End Step
** -----
-
**
** STEP: Step-51
**
*Step, name=Step-51, nlgeom=YES, inc=200,
unsymm=YES
Excavation of the
*Static
0.1, 1., 1e-07, 1.
*CONTROLS, ANALYSIS=DISCONTINUOUS
*MODEL CHANGE, ADD
FEMDDM-1.STOPEN9050P1C155B1, FEMDDM-
1.N9050P1C155UCB1, FEMDDM-
1.STOPEN9225P2C140B1, FEMDDM-
1.N9225P2C140UCB1, FEMDDM-
1.N9250P2C140UCB1
*FIELD
FEMDDM-1.STOPEN9050P1C155BACKFILL1, 1.0
FEMDDM-1.STOPEN9225P2C140BACKFILL1, 1.0
*MODEL CHANGE, REMOVE
FEMDDM-1.STOPEN9050P1C185B1, FEMDDM-
1.STOPEN9200S2C223B1, FEMDDM-
1.STOPEN9225P2C170B1, FEMDDM-
1.SLRS9050C930B3, FEMDDM-1.N9175S1C118UC
**
** OUTPUT REQUESTS
**
*Restart, write, frequency=0

```

```

**
** FIELD OUTPUT: F-Output-2
**
*Output, field
*Element Output, directions=YES
ELEDEN, ELEN, ENER, PEEQMAX, PEEQT
*Contact Output
EFENRRTR, ENRRT
**
** FIELD OUTPUT: F-Output-1
**
*Output, field, variable=PRESELECT
**
** HISTORY OUTPUT: H-Output-1
**
*Output, history, variable=PRESELECT
*End Step
** -----
-
**
** STEP: Step-52
**
*Step, name=Step-52, nlgeom=YES, inc=200,
unsymm=YES
Excavation of the
*Static
0.1, 1., 1e-07, 1.
*CONTROLS, ANALYSIS=DISCONTINUOUS
*MODEL CHANGE, ADD
FEMDDM-1.STOPEN9050P1C185B1, FEMDDM-
1.N9050P1C185UCB1, FEMDDM-
1.STOPEN9200S2C223B1, FEMDDM-
1.N9200S2C223UC, FEMDDM-
1.STOPEN9225P2C170B1, FEMDDM-
1.N9225P2C170UCB1
*FIELD
FEMDDM-1.STOPEN9050P1C185BACKFILL1, 1.0
FEMDDM-1.STOPEN9200S2C223BACKFILL1, 1.0
FEMDDM-1.STOPEN9225P2C170BACKFILL1, 1.0
*MODEL CHANGE, REMOVE
FEMDDM-1.STOPEN9050P1C95B2, FEMDDM-
1.STOPEN9225P2C200B1, FEMDDM-
1.SLRS9050C940B3, FEMDDM-1.N9050P2C200UC,
FEMDDM-1.N9100P1C185UC, FEMDDM-
1.N9175S1C178UC
**
** OUTPUT REQUESTS
**
*Restart, write, frequency=0
**
** FIELD OUTPUT: F-Output-2
**
*Output, field
*Element Output, directions=YES
ELEDEN, ELEN, ENER, PEEQMAX, PEEQT
*Contact Output
EFENRRTR, ENRRT
**
** FIELD OUTPUT: F-Output-1
**
*Output, field, variable=PRESELECT
**
** HISTORY OUTPUT: H-Output-1
**
*Output, history, variable=PRESELECT
*End Step
** -----
-
**
** STEP: Step-54
**
*Step, name=Step-54, nlgeom=YES, inc=200,
unsymm=YES
Excavation of the
*Static
0.1, 1., 1e-07, 1.
*CONTROLS, ANALYSIS=DISCONTINUOUS
*MODEL CHANGE, ADD
FEMDDM-1.STOPEN9050P1C125B2, FEMDDM-
1.N9050P1C125UCB2, FEMDDM-
1.STOPEN9225P2C110B1, FEMDDM-
1.N9225P2C110UCB1, FEMDDM-
1.N9250P2C110UCB1
*FIELD
FEMDDM-1.STOPEN9050P1C125BACKFILL2, 1.0
FEMDDM-1.STOPEN9225P2C110BACKFILL1, 1.0
*MODEL CHANGE, REMOVE
FEMDDM-1.STOPEN9050P1C155B2, FEMDDM-
1.STOPEN9225P2C140B2, FEMDDM-
1.SLRS9050C930B4, FEMDDM-1.N9050P2C80UC,
FEMDDM-1.N9175S1C208UC, FEMDDM-
1.N9075P2C110UC
**
** OUTPUT REQUESTS

```

```

**
**Restart, write, frequency=0
**
** FIELD OUTPUT: F-Output-2
**
**Output, field
**Element Output, directions=YES
ELEDEN, ELEN, ENER, PEEQMAX, PEEQT
**Contact Output
EFENRRTR, ENRRT
**
** FIELD OUTPUT: F-Output-1
**
**Output, field, variable=PRESELECT
**
** HISTORY OUTPUT: H-Output-1
**
**Output, history, variable=PRESELECT
**End Step
** -----
-
**
** STEP: Step-55
**
**Step, name=Step-55, nlgeom=YES, inc=200,
unsymm=YES
Excavation of the
**Static
0.1, 1., 1e-07, 1.
**CONTROLS, ANALYSIS=DISCONTINUOUS
**MODEL CHANGE, ADD
FEMDDM-1.STOPEN9050P1C155B2, FEMDDM-
1.N9050P1C155UCB2, FEMDDM-
1.STOPEN9225P2C140B2, FEMDDM-
1.N9225P2C140UCB2, FEMDDM-
1.N9250P2C140UCB2
**FIELD
FEMDDM-1.STOPEN9050P1C155BACKFILL2, 1.0
FEMDDM-1.STOPEN9225P2C140BACKFILL2, 1.0
**MODEL CHANGE, REMOVE
FEMDDM-1.STOPEN9050P1C185B2, FEMDDM-
1.STOPEN9225P2C170B2, FEMDDM-
1.SLRS9050C940B5, FEMDDM-1.N9075P2C80UC,
FEMDDM-1.N9050P2C140UC
**
** OUTPUT REQUESTS
**
**Restart, write, frequency=0
**
** FIELD OUTPUT: F-Output-2
**
**Output, field
**Element Output, directions=YES
ELEDEN, ELEN, ENER, PEEQMAX, PEEQT
**Contact Output
EFENRRTR, ENRRT
**
** FIELD OUTPUT: F-Output-1
**
**Output, field, variable=PRESELECT
**
** HISTORY OUTPUT: H-Output-1
**
**Output, history, variable=PRESELECT
**End Step
** -----
-
**
** STEP: Step-57
**
**Step, name=Step-57, nlgeom=YES, inc=200,
unsymm=YES
Excavation of the
**Static
0.1, 1., 1e-07, 1.
**CONTROLS, ANALYSIS=DISCONTINUOUS
**MODEL CHANGE, ADD
FEMDDM-1.STOPEN9050P1C95B3, FEMDDM-
1.N9050P1C95UCB3, FEMDDM-
1.STOPEN9225P2C200B2, FEMDDM-
1.N9225P2C200UCB2
**FIELD
FEMDDM-1.STOPEN9050P1C95BACKFILL3, 1.0
FEMDDM-1.STOPEN9225P2C200BACKFILL2, 1.0
**MODEL CHANGE, REMOVE
FEMDDM-1.STOPEN9050P1C125B3, FEMDDM-
1.STOPEN9225P2C110B2, FEMDDM-
1.SLRS9050C970B5, FEMDDM-1.SLRS9050C960B5
**MODEL CHANGE, REMOVE
FEMDDM-1.SLRS9025C960B1, FEMDDM-
1.SLRS9025C950B1, FEMDDM-1.N9075P2C170UC,
FEMDDM-1.S9050XC950T940, FEMDDM-
1.N9200S1C88UC

```

```

**
** OUTPUT REQUESTS
**
*Restart, write, frequency=0
**
** FIELD OUTPUT: F-Output-2
**
*Output, field
*Element Output, directions=YES
ELEDEN, ELEN, ENER, PEEQMAX, PEEQT
*Contact Output
EFENRRTR, ENRRT
**
** FIELD OUTPUT: F-Output-1
**
*Output, field, variable=PRESELECT
**
** HISTORY OUTPUT: H-Output-1
**
*Output, history, variable=PRESELECT
*End Step
** -----
-
**
** STEP: Step-58
**
*Step, name=Step-58, nlgeom=YES, inc=200,
unsymm=YES
Excavation of the
*Static
0.1, 1., 1e-07, 1.
*CONTROLS,ANALYSIS=DISCONTINUOUS
*MODEL CHANGE, ADD
FEMDDM-1.STOPEN9050P1C125B3, FEMDDM-
1.N9050P1C125UCB3, FEMDDM-
1.STOPEN9225P2C110B2, FEMDDM-
1.N9225P2C110UCB2
*FIELD
FEMDDM-1.STOPEN9050P1C125BACKFILL3, 1.0
FEMDDM-1.STOPEN9225P2C110BACKFILL2, 1.0
*MODEL CHANGE, REMOVE
FEMDDM-1.STOPEN9050P1C155B3, FEMDDM-
1.STOPEN9225P2C140B3, FEMDDM-
1.SLRS9050C890B3, FEMDDM-1.SLRS9050C900B3,
FEMDDM-1.SLRS9050C910B3, FEMDDM-
1.S9050XC930T920
*MODEL CHANGE, REMOVE
FEMDDM-1.SLRS9025C935B1, FEMDDM-
1.SLRS9025C920B1, FEMDDM-1.S9050XC940T930,
FEMDDM-1.N9050P2C110UC, FEMDDM-
1.N9200S1C178UC
**
** OUTPUT REQUESTS
**
*Restart, write, frequency=0
**
** FIELD OUTPUT: F-Output-2
**
*Output, field
*Element Output, directions=YES
ELEDEN, ELEN, ENER, PEEQMAX, PEEQT
*Contact Output
EFENRRTR, ENRRT
**
** FIELD OUTPUT: F-Output-1
**
*Output, field, variable=PRESELECT
**
** HISTORY OUTPUT: H-Output-1
**
*Output, history, variable=PRESELECT
*End Step
** -----
-
**
** STEP: Step-59
**
*Step, name=Step-59, nlgeom=YES, inc=200,
unsymm=YES
Excavation of the
*Static
0.1, 1., 1e-07, 1.
*CONTROLS,ANALYSIS=DISCONTINUOUS
*MODEL CHANGE, ADD
FEMDDM-1.STOPEN9050P1C155B3, FEMDDM-
1.N9050P1C155UCB3, FEMDDM-
1.STOPEN9225P2C140B3, FEMDDM-
1.N9225P2C140UCB3
*FIELD
FEMDDM-1.STOPEN9050P1C155BACKFILL3, 1.0
FEMDDM-1.STOPEN9225P2C140BACKFILL3, 1.0
*MODEL CHANGE, REMOVE
FEMDDM-1.STOPEN9050P2C140B1, FEMDDM-
1.STOPEN9075P1C65B1, FEMDDM-
1.STOPEN9225P2C170B3, FEMDDM-
1.SLRS9050C920B4, FEMDDM-1.SLRS9050C930B5,
FEMDDM-1.N9200S1C208UC
**
** OUTPUT REQUESTS
**
*Restart, write, frequency=0
**
** FIELD OUTPUT: F-Output-2
**
*Output, field
*Element Output, directions=YES
ELEDEN, ELEN, ENER, PEEQMAX, PEEQT
*Contact Output
EFENRRTR, ENRRT
**
** FIELD OUTPUT: F-Output-1
**
*Output, field, variable=PRESELECT
**
** HISTORY OUTPUT: H-Output-1
**
*Output, history, variable=PRESELECT
*End Step
** -----
-
**
** STEP: Step-60
**
*Step, name=Step-60, nlgeom=YES, inc=200,
unsymm=YES
Excavation of the
*Static
0.1, 1., 1e-07, 1.
*CONTROLS,ANALYSIS=DISCONTINUOUS
*MODEL CHANGE, ADD
FEMDDM-1.STOPEN9050P2C140B1, FEMDDM-
1.N9050P2C140UCB1, FEMDDM-
1.STOPEN9075P1C65B1, FEMDDM-
1.N9075P1C65UCB1, FEMDDM-
1.STOPEN9225P2C170B3, FEMDDM-
1.N9225P2C170UCB3
*FIELD
FEMDDM-1.STOPEN9050P2C140BACKFILL1, 1.0
FEMDDM-1.STOPEN9075P1C65BACKFILL1, 1.0
FEMDDM-1.STOPEN9225P2C170BACKFILL3, 1.0

```

```

*MODEL CHANGE, REMOVE
FEMDDM-1.STOPEN9050P2C80B1, FEMDDM-
1.STOPEN9075P1C155B1, FEMDDM-
1.STOPEN9225P2C200B3, FEMDDM-
1.SLRS9050C970B5, FEMDDM-1.SLRS9050C920B5,
FEMDDM-1.SLRS9025C975B2
*MODEL CHANGE, REMOVE
FEMDDM-1.SLRS9025C960B2, FEMDDM-
1.SLRS9050C930B5, FEMDDM-1.N9125P1C95UC
**
** OUTPUT REQUESTS
**
*Restart, write, frequency=0
**
** FIELD OUTPUT: F-Output-2
**
*Output, field
*Element Output, directions=YES
ELEDEN, ELEN, ENER, PEEQMAX, PEEQT
*Contact Output
EFENRRTR, ENRRT
**
** FIELD OUTPUT: F-Output-1
**
*Output, field, variable=PRESELECT
**
** HISTORY OUTPUT: H-Output-1
**
*Output, history, variable=PRESELECT
*End Step
** -----
-
**
** STEP: Step-61
**
*Step, name=Step-61, nlgeom=YES, inc=200,
unsymm=YES
Excavation of the
*Static
0.1, 1., 1e-07, 1.
*CONTROLS, ANALYSIS=DISCONTINUOUS
*MODEL CHANGE, ADD
FEMDDM-1.STOPEN9050P2C80B1, FEMDDM-
1.N9050P2C80UCB1, FEMDDM-
1.STOPEN9075P1C155B1, FEMDDM-
1.N9075P1C155UCB1, FEMDDM-
1.STOPEN9225P2C200B3, FEMDDM-
1.N9225P2C200UCB3
*FIELD
FEMDDM-1.STOPEN9050P2C80BACKFILL1, 1.0
FEMDDM-1.STOPEN9075P1C155BACKFILL1, 1.0
FEMDDM-1.STOPEN9225P2C200BACKFILL3, 1.0
*MODEL CHANGE, REMOVE
FEMDDM-1.STOPEN9050P2C110B1, FEMDDM-
1.STOPEN9075P1C185B1, FEMDDM-
1.STOPEN9175S1C148B1, FEMDDM-
1.SLRS9050C960B6, FEMDDM-1.SLRS9050C910B4
*MODEL CHANGE, REMOVE
FEMDDM-1.SLRS9025C910B1, FEMDDM-
1.SLRS9025C910B2, FEMDDM-1.N9125P1C125UC,
FEMDDM-1.SLRS9050C970B6
**
** OUTPUT REQUESTS
**
*Restart, write, frequency=0
**
** FIELD OUTPUT: F-Output-2
**
*Output, field
*Element Output, directions=YES
ELEDEN, ELEN, ENER, PEEQMAX, PEEQT
*Contact Output
EFENRRTR, ENRRT
**
** FIELD OUTPUT: F-Output-1
**
*Output, field, variable=PRESELECT
**
** HISTORY OUTPUT: H-Output-1
**
*Output, history, variable=PRESELECT
*End Step
** -----
-
**
** STEP: Step-62
**
*Step, name=Step-62, nlgeom=YES, inc=200,
unsymm=YES
Excavation of the
*Static
0.1, 1., 1e-07, 1.
*CONTROLS, ANALYSIS=DISCONTINUOUS
*MODEL CHANGE, ADD
FEMDDM-1.STOPEN9050P2C110B1, FEMDDM-
1.N9050P2C110UCB1, FEMDDM-
1.STOPEN9075P1C185B1, FEMDDM-
1.N9075P1C185UCB1, FEMDDM-
1.STOPEN9175S1C148B1, FEMDDM-
1.N9175S1C148UCB1
*FIELD
FEMDDM-1.STOPEN9050P2C110BACKFILL1, 1.0
FEMDDM-1.STOPEN9075P1C185BACKFILL1, 1.0
FEMDDM-1.STOPEN9175S1C148BACKFILL1, 1.0
*MODEL CHANGE, REMOVE
FEMDDM-1.STOPEN9050P2C170B1, FEMDDM-
1.STOPEN9075P1C125B1, FEMDDM-
1.STOPEN9175S1C118B1, FEMDDM-
1.SLRS9050C890B4, FEMDDM-1.SLRS9050C900B4
*MODEL CHANGE, REMOVE
FEMDDM-1.SLRS9025C975B3, FEMDDM-
1.SLRS9025C960B3, FEMDDM-1.N9125P1C65OC,
FEMDDM-1.N9075P2C200UC
**
** OUTPUT REQUESTS
**
*Restart, write, frequency=0
**
** FIELD OUTPUT: F-Output-2
**
*Output, field
*Element Output, directions=YES
ELEDEN, ELEN, ENER, PEEQMAX, PEEQT
*Contact Output
EFENRRTR, ENRRT
**
** FIELD OUTPUT: F-Output-1
**
*Output, field, variable=PRESELECT
**
** HISTORY OUTPUT: H-Output-1
**
*Output, history, variable=PRESELECT
*End Step
** -----
-
**
** STEP: Step-63
**

```

```

*Step, name=Step-63, nlgeom=YES, inc=200,
unsymm=YES
Excavation of the
*Static
0.1, 1., 1e-07, 1.
*CONTROLS, ANALYSIS=DISCONTINUOUS
*MODEL CHANGE, ADD
FEMDDM-1.STOPEN9050P2C170B1, FEMDDM-
1.N9050P2C170UCB1, FEMDDM-
1.STOPEN9075P1C125B1, FEMDDM-
1.N9075P1C125UCB1, FEMDDM-
1.STOPEN9175S1C118B1, FEMDDM-
1.N9175S1C118UCB1
*FIELD
FEMDDM-1.STOPEN9050P2C170BACKFILL1, 1.0
FEMDDM-1.STOPEN9075P1C125BACKFILL1, 1.0
FEMDDM-1.STOPEN9175S1C118BACKFILL1, 1.0
*MODEL CHANGE, REMOVE
FEMDDM-1.STOPEN9050P2C200B1, FEMDDM-
1.STOPEN9075P1C95B1, FEMDDM-
1.STOPEN9175S1C178B1, FEMDDM-
1.SLRS9050C950B6, FEMDDM-1.SLRS9050C940B6
*MODEL CHANGE, REMOVE
FEMDDM-1.SLRS9025C950B2, FEMDDM-
1.SLRS9025C935B2, FEMDDM-1.N9125P1C155UC
**
** OUTPUT REQUESTS
**
*Restart, write, frequency=0
**
** FIELD OUTPUT: F-Output-2
**
*Output, field
*Element Output, directions=YES
ELEDEN, ELEN, ENER, PEEQMAX, PEEQT
*Contact Output
EFENRRTR, ENRRT
**
** FIELD OUTPUT: F-Output-1
**
*Output, field, variable=PRESELECT
**
** HISTORY OUTPUT: H-Output-1
**
*Output, history, variable=PRESELECT
*End Step
** -----
-
**
** STEP: Step-65
**
*Step, name=Step-65, nlgeom=YES, inc=200,
unsymm=YES
Excavation of the
*Static
0.1, 1., 1e-07, 1.
*CONTROLS, ANALYSIS=DISCONTINUOUS
*MODEL CHANGE, ADD
FEMDDM-1.STOPEN9050P2C80B2, FEMDDM-
1.N9050P2C80UCB2, FEMDDM-
1.STOPEN9075P1C155B2, FEMDDM-
1.N9075P1C155UCB2, FEMDDM-
1.STOPEN9175S1C88B1, FEMDDM-
1.N9175S1C88UCB1
*FIELD
FEMDDM-1.STOPEN9050P2C80BACKFILL2, 1.0
FEMDDM-1.STOPEN9075P1C155BACKFILL2, 1.0
FEMDDM-1.STOPEN9175S1C88BACKFILL1, 1.0
*MODEL CHANGE, REMOVE
FEMDDM-1.STOPEN9075P1C125B2, FEMDDM-
1.STOPEN9175S1C208B1, FEMDDM-
1.SLRS9050C910B5, FEMDDM-1.SLRS9050C900B5
*MODEL CHANGE, REMOVE
FEMDDM-1.SLRS9025C950B3, FEMDDM-
1.N9225S1C118UC, FEMDDM-1.N9050S1C208UC
**
** OUTPUT REQUESTS
**
*Restart, write, frequency=0
**
** FIELD OUTPUT: F-Output-2
**
*Output, field
*Element Output, directions=YES
ELEDEN, ELEN, ENER, PEEQMAX, PEEQT
*Contact Output
EFENRRTR, ENRRT

```

```

**
** FIELD OUTPUT: F-Output-1
**
*Output, field, variable=PRESELECT
**
** HISTORY OUTPUT: H-Output-1
**
*Output, history, variable=PRESELECT
*End Step
** -----
-
**
** STEP: Step-66
**
*Step, name=Step-66, nlgeom=YES, inc=200,
unsymm=YES
Excavation of the
*Static
0.1, 1., 1e-07, 1.
*CONTROLS,ANALYSIS=DISCONTINUOUS
*MODEL CHANGE, ADD
FEMDDM-1.STOPEN9075P1C125B2, FEMDDM-
1.N9075P1C125UCB2, FEMDDM-
1.STOPEN9175S1C208B1, FEMDDM-
1.N9175S1C208UCB1
*FIELD
FEMDDM-1.STOPEN9075P1C125BACKFILL2, 1.0
FEMDDM-1.STOPEN9175S1C208BACKFILL1, 1.0
*MODEL CHANGE, REMOVE
FEMDDM-1.STOPEN9050P2C110B2, FEMDDM-
1.STOPEN9075P1C185B2, FEMDDM-
1.STOPEN9175S1C148B2, FEMDDM-
1.SLRS9025C935B3
*MODEL CHANGE, REMOVE
FEMDDM-1.SLRS9025C920B3, FEMDDM-
1.SLRS9025C920B2, FEMDDM-1.N9075S1C208UC
**
** OUTPUT REQUESTS
**
*Restart, write, frequency=0
**
** FIELD OUTPUT: F-Output-2
**
*Output, field
*Element Output, directions=YES
ELEDEN, ELEN, ENER, PEEQMAX, PEEQT
*Contact Output
EFENRRTR, ENRRT
**
** FIELD OUTPUT: F-Output-1
**
*Output, field, variable=PRESELECT
**
** HISTORY OUTPUT: H-Output-1
**
*Output, history, variable=PRESELECT
*End Step
** -----
-
**
** STEP: Step-68
**
*Step, name=Step-68, nlgeom=YES, inc=200,
unsymm=YES
Excavation of the
*Static
0.1, 1., 1e-07, 1.
*CONTROLS,ANALYSIS=DISCONTINUOUS
*MODEL CHANGE, ADD
FEMDDM-1.STOPEN9050P2C140B2, FEMDDM-
1.N9050P2C140UCB2, FEMDDM-
1.STOPEN9075P1C95B2, FEMDDM-
1.N9075P1C95UCB2, FEMDDM-
1.STOPEN9175S1C118B2, FEMDDM-
1.N9175S1C118UCB2
*FIELD
FEMDDM-1.STOPEN9050P2C140BACKFILL2, 1.0
FEMDDM-1.STOPEN9075P1C95BACKFILL2, 1.0
FEMDDM-1.STOPEN9175S1C118BACKFILL2, 1.0
*MODEL CHANGE, REMOVE
FEMDDM-1.STOPEN9050P2C170B2, FEMDDM-
1.STOPEN9075P1C125B3, FEMDDM-
1.STOPEN9175S1C178B2, FEMDDM-
1.SLRS9025C950B4, FEMDDM-1.N9225S1C178UC,
FEMDDM-1.N9100P2C80UC, FEMDDM-
1.N9100P2C200UC
**

```

```

** OUTPUT REQUESTS
**
*Restart, write, frequency=0
**
** FIELD OUTPUT: F-Output-2
**
*Output, field
*Element Output, directions=YES
ELEDEN, ELEN, ENER, PEEQMAX, PEEQT
*Contact Output
EFENRRTR, ENRRT
**
** FIELD OUTPUT: F-Output-1
**
*Output, field, variable=PRESELECT
**
** HISTORY OUTPUT: H-Output-1
**
*Output, history, variable=PRESELECT
*End Step
** -----
-
**
** STEP: Step-69
**
*Step, name=Step-69, nlgeom=YES, inc=200,
unsymm=YES
Excavation of the
*Static
0.1, 1., 1e-07, 1.
*CONTROLS,ANALYSIS=DISCONTINUOUS
*MODEL CHANGE, ADD
FEMDDM-1.STOPEN9050P2C170B2, FEMDDM-
1.N9050P2C170UCB2, FEMDDM-
1.STOPEN9075P1C125B3, FEMDDM-
1.N9075P1C125UCB3, FEMDDM-
1.STOPEN9175S1C178B2, FEMDDM-
1.N9175S1C178UCB2
*FIELD
FEMDDM-1.STOPEN9050P2C170BACKFILL2, 1.0
FEMDDM-1.STOPEN9075P1C125BACKFILL3, 1.0
FEMDDM-1.STOPEN9175S1C178BACKFILL2, 1.0
*MODEL CHANGE, REMOVE
FEMDDM-1.STOPEN9050P2C110B3, FEMDDM-
1.STOPEN9075P1C155B3, FEMDDM-
1.STOPEN9175S1C88B2, FEMDDM-
1.SLRS9025C935B4, FEMDDM-1.N9225S1C208UC
**
** OUTPUT REQUESTS
**
*Restart, write, frequency=0
**
** FIELD OUTPUT: F-Output-2
**
*Output, field
*Element Output, directions=YES
ELEDEN, ELEN, ENER, PEEQMAX, PEEQT
*Contact Output
EFENRRTR, ENRRT
**
** FIELD OUTPUT: F-Output-1
**
*Output, field, variable=PRESELECT
**
** HISTORY OUTPUT: H-Output-1
**
*Output, history, variable=PRESELECT
*End Step
** -----
-
**
** STEP: Step-70
**
*Step, name=Step-70, nlgeom=YES, inc=200,
unsymm=YES
Excavation of the
*Static
0.1, 1., 1e-07, 1.
*CONTROLS,ANALYSIS=DISCONTINUOUS
*MODEL CHANGE, ADD
FEMDDM-1.STOPEN9050P2C110B3, FEMDDM-
1.N9050P2C110UCB3, FEMDDM-
1.STOPEN9075P1C155B3, FEMDDM-
1.N9075P1C155UCB3, FEMDDM-
1.STOPEN9175S1C88B2, FEMDDM-
1.N9175S1C88UCB2
*FIELD
FEMDDM-1.STOPEN9050P2C110BACKFILL3, 1.0
FEMDDM-1.STOPEN9075P1C155BACKFILL3, 1.0
FEMDDM-1.STOPEN9175S1C88BACKFILL2, 1.0
*MODEL CHANGE, REMOVE
FEMDDM-1.STOPEN9050P2C140B3, FEMDDM-
1.STOPEN9075P1C95B3, FEMDDM-
1.STOPEN9175S1C208B2, FEMDDM-
1.SLRS9025C920B4, FEMDDM-1.N9275P1C155OC,
FEMDDM-1.N9100P2C140UC, FEMDDM-
1.N9100P2C170UC
**
** OUTPUT REQUESTS
**
*Restart, write, frequency=0
**
** FIELD OUTPUT: F-Output-2
**
*Output, field
*Element Output, directions=YES
ELEDEN, ELEN, ENER, PEEQMAX, PEEQT
*Contact Output
EFENRRTR, ENRRT
**
** FIELD OUTPUT: F-Output-1
**
*Output, field, variable=PRESELECT
**
** HISTORY OUTPUT: H-Output-1
**
*Output, history, variable=PRESELECT
*End Step
** -----
-
**
** STEP: Step-71
**
*Step, name=Step-71, nlgeom=YES, inc=200,
unsymm=YES
Excavation of the
*Static
0.1, 1., 1e-07, 1.
*CONTROLS,ANALYSIS=DISCONTINUOUS
*MODEL CHANGE, ADD
FEMDDM-1.STOPEN9050P2C140B3, FEMDDM-
1.N9050P2C140UCB3, FEMDDM-
1.STOPEN9075P1C95B3, FEMDDM-
1.N9075P1C95UCB3, FEMDDM-
1.STOPEN9175S1C208B2, FEMDDM-
1.N9175S1C208UCB2
*FIELD
FEMDDM-1.STOPEN9050P2C140BACKFILL3, 1.0
FEMDDM-1.STOPEN9075P1C95BACKFILL3, 1.0
FEMDDM-1.STOPEN9175S1C208BACKFILL2, 1.0

```

```

*MODEL CHANGE, REMOVE
FEMDDM-1.STOPEN9050P2C170B3, FEMDDM-
1.STOPEN9075P2C110B1, FEMDDM-
1.STOPEN9100P1C155B1, FEMDDM-
1.N9100P2C110UC
*MODEL CHANGE, REMOVE
FEMDDM-1.STOPEN9175S1C148B3, FEMDDM-
1.STOPEN9175S1C148B4, FEMDDM-
1.SLRS9025C975B5, FEMDDM-1.N9275P1C125OC
**
** OUTPUT REQUESTS
**
*Restart, write, frequency=0
**
** FIELD OUTPUT: F-Output-2
**
*Output, field
*Element Output, directions=YES
ELEDEN, ELEN, ENER, PEEQMAX, PEEQT
*Contact Output
EFENRRTR, ENRRT
**
** FIELD OUTPUT: F-Output-1
**
*Output, field, variable=PRESELECT
**
** HISTORY OUTPUT: H-Output-1
**
*Output, history, variable=PRESELECT
*End Step
** -----
-
**
** STEP: Step-73
**
*Step, name=Step-73, nlgeom=YES, inc=200,
unsymm=YES
Excavation of the
*Static
0.1, 1., 1e-07, 1.
*CONTROLS, ANALYSIS=DISCONTINUOUS
*MODEL CHANGE, ADD
FEMDDM-1.STOPEN9075P2C140B1, FEMDDM-
1.N9075P2C140UCB1, FEMDDM-
1.STOPEN9175S1C118B3, FEMDDM-
1.N9175S1C118UCB3
*MODEL CHANGE, ADD
FEMDDM-1.STOPEN9200S1C148B1, FEMDDM-
1.N9200S1C148UCB1, FEMDDM-
1.STOPEN9250P1C155B1, FEMDDM-
1.N9250P1C155UCB3, FEMDDM-
1.N9275P1C155OCB1
*FIELD
FEMDDM-1.STOPEN9075P2C140BACKFILL1, 1.0
FEMDDM-1.STOPEN9175S1C118BACKFILL3, 1.0
FEMDDM-1.STOPEN9200S1C148BACKFILL1, 1.0
FEMDDM-1.STOPEN9250P1C155BACKFILL1, 1.0
*MODEL CHANGE, REMOVE
FEMDDM-1.STOPEN9075P2C170B1, FEMDDM-
1.STOPEN9100P1C95B1, FEMDDM-
1.STOPEN9175S1C178B3, FEMDDM-
1.STOPEN9200S1C118B1, FEMDDM-
1.STOPEN9250P1C185B1, FEMDDM-
1.SLRS9025C895B2, FEMDDM-1.N9150P1C125OC
**
** OUTPUT REQUESTS
**
*Restart, write, frequency=0
**
** FIELD OUTPUT: F-Output-2
**
*Output, field
*Element Output, directions=YES
ELEDEN, ELEN, ENER, PEEQMAX, PEEQT
*Contact Output
EFENRRTR, ENRRT
**
** FIELD OUTPUT: F-Output-1
**
*Output, field, variable=PRESELECT

```

```

**
** HISTORY OUTPUT: H-Output-1
**
*Output, history, variable=PRESELECT
*End Step
** -----
-
**
** STEP: Step-74
**
*Step, name=Step-74, nlgeom=YES, inc=200,
unsymm=YES
Excavation of the
*Static
0.1, 1., 1e-07, 1.
*CONTROLS,ANALYSIS=DISCONTINUOUS
*MODEL CHANGE, ADD
FEMDDM-1.STOPEN9075P2C170B1, FEMDDM-
1.N9075P2C170UCB1, FEMDDM-
1.STOPEN9100P1C95B1, FEMDDM-
1.N9100P1C95UCB1, FEMDDM-
1.STOPEN9175S1C178B3, FEMDDM-
1.N9175S1C178UCB3
*MODEL CHANGE, ADD
FEMDDM-1.STOPEN9200S1C118B1, FEMDDM-
1.N9200S1C118UCB1, FEMDDM-
1.STOPEN9250P1C185B1, FEMDDM-
1.N9250P1C185UCB2, FEMDDM-
1.N9275P1C185OCB1
*FIELD
FEMDDM-1.STOPEN9075P2C170BACKFILL1, 1.0
FEMDDM-1.STOPEN9100P1C95BACKFILL1, 1.0
FEMDDM-1.STOPEN9175S1C178BACKFILL3, 1.0
FEMDDM-1.STOPEN9200S1C118BACKFILL1, 1.0
FEMDDM-1.STOPEN9250P1C185BACKFILL1, 1.0
*MODEL CHANGE, REMOVE
FEMDDM-1.STOPEN9075P2C200B1, FEMDDM-
1.STOPEN9100P1C185B1, FEMDDM-
1.STOPEN9175S1C88B3, FEMDDM-
1.STOPEN9200S1C178B1
*MODEL CHANGE, REMOVE
FEMDDM-1.N9225S1C88UC, FEMDDM-
1.STOPEN9250P1C125B1, FEMDDM-
1.SLRS9025C960B5, FEMDDM-1.N9150P1C155OC
**
** OUTPUT REQUESTS
**
*Restart, write, frequency=0
**
** FIELD OUTPUT: F-Output-2
**
*Output, field
*Element Output, directions=YES
ELEDEN, ELEN, ENER, PEEQMAX, PEEQT
*Contact Output
EFENRRTR, ENRRT
**
** FIELD OUTPUT: F-Output-1
**
** OUTPUT REQUESTS
**
*Restart, write, frequency=0
**
** FIELD OUTPUT: F-Output-2
**
*Output, field
*Element Output, directions=YES
ELEDEN, ELEN, ENER, PEEQMAX, PEEQT
*Contact Output
EFENRRTR, ENRRT
**
** FIELD OUTPUT: F-Output-1
**
** OUTPUT REQUESTS
**
*Restart, write, frequency=0
**
** FIELD OUTPUT: F-Output-2
**
*Output, field, variable=PRESELECT
**
** HISTORY OUTPUT: H-Output-1
**
*Output, history, variable=PRESELECT
*End Step
** -----
-
**
** STEP: Step-75
**
*Step, name=Step-75, nlgeom=YES, inc=200,
unsymm=YES
Excavation of the
*Static
0.1, 1., 1e-07, 1.
*CONTROLS,ANALYSIS=DISCONTINUOUS
*MODEL CHANGE, ADD
FEMDDM-1.STOPEN9075P2C200B1, FEMDDM-
1.N9075P2C200UCB1, FEMDDM-
1.STOPEN9100P1C185B1, FEMDDM-
1.N9100P1C185UCB1, FEMDDM-
1.STOPEN9175S1C88B3, FEMDDM-
1.N9175S1C88UCB3
*MODEL CHANGE, ADD
FEMDDM-1.STOPEN9200S1C178B1, FEMDDM-
1.N9200S1C178UCB1, FEMDDM-
1.STOPEN9250P1C125B1, FEMDDM-
1.N9250P1C125UCB3, FEMDDM-
1.N9275P1C125OCB1
*FIELD
FEMDDM-1.STOPEN9075P2C200BACKFILL1, 1.0
FEMDDM-1.STOPEN9100P1C185BACKFILL1, 1.0
FEMDDM-1.STOPEN9175S1C88BACKFILL3, 1.0
FEMDDM-1.STOPEN9200S1C178BACKFILL1, 1.0
FEMDDM-1.STOPEN9250P1C125BACKFILL1, 1.0
*MODEL CHANGE, REMOVE
FEMDDM-1.STOPEN9075P2C80B1, FEMDDM-
1.STOPEN9100P1C65B1, FEMDDM-
1.STOPEN9200S1C88B1, FEMDDM-
1.STOPEN9250P1C215B1, FEMDDM-
1.N9150P1C185OC
*MODEL CHANGE, REMOVE
FEMDDM-1.STOPEN9075P2C80B2, FEMDDM-
1.N9275P2C110OC, FEMDDM-1.N9275P2C140OC
**
** OUTPUT REQUESTS
**
*Restart, write, frequency=0
**
** FIELD OUTPUT: F-Output-2
**
*Output, field
*Element Output, directions=YES
ELEDEN, ELEN, ENER, PEEQMAX, PEEQT
*Contact Output
EFENRRTR, ENRRT
**
** FIELD OUTPUT: F-Output-1
**
** OUTPUT REQUESTS
**
*Restart, write, frequency=0
**
** FIELD OUTPUT: F-Output-2
**
*Output, field, variable=PRESELECT
**
** HISTORY OUTPUT: H-Output-1
**
*Output, history, variable=PRESELECT
*End Step
** -----
-
**
** STEP: Step-76
**
*Step, name=Step-76, nlgeom=YES, inc=200,
unsymm=YES
Excavation of the
*Static
0.1, 1., 1e-07, 1.
*CONTROLS,ANALYSIS=DISCONTINUOUS
*MODEL CHANGE, ADD
FEMDDM-1.STOPEN9075P2C80B2, FEMDDM-
1.N9075P2C80UCB1, FEMDDM-
1.N9075P2C80UCB2, FEMDDM-

```

```

1.STOPEN9100P1C65B1, FEMDDM-
1.N9100P1C65UCB1, FEMDDM-
1.N9125P1C65OCB1
*MODEL CHANGE, ADD
FEMDDM-1.STOPEN9075P2C80B1, FEMDDM-
1.STOPEN9200S1C88B1, FEMDDM-
1.N9200S1C88UCB1, FEMDDM-
1.STOPEN9250P1C215B1, FEMDDM-
1.N9250P1C215UCB1, FEMDDM-
1.N9275P1C215OCB1
*FIELD
FEMDDM-1.STOPEN9075P2C80BACKFILL1, 1.0
FEMDDM-1.STOPEN9075P2C80BACKFILL2, 1.0
FEMDDM-1.STOPEN9100P1C65BACKFILL1, 1.0
FEMDDM-1.STOPEN9200S1C88BACKFILL1, 1.0
FEMDDM-1.STOPEN9250P1C215BACKFILL1, 1.0
*MODEL CHANGE, REMOVE
FEMDDM-1.STOPEN9075P2C110B2, FEMDDM-
1.STOPEN9100P1C95B2, FEMDDM-
1.STOPEN9200S1C208B1, FEMDDM-
1.SLRS9025C910B5, FEMDDM-
1.STOPEN9250P1C185B2, FEMDDM-
1.N9125P1C215UC
*MODEL CHANGE, REMOVE
FEMDDM-1.N9150P1C215OC, FEMDDM-
1.N9175S2C103UC, FEMDDM-1.N9175S2C133UC,
FEMDDM-1.N9275P2C170OC
**
** OUTPUT REQUESTS
**
*Restart, write, frequency=0
**
** FIELD OUTPUT: F-Output-2
**
*Output, field
*Element Output, directions=YES
ELEDEN, ELEN, ENER, PEEQMAX, PEEQT
*Contact Output
EFENRRTR, ENRRT
**
** FIELD OUTPUT: F-Output-1
**
*Output, field, variable=PRESELECT
**
** HISTORY OUTPUT: H-Output-1
**
*Output, history, variable=PRESELECT
*End Step
** -----
-
**
** STEP: Step-78
**
*Step, name=Step-78, nlgeom=YES, inc=200,
unsymm=YES
Excavation of the
*Static
0.1, 1., 1e-07, 1.
*CONTROLS, ANALYSIS=DISCONTINUOUS
*MODEL CHANGE, ADD
FEMDDM-1.STOPEN9050S1C208B1, FEMDDM-
1.N9050S1C208UC, FEMDDM-
1.STOPEN9075P2C140B2, FEMDDM-
1.N9075P2C140UCB2, FEMDDM-
1.STOPEN9100P1C125B1
*MODEL CHANGE, ADD
FEMDDM-1.N9100P1C125UCB1, FEMDDM-
1.STOPEN9200S1C118B2, FEMDDM-
1.N9200S1C118UCB2, FEMDDM-
1.STOPEN9250P1C215B2, FEMDDM-
1.N9250P1C215UCB2, FEMDDM-
1.N9275P1C215OCB2
*FIELD
FEMDDM-1.STOPEN9050S1C208BACKFILL1, 1.0
FEMDDM-1.STOPEN9075P2C140BACKFILL2, 1.0
FEMDDM-1.STOPEN9100P1C125BACKFILL1, 1.0
FEMDDM-1.STOPEN9200S1C118BACKFILL2, 1.0
FEMDDM-1.STOPEN9250P1C215BACKFILL2, 1.0
*MODEL CHANGE, REMOVE
FEMDDM-1.STOPEN9050S1C58B1, FEMDDM-
1.STOPEN9075P2C170B2, FEMDDM-
1.STOPEN9100P1C125B2, FEMDDM-

```

```

1.STOPEN9200S1C148B2, FEMDDM-
1.SLRS9025C960B6
*MODEL CHANGE, REMOVE
FEMDDM-1.STOPEN9250P2C140B1, FEMDDM-
1.N9200S2C103UC, FEMDDM-1.N9200S2C133UC
**
** OUTPUT REQUESTS
**
*Restart, write, frequency=0
**
** FIELD OUTPUT: F-Output-2
**
*Output, field
*Element Output, directions=YES
ELEDEN, ELEN, ENER, PEEQMAX, PEEQT
*Contact Output
EFENRRTR, ENRRT
**
** FIELD OUTPUT: F-Output-1
**
*Output, field, variable=PRESELECT
**
** HISTORY OUTPUT: H-Output-1
**
*Output, history, variable=PRESELECT
*End Step
** -----
-
**
** STEP: Step-79
**
*Step, name=Step-79, nlgeom=YES, inc=200,
unsymm=YES
Excavation of the
*Static
0.1, 1., 1e-07, 1.
*CONTROLS, ANALYSIS=DISCONTINUOUS
*MODEL CHANGE, ADD
FEMDDM-1.STOPEN9050S1C58B1, FEMDDM-
1.N9050S1C58UC, FEMDDM-1.N9075S1C58OC,
FEMDDM-1.STOPEN9075P2C170B2, FEMDDM-
1.N9075P2C170UCB2, FEMDDM-
1.STOPEN9100P1C125B2
*MODEL CHANGE, ADD
FEMDDM-1.N9100P1C125UCB2, FEMDDM-
1.STOPEN9200S1C148B2, FEMDDM-
1.N9200S1C148UCB2, FEMDDM-
1.STOPEN9250P2C140B1, FEMDDM-
1.N9250P2C140UCB3, FEMDDM-
1.N9275P2C140OCB1
*FIELD
FEMDDM-1.STOPEN9050S1C58BACKFILL1, 1.0
FEMDDM-1.STOPEN9075P2C170BACKFILL2, 1.0
FEMDDM-1.STOPEN9100P1C125BACKFILL2, 1.0
FEMDDM-1.STOPEN9200S1C148BACKFILL2, 1.0
FEMDDM-1.STOPEN9250P2C140BACKFILL1, 1.0
*MODEL CHANGE, REMOVE
FEMDDM-1.STOPEN9075P2C110B3, FEMDDM-
1.STOPEN9100P1C185B2, FEMDDM-
1.STOPEN9175S2C103B1, FEMDDM-
1.STOPEN9200S1C178B2, FEMDDM-
1.STOPEN9250P2C170B1, FEMDDM-
1.N9200S2C163UC
*MODEL CHANGE, REMOVE
FEMDDM-1.N9200S2C193UC, FEMDDM-
1.N9050S1C118UC, FEMDDM-1.N9250S2C223UC
**
** OUTPUT REQUESTS
**
*Restart, write, frequency=0
**
** FIELD OUTPUT: F-Output-2
**
*Output, field
*Element Output, directions=YES
ELEDEN, ELEN, ENER, PEEQMAX, PEEQT
*Contact Output
EFENRRTR, ENRRT
**
** FIELD OUTPUT: F-Output-2
**
*Output, field
*Element Output, directions=YES
ELEDEN, ELEN, ENER, PEEQMAX, PEEQT
*Contact Output
EFENRRTR, ENRRT
**
** FIELD OUTPUT: F-Output-1
**
*Output, field, variable=PRESELECT
**
** HISTORY OUTPUT: H-Output-1
**
*Output, history, variable=PRESELECT
*End Step
** -----
-
**
** STEP: Step-80
**
*Step, name=Step-80, nlgeom=YES, inc=200,
unsymm=YES
Excavation of the
*Static
0.1, 1., 1e-07, 1.
*CONTROLS, ANALYSIS=DISCONTINUOUS
*MODEL CHANGE, ADD
FEMDDM-1.STOPEN9075P2C110B3, FEMDDM-
1.N9075P2C110UCB3, FEMDDM-
1.STOPEN9100P1C185B2, FEMDDM-
1.N9100P1C185UCB2, FEMDDM-
1.STOPEN9175S2C103B1
*MODEL CHANGE, ADD
FEMDDM-1.N9175S2C103UCB1, FEMDDM-
1.STOPEN9200S1C178B2, FEMDDM-
1.N9200S1C178UCB2, FEMDDM-
1.STOPEN9250P2C170B1, FEMDDM-
1.N9250P2C170UCB2, FEMDDM-
1.N9275P2C170OCB1
*FIELD
FEMDDM-1.STOPEN9075P2C110BACKFILL3, 1.0
FEMDDM-1.STOPEN9100P1C185BACKFILL2, 1.0
FEMDDM-1.STOPEN9175S2C103BACKFILL1, 1.0
FEMDDM-1.STOPEN9200S1C178BACKFILL2, 1.0
FEMDDM-1.STOPEN9250P2C170BACKFILL1, 1.0
*MODEL CHANGE, REMOVE
FEMDDM-1.STOPEN9075P2C140B3, FEMDDM-
1.STOPEN9100P1C95B3, FEMDDM-
1.STOPEN9175S2C133B1, FEMDDM-
1.STOPEN9200S1C208B2, FEMDDM-
1.STOPEN9250P2C110B1
*MODEL CHANGE, REMOVE
FEMDDM-1.N9050S1C148UC, FEMDDM-
1.N9050S1C178UC, FEMDDM-1.N9125P2C80UC,
FEMDDM-1.N9250S1C88OCB1, FEMDDM-
1.N9250S1C88OCB2
**
** OUTPUT REQUESTS
**
*Restart, write, frequency=0
**
** FIELD OUTPUT: F-Output-2
**
*Output, field
*Element Output, directions=YES
ELEDEN, ELEN, ENER, PEEQMAX, PEEQT
*Contact Output
EFENRRTR, ENRRT

```

```

**
** FIELD OUTPUT: F-Output-1
**
*Output, field, variable=PRESELECT
**
** HISTORY OUTPUT: H-Output-1
**
*Output, history, variable=PRESELECT
*End Step
** -----
-
**
** STEP: Step-81
**
*Step, name=Step-81, nlgeom=YES, inc=200,
unsymm=YES
Excavation of the
*Static
0.1, 1., 1e-07, 1.
*CONTROLS, ANALYSIS=DISCONTINUOUS
*MODEL CHANGE, ADD
FEMDDM-1.STOPEN9075P2C140B3, FEMDDM-
1.N9075P2C140UCB3, FEMDDM-
1.STOPEN9100P1C95B3, FEMDDM-
1.N9100P1C95UCB3, FEMDDM-
1.STOPEN9175S2C133B1, FEMDDM-
1.N9175S2C133UCB1
*MODEL CHANGE, ADD
FEMDDM-1.STOPEN9200S1C208B2, FEMDDM-
1.N9200S1C208UCB2, FEMDDM-
1.STOPEN9250P2C110B1, FEMDDM-
1.N9250P2C110UCB2, FEMDDM-
1.N9275P2C110OCB1
*FIELD
FEMDDM-1.STOPEN9075P2C140BACKFILL3, 1.0
FEMDDM-1.STOPEN9100P1C95BACKFILL3, 1.0
FEMDDM-1.STOPEN9175S2C133BACKFILL1, 1.0
FEMDDM-1.STOPEN9200S1C208BACKFILL2, 1.0
FEMDDM-1.STOPEN9250P2C110BACKFILL1, 1.0
*MODEL CHANGE, REMOVE
FEMDDM-1.STOPEN9075P2C170B3, FEMDDM-
1.STOPEN9100P1C125B3, FEMDDM-
1.STOPEN9175S2C163B1, FEMDDM-
1.STOPEN9200S1C88B2, FEMDDM-
1.STOPEN9250P2C200B1
*MODEL CHANGE, REMOVE
FEMDDM-1.N9075S1C88UC, FEMDDM-
1.N9075S1C118UC, FEMDDM-1.N9125P2C110UC,
FEMDDM-1.N9125P2C200UC, FEMDDM-
1.STOPEN9225S2C223B1
**
** OUTPUT REQUESTS
**
*Restart, write, frequency=0
**
** FIELD OUTPUT: F-Output-2
**
*Output, field
*Element Output, directions=YES
ELEDEN, ELEN, ENER, PEEQMAX, PEEQT
*Contact Output
EFENRRTR, ENRRT
**
** FIELD OUTPUT: F-Output-1
**
*Output, field, variable=PRESELECT
**
** HISTORY OUTPUT: H-Output-1
**
*Output, history, variable=PRESELECT
*End Step
** -----
-
**
** STEP: Step-82
**
*Step, name=Step-82, nlgeom=YES, inc=200,
unsymm=YES
Excavation of the
*Static
0.1, 1., 1e-07, 1.
*CONTROLS, ANALYSIS=DISCONTINUOUS
*MODEL CHANGE, ADD
FEMDDM-1.STOPEN9075P2C170B3, FEMDDM-
1.N9075P2C170UCB3, FEMDDM-
1.STOPEN9100P1C125B3, FEMDDM-
1.N9100P1C125UCB3, FEMDDM-
1.STOPEN9175S2C163B1, FEMDDM-
1.N9175S2C163UCB1
*MODEL CHANGE, ADD
FEMDDM-1.STOPEN9200S1C88B2, FEMDDM-
1.N9200S1C88UCB2, FEMDDM-
1.STOPEN9250P2C200B1, FEMDDM-
1.N9250P2C200UCB1, FEMDDM-
1.N9275P2C200OCB1, FEMDDM-
1.STOPEN9225S2C223B1, FEMDDM-
1.N9225S2C223UC
*FIELD
FEMDDM-1.STOPEN9075P2C170BACKFILL3, 1.0
FEMDDM-1.STOPEN9100P1C125BACKFILL3, 1.0
FEMDDM-1.STOPEN9175S2C163BACKFILL1, 1.0
FEMDDM-1.STOPEN9200S1C88BACKFILL2, 1.0
FEMDDM-1.STOPEN9250P2C200BACKFILL1, 1.0
FEMDDM-1.STOPEN9225S2C223BACKFILL1, 1.0
*MODEL CHANGE, REMOVE
FEMDDM-1.STOPEN9050S1C88B1, FEMDDM-
1.STOPEN9100P1C155B2, FEMDDM-
1.STOPEN9100P1C155B3, FEMDDM-
1.STOPEN9125P1C185B1, FEMDDM-
1.STOPEN9175S2C193B1, FEMDDM-
1.STOPEN9200S1C118B3
*MODEL CHANGE, REMOVE
FEMDDM-1.STOPEN9250P2C200B2, FEMDDM-
1.N9250S1C178UC, FEMDDM-1.N9250S1C178UC1,
FEMDDM-1.N9075S1C148UC, FEMDDM-
1.N9075S1C178UC, FEMDDM-1.N9125P2C140UC
**
** OUTPUT REQUESTS
**
*Restart, write, frequency=0
**
** FIELD OUTPUT: F-Output-2
**
*Output, field
*Element Output, directions=YES
ELEDEN, ELEN, ENER, PEEQMAX, PEEQT
*Contact Output
EFENRRTR, ENRRT
**
** FIELD OUTPUT: F-Output-1
**
*Output, field, variable=PRESELECT
**
** HISTORY OUTPUT: H-Output-1
**
*Output, history, variable=PRESELECT
*End Step
** -----
-
**

```

```

** STEP: Step-83
**
*Step, name=Step-83, nlgeom=YES, inc=200,
unsymm=YES
Excavation of the
*Static
0.1, 1., 1e-07, 1.
*CONTROLS, ANALYSIS=DISCONTINUOUS
*MODEL CHANGE, ADD
FEMDDM-1.STOPEN9050S1C88B1, FEMDDM-
1.N9050S1C88UCB1, FEMDDM-
1.STOPEN9100P1C155B3, FEMDDM-
1.N9100P1C155UCB3, FEMDDM-
1.STOPEN9125P1C185B1, FEMDDM-
1.N9125P1C185UCB1
*MODEL CHANGE, ADD
FEMDDM-1.N9150P1C185OCB1, FEMDDM-
1.STOPEN9175S2C193B1, FEMDDM-
1.N9175S2C193UCB1, FEMDDM-
1.STOPEN9200S1C118B3, FEMDDM-
1.N9200S1C118UCB3
*MODEL CHANGE, ADD
FEMDDM-1.STOPEN9250P2C200B2, FEMDDM-
1.N9250P2C200UCB2, FEMDDM-
1.N9275P2C200OCB2, FEMDDM-
1.STOPEN9100P1C155B2, FEMDDM-
1.N9100P1C155UCB2
*FIELD
FEMDDM-1.STOPEN9050S1C88BACKFILL1, 1.0
FEMDDM-1.STOPEN9100P1C155BACKFILL3, 1.0
FEMDDM-1.STOPEN9100P1C155BACKFILL2, 1.0
FEMDDM-1.STOPEN9125P1C185BACKFILL1, 1.0
FEMDDM-1.STOPEN9175S2C193BACKFILL1, 1.0
FEMDDM-1.STOPEN9200S1C118BACKFILL3, 1.0
FEMDDM-1.STOPEN9250P2C200BACKFILL2, 1.0
*MODEL CHANGE, REMOVE
FEMDDM-1.STOPEN9050S1C118B1, FEMDDM-
1.STOPEN9100P2C80B1, FEMDDM-
1.STOPEN9125P1C125B1, FEMDDM-
1.STOPEN9175S2C103B2, FEMDDM-
1.STOPEN9200S1C148B3
*MODEL CHANGE, REMOVE
FEMDDM-1.STOPEN9225S1C88B1, FEMDDM-
1.N9250S1C118UC, FEMDDM-1.N9250S1C118UC2,
FEMDDM-1.N9125P2C170UC
**
** OUTPUT REQUESTS
**
*Restart, write, frequency=0
**
** FIELD OUTPUT: F-Output-2
**
*Output, field
*Element Output, directions=YES
ELEDEN, ELEN, ENER, PEEQMAX, PEEQT
*Contact Output
EFENRRTR, ENRRT
**
** FIELD OUTPUT: F-Output-1
**
*Output, field, variable=PRESELECT
**
** HISTORY OUTPUT: H-Output-1
**
*Output, history, variable=PRESELECT
**
*End Step
** -----
-
**
** STEP: Step-84
**
*Step, name=Step-84, nlgeom=YES, inc=200,
unsymm=YES
Excavation of the
*Static
0.1, 1., 1e-07, 1.
**
*Step, name=Step-84, nlgeom=YES, inc=200,
unsymm=YES
Excavation of the
*Static
0.1, 1., 1e-07, 1.
*CONTROLS, ANALYSIS=DISCONTINUOUS
*MODEL CHANGE, ADD
FEMDDM-1.STOPEN9050S1C118B1, FEMDDM-
1.N9050S1C118UCB1, FEMDDM-
1.STOPEN9100P2C80B1, FEMDDM-
1.N9100P2C80UCB1, FEMDDM-
1.STOPEN9125P1C125B1, FEMDDM-
1.N9125P1C125UCB1
*MODEL CHANGE, ADD
FEMDDM-1.N9150P1C125OCB1, FEMDDM-
1.STOPEN9175S2C103B2, FEMDDM-
1.N9175S2C103UCB2, FEMDDM-
1.STOPEN9200S1C148B3, FEMDDM-
1.N9200S1C148UCB3, FEMDDM-
1.STOPEN9225S1C88B1, FEMDDM-
1.N9225S1C88UCB1
*FIELD
FEMDDM-1.STOPEN9050S1C118BACKFILL1, 1.0
FEMDDM-1.STOPEN9100P2C80BACKFILL1, 1.0
FEMDDM-1.STOPEN9125P1C125BACKFILL1, 1.0
FEMDDM-1.STOPEN9175S2C103BACKFILL2, 1.0
FEMDDM-1.STOPEN9200S1C148BACKFILL3, 1.0
FEMDDM-1.STOPEN9225S1C88BACKFILL1, 1.0
*MODEL CHANGE, REMOVE
FEMDDM-1.STOPEN9050S1C148B1, FEMDDM-
1.STOPEN9100P2C200B1, FEMDDM-
1.STOPEN9125P1C155B1, FEMDDM-
1.STOPEN9175S2C133B2, FEMDDM-
1.STOPEN9200S1C178B3
*MODEL CHANGE, REMOVE
FEMDDM-1.N9250S1C208UC, FEMDDM-
1.SLRS9025C935B5, FEMDDM-1.N9250S1C148UC,
FEMDDM-1.N9250S1C148UC1
**
** OUTPUT REQUESTS
**
*Restart, write, frequency=0
**
** FIELD OUTPUT: F-Output-2
**
*Output, field
*Element Output, directions=YES
ELEDEN, ELEN, ENER, PEEQMAX, PEEQT
*Contact Output
EFENRRTR, ENRRT
**
** FIELD OUTPUT: F-Output-1
**
*Output, field, variable=PRESELECT
**
** HISTORY OUTPUT: H-Output-1
**
*Output, history, variable=PRESELECT
**
*End Step
** -----
-
**
** STEP: Step-85
**
*Step, name=Step-85, nlgeom=YES, inc=200,
unsymm=YES
Excavation of the
*Static
0.1, 1., 1e-07, 1.

```

```

*CONTROLS,ANALYSIS=DISCONTINUOUS
*MODEL CHANGE, ADD
FEMDDM-1.STOPEN9050S1C148B1, FEMDDM-
1.N9050S1C148UCB1, FEMDDM-
1.STOPEN9100P2C200B1, FEMDDM-
1.N9100P2C200UCB1, FEMDDM-
1.STOPEN9125P1C155B1, FEMDDM-
1.N9125P1C155UCB1
*MODEL CHANGE, ADD
FEMDDM-1.N9150P1C155OCB1, FEMDDM-
1.STOPEN9175S2C133B2, FEMDDM-
1.N9175S2C133UCB2, FEMDDM-
1.STOPEN9200S1C178B3, FEMDDM-
1.N9200S1C178UCB3
*FIELD
FEMDDM-1.STOPEN9050S1C148BACKFILL1, 1.0
FEMDDM-1.STOPEN9100P2C200BACKFILL1, 1.0
FEMDDM-1.STOPEN9125P1C155BACKFILL1, 1.0
FEMDDM-1.STOPEN9175S2C133BACKFILL2, 1.0
FEMDDM-1.STOPEN9200S1C178BACKFILL3, 1.0
*MODEL CHANGE, REMOVE
FEMDDM-1.STOPEN9050S1C178B1, FEMDDM-
1.STOPEN9100P2C110B1, FEMDDM-
1.STOPEN9125P1C95B1, FEMDDM-
1.STOPEN9175S2C163B2
*MODEL CHANGE, REMOVE
FEMDDM-1.STOPEN9225S1C148B1, FEMDDM-
1.SLRS9025C950B5
**
** OUTPUT REQUESTS
**
*Restart, write, frequency=0
**
** FIELD OUTPUT: F-Output-2
**
*Output, field
*Element Output, directions=YES
ELEDEN, ELEN, ENER, PEEQMAX, PEEQT
*Contact Output
EFENRRTR, ENRRT
**
** FIELD OUTPUT: F-Output-1
**
*Output, field, variable=PRESELECT
**
** HISTORY OUTPUT: H-Output-1
**
*Output, history, variable=PRESELECT
*End Step
** -----
-
**
** STEP: Step-87
**
*Step, name=Step-87, nlgeom=YES, inc=200,
unsymm=YES
Excavation of the
*Static
0.1, 1., 1e-07, 1.
*CONTROLS,ANALYSIS=DISCONTINUOUS
*MODEL CHANGE, ADD
FEMDDM-1.STOPEN9050S1C88B2, FEMDDM-
1.N9050S1C88UCB2, FEMDDM-
1.STOPEN9100P2C80B2, FEMDDM-
1.N9100P2C80UCB2, FEMDDM-
1.STOPEN9125P1C185B2, FEMDDM-
1.N9125P1C185UCB2
*MODEL CHANGE, ADD
FEMDDM-1.N9150P1C185OCB2, FEMDDM-
1.STOPEN9175S2C193B2, FEMDDM-
1.N9175S2C193UCB2, FEMDDM-
1.STOPEN9225S1C178B1
*MODEL CHANGE, ADD
FEMDDM-1.N9225S1C178UCB1, FEMDDM-
1.N9250S1C178UC1, FEMDDM-1.N9250S1C178UC2
*FIELD
FEMDDM-1.STOPEN9050S1C88BACKFILL2, 1.0
FEMDDM-1.STOPEN9100P2C80BACKFILL2, 1.0
FEMDDM-1.STOPEN9125P1C185BACKFILL2, 1.0
FEMDDM-1.STOPEN9175S2C193BACKFILL2, 1.0
FEMDDM-1.STOPEN9225S1C178BACKFILL1, 1.0
*MODEL CHANGE, REMOVE
1.N9175S2C163UCB2, FEMDDM-
1.STOPEN9225S1C148B1, FEMDDM-
1.N9225S1C148UCB1
*FIELD
FEMDDM-1.STOPEN9050S1C178BACKFILL1, 1.0
FEMDDM-1.STOPEN9100P2C110BACKFILL1, 1.0
FEMDDM-1.STOPEN9125P1C95BACKFILL1, 1.0
FEMDDM-1.STOPEN9175S2C163BACKFILL2, 1.0
FEMDDM-1.STOPEN9225S1C148BACKFILL1, 1.0
*MODEL CHANGE, REMOVE
FEMDDM-1.STOPEN9050S1C88B2, FEMDDM-
1.STOPEN9100P2C80B2, FEMDDM-
1.STOPEN9125P1C185B2, FEMDDM-
1.STOPEN9175S2C193B2, FEMDDM-
1.STOPEN9225S1C178B1, FEMDDM-
1.SLRS9025C950B6
**
** OUTPUT REQUESTS
**
*Restart, write, frequency=0
**
** FIELD OUTPUT: F-Output-2
**
*Output, field
*Element Output, directions=YES
ELEDEN, ELEN, ENER, PEEQMAX, PEEQT
*Contact Output
EFENRRTR, ENRRT
**
** FIELD OUTPUT: F-Output-1
**
*Output, field, variable=PRESELECT
**
** HISTORY OUTPUT: H-Output-1
**
*Output, history, variable=PRESELECT
*End Step
** -----
-
**
** STEP: Step-86
**
*Step, name=Step-86, nlgeom=YES, inc=200,
unsymm=YES
Excavation of the
*Static
0.1, 1., 1e-07, 1.
*CONTROLS,ANALYSIS=DISCONTINUOUS
*MODEL CHANGE, ADD
FEMDDM-1.STOPEN9050S1C178B1, FEMDDM-
1.N9050S1C178UCB1, FEMDDM-
1.STOPEN9100P2C110B1, FEMDDM-
1.N9100P2C110UCB1, FEMDDM-
1.STOPEN9125P1C95B1, FEMDDM-
1.N9125P1C95UCB1
*MODEL CHANGE, ADD
FEMDDM-1.N9150P1C95OCB1, FEMDDM-
1.STOPEN9175S2C163B2, FEMDDM-

```

```

FEMDDM-1.STOPEN9050S1C118B2, FEMDDM-
1.STOPEN9100P2C140B1, FEMDDM-
1.STOPEN9125P1C95B2, FEMDDM-
1.STOPEN9175S2C103B3, FEMDDM-
1.STOPEN9225S1C118B1, FEMDDM-
1.N9225S2C133UC
**
** OUTPUT REQUESTS
**
**Restart, write, frequency=0
**
** FIELD OUTPUT: F-Output-2
**
**Output, field
**Element Output, directions=YES
ELEDEN, ELEN, ENER, PEEQMAX, PEEQT
**Contact Output
EFENRRTR, ENRRT
**
** FIELD OUTPUT: F-Output-1
**
**Output, field, variable=PRESELECT
**
** HISTORY OUTPUT: H-Output-1
**
**Output, history, variable=PRESELECT
**End Step
** -----
-
**
** STEP: Step-88
**
**Step, name=Step-88, ngeom=YES, inc=200,
unsymm=YES
Excavation of the
**Static
0.1, 1., 1e-07, 1.
**CONTROLS, ANALYSIS=DISCONTINUOUS
**MODEL CHANGE, ADD
FEMDDM-1.STOPEN9050S1C118B2, FEMDDM-
1.N9050S1C118UCB2, FEMDDM-
1.STOPEN9100P2C140B1, FEMDDM-
1.N9100P2C140UCB1, FEMDDM-
1.STOPEN9125P1C95B2, FEMDDM-
1.N9125P1C95UCB2
**MODEL CHANGE, ADD
FEMDDM-1.N9150P1C95OCB2, FEMDDM-
1.STOPEN9175S2C103B3, FEMDDM-
1.N9175S2C103UCB3, FEMDDM-
1.STOPEN9225S1C118B1, FEMDDM-
1.N9225S1C118UCB1, FEMDDM-
1.N9250S1C118UC1, FEMDDM-1.N9250S1C118UC2
**FIELD
FEMDDM-1.STOPEN9050S1C118BACKFILL2, 1.0
FEMDDM-1.STOPEN9100P2C140BACKFILL1, 1.0
FEMDDM-1.STOPEN9125P1C95BACKFILL2, 1.0
FEMDDM-1.STOPEN9175S2C103BACKFILL3, 1.0
FEMDDM-1.STOPEN9225S1C118BACKFILL1, 1.0
**MODEL CHANGE, REMOVE
FEMDDM-1.STOPEN9050S1C148B2, FEMDDM-
1.STOPEN9100P2C170B1, FEMDDM-
1.STOPEN9125P1C125B2, FEMDDM-
1.STOPEN9175S2C133B3, FEMDDM-
1.STOPEN9225S1C208B1, FEMDDM-
1.N9225S2C103UC
**
** OUTPUT REQUESTS
**
**Restart, write, frequency=0
**
** FIELD OUTPUT: F-Output-2
**
**Output, field
**Element Output, directions=YES
ELEDEN, ELEN, ENER, PEEQMAX, PEEQT
**Contact Output
EFENRRTR, ENRRT
**
** FIELD OUTPUT: F-Output-1
**
**Output, field, variable=PRESELECT
**
** HISTORY OUTPUT: H-Output-1
**
**Output, history, variable=PRESELECT
**End Step
** -----
-
**
** STEP: Step-89
**
**Step, name=Step-89, ngeom=YES, inc=200,
unsymm=YES
Excavation of the
**Static
0.1, 1., 1e-07, 1.
**CONTROLS, ANALYSIS=DISCONTINUOUS
**MODEL CHANGE, ADD
FEMDDM-1.STOPEN9050S1C148B2, FEMDDM-
1.N9050S1C148UCB2, FEMDDM-
1.STOPEN9100P2C170B1, FEMDDM-
1.N9100P2C170UCB1, FEMDDM-
1.STOPEN9125P1C125B2, FEMDDM-
1.N9125P1C125UCB2
**MODEL CHANGE, ADD
FEMDDM-1.N9150P1C125OCB2, FEMDDM-
1.STOPEN9175S2C133B3, FEMDDM-
1.N9175S2C133UCB3, FEMDDM-
1.STOPEN9225S1C208B1, FEMDDM-
1.N9225S1C208UCB1
**FIELD
FEMDDM-1.STOPEN9050S1C148BACKFILL2, 1.0
FEMDDM-1.STOPEN9100P2C170BACKFILL1, 1.0
FEMDDM-1.STOPEN9125P1C125BACKFILL2, 1.0
FEMDDM-1.STOPEN9175S2C133BACKFILL3, 1.0
FEMDDM-1.STOPEN9225S1C208BACKFILL1, 1.0
**MODEL CHANGE, REMOVE
FEMDDM-1.STOPEN9050S1C178B2, FEMDDM-
1.STOPEN9100P2C110B2, FEMDDM-
1.STOPEN9125P1C155B2, FEMDDM-
1.STOPEN9175S2C163B3, FEMDDM-
1.STOPEN9225S1C88B2
**MODEL CHANGE, REMOVE
FEMDDM-1.N9225S2C193UC, FEMDDM-
1.N9100S1C88UC, FEMDDM-1.N9150P2C200OC
**
** OUTPUT REQUESTS
**
**Restart, write, frequency=0
**
** FIELD OUTPUT: F-Output-2
**
**Output, field
**Element Output, directions=YES
ELEDEN, ELEN, ENER, PEEQMAX, PEEQT
**Contact Output
EFENRRTR, ENRRT
**
** FIELD OUTPUT: F-Output-1
**
**Output, field, variable=PRESELECT
**
** HISTORY OUTPUT: H-Output-1
**
**Output, history, variable=PRESELECT
**End Step
** -----
-
**

```

```

*Output, field, variable=PRESELECT
**
** HISTORY OUTPUT: H-Output-1
**
*Output, history, variable=PRESELECT
*End Step
** -----
-
**
** STEP: Step-90
**
*Step, name=Step-90, nlgeom=YES, inc=200,
unsymm=YES
Excavation of the
*Static
0.1, 1., 1e-07, 1.
*CONTROLS, ANALYSIS=DISCONTINUOUS
*MODEL CHANGE, ADD
FEMDDM-1.STOPEN9050S1C178B2, FEMDDM-
1.N9050S1C178UCB2, FEMDDM-
1.STOPEN9100P2C110B2, FEMDDM-
1.N9100P2C110UCB2, FEMDDM-
1.STOPEN9125P1C155B2, FEMDDM-
1.N9125P1C155UCB2
*MODEL CHANGE, ADD
FEMDDM-1.N9150P1C155OCB2, FEMDDM-
1.STOPEN9175S2C163B3, FEMDDM-
1.N9175S2C163UCB3, FEMDDM-
1.STOPEN9225S1C88B2, FEMDDM-
1.N9225S1C88UCB2, FEMDDM-
1.N9250S1C88OCB1
*FIELD
FEMDDM-1.STOPEN9050S1C178BACKFILL2, 1.0
FEMDDM-1.STOPEN9100P2C110BACKFILL2, 1.0
FEMDDM-1.STOPEN9125P1C155BACKFILL2, 1.0
FEMDDM-1.STOPEN9175S2C163BACKFILL3, 1.0
FEMDDM-1.STOPEN9225S1C88BACKFILL2, 1.0
*MODEL CHANGE, REMOVE
FEMDDM-1.STOPEN9050S1C88B3, FEMDDM-
1.STOPEN9100P2C140B2, FEMDDM-
1.STOPEN9125P1C95B3, FEMDDM-
1.STOPEN9175S2C193B3, FEMDDM-
1.STOPEN9200S2C103B1, FEMDDM-
1.STOPEN9225S1C208B2
*MODEL CHANGE, REMOVE
FEMDDM-1.N9225S2C163UC, FEMDDM-
1.N9050S2C193UC, FEMDDM-1.N9075S2C193UC,
FEMDDM-1.N9100S1C208UC, FEMDDM-
1.N9150P2C80OC
**
** OUTPUT REQUESTS
**
*Restart, write, frequency=0
**
** FIELD OUTPUT: F-Output-2
**
*Output, field
*Element Output, directions=YES
ELEDEN, ELEN, ENER, PEEQMAX, PEEQT
*Contact Output
EFENRRTR, ENRRT
**
** FIELD OUTPUT: F-Output-1
**
*Output, field, variable=PRESELECT
**
** HISTORY OUTPUT: H-Output-1
**
*Output, history, variable=PRESELECT
*End Step
** -----
-
**
** STEP: Step-91
**
*Step, name=Step-91, nlgeom=YES, inc=200,
unsymm=YES
Excavation of the
*Static
0.1, 1., 1e-07, 1.
*CONTROLS, ANALYSIS=DISCONTINUOUS
*MODEL CHANGE, ADD
FEMDDM-1.STOPEN9050S1C88B3, FEMDDM-
1.N9050S1C88UCB3, FEMDDM-
1.STOPEN9100P2C140B2, FEMDDM-
1.N9100P2C140UCB2, FEMDDM-
1.STOPEN9125P1C95B3, FEMDDM-
1.N9125P1C95UCB3
*MODEL CHANGE, ADD
FEMDDM-1.N9150P1C95OCB3, FEMDDM-
1.STOPEN9175S2C193B3, FEMDDM-
1.N9175S2C193UCB3, FEMDDM-
1.STOPEN9200S2C103B1, FEMDDM-
1.N9200S2C103UCB1, FEMDDM-
1.STOPEN9225S1C208B2, FEMDDM-
1.N9225S1C208UCB2
*FIELD
FEMDDM-1.STOPEN9050S1C88BACKFILL3, 1.0
FEMDDM-1.STOPEN9100P2C140BACKFILL2, 1.0
FEMDDM-1.STOPEN9125P1C95BACKFILL3, 1.0
FEMDDM-1.STOPEN9175S2C193BACKFILL3, 1.0
FEMDDM-1.STOPEN9200S2C103BACKFILL1, 1.0
FEMDDM-1.STOPEN9225S1C208BACKFILL2, 1.0
*MODEL CHANGE, REMOVE
FEMDDM-1.STOPEN9050S1C118B3, FEMDDM-
1.STOPEN9100P2C170B2, FEMDDM-
1.STOPEN9125P1C125B3, FEMDDM-
1.STOPEN9200S2C133B1, FEMDDM-
1.STOPEN9225S1C178B2
*MODEL CHANGE, REMOVE
FEMDDM-1.N9050S2C163UC, FEMDDM-
1.N9075S2C163UC, FEMDDM-1.N9150P2C110OC
**
** OUTPUT REQUESTS
**
*Restart, write, frequency=0
**
** FIELD OUTPUT: F-Output-2
**
*Output, field
*Element Output, directions=YES
ELEDEN, ELEN, ENER, PEEQMAX, PEEQT
*Contact Output
EFENRRTR, ENRRT
**
** FIELD OUTPUT: F-Output-1
**
*Output, field, variable=PRESELECT
**
** HISTORY OUTPUT: H-Output-1
**
*Output, history, variable=PRESELECT
*End Step
** -----
-
**
** STEP: Step-92
**
*Step, name=Step-92, nlgeom=YES, inc=200,
unsymm=YES

```

```

Excavation of the
*Static
0.1, 1., 1e-07, 1.
*CONTROLS,ANALYSIS=DISCONTINUOUS
*MODEL CHANGE, ADD
FEMDDM-1.STOPEN9050S1C118B3, FEMDDM-
1.N9050S1C118UCB3, FEMDDM-
1.STOPEN9100P2C170B2, FEMDDM-
1.N9100P2C170UCB2, FEMDDM-
1.STOPEN9125P1C125B3, FEMDDM-
1.N9125P1C125UCB3
*MODEL CHANGE, ADD
FEMDDM-1.N9150P1C125OCB3, FEMDDM-
1.STOPEN9200S2C133B1, FEMDDM-
1.N9200S2C133UCB1, FEMDDM-
1.STOPEN9225S1C178B2, FEMDDM-
1.N9225S1C178UCB2
*FIELD
FEMDDM-1.STOPEN9050S1C118BACKFILL3, 1.0
FEMDDM-1.STOPEN9100P2C170BACKFILL2, 1.0
FEMDDM-1.STOPEN9125P1C125BACKFILL3, 1.0
FEMDDM-1.STOPEN9200S2C133BACKFILL1, 1.0
FEMDDM-1.STOPEN9225S1C178BACKFILL2, 1.0
*MODEL CHANGE, REMOVE
FEMDDM-1.STOPEN9050S1C148B3, FEMDDM-
1.STOPEN9075S1C88B1, FEMDDM-
1.STOPEN9100P2C110B3, FEMDDM-
1.STOPEN9125P1C155B3, FEMDDM-
1.STOPEN9200S2C163B1, FEMDDM-
1.STOPEN9225S1C88B3
*MODEL CHANGE, REMOVE
FEMDDM-1.N9050S2C103UC, FEMDDM-
1.N9075S2C103UC, FEMDDM-1.N9150P2C140OC
**
** OUTPUT REQUESTS
**
*Restart, write, frequency=0
**
** FIELD OUTPUT: F-Output-2
**
*Output, field
*Element Output, directions=YES
ELEDEN, ELEN, ENER, PEEQMAX, PEEQT
*Contact Output
EFENRRTR, ENRRT
**
** FIELD OUTPUT: F-Output-1
**
*Output, field, variable=PRESELECT
**
** HISTORY OUTPUT: H-Output-1
**
*Output, history, variable=PRESELECT
*End Step
** -----
-
**
** STEP: Step-93
**
*Step, name=Step-93, nlgeom=YES, inc=200,
unsymm=YES
Excavation of the
*Static
0.1, 1., 1e-07, 1.
*CONTROLS,ANALYSIS=DISCONTINUOUS
*MODEL CHANGE, ADD
FEMDDM-1.STOPEN9050S1C148B3, FEMDDM-
1.N9050S1C148UCB3, FEMDDM-
1.STOPEN9075S1C88B1, FEMDDM-
1.N9075S1C88UCB1, FEMDDM-
1.STOPEN9100P2C110B3, FEMDDM-
1.N9100P2C110UCB3, FEMDDM-
1.STOPEN9125P1C155B3, FEMDDM-
1.N9125P1C155UCB3, FEMDDM-
1.STOPEN9200S2C163B1, FEMDDM-
1.N9200S2C163UCB1, FEMDDM-
1.STOPEN9225S1C88B3, FEMDDM-
1.N9225S1C88UCB3, FEMDDM-
1.N9250S1C88OCB2
*FIELD
FEMDDM-1.STOPEN9050S1C148BACKFILL3, 1.0
FEMDDM-1.STOPEN9075S1C88BACKFILL1, 1.0
FEMDDM-1.STOPEN9100P2C110BACKFILL3, 1.0
FEMDDM-1.STOPEN9125P1C155BACKFILL3, 1.0
FEMDDM-1.STOPEN9200S2C163BACKFILL1, 1.0
FEMDDM-1.STOPEN9225S1C88BACKFILL3, 1.0
*MODEL CHANGE, REMOVE
FEMDDM-1.STOPEN9050S2C193B1, FEMDDM-
1.STOPEN9075S1C88B2, FEMDDM-
1.STOPEN9100P2C140B3, FEMDDM-
1.STOPEN9125P2C110B1, FEMDDM-
1.STOPEN9200S2C193B1
*MODEL CHANGE, REMOVE
FEMDDM-1.STOPEN9225S1C118B2, FEMDDM-
1.N9050S2C73UC, FEMDDM-1.N9075S2C73UC
**
** OUTPUT REQUESTS
**
*Restart, write, frequency=0
**
** FIELD OUTPUT: F-Output-2
**
*Output, field
*Element Output, directions=YES
ELEDEN, ELEN, ENER, PEEQMAX, PEEQT
*Contact Output
EFENRRTR, ENRRT
**
** FIELD OUTPUT: F-Output-1
**
*Output, field, variable=PRESELECT
**
** HISTORY OUTPUT: H-Output-1
**
*Output, history, variable=PRESELECT
*End Step
** -----
-
**
** STEP: Step-94
**
*Step, name=Step-94, nlgeom=YES, inc=200,
unsymm=YES
Excavation of the
*Static
0.1, 1., 1e-07, 1.
*CONTROLS,ANALYSIS=DISCONTINUOUS
*MODEL CHANGE, ADD
FEMDDM-1.STOPEN9050S2C193B1, FEMDDM-
1.N9050S2C193UC, FEMDDM-
1.STOPEN9075S1C88B2, FEMDDM-
1.N9075S1C88UCB2, FEMDDM-
1.STOPEN9100P2C140B3, FEMDDM-
1.N9100P2C140UCB3, FEMDDM-
1.STOPEN9125P2C110B1
*MODEL CHANGE, ADD
FEMDDM-1.N9125P2C110UCB1, FEMDDM-
1.N9150P2C110OCB1, FEMDDM-

```

```

1.STOPEN9200S2C193B1, FEMDDM-
1.N9200S2C193UCB1, FEMDDM-
1.STOPEN9225S1C118B2, FEMDDM-
1.N9225S1C118UCB2
*FIELD
FEMDDM-1.STOPEN9050S2C193BACKFILL1, 1.0
FEMDDM-1.STOPEN9075S1C88BACKFILL2, 1.0
FEMDDM-1.STOPEN9100P2C140BACKFILL3, 1.0
FEMDDM-1.STOPEN9125P2C110BACKFILL1, 1.0
FEMDDM-1.STOPEN9200S2C193BACKFILL1, 1.0
FEMDDM-1.STOPEN9225S1C118BACKFILL2, 1.0
*MODEL CHANGE, REMOVE
FEMDDM-1.STOPEN9050S2C73B1, FEMDDM-
1.STOPEN9075S1C208B1, FEMDDM-
1.STOPEN9125P2C200B1, FEMDDM-
1.STOPEN9200S2C103B2, FEMDDM-
1.STOPEN9225S1C148B2
*MODEL CHANGE, REMOVE
FEMDDM-1.N9050S2C133UC, FEMDDM-
1.N9075S2C133UC, FEMDDM-1.N9100S1C118UC,
FEMDDM-1.N9150P2C170OC, FEMDDM-
1.N9250S2C133UC, FEMDDM-1.N9250S2C133UC1
**
** OUTPUT REQUESTS
**
*Restart, write, frequency=0
**
** FIELD OUTPUT: F-Output-2
**
*Output, field
*Element Output, directions=YES
ELEDEN, ELEN, ENER, PEEQMAX, PEEQT
*Contact Output
EFENRRTR, ENRRT
**
** FIELD OUTPUT: F-Output-1
**
*Output, field, variable=PRESELECT
**
** HISTORY OUTPUT: H-Output-1
**
*Output, history, variable=PRESELECT
*End Step
** -----
-
**
** STEP: Step-96
**
*Step, name=Step-96, nlgeom=YES, inc=200,
unsymm=YES
Excavation of the
*Static
0.1, 1., 1e-07, 1.
*CONTROLS, ANALYSIS=DISCONTINUOUS
*MODEL CHANGE, ADD
FEMDDM-1.STOPEN9050S2C103B1, FEMDDM-
1.N9050S2C103UCB1, FEMDDM-
1.STOPEN9075S1C118B1, FEMDDM-
1.N9075S1C118UCB1, FEMDDM-
1.STOPEN9125P1C215B1, FEMDDM-
1.N9125P1C215UC
*MODEL CHANGE, ADD
FEMDDM-1.N9150P1C215OCB1, FEMDDM-
1.STOPEN9200S2C133B2, FEMDDM-
1.N9200S2C133UCB2, FEMDDM-
1.STOPEN9225S1C178B3, FEMDDM-
1.N9225S1C178UCB3
*FIELD
FEMDDM-1.STOPEN9050S2C103BACKFILL1, 1.0
FEMDDM-1.STOPEN9075S1C118BACKFILL1, 1.0
FEMDDM-1.STOPEN9125P1C215BACKFILL1, 1.0
FEMDDM-1.STOPEN9200S2C133BACKFILL2, 1.0
FEMDDM-1.STOPEN9225S1C178BACKFILL3, 1.0
*MODEL CHANGE, REMOVE
FEMDDM-1.STOPEN9050S2C133B1, FEMDDM-
1.STOPEN9075S1C148B1, FEMDDM-

```

```

1.STOPEN9125P2C140B1, FEMDDM-
1.STOPEN9200S2C163B2
*MODEL CHANGE, REMOVE
FEMDDM-1.N9250S2C193UC, FEMDDM-
1.N9275S1C178OC, FEMDDM-1.N9275S2C223OC
**
** OUTPUT REQUESTS
**
*Restart, write, frequency=0
**
** FIELD OUTPUT: F-Output-2
**
*Output, field
*Element Output, directions=YES
ELEDEN, ELEN, ENER, PEEQMAX, PEEQT
*Contact Output
EFENRRTR, ENRRT
**
** FIELD OUTPUT: F-Output-1
**
*Output, field, variable=PRESELECT
**
** HISTORY OUTPUT: H-Output-1
**
*Output, history, variable=PRESELECT
*End Step
** -----
-
**
** STEP: Step-98
**
*Step, name=Step-98, nlgeom=YES, inc=200,
unsymm=YES
Excavation of the
*Static
0.1, 1., 1e-07, 1.
*CONTROLS, ANALYSIS=DISCONTINUOUS
*MODEL CHANGE, ADD
FEMDDM-1.STOPEN9050S2C163B1, FEMDDM-
1.N9050S2C163UCB1, FEMDDM-
1.STOPEN9075S1C178B1, FEMDDM-
1.N9075S1C178UCB1, FEMDDM-
1.STOPEN9125P2C80B1, FEMDDM-
1.N9125P2C80UCB1, FEMDDM-1.N9275S2C223OC
*MODEL CHANGE, ADD
FEMDDM-1.N9150P2C80OCB1, FEMDDM-
1.STOPEN9200S2C193B2, FEMDDM-
1.N9200S2C193UCB2, FEMDDM-
1.STOPEN9225S1C148B3, FEMDDM-
1.N9225S1C148UCB3, FEMDDM-
1.STOPEN9250S2C223B1, FEMDDM-
1.N9250S2C223UC
*FIELD
FEMDDM-1.STOPEN9050S2C163BACKFILL1, 1.0
FEMDDM-1.STOPEN9075S1C178BACKFILL1, 1.0
FEMDDM-1.STOPEN9125P2C80BACKFILL1, 1.0
FEMDDM-1.STOPEN9200S2C193BACKFILL2, 1.0
FEMDDM-1.STOPEN9225S1C148BACKFILL3, 1.0
FEMDDM-1.STOPEN9250S2C223BACKFILL1, 1.0
*MODEL CHANGE, REMOVE
FEMDDM-1.STOPEN9050S2C73B2, FEMDDM-
1.STOPEN9075S1C88B3, FEMDDM-
1.STOPEN9100S1C208B1, FEMDDM-
1.STOPEN9125P2C170B1, FEMDDM-
1.STOPEN9200S2C103B3
*MODEL CHANGE, REMOVE
FEMDDM-1.STOPEN9250S1C118B1, FEMDDM-
1.N9275S1C148OC
**
** OUTPUT REQUESTS
**
*Restart, write, frequency=0
**
** FIELD OUTPUT: F-Output-2
**
*Output, field
*Element Output, directions=YES
ELEDEN, ELEN, ENER, PEEQMAX, PEEQT
*Contact Output
EFENRRTR, ENRRT
**

```

```

** FIELD OUTPUT: F-Output-1
**
*Output, field, variable=PRESELECT
**
** HISTORY OUTPUT: H-Output-1
**
*Output, history, variable=PRESELECT
*End Step
** -----
-
**
** STEP: Step-99
**
*Step, name=Step-99, nlgeom=YES, inc=200,
unsymm=YES
Excavation of the
*Static
0.1, 1., 1e-07, 1.
*CONTROLS, ANALYSIS=DISCONTINUOUS
*MODEL CHANGE, ADD
FEMDDM-1.STOPEN9050S2C73B2, FEMDDM-
1.N9050S2C73UCB2, FEMDDM-
1.STOPEN9075S1C88B3, FEMDDM-
1.N9075S1C88UCB3, FEMDDM-
1.STOPEN9100S1C208B1
*MODEL CHANGE, ADD
FEMDDM-1.STOPEN9125P2C170B1, FEMDDM-
1.N9125P2C170UCB1, FEMDDM-
1.N9150P2C170OCB1, FEMDDM-
1.STOPEN9200S2C103B3, FEMDDM-
1.N9200S2C103UCB3
*MODEL CHANGE, ADD
FEMDDM-1.STOPEN9250S1C118B1, FEMDDM-
1.N9250S1C118UCB3, FEMDDM-
1.N9100S1C208UC, FEMDDM-1.N9275S1C118OC
*FIELD
FEMDDM-1.STOPEN9050S2C73BACKFILL2, 1.0
FEMDDM-1.STOPEN9075S1C88BACKFILL3, 1.0
FEMDDM-1.STOPEN9100S1C208BACKFILL1, 1.0
FEMDDM-1.STOPEN9125P2C170BACKFILL1, 1.0
FEMDDM-1.STOPEN9200S2C103BACKFILL3, 1.0
FEMDDM-1.STOPEN9250S1C118BACKFILL1, 1.0
*MODEL CHANGE, REMOVE
FEMDDM-1.STOPEN9050S2C103B2, FEMDDM-
1.STOPEN9075S1C178B2, FEMDDM-
1.STOPEN9125P2C80B2, FEMDDM-
1.STOPEN9200S2C133B3, FEMDDM-
1.STOPEN9225S2C103B1
*MODEL CHANGE, REMOVE
FEMDDM-1.STOPEN9250S1C148B1, FEMDDM-
1.N9100S2C73UC
**
** OUTPUT REQUESTS
**
*Restart, write, frequency=0
**
** FIELD OUTPUT: F-Output-2
**
*Output, field
*Element Output, directions=YES
ELEDEN, ELEN, ENER, PEEQMAX, PEEQT
*Contact Output
EFENRRTR, ENRRT
**
** FIELD OUTPUT: F-Output-1
**
*Output, field, variable=PRESELECT
**
** HISTORY OUTPUT: H-Output-1
**
*Output, history, variable=PRESELECT
*End Step
** -----
-
**
** STEP: Step-100
**
*Step, name=Step-100, nlgeom=YES, inc=200,
unsymm=YES
Excavation of the
*Static
0.1, 1., 1e-07, 1.
*CONTROLS, ANALYSIS=DISCONTINUOUS
*MODEL CHANGE, ADD
FEMDDM-1.STOPEN9050S2C103B2, FEMDDM-
1.N9050S2C103UCB2, FEMDDM-
1.STOPEN9075S1C178B2, FEMDDM-
1.N9075S1C178UCB2, FEMDDM-
1.STOPEN9125P2C80B2, FEMDDM-
1.N9125P2C80UCB2
*MODEL CHANGE, ADD
FEMDDM-1.N9150P2C80OCB2, FEMDDM-
1.STOPEN9200S2C133B3, FEMDDM-
1.N9200S2C133UCB3, FEMDDM-
1.STOPEN9225S2C103B1, FEMDDM-
1.N9225S2C103UCB1
*MODEL CHANGE, ADD
FEMDDM-1.STOPEN9250S1C148B1, FEMDDM-
1.N9250S1C148UCB3, FEMDDM-
1.N9275S1C148OC
*FIELD
FEMDDM-1.STOPEN9050S2C103BACKFILL2, 1.0
FEMDDM-1.STOPEN9075S1C178BACKFILL2, 1.0
FEMDDM-1.STOPEN9125P2C80BACKFILL2, 1.0
FEMDDM-1.STOPEN9200S2C133BACKFILL3, 1.0
FEMDDM-1.STOPEN9225S2C103BACKFILL1, 1.0
FEMDDM-1.STOPEN9250S1C148BACKFILL1, 1.0
*MODEL CHANGE, REMOVE
FEMDDM-1.STOPEN9050S2C133B2, FEMDDM-
1.STOPEN9075S1C118B2, FEMDDM-
1.STOPEN9125P2C110B2, FEMDDM-
1.STOPEN9200S2C163B3, FEMDDM-
1.STOPEN9225S2C133B1, FEMDDM-
1.STOPEN9250S1C178B1
**
** OUTPUT REQUESTS
**
*Restart, write, frequency=0
**
** FIELD OUTPUT: F-Output-2
**
*Output, field
*Element Output, directions=YES
ELEDEN, ELEN, ENER, PEEQMAX, PEEQT
*Contact Output
EFENRRTR, ENRRT
**
** FIELD OUTPUT: F-Output-1
**
*Output, field, variable=PRESELECT
**
** HISTORY OUTPUT: H-Output-1
**
*Output, history, variable=PRESELECT
*End Step
** -----
-
**
** STEP: Step-101
**

```

```

*Step, name=Step-101, nlgeom=YES, inc=200,
unsymm=YES
Excavation of the
*Static
0.1, 1., 1e-07, 1.
*CONTROLS, ANALYSIS=DISCONTINUOUS
*MODEL CHANGE, ADD
FEMDDM-1.STOPEN9050S2C133B2, FEMDDM-
1.N9050S2C133UCB2, FEMDDM-
1.STOPEN9075S1C118B2, FEMDDM-
1.N9075S1C118UCB2, FEMDDM-
1.STOPEN9125P2C110B2, FEMDDM-
1.N9125P2C110UCB2
*MODEL CHANGE, ADD
FEMDDM-1.N9150P2C110OCB2, FEMDDM-
1.STOPEN9200S2C163B3, FEMDDM-
1.N9200S2C163UCB3, FEMDDM-
1.STOPEN9225S2C133B1, FEMDDM-
1.N9225S2C133UCB1
*MODEL CHANGE, ADD
FEMDDM-1.STOPEN9250S1C178B1, FEMDDM-
1.N9250S1C178UCB2, FEMDDM-
1.N9275S1C178OCB1
*FIELD
FEMDDM-1.STOPEN9050S2C133BACKFILL2, 1.0
FEMDDM-1.STOPEN9075S1C118BACKFILL2, 1.0
FEMDDM-1.STOPEN9125P2C110BACKFILL2, 1.0
FEMDDM-1.STOPEN9200S2C163BACKFILL3, 1.0
FEMDDM-1.STOPEN9225S2C133BACKFILL1, 1.0
FEMDDM-1.STOPEN9250S1C178BACKFILL1, 1.0
*MODEL CHANGE, REMOVE
FEMDDM-1.STOPEN9050S2C163B2, FEMDDM-
1.STOPEN9075S1C148B2, FEMDDM-
1.STOPEN9125P2C140B2, FEMDDM-
1.STOPEN9200S2C193B3, FEMDDM-
1.STOPEN9225S2C163B1, FEMDDM-
1.STOPEN9250S1C208B1
**
** OUTPUT REQUESTS
**
*Restart, write, frequency=0
**
** FIELD OUTPUT: F-Output-2
**
*Output, field
*Element Output, directions=YES
ELEDEN, ELEN, ENER, PEEQMAX, PEEQT
*Contact Output
EFENRRTR, ENRRT
**
** FIELD OUTPUT: F-Output-1
**
*Output, field, variable=PRESELECT
**
** HISTORY OUTPUT: H-Output-1
**
*Output, history, variable=PRESELECT
*End Step
** -----
-
**
** STEP: Step-102
**
*Step, name=Step-102, nlgeom=YES, inc=200,
unsymm=YES
Excavation of the
*Static
0.1, 1., 1e-07, 1.
*CONTROLS, ANALYSIS=DISCONTINUOUS
*MODEL CHANGE, ADD
FEMDDM-1.STOPEN9050S2C103B3, FEMDDM-
1.N9050S2C103UCB3, FEMDDM-
1.STOPEN9075S1C118B3, FEMDDM-
1.N9075S1C118UCB3, FEMDDM-
1.STOPEN9125P2C170B2, FEMDDM-
1.N9125P2C170UCB2
*MODEL CHANGE, ADD
FEMDDM-1.STOPEN9050S2C163B2, FEMDDM-
1.N9050S2C163UCB2, FEMDDM-
1.STOPEN9075S1C148B2, FEMDDM-
1.N9075S1C148UCB2, FEMDDM-
1.STOPEN9125P2C140B2, FEMDDM-
1.N9125P2C140UCB2, FEMDDM-
1.N9275S1C208OCB1
*MODEL CHANGE, ADD
FEMDDM-1.N9150P2C140OCB2, FEMDDM-
1.STOPEN9200S2C193B3, FEMDDM-
1.N9200S2C193UCB3, FEMDDM-
1.STOPEN9225S2C163B1, FEMDDM-
1.N9225S2C163UCB1, FEMDDM-
1.STOPEN9250S1C208B1, FEMDDM-
1.N9250S1C208UCB1
*FIELD
FEMDDM-1.STOPEN9050S2C163BACKFILL2, 1.0
FEMDDM-1.STOPEN9075S1C148BACKFILL2, 1.0
FEMDDM-1.STOPEN9125P2C140BACKFILL2, 1.0
FEMDDM-1.STOPEN9200S2C193BACKFILL3, 1.0
FEMDDM-1.STOPEN9225S2C163BACKFILL1, 1.0
FEMDDM-1.STOPEN9250S1C208BACKFILL1, 1.0
*MODEL CHANGE, REMOVE
FEMDDM-1.STOPEN9050S2C103B3, FEMDDM-
1.STOPEN9075S1C118B3, FEMDDM-
1.STOPEN9125P2C170B2, FEMDDM-
1.STOPEN9225S2C193B1, FEMDDM-
1.STOPEN9250S1C178B2, FEMDDM-
1.N9100S2C193UC
**
** OUTPUT REQUESTS
**
*Restart, write, frequency=0
**
** FIELD OUTPUT: F-Output-2
**
*Output, field
*Element Output, directions=YES
ELEDEN, ELEN, ENER, PEEQMAX, PEEQT
*Contact Output
EFENRRTR, ENRRT
**
** FIELD OUTPUT: F-Output-1
**
*Output, field, variable=PRESELECT
**
** HISTORY OUTPUT: H-Output-1
**
*Output, history, variable=PRESELECT
*End Step
** -----
-
**
** STEP: Step-103
**
*Step, name=Step-103, nlgeom=YES, inc=200,
unsymm=YES
Excavation of the
*Static
0.1, 1., 1e-07, 1.
*CONTROLS, ANALYSIS=DISCONTINUOUS
*MODEL CHANGE, ADD
FEMDDM-1.STOPEN9050S2C103B3, FEMDDM-
1.N9050S2C103UCB3, FEMDDM-
1.STOPEN9075S1C118B3, FEMDDM-
1.N9075S1C118UCB3, FEMDDM-
1.STOPEN9125P2C170B2, FEMDDM-
1.N9125P2C170UCB2
*MODEL CHANGE, ADD

```

```

FEMDDM-1.N9150P2C170OCB2, FEMDDM-
1.STOPEN9225S2C193B1, FEMDDM-
1.N9225S2C193UCB1, FEMDDM-
1.STOPEN9250S1C178B2, FEMDDM-
1.N9250S1C178UCB3, FEMDDM-
1.N9275S1C178OCB2
*FIELD
FEMDDM-1.STOPEN9050S2C103BACKFILL3, 1.0
FEMDDM-1.STOPEN9075S1C118BACKFILL3, 1.0
FEMDDM-1.STOPEN9125P2C170BACKFILL2, 1.0
FEMDDM-1.STOPEN9225S2C193BACKFILL1, 1.0
FEMDDM-1.STOPEN9250S1C178BACKFILL2, 1.0
*MODEL CHANGE, REMOVE
FEMDDM-1.STOPEN9050S2C133B3, FEMDDM-
1.STOPEN9075S1C148B3, FEMDDM-
1.STOPEN9125P2C80B3, FEMDDM-
1.STOPEN9225S2C103B2, FEMDDM-
1.STOPEN9250S1C208B2, FEMDDM-
1.N9100S2C103UC
**
** OUTPUT REQUESTS
**
*Restart, write, frequency=0
**
** FIELD OUTPUT: F-Output-2
**
*Output, field
*Element Output, directions=YES
ELEDEN, ELEN, ENER, PEEQMAX, PEEQT
*Contact Output
EFENRRTR, ENRRT
**
** FIELD OUTPUT: F-Output-1
**
*Output, field, variable=PRESELECT
**
** HISTORY OUTPUT: H-Output-1
**
*Output, history, variable=PRESELECT
*End Step
** -----
-
**
** STEP: Step-104
**
*Step, name=Step-104, nlgeom=YES, inc=200,
unsymm=YES
Excavation of the
*Static
0.1, 1., 1e-07, 1.
*CONTROLS, ANALYSIS=DISCONTINUOUS
*MODEL CHANGE, ADD
FEMDDM-1.STOPEN9050S2C133B3, FEMDDM-
1.N9050S2C133UCB3, FEMDDM-
1.STOPEN9075S1C148B3, FEMDDM-
1.N9075S1C148UCB3, FEMDDM-
1.STOPEN9125P2C80B3, FEMDDM-
1.N9125P2C80UCB3, FEMDDM-
1.N9150P2C80OCB3
*MODEL CHANGE, ADD
FEMDDM-1.STOPEN9225S2C103B2, FEMDDM-
1.N9225S2C103UCB2, FEMDDM-
1.N9250S2C103OC1, FEMDDM-
1.N9250S2C103OC2, FEMDDM-
1.STOPEN9250S1C208B2, FEMDDM-
1.N9250S1C208UCB2, FEMDDM-
1.N9275S1C208OCB2
*FIELD
FEMDDM-1.STOPEN9050S2C133BACKFILL3, 1.0
FEMDDM-1.STOPEN9075S1C148BACKFILL3, 1.0
FEMDDM-1.STOPEN9125P2C80BACKFILL3, 1.0
FEMDDM-1.STOPEN9225S2C103BACKFILL2, 1.0
FEMDDM-1.STOPEN9250S1C178BACKFILL2, 1.0
*MODEL CHANGE, REMOVE
FEMDDM-1.STOPEN9050S2C163B3, FEMDDM-
1.STOPEN9075S2C193B1, FEMDDM-
1.STOPEN9125P2C110B3, FEMDDM-
1.STOPEN9225S2C133B2, FEMDDM-
1.N9100S2C133UC, FEMDDM-1.N9100S2C163UC
**
** OUTPUT REQUESTS
**
*Restart, write, frequency=0
**
** FIELD OUTPUT: F-Output-2
**
*Output, field
*Element Output, directions=YES
ELEDEN, ELEN, ENER, PEEQMAX, PEEQT
*Contact Output
EFENRRTR, ENRRT
**
** FIELD OUTPUT: F-Output-1
**
*Output, field, variable=PRESELECT
**
** HISTORY OUTPUT: H-Output-1
**
*Output, history, variable=PRESELECT
*End Step
** -----
-
**
** STEP: Step-105
**
*Step, name=Step-105, nlgeom=YES, inc=200,
unsymm=YES
Excavation of the
*Static
0.1, 1., 1e-07, 1.
*CONTROLS, ANALYSIS=DISCONTINUOUS
*MODEL CHANGE, ADD
FEMDDM-1.STOPEN9050S2C163B3, FEMDDM-
1.N9050S2C163UCB3, FEMDDM-
1.STOPEN9075S2C193B1, FEMDDM-
1.N9075S2C193UC, FEMDDM-
1.STOPEN9125P2C110B3, FEMDDM-
1.N9125P2C110UCB3
*MODEL CHANGE, ADD
FEMDDM-1.N9150P2C110OCB3, FEMDDM-
1.STOPEN9225S2C133B2, FEMDDM-
1.N9225S2C133UCB2, FEMDDM-
1.N9250S2C133UC1, FEMDDM-1.N9250S2C133UC2
*FIELD
FEMDDM-1.STOPEN9050S2C163BACKFILL3, 1.0
FEMDDM-1.STOPEN9075S2C193BACKFILL1, 1.0
FEMDDM-1.STOPEN9125P2C110BACKFILL3, 1.0
FEMDDM-1.STOPEN9225S2C133BACKFILL2, 1.0
*MODEL CHANGE, REMOVE
FEMDDM-1.STOPEN9075S2C73B1, FEMDDM-
1.STOPEN9125P2C140B3, FEMDDM-
1.STOPEN9225S2C163B2, FEMDDM-
1.N9125S2C193UC, FEMDDM-1.N9125S1C88UC
**
** OUTPUT REQUESTS
**
*Restart, write, frequency=0
**
** FIELD OUTPUT: F-Output-2
**

```

```

*Output, field
*Element Output, directions=YES
ELEDEN, ELEN, ENER, PEEQMAX, PEEQT
*Contact Output
EFENRRTR, ENRRT
**
** FIELD OUTPUT: F-Output-1
**
*Output, field, variable=PRESELECT
**
** HISTORY OUTPUT: H-Output-1
**
*Output, history, variable=PRESELECT
*End Step
** -----
-
**
** STEP: Step-106
**
*Step, name=Step-106, nlgeom=YES, inc=200,
unsymm=YES
Excavation of the
*Static
0.1, 1., 1e-07, 1.
*CONTROLS, ANALYSIS=DISCONTINUOUS
*MODEL CHANGE, ADD
FEMDDM-1.STOPEN9075S2C73B1, FEMDDM-
1.N9075S2C73UCB1, FEMDDM-
1.STOPEN9125P2C140B3, FEMDDM-
1.N9125P2C140UCB3, FEMDDM-
1.N9150P2C140OCB3
*MODEL CHANGE, ADD
FEMDDM-1.STOPEN9225S2C163B2, FEMDDM-
1.N9225S2C163UCB2, FEMDDM-
1.N9250S2C163UC1, FEMDDM-1.N9250S2C163UC2
*FIELD
FEMDDM-1.STOPEN9075S2C73BACKFILL1, 1.0
FEMDDM-1.STOPEN9125P2C140BACKFILL3, 1.0
FEMDDM-1.STOPEN9225S2C163BACKFILL2, 1.0
*MODEL CHANGE, REMOVE
FEMDDM-1.STOPEN9075S2C103B1, FEMDDM-
1.STOPEN9100S1C88B1, FEMDDM-
1.STOPEN9125P2C170B3, FEMDDM-
1.STOPEN9225S2C193B2, FEMDDM-
1.N9125S1C118UC
**
** OUTPUT REQUESTS
**
*Restart, write, frequency=0
**
** FIELD OUTPUT: F-Output-2
**
*Output, field
*Element Output, directions=YES
ELEDEN, ELEN, ENER, PEEQMAX, PEEQT
*Contact Output
EFENRRTR, ENRRT
**
** FIELD OUTPUT: F-Output-1
**
*Output, field, variable=PRESELECT
**
** HISTORY OUTPUT: H-Output-1
**
*Output, history, variable=PRESELECT
*End Step
** -----
-
**
** STEP: Step-108
**
*Step, name=Step-108, nlgeom=YES, inc=200,
unsymm=YES
Excavation of the
*Static
0.1, 1., 1e-07, 1.
*CONTROLS, ANALYSIS=DISCONTINUOUS
*MODEL CHANGE, ADD
FEMDDM-1.STOPEN9075S2C133B1, FEMDDM-
1.N9075S2C133UCB1, FEMDDM-
1.STOPEN9100S1C118B1, FEMDDM-
1.N9100S1C118UCB1
*MODEL CHANGE, ADD
FEMDDM-1.STOPEN9225S2C103B3, FEMDDM-
1.N9225S2C103UCB3, FEMDDM-
1.N9250S2C103OCB3
*FIELD

```

```

FEMDDM-1.STOPEN9075S2C133BACKFILL1, 1.0
FEMDDM-1.STOPEN9100S1C118BACKFILL1, 1.0
FEMDDM-1.STOPEN9225S2C103BACKFILL3, 1.0
*MODEL CHANGE, REMOVE
FEMDDM-1.STOPEN9075S2C163B1, FEMDDM-
1.STOPEN9100S1C148B1, FEMDDM-
1.STOPEN9125S1C208B1, FEMDDM-
1.STOPEN9225S2C133B3, FEMDDM-
1.N9125S1C178UC, FEMDDM-1.N9275S2C133OC
**
** OUTPUT REQUESTS
**
*Restart, write, frequency=0
**
** FIELD OUTPUT: F-Output-2
**
*Output, field
*Element Output, directions=YES
ELEDEN, ELEN, ENER, PEEQMAX, PEEQT
*Contact Output
EFENRRTR, ENRRT
**
** FIELD OUTPUT: F-Output-1
**
*Output, field, variable=PRESELECT
**
** HISTORY OUTPUT: H-Output-1
**
*Output, history, variable=PRESELECT
*End Step
** -----
-
**
** STEP: Step-110
**
*Step, name=Step-110, nlgeom=YES, inc=200,
unsymm=YES
Excavation of the
*Static
0.1, 1., 1e-07, 1.
*CONTROLS, ANALYSIS=DISCONTINUOUS
*MODEL CHANGE, ADD
FEMDDM-1.STOPEN9075S2C73B2, FEMDDM-
1.N9075S2C73UCB2, FEMDDM-
1.STOPEN9100S1C178B1, FEMDDM-
1.N9100S1C178UCB1, FEMDDM-
1.STOPEN9225S2C163B3, FEMDDM-
1.N9225S2C163UCB3
*MODEL CHANGE, ADD
FEMDDM-1.STOPEN9250S2C133B1, FEMDDM-
1.N9250S2C133UCB3, FEMDDM-
1.N9275S2C133OC, FEMDDM-
1.STOPEN9225S2C163B4, FEMDDM-
1.N9225S2C163UCB4
*FIELD
FEMDDM-1.STOPEN9075S2C73BACKFILL2, 1.0
FEMDDM-1.STOPEN9100S1C178BACKFILL1, 1.0
FEMDDM-1.STOPEN9225S2C163BACKFILL3, 1.0
FEMDDM-1.STOPEN9225S2C163BACKFILL4, 1.0
FEMDDM-1.STOPEN9250S2C133BACKFILL1, 1.0
*MODEL CHANGE, REMOVE
FEMDDM-1.STOPEN9075S2C103B2, FEMDDM-
1.STOPEN9100S1C178B2, FEMDDM-
1.STOPEN9225S2C193B3, FEMDDM-
1.STOPEN9250S2C163B1, FEMDDM-
1.N9275S2C193OC
**
** OUTPUT REQUESTS
**
*Restart, write, frequency=0
**
** FIELD OUTPUT: F-Output-2
**
*Output, field
*Element Output, directions=YES
ELEDEN, ELEN, ENER, PEEQMAX, PEEQT
*Contact Output
EFENRRTR, ENRRT
**
** FIELD OUTPUT: F-Output-1
**
*Output, field, variable=PRESELECT
**
** HISTORY OUTPUT: H-Output-1
**

```

```

*Output, history, variable=PRESELECT
*End Step
** -----
-
**
** STEP: Step-111
**
*Step, name=Step-111, nlgeom=YES, inc=200,
unsymm=YES
Excavation of the
*Static
0.1, 1., 1e-07, 1.
*CONTROLS,ANALYSIS=DISCONTINUOUS
*MODEL CHANGE, ADD
FEMDDM-1.STOPEN9075S2C103B2, FEMDDM-
1.N9075S2C103UCB2, FEMDDM-
1.STOPEN9100S1C178B2, FEMDDM-
1.N9100S1C178UCB2, FEMDDM-
1.STOPEN9225S2C193B3, FEMDDM-
1.N9225S2C193UCB3
*MODEL CHANGE, ADD
FEMDDM-1.STOPEN9250S2C163B1, FEMDDM-
1.N9250S2C163UCB3, FEMDDM-
1.N9275S2C163OC
*FIELD
FEMDDM-1.STOPEN9075S2C103BACKFILL2, 1.0
FEMDDM-1.STOPEN9100S1C178BACKFILL2, 1.0
FEMDDM-1.STOPEN9225S2C193BACKFILL3, 1.0
FEMDDM-1.STOPEN9250S2C163BACKFILL1, 1.0
*MODEL CHANGE, REMOVE
FEMDDM-1.STOPEN9075S2C103B3, FEMDDM-
1.STOPEN9100S1C88B2, FEMDDM-
1.STOPEN9250S2C193B1
**
** OUTPUT REQUESTS
**
*Restart, write, frequency=0
**
** FIELD OUTPUT: F-Output-2
**
*Output, field
*Element Output, directions=YES
ELEDEN, ELEN, ENER, PEEQMAX, PEEQT
*Contact Output
EFENRRTR, ENRRT
**
** FIELD OUTPUT: F-Output-1
**
*Output, field, variable=PRESELECT
**
** HISTORY OUTPUT: H-Output-1
**
*Output, history, variable=PRESELECT
*End Step
** -----
-
**
** STEP: Step-112
**
*Step, name=Step-112, nlgeom=YES, inc=200,
unsymm=YES
Excavation of the
*Static
0.1, 1., 1e-07, 1.
*CONTROLS,ANALYSIS=DISCONTINUOUS
*MODEL CHANGE, ADD
FEMDDM-1.STOPEN9075S2C103B3, FEMDDM-
1.N9075S2C103UCB3, FEMDDM-
1.STOPEN9100S1C88B2, FEMDDM-
1.N9100S1C88UCB2
**
** STEP: Step-113
**
*Step, name=Step-113, nlgeom=YES, inc=200,
unsymm=YES
Excavation of the
*Static
0.1, 1., 1e-07, 1.
*CONTROLS,ANALYSIS=DISCONTINUOUS
*MODEL CHANGE, ADD
FEMDDM-1.STOPEN9075S2C133B2, FEMDDM-
1.N9075S2C133UCB2, FEMDDM-
1.STOPEN9100S1C88B3, FEMDDM-
1.N9100S1C88UCB3, FEMDDM-
1.N9075S2C133UCB3
*MODEL CHANGE, ADD
FEMDDM-1.STOPEN9250S2C193B2, FEMDDM-
1.N9250S2C193UCB2, FEMDDM-
1.N9275S2C193OCB2, FEMDDM-
1.STOPEN9075S2C133B3
*FIELD
FEMDDM-1.STOPEN9075S2C133BACKFILL2, 1.0
FEMDDM-1.STOPEN9075S2C133BACKFILL3, 1.0
FEMDDM-1.STOPEN9100S1C88BACKFILL3, 1.0
FEMDDM-1.STOPEN9250S2C193BACKFILL2, 1.0
*MODEL CHANGE, REMOVE
FEMDDM-1.STOPEN9075S2C163B2, FEMDDM-
1.STOPEN9075S2C163B3, FEMDDM-
1.STOPEN9100S1C118B2, FEMDDM-
1.STOPEN9100S1C118B3, FEMDDM-
1.N9125S2C73UC
**
** OUTPUT REQUESTS

```

```

**
**Restart, write, frequency=0
**
** FIELD OUTPUT: F-Output-2
**
**Output, field
**Element Output, directions=YES
ELEDEN, ELEN, ENER, PEEQMAX, PEEQT
**Contact Output
EFENRRTR, ENRRT
**
** FIELD OUTPUT: F-Output-1
**
**Output, field, variable=PRESELECT
**
** HISTORY OUTPUT: H-Output-1
**
**Output, history, variable=PRESELECT
**End Step
** -----
-
**
** STEP: Step-114
**
**Step, name=Step-114, nlgeom=YES, inc=200,
unsymm=YES
Excavation of the
**Static
0.1, 1., 1e-07, 1.
**CONTROLS, ANALYSIS=DISCONTINUOUS
**MODEL CHANGE, ADD
FEMDDM-1.STOPEN9075S2C163B2, FEMDDM-
1.N9075S2C163UCB2, FEMDDM-
1.STOPEN9075S2C163B3, FEMDDM-
1.N9075S2C163UCB3
**MODEL CHANGE, ADD
FEMDDM-1.STOPEN9100S1C118B2, FEMDDM-
1.N9100S1C118UCB2, FEMDDM-
1.STOPEN9100S1C118B3, FEMDDM-
1.N9100S1C118UCB3
**FIELD
FEMDDM-1.STOPEN9075S2C163BACKFILL2, 1.0
FEMDDM-1.STOPEN9075S2C163BACKFILL3, 1.0
FEMDDM-1.STOPEN9100S1C118BACKFILL2, 1.0
FEMDDM-1.STOPEN9100S1C118BACKFILL3, 1.0
**MODEL CHANGE, REMOVE
FEMDDM-1.STOPEN9100S1C148B2, FEMDDM-
1.STOPEN9100S1C148B3, FEMDDM-
1.STOPEN9125S1C88B1, FEMDDM-
1.STOPEN9125S1C88B2, FEMDDM-
1.STOPEN9125S1C88B3, FEMDDM-
1.N9125S2C103UC, FEMDDM-1.N9150S1C118OC
**
** OUTPUT REQUESTS
**
**Restart, write, frequency=0
**
** FIELD OUTPUT: F-Output-2
**
**Output, field
**Element Output, directions=YES
ELEDEN, ELEN, ENER, PEEQMAX, PEEQT
**Contact Output
EFENRRTR, ENRRT
**
** FIELD OUTPUT: F-Output-1
**
**Output, field, variable=PRESELECT
**
** HISTORY OUTPUT: H-Output-1
**
**Output, history, variable=PRESELECT
**End Step
** -----
-
**
** STEP: Step-115
**
**Step, name=Step-115, nlgeom=YES, inc=200,
unsymm=YES
Excavation of the
**Static
0.1, 1., 1e-07, 1.
**CONTROLS, ANALYSIS=DISCONTINUOUS
**MODEL CHANGE, ADD
FEMDDM-1.STOPEN9100S1C148B2, FEMDDM-
1.N9100S1C148UCB2, FEMDDM-
1.STOPEN9100S1C148B3, FEMDDM-
1.N9100S1C148UCB3
**MODEL CHANGE, ADD
FEMDDM-1.STOPEN9125S1C88B1, FEMDDM-
1.N9125S1C88UCB1, FEMDDM-
1.N9150S1C88OCB1, FEMDDM-
1.STOPEN9125S1C88B2, FEMDDM-
1.N9125S1C88UCB2, FEMDDM-
1.N9150S1C88OCB2
**MODEL CHANGE, ADD
FEMDDM-1.STOPEN9125S1C88B3, FEMDDM-
1.N9125S1C88UCB3, FEMDDM-
1.N9150S1C88OCB3
**FIELD
FEMDDM-1.STOPEN9100S1C148BACKFILL2, 1.0
FEMDDM-1.STOPEN9100S1C148BACKFILL3, 1.0
FEMDDM-1.STOPEN9125S1C88BACKFILL1, 1.0
FEMDDM-1.STOPEN9125S1C88BACKFILL2, 1.0
FEMDDM-1.STOPEN9125S1C88BACKFILL3, 1.0
**MODEL CHANGE, REMOVE
FEMDDM-1.STOPEN9100S2C73B1, FEMDDM-
1.STOPEN9100S2C73B2, FEMDDM-
1.STOPEN9125S1C118B1, FEMDDM-
1.STOPEN9125S1C118B2, FEMDDM-
1.STOPEN9125S1C118B3
**MODEL CHANGE, REMOVE
FEMDDM-1.N9125S2C133UC, FEMDDM-
1.N9125S2C163UC, FEMDDM-1.N9150S1C178OC,
FEMDDM-1.N9150S1C148OC
**
** OUTPUT REQUESTS
**
**Restart, write, frequency=0
**
** FIELD OUTPUT: F-Output-2
**
**Output, field
**Element Output, directions=YES
ELEDEN, ELEN, ENER, PEEQMAX, PEEQT
**Contact Output
EFENRRTR, ENRRT
**
** FIELD OUTPUT: F-Output-1
**
**Output, field, variable=PRESELECT
**
** HISTORY OUTPUT: H-Output-1
**
**Output, history, variable=PRESELECT
**End Step
** -----
-
**

```



```

1.STOPEN9100S2C133B3, FEMDDM-
1.N9100S2C133UCB3
*MODEL CHANGE, ADD
FEMDDM-1.STOPEN9125S2C73B1, FEMDDM-
1.N9125S2C73UCB1, FEMDDM-
1.N9150S2C73OCB1, FEMDDM-
1.STOPEN9125S2C73B2, FEMDDM-
1.N9125S2C73UCB2, FEMDDM-
1.N9150S2C73OCB2
*FIELD
FEMDDM-1.STOPEN9100S2C133BACKFILL1, 1.0
FEMDDM-1.STOPEN9100S2C133BACKFILL2, 1.0
FEMDDM-1.STOPEN9100S2C133BACKFILL3, 1.0
FEMDDM-1.STOPEN9125S2C73BACKFILL1, 1.0
FEMDDM-1.STOPEN9125S2C73BACKFILL2, 1.0
*MODEL CHANGE, REMOVE
FEMDDM-1.STOPEN9100S2C163B1, FEMDDM-
1.STOPEN9100S2C163B2, FEMDDM-
1.STOPEN9100S2C163B3, FEMDDM-
1.STOPEN9125S2C103B1
*MODEL CHANGE, REMOVE
FEMDDM-1.STOPEN9125S2C103B2, FEMDDM-
1.STOPEN9125S2C103B3, FEMDDM-
1.N9150S2C133OC
**
** OUTPUT REQUESTS
**
*Restart, write, frequency=0
**
** FIELD OUTPUT: F-Output-2
**
*Output, field
*Element Output, directions=YES
ELEDEN, ELEN, ENER, PEEQMAX, PEEQT
*Contact Output
EFENRRTR, ENRRT
**
** FIELD OUTPUT: F-Output-1
**
*Output, field, variable=PRESELECT
**
** HISTORY OUTPUT: H-Output-1
**
*Output, history, variable=PRESELECT
*End Step
** -----
-
**
** STEP: Step-119
**
*Step, name=Step-119, nlgeom=YES, inc=200,
unsymm=YES
Excavation of the
*Static
0.1, 1., 1e-07, 1.
*CONTROLS, ANALYSIS=DISCONTINUOUS
*MODEL CHANGE, ADD
FEMDDM-1.STOPEN9100S2C163B1, FEMDDM-
1.N9100S2C163UCB1, FEMDDM-
1.STOPEN9100S2C163B2, FEMDDM-
1.N9100S2C163UCB2, FEMDDM-
1.STOPEN9100S2C163B3, FEMDDM-
1.N9100S2C163UCB3
*MODEL CHANGE, ADD
FEMDDM-1.STOPEN9125S2C103B1, FEMDDM-
1.N9125S2C103UCB1, FEMDDM-
1.N9150S2C103OCB1, FEMDDM-
1.STOPEN9125S2C103B2, FEMDDM-
1.N9125S2C103UCB2, FEMDDM-
1.N9150S2C103OCB2
*MODEL CHANGE, ADD
FEMDDM-1.STOPEN9125S2C133B1, FEMDDM-
1.N9125S2C133UCB1, FEMDDM-
1.N9150S2C133OCB1, FEMDDM-
1.STOPEN9100S2C163BACKFILL1, 1.0
FEMDDM-1.STOPEN9100S2C163BACKFILL2, 1.0
FEMDDM-1.STOPEN9100S2C163BACKFILL3, 1.0
FEMDDM-1.STOPEN9125S2C103BACKFILL1, 1.0
FEMDDM-1.STOPEN9125S2C103BACKFILL2, 1.0
FEMDDM-1.STOPEN9125S2C103BACKFILL3, 1.0
*MODEL CHANGE, REMOVE
**
** STEP: Step-120
**
*Step, name=Step-120, nlgeom=YES, inc=200,
unsymm=YES
Excavation of the
*Static
0.1, 1., 1e-07, 1.
*CONTROLS, ANALYSIS=DISCONTINUOUS
*MODEL CHANGE, ADD
FEMDDM-1.STOPEN9100S2C193B1, FEMDDM-
1.N9100S2C193UC, FEMDDM-
1.STOPEN9125S2C133B1, FEMDDM-
1.N9125S2C133UCB1, FEMDDM-
1.N9150S2C133OCB1
*MODEL CHANGE, ADD
FEMDDM-1.STOPEN9125S2C133B2, FEMDDM-
1.N9125S2C133UCB2, FEMDDM-
1.N9150S2C133OCB2, FEMDDM-
1.STOPEN9125S2C133B3, FEMDDM-
1.N9125S2C133UCB3, FEMDDM-
1.N9150S2C133OCB3
*FIELD
FEMDDM-1.STOPEN9100S2C193BACKFILL1, 1.0
FEMDDM-1.STOPEN9125S2C133BACKFILL1, 1.0
FEMDDM-1.STOPEN9125S2C133BACKFILL2, 1.0
FEMDDM-1.STOPEN9125S2C133BACKFILL3, 1.0
*MODEL CHANGE, REMOVE

```

```

FEMDDM-1.STOPEN9125S1C178B1, FEMDDM-
1.STOPEN9125S1C178B2, FEMDDM-
1.N9150S2C193OC
**
** OUTPUT REQUESTS
**
*Restart, write, frequency=0
**
** FIELD OUTPUT: F-Output-2
**
*Output, field
*Element Output, directions=YES
ELEDEN, ELEN, ENER, PEEQMAX, PEEQT
*Contact Output
EFENRRTR, ENRRT
**
** FIELD OUTPUT: F-Output-1
**
*Output, field, variable=PRESELECT
**
** HISTORY OUTPUT: H-Output-1
**
*Output, history, variable=PRESELECT
*End Step
** -----
-
**
** STEP: Step-121
**
*Step, name=Step-121, nlgeom=YES, inc=200,
unsymm=YES
Excavation of the
*Static
0.1, 1., 1e-07, 1.
*CONTROLS, ANALYSIS=DISCONTINUOUS
*MODEL CHANGE, ADD
FEMDDM-1.STOPEN9125S1C178B1, FEMDDM-
1.N9125S1C178UCB1, FEMDDM-
1.STOPEN9125S1C178B2, FEMDDM-
1.N9125S1C178UCB2, FEMDDM-
1.N9150S1C178OC
*FIELD
FEMDDM-1.STOPEN9125S1C178BACKFILL1, 1.0
FEMDDM-1.STOPEN9125S1C178BACKFILL2, 1.0
*MODEL CHANGE, REMOVE
FEMDDM-1.STOPEN9125S2C193B1
**
** OUTPUT REQUESTS
**
*Restart, write, frequency=0
**
** FIELD OUTPUT: F-Output-2
**
*Output, field
*Element Output, directions=YES
ELEDEN, ELEN, ENER, PEEQMAX, PEEQT
*Contact Output
EFENRRTR, ENRRT
**
** FIELD OUTPUT: F-Output-1
**
*Output, field, variable=PRESELECT
**
** HISTORY OUTPUT: H-Output-1
**
*Output, history, variable=PRESELECT
*End Step
** -----
-
**
** STEP: Step-122
**
*Step, name=Step-122, nlgeom=YES, inc=200,
unsymm=YES
Excavation of the
*Static
0.1, 1., 1e-07, 1.
*CONTROLS, ANALYSIS=DISCONTINUOUS
*MODEL CHANGE, ADD
FEMDDM-1.STOPEN9125S2C193B1, FEMDDM-
1.N9125S2C193UC, FEMDDM-1.N9150S2C193OC
*FIELD
FEMDDM-1.STOPEN9125S2C193BACKFILL1, 1.0
*MODEL CHANGE, REMOVE
FEMDDM-1.STOPEN9125S2C163B1, FEMDDM-
1.STOPEN9125S2C163B2, FEMDDM-
1.STOPEN9125S2C163B3,
**
** OUTPUT REQUESTS
**
*Restart, write, frequency=0
**
** FIELD OUTPUT: F-Output-2
**
*Output, field
*Element Output, directions=YES
ELEDEN, ELEN, ENER, PEEQMAX, PEEQT
*Contact Output
EFENRRTR, ENRRT
**
** FIELD OUTPUT: F-Output-1
**
*Output, field, variable=PRESELECT
**
** HISTORY OUTPUT: H-Output-1
**
*Output, history, variable=PRESELECT
*End Step
** -----
-
**
** STEP: Step-123
**
*Step, name=Step-123, nlgeom=YES, inc=200,
unsymm=YES
Excavation of the
*Static
0.1, 1., 1e-07, 1.
*CONTROLS, ANALYSIS=DISCONTINUOUS
*MODEL CHANGE, ADD
FEMDDM-1.STOPEN9125S2C163B1, FEMDDM-
1.N9125S2C163UCB1, FEMDDM-
1.N9150S2C163OCB1, FEMDDM-
1.STOPEN9125S2C163B2, FEMDDM-
1.N9125S2C163UCB2, FEMDDM-
1.N9150S2C163OCB2
*MODEL CHANGE, ADD
FEMDDM-1.STOPEN9125S2C163B3, FEMDDM-
1.N9125S2C163UCB3, FEMDDM-
1.N9150S2C163OCB3
*FIELD
FEMDDM-1.STOPEN9125S2C163BACKFILL1, 1.0
FEMDDM-1.STOPEN9125S2C163BACKFILL2, 1.0
FEMDDM-1.STOPEN9125S2C163BACKFILL3, 1.0
**
** OUTPUT REQUESTS
**
*Restart, write, frequency=0
**
** FIELD OUTPUT: F-Output-2

```

```
**
*Output, field
*Element Output, directions=YES
ELEDEN, ELEN, ENER, PEEQMAX, PEEQT
*Contact Output
EFENRRTR, ENRRT
**
** FIELD OUTPUT: F-Output-1
**

*Output, field, variable=PRESELECT
**
** HISTORY OUTPUT: H-Output-1
**
*Output, history, variable=PRESELECT
*End Step
```